

12-72

DTIC

AD-A279 880



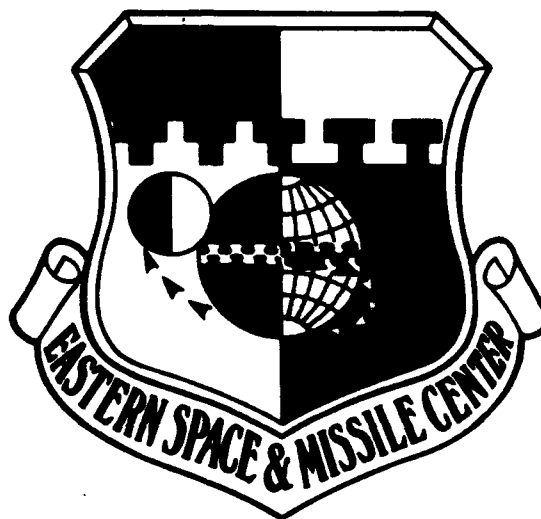
DTIC
ELECTE
MAY 31 1994
S F D

45 SPW/SEMB -TR-92-001

O

1-13

FINAL REPORT KEVLAR OVERWRAP STUDY



K

APRIL 1992

94-16123



SASB

This document has been approved
for public release and sale; its
distribution is unlimited.

Arde Inc.
500 Walnut Street
Norwood, N.J. 07648

Eastern Space and Missile Center
/Air Force Systems Command
Patrick Air Force Base, Florida

DTIC QUALITY INSPECTED 1

94 5 22 009

NOTICE

When government specifications, or other data are used for any purpose other than in connection with a definitely related government procurement operation, the United States Government thereby incurs no responsibility nor any obligation whatsoever; and the fact that the government may have formulated, furnished, or in any way supplied the said specifications, or other data, is not to be regarded by implication or otherwise as in any manner licensing the holder of any other person or corporation, or conveying any right or permission to manufacture use, or sell any patented invention that may in any way be related thereto.

This report has been reviewed by the Office of Public Affairs (ESMC/PA) and is releasable to the National Technical Information Service (NTIS). At NTIS, it will be available to the general public, including foreign nations.

This technical report has been reviewed and is approved for publication.



PETER TADDIE
Project Manager



LOUIS J. ULLIAN
Deputy Director, Range Safety

**FINAL REPORT
KEVLAR OVERWRAP STUDY**

April 1992

Prepared by

**Arde Inc.
500 Walnut Street
Norwood, N.J. 07648**

D. Gleich

Accession For	
NTIS CRA&I	<input checked="checked" type="checkbox"/>
DTIC TAB	<input type="checkbox"/>
Unannounced	<input type="checkbox"/>
Justification	
By	
Distribution /	
Availability Codes	
Dist	Avail and/or Special
A-1	

**for
Eastern Space and Missile Center
Air Force Systems Command
Patrick Air Force Base, Florida**

FOREWARD

This final report was submitted by ARDE, INC. to the Eastern Space Missile Command (ESMC), Patrick Air Force Base, under Contract No. FO 8606-84-0029.

This report summarizes the experience and knowledge base for predicting the fail safe features of a Kevlar Overwrap Vessel and has been reviewed and is approved for release and distribution in accordance with the distribution statement on the cover and on the Standard Form 298.


PETER TADDIE
Project Manager


LOUIS J. ULLIAN
Deputy Director, Range Safety

REPORT DOCUMENTATION PAGE

Form Approved
OMB No. 0704-0188

Public reporting burden for this collection of information is estimated to average 1 hour per response, including the time for reviewing instructions, searching existing data sources, gathering and maintaining the data needed, and completing and reviewing the collection of information. Send comments regarding this burden estimate or any other aspect of this collection of information, including suggestions for reducing this burden, to Washington Headquarters Services, Directorate for Information Operations and Reports, 1215 Jefferson Davis Highway, Suite 1204, Arlington, VA 22202-4302, and to the Office of Management and Budget, Paperwork Reduction Project (0704-0188), Washington, DC 20503.

1. AGENCY USE ONLY (Leave blank)		2. REPORT DATE		3. REPORT TYPE AND DATES COVERED Feb., 1992 Research & Development, Sept. 1984 to	
4. TITLE AND SUBTITLE Final Report Kevlar Overwrap Study				5. FUNDING NUMBERS FO-8606-84-C-0029	
6. AUTHOR(S) David Gleich					
7. PERFORMING ORGANIZATION NAME(S) AND ADDRESS(ES) ARDE, INC. 500 Walnut Street Norwood, N.J. 07648				8. PERFORMING ORGANIZATION REPORT NUMBER EG 42001-14	
9. SPONSORING/MONITORING AGENCY NAME(S) AND ADDRESS(ES) Department of the Air Force Eastern Space & Missile Center Patrick AFB FL 32925-5472				10. SPONSORING/MONITORING AGENCY REPORT NUMBER 45 SPW/SEMB-TR-92-001	
11. SUPPLEMENTARY NOTES					
12a. DISTRIBUTION/AVAILABILITY STATEMENT Distribution Unlimited				12b. DISTRIBUTION CODE	
13. ABSTRACT (Maximum 200 words) A guide to the design of a Kevlar -49 fiber overwrapped metal composite tank that would "fail safe" in the event the metal liner ruptured suddenly at operating pressure was developed based on the analytic and experimental program performed. The fail safe mode is defined by containment of any ruptured metal liner fragments by the intact fiber shell and benign venting of the contained fluid. Two sudden metal liner failure modes were investigated experimentally and analytically; stable ductile liner crack growth (leak-before-burst, LBB) and liner unstable brittle crack growth/rupture failure mode. The tankage investigated in the program is Kevlar -49 overwrapped cryoformed 301 stainless steel spherical pressure vessels. Liner failure models were postulated and failure predictions made based on tankage dynamic response computer calculations and simple one-dimensional model computation presuming two (2) percent Kevlar -49 fiber strain to failure. Tanks of 16, 22 and 11 inch diameter were tested with high pressure helium gas to compare theory with experiment. The LBB liner failure mode was experimentally investigated by operating pressure cycle testing tanks having liners with intentionally machined defects. Further liner LBB data was obtained from uniaxial R-Curve fracture mechanics tests. The unstable crack growth "catastrophic" failure mode was achieved experimentally by intentionally hydrogen embrittling the liner by charging it with hydrogen gas followed by operating pressure loading.					
14. SUBJECT TERMS brittle fracture, composite, crack growth, cryoformed, dynamic response, fail safe, fiber, fracture mechanics, fragment containment, high pressure gas, hydrogen embrittlement, Kevlar, leak-before-burst, liner, pressure vessel, prestressed, R-curve, stainless steel, safety				15. NUMBER OF PAGES	
				16. PRICE CODE	
17. SECURITY CLASSIFICATION OF REPORT Unclassified	18. SECURITY CLASSIFICATION OF THIS PAGE Unclassified	19. SECURITY CLASSIFICATION OF ABSTRACT Unclassified	20. LIMITATION OF ABSTRACT None		

ACKNOWLEDGEMENT

The program team that performed this research and development effort consisted of Pete Taddie, Patrick AFB (ESMC/SEM), Program Manager, ARDE, INC. as Prime Contractor/Principal Investigator, Physics International as subcontractor for failure modeling computer calculations and Air Force Astronautics Laboratory (EAFB) for full scale composite vessel testing. In addition, important contributions were made by Dr. Yen Pan, Aerospace Corporation and Ray Lark, NASA Lewis Research Laboratory, who acted as program advisors/monitors. Larry Tolley, AL(AFSC) and John Marshall, General Physics Corporation, provided valuable editorial review and comment regarding the report manuscript.

TABLE OF CONTENTS

<u>PARA. NO.</u>	<u>TITLE</u>	<u>PAGE</u>
	FOREWARD	i
	REPORT DOCUMENTATION PAGE (STANDARD FORM 298)	ii
	ACKNOWLEDGEMENT	iii
	TABLE OF CONTENTS	iv
	LIST OF FIGURES AND TABLES	vii
	GLOSSARY OF TERMS	viii
	SUMMARY	ix
1.0	INTRODUCTION	1-1
2.0	TECHNICAL DISCUSSION	2-1
2.1	OVERVIEW	2-1
2.2	FAILURE MODE POSTULATION AND ANALYSIS	2-3
2.3	FIBER ULTIMATE STRAIN VERIFICATION	2-6
2.4	LINER HYDROGEN EMBRITTLEMENT PARAMETER DEFINITION	2-12
2.5	FRACTURE MECHANICS R-CURVE TEST DATA AND LEAK- BEFORE-BURST (LBB) VERIFICATION	2-12
2.6	FULL SCALE 16" ϕ PSC VESSEL TESTS	2-13
2.6.1	OVERALL TEST DESCRIPTION	2-13
2.6.2	TEST PROCEDURE, SET-UP, INSTRUMENTATION	2-13

TABLE OF CONTENTS

<u>PARA. NO.</u>	<u>TITLE</u>	<u>PAGE</u>
2.6.3	16" ϕ AND 22" ϕ PSC VESSEL TEST RESULTS	2-22
2.6.4	PSC VESSEL TEST DATA CORRELATION	2-28
2.7	FAIL SAFE DESIGN GUIDE	2-30
3.0	CONCLUSIONS AND RECOMMENDATIONS	3-1
4.0	REFERENCES	4-1
	APPENDIX A - ANALYTICAL MODELS	A-1
	APPENDIX B - HYDROGEN EMBRITTLEMENT PARAMETERS	B-1
	APPENDIX C - FRACTURE MECHANICS	C-1
	APPENDIX D - 6 INCH DIAMETER KEVLAR -49 FIBER WRAPPED CYLINDER	D-1
	APPENDIX E - 16" ϕ AND 22" ϕ PSC VESSEL TESTS	E-1
	E.1 - FULL SCALE COMPOSITE VESSEL TESTS - INSTRUMENTATION REQUIREMENTS/PROCEDURES	E-1
	E.2 - 16" ϕ AND 22" ϕ PSC VESSEL TEST MATRIX	E-33
	E.3 - RV-4, 4A TESTS	E-37
	E.4 - RV-5 TEST	E-59
	E.5 - RV-7 TEST	E-81
	E.6 - RV-9 TEST	E-112
	E.7 - RV-10 TEST	E-138
	E.8 - RV-11 TEST	E-166
	E.9 - RV-12 TEST	E-196

TABLE OF CONTENTS

<u>PARA. NO.</u>	<u>TITLE</u>	<u>PAGE</u>
E.10-	RV-12A TEST	E-204
E.11-	RV-14 TEST	E-234
E.12-	RV-14A TEST	E-E-252
	APPENDIX F - FULL SCALE TEST DATA CORRELATION	F-1
	APPENDIX G - DETAILED LIST OF FIGURES AND TABLES	G-1

LIST OF FIGURES AND TABLES

This report contains a very large number of figures and tables to support and clarify the text. In order to preserve ready continuity of technical discussion, and for reader convenience, the large detailed list of figures and tables is placed at the end of the report in Appendix G.

For convenience of reference, the following scheme is used to aid figure/table ready identification/location.

1. In general, the first character (number or letter) of a figure or table number (e.g., 1-2, 2-3, A-1, C-2, etc.) identifies the report section or appendix in which it is located.
2. An exception is figure and table numbers with letters (A, B, C ... G) after the numerical diget (e.g., 3C) which refer to figures and/or tables in prior independently prepared documentation used to support this report text.

GLOSSARY OF TERMS

Acronyms (abbreviations) are used throughout the text. They are defined in most instances when first used. For convenience of reference, they are listed below.

AE - Acoustic emission
BM - Base metal
CCT - Center cracked tension panel R-Curve test specimen
CRES - Corrosion resistant steel
Cryo - Cryoformed
Cryoformed - A plastic deformation forming process at cryogenic (-320°F) temperature
CT - Compact tension R-Curve test specimen
EDM - Electron discharge machining
Elox - another name for EDM
FPS - Frames per second
GHe - Gaseous helium
HAZ - Heat affected zone (of weld)
Hi - Cams - High speed cameras
J_R Curve - A plot of J-integral values proportional to the areas under the load-displacement curves vs. crack growth generated during tests of pre-cracked material specimens.
LBB - Leak-before-burst (failure mode)
PICES 2D - Physics International Corporation two-dimensional transient computer program
PC - Chamber pressure
PSC - Prestressed composite
PV - Vessel pressure
R-Curve - A continuous record of toughness development in terms of crack growth resistance K_R plotted against crack extension in the material as a crack is driven under a continuously increased stress intensity factor, K
SG - Strain gage
SPP - Samples per second
TC - Thermocouple
VHS - Very high speed
WM - Weld metal
2D - Two dimensional
1D - One dimensional
φ - Diameter

SUMMARY

Key program results are briefly summarized below. They are more fully described in the main text.

1. Fail Safe Demonstrated

"Fail Safe" (leak/fiber retention of liner fragments) has been demonstrated experimentally at 2500 - 5600 psig gaseous helium (GHe) operating pressure for 16" and 22" diameter (ϕ) prestressed composite (PSC) Kevlar overwrapped tanks. The 301 Cryoformed corrosion resistant steel (CRES) liners were intentionally hydrogen embrittled to achieve a brittle failure mode at operating pressures. Measured fiber strains are predicted by "static" structural response for liner global embrittlement mode. Here, global refers to the entire liner inside surface less bosses. Significant dynamic structural response (about 1.5 - 1.7 dynamic amplification factors) was noted for the liner local girth weld heat affected zone (HAZ) embrittlement mode which experimentally simulated the transient worst case structural model. Similar dynamic fiber strain amplification was measured for local boss/head weld HAZ embrittlement of the liner. Girth embrittlement is considered more critical since the liner fragmented into two pieces at the girth. The embrittled boss region, although cracked, was still attached to the rest of the liner (no fragments) and the liner could still resist some load as an "intact" one piece shell.

A single small fragment metal liner brittle rupture failure mode was also investigated. Analytic considerations and experimental evidence, as detailed in Appendices E.5, E.6 and F, showed this failure mode to be less critical than local girth or boss embrittled failure modes discussed above.

2. Failure Modes Predicted

Failure pressure and failure mode (metal plus fiber) were predicted and experimentally verified for 16" ϕ PSC sphere "sure fail" designed unit with local girth weld embrittled liner and 50% of baseline fiber thickness. Margin test 16" ϕ vessel (83% fiber thickness and local girth weld embrittlement) gave experimental results very close to expected failure/retention mode values. Dynamic amplification at liner brittle rupture was slightly higher than anticipated. 16" ϕ 90% fiber thickness and 22" ϕ PSC tanks demonstrated fail safe behavior, as predicted.

3. Leak-Before-Burst (LBB) Mode Demonstrated by Test

Operating pressure cycle tests of vessels with Elox (EDM) machined defects in 301 cryoformed CRES liner walls showed benign leak mode for GHe and hydraulic pressurants. A globally embrittled PSC vessel cryoformed 301 CRES liner with hundreds of thru, continuous cracks showed benign leak mode for a GHe operating pressure test. R-Curve and vessel fracture mechanics tests demonstrated that cryoformed 301 CRES

is a tough, high strength material that gives LBB mode. Significant results obtained were a plane stress critical R-Curve stress intensity

of $180 \text{ ksi} \sqrt{\text{in}}$ for parent material, weld and HAZ at high tensile strength (200 - 260 ksi). Metal vessel thru cracks grew in a stable manner up to four (4) times the wall thickness before reaching critical size. This indicated significant LBB safety margin since LBB is considered demonstrated if thru cracks grow to two (2) times wall thickness before becoming unstable.

4. Analytic Predictions Verified

Analytic predictions of fiber strains/failure modes were in reasonable agreement with experimental results. Computer two-dimensional (2D) structural models and a simplified one-dimensional (1D) analytic model were thus verified.

5. A "Fail Safe" Tank Design Guide Developed

A guide for the design of Kevlar -49 fiber overwrapped metal composite tanks that will "fail safe" if the metal liner ruptures suddenly at operating pressure was developed based on structural theory and test data. The design guide simply relates fiber operating stress and metal stress increment (operating stress minus initial stress) to the required fiber to metal thickness ratio to achieve retention by the intact fiber shell of any metal fragments generated. Here, fiber stress refers to the fiber load divided by the fiber less resin cross-sectional area. The resin is presumed to carry zero load.

6. Key Experimental Techniques Developed

Test procedures/technique/set-up/instrumentation were developed as required to accomplish successful transient GHe pressure testing of fiber overwrapped prestressed composite pressure vessels and to accurately monitor the extremely short time fiber strain response/pressure/temperatures. In addition, techniques and parameters required to intentionally hydrogen embrittle the PSC 301 cryoformed (Cryo) CRES liners in a controlled manner so that they failed in a predetermined brittle way at predetermined/pressure/stress/time were developed and experimentally verified.

1.0 INTRODUCTION

Prestressed composite (PSC) fiber overwrapped metal pressure vessels^{2, 3*} have wide use for gas storage because of their light weight. Typical maximum operating pressures are in the range of 3000 - 5000 psig which could cause catastrophic damage in the event of tank rupture. Therefore, safety considerations for personnel working in the vicinity of PSC tanks are very important. PSC tanks because of their two load carrying members (fiber and metal) have a potential safety advantage. In the event that the metal component was to fail catastrophically during operation (metal liner ruptures at operating pressure), the load carried by the liner could be possibly transferred to the non-failed fibers so that the metal liner fragments (if any) would be non-hazardously contained and the pressure vented by leaking gas through the porous outer fiber shell.

Up to the present, no appropriate experimental evidence was available to prove these potential safety advantages of PSC tankage and no systematic study had been made to analytically define the pertinent tank parameters relating to fail safe behavior. The Air Force, therefore, funded a research and development program to establish and verify the design basis of PSC pressure vessel construction that can exhibit the desired safety advantages. ARDE, INC., under Patrick Air Force Base Contract No. FO-8606-84-C-0029, "Kevlar Overwrap Study", investigated experimentally and analytically the circumstances under which PSC tankage will "fail safe" at operating pressure load. The objective being to define a test-verified "generic" rationale for the design of fail safe PSC tankage consisting of a metal liner overwrapped with Kevlar -49.

Two sudden metal liner failure modes were investigated; a brittle liner (unstable, crack growth) failure and a ductile liner (stable, leak-before-burst) failure. The metal liner failure mode depends to a large extent upon liner toughness. Fiber toughness is not germane since a basic ground rule of this study is that the fiber wrap has no "initial flaws". The discussion of toughness in this report, therefore, relates entirely to the metal liner. The PSC tankage used in the program is Kevlar -49 fiber overwrapped cryoformed 301 CRES spherical pressure vessels. The cryoformed 301 CRES liner selection was for convenience. The target was to have the program output relate to any liner material. Both 11 inch diameter subscale and 16 and 22 inch diameter full scale vessels were tested. The full scale 16 inch PSC tanks are similar in size and configuration to those produced for high pressure gas storage on British Aerospace's Olympus Satellite (Fig. 1-1). The 22 inch full scale PSC tanks are similar to those built for high pressure helium gas storage on General Dynamics Centaur vehicle (Fig. 1-2). Fiber thicknesses were modified to suit test program requirements. The brittle liner failure mode was achieved through intentional embrittlement of the metal liner by establishing a "battery" for charging the metal liner with hydrogen gas for an extended period to

* Numbers in superscript refer to references listed in section 4.0.

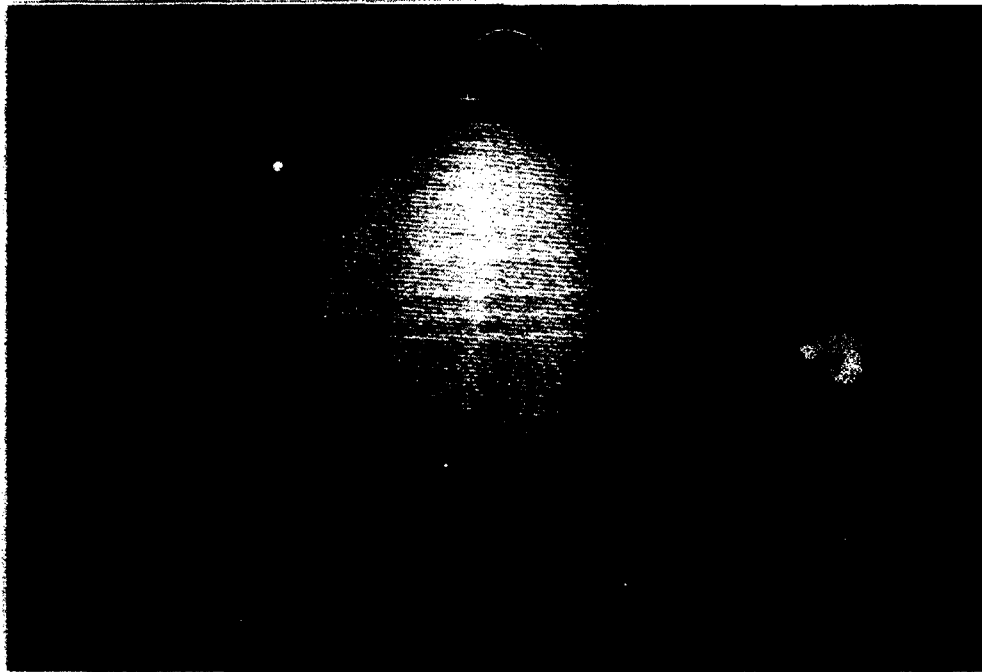


Fig. 1-1

**Olympus Cryoformed 301 S/S
Kevlar 49 Overwrap Prestressed
Composite Pressure Vessel**

assure saturation and then applying operating pressure to the tank. In addition, the liner inside surface was "sensitized" by pickling and the hydrogen embrittlement reaction enhanced by the addition of sodium arsenite to the "battery" electrolyte solution. Subscale all metal vessels were tested first to develop hydrogen embrittlement parameters, followed by testing of subscale and full scale PSC tanks. The leak-before-burst (LBB) stable crack growth mode was induced by EDM machining appropriate defects in the liner wall followed by cycling at operating pressure to produce crack wall breakthrough. Both subscale and full scale PSC tanks were tested. In addition, uniaxial tensile R curve tests of appropriate cryoformed CRES specimens were conducted to provide additional liner fracture mechanics data for LBB verification.



Fig. 1-2

CENTAUR CRYOFORMED 301 S/S KEVLAR 49 OVERWRAP
PRESTRESSED COMPOSITE PRESSURE VESSEL

2.0 TECHNICAL DISCUSSION

This section discusses the various technical program tasks and provides details of analytic and test approaches and results. Both successful and unsuccessful approaches are described since one can learn as much, if not more, from failure compared to success. As an aid to subsequent discussions, Figure 2-1 defines PSC tank components and regions.

2.1 Overview

The basic objective of the program was to provide valid data enabling definition of "fail safe" design criteria for Kevlar -49 fiber overwrapped metal PSC vessels in the event that the metal liner should fail suddenly at operating pressure. To accomplish this objective, program effort involved the tasks outlined below. These tasks and their results are more fully discussed subsequently in the order listed below.

1. Postulate failure models/modes
2. Verify fiber ultimate strain
3. Define and verify metal liner hydrogen embrittlement techniques/parameters.
4. Obtain experimental uniaxial R-Curve fracture mechanics data for the liner and verify its leak-before-burst failure mode by vessel tests.
5. Obtain "fail safe" data for brittle liner failure mode by full scale PSC vessel tests for liner global hydrogen embrittlement, local girth weld heat affected zone and local boss/head weld heat affected zone hydrogen embrittlement cases.
6. Correlate test results and refine structural models/failure modes as required by experiment to facilitate definition of "fail safe" PSC vessel design criteria.

2.2 Failure Mode Postulation and Analysis

The objective of the analysis is to predict the onset of Kevlar -49 fiber overwrap failure in response to an instantaneous metal liner failure of a PSC spherical vessel. This PSC tank structural analysis and failure mode modeling was accomplished by a two-dimensional transient stress analysis using PISCES 2 DELK computer program⁴ and a simplified one dimensional lumped transient model as described in Appendix A. One-dimensional static calculations based on a prior formulation³ were also used in the test data correlation, as appropriate.

Fiber failure was presumed at the test verified 2% fiber less resin ultimate strain value. Two (2) liner failure modes were considered in the PISCES transient analysis; an instantaneous unstable brittle liner girth crack and an instantaneous liner stable polar hole.

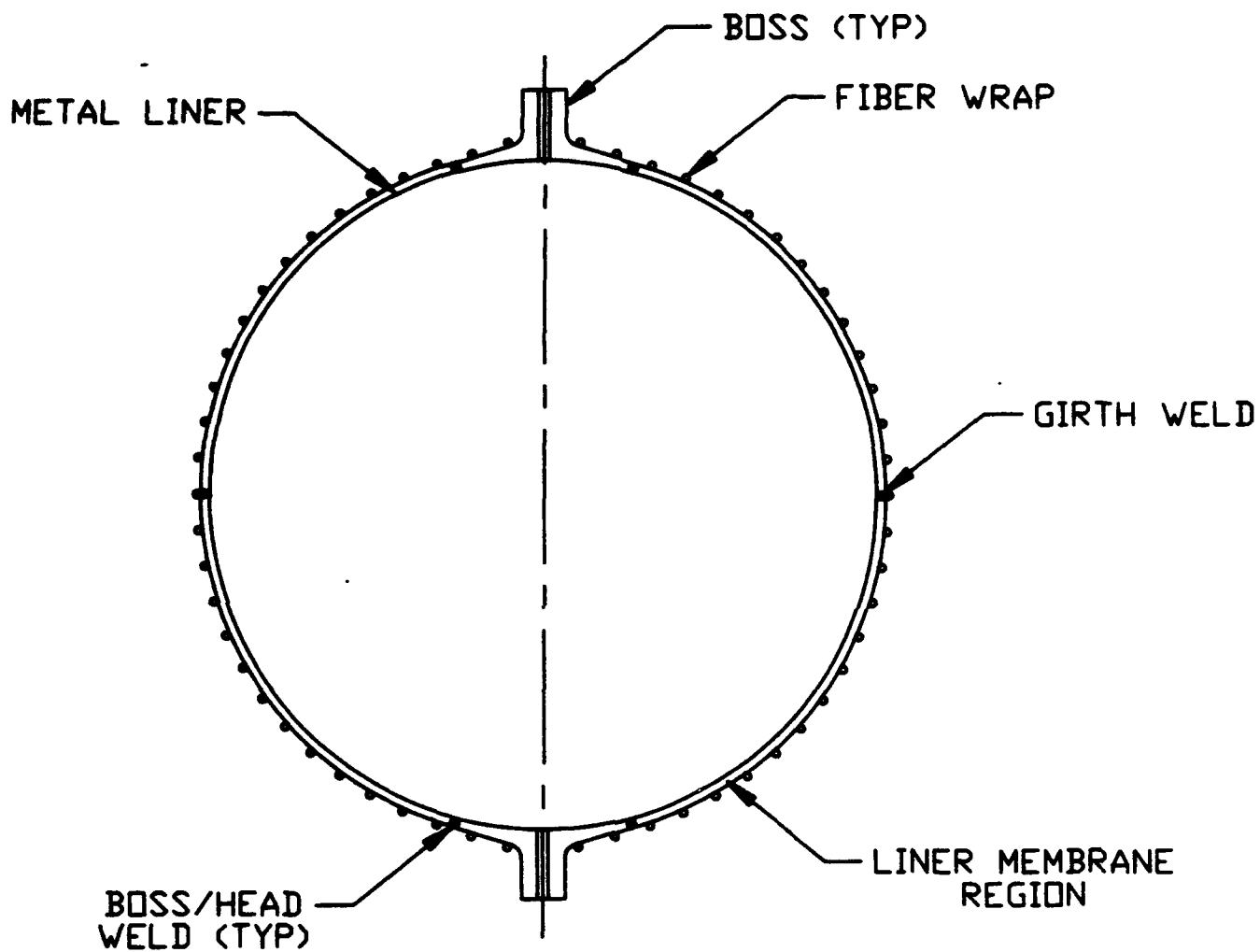


FIG. 2-1 PRESTRESSED COMPOSITE TANK COMPONENTS AND REGIONS

As subsequently discussed, agreement between PISCES analysis predicted and measured strains was reasonable. The one-dimensional models also gave good agreement with test results and failure modes predicted were verified by test.

2.3 - Fiber Ultimate Strain Verification

A fiber ultimate strain of 2% was verified experimentally, in agreement with other data⁸, by burst pressure tests of strain gage instrumented 6" ϕ fiber wrapped cylinders having small angle helical fibers in addition to hoop fibers, as sketched on Figure 2-2. The test specimens were designed to fail in the hoop fibers. The hoop fibers correspond to the theoretical "isotensoid" great circle fibers of a spherical fiber wrap. The classical stress/strain transformations⁹ for fibers at different orientations and fiber less resin Young's Modulus used in the failure modeling analysis were also confirmed by these tests. Details of the experiments and test data correlation are given in ARDE Report EG 42001-1, contained in Appendix D.

2.4 Liner Hydrogen Embrittlement Parameter Definition and Verification

The requirements/objectives of the intentional liner hydrogen embrittlement were to cause a brittle liner "catastrophic" failure at typical operating stress levels of 45 - 50% of ultimate (100 - 110 ksi) within eight minutes of pressurization. This requirement was dictated by the limited run time of the high speed recording tape or camera film during the test. To meet these objectives, numerous hydrogen embrittlement tests of subscale 11" ϕ all metal and 16" and 22" ϕ PSC spheres were made to define and confirm the appropriate liner embrittlement processing parameters. Liner global embrittlement and local girth and boss weld zone embrittlement modes were investigated. The basic technique used is schematically indicated on Figure 2-3. A lead anode is immersed in the dilute sulphuric acid solution electrolyte contained in the tank interior with the metal liner functioning as the cathode. A controlled source of current is used to complete the circuit generating hydrogen gas which diffuses into the liner wall. These hydrogen embrittlement experiments led to the parameters given in Appendix B. Details of the all metal subscale 11" ϕ vessel and the 16" ϕ and 22" ϕ PSC sphere hydrogen embrittlement tests are given in the Appendices B and E, respectively.

In early experiments, the metal tank (liner) was embrittled in the horizontal position and rotated about the bosses to preclude boss embrittlement. This proved to be impractical and the vertical embrittling mode shown in Figure 2-3 was used for testing. Maskant was utilized to protect selected liner regions against embrittlement.

Acoustic emission monitoring was used initially in attempts to define characteristic acoustic signals indicating sub-critical cracking and onset of brittle liner failure. No characteristic signal(s) indicating onset of brittle liner failure could be determined from the acoustic data obtained.

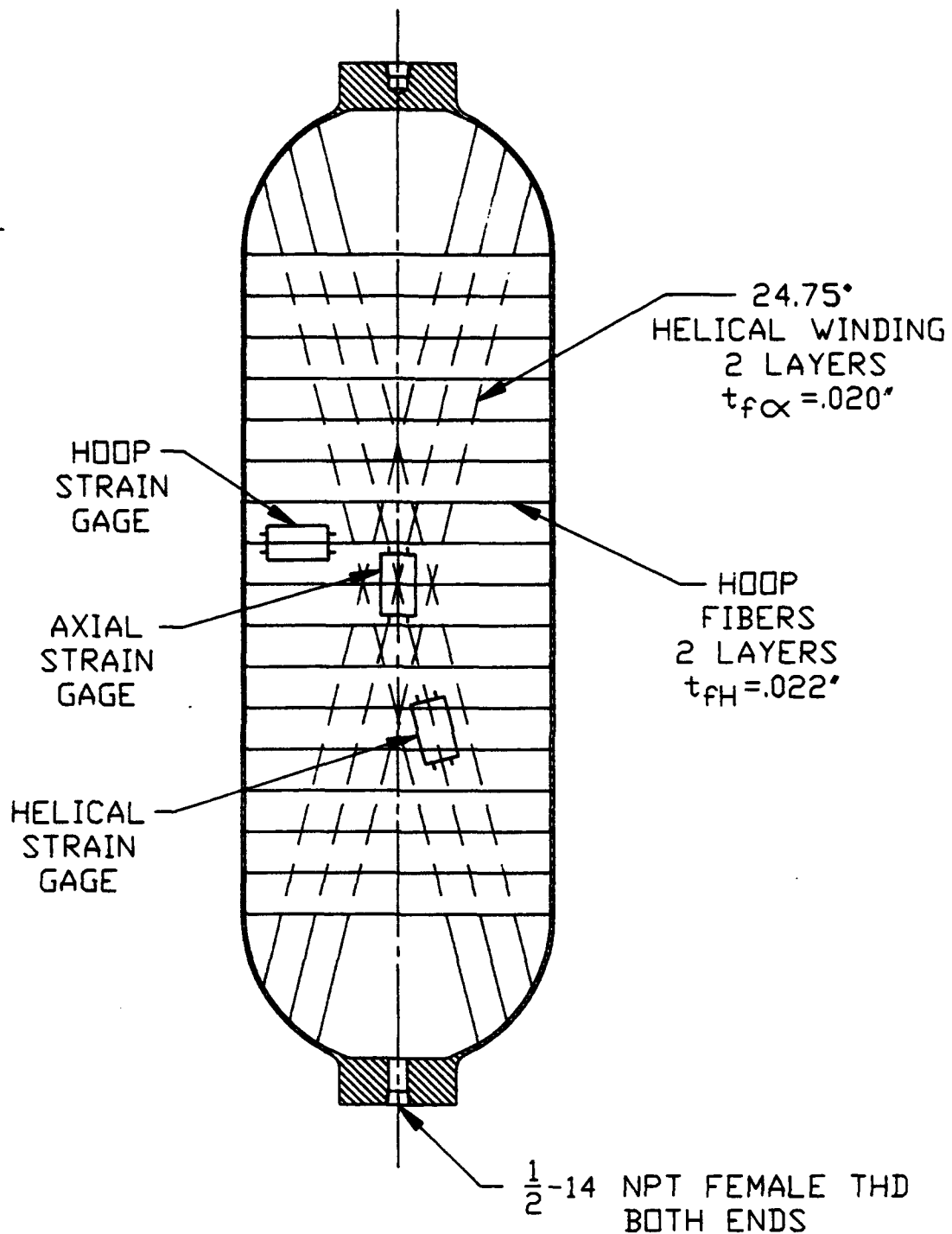


FIG. 2-2 6" Ø KEVLAR 49 FIBER WRAP MATERIAL EVALUATION CYLINDER

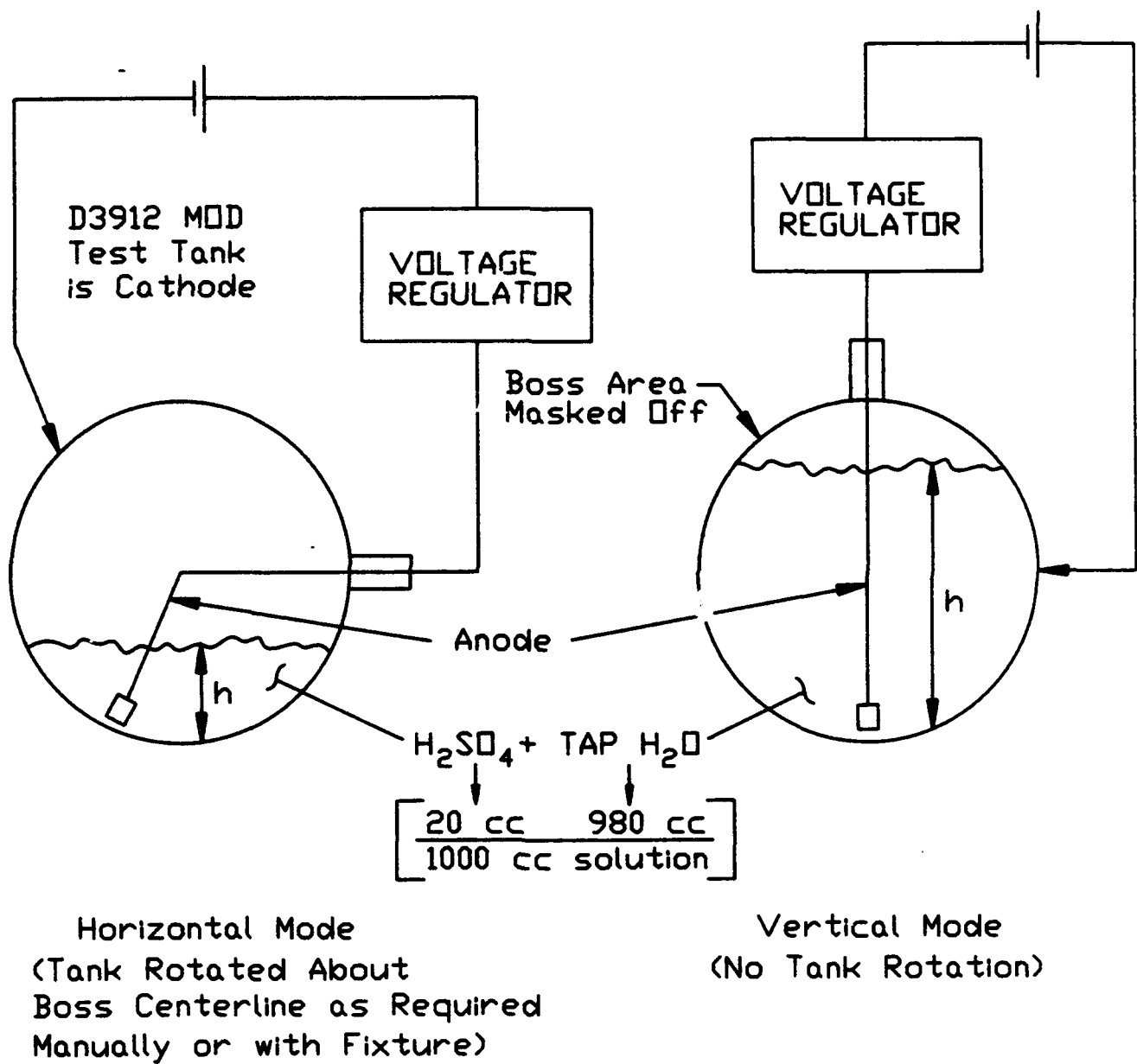


FIG. 2-3 SUBSCALE HYDROGEN EMBRITTLEMENT TEST MODES

This effort was discontinued because brittle liner failure control had improved due to better hydrogen embrittlement techniques and, in addition, the significant work needed to develop appropriate acoustic emission technology for this application was beyond the scope of the program.

Different brittle failure modes were noted for the globally embrittled all metal tanks and the globally embrittled fiber overwrapped PSC metal tanks. The embrittled all metal tanks fragmented whereas metal liner fragmentation was suppressed by load transfer of the cracking embrittled metal liner to the fibers. This highlights the advantage of a structure with two members capable of carrying load compared to a structure with a single load resisting element. Figure 2-4 shows a cut apart intentionally globally hydrogen embrittled PSC liner after test. The fiber overwrapped spherical liner was intact in one piece despite the hundreds of continuous through cracks shown. This is in contrast to the post burst test view of a similarly intentionally embrittled all metal single load resisting member tank given on Figure 2-5.

2.5 Fracture Mechanics R-Curve Test Data and Leak-Before-Burst (LBB) Verification

Leak-before-burst (LBB) tests were conducted on 11" ϕ .06 thick prestressed composite (PSC) 301 cryo CRES spherical liners overwrapped with Kevlar -49 fibers and on 11" ϕ and 23" ϕ all 301 Cryo CRES spherical vessels. Elliptical part through thickness flaws were elox machined (EDM) on the O.D. surface of the all metal vessels and on the I.D. surface of the PSC tanks. Typical flaw geometry is shown on Figure 2-6 for the 23" ϕ tank. Operating pressure cycling tests (3500 - 5000 psig) were performed with pressurizing media of hydraulic fluid and gaseous helium. Failure mode was benign leak in all cases with through crack stable growth as long as four (4) times wall thickness before failure. Since LBB is considered proven by stable through crack growth of two (2) times wall thickness before failure, a large LBB safety factor has been demonstrated.

Sustained load tests of all metal 301 Cryo CRES tanks at 4000 psig pressure level were conducted after pressure cycling experiments for durations up to 48 hours without any additional crack growth. This result verified the safe, stable mode of the through cracked tanks under constant operating load.

Uniaxial R-Curve tests were performed on 301 cryo CRES through center cracked tension panels and compact tensile specimens. Figures 2-7 and 2-8 show test specimen geometry. The R-Curve test results gave a plane stress

critical stress intensity, K_{IC} of 180 ksi $\sqrt{\text{in}}$ for parent material, weld or heat affected zone as well as a crack initiation stress intensity, $K_{IE} >$

100 ksi $\sqrt{\text{in}}$ for uniaxial strengths as high as 260 ksi. These uniaxial R-Curve tests, verified by vessel tests, showed that 301 cryo CRES is a tough, high strength material that demonstrates leak-before-burst (LBB).

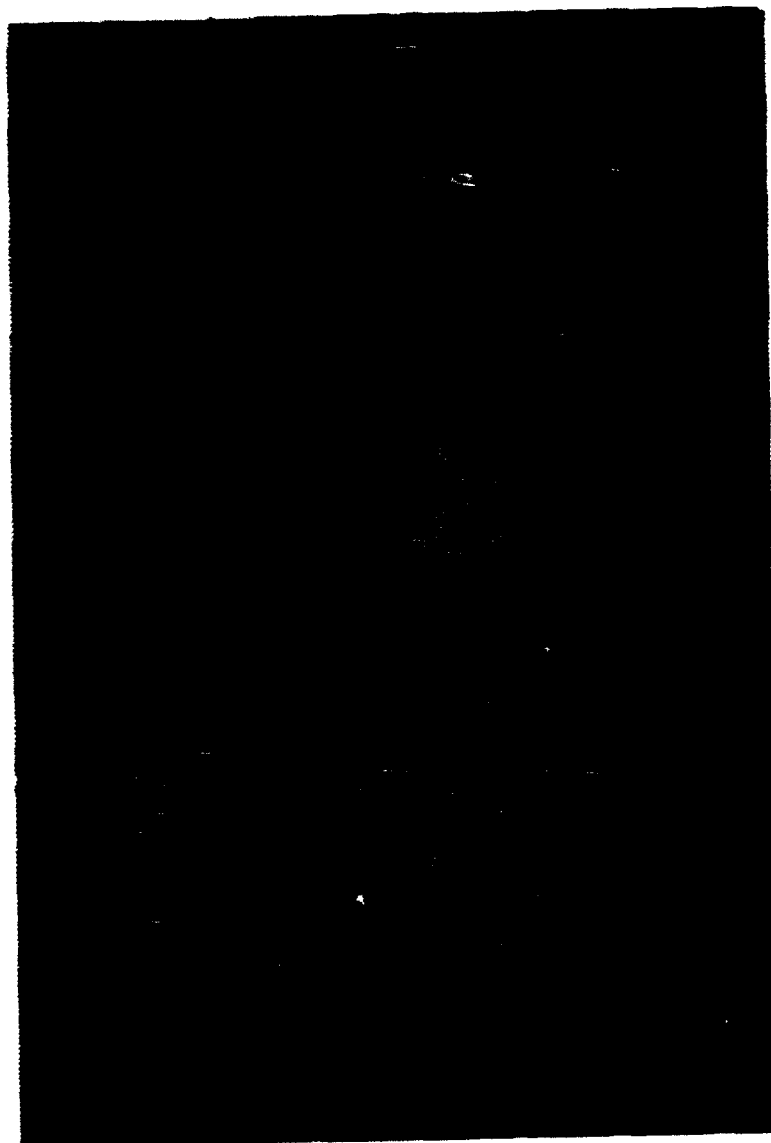


FIG. 2-4 GLOBALLY HYDROGEN EMERITTLED PSC LINER AFTER TEST



FIG. 2-5 POST TEST VIEW OF HYDROGEN EMBRITTLED ALL METAL

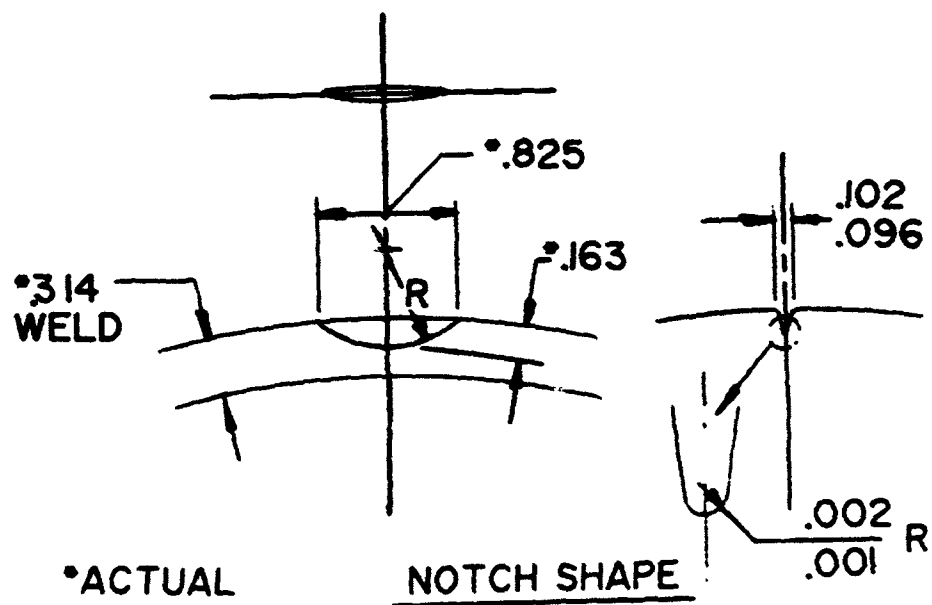


FIG. 2-6 PRESSURANT TANK, 23" DIA.

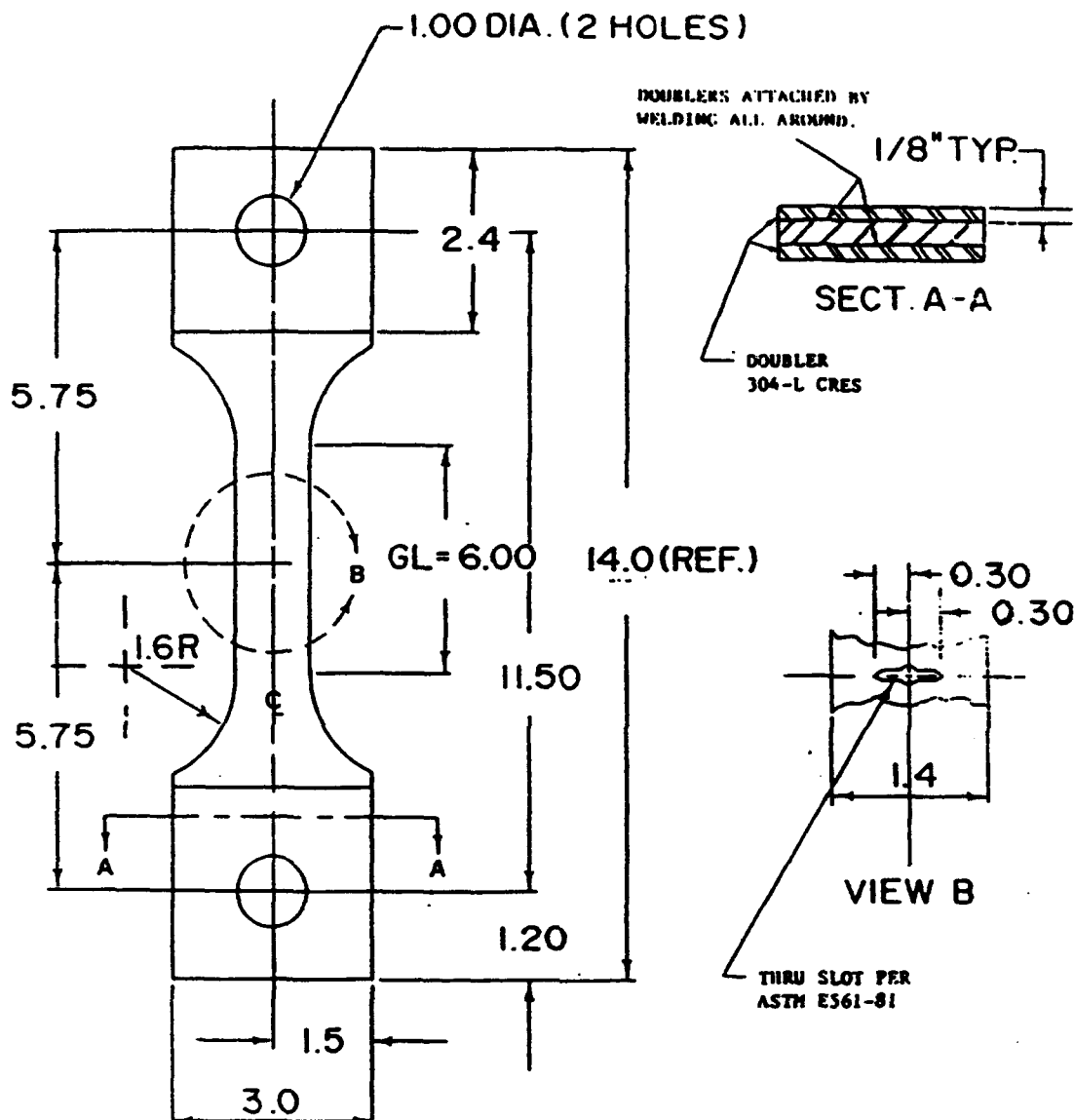
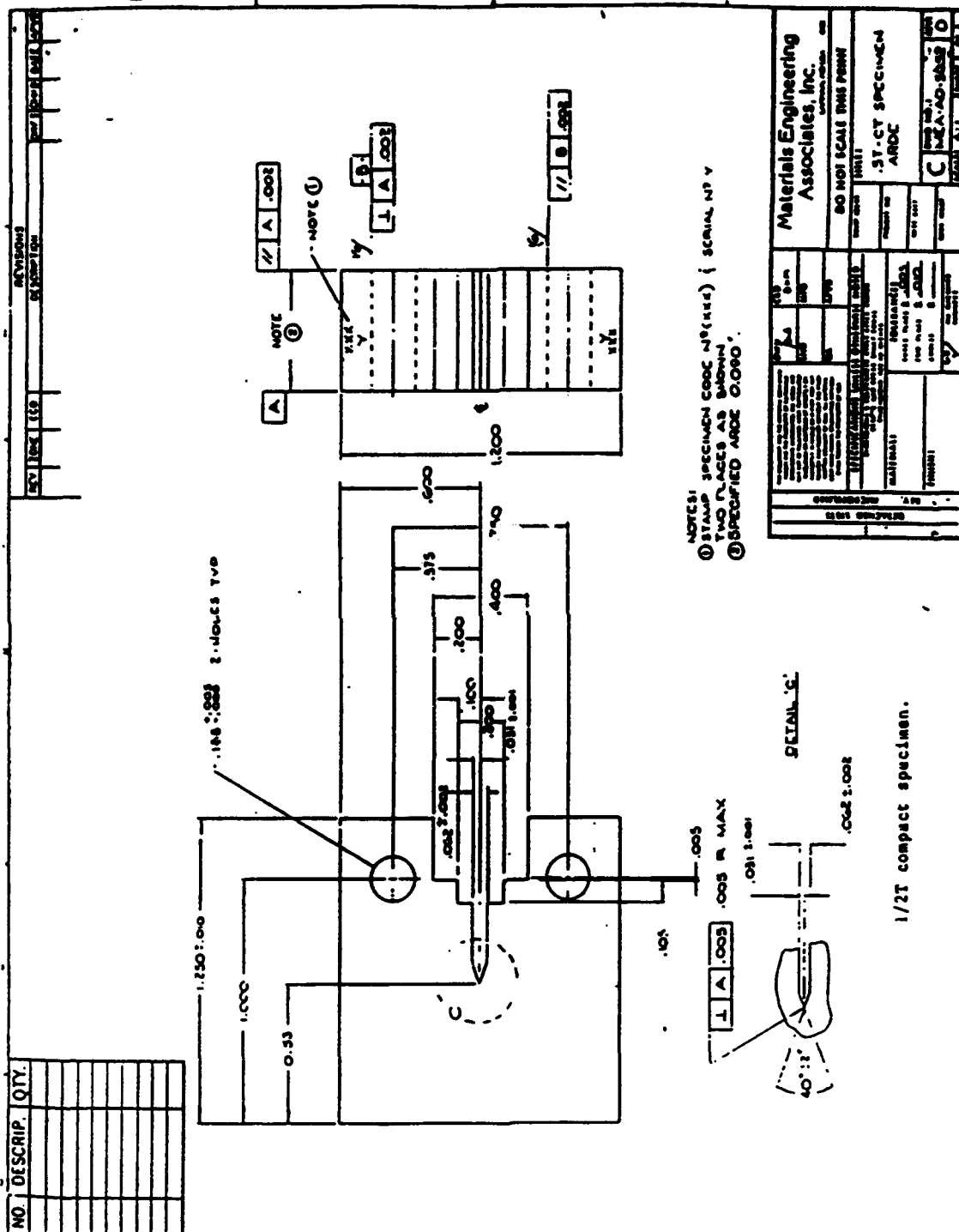


FIG. 2-7 Center cracked tension panel. Dimensions in inches.



Details of the vessel LBB experiments and the uniaxial R-Curve tests are given in ARDE Report EG 42001-14 contained in Appendix C.

2.6 Full Scale 16" ϕ and 22" ϕ PSC Vessel Tests

2.6.1 Overall Test Description

2.6.1.1 Test Vessel Description

Full scale (16" and 22" ϕ) PSC operating pressure tests with 2500 - 5600 psig gaseous helium were conducted by AFAL, Edwards AFB, California, at Area 1-52, D-Pad. The Kevlar overwrapped 301 cryo CRES spherical composite vessels, Figures 1-1 and 1-2, had intentionally hydrogen embrittled liners. The 16" ϕ tank liner thickness was kept constant at .05 inch, nominal. Kevlar -49 fiber thickness was varied to suit program needs. The baseline 16" ϕ tank fiber (less resin) "average" thickness (100%) was .154 inch, the same as the flight units delivered to British Aerospace for their Olympus Satellite high pressure gas tank. The 22" ϕ composite tank configuration, Figure 1-2, was the same as the flight high pressure gas tanks delivered to General Dynamics for their Centaur vehicle. Average Kevlar fiber (less resin) thickness was .192 inch with a .044 inch thick 301 cryo CRES liner. The original program plan called for the use of all 16" ϕ full scale test tanks for consistency of data base, but one 16" ϕ tank was ruptured in fabrication due to inadvertent damage during the resin cure operation of the fiber wrapped tank. The failed 16" ϕ tank was replaced by an existing 22" ϕ tank asset to minimize schedule and cost impact.

2.6.1.2 Measurements

Pressures, fiber strains, girth diametral displacements and temperatures were monitored to provide "fail safe" brittle liner failure mode test data. In some instances, air blast and fragmentation data was obtained. The 16" and 22" ϕ PSC vessel test matrix is given in Appendix E.2.

2.6.2 Test Procedure. Set-up. Instrumentation

2.6.2.1 Overview

Testing and monitoring PSC vessel structural response after sudden brittle liner failure presented some experimental technique challenges. Primary areas of concern were the monitoring of the extremely short fiber strain transient events of interest (the order of 10^{-4} to 10^{-6} seconds) and the mounting of strain gages on the uneven, bumpy, fiber matrix surface to measure the strains. In addition, gas compression work, due to the necessary rapid pressurization rate to reach operating pressure before embrittled liner failure, could raise test tank temperatures to unacceptable levels. These primary test challenges were successfully met by development of a suitable strain gage mounting technique and utilization of high strain response, post yield strain gages coupled to a

high frequency response recording system. In addition, use of a liquid nitrogen heat exchanger and properly sequenced pressurization mode provided sufficiently cool helium gas into the test tank.

2.6.2.2 System Checkout Tests

The instrumentation requirements/test procedure guidelines to achieve the testing objectives were defined by ARDE document EG 42001-5, given in Appendix E.1. These requirements/procedures were modified, as required, based on a series of system checkout tests using various size/configuration vessels. Initial system checkout utilizing a practice vessel approximating the size of the actual test articles determined the selection of gaseous helium in lieu of gaseous nitrogen as a pressurizing agent. Initial checkout tests showed that helium reduced cycling time and/or time to operating pressure by more than 50%. Additionally, many of the vessel tests required high pressurization rates to obtain 5000 psig test vessel pressure within 90 seconds, which gaseous nitrogen could not achieve.

Follow-on system checkout tests, described in ARDE letters 52001-KOS-084 (3 Feb. 1986) contained in Appendix E.1, herein, defined test system operational parameters and resolved testing problems. As aforementioned in section 2.6.2.1, test vessel temperatures during pressurization were expected to exceed the maximum allowed value (140°F). To prevent damage to the Kevlar fiber overwrap, a heat exchanger was installed to cool the incoming helium pressurizing gas. Many tests were needed to determine the required heat exchanger tube length and cooling medium. Only liquid nitrogen was found to be able to safely and adequately supercool the gaseous helium to overcome the compression heating.

Additional problems were encountered during initial pressurization due to the volume of ambient air trapped in the system and test vessel. Two vent valves were installed, one to vent warm air from the system and one to vent incoming gas from the test vessel. When these valves were cycled in series with the pressurization valve, the test vessel metal boss temperature could be reduced to 60° F and the test vessel gas temperature to 20° F. These temperatures were required in order not to exceed the maximum allowable test vessel temperature of 140° F during final pressurization.

2.6.2.3 Test System Description/Schematics

Figure 2-9 is a schematic sketch of the instrumentation/test set-up initial projected. The actual plumbing and component placement used, as influenced by the system checkout test experiences, are shown on Figure 2-10.

PSC SAFETY PROGRAM

KEY

C = connector

Signal

SG = strain gage (brittle failure) - (12) bi-axial gages - equipped on 10° great circles

SCD = strain gage (ductile failure) - (4) as - one (1) over flow and three (3) 1" away

DSG = dummy strain gage close to active gages

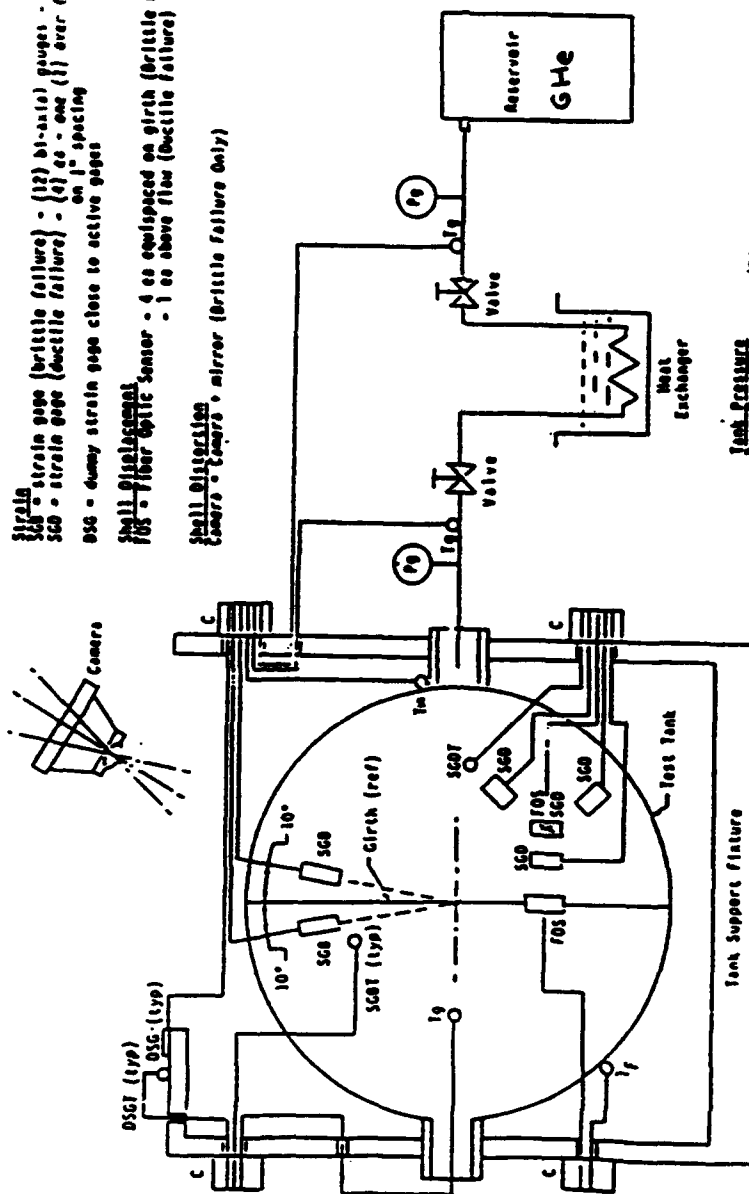
Shell Distortion

ROS = fiber optic sensor - 4 as equipped on girth (brittle failure)

ROS = fiber optic sensor - 1 as above flow (ductile failure)

Shell Distortion

Camera = Camera, mirror (brittle failure only)



Test Features
P1 = Pressure gage (Piezo... resistive)

Temperature (Thermocouples)

Tg = gas temp

Ta = tank metal temp

SGST = strain gage (brittle failure) temp

SCST = strain gage (ductile failure) temp

DSST = dummy strain gage temp

Valves
Valve closures identified and sensed (microswitches)

SCHEMATIC
TEST TANK INSTRUMENTATION

FIG. 2-9 SCHEMATIC, TEST TANK INSTRUMENTATION

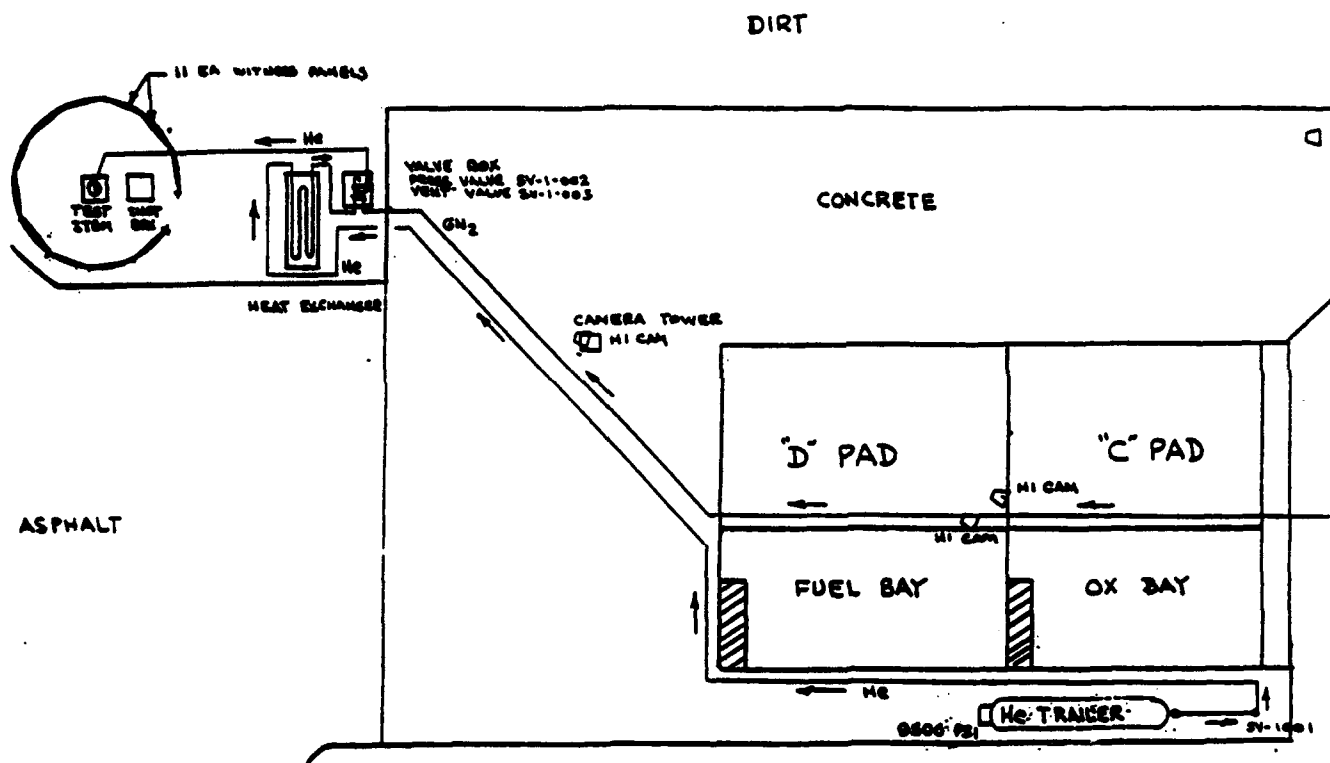


FIG. 2-10 SKETCH, TEST SETUP AREA 1-52, D PAD

2.6.2.3.1 Mechanical System Components

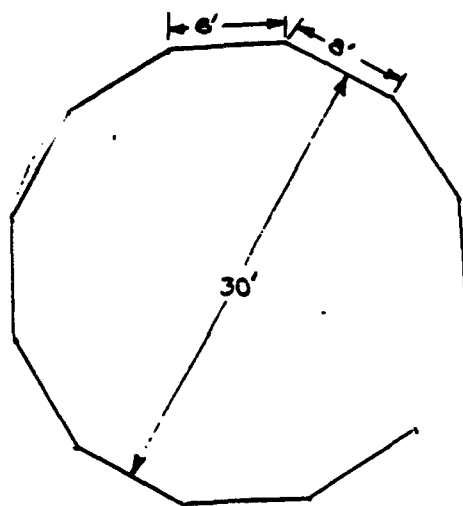
Helium for testing was provided by a dual bank trailer. Bank 1 was pressurized to 6,000 psi and bank 2 was pressurized to 8,000 psi. Total trailer volume is 100 cubic feet at 10,000 psi. Gaseous nitrogen for valve actuation was obtained from a 120 psi source on D-Pad. Valve SV-0-001 is a 20,000 psi remote actuated 3/8 inch valve and is used as a system isolation valve only. Valves SV-0-002, SV-0-003, and SV-0-004, located in the valve box, are remote single action valves rated at 10,000 psi. Their port orifices are 0.125 inch, with seat orifices of 0.093 inch, and have a flow coefficient of 0.135. Valve SV-0-002 is the vessel pressurization valve, while SV-0-003 and SV-0-004 are the line and vessel vent valves respectively. All pressure lines are 3/8 inch outside and 1/8 inch inside diameters and are rated at 10,000 psi. Total length of line from the isolation valve to the test article is 280 +/- 5 feet. A series of three complete loops totaling 60 feet is contained in the heat exchanger box.

2.6.2.3.2 Witness Panels

The witness panels, as shown on Figure 2-11, consist of an angle iron frame measuring 8 x 8 feet. Each panel contains two 4 x 8 foot sheets of 1 inch thick "Celotex" (TM) backed by 0.0940 inch aluminum. This configuration closely approximates the environment where the vessels to be tested are currently utilized. Each panel assembly is anchored to hinge points imbedded in concrete and are mounted approximately one foot above ground level. They connect at the top to form a 12 sided polygon 30 feet in diameter with one section deleted to facilitate camera viewing. The frames are designed to break away and fold back to prevent excessive damage due to overpressure or for stowage in high winds.

2.6.2.3.3 Photographic Coverage

Pre and post test stills were taken, of each vessel tested. Three Hi-Cams (1000 FPS) were used in an attempt to record events. The cameras were activated in series along the pressure curve at points selected by the test engineer as the most likely to be the start of an event. Early attempts were not always successful. The unknown behavior of the test article combined with the short run time of the cameras resulted in many missed events. The addition of a high speed video monitor connected to a very high speed (VHS) recorder allowed for more continuous coverage. Exposure at 1/60th of a second, combined with the slow motion play back capability provided excellent fragmentation coverage.



11 EA 8'x8' WITNESS
PANELS. 1 FT ABOVE
GROUND LEVEL

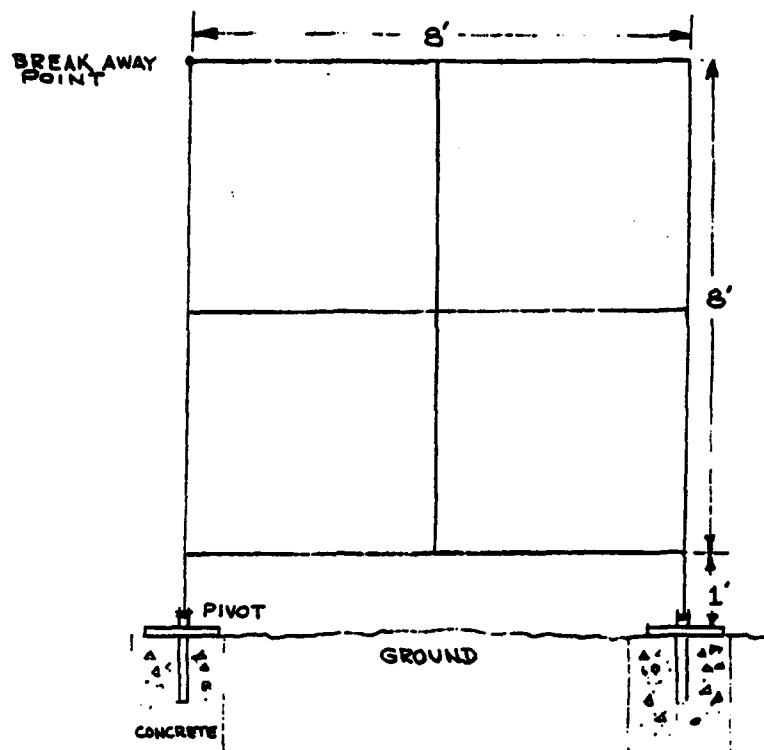


FIGURE 2-11 WITNESS PANEL SKETCH

2.6.3 16" and 22" ϕ PSC Vessel Test Results

The full scale 16" ϕ and 23" ϕ PSC vessel GHe pressure test results are summarized in Table E-1 of Appendix E.2. The effects of varying hydrogen embrittlement electrolyte solution charging current density, pickling the liner I.D. and adding sodium arsenite to enhance the embrittlement reaction and global versus local girth and boss weld area embrittlement were investigated in the experiments. The investigation was limited in nature since hydrogen embrittlement, by itself, was not the primary research and development issue. Fiber thickness was varied as required to achieve "fail safe" liner fragment retention/benign pressure venting mode, "sure failure" of liner plus fibers and "fail safe" margin data at operating pressure.

As shown in Table E-1, tests RV-4 and RV-5 demonstrated fail safe mode at operating pressure for the globally embrittled 100% fiber thickness 16" ϕ PSC vessel configuration. Test RV-5 showed the enhanced intentional embrittlement effect due to increased GHe charging time, pickling of liner I.D. and adding sodium arsenite to the electrolyte solution. Fiber strain response data was correlated by static structural behavior. A photograph of prior discussed cut apart RV-5 "fail safe mode" test tank is shown on Figure 2-4. The enhancement in the intentional hydrogen embrittlement is evidenced by the multitudes of connected through cracks seen in the photograph.

Experiments RV-7 and RV-9 with 16" ϕ tanks demonstrated the fail safe/fragmentation retention/benign leak mode at operating pressure with local girth weld heat affected zone (HAZ) intentionally embrittled liners. These tests simulated the worst case structural model which assumes an instantaneous unstable crack of the entire girth weld. The liners broke at the girth and separated into two halves during the test. The fibers were intact. Large dynamic fiber strain spikes were observed. Figure 2-12 shows the strain spike monitored by strain gage 12. Tension is negative.

The as designed intended "catastrophic" brittle liner and fiber both fail mode was demonstrated by test RV-10 of a local girth region 16" ϕ PSC test sphere at design operating pressure with reduced fiber thickness (50% of baseline). Liner separation/fragments were as predicted. Large fiber strain spikes were observed at/near failure. Fragmentation and overpressure data were obtained. Typical fragments are shown on Figure 2-13.

Both the fibers and the local girth area embrittled liner failed in the RV-11 experiment with the 83% of baseline fiber thickness 16" ϕ PSC test vessel. The failure pressure was very close to the predicted value. The expected large fiber dynamic strain spikes were observed. Overpressure and fragmentation data were obtained. Strain gage measurements indicate that the fibers came very close to remaining intact per the no failure prediction.

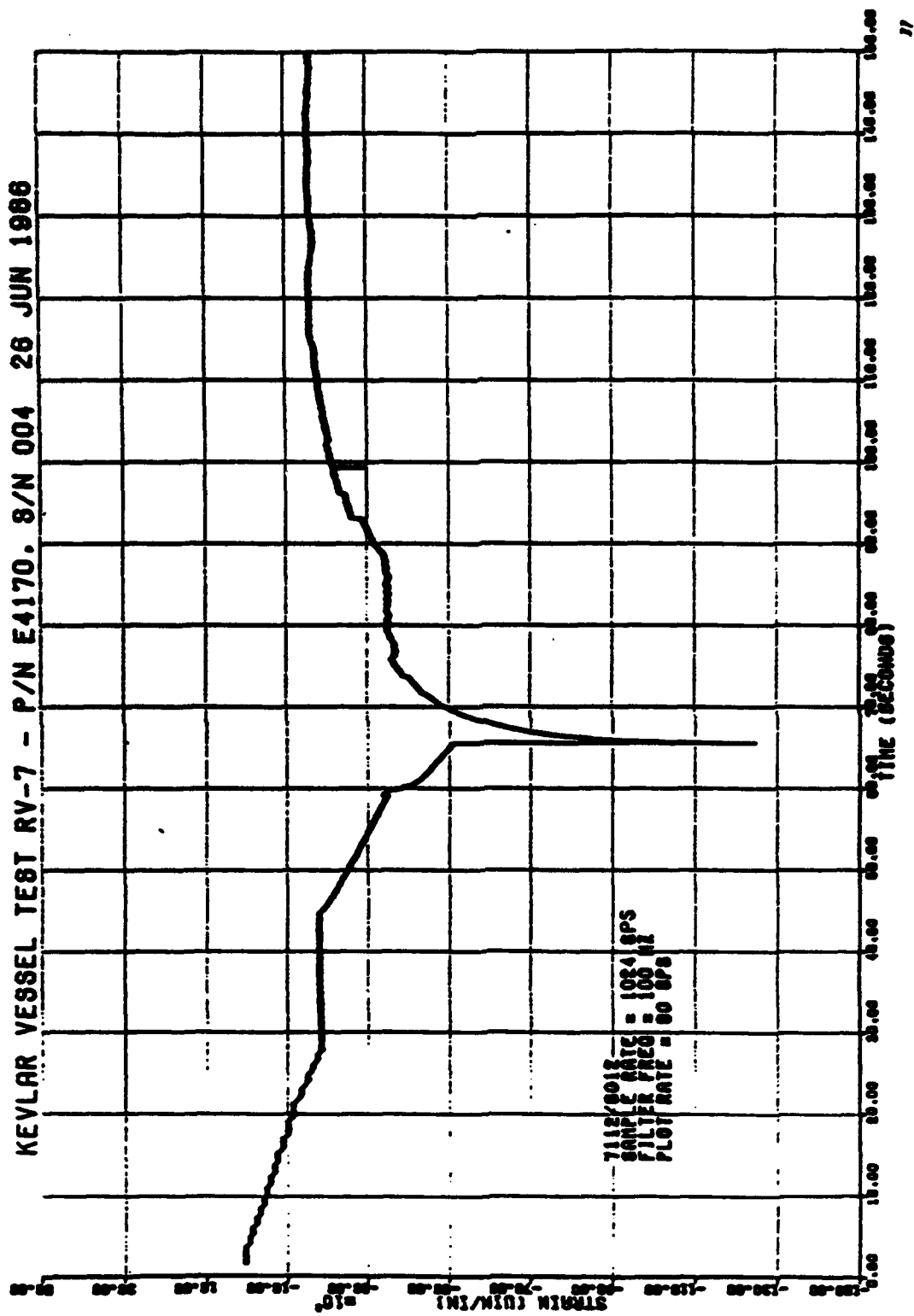


FIG. 2-12 DYNAMIC FIBER STRAIN SPIKE RV-7 TEST

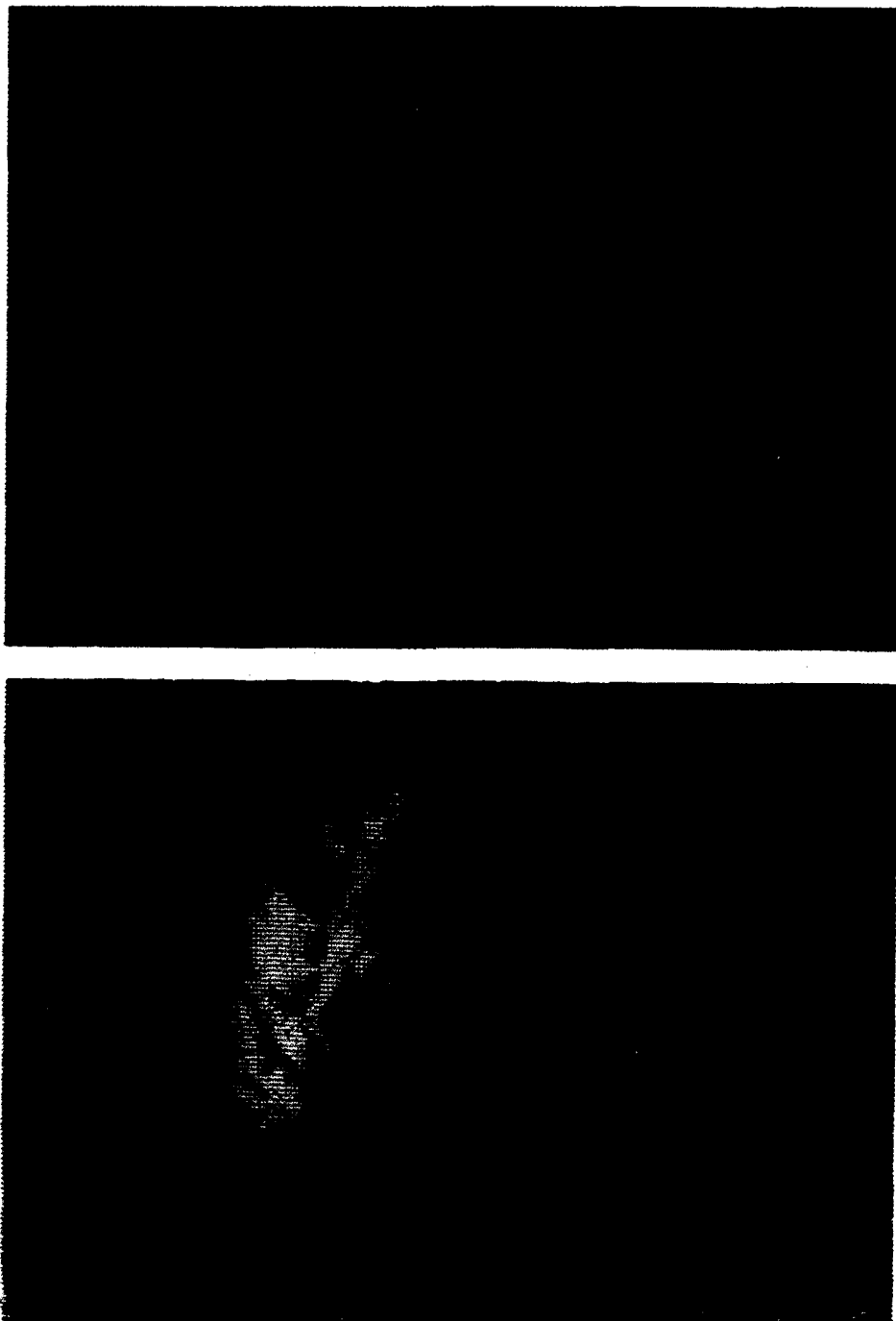


FIG. 2-13 INTENTIONAL "SURE FAIL" BRITTLE LINER RV-10
TEST TANK FRAGMENTS

A "fail safe" benign leak failure mode was demonstrated by RV-14A tests with 90% of baseline fiber thickness 16" ϕ test vessels. Based on RV-7 to RV-11 and RV-14 and 14-A tests, one estimates that the "dividing line" between "fail safe" fragment retention and catastrophic failure for the critical girth weld embrittled liner mode 16" ϕ test tanks is at a fiber thickness slightly greater than 83% of baseline (say 85% of baseline). A more meaningful and proper "fail safe" criterion in terms of fiber stress and metal stress increment at operating pressure and fiber to metal thickness ratio is detailed in section 2.7 based on the test data correlations discussed in section 2.6.4 which follows.

Tests RV-12 and RV-12A demonstrated fail safe modes for local boss/head weld embrittled liners of the 22" ϕ PSC test tanks. Although significant liner cracking occurred in the local boss/head weld embrittled region, the boss did not separate from the liner head. Dynamic fiber strain amplification effects were similar to those measured in the local girth weld embrittled tests. Girth embrittlement is considered more critical since the liner fragmented at the girth into two pieces whereas the boss embrittled liner was still in one piece and could resist load as an "intact" shell.

2.6.4 PSC Vessel Test Data Correlation

The full scale PSC test data was correlated utilizing the two-dimensional finite difference transient computer program PISCES 2 DELK⁴ and simplified one-dimensional models as discussed in Appendix A. The test data was used to refine the models and derive equivalent dynamic amplification factors that would result in 2% fiber ultimate strain. In general, agreement between strains calculated from theory and strains measured during test was reasonably good. Predicted failure modes were verified by the experiments. Sample test data correlation calculations and pressure and strain versus time plots are given in Appendix F.

Agreement between measured strains and values predicted by PISCES computer program was reasonable. PISCES computed results were conservative since they were greater than the measured strains. Typical results obtained were 13505 to 13870 maximum computed meridional micro delta strains compared to the 10600 to 11900 maximum micro delta meridional strains measured as detailed in Appendix F. Predicted PICES 2D strains were thus 22% higher on average compared to measured strains. Improved strain test data correlation was obtained using a slip boundary condition at the fiber/metal interface, rather than a completely bonded condition. The slip condition gave higher strains than the completely bonded case as shown on Figure 2-15.

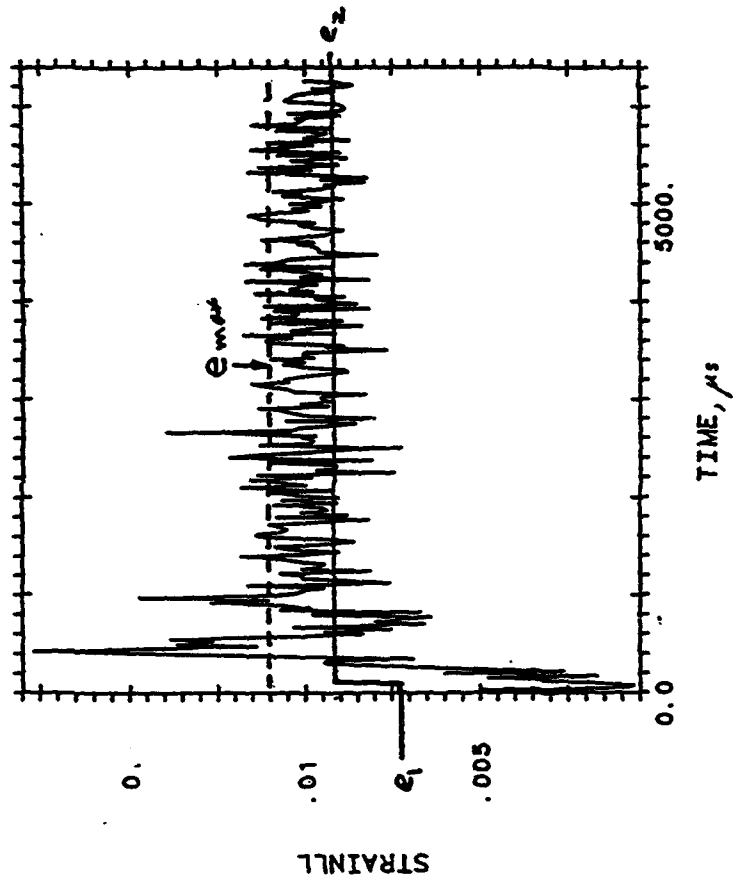
The simple one-dimensional (1D) transient model which presumed instantaneous total liner loss of strength/stiffness gave even better results. The strains predicted by the simple 1D model, while still generally conservative, were less than the PISCES results (Figure 2-14) and, therefore, closer to the measured strains. Figures 2-16 to 2-19 show typical measured transient fiber strains for experiments RV-7, RV-9 and RV-11. Tensile strain is negative. Superposed on these figures are the strains computed from the one-dimensional transient model. The quantity e_{max} is the maximum transient fiber strain after liner failure, e_1 the static fiber strain prior to liner failure and e_2 the static equilibrium fiber strain presuming liner loss of strength/stiffness. It is seen that agreement between simple one-dimensional theory and test is quite good.

The one-dimensional equivalent static model constructed, based on prior developments³, assumes that the pressure to cause 2% ultimate fiber strain is composed of the static pressure the fibers were carrying before liner sudden failure plus a dynamic amplification factor, Φ , times the static pressure the liner was carrying before it failed. Based on the test data, dynamic amplification factors in the range of $\Phi = 1.5 - 1.7$ were derived for the critical local girth weld heat affected zone (HAZ) embrittlement and the local boss/head weld embrittled liner failure modes. Measured fiber strains for the liner global embrittled failure mode were correlated by static structural behavior ($\Phi = 1$). This equivalent static model, together with the test derived Φ values were used to derive the design guides discussed in section 2.7.

PISCES CALCULATION WITH ZERO FRICTION BETWEEN LINER AND OVERWRAP
GIVES HIGHER STRAINS THAN PREDICTED BY THE ANALYTICAL MODEL

MERIDIONAL STRAIN

4000 PSI BURST WITH FULL SLIP
COLUMN 1 ROW 2 SUBGRID 3



HOOP STRAIN

4000 PSI BURST WITH FULL SLIP
COLUMN 1 ROW 2 SUBGRID 3

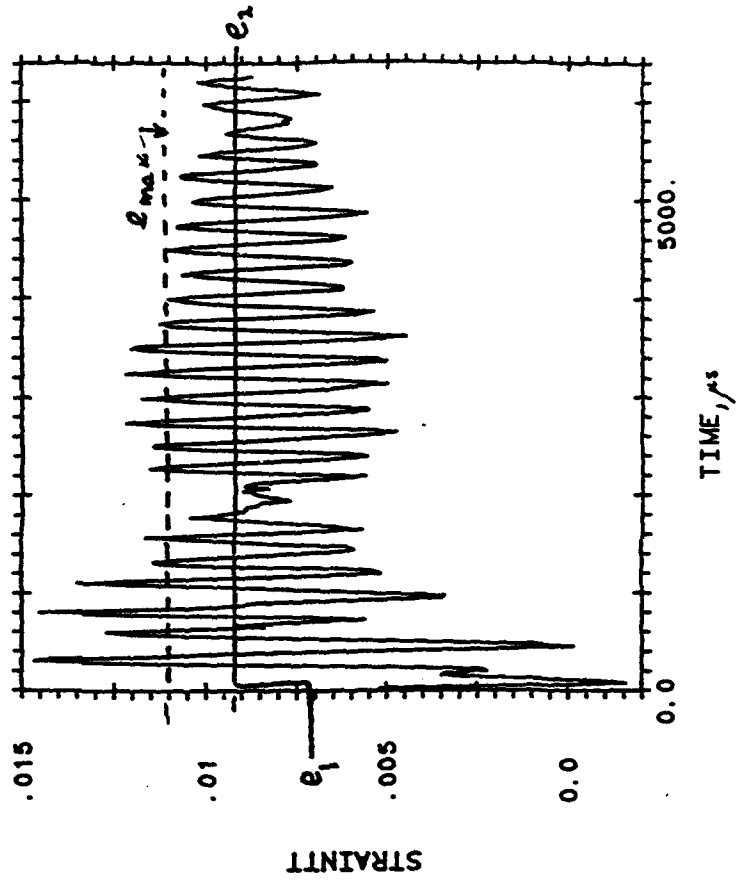
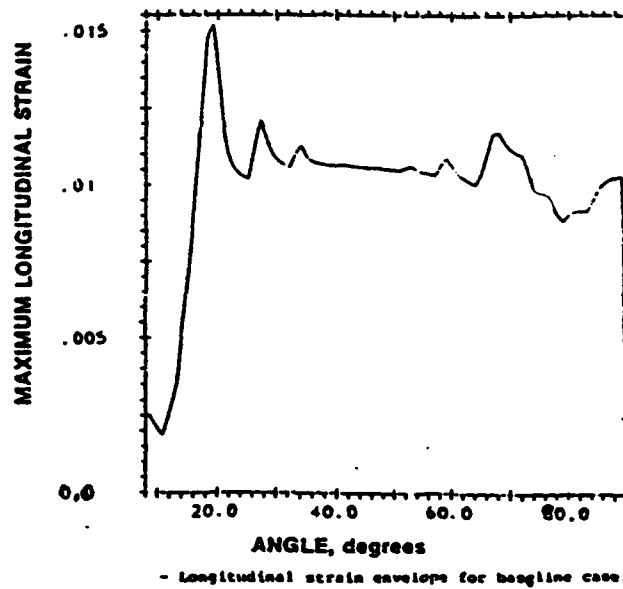


FIG. 2-14 PISCES 2D vs. 1D ANALYTIC MODEL COMPUTED STRAINS

TWO-DIMENSIONAL CALCULATIONS AT 4000 PSI
PEAK MERIDIONAL STRAIN VS. ANGLE

OVERWRAP IS ATTACHED TO THE LINER



ZERO FRICTION
OVERWRAP IS NOT ATTACHED TO THE LINER

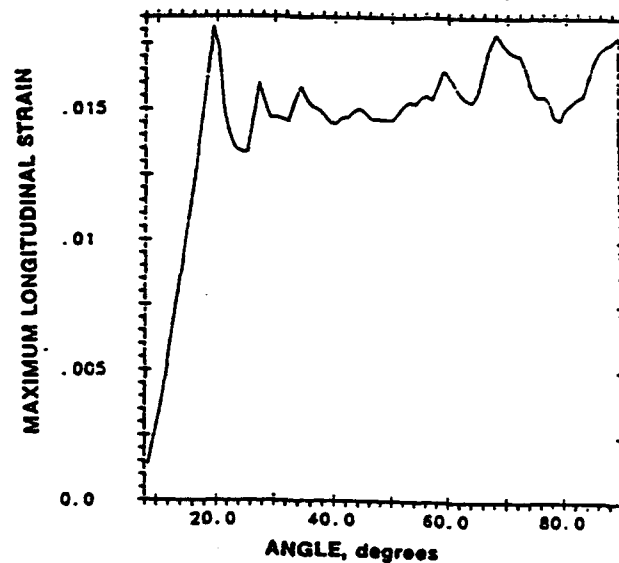


FIG. 2-15 TWO-DIMENSIONAL CALCULATION PEAK MERIDIONAL STRAIN VS. ANGLE

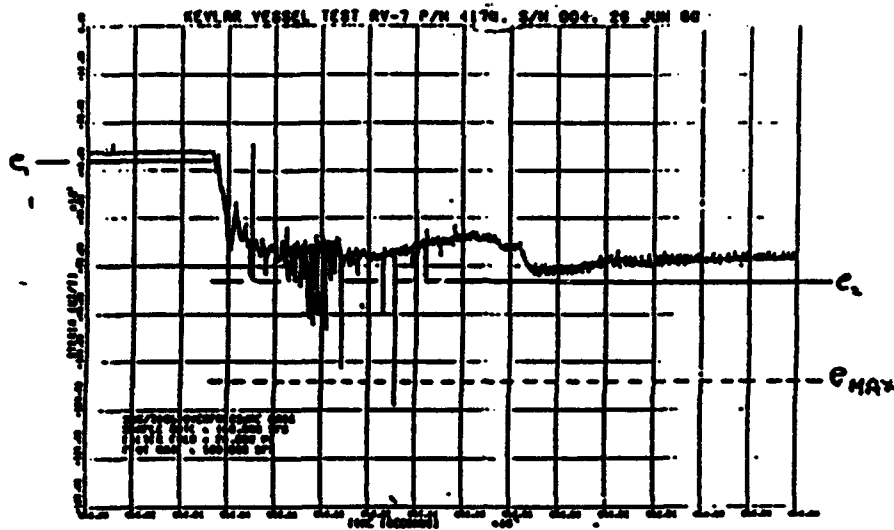


FIG. 2-16 FIBER STRAIN VS. TIME, TEST RV-7,
STRAIN GAGE NO. 6

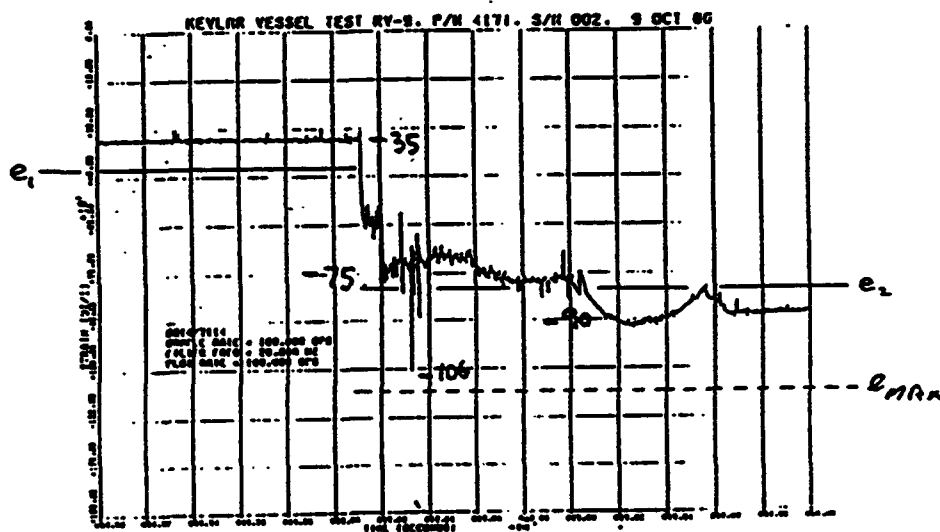


FIG. 2-17 FIBER STRAIN VS. TIME, TEST RV-9
STRAIN GAGE NO. 14

TEST RV-11, SG 4, 12, 20

N Equator Meridional

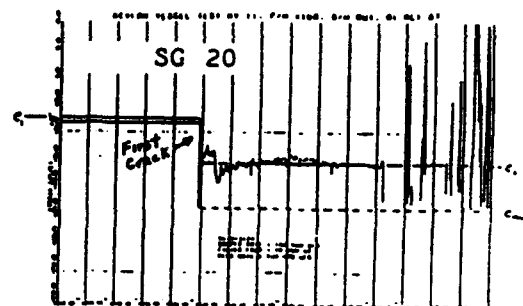
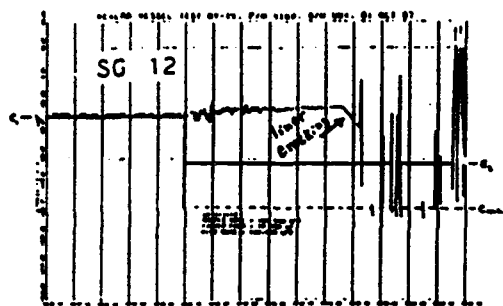
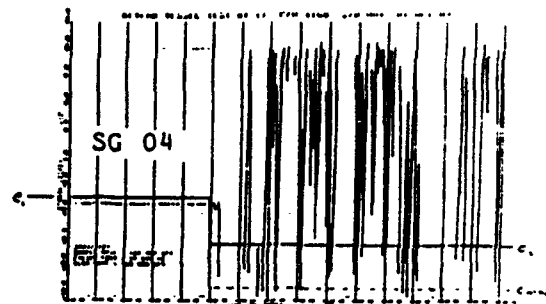


FIG. 2-18 FIBER STRAIN VS. TIME, TEST RV-11,
STRAIN GAGES 4, 12, 20

TEST RV-11, SG 2, 10, 18

N Pole Meridional

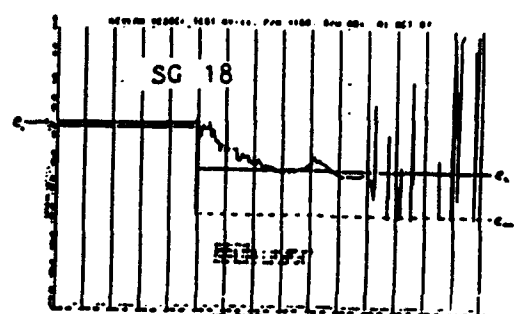
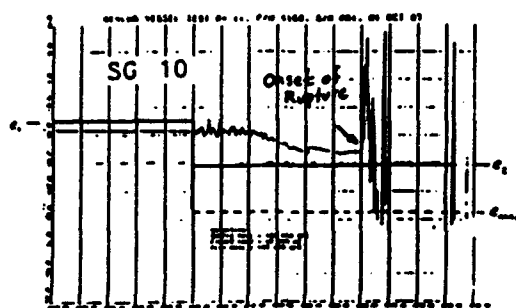
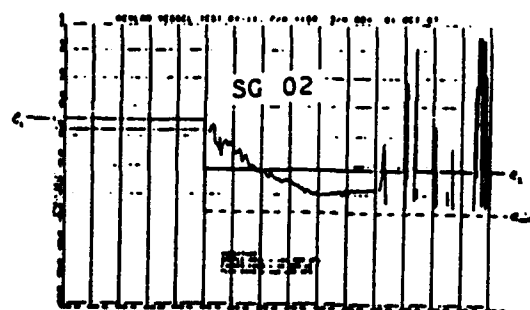


FIG. 2-19 FIBER STRAIN VS. TIME, TEST RV-11,
STRAIN GAGES 2, 10, 18

2.7 Fail Safe Design Guide

2.7.1 Spherical Vessels

A "fail safe" spherical prestressed Kevlar fiber overwrapped tank design guide, based on test data and structural models obtained/utilized on this program is derived and defined in Appendix A. The pertinent equation, given below again for convenience, is plotted on Figure 2-20.

$$\sigma_{fo} = 345 - \frac{3.4}{t_f/t_M} \Delta\sigma_{MO} \quad \text{--- (A-24)}$$

Here,

σ_{fo} = maximum allowable fiber (less resin) stress (ksi) at operating pressure for "fail safe" fiber retention of liner fragments generated by sudden liner brittle failure at operating pressure.

σ_{MO} = design metal stress at operating pressure (ksi)

σ_{Mi} = Metal initial stress (ksi)

$\Delta\sigma_{MO} = \sigma_{MO} - \sigma_{Mi}$ = Metal operating stress increment

t_f/t_M = fiber (less resin) to metal liner thickness ratio.

This design guide enables one to check a given prestressed composite vessel design for fail safe liner fragment retention if the liner fails suddenly in a brittle manner at operating pressure. Referring to Figure 2-20 or equation (A-24), if for example, $\Delta\sigma_{MO} = 100$ ksi for $t_f/t_M = 3$, the maximum allowable fiber operating stress, σ_{fo} , is 231 ksi. Liner fragment retention by the fibers at operating pressure is thus indicated for fiber operating stress, $\sigma_{fo} \leq 231$ ksi. Conversely, one can find the minimum fiber to metal thickness ratio for "fail safe" mode, given the fiber and metal operating stresses. if $\sigma_{fo} = 250$ ksi and $\Delta\sigma_{MO} = 100$ ksi, the required minimum fiber (less resin) to metal thickness ratio from equation A-24 is 3.58.

The fail safe design guide defined by equation (A-24) of Appendix A is based on test data for Kevlar -49 fibers and cryoformed 301 CRES liners. Test data for other fibers, especially graphite, are needed in order to define applicable design guides.

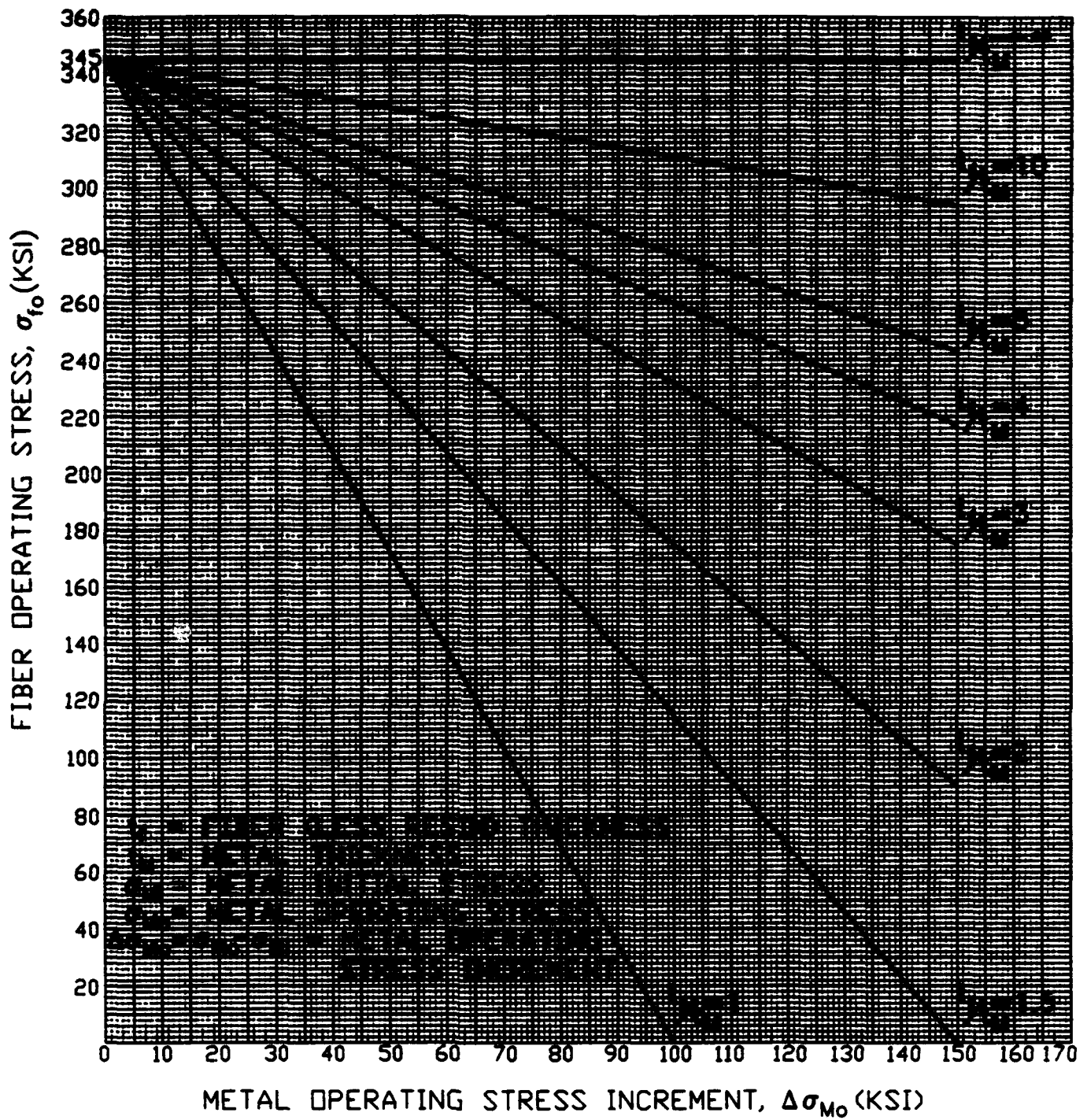


FIG. 2-20 KEVLAR OVERWRAPPED COMPOSITE SPHERE "FAIL SAFE" FIBER OPERATING STRESS VS. METAL OPERATING STRESS INCREMENT

A program objective was to develop a "generic" prestressed composite vessel design guide, valid for any liner material overwrapped with Kevlar - 49 fibers, that would describe the circumstances under which the Kevlar fibers would retain any fragments generated by sudden liner brittle failure at operating pressure and permit benign venting to ambient of the contained gas. Test data generated on the current program indicate that the results are a function of the specific liner failure mode. Globally embrittled 301 cryo-CRES spherical liners with multitudes of through the thickness cracks remained in one piece as load carrying shells at operating pressure and the fiber structural response was essentially static. On the other hand, locally girth weld heat affected zone embrittled liners separated into two pieces and there was significant dynamic amplification of fiber static operating pressure strains. It seems likely, therefore, that liner failure modes for different liner materials would be a function of their material properties, particularly toughness, which relate to the number and size of fragments generated by the sudden liner brittle rupture at operating pressure, corresponding to different levels of fiber strain dynamic amplification. Additional tests with different liner materials wrapped with Kevlar -49 fibers would be required to define/verify the appropriate structural behavior/fail safe scenario and check the validity of the design guide presented in this report.

2.7.2 Cylindrical Vessels

A preliminary "first cut" design guide for fail safe liner fragment containment by the fibers of a prestressed composite cylindrical vessel whose metal liner fails suddenly in a brittle manner at operating pressure is derived in Appendix A. It is plotted on Figure 2-22 and set forth again below for continuity of text in equations A-31 and A-32. The equation is based on the assumptions that the structural models/test data generated on this program for spheres and 6" ϕ fiber wrapped cylinders are valid and that the hoop fibers in the cylindrical region fail at .02 hoop strain subsequent to sudden liner brittle failure at operating pressure. Test data for Kevlar -49 overwrapped prestressed composite cylindrical vessels are obviously needed to verify/improve the preliminary design guide postulated.

$$\sigma_{FHO} + \frac{1.7}{\beta} (\Delta\sigma_{MHO}) \leq 345 \quad \text{--- (A-31)}$$

$$\beta = \frac{n_f A_{FH}}{L t_M} \quad \text{--- (A-32)}$$

As defined in the nomenclature of Appendix A and Figure 2-21,

A_{FH} - hoop fiber (less resin) cross-sectional area per fiber (in²)

L - cylindrical length (in)

n_f - number of hoop fiber turns

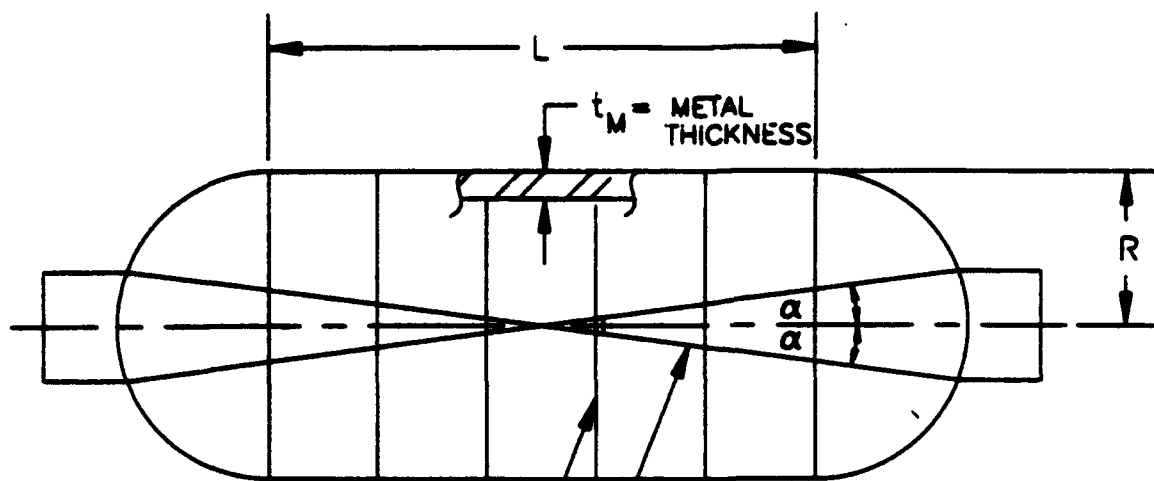
t_M - metal liner thickness (in)

σ_{FHO} - hoop fiber (less resin) operating stress (ksi)

σ_{MHO} - metal liner hoop operating stress (ksi)

σ_{MHi} - metal liner hoop initial stress (ksi)

$\Delta\sigma_{MHO} = (\sigma_{MHO} - \sigma_{MHi})$ - metal liner hoop operating stress increment (ksi)



HOOP FIBER (n_θ TURNS)

AREA/FIBER = A_{fh}

NUMBER OF HOOP FIBER TURNS

PER UNIT LENGTH = $\frac{n_\theta}{L}$

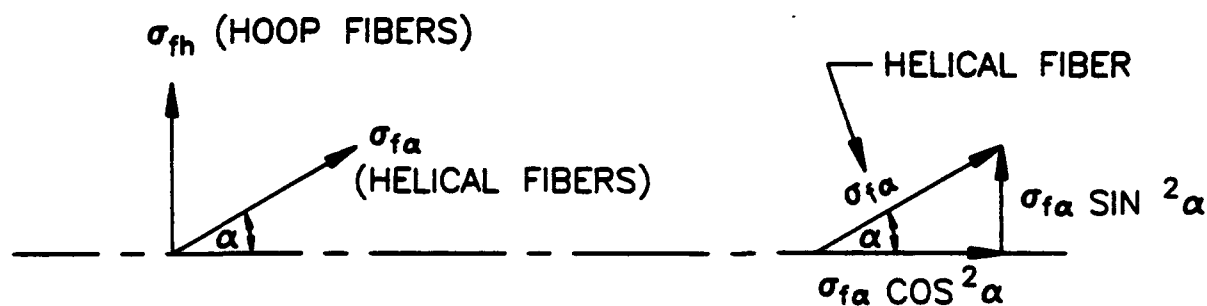
HELICAL FIBER (n_α TURNS)

AREA/FIBER = $A_{f\alpha}$

NUMBER OF HELICAL FIBER TURNS PER

UNIT CIRCUMFERENTIAL LENGTH = $\frac{n_\alpha}{2\pi R}$

a) CYLINDER FIBER WRAP GEOMETRY



b) CYLINDER FIBER WRAP STRESSES

FIG. 2-21 FIBER OVERWRAPPED CYLINDER GEOMETRY AND STRESSES

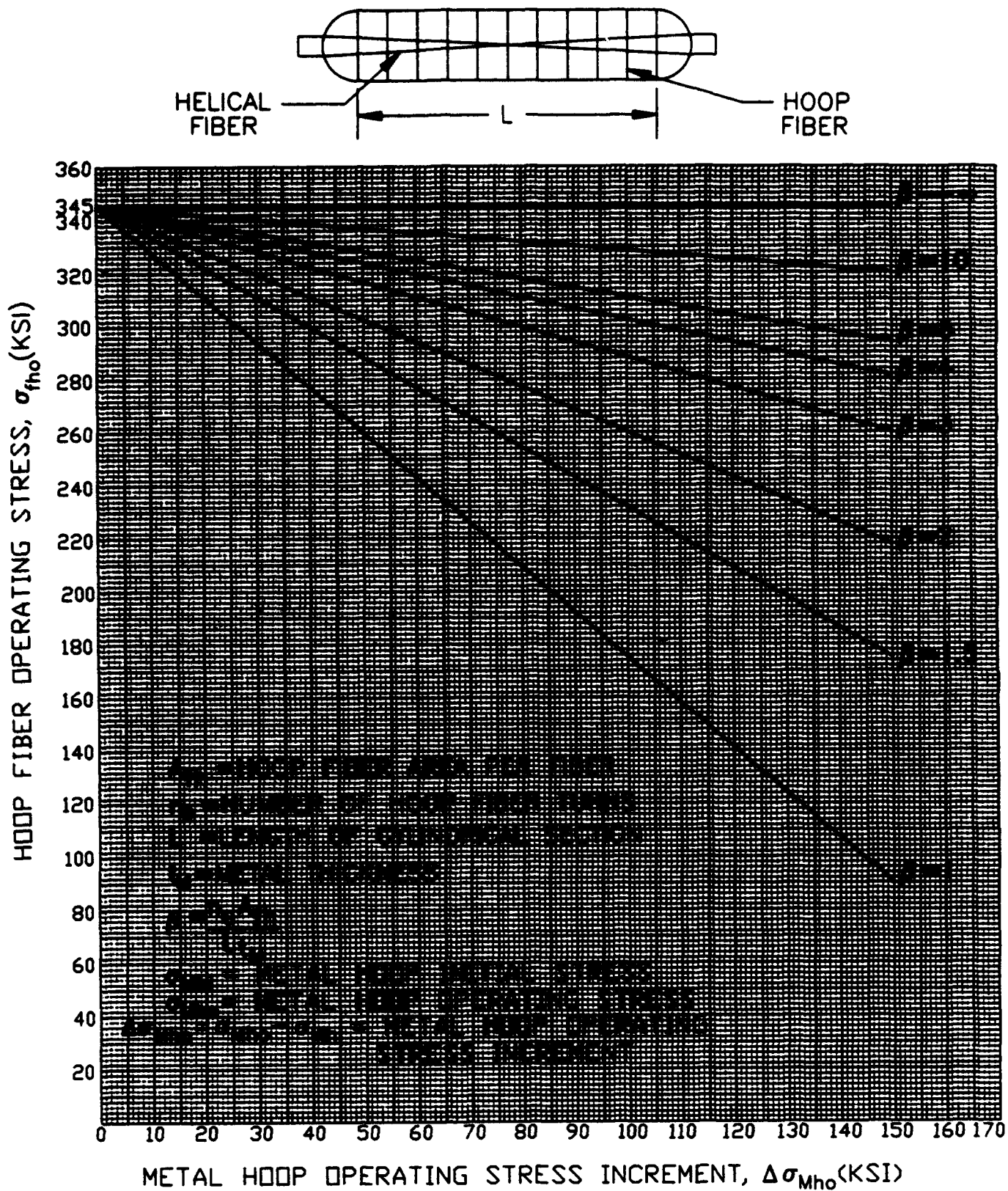


FIG. 2-22 KEVLAR OVERWRAPPED COMPOSITE CYLINDER "FAIL SAFE"
HOOP FIBER OPERATING STRESS VS. METAL HOOP OPERATING
STRESS INCREMENT

3.0 CONCLUSIONS AND RECOMMENDATIONS

3.1 Conclusions

3.1.1 Fail Safe Demonstrated

"Fail Safe", benign leak/fiber retention of liner fragments has been demonstrated experimentally for a range of tank structural and geometric parameters at 2500 to 5600 psig GHe operating test pressures for PSC Kevlar fiber overwrapped 301 cryo CRES spherical liners. The liners were intentionally hydrogen embrittled to achieve sudden brittle failure modes at operating pressure.

3.1.2 Fail Safe Design Guides Defined

Based on structural theory and test data obtained in this program, "Fail Safe", benign leak/fiber retention of liner fragments at operating pressure for Kevlar overwrapped metal composite tanks is a function of fiber operating stress, metal stress increment (operating minus initial) and fiber to metal thickness ratio. Guides to fail safe composite tank design are defined in terms of these parameters for both spheres and cylinders. It is presumed that test data generated for spherical geometry is valid for cylinders. This hypothesis is based on similarity between geodesic isotensoid fiber wraps (great circle sphere and hoop cylinder) and validity of the dynamic amplification factor model. Tests are obviously required to verify these assumptions.

3.1.3 Leak-Before-Burst (LBB) Mode Demonstrated by Test for 301 Cryoformed CRES

Operating pressure cycle tests of composite tanks with Elox machined defects in 301 cryoformed CRES liner walls showed benign leak mode for GHe and hydraulic pressurants. R-Curve and vessel fracture mechanics tests demonstrated that cryoformed 301 CRES is a tough, high strength material that gives LBB mode. Significant results obtained were a plane stress

critical R-Curve stress intensity of 180 ksi $\sqrt{\text{in}}$ for parent material, weld and HAZ at high tensile strength (200 - 260 ksi). Metal vessel thru cracks grew up to four (4) times the wall thickness before reaching critical size, demonstrating a large LBB safety factor. No further crack growth occurred after up to 48 hours of sustained operating pressure subsequent to benign leak. This verified the safe, stable mode of the thru cracked tank under constant operating load.

3.1.4 Analytic Predictions/Models Verified

Analytic predictions by 2D transient computer code model and simple 1D lumped models of fiber strains/failure modes were in reasonable agreement with experimental results.

3.1.5 Key Experimental Techniques Developed/Verified

Test procedures/techniques/set-up/instrumentation were developed to accomplish successful transient high pressure GHe testing of fiber overwrapped prestressed composite pressure vessels and to accurately monitor the extremely short time fiber strain response/ pressure/ temperatures. Accurate experimental simulation of sudden metal liner brittle failure computer model was accomplished. Techniques and parameters required to intentionally embrittle the PSC Cryo CRES liners in a controlled manner so that they failed in a predetermined brittle way at predetermined pressure/stress/time were developed and experimentally verified.

3.2 Recommendations

3.2.1 The use of high strength and high modulus graphite fiber overwrap for PSC vessel construction is becoming more and more prevalent because of the significant weight reduction possible. Indications are that graphite fiber behavior may be different from Kevlar. Continuation of the "fail safe" data base work of this program to encompass graphite fiber overwrapped PSC vessels appears warranted and mandatory.

3.2.2 Tests of cylindrical fiber overwrapped PSC composite tanks are recommended to verify the fail safe design guide for cylindrical geometry defined herein which was extrapolated from results on spheres.

3.2.3 Test data obtained on the program indicate that fiber dynamic strain amplification is a function of the failure mode of the liner. Large dynamic strain amplification occurred when the liner fragmented into two pieces. On the other hand, essentially static behavior was observed for the cracked liner which remained intact and capable of resisting load as a whole shell. It is anticipated that more severe fragmentation would occur, all else the same, for a less tough liner material compared to a more tough liner material. It is recommended, therefore, that PSC fiber overwrapped tanks with different liner materials be tested to evaluate this effect.

4.0 REFERENCES

1. Gleich, D., "Report on Kevlar -49 Composite Pressure Vessel Safety Technology Program", Presented at the 1985 JANNAF Propulsion Meeting, San Diego, CA 9 - 12 April 1985.
2. Gleich, D., "High Performance Positive Expulsion Tankage and Pressure Vessel Constructions", Paper 78-WA/Aero-19, Presented at the ASME Winter Annual Meeting, San Francisco, CA, December 10 - 15, 1978.
3. Gleich D., "Design Considerations and Structural Performance of Prestressed Composite Pressure Vessels", Paper AIAA-82-1230, AIAA/SAE/ASME 18th Joint Propulsion Conference, June 21 - 23, 1982, Cleveland, Ohio.
4. PISCES, "Physics International's Scientific Codes for Engineering Service", Physics International Co., San Leandro, CA.
5. Gerstle, F. P., "Analysis of Filament Reinforced Spherical Pressure Vessels", ASTM STP 546, pp. 604-631, Composite Materials 3rd ASTM Conference, Williamsburg, VA., 21 - 22 March, 1973.
6. Tsai, W. W. and Pagano, N.J., "Invariant Properties of Composite Materials" in "Composite Materials Workshop", Technomic, 1968, pp. 233-253.
7. Kevlar 49 Data Manual, E. T. DuPont De Nemours and Co., Wilmington, Del.
8. Handbook of Engineering Mechanics, edited by W. Flugge, First Ed., pp. 61-27, McGraw-Hill Book Co., 1962.

APPENDICES

This section contains the Appendices used to amplify the discussions given in the main text.

The Appendices consist of newly generated text and reference documents that were prior generated on the program. For purposes of clarity and ease of reference, figures/tables in the prior generated reference documents have letters following the figure or table number, e.g., Figure 1A, Figure 2B, etc. The newly generated appendices text figures/tables numbers have letters preceding the algebraic digits (e.g., A-1, B-2, C-2, etc.) indicating their specific appendix location. A complete list of figures and tables together with their locations is given in Appendix G, herein.

Appendix A - Analytic Models

This appendix describes the analytic models used to investigate the "fail safe" potential of Kevlar fiber overwrapped PSC tanks at operating pressure and to evaluate and correlate the experimental data obtained in the program.

The following items are treated in detail herein.

- A.1 Nomenclature
- A.2 Two-Dimensional Spherical PICES Computer Model
- A.3 One-Dimensional Transient and Static Models and
"Fail Safe" Design Guides

A.1 Nomenclature

A_{fH} = Hoop Fiber Area

$A_{f\alpha}$ = Helical Fiber Area

d = Distance

E_1 = Composite (fiber + Resin) Young's Modulus in Fiber Direction

E_2 = Composite Young's Modulus Perpendicular to Fiber Direction

E_f = Fiber Less Resin Young's Modulus in Fiber Direction

E_M = Metal Young's Modulus

$\Delta_{E_M} = E_M / (1 - \nu_M)$ = Metal Effective Young's Modulus for Spherical

Membrane

E_W = Effective Isotropic Composite Young's Modulus

F.S. = Factor of Safety

G = Composite Average Shear Modulus

h_M = Metal Thickness

h_W = Composite Thickness

k_f = Fiber Less Resin Extensional Stiffness = $\frac{E_f t_f}{2}$

$k_M = \Delta_{E_M} =$ Metal Extensional Stiffness

L = Length

n_θ = Number of hoop Fiber Turns

n_α = Number of Helical Fiber Turns

P = Pressure

P_i = Initial Stress Pressure

P_o = Operating Pressure

P_f = Pressure Carried by Fiber Less Resin

P_{fo} = Operating Pressure Carried by Fiber Less Resin

P_M = Pressure Carried by Metal

P_{Mo} = Operating Pressure Carried by Metal

$P_{f\theta o}$ = Portion of Operating Pressure Resisted by Fibers in Hoop

Direction

$P_{M\theta o}$ = Portion of Operating Pressure Resisted by Metal in Hoop

Direction

Δ = Pressure Hoop Fibers Have to resist Upon Sudden Liner

$P_{\theta f}$

Failure

P^* = Static Fiber Stress Pressure

P_W = Equivalent Static Pressure Metal Transmits to Fiber Wrap

Q = Average Composite Stiffness in the Principal Directions

R = Radius

t = Time

t_f = Fiber Less Resin Thickness

t_M = Metal Thickness

u = Radial Displacement

V = Volume

α = Helix Fiber Winding Angle

$$\alpha_M = E_M / 1 - \nu_M$$

$$\alpha_W = E_W / 1 - \nu_W$$

$$\beta = \frac{n_\theta A_{FH}}{L t_M}$$

Δ = Increment

γ = Shear Strain

ϵ = Strain

$$\epsilon_i = \frac{1}{3} \frac{\Delta V}{V} = \text{prestrain (initial strain)}$$

ϵ_1, ϵ_1 = Fiber Equilibrium Strain Prior to Liner Failure

ϵ_2, ϵ_2 = Fiber Equilibrium Strain After Liner Failure

ϵ_{MAX} = Maximum Fiber Strain

$\frac{\Lambda}{\epsilon_f}$ = Effective Static Fiber Less Resin Strain

$\frac{\Lambda}{\epsilon_{\theta f}}$ = Effective Static Hoop Fiber Less Resin Strain

μ = Mass Density Per Unit Area

ν_M = Poisson's Ratio of Metal

ν_W = Effective Isotropic Composite Poisson's Ratio

σ_f = Fiber Less Resin Stress

σ_{fo} = Operating Fiber Less Resin Stress

σ_{fHo} = Operating Hoop Fiber Less Resin Stress

σ_{fao} = Operating Helical Fiber Less Resin Stress

σ_{fai} = Initial Helical Fiber Less Resin Stress

σ_{fi} = Initial Fiber Less Resin Stress

σ_{fHi} = Initial Fiber Less Resin Hoop Stress

$\frac{\Lambda}{\sigma_f}$ = Equivalent Static Fiber Less Resin Stress

σ_M = Metal Stress

σ_{MO} = Operating Metal Stress Before Liner Failure

σ_{MHO} = Operating Metal Hoop Stress Before Liner Failure

σ_w = Composite Fiber Wrap Stress

σ_{Mi} = Metal Initial Stress

σ_{MHi} = Metal Hoop Initial Stress

σ_{Wi} = Composite Fiber Wrap Initial Stress

τ = Shear Stress

Φ = Dynamic Amplification Factor

ω = Natural Frequency

A.2 Two-Dimensional Model

The description of the two-dimensional spherical model used for the brittle liner failure mode analysis is outlined on Figure A-1. It is based on the use of PISCES finite difference transient computer program⁴. A worst case scenario assumes an instantaneous complete girth crack in the brittle liner at zero time. A set of simplified Kevlar/epoxy composite isotropic material constants used in the calculations are based on the equations of Tsai and Pagano⁶:

$$Q = \frac{1}{8} (3E_1 + 5E_2) \dots (A-1)^*$$

$$G = \frac{1}{8} (E_1 + 2E_2) \dots (A-2)$$

$$\text{For } E_1 = 2/3 \times 19 \times 10^6 = 12.67 \times 10^6 \text{ psi,}$$

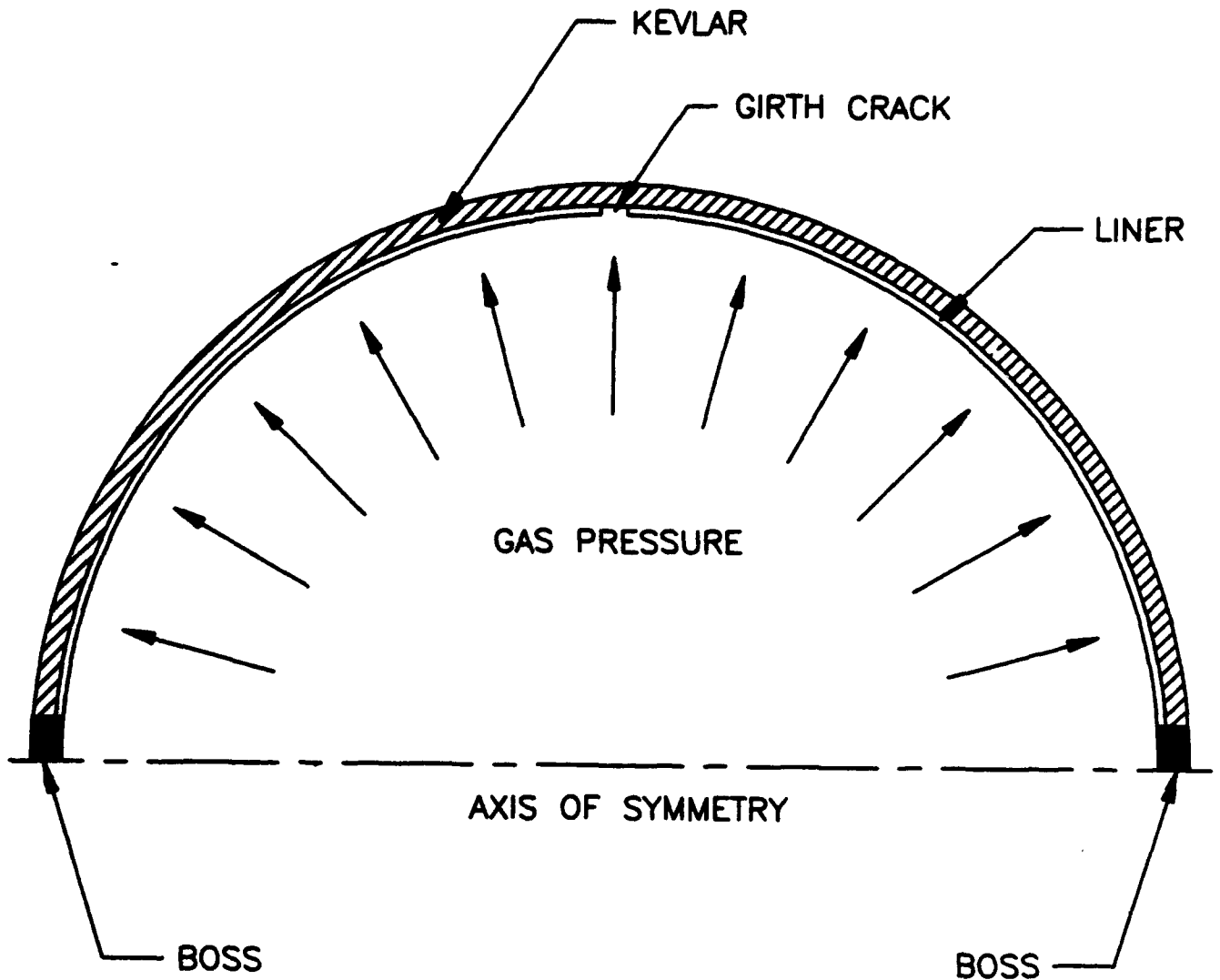
$$\text{and } E_2 = 2/3 (0.95 \times 10^6) = .633 \times 10^6 \text{ psi, we obtain}^7$$

from A-1 and A-2,

$$Q = 5.15 \times 10^6 \text{ psi}$$

$$G = 1.74 \times 10^6 \text{ psi}$$

* Refers to equation numbers (typical)



- TWO-DIMENSIONAL TRANSIENT STRESS ANALYSIS USING PISCES 2DELK
- THIN-SHELL AXISYMMETRIC ELEMENTS
- KEVLAR - SINGLE SHELL
- LINER - ISOTROPIC THIN SHELL
- CRACK CAN BE POSITIONED TO CONSIDER WORST CASE

FIG. A-1 BRITTLE LINER ANALYSIS

The equivalent isotropic Young's modulus and Poisson's ratio are found from,

$$\frac{E_w}{1-\nu_w^2} = Q \quad \dots (A-3)$$

$$\frac{E_w}{2(1+\nu_w)} = G \quad \dots (A-4)$$

yielding upon substitution of above numerical values,

$$E_w = \frac{4G}{1-G/Q} = 4.6 \times 10^6 \text{ psi}$$

$$\nu_w = \frac{1-2G}{Q} = 0.32$$

as the effective isotropic constants for Kevlar/epoxy overwrap. Computer calculations were carried out for the structural model schematically shown on Figure A-2 using appropriate test PSC vessel pressures, geometries and materials properties assuming complete slip and complete bonding at the fiber/metal interface. The complete slip interface condition resulted in higher fiber strains and better agreement with the strains measured in the tests.

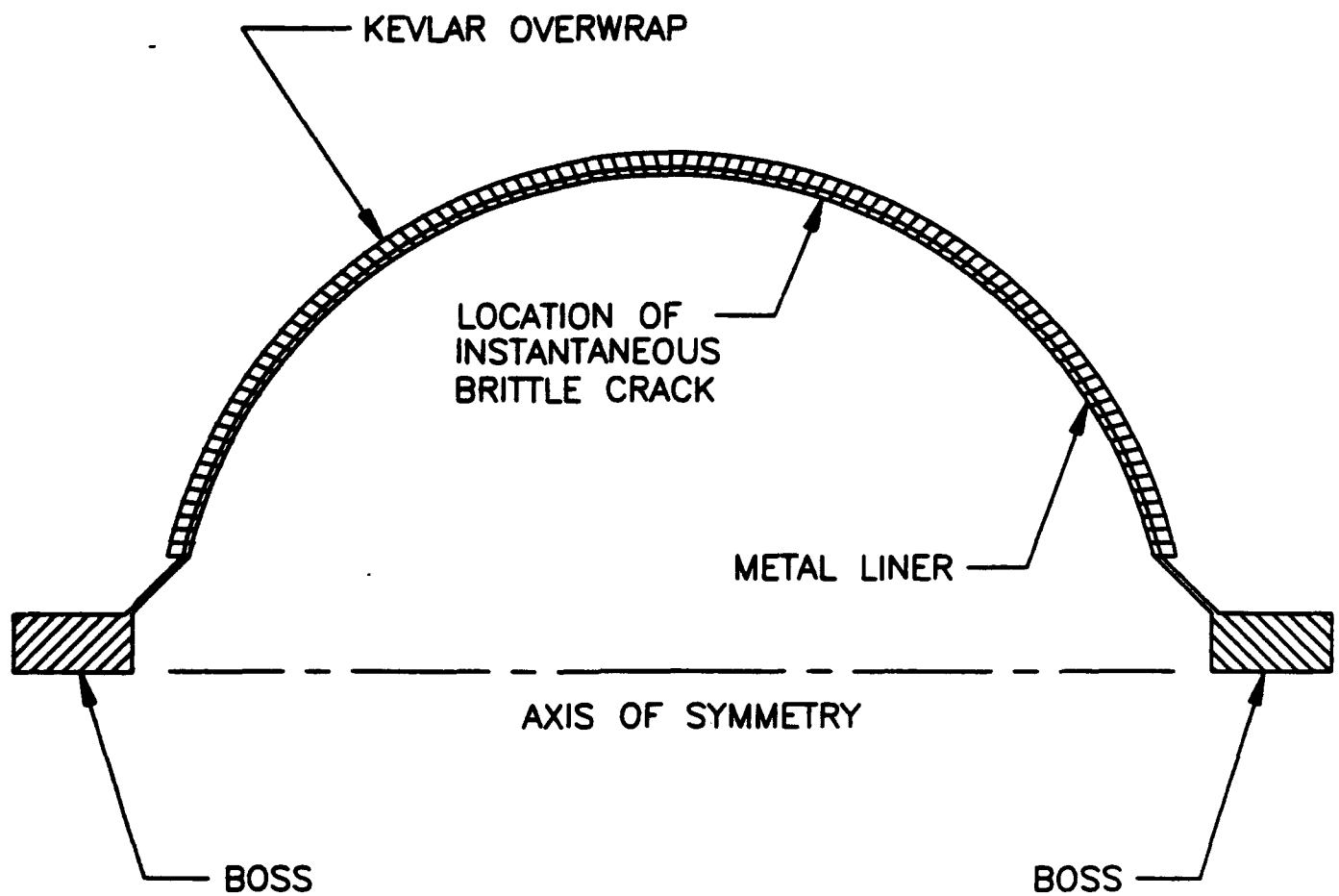


FIG. A-2 PISCES SHOCK-RESPONSE MODEL DEVELOPMENT

A.3 One-Dimensional Models

A.3.1 Transient Model

A.3.1.1 Static State

For static equilibrium at pressures P and zero (prestress state) we have,

$$\sigma_M h_M + \sigma_w h_w = \frac{PR}{2} \dots (A-5)$$

$$\sigma_{Mi} h_M + \sigma_{wi} h_w = 0 \dots (A-6)$$

Assuming linear elasticity, strain compatibility between pressure P and zero requires,

$$\frac{\sigma_M - \sigma_{Mi}}{\sigma_M} = \frac{\sigma_w - \sigma_{wi}}{\alpha_w} \dots (A-7)$$

From (A-5) \rightarrow (A-7) one obtains for the static composite shell,

$$\sigma_M - \sigma_{Mi} = \frac{PR}{2h_M} \frac{1}{1 + \frac{h_w \alpha_w}{h_M \alpha_M}} \dots (A-8)$$

$$\frac{\sigma_w - \sigma_{wi}}{\alpha_w} = \frac{PR/2}{h_M \alpha_M + h_w \alpha_w} = \epsilon_1 - \epsilon_i \dots (A-9)$$

If the fiber wrap is intact and the liner loses strength ($\sigma_M = 0$), we determine from (A-5) and the fiber stress/strain relation, the static fiber strain, ϵ_2 , referenced to the fiber zero stress state as,

$$\epsilon_2 = \frac{\sigma_w}{\alpha_w} = \frac{PR}{2h_w \alpha_w} \dots (A-10)$$

A.3.1.2 Transient State

Assuming the entire liner instantly loses strength, the equation of motion for a spherical shell for rotationally symmetric radial motion, u and extensional strain, $\epsilon = u/R$, loaded with time varying pressure can be written⁸,

$$\ddot{\epsilon} + \omega^2 \epsilon = \frac{p}{R\mu} \dots (A-11)$$

$$\text{with } \omega^2 = \frac{2hw\alpha_w}{R^2\mu} \dots (A-12)$$

The mass per unit area, μ , contains the liner mass only if the liner remains attached to the overwrap and participates in the motion.

The solution of (A-11) with the initial condition, $\epsilon = \epsilon_1$ at $t = 0$, is,

$$\epsilon = \epsilon_2 + (\epsilon_1 - \epsilon_2) \cos \omega t \dots (A-13)$$

The maximum strain occurs for $\cos \omega t = -1$ and is given by,

$$\epsilon_{\text{MAX}} = \epsilon_2 + (\epsilon_2 - \epsilon_1) \dots (A-14)$$

The peak strain is the same regardless of the amount of liner mass participating in the motion; only the frequency differs.

Test data fiber strain correlation calculations were made using equations A-9, A-10 and A-14, together with PSC test vessel geometry, effective fiber wrap isotropic constants, 301 cryo CRES liner material properties and fiber prestrain values, ϵ_i . Typical results are illustrated by the ϵ_1 , ϵ_2 and ϵ_{MAX} values given on Figures 2-17, 2-18 and 2-19.

A.3.2 Static One-Dimensional Model - Dynamic Amplification Factor/"Fail Safe" Design Guide

A.3.2.1 Dynamic Amplification factor

Just prior to composite vessel liner failure at pressure, P, the fiber stress is σ_f and it resists a pressure P_f , while the metal liner carries the balance of the pressure, $P_M = P - P_f$. When the liner fails suddenly, the fibers have to carry an additional pressure, P_1 , and their stress and strain are increased to $\frac{\Delta}{\sigma_f}$ and $\frac{\Delta}{\epsilon_f}$, respectively. It is postulated that the additional fiber pressure P_1 is given by a dynamic amplification factor Φ times the static pressure P_M that the metal was carrying just before it failed. If P_1 is large enough, fiber failure will occur at the test verified 2% ultimate strain value. This model is formulated analytically below using, for convenience, the results of prior work³. Terms are defined in the nomenclature.

$$\frac{\Delta}{\sigma_f} = \sigma_f + \frac{\Phi P_M}{t_f} = \sigma_{fi} + \frac{\Delta \sigma_f \Delta P}{\Delta P} + \frac{\Phi P_M}{t_f} = E_f \frac{\Delta}{\epsilon_f} \dots (A-15)$$

with,

$$\frac{\Delta \sigma_f}{\Delta p} = \frac{E_f}{E_m} \times \frac{R/2t_m}{1 + k_f/k_m} \dots (A-16)$$

$$\frac{P_m}{P} = \frac{1}{1 + k_f/k_m} \dots (A-17)$$

$$\sigma_{fi} = E_f \epsilon_i = E_f \frac{1}{3} \frac{\Delta V}{V} \dots (A-18)$$

Correlation of pertinent test data to date, using

$$\frac{\Delta}{\epsilon_f} = .02, \text{ gave values of dynamic amplification factor } \Phi$$

range of 1.5 - 1.7 for the local girth and boss weld regions embrittled liner failure modes. Measured fiber strains for the spherical liner global embrittled failure mode were correlated by static structural behavior ($\Phi = 1$).

A.3.2.2 "Fail Safe" Design Guide

A.3.2.2.1 Spheres

Recasting (A-15) specifically at operating pressure, with subscripts, o, as defined in the nomenclature and specifying fiber and metal operating pressures in terms of their static operating stress increments (measured from the prestressed state) yields,

$$P_{fo} = \Delta \sigma_{fo} \frac{t_f}{R} \dots (A-19)$$

$$P_{MO} = 2\Delta \sigma_{MO} \frac{t_M}{R} \dots (A-20)$$

with $P_{fo} + P_{MO} = P_o \dots (A-21)$

Here,

$$\Delta\sigma_{fo} = \sigma_{fo} - \sigma_{fi}$$

$$\Delta\sigma_{MO} = \sigma_{MO} - \sigma_{Mi} \dots (A-22)$$

Substituting in (A-15) one obtains,

$$E_f \epsilon_f = \frac{R}{t_f} \sigma_{fo} \frac{t_f}{R} + \phi 2 \Delta\sigma_{MO} \frac{t_M}{R} \dots (A-23)$$

Taking for Kevlar -49, $E_f = 19000$ ksi,

$\epsilon_f = .02$ fiber less resin ultimate strain and allowing for a design

factor of safety, F.S., we have from (A-23) the relation between

allowable static fiber operating stress, given metal static operating

rating stress increment and fiber to metal thickness ratio for "fail

safe" liner fragment retention by the fibers as,

$$\sigma_{fo} = \frac{380}{F.S.} - \frac{2\phi\Delta\sigma_{MO}}{t_f/t_M} \dots (A-24)$$

Taking now, $\Phi = 1.7$ (worst case embrittled dynamic amplification factor) and $FS = 1.1$, we obtain as a spherical prestressed composite tank "fail safe" design guide the allowable static fiber operating stress,

$$\sigma_{fo} = 345 - \frac{3.4\Delta\sigma_{MO}}{t_f t_M} \dots (A-25)$$

This relation is plotted on Figure 2-20 of section 2. Values of fiber operating stress, σ_{fo} , equal to or less than the values shown on the figure for given metal operating stress increment $\Delta\sigma_{MO}$, and specified fiber to metal thickness ratio, t_f/t_M , indicate "fail safe" retention of spherical liner fragments by the Kevlar -49 fibers and benign pressure venting to ambient. For example, at $\Delta\sigma_{MO} = 100$ ksi and $t_f/t_M = 3$, values of fiber operating stress, $\sigma_{fo} \leq 231$ ksi indicate "fail safe" fragment retention behavior for sudden spherical liner failure at operating pressure.

A.3.2.2.2 Cylinders

Based on the structural models/test data obtained for spheres and successful test data correlation of 6" ϕ fiber wrapped cylinders on the current program, we derive below a simplified "first cut" liner fragment retention design guide for cylindrical shapes, assuming a hoop fiber failure mode in the cylindrical (non-head) region when the metal liner fails suddenly at operating pressure. Differences in geometry and fiber wrap pattern between spherical and cylindrical configurations may affect

the accuracy of the results. Test data are obviously needed to verify/improve the model.

The cylindrical vessel of radius, R and cylindrical length, L , has a metal liner of thickness, t_M , as sketched on Figure 2-21 of section 2. The liner is fiber wrapped with hoop fibers with fiber area A_{fh} per fiber, having $\frac{n_\theta}{L}$ turns per unit of cylindrical length as well as helical fibers of area $A_{f\alpha}$ per fiber, inclined at an angle, α , with the axial centerline of the cylinder as shown on the figure. The helical fiber turns per circumferential length is $n_\alpha/2\pi R$ as noted. The composite tank is prestressed. At zero pressure, the metal liner is in hoop compression, σ_{MHi} , and the hoop and helical fibers are in tensions, σ_{fHi} and $\sigma_{f\alpha i}$, respectively. The composite cylindrical vessel with closed ends is then loaded with an internal operating pressure, P_o .

Using netting analysis theory and measuring stress increments (operating minus initial stress) from the zero stress state, we write the well known hoop equilibrium equation in the form,

$$\Delta\sigma_{MHO} \frac{t_M}{R} + \frac{n_\theta A_{fh} \Delta\sigma_{fHO}}{LR} + \frac{n_\alpha A_{f\alpha} \sin\alpha \tan\alpha \Delta\sigma_{f\alpha o}}{2\pi R^2} = \Delta P_o = P_o$$

... (A-26)

The first term on the left hand side of (A-26) is the "hoop pressure" resisted by the metal. The second term represents the hoop pressure reacted by the combined hoop plus helical fibers. Symbolically, (A-26) then becomes,

$$\Delta P_{M\theta O} + \Delta P_{f\theta O} = \Delta P_O = P_O \dots (A-27)$$

Assuming, as for spheres, that the pressure, $\Delta P_{\theta f}$, the fibers have to resist at sudden liner failure is the sum of the static pressure it carried before liner failure plus a dynamic amplification factor, Φ , times the pressure the metal was carrying before liner failure, we have,

$$\Delta P_{\theta f} = \Delta P_{\theta O} + \Phi \Delta P_{M\theta O} \dots (A-28)$$

Noting that the hoop fiber strain increment is given by,

$$\Delta \epsilon_f = \frac{\Delta \sigma_f}{E_f} = \frac{1}{E_f} \frac{\Delta P_{\theta f} R}{n_{\theta} A_{fH/L}} \dots (A-29)$$

and using A-26 through A-28, we obtain,

$$E_f \Delta \epsilon_f = \Delta \sigma_{fHo} + \frac{n_{\alpha} A_{f\alpha/2\pi R}}{n_{\theta} A_{fH/L}} \sin \alpha \tan \alpha \Delta \sigma_{fao} \dots (A-30)$$

For practical designs, $\frac{n_{\alpha} A_{f\alpha/2\pi R}}{n_{\theta} A_{fH/L}}$ is the order of unity,

$\Delta\sigma_{fho} = \frac{3}{4} \Delta\sigma_{fH}$ and α is a small angle, 15° or less. The second term on the left hand side of (A-30) is then about 5% or less of the first term and is conservatively neglected.

Adding now the effect of initial fiber strain, $\epsilon_{fHi} = \sigma_{fHi}/E_f$, to obtain the total fiber strain, $\epsilon_f = \Delta\epsilon_f + \epsilon_{fHi}$ and noting that $\sigma_{fHo} = \Delta\sigma_{fHo} + \sigma_{fHi}$, we obtain,

$$E_f \epsilon_f = \sigma_{fHo} + \frac{\phi t_M}{n_\theta A_{fH}/L} \Delta\sigma_{MHo} \dots (A-31)$$

Taking in A-31 $E_f = 19000$ ksi, $\epsilon_f = .02$, $\phi = 1.7$ and allowing for a factor of safety, $FS = 1.1$ yields,

$$\sigma_{fHo} + \frac{1.7}{\beta} \Delta\sigma_{MHo} \leq 345 \dots (A-32)$$

with the effective hoop fiber to metal thickness ratio, β , given by,

$$\beta = \frac{n_\theta A_{fH}}{Lt_M} \dots (A-33)$$

Equation (A-32), the preliminary design guide for cylindrical liner fragment retention by Kevlar fibers is plotted on Figure 2-22 of section 2. It defines the maximum allowable hoop fiber operating stress for given metal operating hoop stress increment and effective hoop fiber to metal thickness ratio, β . Fragment retention and fail safe behavior is defined by the region bounded by the applicable $\beta = \text{constant}$ curves.

APPENDIX B - Hydrogen Embrittlement Parameters/Test Data

This appendix discusses in detail the derivation of the hydrogen embrittlement parameters used in the controlled intentional embrittlement of the 301 Cryo CRES liners of the Kevlar fiber overwrapped PSC tanks. Hydrogen embrittlement was used to provide the sudden brittle liner failure mode at operating pressure required to obtain "fail safe" experimental data as described in section 2 of the text.

Hydrogen embrittlement parameters and test data are summarized and they are discussed in detail in ARDE Report EG 42001-3 "Interim Report Kevlar 49 Overwrap Study Liner Failure Inducement by Hydrogen Embrittlement Sub Scale Tests," contained in this appendix.

B.1 Hydrogen Embrittlement Parameters

Intentional 301 CRES liner hydrogen embrittlement parameters derived from the 11" ϕ and full scale 16" ϕ PSC vessel tests are listed below.

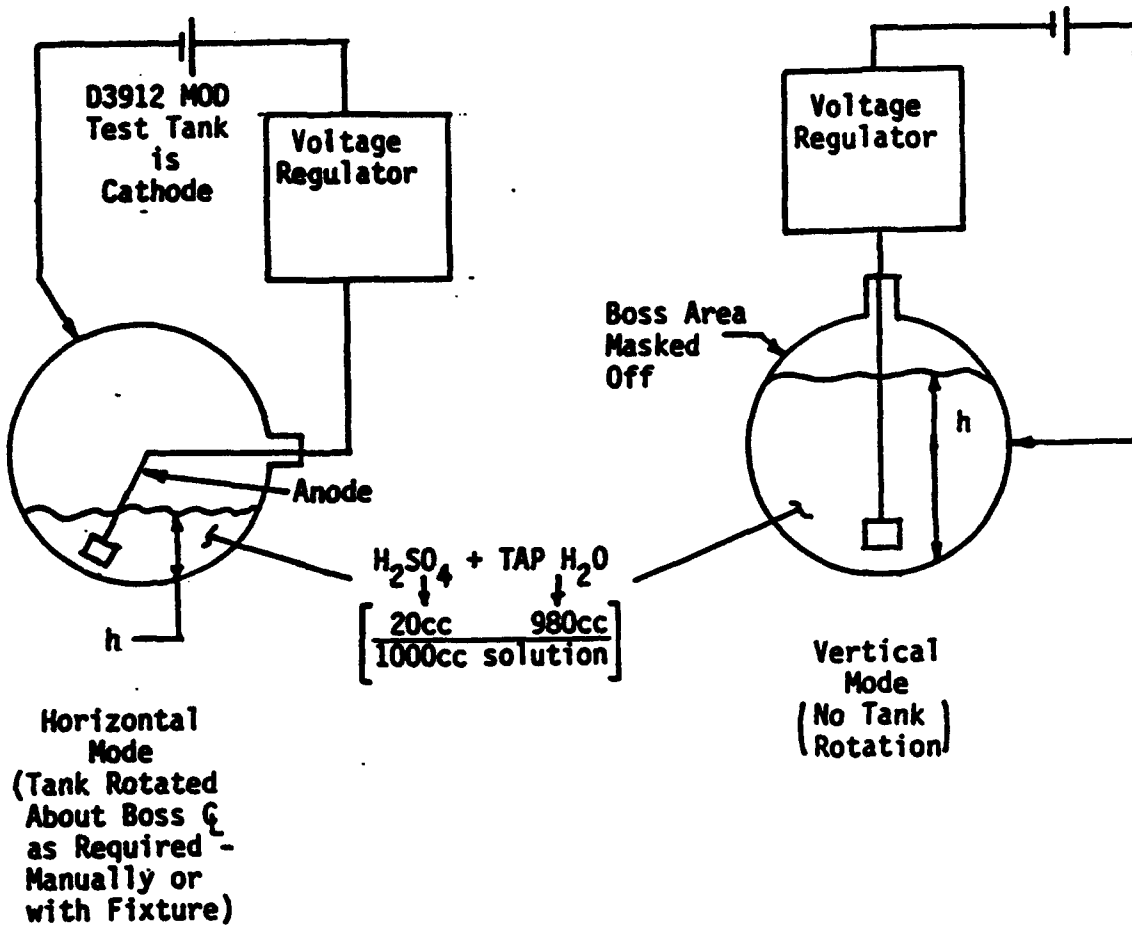
- . Electrolyte solution: 20cc H_2SO_4 + 980cc tap water + 500 mg $NaAsO_2$. Additional solution volumes in same proportions.
- . Sensitize liner inside surface: cold pickle - nitric/hydrofluoric acid solution (70°F-90°F).
- . Charging current: 6 mili amps/in² of surface to be embrittled.
- . Charging time: 72 hours
- . Hold time after charging: Pressure test within 3 hours after end of charging.
- . Mask off areas not to be embrittled: Adcoat AC818T liquid maskant

B.2 11" ϕ Hydrogen Embrittlement Test Data Summary

Subscale (11" ϕ) hydrogen embrittlement test data for 301 cryo CRES spheres, P/N D391, Figure B-1, are given in Table B-1. Hydrogen embrittlement test modes and hydrogen embrittlement vessel burst test schematic are sketched on Figures B-2 and B-3, respectively. Additional test details are given in ARDE Interim Report EG 42001-3 contained in this Appendix.

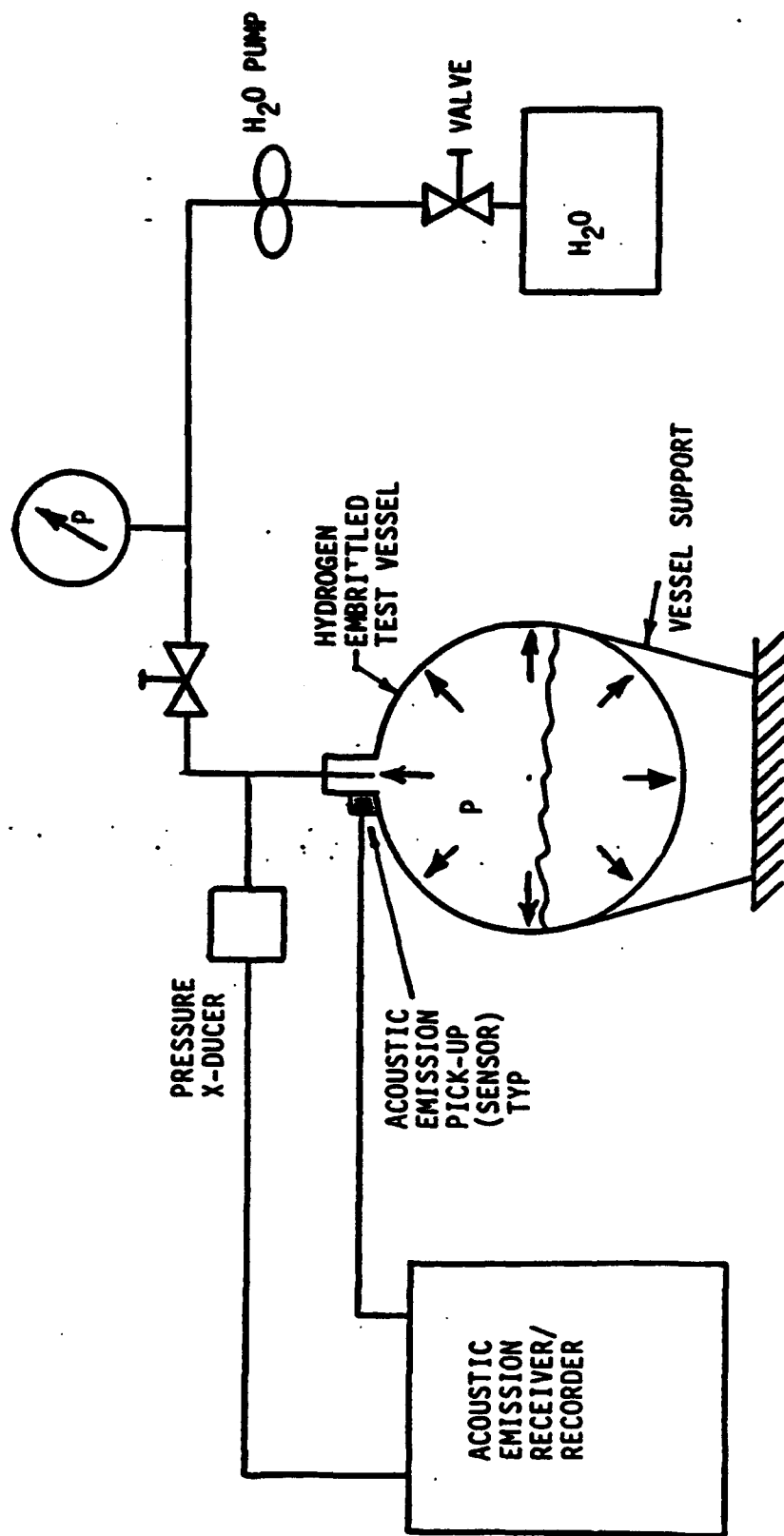
SUB-SALT INTRACON ENLIGHTENMENT TEST DATA (P/N D3012 MOD)

S/N	QOL CHANGE NO.	CHG SOLUTION BOTTLE IN TANK (1st) VOL. (ML.)	DILUTION TIME	TANK POS-ROTATED MARKED	DOGS CHMS	CORRECTION CHANGE TIME	HOLD TIME AFTER CHARGE (HRS)	TIME OF PRESSURE EST. OF C ₀	ACUSTIC SIGNALS	FAILURE MODE IDENTIFICATIONALLY	REMARKS
004	88470 2850	3.5	Ver	Yes No	0/16/ 400	3.2	24	3000	.40 Single Sensor, low sensitivity	Did not fail	Overlap change 4.9, 12.16, 20 & 31 hrs
004	2850	3.5	Ver	No	48	600	24	2240	.45 Single Sensor, sensitivity (12 sec) (Hold)	Hydrogen Substitution Pressure over local ductile SMI crane/POE about	One place
006	2850	3.5	Ver	Gas-bleed	90	600	24	3400	.4C Four Sensor Low Sensitivity	Did not fail	Rotation used to preclude base area from being submitted
006	11400	9.125	Vert	No Yes	48	1600	24	2760	.4D Two Sensor Linear, Low Sensitivity	Hydrogen Substitution Pressure burr broke into three face same as plane A	Hubert area not considered. Tank pressure burr broke into three plane A
003	1140	9.125	Vert	No Yes	48	1600	24	2810	.3B Two Sensor Linear, Low Sensitivity	Did not fail	Same subcritical crack growth detected by microscope/radiography
003	11400	9.125	Vert	No Yes	48	1600	24	2260	.4F Two Sensor Linear, low and high sensitivity	Hydrogen Substitution works pre-substitution cracks face has no even cracking. Bottle clear there washed area	Hubert clearly substituted work pre-substitution cracks
008	88470 1450	2.4	Vert	No	53	4000	0	3300	(5 sec.) .4C (10 min) Hold	None	Poor (4) amp Substitution battery charge as fracture bar-power source facing singular 14-29-53 hrs. to 2/11/64
009	88470 11400	9.125	Vert	No Yes	60	1600	12	2720	.50 Two Sensor, High Sensitivity (1.3 min) (Hold)	Hydrogen Substitution	Two pieces
013	88470 11400	9.125	Vert	No Yes	60	1600	12	2700	.50 Two sensor, High Sensitivity (1.0 min) Hold	Hydrogen Substitution	Single piece
004	90740 11400	9.125	Vert	No Yes	72	1600	24	3260	.50 sec. (20 sec) (Hold)	None	Cold Finished Hydrogen Substitution 10 min. 6 pieces
109	1X7395 W/A	Girth Band	Vert	No Girth Band	72	1150	6	2750	.50 min. 4.7 min. hold	None	Hydrogen Substitution Fragmentation
10	88470 1140	9.125	Vert.	No	72	1400	3	3400	.50 sec. 20 sec. 20 sec. 20 sec.	Gas. Hydrogen Substitution	Fragmented



SUB SCALE
HYDROGEN EMBRITTLEMENT
TEST MODES

FIGURE B-2



SUB - SCALE
HYDROGEN EMBRITTLEMENT VESSEL
BURST TEST SCHEMATIC

FIGURE B-3
B-6

INTERIM REPORT
KEVLAR 49 OVERWRAP STUDY
LINER FAILURE INDUCEMENT
BY
HYDROGEN EMBRITTLEMENT
SUB SCALE TESTS

Submitted to:

PATRICK AFB
Eastern Space and Missile Command
Florida 32925

Contract: FO8606-84-C-0029

Prepared By:

S. M. Berko
S. M. Berko
Project Engineer

Approvals:

David Gleich
D. Gleich
Principal Investigator

A. Cozewith
A. Cozewith
Vice President
Program Management

ARDE, INC.
19 Industrial Avenue
Mahwah, N.J. 07430

TABLE OF CONTENTS

<u>PARA.</u>	<u>TITLE</u>	<u>PAGE</u>
1.0	INTRODUCTION	B-10
1.1	PURPOSE	B-10
1.2	APPROACH AND SUMMARY OF RESULTS.	B-11
	1.2.1 TANK EMBRITTLEMENT.	B-11
	1.2.2 ACOUSTIC EMISSION TESTING AND SUMMARY OF RESULTS	B-11
1.3	SUMMARY OF CONCLUSIONS TO DATE AND CONTINU- ATION OF TESTING	B-12
2.0	TEST SET-UP.	B-13
2.1	TEST ARTICLES	B-13
2.2	TEST EQUIPMENT	B-13
2.3	BASELINE PARAMETERS.	B-15
3.0	SPECIFIC TESTS AND RESULTS	B-15
3.1	HEAT #88470 S/N 008	B-16
3.2	HEAT #88019 S/N 004	B-16
3.3	HEAT #88019 S/N 006	B-18
3.4	HEAT #88019 S/N 003	B-19

APPENDICES

APPENDIX B-1	HYDROGEN CONCENTRATION IN THE WALL OF THE PRESSURE VESSEL DURING CHARGING, HOLD AND TEST	B-42
APPENDIX B-2	PRE-PROPOSAL TEST OF HYDROGEN ENDUCED FAILURE ARDE AMR #279	B-46
APPENDIX B-3	HYDROGEN EMBRITTLEMENT PROCEDURE	B-51
APPENDIX B-4	MATERIAL EVALUATION OF HEAT 88470	B-55

LIST OF FIGURES

<u>FIGURE</u>	<u>TITLE</u>	<u>PAGE</u>
1A	SPHERE MATERIAL EVALUATION SKC 11341	B-27
2A	SUBSCALE HYDROGEN EMBRITTLEMENT VESSEL BURST TEST SCHEMATIC	B-28
3A	SUBSCALE HYDROGEN EMBRITTLEMENT TEST MODES	B-29
4A	HYDROGEN EMBRITTLEMENT TEST 2 PN D3912, SN4	B-31
5A	HYDROGEN EMBRITTLEMENT SUBSCALE TEST D3912 SN 006	B-32
6A	HYDROGEN EMBRITTLEMENT SUBSCALE TEST D3912 MOD SN 006	B-33
7A	HYDROGEN EMBRITTLEMENT SUBSCALE TEST D3912 MOD SN 006	B-34
8A	HYDROGEN EMBRITTLEMENT SUBSCALE TEST D3912 MOD SN 006	B-35
9A	HYDROGEN EMBRITTLEMENT SUBSCALE TEST D3912 MOD SN 3 HT 88019	B-36
10A	HYDROGEN EMBRITTLEMENT SUBSCALE TEST D3912 MOD SN 3 HT 88019	B-37
11A	HYDROGEN EMBRITTLEMENT SUBSCALE TEST D3912 SN 3 HT 88019	B-38
12A	HYDROGEN EMBRITTLEMENT SUBSCALE TEST D3912 SN 3 HT 88019	B-39
13A	HYDROGEN EMBRITTLEMENT SUBSCALE TEST D3912 SN 3 HT 88019	B-40
14A	HYDROGEN EMBRITTLEMENT SUBSCALE TEST D3912 SN 3 HT 88019	B-41
15A	LINER INDUCED FAILURE TEST	B-50

TABLE

1A	SUBSCALE HYDROGEN EMBRITTLEMENT TEST DATA	B-14
----	---	------

1.0 Introduction

1.1 Purpose

The "catastrophic" failure mode testing program of the Kevlar Overwrap Study requires that the vessel liner fail in a brittle, unstable manner at a stress range of 35% to 50% of metal liner UTS, which is the liner operating pressure stress range for practical composite vessel designs. For controlled testing, it is desired that gas pressure cycling requirements be minimized in order to be at the desired stress when the vessel fails. The approach for achieving this is to intentionally charge a cryoformed Cres liner with hydrogen such that gas can be charged during a single cycle to the desired pressure and that this pressure cause rupture of the hydrogen embrittled structure. A second aspect of the test program is to establish the appropriate vessel signature which indicates onset of failure. This interim report describes the results of testing three (3) sub-scale all metal vessels and the readout obtained by acoustic emission equipment. This testing effort is part of contract Task II, Liner Failure Inducement Study (subscale validation tests).

A difficult aspect of the test program was the need to:

- a) Not embrittle the boss area so as to insure membrane failure.
- b) Balance time between post charging and test such that hydrogen does not leave the vessel during test set-up.

- c) Pick up acoustic emission signals with probes attached to the boss extensions only.

1.2 - Approach and Summary of Results

1.2.1 Tank Embrittlement

In order not to embrittle the boss area, Arde intentionally partially filled and rotated the tank on a continuous basis. It was, however, determined that metal membrane exposure to hydrogen gas was not sufficient to balance out the rate of gas escape from the unexposed area. The solution to the problem was to apply a common strippable coating to the desired area on the tank inside surface. All vessels were held 24 hours prior to pressure test.

1.2.2 Acoustic Emission Testing and Summary of Results

Utilizing Arde equipment, AET Model - 5000, hydrogen embrittled tanks were monitored to try and discern onset of failure. Initial difficulties were associated with efforts to establish correct gain settings and to find the best locations for "taping" off the equipment circuitry. Results to date indicate that meaningful signals can be generated from the acoustic emission equipment.

1.3 Summary of Conclusions to Date and Continuation of Testing

All tanks tested to date indicate achievement of rapid crack growth within the stress range of interest while Acoustic Emission equipment demonstrates an ability to discern the onset of failure, but not without problems.

With the exception of the pre-proposal test vessel, which had no 24 hour hold period after charging, all vessels were charged and pressurized twice before operating stress rupture occurred. It has become apparent that a more reliable approach to virgin vessel rupture can only occur by an over-kill set of parameters. This will result in shorter pressurization periods which AF/RPL must consider in their pneumatic system while assuring that pressurization rate will not result in vessel over heating. This could well require a heat exchanger. It is suggested that set-up vessels be used in the program for the pneumatic and other instrumentation shake downs.

Final resolution of the charging parameters will be achieved by additional sub-scale testing. The thrust of further testing will hinge on the following aspects:

1. more charging and less hold time with virgin (one pressurization) rupture as an objective.

2. further development of Acoustic Emission techniques to reliably detect sub-critical crack growth so that rupture prediction can be definitized.

A summary of test results follows in Table 1A.

2.0 Test Set-Up

2.1 Test Articles

Arde's standard material evaluation spheres P/N D3912 (Figure 1) were used for hydrogen induced failure demonstration. Existing vessels used to evaluate specific heats of material were electrolytically charged with hydrogen and hydrostatically pressurized to failure. Arde's pre-proposal test was heat #88470, annealed for this investigation, and tested as described in Appendix . Three (3) post award subscale vessels were fabricated from Heat #88019.

2.2 Test Equipment:

- 2.2.1 Flasks capable of mixing electrolyte, .1 molar solution of sulphuric acid. Add 10 ml. of conc. H_2SO_4 to make 1000 ml. solution.
- 2.2.2 Power Supply: Lambda LA-200
- 2.2.3 Lead Anode: 3 in. long x 3/8" diameter, approx. dimensions. It is important that anode current densities remain constant from test to test. Full scale vessels will require larger anodes.

- 2.2.4 Maskant: Adcoat AC-818-T
- 2.2.5 Acoustic Emission Monitor System: AET 5000
- 2.2.6 Appropriate pre-cautionary measures for hydrogen generation.
- 2.3 Baseline Parameters
- 2.3.1 Current densities: Anode (lead) density varied depending on amount of electrolyte, but, cathodic (vessel) density remained constant.
Two (2) cases of tests were performed. One in which a 3½" electrolyte level was used; another where 9-1/8" level was used. The vessels are eleven (11) inch diameter and the current was 0.6 amps at the 3½" level/1.6 amps at 9-1/8 level.
- 2.3.2 Electrolyte concentration: Same for all tests, 10 ml. of conc. H₂SO₄ to make 1000 ml. of solution.
- 3.0 Specific Tests and Results

After hydrogen charging, all vessels were subjected to burst testing as shown in Figure 2A. With the exception of the pre-proposal test article, all tests utilized Acoustic Emission monitoring techniques. Hydrogen charging fell into two basic categories as shown in Figure 3A. Discussion as to the reason for each mode is presented under the specifics below.

3.1 Heat #88470 S/N 008

Pre-proposal test article; results of which are contained in Appendix 2. Basically, current densities were very high. Vessel was charged in vertical mode and immediately hydrostatic burst tested after charging. The vessel burst 5 seconds after achieving 110 ksi or 46% of burst.

Acoustic Emission monitoring techniques were not used for this vessel. Post test examination revealed approximately 50% through-wall embrittlement. Vessel remained in one piece.

3.2 Heat #88019 S/N 004

This is the first subscale test of a series of three performed under contract. This test article took two (2) separate chargings and pressurizations to cause "operating pressure failure". The first charging was in the horizontal mode shown in Fig. 3A and Photo #1. An attempt was made to zero in on an appropriate charging time by manually rotating the vessel over a 28 hour period. The vessel was rotated three times (120° apart) for 8 hours, 16 hours, and finally 4 hours to provide over-lap chargings of 4, 8, 12, 16, 20, and 24 hours duration. The cathodic (vessel) current density was such that the 11" diameter vessel was filled with 3½" of electrolyte and charged with 0.4 amps. The vessel was then given

a 24 hour hold period before pressurization.

Pressurization occurred on December 5, 1984. The vessel was pressurized to a maximum pressure of 3000 psig or 60% of calculated burst. The test set-up is shown in Fig. 2A and Photo #2. The vessel did not rupture after approximately 50 minutes under pressurization.

Acoustic Emission monitoring was attempted with a single transducer mounted on the inlet pole. Gain settings were such that too high a sensitivity was achieved where false events due to background noise were a problem.

Since the vessel did not rupture, a second charging and test was initiated. The horizontal charging mode was used again, but, no rotation and current level increased to 0.6 amps for 48 hours. The 24 hour hold period was maintained and vessel pressurization/rupture occurred on December 10, 1984. The rupture pressure was 2240 psig which is approximately 45% of burst. The pressurization time to failure was approximately 2½ minutes. This is cumulative time from 0 to 2240 psig, including a 12 second hold at 2240 psig.

The single probe, high sensitivity, Acoustic Emission technique was used. Again, many noise level events were recorded so that in arriving at a reasonable data presentation, all events with "ring-down" counts less than

10 were discriminated. "Ring-down" count is a measurement of how many times the decaying sinusoid crosses the threshold voltage. Strong AE signals have many "ring-down" counts, whereas system noise will have few. See Fig. 4A for Acoustic signature.

3.3 -Heat #88019 S/N 006

Since the previous vessel indicated that a 24 hour hold period was feasible, this vessel's first charging was done in a configuration that would embrittle the entire vessel membrane less bosses. The vessel was rotated during charging. See Photo #4. The cathodic current density remained at 0.6 amps at the 3½" electrolyte level, but, the time was increased to 90 hours to adjust for approximately 3 times surface area. Normalized to the prior test, this represented 30 hours effective versus the 48 hours used in the successful test of S/N 004. The vessel was pressurized on 16 January 1985 to the pressure profile shown in Fig. 5A.

The set-up and Acoustic Mission sensor location is shown in Photo #5. The Acoustic Emission sensitivity level was decreased for this test to be above noise. The vessel did not rupture. There was no acoustic activity recorded.

A second charging was initiated where the vertical mode of charging was used. (Same position as pre-proposal article) In this case, the bottom of the vessel was protected from electrolyte/hydrogen via Adcoat Maskant AC 818-T. The vessel was filled to a 9-1/8" electrolyte

level and the cathodic current density remained the same, i.e., 0.6 amps: 3½" as 1.6 amps: 9-1/8".

Charging time 48 hours with 24 hour hold before rupture test.

Vessel pressurization/rupture occurred on 21 January 1985. Test set-up is shown in Photo #6. The ruptured vessel is shown in Photos #7 and #8. There is an extensive network of sub-critical crack growth at the vessel I.D. The vessel broke into three pieces even under hydrostatic pressure. The pressure profile is shown in Figure 6A; rupture occurred at 2760 psig or approximately 49% of burst after 85 seconds of pressurization.

Figures 7A and 8A show the acoustic signature of this test. The same decreased sensitivity level was used as above. A linear type two sensor test was set up. Figure 8A shows a distribution of acoustic activity, 0 represents port boss sensor and 98 represents the opposite dome. Significant acoustic activity initiated at 2000 psig or 30 seconds prior to rupture.

3.4 Heat #88019 S/N 003

This vessel was first charged to the 1.6 amp/9-1/8" electrolyte level in the vertical mode. Maskant of apex again used. 48 hour charging with 24 hour dwell before pressurization. This test was a duplicate of the prior test with S/N 006.

Pressurization occurred on 28 January 1985 to the profile shown in Figure 9A. The maximum pressure achieved was 2810 psig or 52 % of estimated burst for approximately 6 minutes. No failure; no Acoustic signals.

Acoustic Emission technique was a two sensor linear type test at low sensitivity. The same test as S/N 006 failure.

Post test examination via borescope and radiography revealed some sub-critical crack growth.

The vessel was then recharged in a similar manner as the first charging. Two acoustic emission techniques, high (Test #2) and low (Test #1) sensitivity were used during pressurization/rupture test. Sensor location is shown in Photo #9. The pressurization profile is shown in Figure 10A. Failure occurred after approximately 35 seconds from start of pressurization. Rupture occurred at 2260 psig or 42% of ultimate. See Photo #10 and Figure 10.

Figures 11A, 12A, 13A and 14A show the acoustic signatures and distribution of events by the two sensor linear location software. It is noted that this data discriminates ring-down counts less than 10.

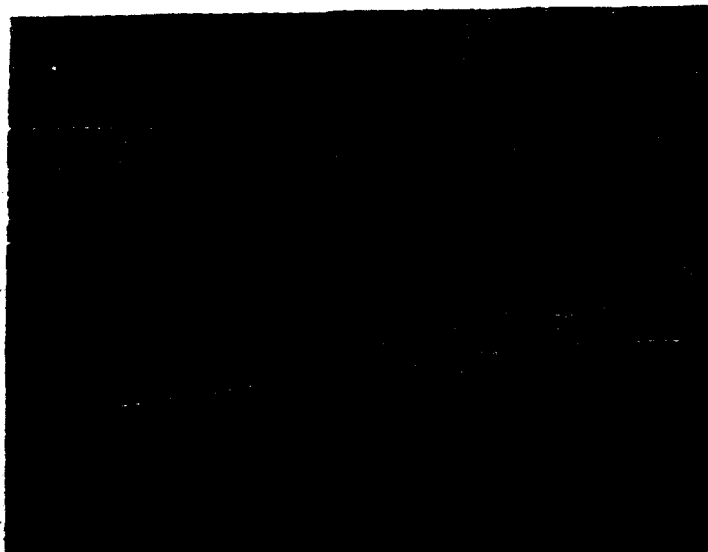


PHOTO #1
Heat #88019 S/N 004

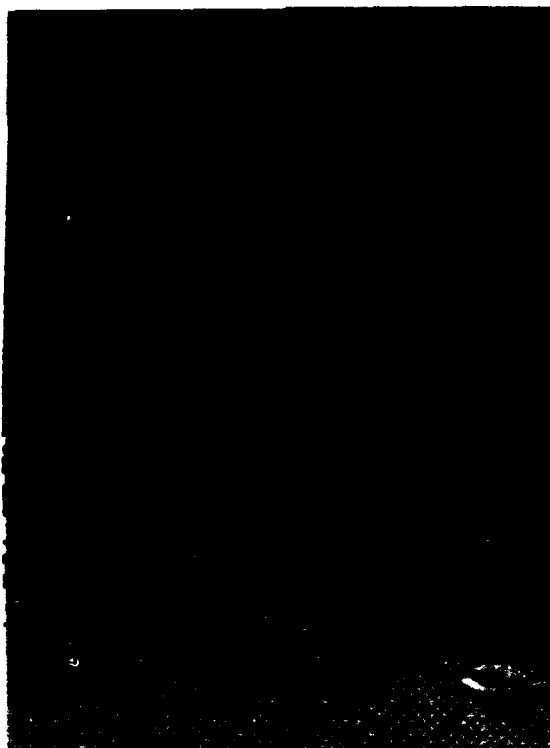


PHOTO #2
Heat #88019 S/N 004

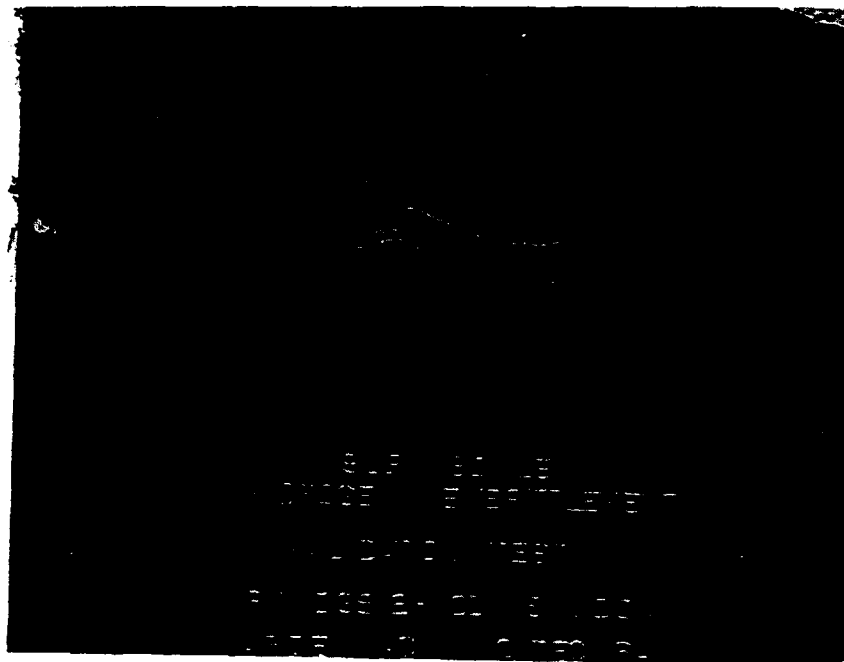


PHOTO #3
Heat #88019 S/N 004

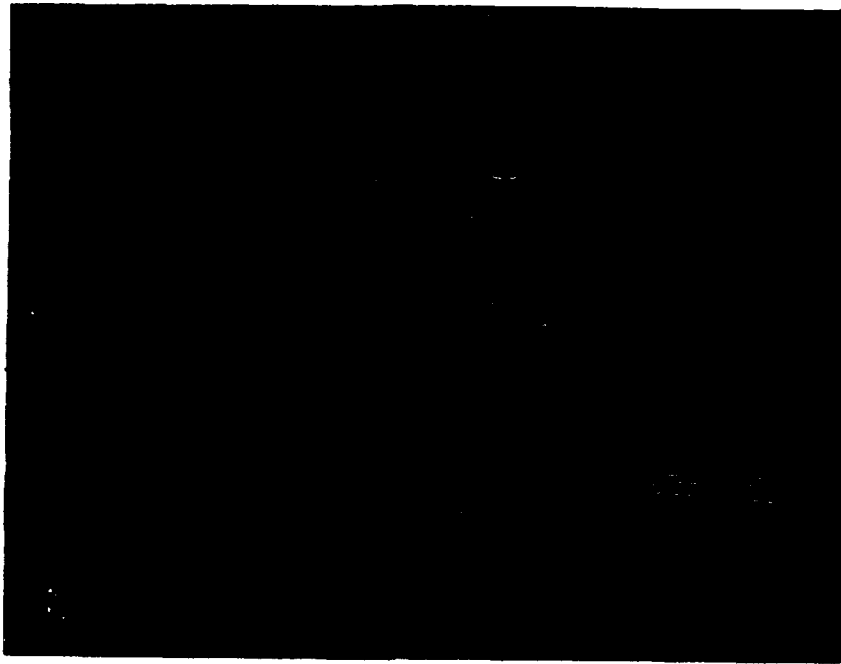


PHOTO #4
Heat #88019 S/N 006

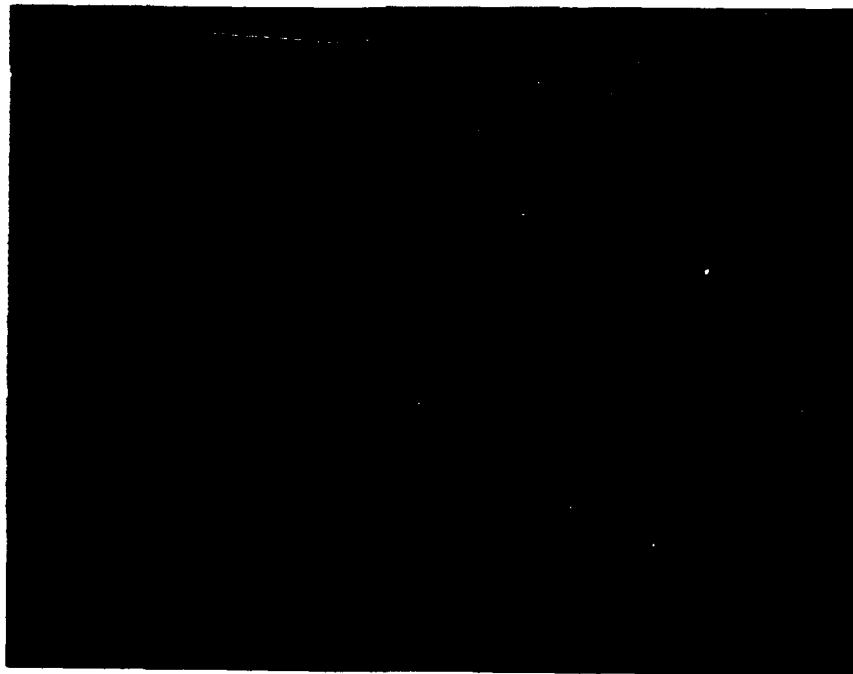


PHOTO #5
Heat #88019 S/N 006

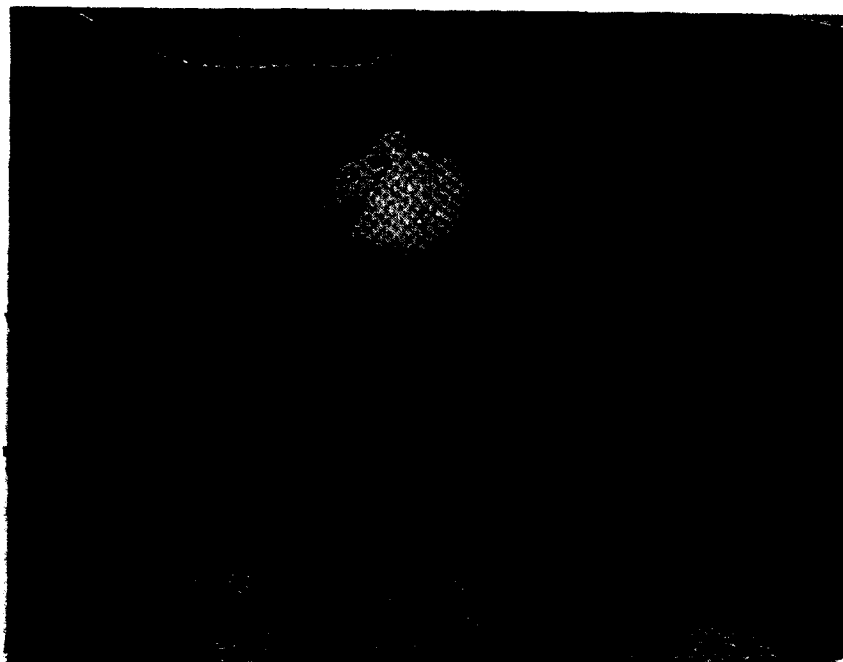


PHOTO #6
Heat #88019 S/N 006

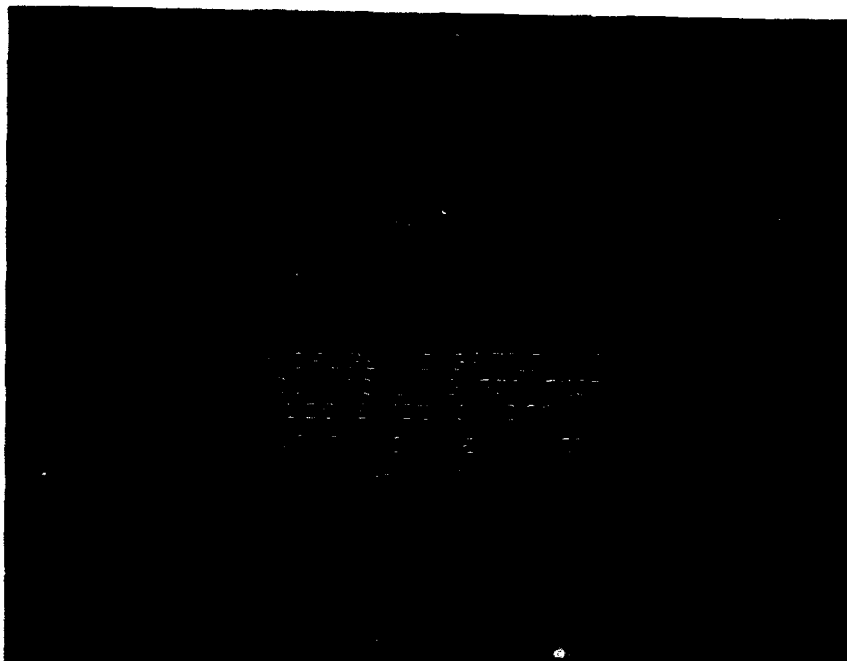


PHOTO #7
Heat #88019 S/N 006

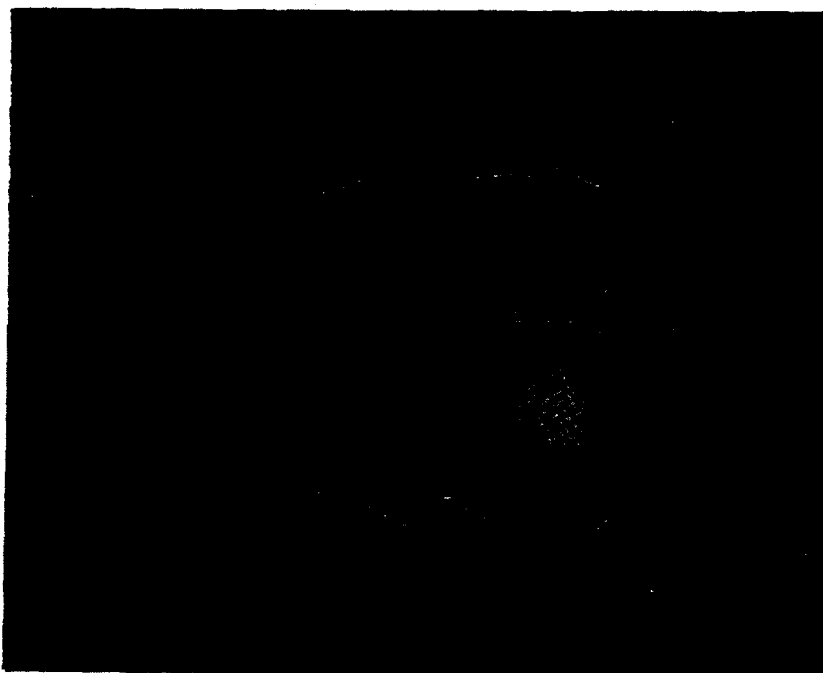


PHOTO #8
Heat #88019 S/N 006

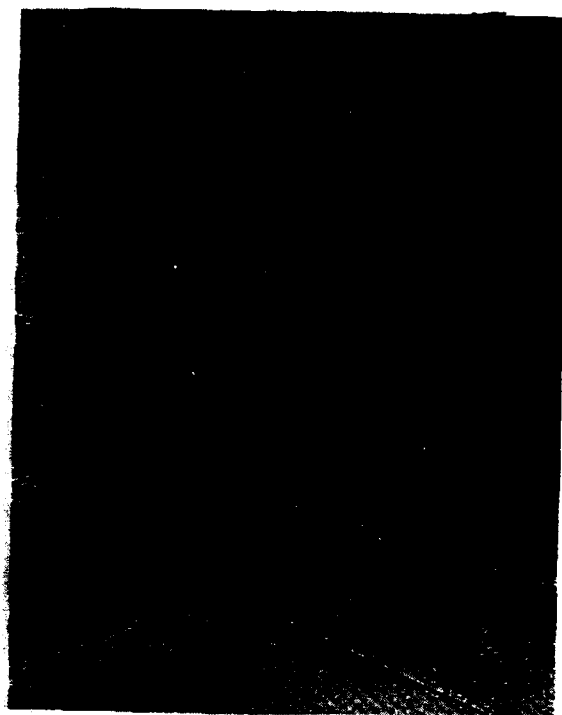


PHOTO #9
Heat #88019 S/N 003

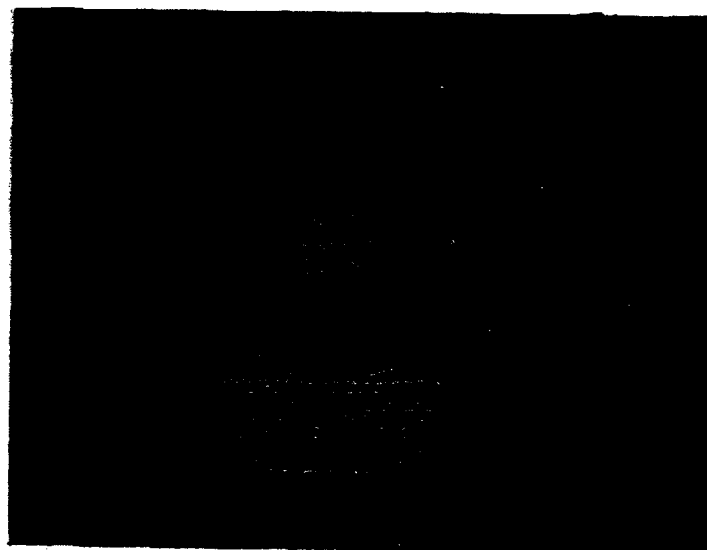
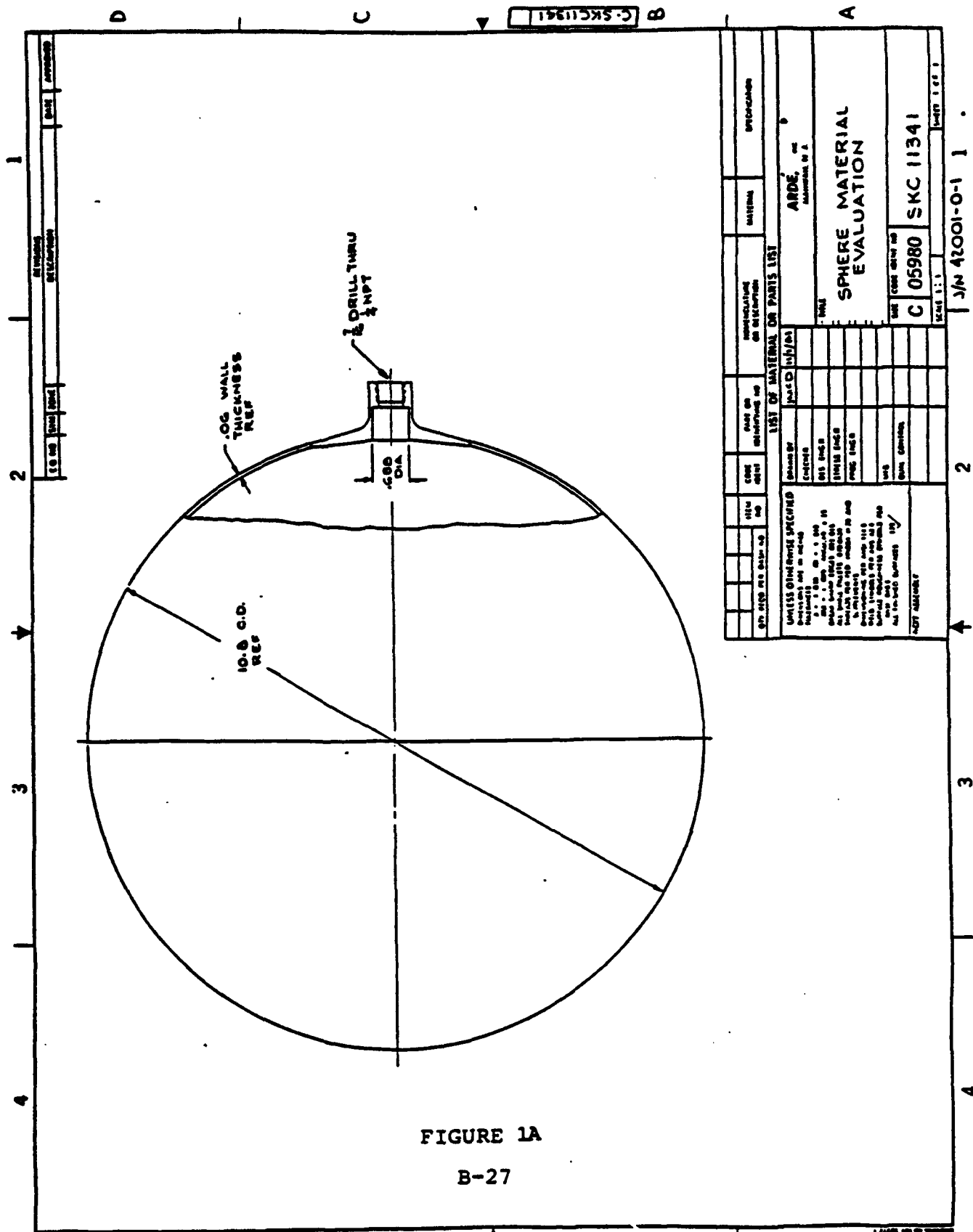
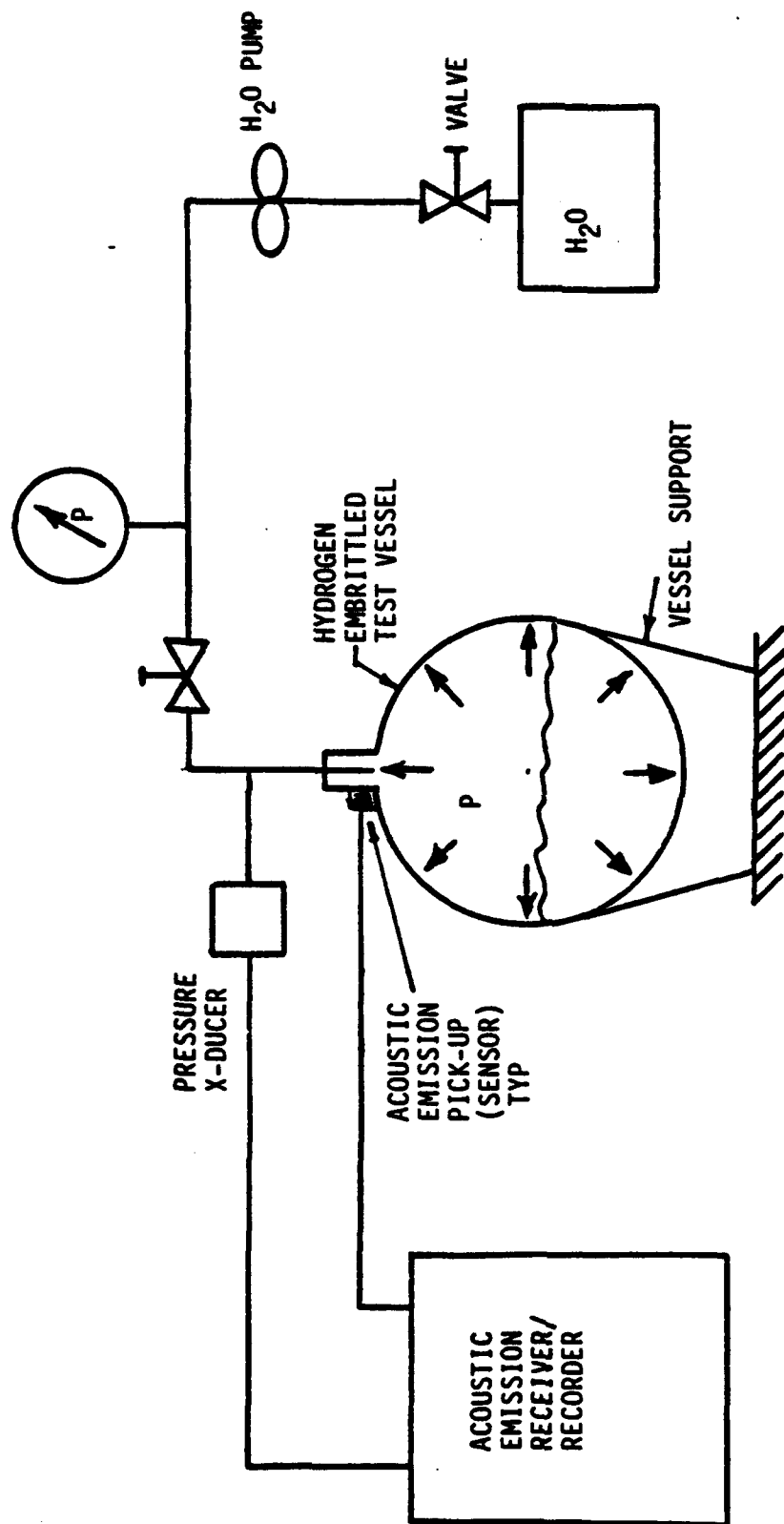


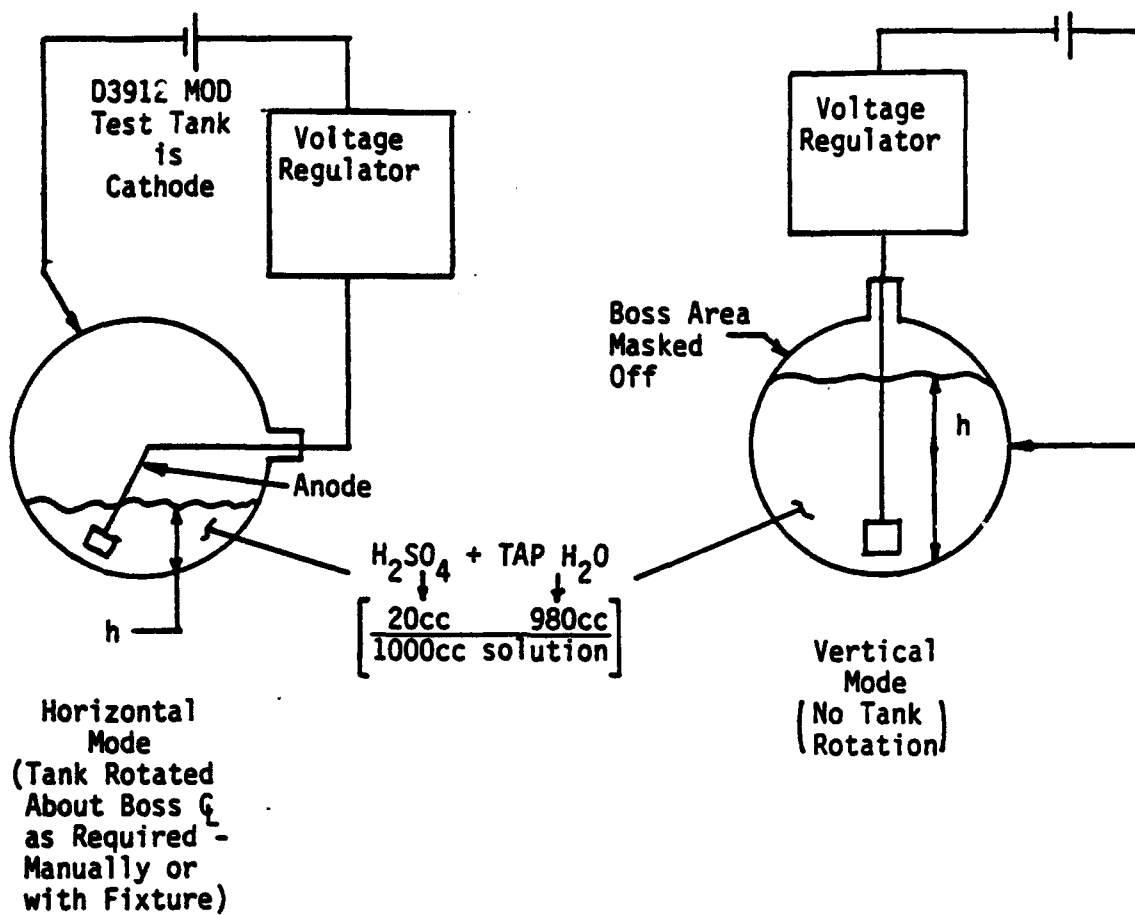
PHOTO #10
Heat #88019 S/N 003





SUB - SCALE
HYDROGEN EMBRITTLEMENT VESSEL
BURST TEST SCHEMATIC

FIGURE 2A



SUB SCALE
HYDROGEN EMBRITTLEMENT
TEST MODES

FIGURE 3A

● SUB-SCALE HYDROGEN EMBRITTLEMENT TEST
DATA ANALYSIS SUMMARY

(+)

- CAN HYDROGEN EMBRITTLE CRYOFORMED 301 CRES LINER TO CAUSE SUDDEN BRITTLE RUPTURE AT $P/P_{ult} \approx .4 \rightarrow .5$ (REQUIRED $P/P_{ult} = .35 \rightarrow .55$)
- CRACK GROWTH/RUPTURE READILY DETECTED BY ACOUSTIC EMISSION SIGNALS.
- CAN PREVENT HYDROGEN EMBRITTLEMENT OF LOCAL REGIONS (E.G. BOSSES) BY USE OF MASKING. TANK ROTATION NOT REQUIRED.

(-)

- NOT ENOUGH HYDROGEN IN VESSEL WALL TO CAUSE BRITTLE RUPTURE IN A TIMELY FASHION AT REASONABLE PRESSURE LEVELS AFTER FIRST CHARGING CYCLE AND 24 HR. HOLD (HYDROGEN LEAK RATE OVERPOWERED HYDROGEN CHARGED).
- JUST STABLE SUB-CRITICAL CRACKS FORMED.
- AFTER SECOND CHARGE CYCLE AND 24 HR. HOLD, BRITTLE RUPTURE MOST OFTEN OCCURRED IN A SHORT TIME ON THE WAY UP TO DESIRED TEST "BURST" PRESSURE.

PROJECTED CORRECTIVE ACTION

- ADDITIONAL TESTS REQUIRED TO REFINE BURST PRESSURE PREDICTION
 - OBJECTIVE: PREDICT BURST PRESSURE REASONABLY CLOSE AND REPEATABLY.
 - HAVE RELEASED THREE (3) MORE SUB-SCALE VESSELS FOR FABRICATION.
 - CHARGING PARAMETER OPTIONS
 - LONGER CHARGING TIMES (> 48 HOURS)
 - HIGHER CHARGING AMPS ($> .6$ AMPS)
 - LESS HOLD TIME (< 24 HOURS)

84 DEC 10 11:05:41 ELAPSED TIME = 00:03:40
HYDROGEN ENBRITTLEMENT TEST 2 PN 03912, SN4 1

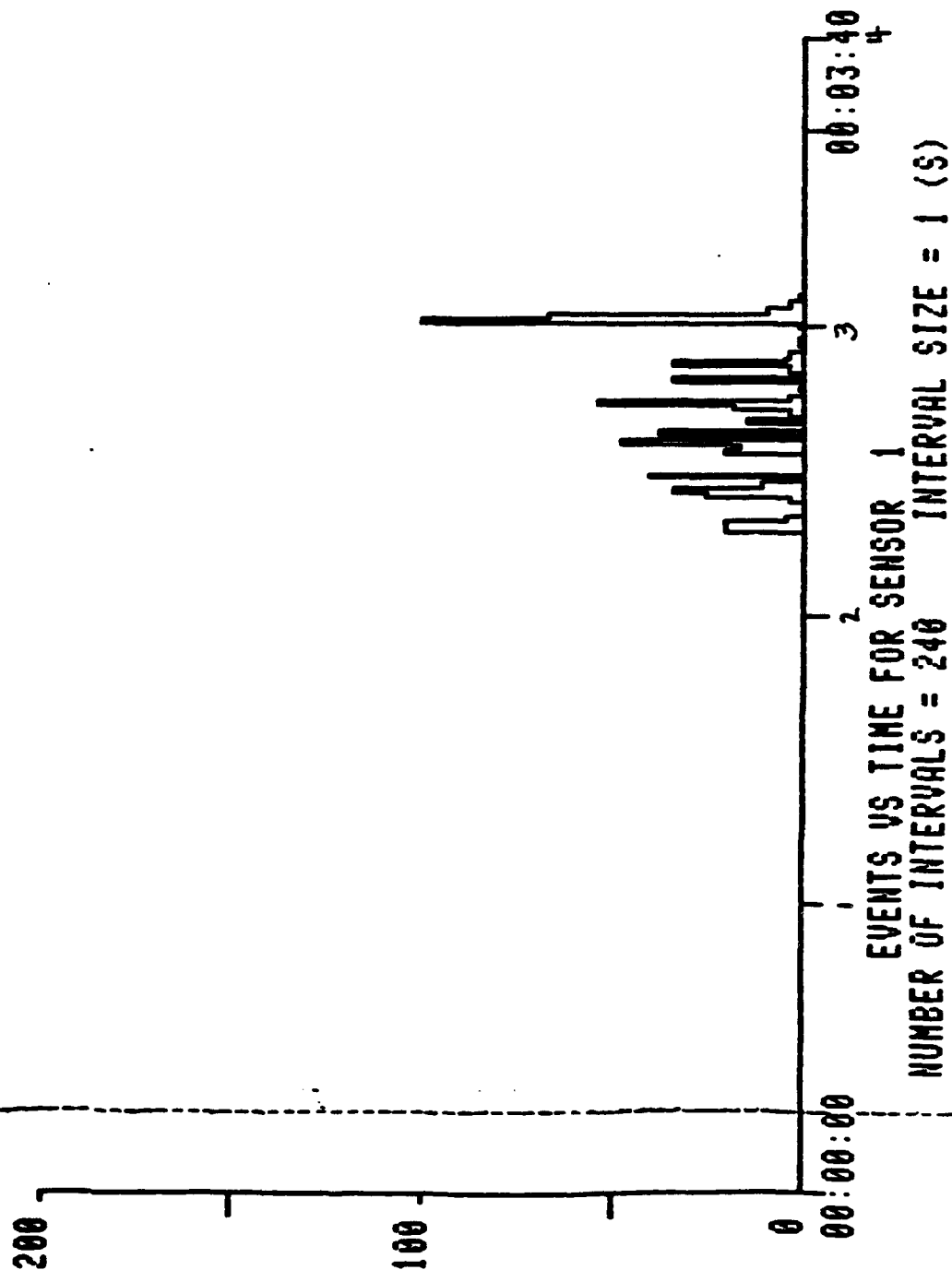


FIGURE 4A

85 JAN 16 02:12:32 ELAPSED TIME = 00:32:15
HYDROGEN ENBRITTLEMENT SUBSCALE TEST 03912 N00 SN 006

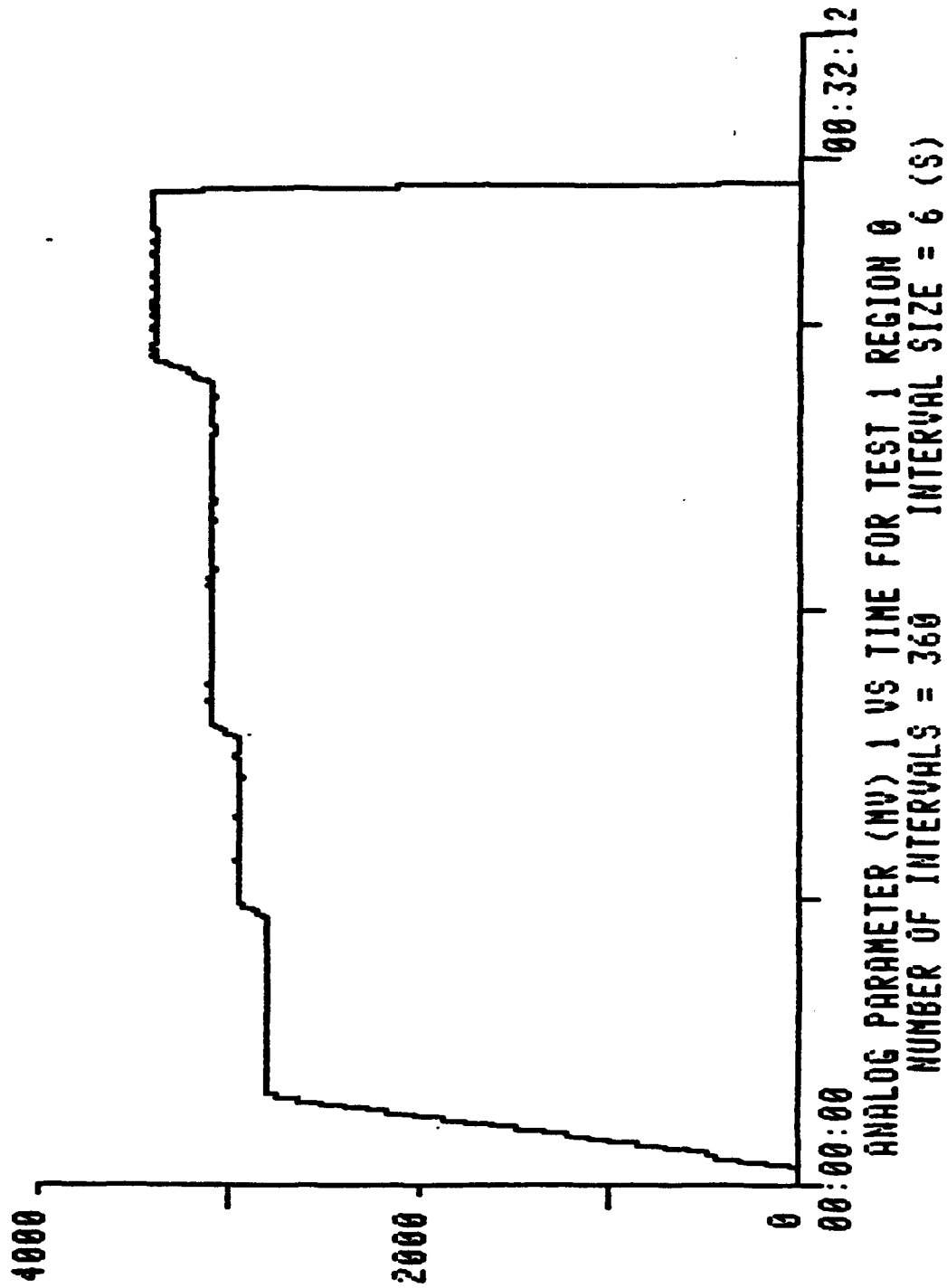


FIGURE 5A

85 JAN 21 03:50:04 ELAPSED TIME = 00:01:59
 HYDROGEN EMBRITTLEMENT SUBSCALE TEST 03912 MOD SN 006

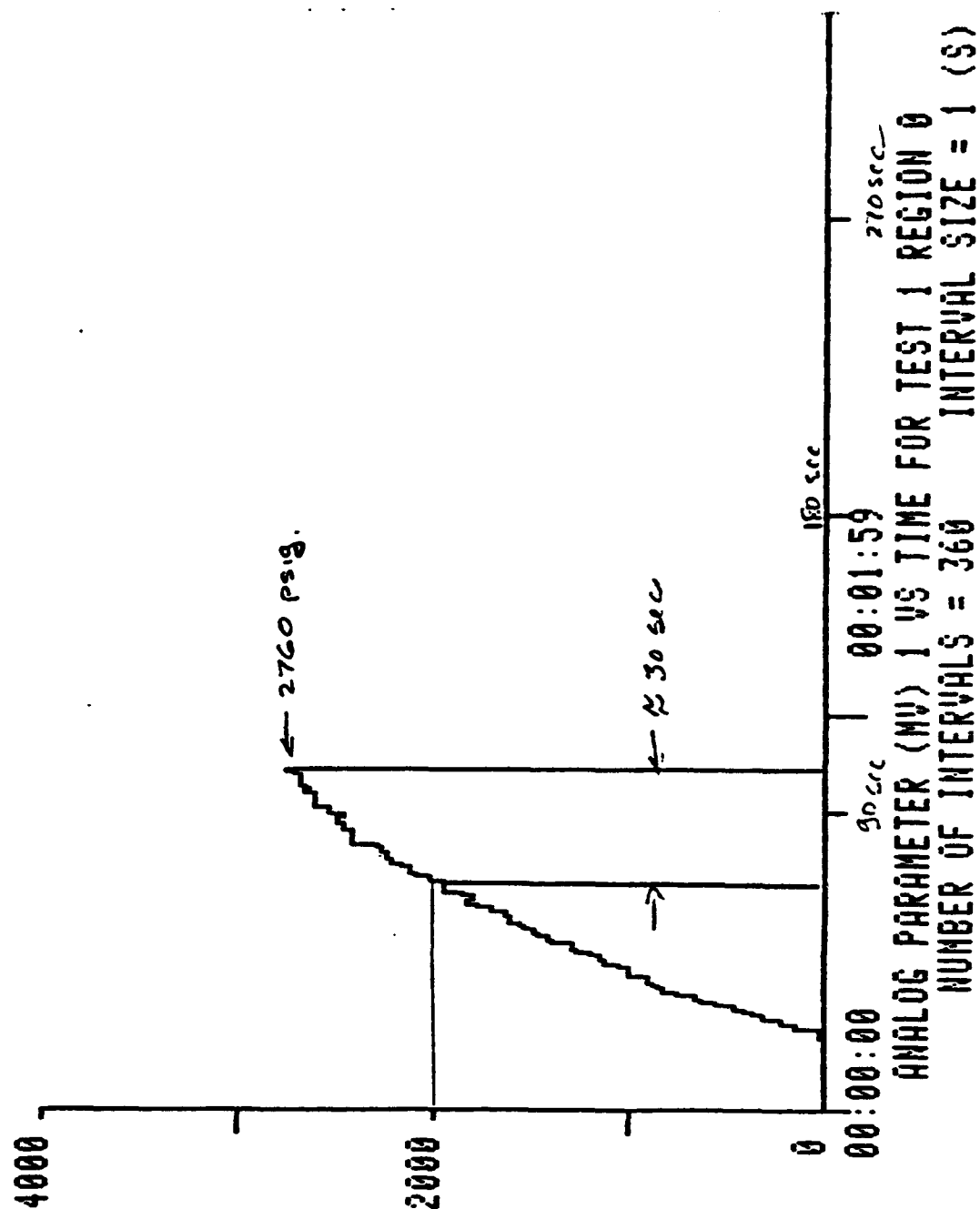


FIGURE 6A

85 JAN 21 03:44:53 ELAPSED TIME = 00:01:59
 HYDROGEN ENBRITTLEMENT SUBSCALE TEST D3912 MOD SN 006

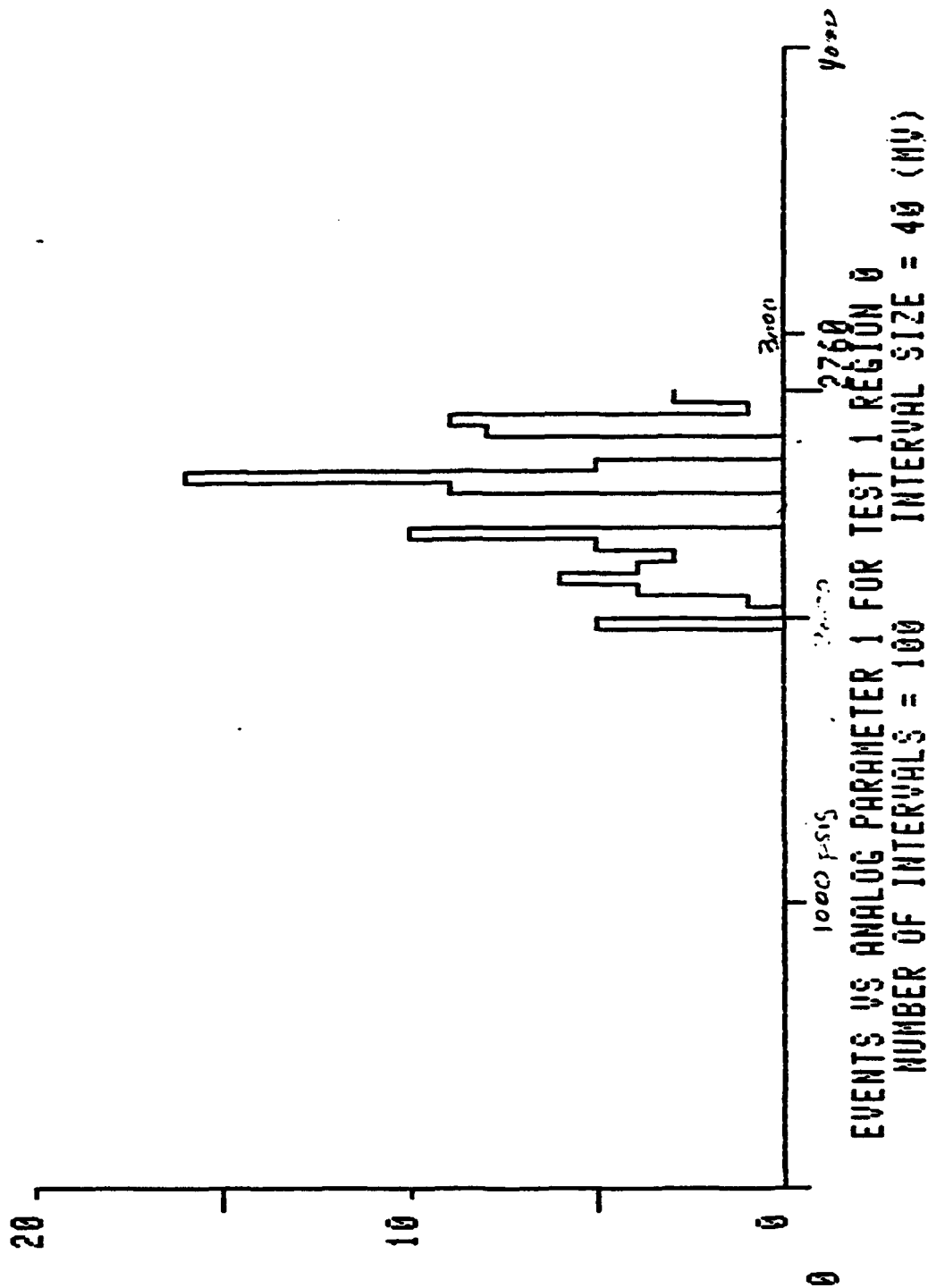


FIGURE 7A

85 JAN 21 04:19:23 ELAPSED TIME = 00:01:59
 HYDROGEN EMBRITTLEMENT SUBSCALE TEST D3912 MOD SN 006

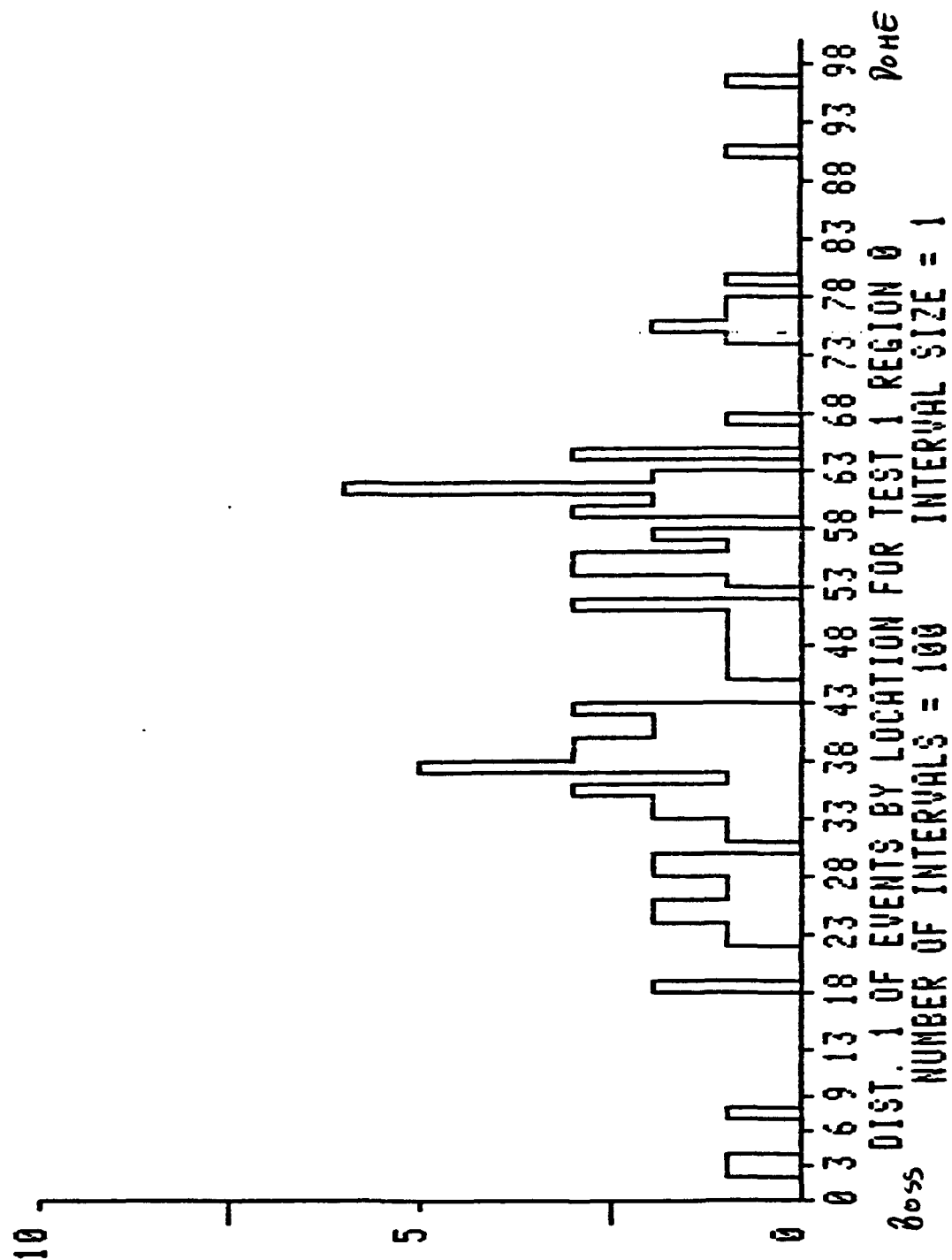


FIGURE 8A

85 JAN 28 10:16:29 ELAPSED TIME = 00:06:38
 HYDROGEN ENBRITTLEMENT SUBSCALE TEST 03912 MOD SN 3 HT 8801

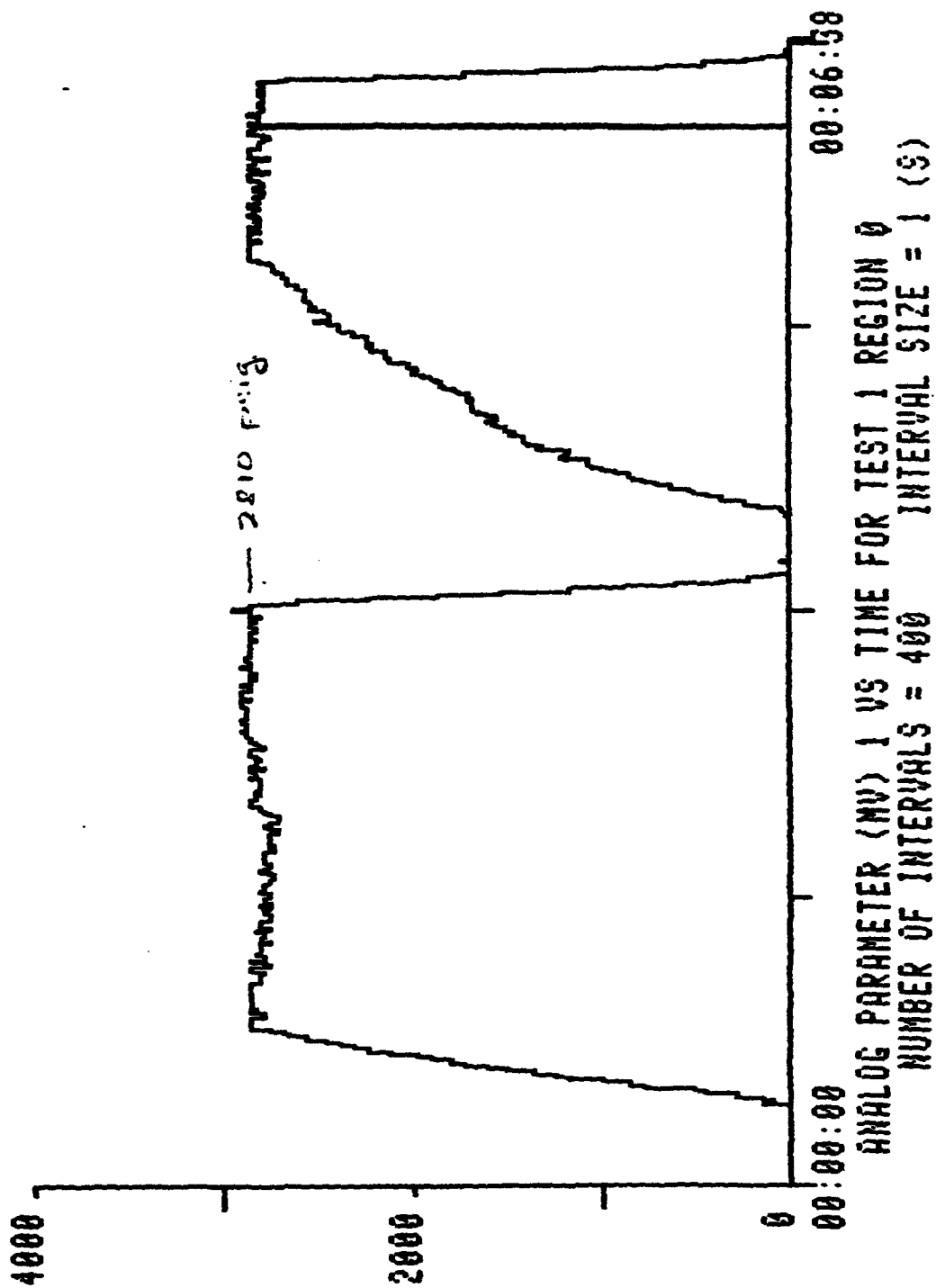


FIGURE 9A
 B-36

85 FEB 01 04:15:31 ELAPSED TIME = 00:01:27
 HYDROGEN EMBRITTLEMENT SUBSCALE TEST 03912 SN 3 HT 88019

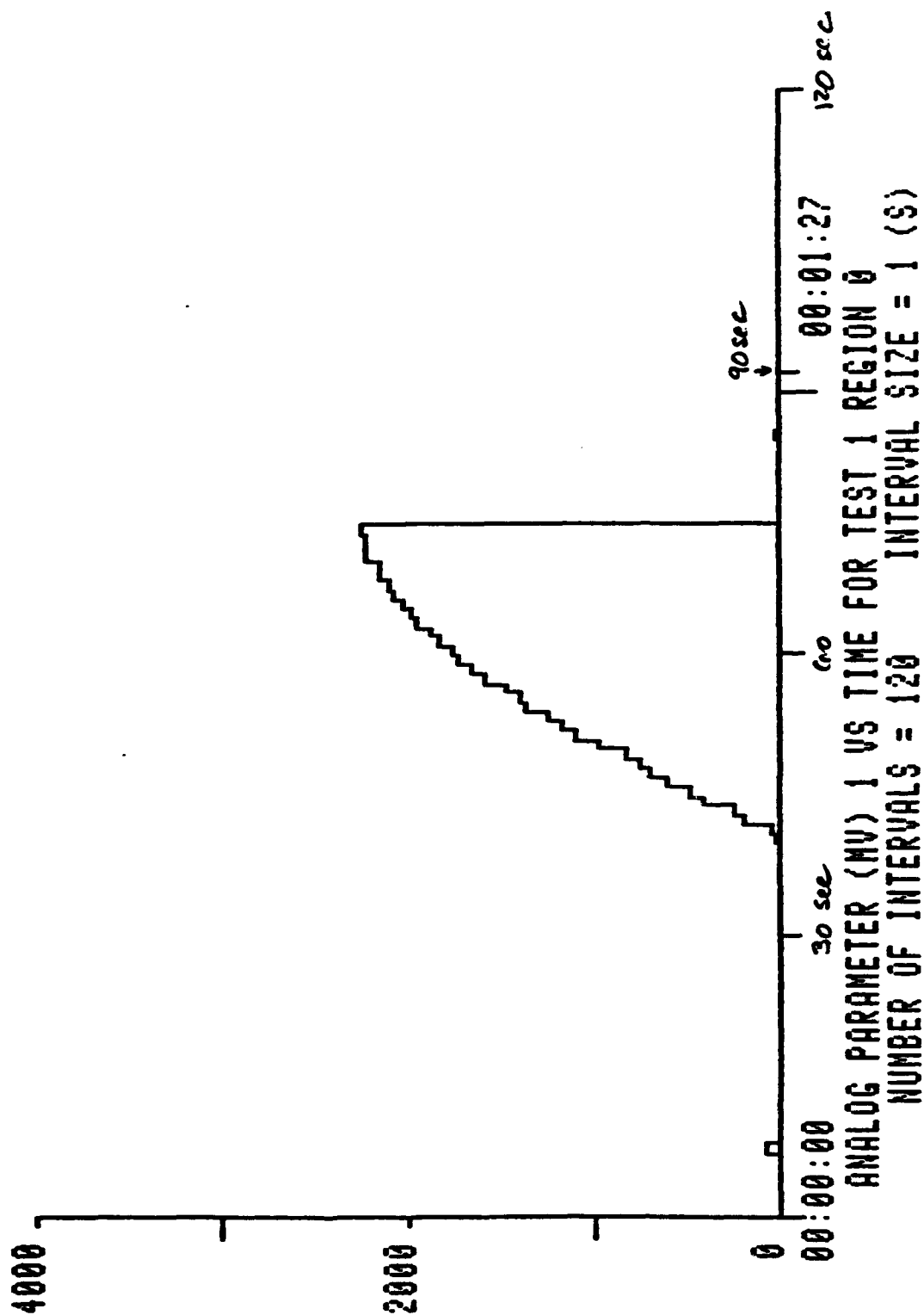


FIGURE 10A

35 FEB 01 04:04:24 ELAPSED TIME = 00:01:27
HYDROGEN ENBRITTTLEMENT SUBSCALE TEST 03912 SN 3 HT 88019

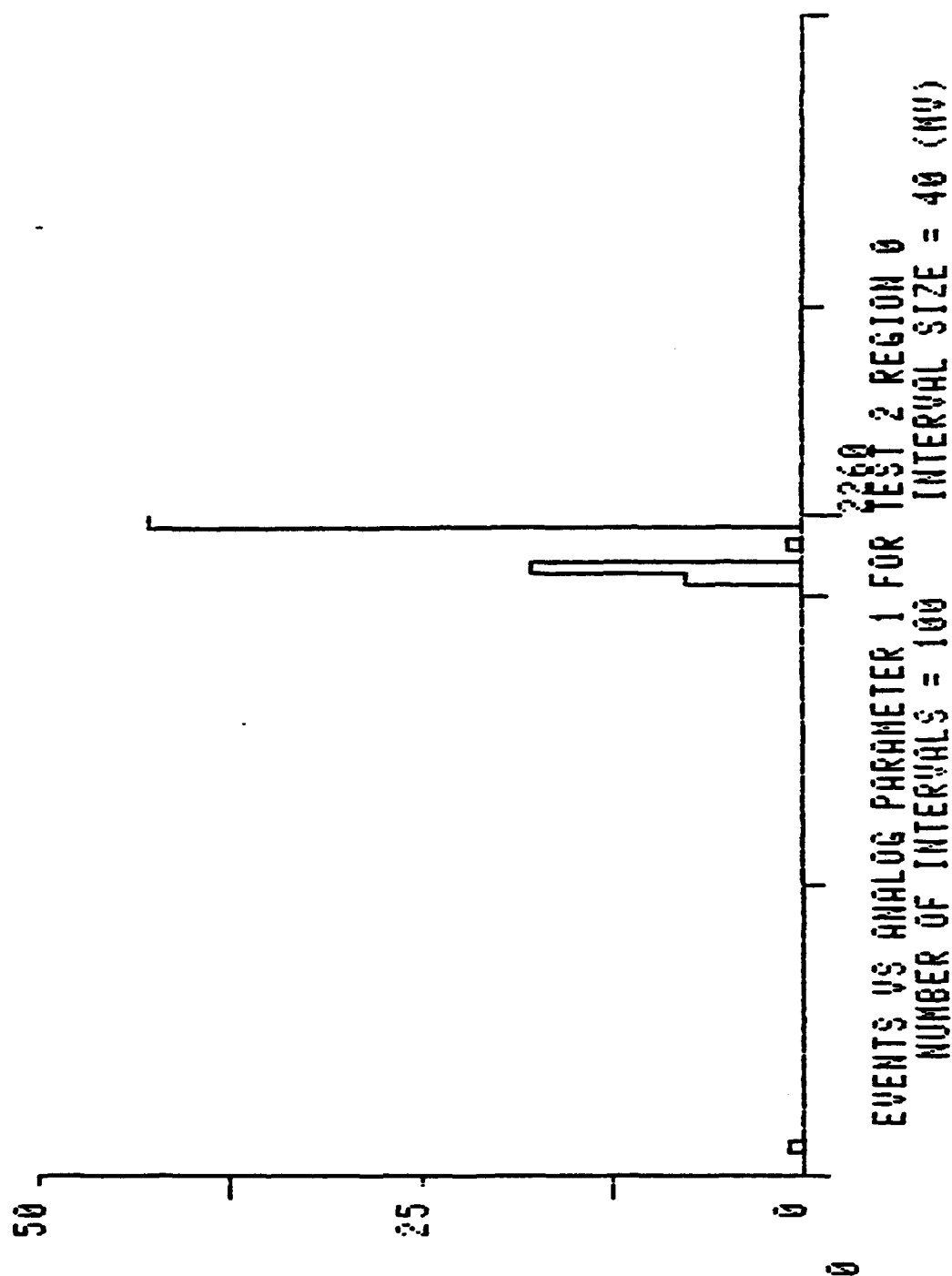


FIGURE 11A

85 FEB 01 04:01:48 ELAPSED TIME = 00:01:27
 HYDROGEN ENBRITTTLEMENT SUBSCALE TEST D3912 SN 3 HT 88019

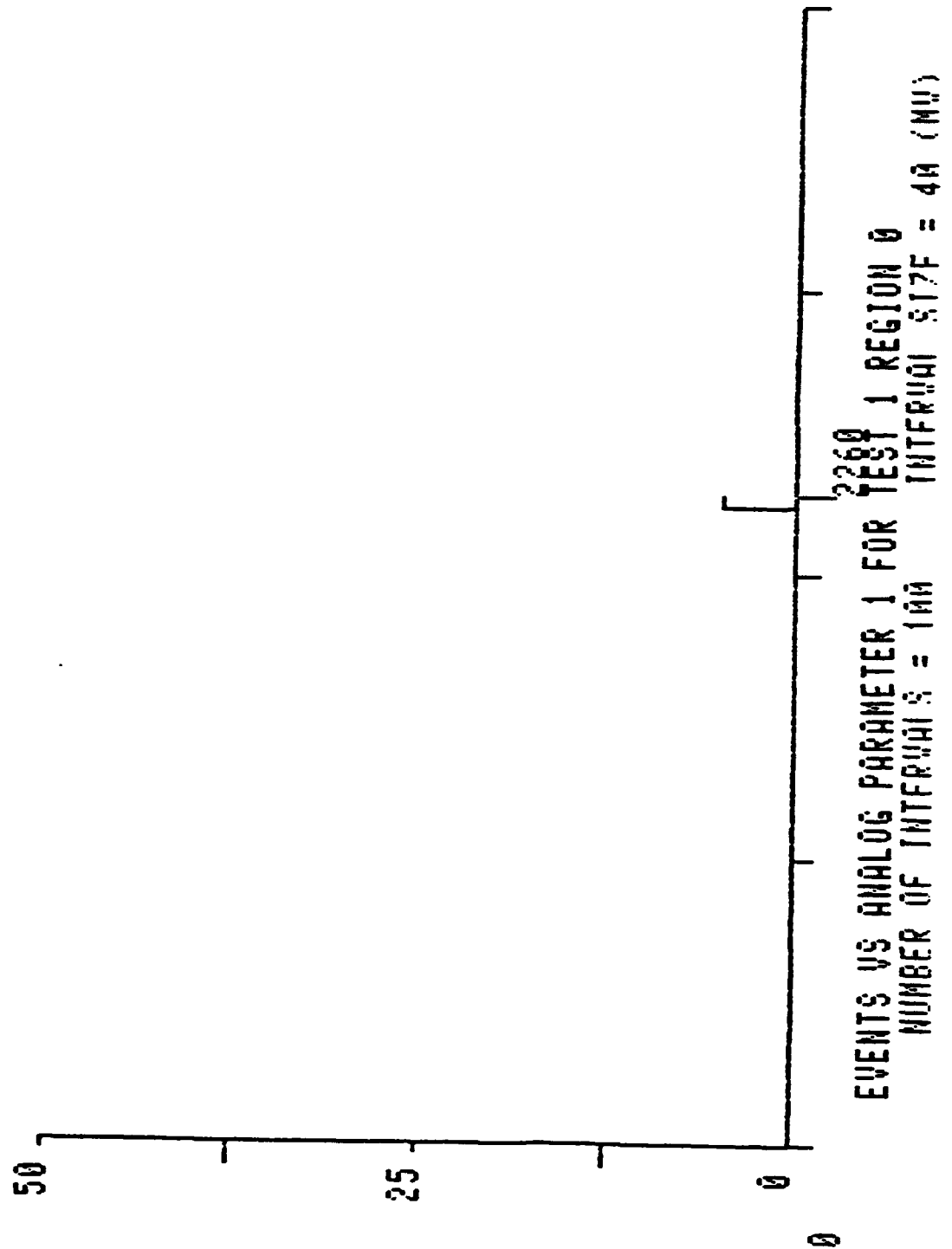


FIGURE 12A

85 FEB 01 04:36:50 ELAPSED TIME = 00:01:27
 HYDROGEN EMBRITTLEMENT SUBSCALE TEST 03912 SN 3 HT 88019

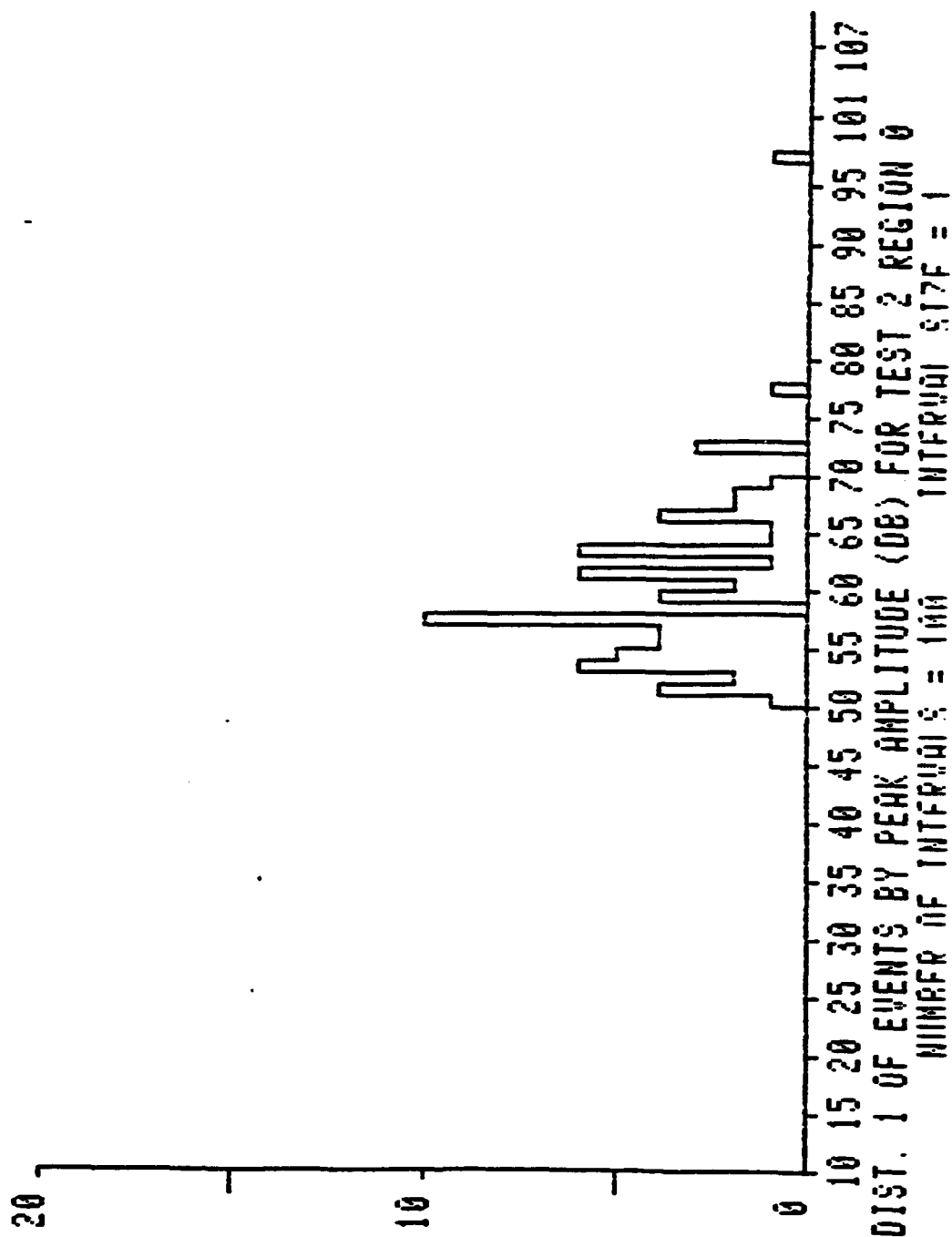


FIGURE 13A

85 FEB 01 04:34:17 ELAPSED TIME = 00:01:27
 HYDROGEN EMBRITTLEMENT SUBSCALE TEST 03912 SN 3 HT 88019

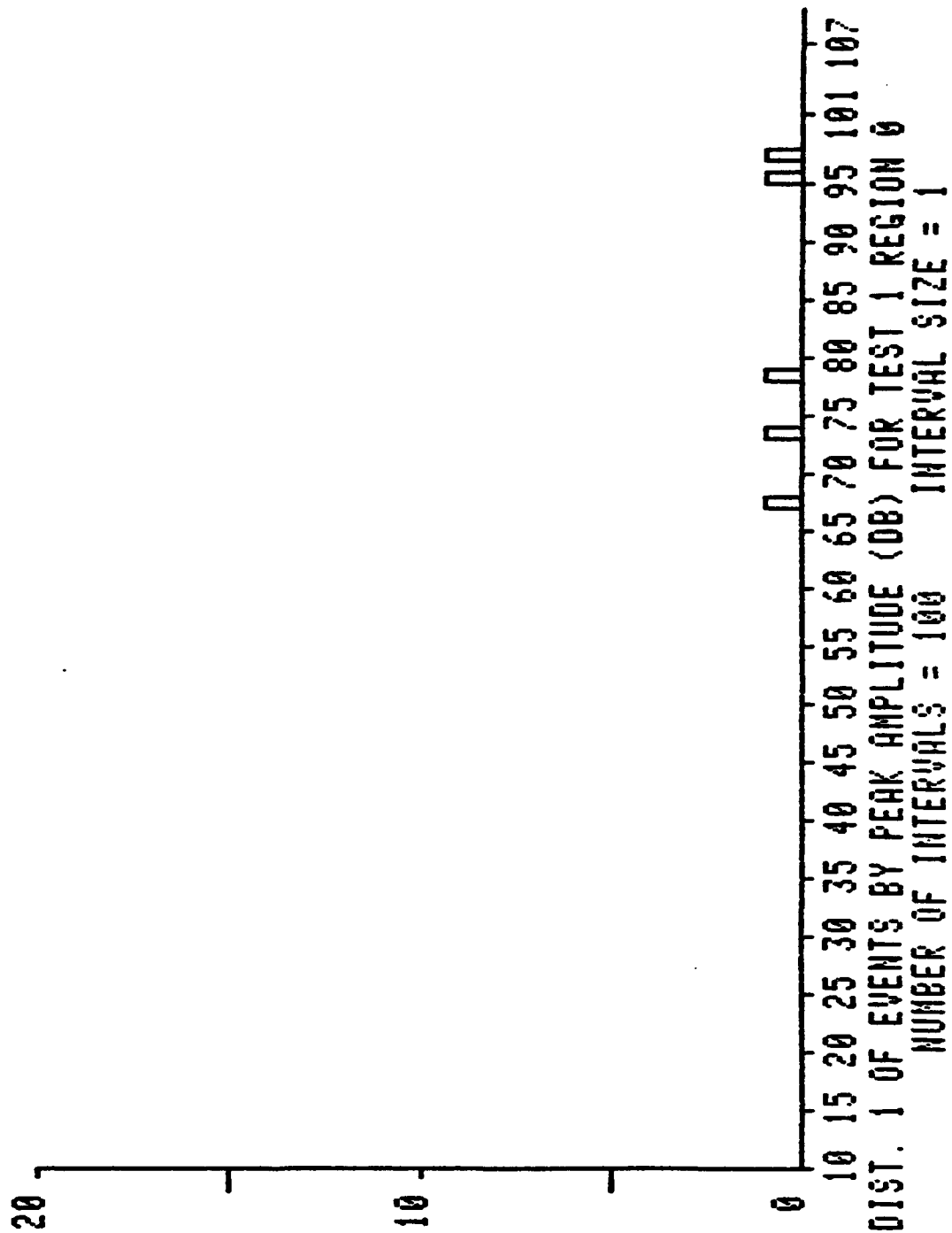


FIGURE 14A

APPENDIX B-1

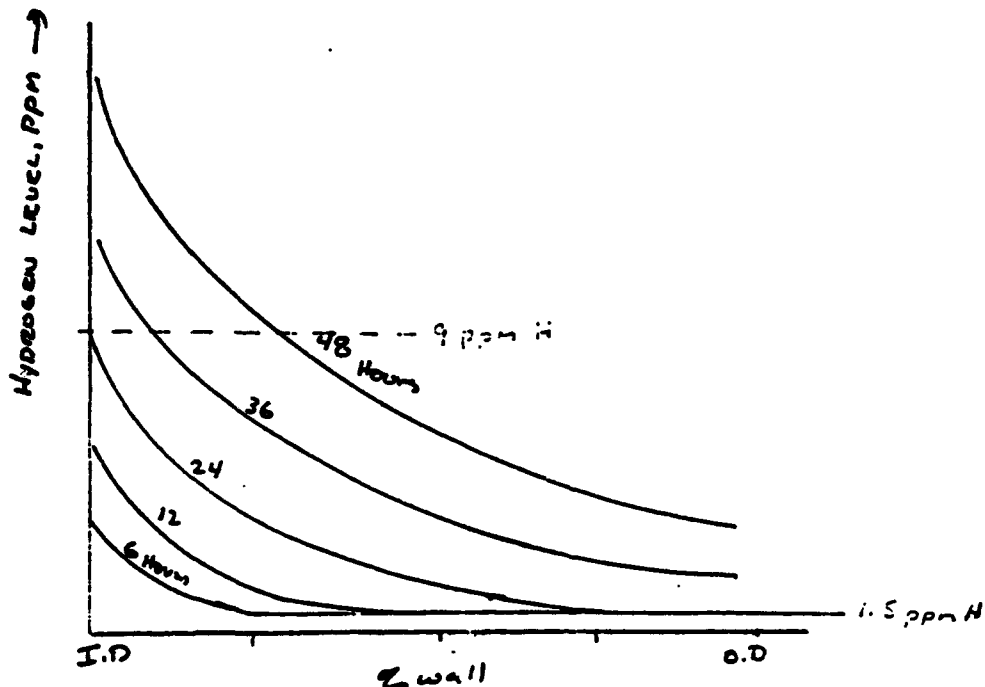
**Hydrogen Concentration in the Wall
of the Pressure Vessel During
Charging, Hold and Test**

TO: DAVE GLEICH & STEVE BERKO

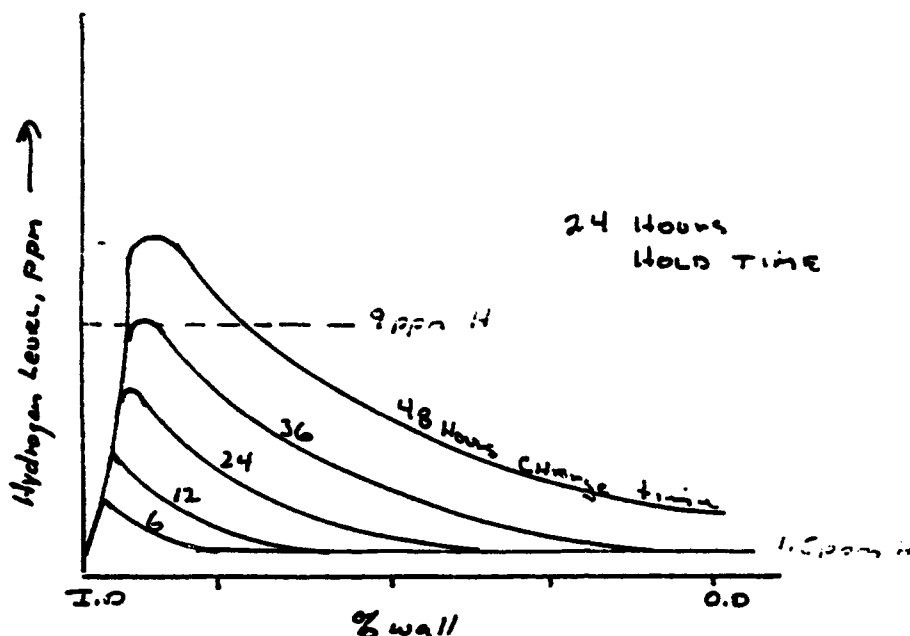
FROM: NORMAN FEIGE

SUBJECT: HYDROGEN CONCENTRATION IN THE WALL OF THE PRESSURE VESSEL DURING THE CHARGING, HOLD CYCLE AND TEST CYCLE.

The hydrogen diffusion reaction rates are defined by Fick's Law for the concentration of hydrogen through the steel wall of the vessel. The rate reaction is an exponential function. Equilibrium or constant hydrogen levels are never established because the hydrogen is charged from the inside diameter surface only and the gas readily leaks out of the vessel wall at the outside diameter surface. The net effect is a very high concentration of hydrogen at the inside surface which readily embrittles the metal and a outside surface which is highly ductile. Based on very limited experimental data combined with the rate reaction equations the best guess as to the shape and concentration of hydrogen in the vessel wall is as follows:



With the rather dilute acid used in the experiment the charging time must exceed 24 hours to obtain a sufficient hydrogen gradient to initiate the cracking of the vessel near the inside diameter surface. As the bottle is stored in air the hydrogen continues to diffuse out or leak out from both the inside and outside surfaces and no hydrogen effects are observed. Fick's Law also controls the loss of hydrogen with time. The predicted shape of the hydrogen concentration curve verses wall thickness and time is shown as follows:



As the bottle is pressurized the region of the bottle exceeding 9 ppm hydrogen will rupture almost immediately at approximately 35% of the predicted burst pressure. The flaws created are subcritical in size for bottle burst and the flaws blunt with the observed crazed pattern on the bottle inside diameter surface and the lateral contraction of the outside diameter of the surface of the shell wall. Of the bottles burst to date the region exceeding 9 ppm hydrogen represents between 40 to 60% of the vessel wall thickness.

Based upon very limited test data it appears that the sonic indications initially increase in intensity as the bottle breaks up into platelets supported by an outer ductile surface. As the strain is redistributed the sonic indications decrease with increasing pressure. The burst pressure of the bottle is now dependent upon the ductile ligaments between the platelets to support the load. If the critical hydrogen level has exceeded 50% of the wall the burst pressure will be reduced accordingly.

The rate controlling reaction to failure with a subcritical flaw now becomes dependent upon the rate of diffusion of the hydrogen in the lattice diffusing to the crack tip, and the stress intensity of the crack tip which lowers the critical hydrogen level to cause rupture. One has the following three options to reduce the rate of the reaction:

1. Lower the hold pressure to reduce the stress intensity at the crack tip to increase the time to failure.

2. Attempt to reduce the size of the high hydrogen region to reduce the initial flaw size.
3. Pressurize the bottle quickly to override hydrogen diffusion which extends the flaw length and reduces the section thickness supporting the load.

In the first case the frequency of cracking should slowly increase with time at the lower hold pressure as the increasing stress intensity at the crack tip lowers the required hydrogen level at the tip to extend the flaw. In the second case the initial number of sonic indications should be lower with the time to failure extended. The limiting factor is the control of the amount of hydrogen charged. If the hydrogen level is below 5 ppm, no initial flaw is created at the inside diameter surface. In the third case the ability to reach the desired burst pressure of 50% of design burst may not be achieved.

It would appear that through wall tank embrittlement can only be obtained by simultaneously charging hydrogen on both the inside diameter and outside diameter surfaces of the vessel. The time to failure will be abrupt at 35% of the design burst pressure if the hydrogen level exceeds 9 ppm at the surfaces. The experiment in a practical sense is difficult with a fiber wound bottle.

Increasing the hold time after charging does not establish an equilibrium hydrogen level throughout the vessel wall. Plating the vessel with copper, aluminum or silver to prevent hydrogen adsorption has been reported successful. However, the technique does not work in the reverse as the hydrogen either diffuses through the coating or comes out at defects forming gas blisters under the plate. Therefore, plating the outside diameter surface of the vessel to prevent the loss of hydrogen does not appear feasible.

If bottle fragmentation is desired in the bottle burst experiment the most pragmatic approach is to craze the inside diameter wall surface with brittle hydrogen cracks and obtain burst between 35% to 50% of predicted burst by rapid pressurization.

Of the options available the most reliable appears to be the rapid pressurization of the vessel above 35% of the design burst pressure of the vessel or just after the first sonic indication is recorded. Lowering the hold pressure to increase the time to failure has no technical advantages other than guaranteeing a lower gas temperature in the bottle at burst. Lowering the hydrogen level runs the risk that no failure occurs, requiring recharging with hydrogen.

APPENDIX B-2

**PRE-PROPOSAL TEST
OF
HYDROGEN ENDUCED FAILURE
ARDE AMR #279**

AMR #279

HYDROGEN EMBRITTLEMENT TEST
OF
CRYOFORMED VESSEL

Prepared by:

AKV 7/30/84

1.0 SCOPE

To demonstrate the effect of hydrogen contamination to cryoformed vessel.

2.0 DISCUSSION

A cryoformed, unaged spherical vessel per P/N 3912, S/N 008 of Heat No. 88470 was charged with hydrogen from its internal surface per procedure defined in Appendix 3. This vessel was leftover from the material evaluation where it was cryostrained at 8.36% and hydrotested at room temperature to a maximum yielding pressure of 7160 psi and vented when it dropped to 7060 psi. The vessel did not break and its computed burst strength was 238 ksi. See Appendix 4, Heat 88470 Material Evaluation Test Report.

Hydrogen was then charged to the vessel as outlined in Appendix 3 and hydrotested at 3300 psi to simulate the working pressure stress of 110 ksi when used as a liner in Prestress Composite Assembly. The vessel burst in a brittle manner after holding for about five (5) seconds. The brittle fracture surface was clearly evident and it extended about 50% of the wall thickness around the electrolyte/air interface. The vessel did not break into pieces (See Figure 15A) as compared to the normal material evaluation failure where it usually breaks into 2 or 3 pieces. The fracture line followed the hydrogen

penetration at the electrolyte/air interface with secondary fracture beyond this hydrogen attack. There was no indication of stress corrosion or prior damage of the vessel wall prior to brittle fracture. The burst at 3300 psi was about 47% of the estimated strength indicating a 53% deterioration of strength which coincided with the degree of hydrogen attack through the wall.

3.0 CONCLUSION

Hydrogen contamination of the cryoformed vessel promotes a brittle manner of failure. The procedure of hydrogen introduction to the vessel is defined in Appendix A.

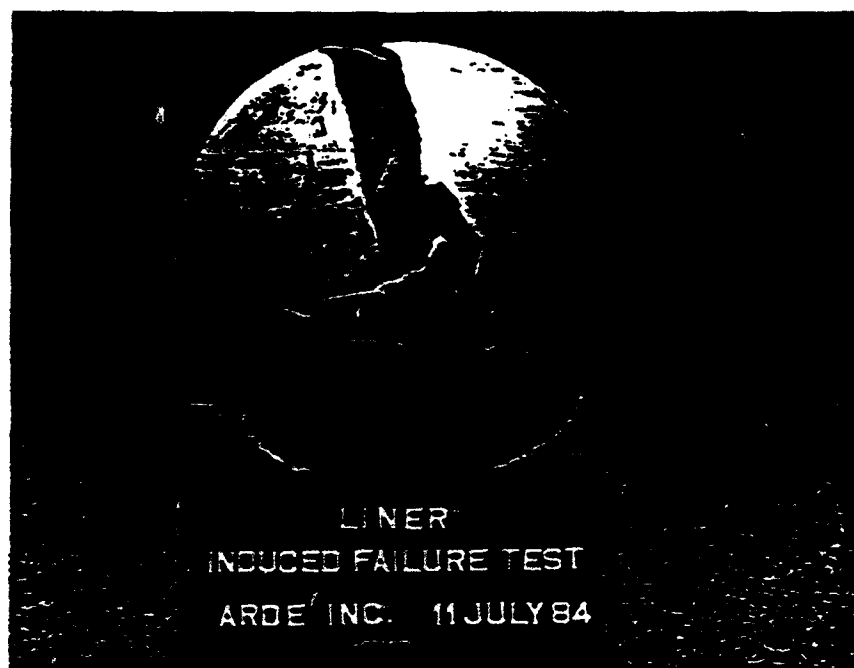


FIGURE 15A

APPENDIX B-3

HYDROGEN EMBRITTLEMENT PROCEDURE

HOFFMANN & FEIGE, INC.
MATERIALS AND METALLURGICAL ENGINEERING
QUALITY ASSURANCE
223 KATONAH AVENUE, KATONAH, NEW YORK 10536

RICHARD A. HOFFMANN
NORMAN G. FEIGE

TELEPHONE
(914) 232-5733
(914) 232-7773

July 13, 1984
435-LTR-25

Mr. Tony Orsini
Arde, Inc.
19 Industrial Avenue
Mahwah, New Jersey 07430

RE: HYDROGEN EMBRITTLEMENT OF SMALL TANK

Dear Tony:

To document the experimental procedures, the following conditions were established:

1. ELECTROLYTE

The established standards are sufficient sulfuric acid must be added to obtain electrical conductivity. The concentration must also be sufficiently diluted so that one's finger may be dunked in the solution without an acid burn. Dilute sulfuric acid, the initial concentration was 20 cc. concentrated sulfuric acid in 1000 cc. water. The concentration after the initial charge was highly variable depending upon dilution and concentration of electrolyte during operation.

2. POWER SOURCE

Inexpensive battery charger, 4 amp. max. capacity. The vessel was the cathode (black wire), and the anode was lead and connected to the red wire. Place the anode 2" from the bottom surface and immerse the anode approximately 2" in the initial electrolyte.

3. CURRENT DENSITY AND TIME OF CHARGE

The cathodic current density for the first 24 hrs. was 8 milliamps/in.sq. The second half of the charge cycle

for 29 hrs. was at 16 milliamps/in.sq. The anodic current density for the first 24 hrs. was 1/2-amp/sq.in. and the balance of the 29 hrs. varied from 1 amp/in.sq. to 1.2 amps/in.sq. as the anode slowly dissolved. The anode was being operated somewhat beyond its maximum current density. The usual accepted figure would be less than 1 amp/in.sq.

4. MODE OF BOTTLE FAILURE WAS BY HYDROGEN EMBRITTLEMENT

Brittle fracture extended approximately 50% of the wall thickness for an extended length at the electrolyte/air interface. There was no indication of stress corrosion or prior perforation of the vessel wall prior to brittle fracture. Analysis of the brittle fracture length indicates that the time and current density of charging was way in excess of that required and will result in short term fracture at less than 50% of the designed burst strength of the vessel.

Yours truly,

HOFFMANN & FEIGE, INC.



Norman G. Feige

NGF:ird

0.98075

A BROKE TO THE DONG

1 2 3 4 5 6 7 8 9 10 11 12 13 14 15 16 17 18 19 20 21 22 23 24 25 26 27 28 29 30 31 32 33 34 35 36 37 38 39 40 41 42 43 44 45 46 47 48 49 50 51 52 53 54 55 56 57 58 59 60 61 62 63 64 65 66 67 68 69 70 71 72 73 74 75 76 77 78 79 80 81 82 83 84 85 86 87 88 89 90 91 92 93 94 95 96 97 98 99 100

HYPHENATION SYSTEM FOR TEST
INTEGRITY & ACCESS
CIRCUIT AND/OR PORTS
A CIRCULAR T.T. 1.5

APPENDIX 4

MATERIAL EVALUATION OF HEAT 88470

MATERIAL EVALUATION TEST REPORT

Heat No. 88470

Date 2/10/84

Specimen: Sphere

Tested by: ML

* *
Aged/Unaged

(E_{avg}) (P_{avg}) (E_{pass})

S/N	Pcryo (psi)	D ₀ (in.)	t ₀ (in.)	S ₂ (ksi)	E _{np} (%)	D _F (in.)	t _f (in.)	P _y (psi)	P _B (psi)	σ _y (ksi)	σ _B (ksi)	P _B /P _C	
008**	8450	10.19	(.0125)	230	(7.57) 8.36	(.0533) .0557	(.08125) .0836	27060	7160	(2337) 235	(237.1) 238.3		Not Backed But Yielded F = 39.2 X 10 ⁶
009*	8300	10.19	(.01205)	220	(7.33) 7.72	(.0515) .0531	(.08205) .0824	8000	8060	(262) 261	(264) 263		Not Backed But Yielded F = 39.2 X 10 ⁶
010*	8650	10.19	(.01202)	230	(7.80) 8.59	(.0555) .0576	(.08075) .08082	8000	8030	(266.6) 265	(267.6) 266		Not Backed But Yielded F = 39.8 X 10 ⁶
011	9100	10.19	(.0137)	244	11%	(.0498115)		- Broken AT					
012**	7900	10.19	(.01195)	210	(6.74) 7.29	(.0166) .01823	(.08276) .0815		6870	(218.2) 221	(222.1) 224.6		Backed But Yielded F = 36.3 X 10 ⁶
013*	8100	10.19	(.0135)	215	(6.96) 7.41	(.0182) .01846	(.0826) .08288	7900	8050	(256) 254	(261) 259		Not Backed But Yielded F = 36.7 X 10 ⁶
014**	7150	10.19	(.01075)	170	(6.06) 6.03	(.0180) .01648	(.08175) .08406	6210	6740	(203) 195	(219) 210		Backed But Yielded F = 35.6 X 10 ⁶

** UNAGED SPHERE WERE TESTED 7 DAYS AFTER CAST

APPENDIX C - leak-Before-Burst Data and R-Curve Tests for Cryoformed
301 CRES

ANDE Interim Report EG 42001-14, which details the leak-before-burst (LEB) vessel experiments and the uniaxial R-Curve tests of cryoformed 301 CRES, is contained in this section. This report includes Appendices C-I and C-II described on page C-3, herein.

EG 42001-14
Date of Original
Issue: 9/19/86

INTERIM REPORT
R-CURVE TESTING AND
LEAK-BEFORE-BURST DATA
FOR CRYOFORMED 301 CRES

Submitted to:

Patrick Air Force Base, FLA
Contract No. FO 8606-84-C-0029

Prepared by:


D. Gleich
Principal Investigator

Approved by:


Program Management

Interim Report of CCN P00002 Effort Under Contract FO8606-84-C-0029

ARDE, INC.
Norwood, N. J.

TABLE OF CONTENTS

	<u>PAGE</u>
1. INTRODUCTION	C-6
2. SUMMARY	C-8
3. CONCLUSIONS	C-27
4. REFERENCES	C-28
5. APPENDICES	C-29
5.1 APPENDIX C-I	C-30
McCabe, D. E., "Final Report R-Curve Testing of 301 CRES Material," July 14, 1986	
5.2 APPENDIX C-II	C-106
Cotter, K. H., "Leak-Before-Burst Criteria Applied to Cryoformed Pressurant Tanks," paper AIAA-86-1503, presented at AIAA/ASME/SAE/ASEE 22nd Joint Propulsion Conference, June 16-18, 1986/Huntsville, Alabama	

LIST OF FIGURES

<u>FIGURE NO.</u>		<u>PAGE</u>
1 ♂	Center Cracked Tension Panel	C-12
2 ♂	.5T - CT Specimen ARDE	C-13
3 ♂	11"⌀ Cryoformed 301 CRES Sphere	C-17
4 ♂	11"⌀ Kevlar-49 Overwrapped Cryoformed 301 CRES Sphere	C-18
5 ♂	Pressurant Tank, 23" Dia.	C-19
6 ♂	Pressurant Tank, 23" Dia., Initial Flaw Geometry	C-20
7 ♂	LBB Evaluation Cryoformed 301 CRES Spherical Tank S/N 113, D = 23 in., Flaw in Weld Metal	C-21
8 ♂	I.D. Crack After LBB Demonstration, Pressurant Tank, 23" Dia.	C-23
9 ♂	LBB Test, Pressurant Tank, 23" Dia.	C-24
10 ♂	Base Metal (500X - Electrolytic Oxalic Acid Etch)	C-25
11 ♂	Single Pass Square Butt Weld, Multi Pass Modified U-Prep Weld (500X - Electrolytic Oxalic Acid Etch)	C-26

LIST OF TABLES

TABLE NO.

PAGE

1 B	Test Matrix - Specimen Identification	C-9
2 B	Summary Data From R-Curve Tests of CTT SPECIMENS	C-10
3 B	Summary Data Comparing CCT and CT Results	C-11
4 B	Room Temperature Fracture Toughness Data	C-16
5 B	Test Parameters	C-22
6 B	Cycles to Leak	C-22
7 B	Sustained Load Tests	C-22
8 B	LBB Verification	C-22

1. INTRODUCTION

This report describes R-Curve and other fracture mechanics experiments and presents test and analytic fracture mechanics data for cryoformed 301 CRES. Unaged cryoformed 301 CRES is used as the metal liner for the Kevlar-49 fiber overwrapped composite prestressed spheres utilized on the Kevlar Overwrap Study under Contract No. F08606-84-C-0029, Patrick Air Force Base, Florida. Fracture mechanics data was, therefore, needed to characterize 301 CRES toughness and leak-before-burst failure mode potential as an aid in defining a "fail safe" composite vessel configuration required under the Kevlar Overwrap Study contract.

Both tensile coupon and vessel test data are analyzed and reported. Aged as well as unaged cryoformed 301 CRES base metal, heat affected zone (HAZ) and weld metal results are presented for completeness. R-Curve experiments were performed using through cracked center tension panels (CCT) and compact tension specimens (CT) of unaged and aged 301 CRES. Vessel leak-before-burst (LBB) tests were conducted on 11"φ aged and unaged all metal 301 CRES spheres, 11"φ prestressed Kevlar-49 overwrapped unaged 301 CRES spherical liners and a 23"φ aged 301 CRES spherical tank. Elliptical-shaped part through defects were EDM machined in the 301 CRES liner surfaces and the vessels were cycle tested at operating pressure using oil or oil followed by gaseous helium (GHe). Sustained load and overpressure experiments were also included in the test program.

Unaged 301 CRES CCT panel experiments and 11" ϕ unaged 301 CRES all metal and composite vessel tests were funded by the Air Force under PAFB Contract No. FO8606-84-C-0029 with ARDE, INC. while the aged CCT and aged and unaged CT tensile specimens as well as the 11" ϕ and 23" ϕ aged vessel experiments were funded by ARDE. For completeness, all test data are presented and discussed in this report written in fulfillment of a PAFB Contract No. FO8606-84-C-0029 (CCN P00002) task requirement.

R-Curve fracture mechanics test panel data are discussed in detail in the final report, "R-Curve Testing of 301 CRES Material," prepared for ARDE by D. E. McCabe of Materials Engineering Associates. This report is included herein as Appendix I. Part through and through the thickness tensile and vessel 301 CRES fracture mechanics data, together with analytic assessments of leak-before-burst (LBB) mode and experimental verification of LBB by vessel tests, are given in Appendix II in an AIAA-86-1503 paper by Dr. K. H. Cotter of Fracture Proof Design Corporation.

2.0

SUMMARY

2.1

301 Cryostretched *CRES R-Curve Tests

Fifteen (15) center cracked tensile (CCT) panels and six (6) compact specimens were tested with cracks machined in base metal (BM), weld heat affected zone (HAZ) and weld metal (WM). Test samples were strengthened by cryostretching only as well as by cryostretching and ageing, thus covering an ultimate strength range from 204 ksi to 265 ksi.

J_R - curve development was made by recording load versus displacement of the test specimens. Stable crack growth initiation toughness, $K(J_{Ic})$, and crack instability toughness, K_c , were calculated from the R-curve data. The test results summarized in Table 1B and 2B on the following pages show retention of equivalent toughness in BM, HAZ, WM with approximate equivalence of $K(J_{Ic})$ over the total strength range and some improvement of K_c for the higher strength levels as enhanced by the ageing process. The test matrix is shown in Table 3B while the test samples are shown in Figure 1B and 2B. Complete test data are given in Appendix I.

* Work hardened at -320°F to achieve high strength

Table 1B Summary Data Comparing CCT and CT Results

	Power Law, $K(J_{IC})$ (ksi in.)	Δa_p (in.)	K_c (ksi in.)	Yield Strength (ksi)
Base Metal Aged				
CCT Avg.	96.1	0.036	180	261
CT	162.3	0.247	224	
Weld Metal Aged				
CCT Avg.	98.8	0.040	190	229
CT	133	0.210	187	
CT	102.2	0.216	219	
Weld Metal Unaged				
CCT Avg.	101.4	0.036	177	198
CT	114.7	0.237	171	
CT	116.2	0.240	185	
Base Metal Unaged				
CCT	108.2	0.032	163	207
CT	132.9	0.247	169	

Table 20 Summary Data From R-Curve Tests of CCT Specimens

Specimen Number	K(J _{IC}) Power Law (ksi√in.)	(Δa _p)		(K _C) (ksi√in.)	(σ _n ^a) (ksi)	Yield Strength (ksi)
		Clip Gage (in.)	Visual (in.)			
BH006A	108.1	0.032	0.0395	191	238	
007A	88.0	0.044	0.017	180	238	261
008A	92.2	0.032	0.025	169	238	
WH006A	118.3	0.040	0.040	194	240	
007A	87.6	0.052	0.037	204	240	229
008A	90.5	0.028	0.025	171	235	
HAZ009A	136.2	0.026	0.015	213	256	
WH001	101.5	0.043	0.050	183	214	
002	98.5	0.040	0.011	168	223	192
003	104.3	0.025	0.022	179	207	
BH001	130.9	0.036	0.021	185	217	
002	103.5	0.024	0.020	147	218	207
003	90.1	0.035	0.038	157	213	
HAZ004	116.5	0.022	0.015	184	228	
005	126.6	0.017	0.022	174	223	

$$(\sigma_n)_{\text{net cross-section stress}} = \frac{P/B}{W - 2(a_0 + \Delta a_p)}$$

A - Aged

Table 30 Test Matrix - Specimen Identification

Conditions	Specimen Type	Base Metal	Weld Metal	HAZ
Aged	CCT	40-006	40W-006	40W-009
	CCT	40-007	40W-007	
	CCT	40-008	40W-008	
	CT	BM-008	WM 13A	
	CT		WM 14A	
Unaged	CCT	40-001	40W-001	40W-004
	CCT	40-002	40W-002	40W-005
	CCT	40-003	40W-003	
	CT	BM-003	WM 11	
	CT		WM 12	

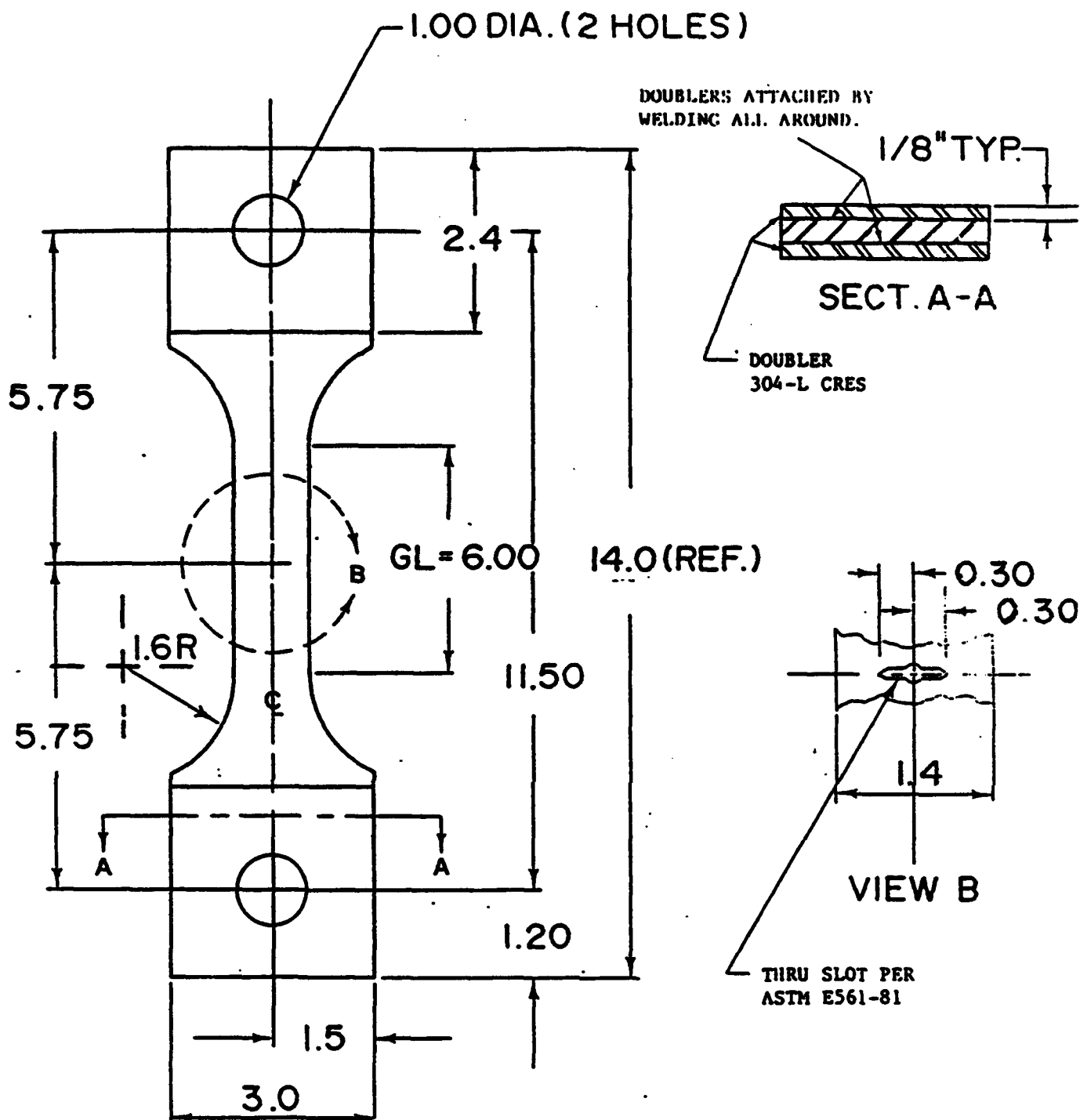


Fig. 1b Center cracked tension panel. Dimensions in inches.

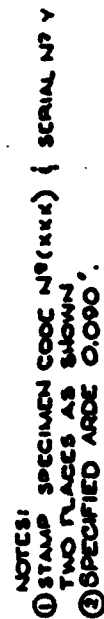
[illegible]

Fig. 2B 1/2T compact specimen.

2.2 Part Through and Through Crack Tensile and Vessel Data and Leak-Before-Burst Assessment

Part through and through thickness crack 301 CRES tensile fracture mechanics data obtained by various investigators⁽¹⁾⁻⁽⁷⁾ (Table 4~~8~~) was reviewed and analyzed. Based on this data, crack stability and LBB predictions were made for 11" ϕ and 23" ϕ cryoformed 301 CRES spherical vessels and LBB tests were run to confirm the analytical results. Figures 3~~6~~, 4~~8~~, 5~~8~~ show 11" ϕ all 301 CRES, 11" ϕ Kevlar-49 overwrapped 301 CRES composite and 23" ϕ all 301 CRES spherical test vessels. Elliptical surface flaws (part through defects) were EDM machined in the tank walls and the tanks were cycle and sustained load tested at operating pressures. Figure 6~~8~~ depicts a typical EDM initial flaw geometry.

The analytic LBB predictions were verified by these vessel tests. The test data/results are given in Tables 5-8~~8~~. The stable LBB mode was maintained for wall break-through surface crack lengths $2C_{eff}$, 2.83 to 4.30 times wall thickness. This is contrasted with an expected length at breakthrough for in-service defects of 2 times the wall thickness. Figure 7~~6~~, a plot of the analytic prediction for the 23" ϕ aged 301 CRES vessel with an EDM flaw in the weld shows that the stable crack growth length after wall breakthrough is more than 5 wall thicknesses (5t). The test points at stable crack breakthrough length 4.3t are shown on the figure. Magnified views of the I.D. weld crack and fracture surface after crack breakthrough and LBB demonstration are given on Figures 8~~8~~ and 9~~8~~, respectively. Note the EDM flaw (Figure 9~~8~~), showing the

fatigue crack growth and the shear lips associated with a tough material, that were generated at crack breakthrough.

Stable crack growth initiation toughness and crack instability toughness values obtained ranged from 96 to 108 ksi $\sqrt{\text{in}}$ and 163 to 190 ksi $\sqrt{\text{in}}$, respectively, in reasonable agreement with R-Curve test results. Figures 106 and 118 show typical cryoformed base and weld metal microstructures at 500X. The weld and base metal microstructures are similar, consisting of a tough austenitic matrix with interlocking platelets of high strength martensite. The high toughness exhibited by cryoformed 301 CRES results from this favorable microstructure configuration.

Table 4B Room Temperature Fracture Toughness Data

Material (1)	Weld Wire	Specimen type (2)	Number of tests	Average Toughness (ksi-√in)	σ_y (ksi)	σ_u (ksi)	t (in)	Source
BM/A		CTC	3	188	287	286	.084	Ref. 1
WM/A	308L	CTC	3	190	229	231	.084	
HAZ/A		CTC	3	213			.084	
WM/A	308L	CTC	3	196	220	231	.084	
BM/UA		CTC	3	163	287	215	.084	
BM/UA		PTC/TC	1	188	188	188	.125	Ref. 2
BM/UA		PTC	1	74	188	188	.125	
WM/UA	308L	PTC	1	86			.125	
WM/UA	308L	PTC	1	94			.125	
WM/UA	308L	PTC/TC	1	124			.125	
WM/UA	308L	PTC/TC	1	137			.125	
WM/UA	308L	PTC	1	87			.125	
BM/A		PTC(PV)	1	98.5	~200		.084	Ref. 4
BM/A		PTC	1	102.8	220		~.200	Ref. 5
BM/A		PTC	1	108.8	220		~.200	
WM/A	308L	PTC	1	103.8	218		~.200	
WM/UA	308L	PTC	3	88.5	175		.063	Ref. 6
HAZ/UA		PTC	3	88.8	~205		.063	
BM/UA		PTC	2	88.5	215		.063	
WM/A	308L	PTC	2	83.0	235		.063	
HAZ/A		PTC	2	87.3	~254		.063	
BM/A		PTC	2	102.8	258		.063	
BM/UA		PTC	10	118.5	174	210	(.100	Ref. 7
WM/UA	308L	PTC	7	92.3	181		2.028)	

1) BM- base metal; WM- weld metal; HAZ- heat-affected zone; /A- aged;
and, /UA- unaged

2) CTC- center through-crack; PTC- part-through crack; PTC/TC- PTC became TC
after penetrating thickness; and, CT- compact tension

3) ~ approximately



Fig. 3B 11" ϕ CRYOFORMED 301 CRES SPHERE

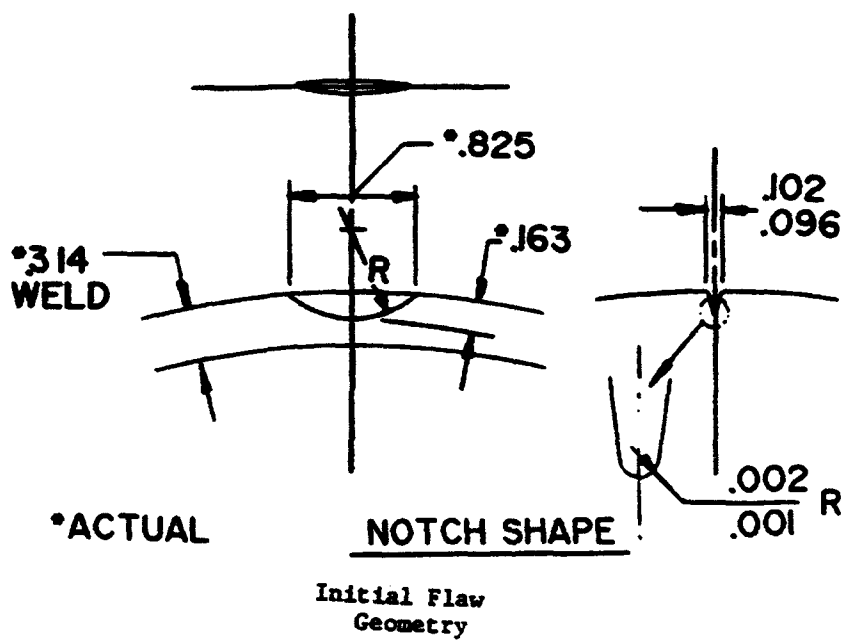


Fig. 4B



DESIGN BURST PRESSURE	: 9800 PSI MINIMUM
DESIGN MEOP	: 4900 PSI
SERVICE MEOP	: < 3800 PSI
MINIMUM WALL	: 0.215 INCH THICK
TYPE OF WELD	: TIG, MODIFIED U-PREP (0.215 INCH THICK)

PRESSURANT TANK, 23" DIA.



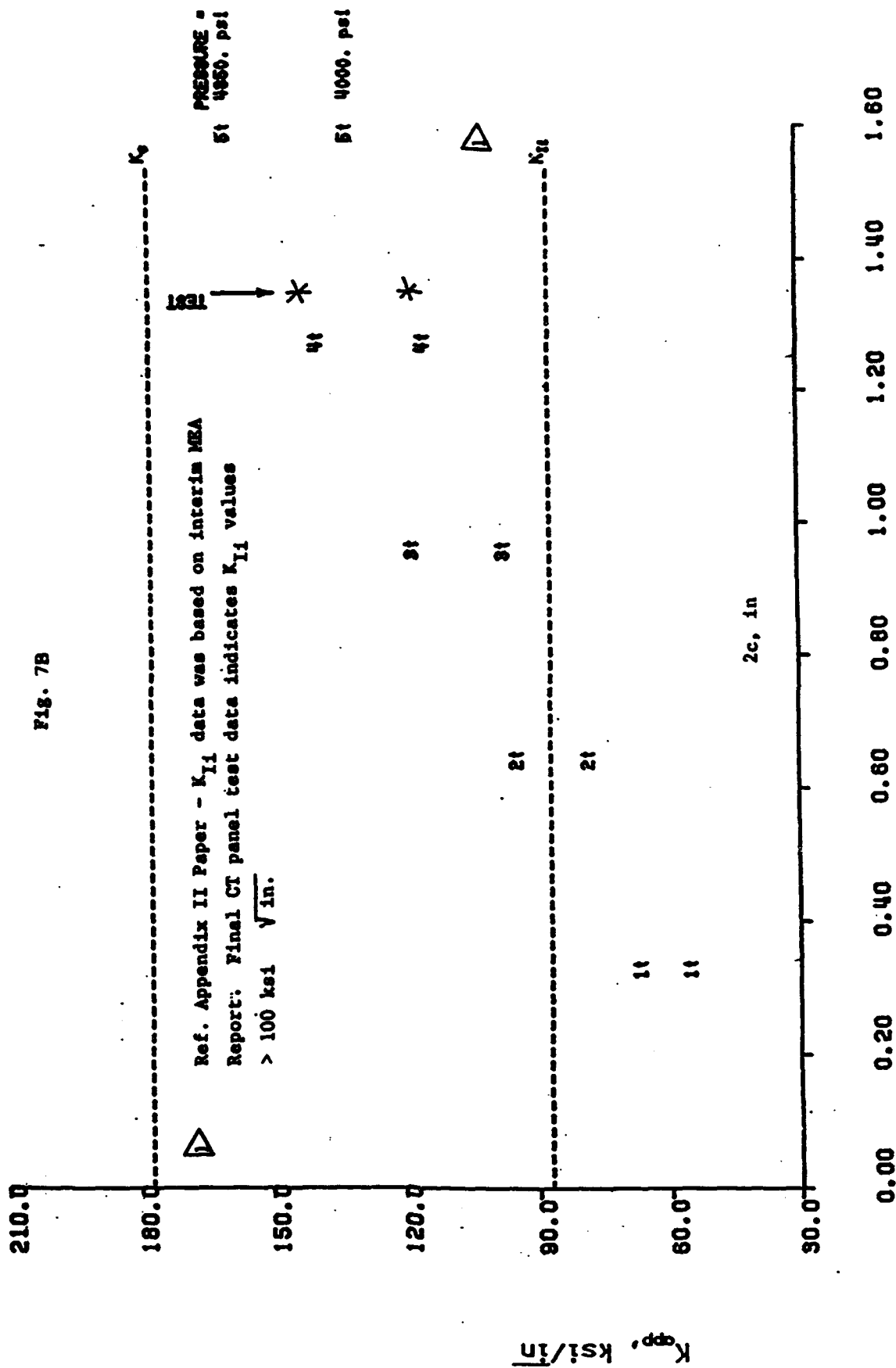
Initial Flaw
Geometry

PRESSURANT TANK, 23" DIA.

Fig. 6B
C-20

LBB EVALUATION
CRYOFORMED TP301 STAINLESS STEEL SPHERICAL TANK
3/N 113, D = 29 IN, FLAW IN WELD METAL

Fig. 7B



3302/18
TWENTY

TANK NO.	TANK P/N	TYPE	TANK S/N	SOI WEAT	CONDITION	FLAW LOCATION	DIAMETER (IN)
1	SKA11419A	Metal	105	89019	Aged	OD-DM	11
2	SKA11458	Metal	003	90740	Aged	OD-DM	11
3	SKA11425	Metal	104	89019	Aged	OD-DM	11
4	SKA11463	Metal	113	89370	Aged	OD-DM	23
5	D3912 MOD	Metal	003	88690	Unaged	ID-DM	11
6	D4163	Composite	001	88690	Unaged	ID-DM	11
7	D4163	Composite	002	88690	Unaged	ID-DM	11

TABLE 6B: CYCLES TO LEAK

TRANK NO.	Power (psi)	τ_{off} (in)	(s/e/c) ₂	a_1 (in)	N (Cycles)
1	4200	.089	.21	.041	2590
2	4000	.121	.24	.074	2548
3	3900	.090	.23	.044	2338
4	4000	.314	.20	.163	2377
5	2450		.20	.038	540
6	4000-7000-4000	.057	.20	.038	1140
7	3000-6000-3000	.057	.17	.034	1987

TABLE 7D: SUSTAINED LOAD TESTS

TANK NO.	DURATION (HR)	P _{oper} (psi)	K _{app} (ksi \sqrt{in})	CRACK GROWTH
1	27	3475 to 4130	84.9	None
3	48	3850 to 4000	82.2	None
5	5	4050	71.0	None

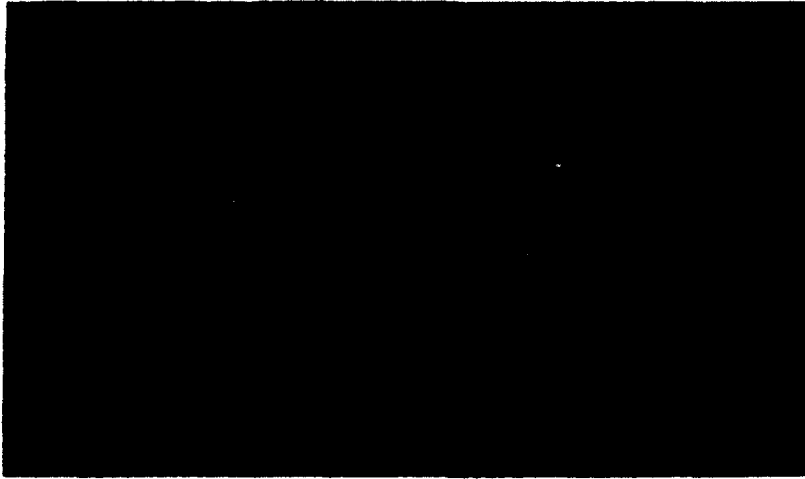
TABLE 9B: LBB VERIFICATION

PANK NO.	$2c_{eff} \text{ (in)}$	$\frac{2c_{eff}}{c_{eff}}$	$P_{max} \text{ (psi)}$	AREA VOLUME VENTILATION		REFRIGERANT
				$K_{app} \text{ (hcf } \sqrt{\text{in}})$	$K_T \text{ (hcf } \sqrt{\text{in}})$	
-					$K_g \text{ (hcf } \sqrt{\text{in}})$	
1	.252	2.83	6100	131.7	96.1	180 OIL
2	.363	3.00	6800	119.2	96.8	190 OIL
3	.266	2.96	4050	80.9	96.1	180 OIL THEN GAS
4	1.350	4.30	4850	135.9	96.8	190 OIL THEN WATER
5	.090	1.58	2600	64.8	108.2	163 OIL
6	.193	3.39	7150	88.4	108.2	163 OIL
7	.200	3.51	6150	93.1	108.2	163 OIL

△ Cryoformed 301 CRPS per ARDE AIS 258

Unaged Cryo CRES 301 Plus Kevlar 49 Type 969 Per DHS-1

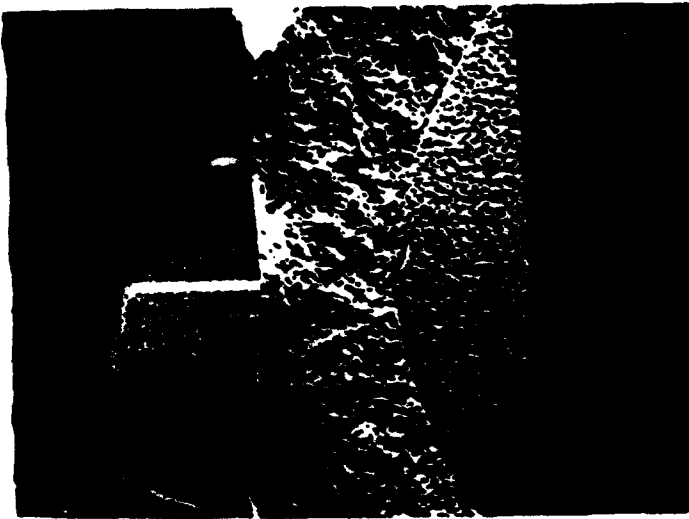
3. Toughness Value is an Average of Three Tests per Condition/Flaw Location Type - See NEA Final Report NEA-2151 (Appendix I)



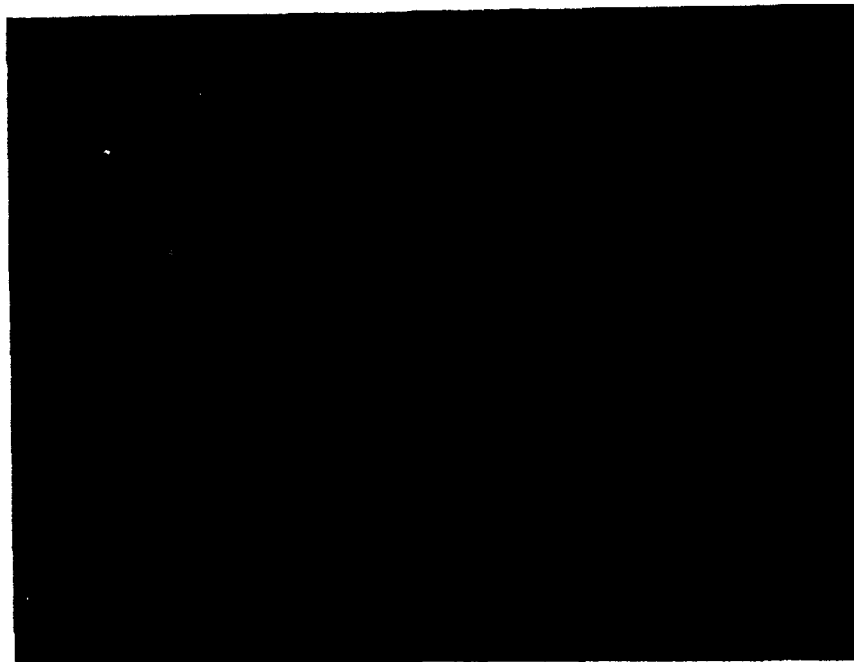
- I.D. CRACK AFTER LEAK BEFORE BURST DEMONSTRATION
- MAX PRESSURE : 4850 PSI
- CRACK LENGTH : 0.71 INCH
- LOCATION : WELD

PRESSURANT TANK, 23" DIA.

LEAK BEFORE BURST TEST



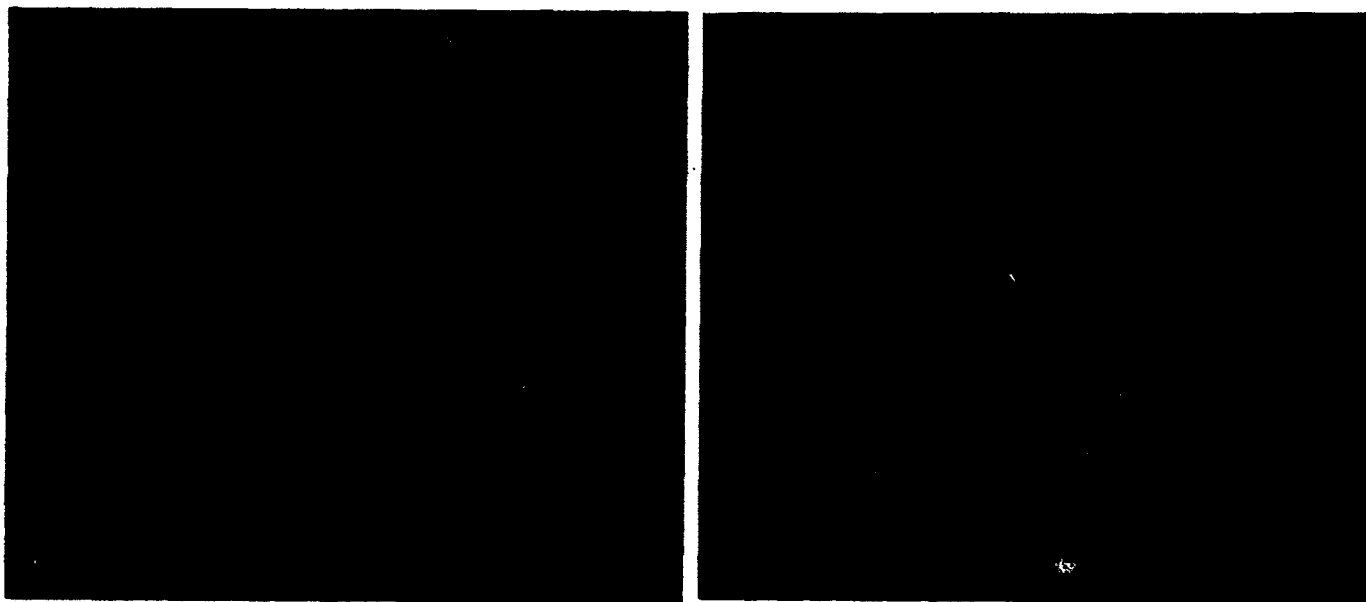
- EDM FLAW ON VESSEL O.D.
- FATIGUE REGION IN CENTER
- SHEAR LIPS ON VESSEL I.D.



BASE METAL

(500X—Electrolytic Oxalic Acid Etch)

- **ORIGINAL AUSTENITIC GRAIN BOUNDARIES ARE CLEARLY RETAINED**
- **NO VISIBLE PRECIPITATES ALONG GRAIN BOUNDARIES**
- **UNIFORM TRANSFORMATION THROUGHOUT STRUCTURE**
- **AUSTENITIC MATRIX WITH INTERLOCKING PLATELETS OF HIGH STRENGTH MARTENSITE**



SINGLE PASS SQUARE BUTT WELD

MULTI PASS MODIFIED U-PREP WELD

(500X —Electrolytic Oxalic Acid Etch)

- **WELDS TRANSFORM IN UNIFORM MANNER**
- **NO EVIDENCE OF RESIDUAL AS CAST STRUCTURE**
- **NOTE SIMILARITY TO BASE METAL**

3. CONCLUSIONS

- 3.1 Cryoformed 301 CRES is a high strength material with very excellent toughness.
- 3.2 Leak-before-burst (LBB) mode with large margins has been confirmed by vessel tests for wall breakthrough surface crack lengths much greater than 2 times wall thickness, the expected breakthrough LBB crack length for in-service defects.
- 3.3 Cryoformed 301 CRES material toughness is independent of flaw location. Essentially, no difference in tolerance to defects was noted between base metal, weld metal or HAZ material.

4. REFERENCES

1. McCabe, D. E., preliminary fracture properties of cryoformed TP301 stainless steel, March 21, 1986, Materials Engineering Associates, Inc., Lanham, MD, to be published.
2. Beck, E. J. & Schwartzberg, F. R., "Fracture Behavior of Cryogenically Stretched 301 Stainless Steel Used in the M-509 Pressure Vessel," Martin Marietta Report MCR-71-53, February 1971, prepared under NASA Contract NAS 9-9339.
3. Private communication with A. Cozewith, Arde, Inc., Mahwah, NJ, March 1986.
4. Campbell, J. E., DMIC Review of Recent Developments - Mechanical Properties of Metals, DMIC, Battelle Memorial Institute, Columbus, OH, February 16, 1968.
5. Tests conducted by Thiokol Chemical Corporation under NASA Contract NAS 8-11977.
6. Forman, R. G., "Environmental Crack Growth Behavior of High Strength Pressure Vessel Alloys," NASA TN D-7952, April 1975.
7. Bixler, W. D., "Fracture Control Method for Composite Tanks with Load Sharing Liners," "NASA CR-134758, July 1975.

5. APPENDICES

5.1 APPENDIX C-1

**R-CURVE TESTING OF
301 CRES MATERIAL**

Prepared by

D.E. McCabe

**Materials Engineering Associates, Inc.
9700B Martin Luther King, Jr. Highway
Lanham, Maryland 20706-1837**

July 14, 1986

Prepared for

**ARDE, Inc.
19 Industrial Avenue
Mahwah, New Jersey 07430**

**Contract
#FO-8606-84-C-0029**

TABLE OF CONTENTS

	<u>Page</u>
INTRODUCTION.....	C-34
TOUGHNESS CALCULATIONS - CCT PANELS.....	C-35
TOUGHNESS CALCULATIONS - CT SPECIMENS.....	C-36
FRACTURE TOUGHNESS CRITERIA.....	C-37
RESULTS.....	C-38
CONCLUSIONS.....	C-39
REFERENCES.....	C-40
ACKNOWLEDGEMENTS.....	C-41
APPENDIX III - R-CURVES AND TABULATED DATA	C-58
APPENDIX IV - EXAMPLE CALIBRATION INFORMATION	C-102

FIGURE CAPTIONS

- Fig. 1 C Center cracked tension panel. Dimensions in inches.
- Fig. 2 C Clip gage attachment setup for 6-inch gage length.
- Fig. 3 C View of DSST gage and traveling stage microscope for measuring slow-stable crack growth.
- Fig. 4 C 1/2T compact specimen.
- Fig. 5 C Representative load-displacement record, CCT panel.
- Fig. 6 C Representative load-displacement record, compact specimen.
- Fig. 7 C Magnified view of crack tip region after considerable slow-stable crack extension.
- Fig. 8 C Compact specimen and center cracked panel J_R -curves for unaged base metal.
- Fig. 9 C Compact specimen and center cracked panel J_R -curves for aged base metal.
- Fig. 10 C Compact specimen and center cracked panel J_R -curves for unaged weld metal.
- Fig. 11 C Compact specimen and center cracked panel J_R -curves for aged weld metal.

Introduction

The purpose of this program was to test specimens of CRES ³⁰¹100 material provided by ARDE for J_R -curve and for J_{IC} -like values that can be obtained from J_R -curves. The material is an extremely high strength stainless steel that has good toughness by ultra-high strength materials standards.

Center cracked tension panels (CCT) were prepared by ARDE; 1/2T (plan view) compact specimens were machined under MEA control. All specimens were nominally 0.090-in. to 0.095-in. (2.3 mm to 2.4 mm) thickness. Doubler pads had been welded on the ends of the CCT specimens, the fabrication of which caused various degrees of kinking at the ends of the specimens. Fifteen CCT panels and six compact specimens were tested in conditions representing base metal, weld metal and HAZ in aged and unaged conditions (Table 12). The compact specimens of base metal were made from broken halves of CCT specimens.

J_R -curve development was made by recording load vs. displacement, measuring work done on the specimens. The CCT panels were 1.4-in. (35.5 mm) wide with a 6-in. (152 mm) parallel section and a nominal 0.4-in. starting fatigue crack for a crack size ratio, $2a_0/W$ of 0.43 (Fig. 1E). Extension arms and an MTS clip gage were used to measure elongation over the 6-in. gage length. The attachment points for the clip gage were razor blade tips (Fig. 2E). A second gage (DSST-type) was attached across the crack mouth at a span of 0.5-in. (12.7 mm) to measure crack growth by unloading compliance (Fig. 3E). The 1/2T compact specimen is shown in Fig. 4C, and in this case, displacement is measured under the loading pins (on the load line) in the region of the cutout. Again, the clip gage was attached across razor blade tips. Load coupled with displacement measurement indicates work done.

All of the clip gages discussed above were calibrated and example calibration information is enclosed in Appendix IV.

Periodic partial unloading of specimens gives linear unloading traces, the slope of which corresponds to currently existing physical crack sizes (Figs. 5C and 6E). Linear regression was used to fit the unloading slope and elastic compliance was used to calculate crack size. All of the above had been performed during the test using a computer. Generally the unloading slopes were linear, having correlation coefficients of the order of 0.999XX. For the CCT panels, the crack size measurement accuracy was within 0.002 to 0.005-in., depending upon the initial distortion of the specimens at the doubler plates. Sensitivity, which is important for the R -curve accuracy, was usually good to 0.002 in. of crack growth increment. The compact specimens had been initially ground flat and both precision and accuracy were of high resolution.

To verify the unloading compliance measurements, we also used visual measurements on one of the two surfaces using a traveling stage microscope. This was definitely less precise compared to unloading compliance because the crack tunnels at midthickness which cannot be seen on the surface. Additionally, surface growth tended to be slightly uneven from front to back of the specimens. Also, when plastic zones of appreciable size develop at the crack tips, as they did here, the exact location of the physical crack tip becomes a matter of judgment. The situation is illustrated in Fig. 7C.

Toughness Calculations - CCT Panels

The fracture toughness of the material was evaluated in terms of J-integral. The J solutions for the CCT geometry [M(T)] have not been as thoroughly developed and standardized to the extent that they have been for the compact specimen, [C(T)]. Therefore we had selected a compromise computational procedure that is most likely to lead to geometry independent J. Here we use the term Merkle-Corten J_{mc} for the reason that it resembles the Merkle Corten computational approach used on compact specimens. Specifically all load vs. displacement measurements are treated as total work done on the specimen, and no special provision is used to correct for the slow-stable crack growth. Following Reference 1:

$$J_p = \frac{2 (\text{Area} - 1/2 P v)}{B (W-2a)} \quad (1)$$

where:

J_p	=	the plastic component of J
Area	=	total work done
a	=	initial half-crack size
P	=	load
v	=	total displacement
W	=	specimen width
B	=	specimen thickness

Total J (i.e., J_{mc}) is obtained after adding elastic J calculated as follows:

$$J_e = \frac{K^2}{E} = \frac{\sigma^2 v_a}{E} \text{Sec} \frac{v_a}{W} \quad (2)$$

σ	=	gross stress
E	=	elastic modulus

$$J_{mc} = J_e + J_p \quad (3)$$

As had been stated before, dimension "a" is not updated for crack growth. Nevertheless, the above procedure is likely to give J_{mc} near in value to modified J (Ref. 2) as opposed to deformation theory J (Ref. 3).

As an exercise to assure the reasonableness of the J for R-curve plots and to verify the performance of the instrumentation, two alternative fracture toughness computations were made. See the tabulated data in Appendix III. One was a plasticity corrected stress intensity factor, K_r , obtained using a procedure described in ASTM method E561 (Ref. 4). The equations are as follows:

$$K_r = \sigma \left[v_a \text{Sec} \frac{v_a}{W} \right]^{1/2} \quad (4)$$

where a_e is plastic zone corrected crack size, and:

$$J(K_r) = K_r^2/E \quad (5)$$

A second alternative (J_{bt}) procedure that we added violates accepted J analysis testing practices but the results were found useful here to evaluate the compatibility of displacement measurement between the two gages. Displacement from the DSST mouth gage was used in place of total displacement (v), to calculate work done (Area) and the plastic component of work done (Area - $1/2 P v$) in Eq. 1. Values of " J_{bt} " were calculated using Eqs. -1 through 3. Comparison of J_{mc} , $J(K_r)$ and J_{bt} are included in the tabulations of Appendix III.

Toughness Calculations - CT Specimens

The CT specimen, C[T] is the most thoroughly studied fracture mechanics specimen. Testing techniques have been highly refined and J can be calculated with better conformance to theoretical considerations. However, from the three computational options available, (Merkle-Corten, Deformation Theory J, and Modified J) we will again choose Merkle-Corten J_{mc} as the primary one simply to make comparisons to the CCT panel results. In this case, the J_{mc} values can be verified through a comparison to modified J values which are better justified by theory. Modified J (J_M) will be treated herein as the alternative method number 1.

For the compact specimen, it is not necessary to subdivide the computation of J_{mc} into its elastic and plastic components and so the following simple formula can be used to calculate total J_{mc} .

$$J_{mc} = \frac{\eta \text{ Area}}{B b} \quad (6)$$

where,

Area = total area under load vs. displacement
 b = $W - a$
 a = initial crack size
 B = specimen thickness
 η = $2 + 0.522b/W$

Modified J had been developed to handle cases where there is substantial crack growth with respect to the initial remaining ligament size. It is computed from the following equations:

$$J_M = G + \frac{1}{B} \int_0^v P \frac{\eta}{b} P dv_p \quad (7)$$

where:

b = $W - a_i$
 a_i = updated crack size
 n = $2 + 0.522 b/W$
 v^p = plastic component of displacement
 G^p = J (elastic)

Despite the fact that equations (6) and (7) differ a great deal in computational approach, it can be seen in the tabulations in Appendix III that the values are nearly the same over the full range of the J_R -curves.

Fracture Toughness Criteria

The work statement of ARDE had asked for material toughness evaluation by J_R curve and for J_{IC} by ASTM Method E813, "J_{IC}, A Measure of Fracture Toughness" (Ref. 5). This standard has been revised recently and is currently being balloted within ASTM. The revised practice is used herein as the primary data evaluation procedure. It should be kept in mind that the J_{IC} values obtained cannot be validated according to the old nor the revised versions of the standard because we will be ignoring the thickness requirements and specimen design recommendations in the case of the CCT specimens.

The procedure for determining provisional values of J_{IC} involves several procedural steps. A blunting line is developed which is defined by the following equation:

$$\Delta a_p = J/2\sigma_f \quad (8)$$

where $\sigma_f = (\sigma_{ys} + \sigma_{ts}) / 2$.

Equation 8 predicts a material crack tip blunting behavior that is graphically constructed. Two "exclusion lines" are drawn parallel to the blunting line, offset by 0.006-in. (0.15 mm) and 0.060-in. (1.5 mm). The purpose of the lower bound exclusion line is to exclude from the J_R -curve model all of the slow stable crack growth near initiation, where Δa_p is very nebulously defined. These data as a general rule cannot be reliably reproduced between investigators. The upper bound exclusion line restricts the Δa_p range so that a simple power law produces a good fit to the data. Hence the qualified data within the exclusion lines is fit with the following power law equation:

$$J_{P1} = C (\Delta a_p)^n \quad (9)$$

where:

C = fitting constant
 Δa_p = physical crack growth

In the revised standard, a third parallel offset line is made at 0.008-in. (0.2 mm) of Δa_p and J_{IC} is defined as the intersection of J_{P1} with this offset line. This new approach establishes J_{IC} as a real definable point on the J_R -curve which was not necessarily the case with the practice that is presently in place. It is felt that the 0.008-in. of stable growth necessary to be on the J_R curve will not be relevant to engineering concerns.

Results

Appendix A presents J_R -curves and tabulations of J_R values at each unloading event for all specimens. The units of measure used here were purposely chosen to be English units. To convert to metric use the following:

$$K_I: \text{ksi}\sqrt{\text{in.}} \times 1.1 = \text{MPa}\sqrt{\text{m}}$$

$$J_I: \text{in.-lb/in.}^2 \times 0.175 = \text{kJ/m}^2$$

$$\sigma: \text{ksi} \times 6.894 = \text{MPa}$$

$$\Delta a_p = \text{in.} \times 25.4 = \text{mm}$$

Table 2C summarizes the fracture toughness parameters obtained from CCT panels. The symbol $K (J_{IC})$ used here suggests only that the J_{IC} procedure and conversion equality $K_{IC}^2 = J_{IC}E$ had been used. The values do not necessarily meet all of the validity requirements of standard E813 (new or old version) nor standard E399. For K_S values, the numbers are K converted from J_{IC} and they correspond to the unloading at or just prior to maximum load. For almost all of the CCT panels, maximum load was a crack instability load which terminated the J_R -curve development. The net stress calculations were based on crack size including slow stable crack growth.

Tests on CT specimens can be easily identified in Appendix A by the 0.2-in. or more of slow-stable growth in the J_R curves. This is possible because the compact specimen is an inherently stable geometry. The J_R -curves are the same as those that had been obtained with CCT specimens, however (Figs. 8-11C). The $K (J_{IC})$ values indicated from the CT specimens appear to be slightly higher on average than those obtained with CCT panels, as can be seen in Table 3C. The reason for this becomes clear when we realize that only half of the J_R -curve data between the exclusion lines is developed before instability with CCT specimens. As a result, the power law fits were biased slightly toward higher slopes and lower J_R predictions at the 0.008-in. (0.2 mm) offset line.

Table 4C compares compliance indicated crack growth for CCT panels as measured by the DSST gage to the visually measured growth. In some cases, the compliance-indicated crack growth had been transposed or offset along the abscissa by an amount indicated in the last column. The same visual vs. compliance comparison is made for compact specimen tests in Table 5C. With these specimens, however, the testing practice and specimen machining methods are thoroughly refined and initial offset adjustment was not necessary.

Precracking data are given in Table 6C. The total cycles for base metal specimen 002 had been inadvertently not recorded.

Conclusions

J_R -curves were obtained on CRES base metal, weld metal, and HAZ in the aged and unaged conditions. For CCT panels, each J_R -curve was terminated by an onset of crack instability, usually with less than 0.05-in. (1.27 mm) of crack growth. Compact specimens produced essentially the same J_R -curves except there was no instability and the J_R -curve up to 0.20-in. (5 mm) of crack growth was obtained. The J_{IC} -like crack initiation values resulting from CCT J_R -curves were slightly lower than the J_{IC} -like values of CT specimens. Apparently, the existence of fewer data points in the zone of data inclusion which are clustered near to the crack growth initiation biases the power law curve to lower J_R values at the 0.008-in. intercept.

References

1. Rice, J.R., Paris, P.C., and Merkle J.G., "Some Further Results of J-Integral Analysis and Estimates", Progress in Flaw Growth and Fracture Toughness Testing, ASTM STP 536, 1973, pp. 231-245.
2. Ernst, H.A. "Material Resistance and Instability Beyond J Controlled Crack Growth", ASTM STP 803, Vol. 1983.
3. Paris, P.C. "Fracture Mechanics in the Elastic-Plastic Regime", Flaw Growth and Fracture, ASTM STP 631, 1977, pp. 3-27.
4. ASTM Standard E561-81, "R-Curve Determination", ASTM Annual Book of Standards, Section 3, Vol. 03.01, 1985.
5. ASTM Standard E813-81, " J_{IC} , A Measure of Fracture Toughness", ASTM Annual Book of Standards, Section 3, Vol. 03.01, 1985.

Acknowledgments

The author would like to acknowledge Messrs R. Taylor and H. Sanders for their contributions in equipment development and for help in the test technique refinements. The tests were conducted with good techniques by Ms. D'Ambrosio and Ms. Fletcher. The computations and graphics work was performed by Mr. Tim Ramey. Preparation of the manuscript was by Ms. L. Wahler.

Table 1C Test Matrix - Specimen Identification

Conditions	Specimen Type	Base Metal	Weld Metal	HAZ
Aged	CCT	40-006	40W-006	40W-009
	CCT	40-007	40W-007	
	CCT	40-008	40W-008	
	CT	BM-008	WM 13A	
	CT		WM 14A	
Unaged	CCT	40-001	40W-001	40W-004
	CCT	40-002	40W-002	40W-005
	CCT	40-003	40W-003	
	CT	BM-003	WM 11	
	CT		WM 12	

Table 2C Summary Data from R-Curve Tests of CGT Specimens

Specimen Number	K(J _{IC}) Power Law (ksi√in.)	(Δa _p)		(K _{IC}) (ksi√in.)	(σ _n ^a) (ksi)	Yield Strength (ksi)
		Clip Gage (in.)	Visual (in.)			
BH006A	108.1	0.032	0.0395	191	238	
007A	88.0	0.044	0.017	180	238	261
008A	92.2	0.032	0.025	169	238	
BH006A	118.3	0.040	0.040	194	240	
007A	87.6	0.052	0.037	204	240	229
008A	90.5	0.028	0.025	171	235	
HAZ009	136.2	0.026	0.015	213	256	
BH001	101.5	0.043	0.050	183	214	
002	98.5	0.040	0.011	168	223	192
003	104.3	0.025	0.022	179	207	
BH001	130.9	0.036	0.021	185	217	
002	103.5	0.024	0.020	147	218	207
003	90.1	0.035	0.038	157	213	
HAZ004	116.5	0.022	0.015	184	228	
005	126.6	0.017	0.022	174	223	

Net cross-section stress
$$\frac{P/B}{W - 2(a_0 + \Delta a_p)}$$

Table 3C. Summary Data Comparing CCT and CT Results

	Power Law, $K(J_{IC})$ (ksi in.)	A_{a_p} (in.)	K_c (ksi in.)	Yield Strength (ksi)
Base Metal-Aged				
CCT Avg.	96.1	0.036	180	261
CT	162.3	0.247	224	
Weld Metal Aged				
CCT Avg.	98.8	0.040	190	229
CT	133	0.210	187	
CT	102.2	0.216	219	
Weld Metal Unaged				
CCT Avg.	101.4	0.036	177	198
CT	114.7	0.237	171	
CT	116.2	0.240	183	
Base Metal Unaged				
CCT	108.2	0.032	163	207
CT	132.9	0.247	169	

Table 4C Comparison of Visual (V) vs. Compliance Indicated (C) Crack Growth (Δa_p) At Selected Unloading Points for CCI Specimens

Specimen No.	Crack Length Differences (in.)																Offset Mills
40-006 (V)	0	0	0.002	0.001	0.003	0.004	0.005	0.004	0.005	0.007	0.007	0.007	0.007	0.007	0.007	0.007	0.007
40-006 (C)	0	0.001	0.003	0.005	0.005	0.006	0.006	0.006	0.006	0.007	0.007	0.007	0.007	0.007	0.007	0.007	0.007
40-007 (V)	0	0	0	0	0	0.005	0.005	0.005	0.005	0.005	0.005	0.005	0.005	0.005	0.005	0.005	0.005
40-007 (C)	0	0.002	0.002	0.005	0.005	0.005	0.005	0.005	0.005	0.005	0.005	0.005	0.005	0.005	0.005	0.005	0.005
40-008 (V)	0	0	0.0015	0.002	0.0025	0.003	0.003	0.003	0.003	0.003	0.003	0.003	0.003	0.003	0.003	0.003	0.003
40-008 (C)	0	0.001	0.0035	0.005	0.005	0.005	0.005	0.005	0.005	0.005	0.005	0.005	0.005	0.005	0.005	0.005	0.005
40-009 (V)	0	0.0015	0.0025	0.003	0.0035	0.0035	0.0035	0.0035	0.0035	0.0035	0.0035	0.0035	0.0035	0.0035	0.0035	0.0035	0.0035
40-009 (C)	0	0	0	0.0015	0.003	0.003	0.004	0.004	0.004	0.004	0.004	0.004	0.004	0.004	0.004	0.004	0.004
40-007 (V)	0	0.002	0.004	0.004	0.004	0.004	0.005	0.005	0.005	0.005	0.005	0.005	0.005	0.005	0.005	0.005	0.005
40-007 (C)	0	0.001	0.003	0.005	0.005	0.005	0.005	0.005	0.005	0.005	0.005	0.005	0.005	0.005	0.005	0.005	0.005
40-008 (V)	0	0.002	0.002	0.004	0.004	0.004	0.004	0.004	0.004	0.004	0.004	0.004	0.004	0.004	0.004	0.004	0.004
40-008 (C)	0	0	0	0	0.001	0.001	0.001	0.001	0.001	0.001	0.001	0.001	0.001	0.001	0.001	0.001	0.001
40-009 (V)	0	0.002	0.002	0.003	0.0035	0.0035	0.0035	0.0035	0.0035	0.0035	0.0035	0.0035	0.0035	0.0035	0.0035	0.0035	0.0035
40-009 (C)	0	0	0.001	0.003	0.004	0.004	0.004	0.004	0.004	0.004	0.004	0.004	0.004	0.004	0.004	0.004	0.004
40-001 (V)	0	0	0.001	0.002	0.002	0.004	0.005	0.005	0.005	0.005	0.005	0.005	0.005	0.005	0.005	0.005	0.005
40-001 (C)	0	0	0	0	0	0.001	0.001	0.001	0.001	0.001	0.001	0.001	0.001	0.001	0.001	0.001	0.001
40-002 (V)	0	0	0	0	0	0.001	0.001	0.001	0.001	0.001	0.001	0.001	0.001	0.001	0.001	0.001	0.001
40-002 (C)	0	0	0.001	0.003	0.0035	0.004	0.004	0.004	0.004	0.004	0.004	0.004	0.004	0.004	0.004	0.004	0.004
40-003 (V)	0	0.003	0.005	0.005	0.005	0.0045	0.0045	0.0045	0.0045	0.0045	0.0045	0.0045	0.0045	0.0045	0.0045	0.0045	0.0045
40-003 (C)	0	0	0.002	0.003	0.004	0.004	0.004	0.004	0.004	0.004	0.004	0.004	0.004	0.004	0.004	0.004	0.004
40-001 (V)	0	0	0	0	0	0.001	0.002	0.002	0.002	0.002	0.002	0.002	0.002	0.002	0.002	0.002	0.002
40-001 (C)	0	0	0	0	0	0.001	0.002	0.002	0.002	0.002	0.002	0.002	0.002	0.002	0.002	0.002	0.002
40-002 (V)	0.003	0.002	0.003	0.003	0.003	0.003	0.003	0.003	0.003	0.003	0.003	0.003	0.003	0.003	0.003	0.003	0.003
40-002 (C)	0	0.001	0.002	0.002	0.002	0.002	0.002	0.002	0.002	0.002	0.002	0.002	0.002	0.002	0.002	0.002	0.002
40-003 (V)	0	0	0	0	0	0.001	0.001	0.001	0.001	0.001	0.001	0.001	0.001	0.001	0.001	0.001	0.001
40-003 (C)	0.001	0.001	0.001	0	0.002	0.002	0.002	0.002	0.002	0.002	0.002	0.002	0.002	0.002	0.002	0.002	0.002
40-004 (V)	0	0.003	0.004	0.005	0.005	0.004	0.005	0.005	0.005	0.005	0.005	0.005	0.005	0.005	0.005	0.005	0.005
40-004 (C)	0	0.001	0.002	0.003	0.004	0.004	0.004	0.004	0.004	0.004	0.004	0.004	0.004	0.004	0.004	0.004	0.004
40-005 (V)	0.001	0.0015	0.0025	0.004	0.005	0.005	0.005	0.005	0.005	0.005	0.005	0.005	0.005	0.005	0.005	0.005	0.005
40-005 (C)	0	0	0	0	0.001	0.001	0.001	0.001	0.001	0.001	0.001	0.001	0.001	0.001	0.001	0.001	0.001

a) Initial bias in Δa_p from panel straightening

Table 5C Comparison of Visual (V) vs. Compliance Indicated (C) Crack Growth (Δa_p)
at Selected Unloading Points for CT Specimens

Specimen Number	Crack Length Difference (in.)												
	V	C	0	.001	.0005	0	.002	.005	.037	.060	.067	.160	.259
BH003													
	V	C	0	.001	.0005	.001	.003	.007	.010	.030	.063	.147	.247
BH008													
	V	C	0	.0005	0	.001	.003	.006	.012	.020	.112	.164	.260
WH-11													
	V	C	0	.001	.0005	.001	.003	.029	.062	.109	.222	.216	.237
WH-12													
	V	C	0	.002	.008	.006	.031	.058	.103	.126	.157	.206	.247
WH-13A													
	V	C	0	.001	.007	.010	.020	.041	.067	.114	.135	.163	.187
WH-14A													
	V	C	0	.014	.013	.026	.050	.062	.105	.166	.203	.218	.249

Table 6 C Fatigue Precracking Information

Product Form	Spec. No.	<u>Load</u>		<u>Crack Length</u>		<u>Cycles</u>
		P_{max}	P_{min}	a_{rear}	a_{front}	N
		(lb)	(lb)	(in.)	(in.)	
WM-CCT	001	2500	250	0.038	0.041	29,000
	002	2500	250	0.035	0.040	35,000
	003	2500	250	0.045	0.049	35,000
	004	2500	250	0.035	0.040	35,000
	005	2500	250	0.035	0.039	31,000
	006	2840	284	0.041	0.037	25,000
	007	2500	250	0.036	0.038	29,000
	008	2500	250	0.040	0.040	30,000
	009	2500	250	0.039	0.036	30,000
BM-CCT	001	2500	250	0.035	0.038	20,000
	002	2500	250	0.042	0.042	-
	003	2500	250	0.040	0.040	28,000
	004	-	-	-	-	-
	005	2850	285	0.038	0.039	30,000
	006	2500	250	0.038	0.043	30,000
	007	2500	250	0.037	0.037	25,000
	008	2500	250	0.035	0.038	28,000
	009	2840	284	0.044	0.040	25,000
WM-CT	WM11	270	100	0.050	0.050	15,000
	WM12	270	100	0.050	0.054	15,750
	WM13A	270	100	0.053	0.046	18,500
	WM14A	270	100	0.050	0.050	16,500
BM-CT	BM003	270	100	0.050	0.050	16,000
	BM008	270	100	0.050	0.050	16,500

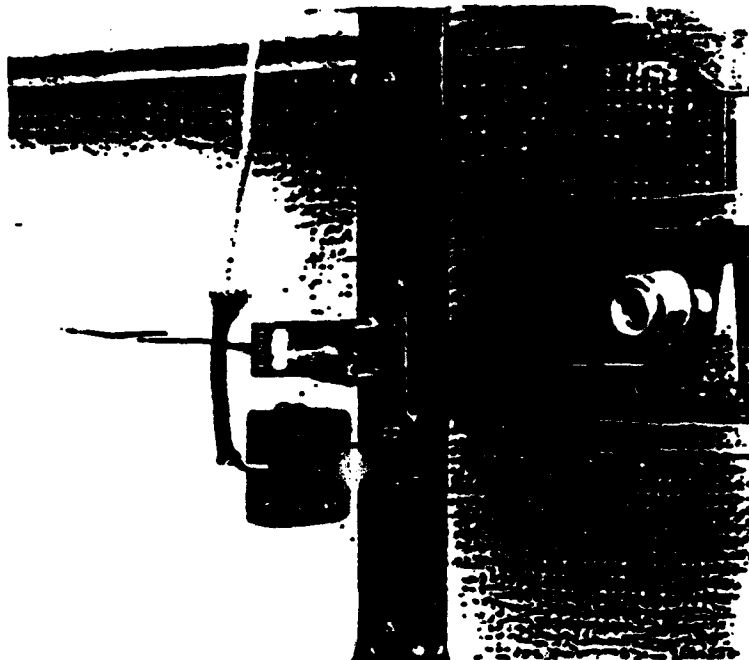


Fig. 2C Clip gage attachment setup for
6-inch gage length.

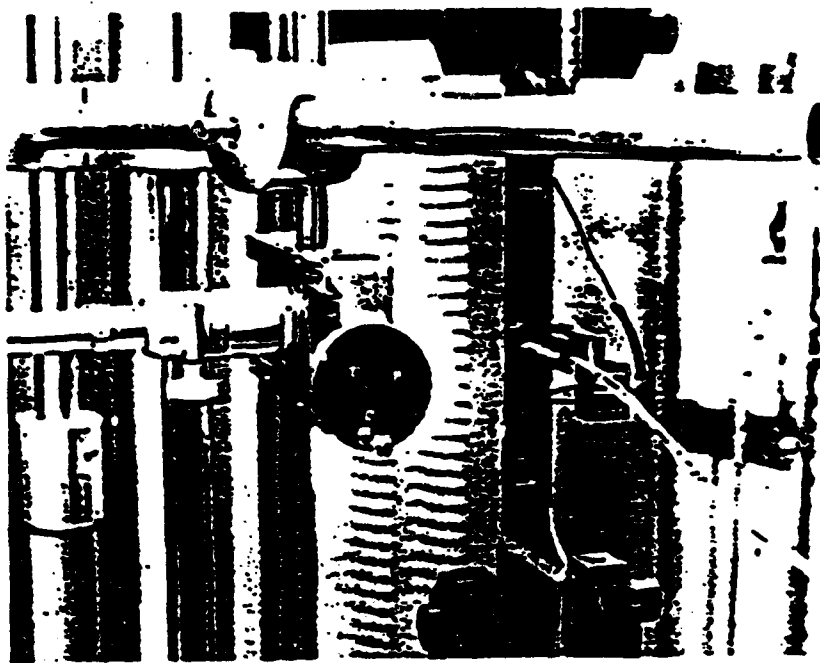
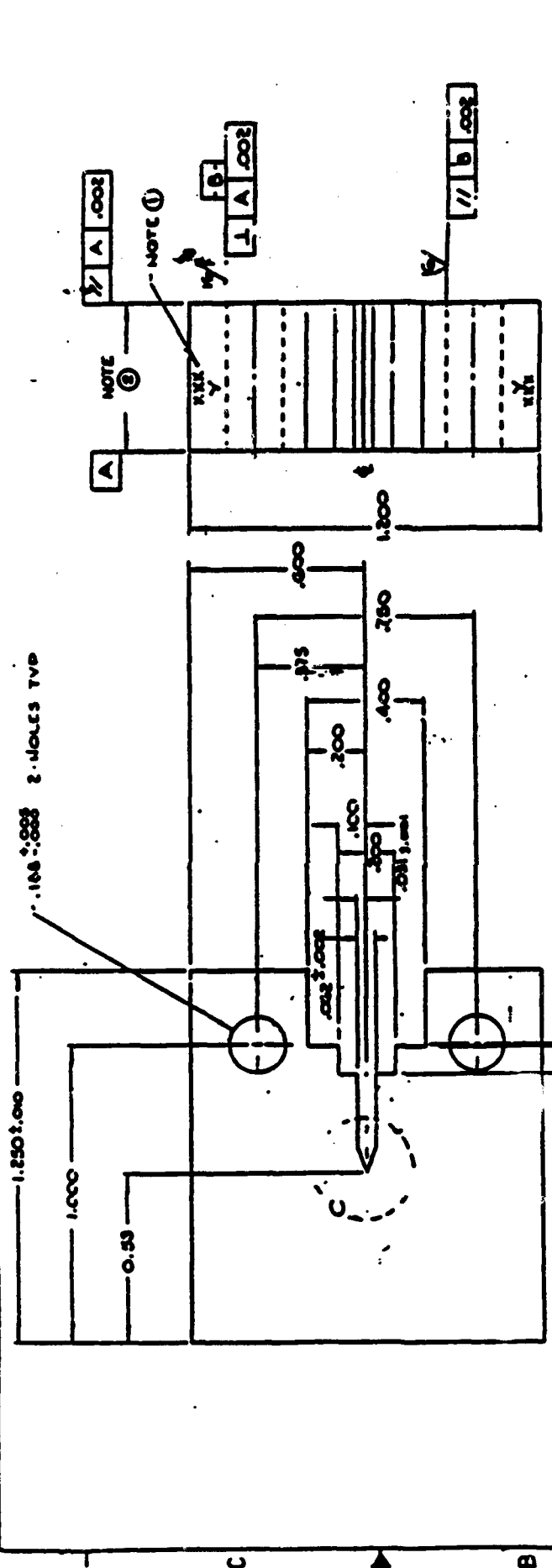


Fig. 3C View of DSST gage and traveling stage
microscope for measuring slow-stable
crack growth.

[illegible]

NOTES:
 ① TAMP SPECIMEN CODE N9(NNE)
 TWO PLACES AS SHOWN
 ② SPECIFIED ARGE 0.090".

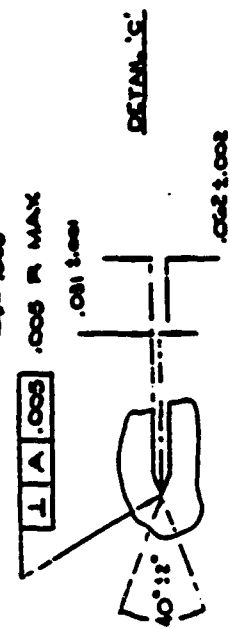


Fig. 4C 1/2T compact specimen.

ATTACHING LABEL 007. MICROFILMED		1. STANDARDIZATION This document is a standard for the purpose of establishing uniformity in the use of the term "standardization" and its derivatives. It is not intended to be used as a basis for legal action.		2. SCOPE This document applies to the use of the term "standardization" and its derivatives in the field of information science.		3. DEFINITIONS For the purposes of this document, the following definitions apply: 3.1 Standardization is the process of establishing and applying standards. 3.2 Standard is a document which provides a basis for uniformity in the use of a term or a process.		4. TERMINOLOGY The following terms are defined in this document: 4.1 Standardization is the process of establishing and applying standards. 4.2 Standard is a document which provides a basis for uniformity in the use of a term or a process.		5. REFERENCES The following references are cited in this document: 5.1 ISO 15924:1980 - Information science - Standardization - Vocabulary		6. NOTES The following notes are included in this document: 6.1 NOTE 1 - This document is a standard for the purpose of establishing uniformity in the use of the term "standardization" and its derivatives. It is not intended to be used as a basis for legal action.		7. APPENDIX The following appendix is included in this document: 7.1 APPENDIX A - List of standardization organizations		8. INDEX The following index is included in this document: 8.1 INDEX - List of terms and their definitions		9. FIGURES The following figures are included in this document: 9.1 FIGURE 1 - Diagram of the standardization process		10. TABLES The following tables are included in this document: 10.1 TABLE 1 - List of standardization organizations		11. FORMS The following forms are included in this document: 11.1 FORM 1 - Standardization form		12. OTHER The following other information is included in this document: 12.1 OTHER - List of standardization organizations																																																																															
13. REVISIONS The following revisions are included in this document: 13.1 REVISION 1 - First revision		14. APPROVALS The following approvals are included in this document: 14.1 APPROVAL 1 - First approval		15. REVISIONS The following revisions are included in this document: 15.1 REVISION 1 - First revision		16. APPROVALS The following approvals are included in this document: 16.1 APPROVAL 1 - First approval		17. REVISIONS The following revisions are included in this document: 17.1 REVISION 1 - First revision		18. APPROVALS The following approvals are included in this document: 18.1 APPROVAL 1 - First approval		19. REVISIONS The following revisions are included in this document: 19.1 REVISION 1 - First revision		20. APPROVALS The following approvals are included in this document: 20.1 APPROVAL 1 - First approval		21. REVISIONS The following revisions are included in this document: 21.1 REVISION 1 - First revision		22. APPROVALS The following approvals are included in this document: 22.1 APPROVAL 1 - First approval		23. REVISIONS The following revisions are included in this document: 23.1 REVISION 1 - First revision		24. APPROVALS The following approvals are included in this document: 24.1 APPROVAL 1 - First approval		25. REVISIONS The following revisions are included in this document: 25.1 REVISION 1 - First revision		26. APPROVALS The following approvals are included in this document: 26.1 APPROVAL 1 - First approval		27. REVISIONS The following revisions are included in this document: 27.1 REVISION 1 - First revision		28. APPROVALS The following approvals are included in this document: 28.1 APPROVAL 1 - First approval		29. REVISIONS The following revisions are included in this document: 29.1 REVISION 1 - First revision		30. APPROVALS The following approvals are included in this document: 30.1 APPROVAL 1 - First approval		31. REVISIONS The following revisions are included in this document: 31.1 REVISION 1 - First revision		32. APPROVALS The following approvals are included in this document: 32.1 APPROVAL 1 - First approval		33. REVISIONS The following revisions are included in this document: 33.1 REVISION 1 - First revision		34. APPROVALS The following approvals are included in this document: 34.1 APPROVAL 1 - First approval		35. REVISIONS The following revisions are included in this document: 35.1 REVISION 1 - First revision		36. APPROVALS The following approvals are included in this document: 36.1 APPROVAL 1 - First approval		37. REVISIONS The following revisions are included in this document: 37.1 REVISION 1 - First revision		38. APPROVALS The following approvals are included in this document: 38.1 APPROVAL 1 - First approval		39. REVISIONS The following revisions are included in this document: 39.1 REVISION 1 - First revision		40. APPROVALS The following approvals are included in this document: 40.1 APPROVAL 1 - First approval		41. REVISIONS The following revisions are included in this document: 41.1 REVISION 1 - First revision		42. APPROVALS The following approvals are included in this document: 42.1 APPROVAL 1 - First approval		43. REVISIONS The following revisions are included in this document: 43.1 REVISION 1 - First revision		44. APPROVALS The following approvals are included in this document: 44.1 APPROVAL 1 - First approval		45. REVISIONS The following revisions are included in this document: 45.1 REVISION 1 - First revision		46. APPROVALS The following approvals are included in this document: 46.1 APPROVAL 1 - First approval		47. REVISIONS The following revisions are included in this document: 47.1 REVISION 1 - First revision		48. APPROVALS The following approvals are included in this document: 48.1 APPROVAL 1 - First approval		49. REVISIONS The following revisions are included in this document: 49.1 REVISION 1 - First revision		50. APPROVALS The following approvals are included in this document: 50.1 APPROVAL 1 - First approval		51. REVISIONS The following revisions are included in this document: 51.1 REVISION 1 - First revision		52. APPROVALS The following approvals are included in this document: 52.1 APPROVAL 1 - First approval		53. REVISIONS The following revisions are included in this document: 53.1 REVISION 1 - First revision		54. APPROVALS The following approvals are included in this document: 54.1 APPROVAL 1 - First approval		55. REVISIONS The following revisions are included in this document: 55.1 REVISION 1 - First revision		56. APPROVALS The following approvals are included in this document: 56.1 APPROVAL 1 - First approval		57. REVISIONS The following revisions are included in this document: 57.1 REVISION 1 - First revision		58. APPROVALS The following approvals are included in this document: 58.1 APPROVAL 1 - First approval		59. REVISIONS The following revisions are included in this document: 59.1 REVISION 1 - First revision		60. APPROVALS The following approvals are included in this document: 60.1 APPROVAL 1 - First approval		61. REVISIONS The following revisions are included in this document: 61.1 REVISION 1 - First revision		62. APPROVALS The following approvals are included in this document: 62.1 APPROVAL 1 - First approval		63. REVISIONS The following revisions are included in this document: 63.1 REVISION 1 - First revision		64. APPROVALS The following approvals are included in this document: 64	

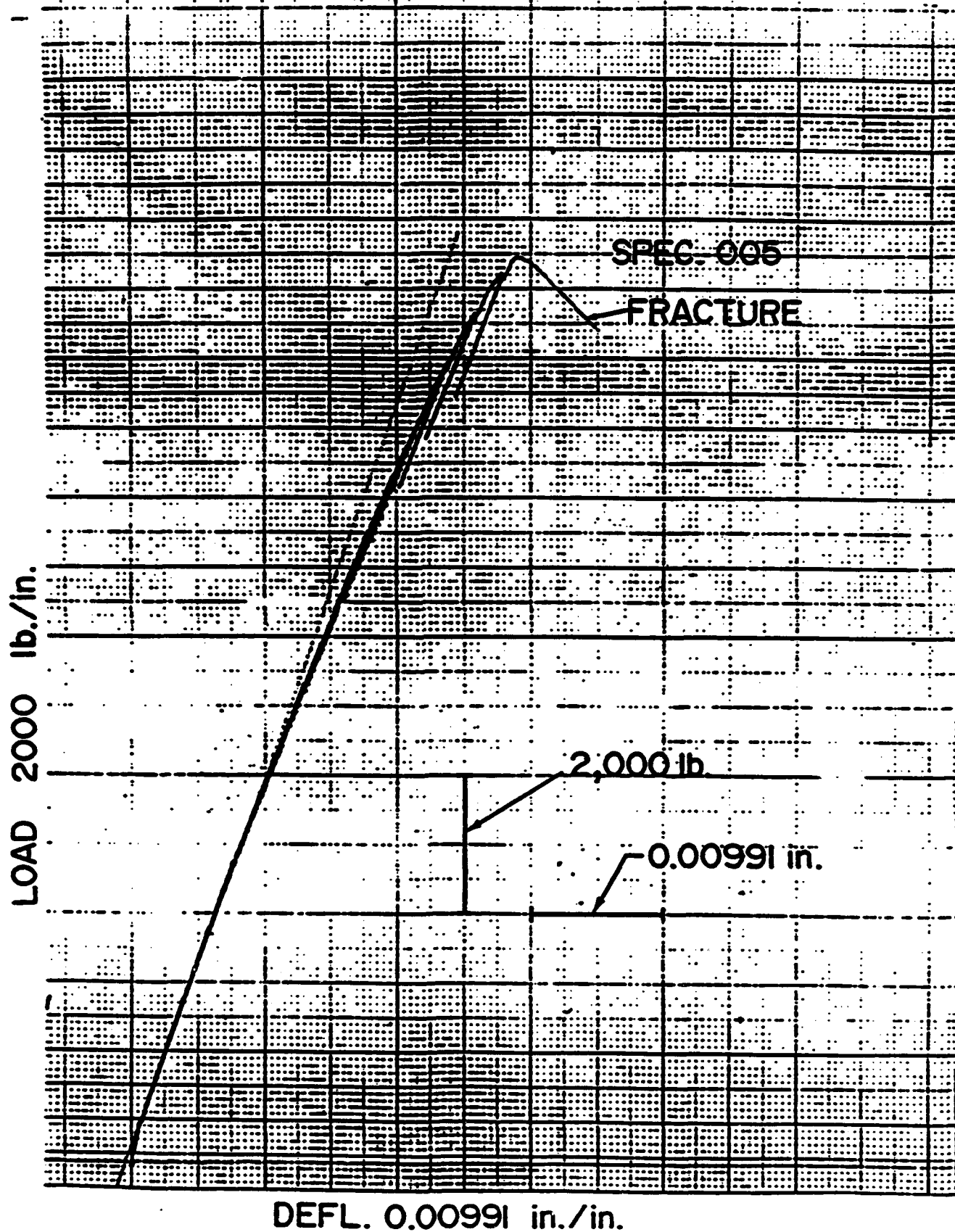
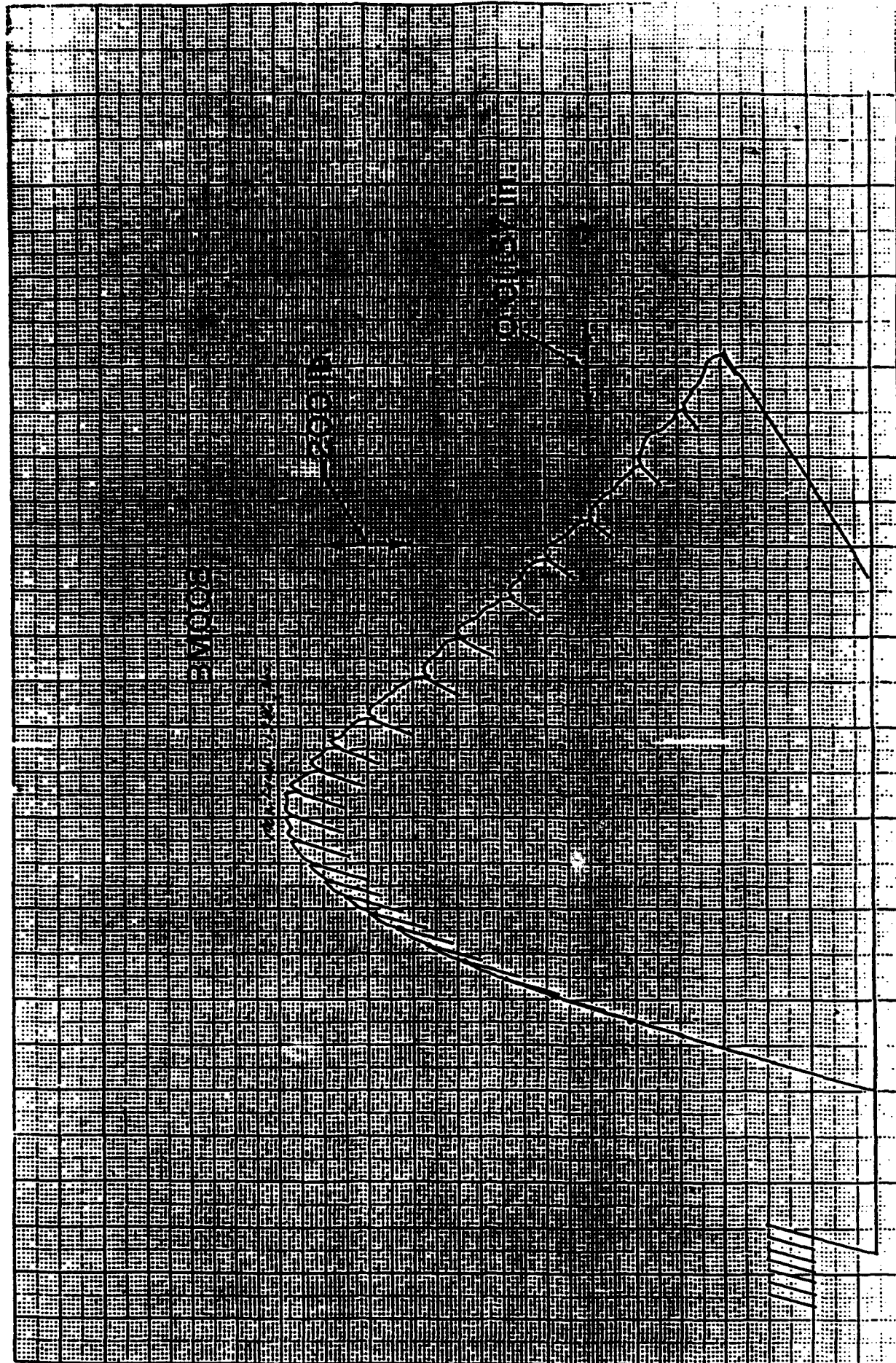


Fig. 5C Representative load-displacement record, CCT panel.
C-51

LOAD 200 lb./in.



DEFL. 0.01137 in./in

Fig. 6C Representative load-displacement record, compact specimen.

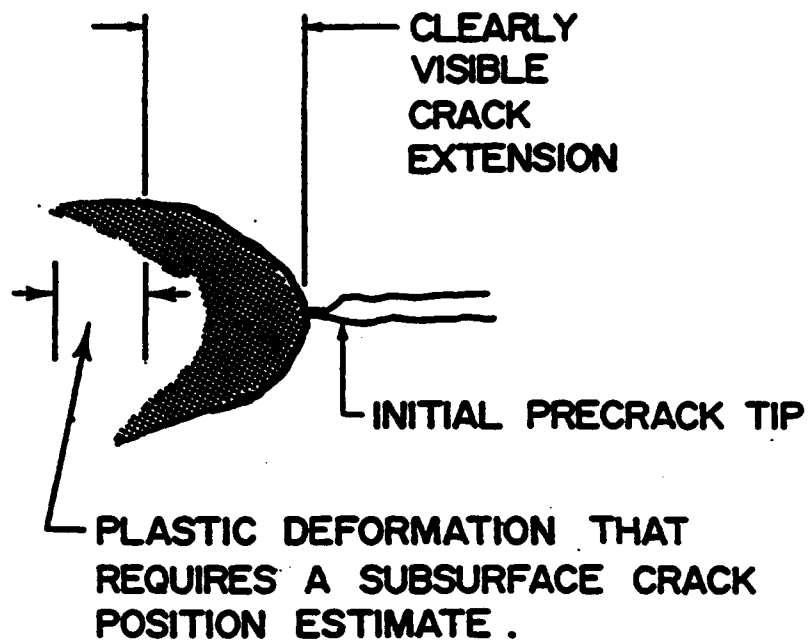


Fig. 7C Magnified view of crack tip region after considerable slow-stable crack extension.

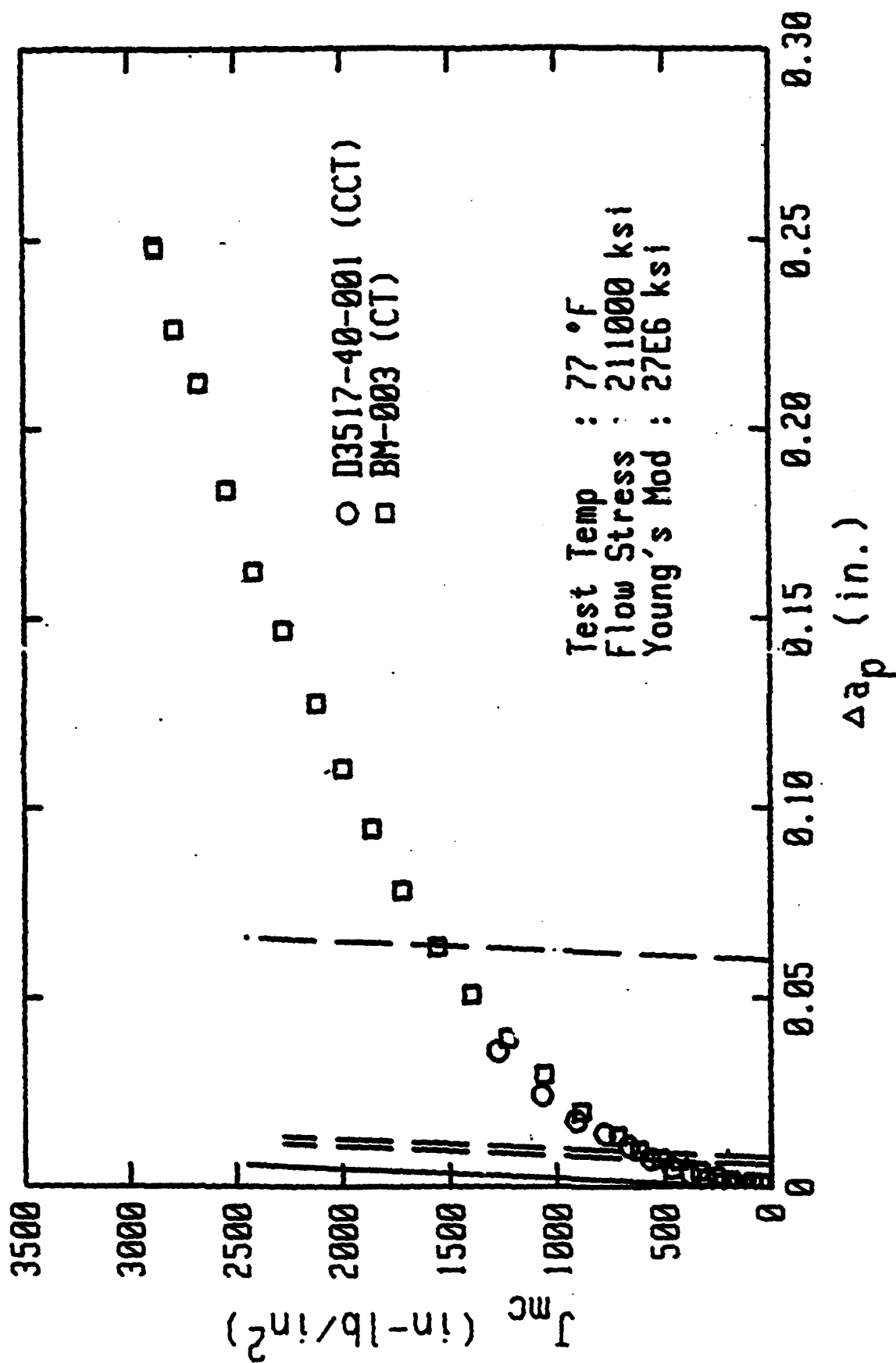


Fig. 8C Compact specimen and center cracked panel J_R -curves for unaged base metal.

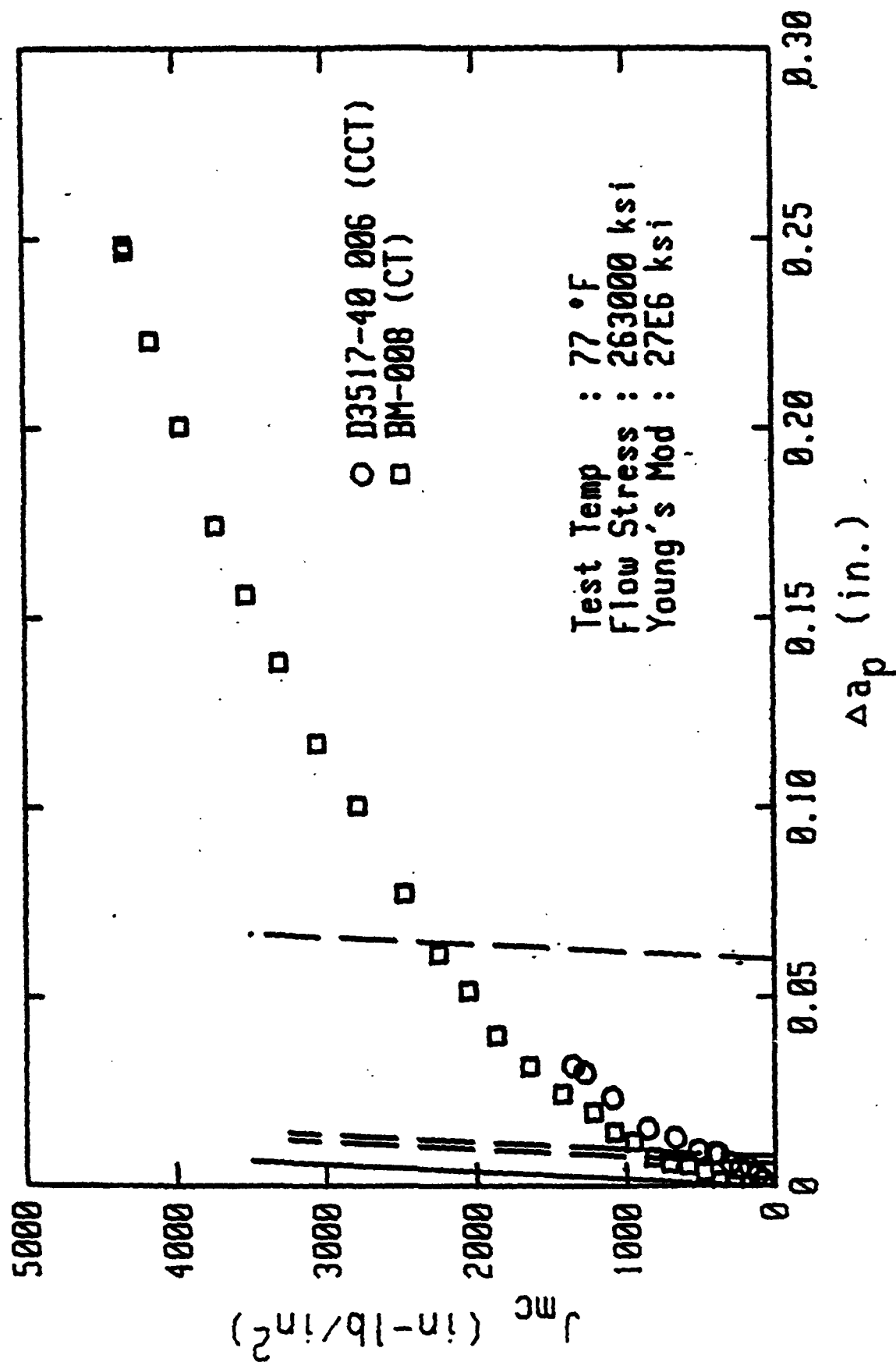


Fig. 9C Compact specimen and center cracked panel J_g -curves for aged base metal.

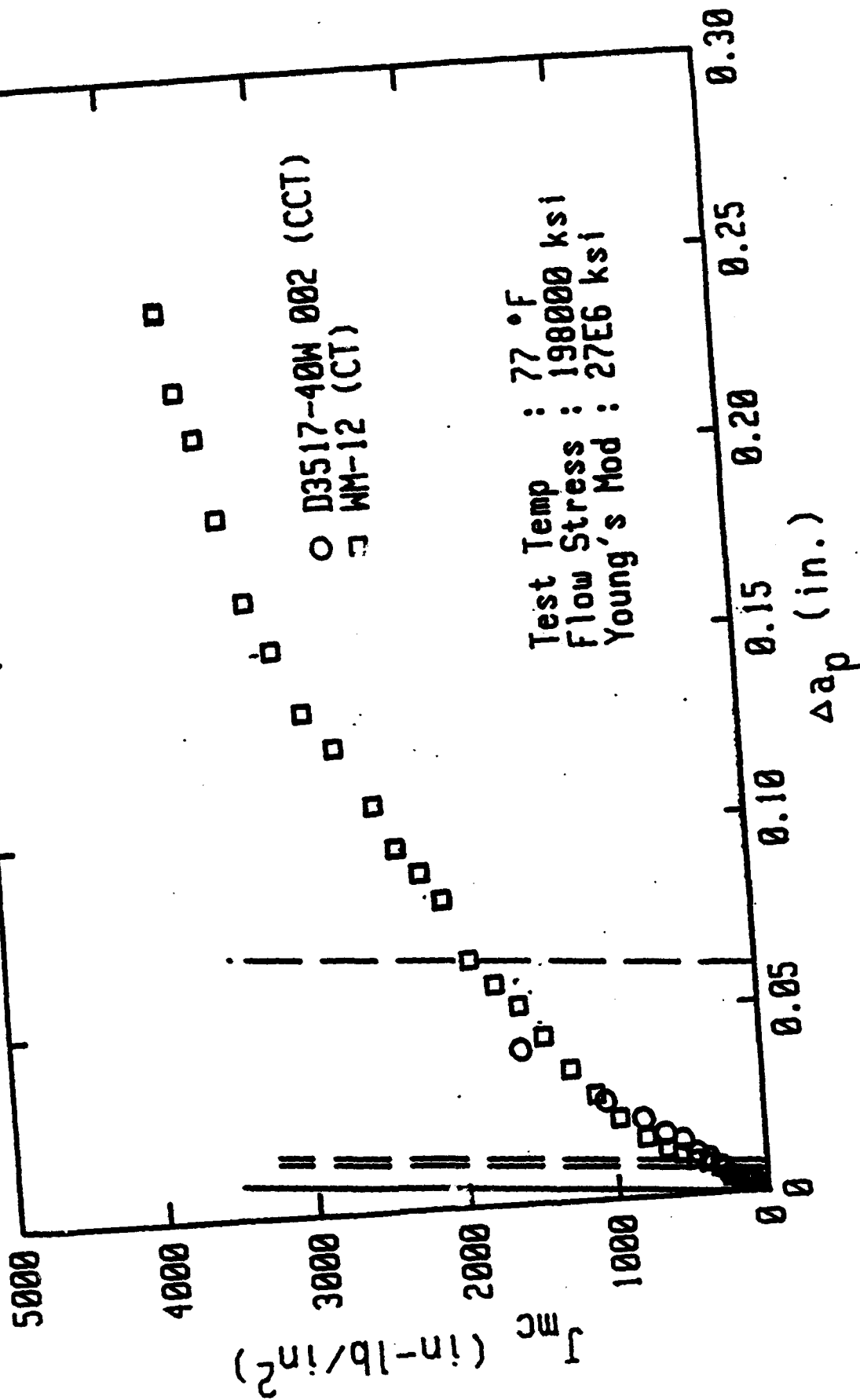


Fig. 10C Compact specimen and center cracked panel J_{IC} -curves for
 unused weld metal.

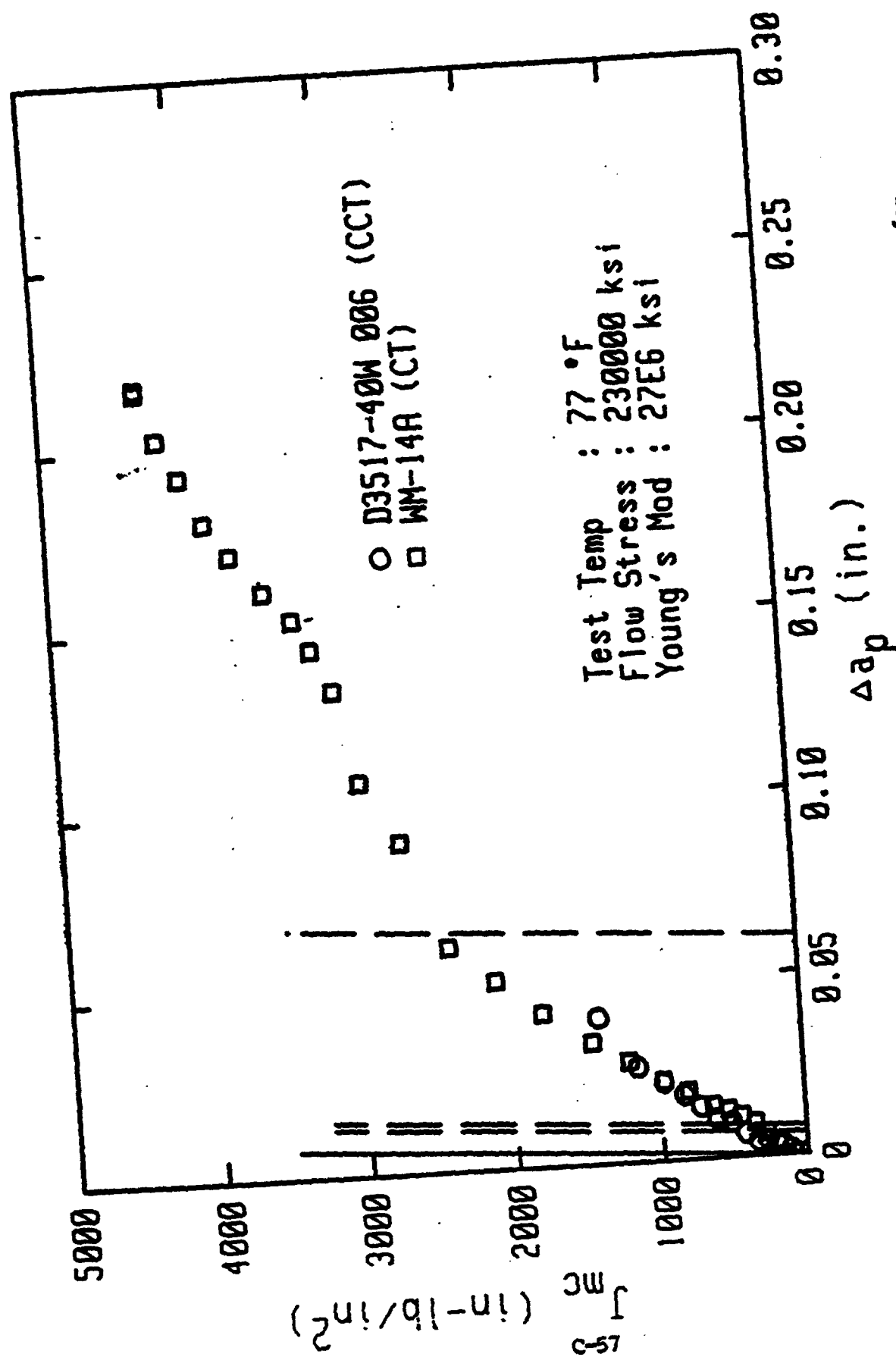
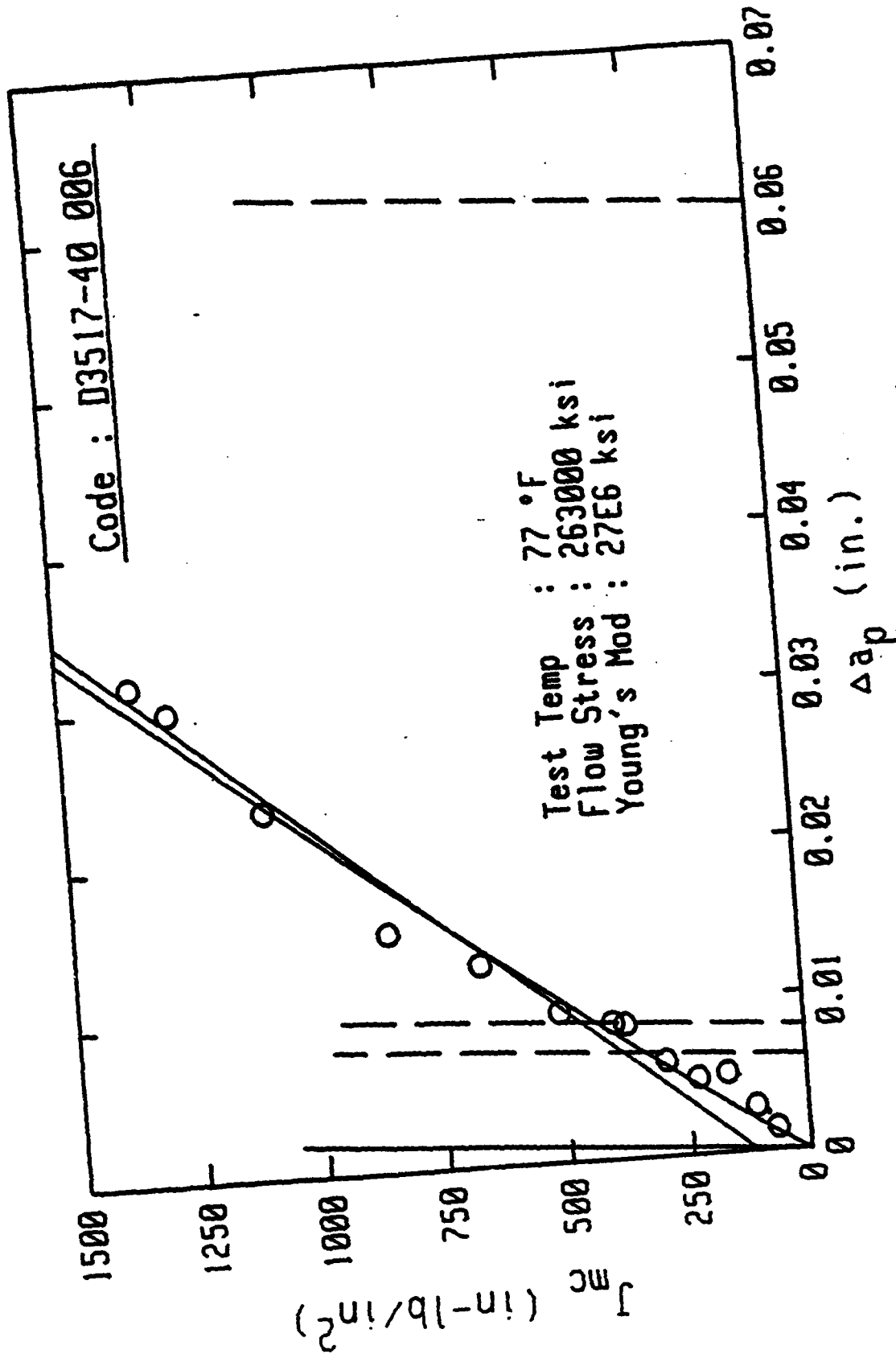


Fig. 11C Compact specimen and center cracked panel J_R-curves for aged weld metal.

APPENDIX III
R-CURVES AND TABULATED DATA

Definitions:

- J_{pl} The intersection of the power law curve, Eq. 6, with the 0.008-in. offset.
- K_{pl} $\sqrt{J_{pl}E}$
- r Correlation coefficient of regression analysis.
- J_{ic} The intersection of the linear regression line with the blunting line. Not validated by E813.
- K_{ic} $\sqrt{J_{ic}E}$ not E399 validated.
- J_{mc} J by Eq. 1
- J_{bt} J by Eqs. 1 through 3 using DSST gage output
- $J(K_p)$ J by Eq. 4
- K_c $\sqrt{J_{mc}E}$ at last unload prior to instability.
- J_H Modified J



Thickness : 0.094 in.
Initial a : 0.292 in.

$J_{p1} = 433.1 \text{ in-lb/in}^2$
 $K_{p1} = 108.1 \text{ ksi}\sqrt{\text{in}}$
 $r = 0.982$

$J_{Ic} = 120.6 \text{ in-lb/in}^2$
 $K_{Ic} = 57.1 \text{ ksi}\sqrt{\text{in}}$
 $r = 0.9849$

Toughness 3

Event	Load lb	Jac in-lb/in ²	Jbt in-lb/in ²	J(Kr) in-lb/in ²	del-ap in.
1	2522	16.4	16.4	34.3	0.0000
2	3406	34.7	21.3	53.2	0.0000
3	4454	66.4	33.3	82.6	0.0014
4	5603	100.2	52.2	120.8	0.0029
5	6739	166.3	79.8	166.6	0.0051
6	7722	227.7	110.7	214.4	0.0048
7	8717	293.3	143.3	269.9	0.0061
8	9711	373.1	195.2	336.5	0.0085
9	10256	397.7	209.4	356.3	0.0086
10	11282	506.9	278.0	449.4	0.0095
11	12712	662.8	382.1	582.4	0.0120
12	14065	847.6	519.8	746.2	0.0152
13	15257	1088.8	742.0	979.9	0.0233
14	15967	1275.7	926.2	1175.0	0.0298
15	16146	1349.7	992.6	1248.3	0.0316

$P_{max} = 16340 \text{ (lb)}$
 $\% \text{ Stress} = 237866 \text{ (psi)}$

Code : D33517-40 007

J (in-lb/in²)

C-62

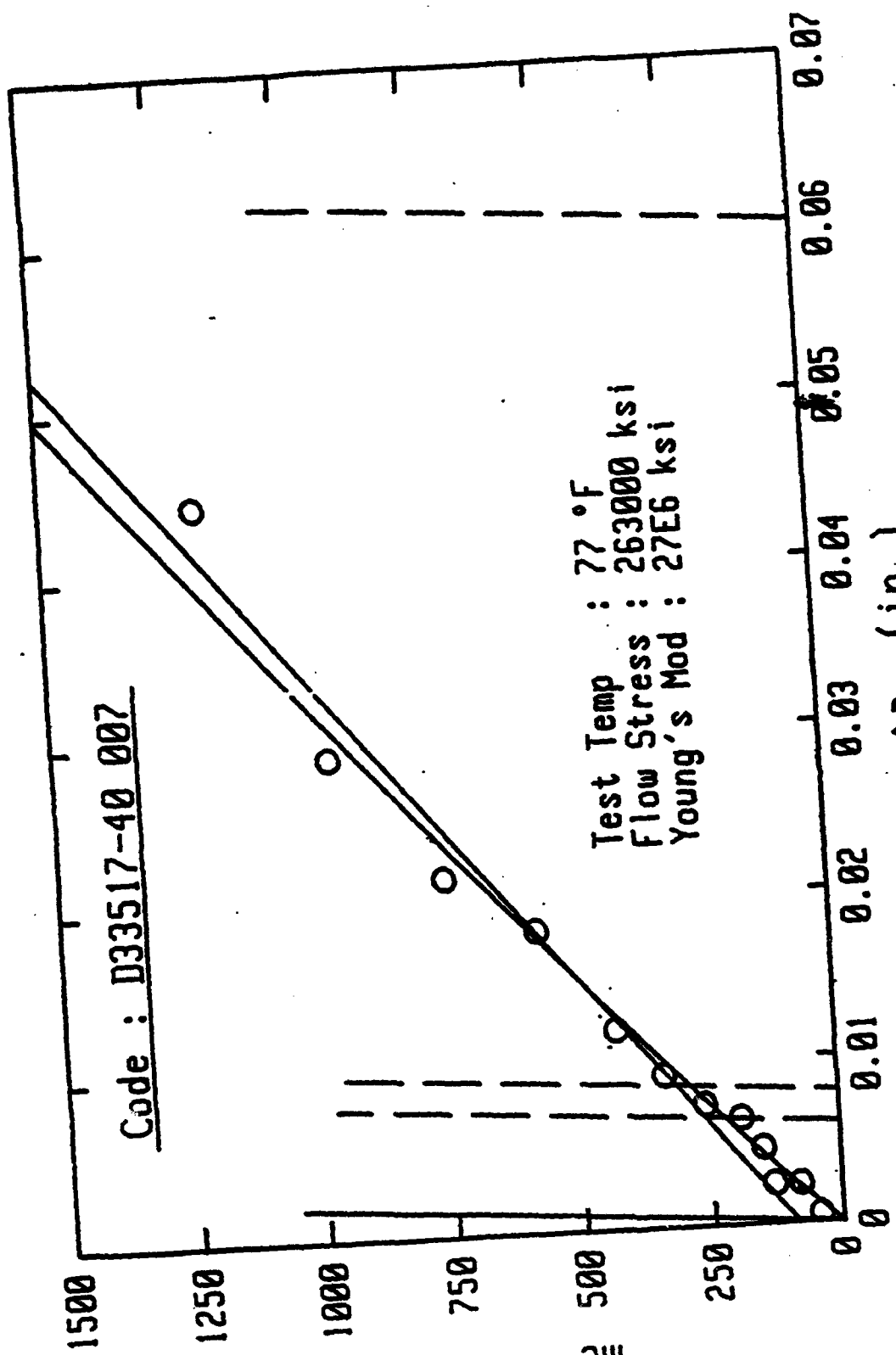
Test Temp : 77 °F
 Flow Stress : 263000 ksi
 Young's Mod : 27E6 ksi

Δa_p (in.)

$J_{p1} = 286.9 \text{ in-lb/in}^2$
 $K_{p1} = 88 \text{ ksi}\sqrt{\text{in}}$
 $r = 0.9892$

$J_{Ic} = 90.5 \text{ in-lb/in}^2$
 $K_{Ic} = 49.4 \text{ ksi}\sqrt{\text{in}}$
 $r = 0.9848$

Thickness : 0.092 in.
 Initial a : 0.293 in.



Specimen Code : D33517-42 037

Toughness J

Event	Load lb	Jac in-lb/in ²	Jbt in-lb/in ²	J(Kr) in-lb/in ²	del-ap in.
1	4003	43.0	43.0	151.2	0.0005
2	4984	79.5	36.2	190.5	0.0024
3	6034	129.7	35.6	240.4	0.0024
4	6484	148.4	35.2	257.9	0.0046
5	7088	188.3	40.6	296.4	0.0064
6	8117	257.4	55.9	362.1	0.0073
7	9087	335.6	76.9	431.5	0.0091
8	10846	423.1	108.9	511.9	0.0120
9	11445	568.9	177.5	653.3	0.0181
10	12767	741.6	265.7	815.0	0.0215
11	13978	955.0	390.8	1010.9	0.0289
12	15133	1195.6	582.9	1277.6	0.0442

Pmax = 15500 (lb)
Net Stress = 238120 (psi)

Code : D3517-40 008

J_{IC} (in-lb/in²)

C-64

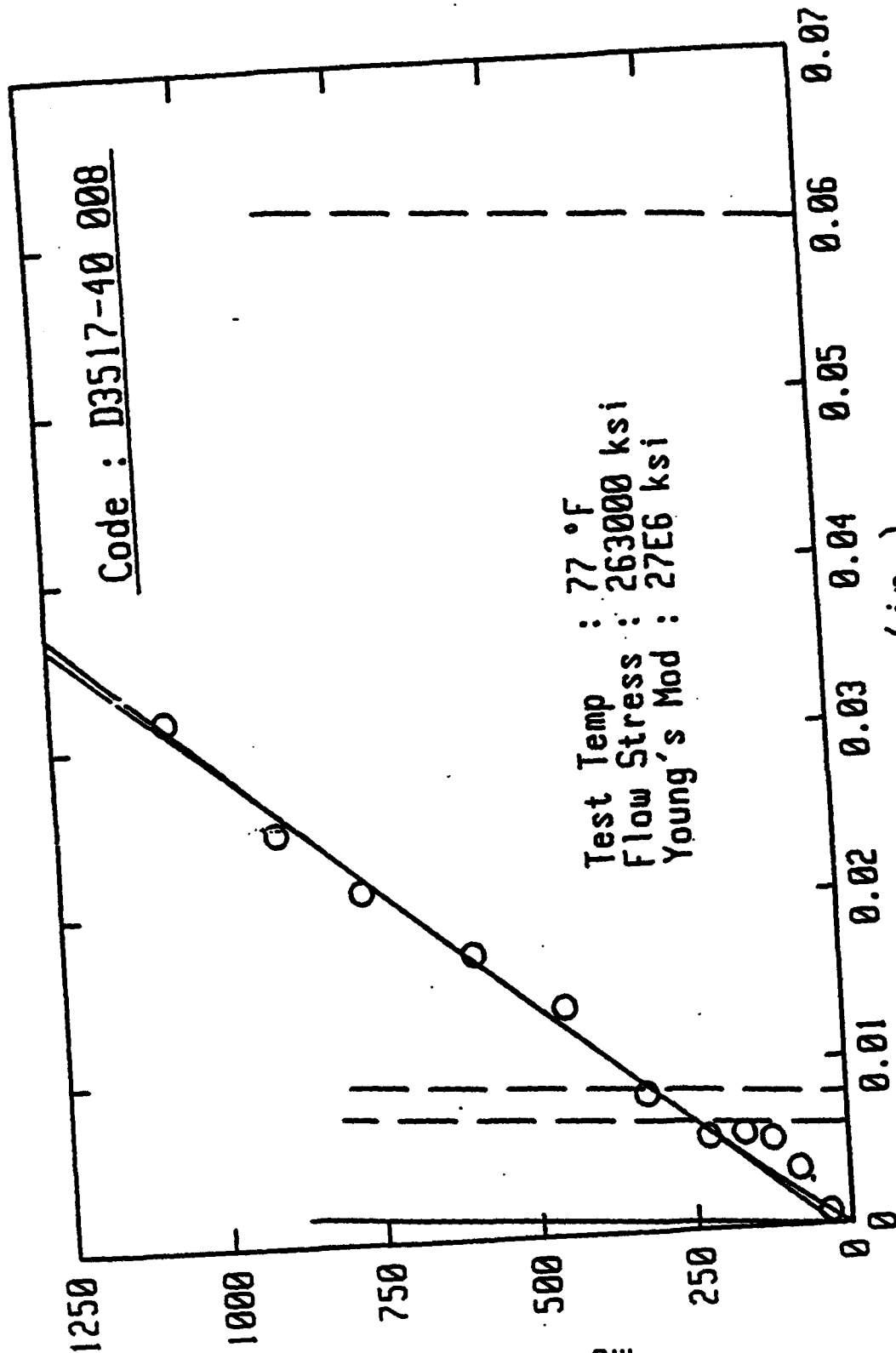
Test Temp : 77 °F
Flow Stress : 263000 ksi
Young's Mod : 27E6 ksi

Δa_p (in.)

$J_{IC} = 31.6$ in-lb/in²
 $K_{IC} = 29.1$ ksi√in
 $r = 0.9936$

$J_{p1} = 315.1$ in-lb/in²
 $K_{p1} = 92.2$ ksi√in
 $r = 0.9922$

Thickness : 0.092 in.
Initial a : 0.289 in.

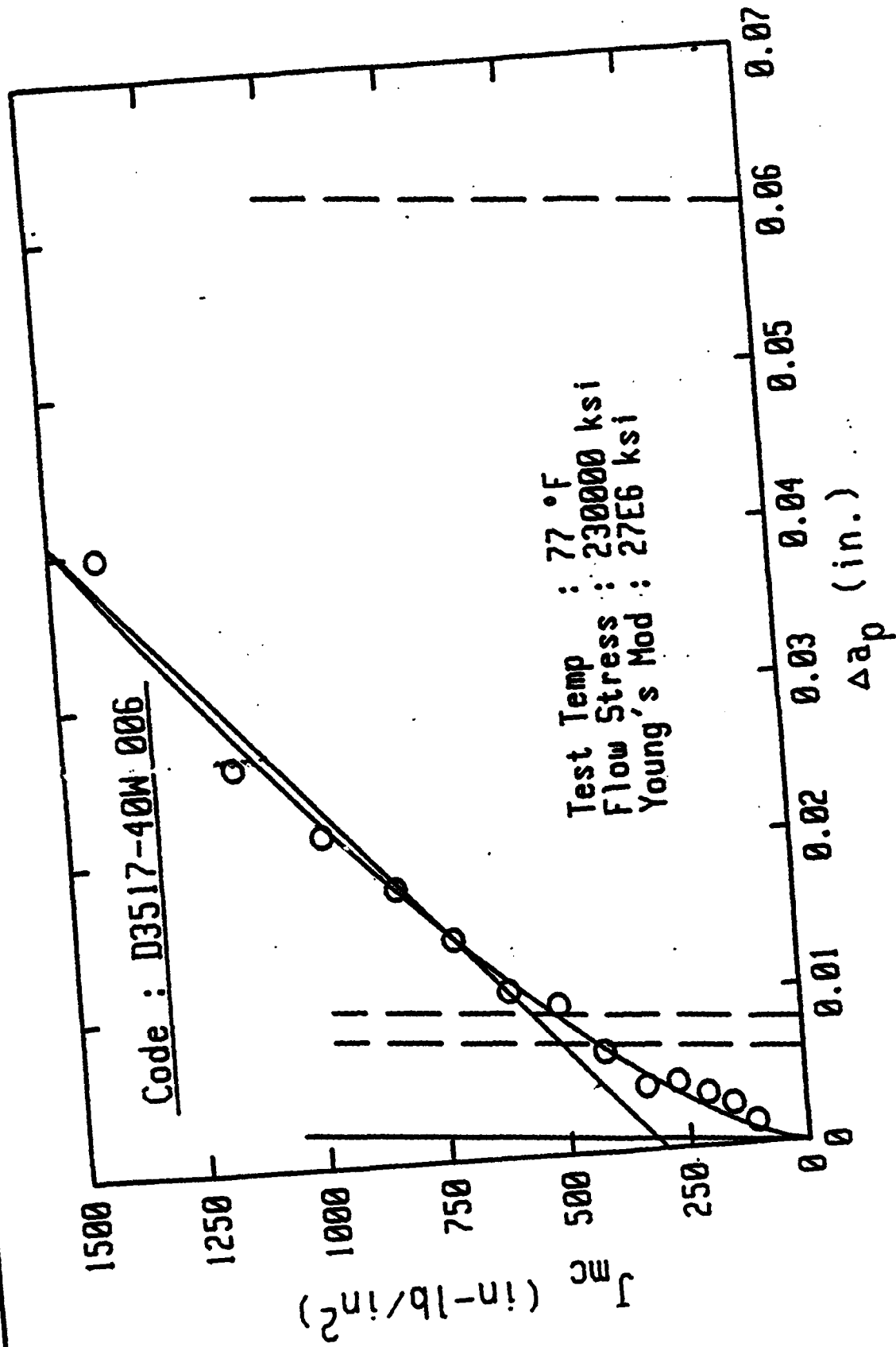


Specimen Code : B3517-4E C8E

Toughness J

Event	Load lb	Jac in-lb/in ²	Jbt in-lb/in ²	J(Kr) in-lb/in ⁴	del-ap in.
1	2529	16.9	16.9	38.2	0.0000
2	3428	34.8	20.1	57.4	0.0008
3	5083	80.7	39.3	105.6	0.0035
4	6167	121.5	59.2	144.7	0.0053
5	7144	166.7	84.7	187.2	0.0057
6	8208	224.3	118.3	239.8	0.0055
7	9679	321.7	183.3	329.9	0.0082
8	11146	-447.8	271.7	443.6	0.0136
9	12558	588.7	382.8	579.7	0.0170
10	13835	763.8	516.2	738.9	0.0210
11	14658	896.8	628.3	867.5	0.0246
12	15442	1065.6	778.8	1031.1	0.0315

Pmax = 16200 (lb)
Net Stress = 238310 (psi)



Thickness : 0.095 in.
Initial a : 0.298 in.

$J_{pl} = 518.4 \text{ in-lb/in}^2$
 $K_{pl} = 118.3 \text{ ksi}\sqrt{\text{in}}$
 $r = 0.9919$

$J_{Ic} = 319.3 \text{ in-lb/in}^2$
 $K_{Ic} = 92.8 \text{ ksi}\sqrt{\text{in}}$
 $r = 0.9825$

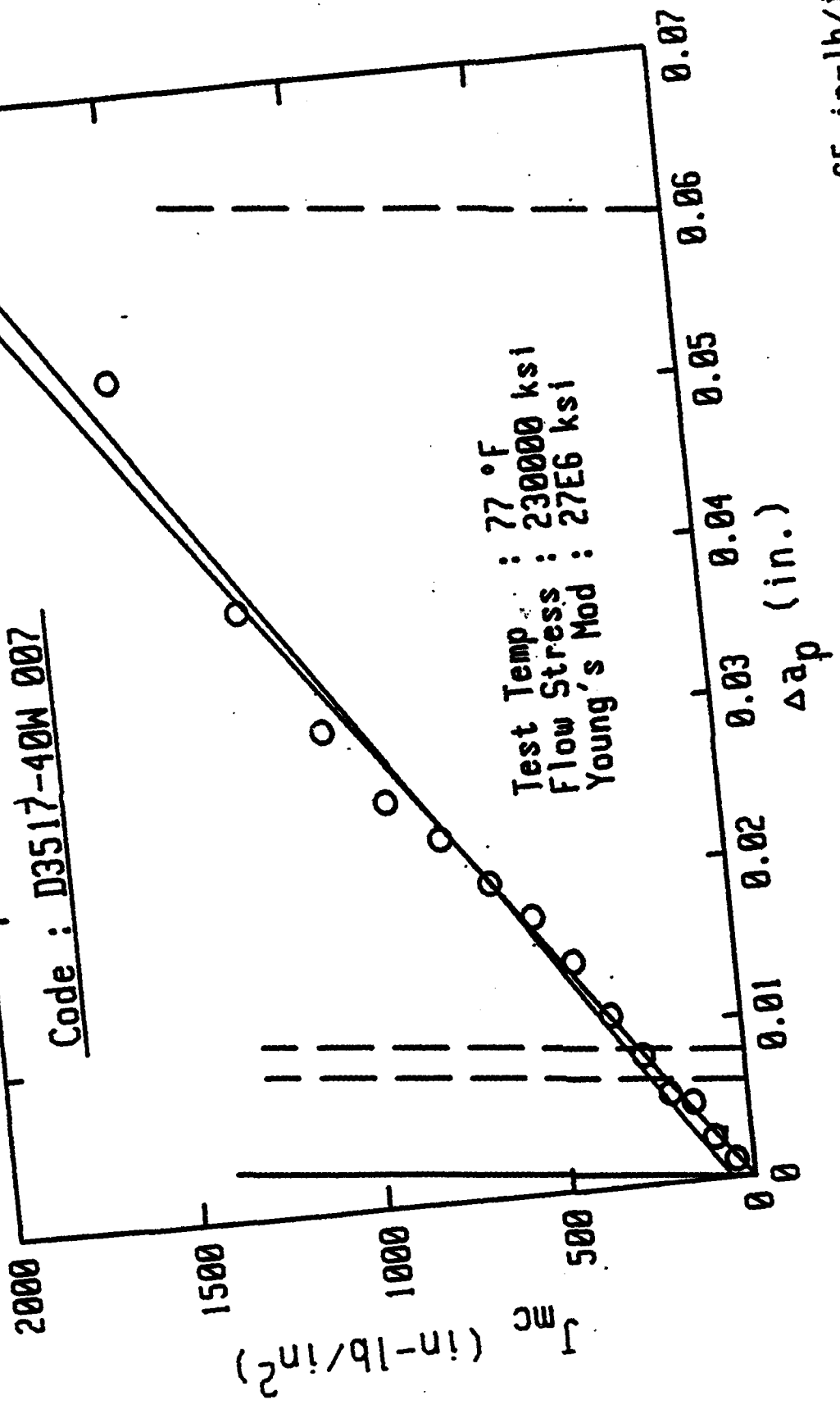
Specimen Code : D3517-46W 026

Toughness J

Event	Load lb	Jac in-lb/in ²	Jbt in-lb/in ²	J(Kr) in-lb/in ²	del-ap in.
1-	2537	16.6	16.6	35.6	0.0000
2	3523	37.7	22.3	57.5	0.0000
3	4579	67.9	34.6	87.5	0.0000
4	5627	106.0	52.4	123.5	0.0015
5	6631	151.8	75.7	164.7	0.0027
6	7643	204.6	105.2	212.7	0.0034
7	8621	266.9	141.4	267.0	0.0042
8	9520	333.5	181.0	323.8	0.0041
9	10497	416.6	234.3	395.6	0.0064
10	11407	507.1	298.0	476.1	0.0096
11	12301	607.8	373.7	569.0	0.0106
12	13166	715.2	463.9	676.4	0.0141
13	13972	827.2	559.8	798.7	0.0176
14	14791	972.7	686.1	937.1	0.0212
15	15504	1149.0	850.3	1115.7	0.0258
16	16008	1401.3	1109.5	1372.8	0.0398

P_{max} = 16100 (lb)
Net Stress = 239800 (psi)

Code : D3517-40W 007



Test Temp : 77 °F
 Flow Stress : 230000 ksi
 Young's Mod : 27E6 ksi

$J_{Ic} = 65 \text{ in-lb/in}^2$
 $K_{Ic} = 41.9 \text{ ksi}\sqrt{\text{in}}$
 $r = 0.9875$

$J_{pl} = 284 \text{ in-lb/in}^2$
 $K_{pl} = 87.6 \text{ ksi}\sqrt{\text{in}}$
 $r = 0.9938$

Thickness : 0.092 in.
 Initial a : 0.2885 in.

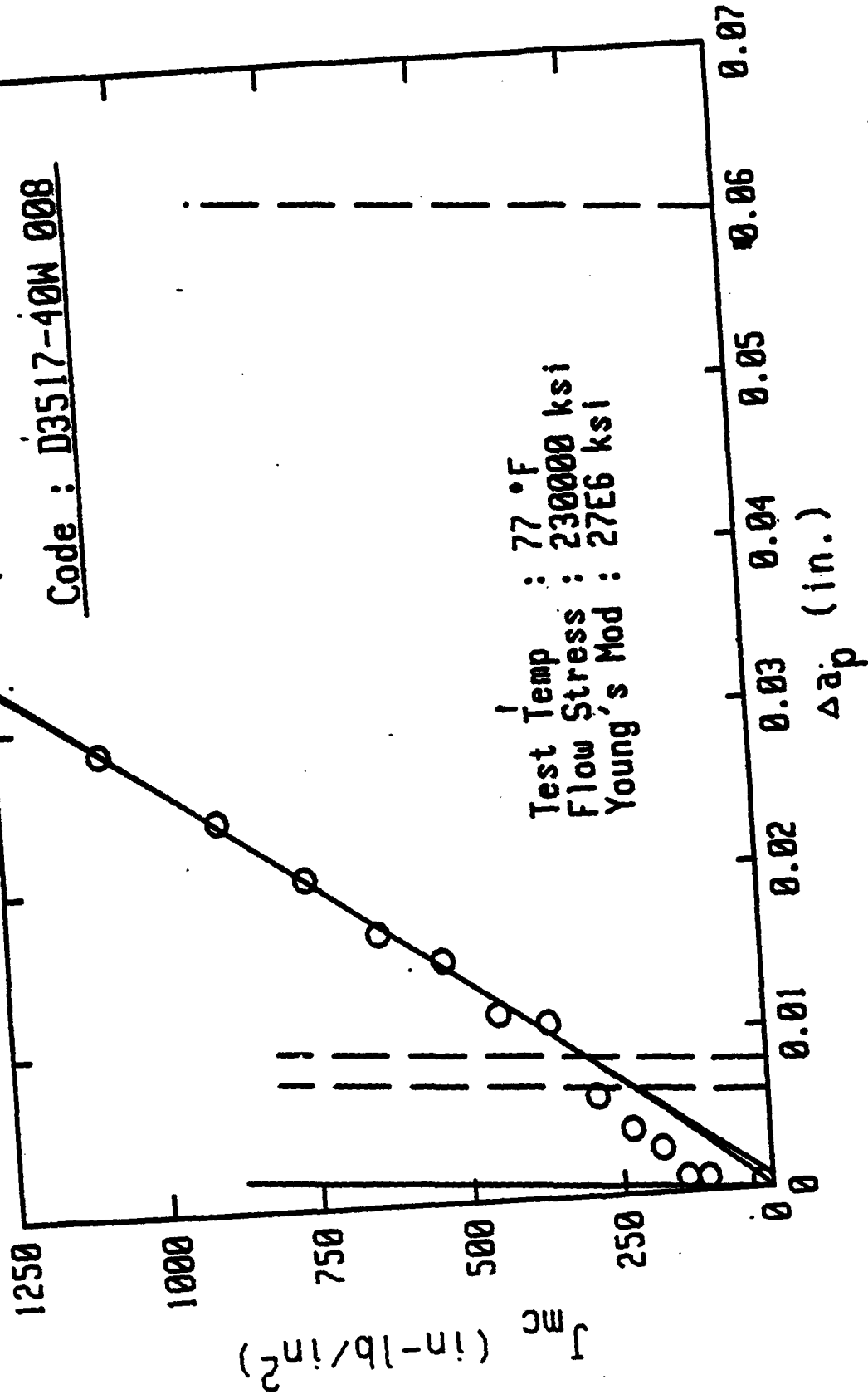
Specimen Code : 83517-42X 837

Toughness J

Event	Load lb	Jac in-lb/in ²	Jbt in-lb/in ²	J(Kr) in-lb/in ²	del-ap in.
1	2449	15.8	15.8	35.1	0.0000
2	3602	46.5	22.7	61.8	0.0011
3	5008	98.7	41.3	105.3	0.0026
4	6870	148.2	60.3	144.6	0.0049
5	7134	208.6	86.9	191.2	0.0055
6	9146	273.1	120.1	243.5	0.0080
7	9141	350.9	165.4	306.7	0.0107
8	10897	439.2	220.9	379.6	0.0142
9	11043	538.0	283.3	461.4	0.0171
10	11920	647.0	354.5	551.3	0.0194
11	12770	767.1	436.9	653.6	0.0225
12	13615	901.8	540.7	777.2	0.0250
13	14373	1055.7	650.6	915.8	0.0297
14	15033	1251.0	829.9	1099.8	0.0376
15	15476	1540.2	1115.9	1303.4	0.0525

Pmax = 15400 (lb)
Net Stress = 239810 (psi)

Code : D3517-40W 008



Test Temp : 77 °F
 Flow Stress : 230000 ksi
 Young's Mod : 27E6 ksi

$J_{p1} = 303.6 \text{ in-lb/in}^2$
 $K_{p1} = 90.5 \text{ ksi}\sqrt{\text{in}}$
 $r = 0.9936$

$J_{Ic} = -32.9 \text{ in-lb/in}^2$
 $K_{Ic} = 0 \text{ ksi}\sqrt{\text{in}}$
 $r = 0.9971$

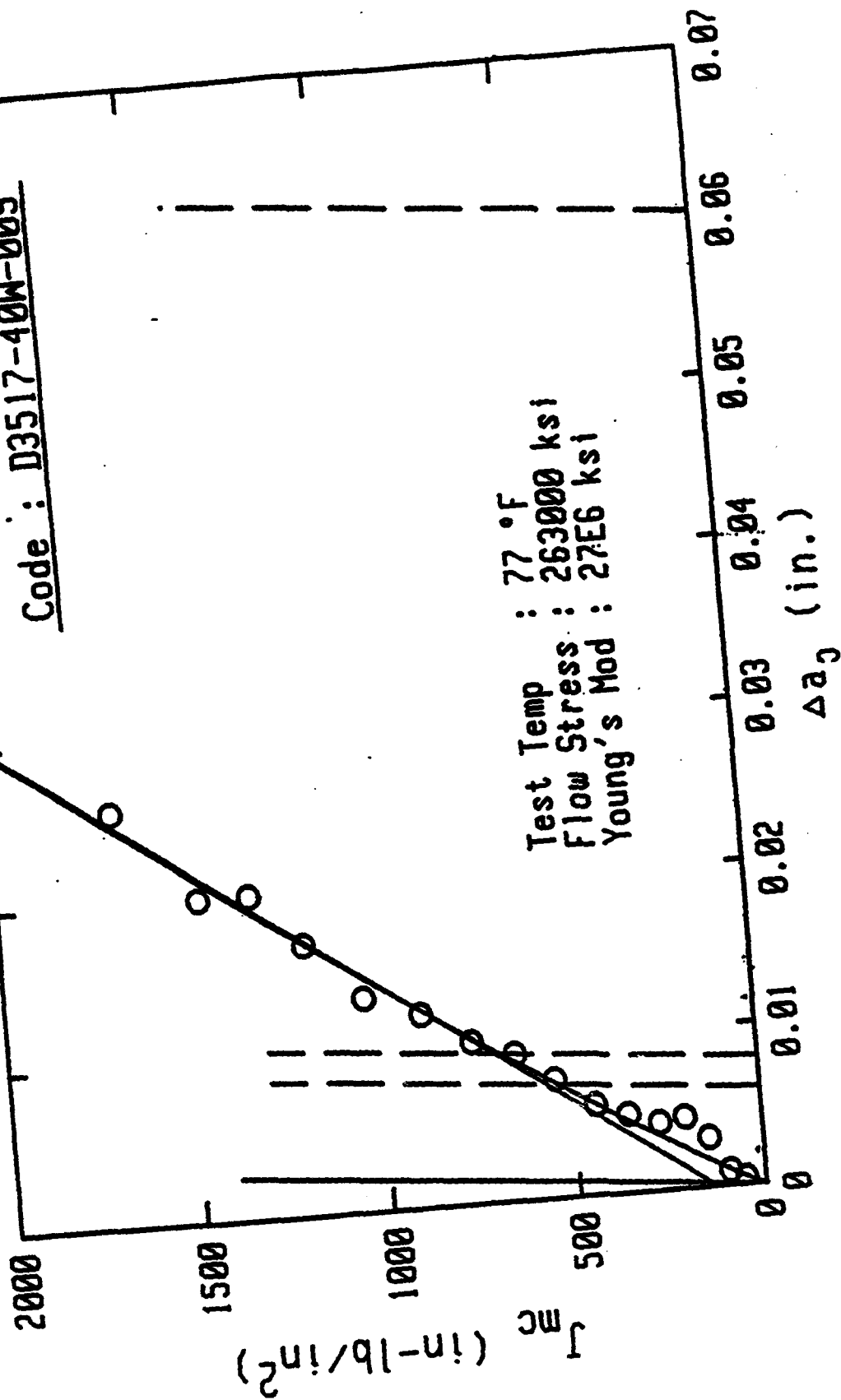
Thickness : 0.095 in.
 Initial a : 0.2915 in.

Toughness J

Event	Load lb	Jac in-lb/in ²	Jbt in-lb/in ²	J(Kr) in-lb/in ²	del-ap in.
1	2529	16.0	16.0	30.3	0.0004
2	3545	31.9	23.8	51.1	0.0008
3	4469	50.9	35.3	74.8	0.0008
4	5513	77.3	54.7	108.8	0.0008
5	6490	106.3	78.0	144.9	0.0009
6	7493	141.8	107.4	188.8	0.0009
7	8491	182.2	142.5	238.7	0.0027
8	9491	229.7	185.4	296.7	0.0040
9	10432	286.6	236.2	361.2	0.0061
10	11384	361.0	304.4	441.9	0.0107
11	12292	443.0	381.9	532.4	0.0114
12	13158	530.1	464.2	629.9	0.0148
13	13998	634.0	558.5	748.8	0.0167
14	14790	751.1	672.3	870.1	0.0202
15	15525	892.0	813.5	1025.8	0.0240
16	16125	1080.7	1006.2	1225.4	0.0284

Pmax = 16508 (lb)
Net Stress = 234670 (psi)

Code : D3517-40W-009



$J_{Ic} = 148.9 \text{ in-lb/in}^2$
 $K_{Ic} = 63.4 \text{ ksi}\sqrt{\text{in}}$
 $r = 0.9896$

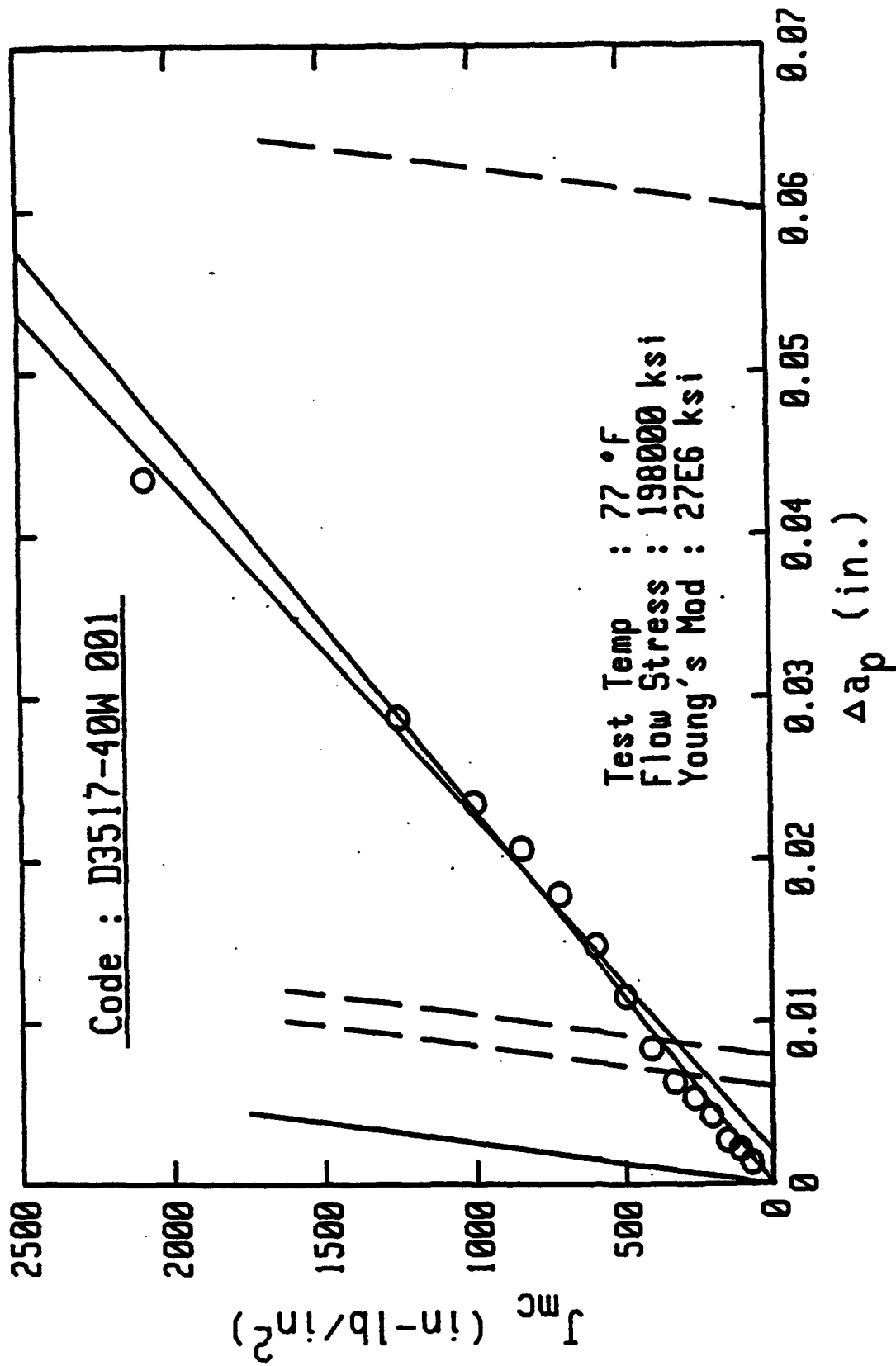
$J_{p1} = 687 \text{ in-lb/in}^2$
 $K_{p1} = 136.2 \text{ ksi}\sqrt{\text{in}}$
 $r = 0.9925$

Thickness : 0.094 in.
Initial a : 0.294 in.

Toughness J

Event	Load lb	Jac in-lb/in ²	Jbt in-lb/in ²	J(Kr) in-lb/in ²	del-ap in.
1	2530	16.6	16.6	41.6	0.0000
2	4021	50.6	23.8	78.4	0.0005
3	5165	93.3	39.7	115.5	0.0010
4	6292	146.3	61.1	159.3	0.0031
5	7360	207.0	88.1	208.0	0.0044
6	8373	275.4	120.8	261.0	0.0042
7	9447	356.6	162.0	325.8	0.0049
8	10420	448.7	206.2	391.4	0.0056
9	11522	545.6	264.6	475.0	0.0073
10	12441	647.3	323.5	555.3	0.0091
11	13351	759.5	392.4	646.0	0.0100
12	14262	888.9	476.6	752.4	0.0119
13	15149	1036.6	580.7	878.6	0.0132
14	16015	1186.6	687.8	1012.7	0.0167
15	16642	1320.8	798.7	1141.6	0.0200
16	17130	1459.0	916.8	1273.5	0.0200
17	17638	1675.1	1119.8	1489.2	0.0257

Pmax = 17800 (lb)
Net Stress = 25560 (psi)



$$J_{IC} = -109.2 \text{ in-lb/in}^2$$

$$K_{IC} = 0 \text{ ksi}\sqrt{\text{in}}$$

$$r = 0.9935$$

$$J_{p1} = 381.8 \text{ in-lb/in}^2$$

$$K_{p1} = 101.5 \text{ ksi}\sqrt{\text{in}}$$

$$r = 0.9901$$

Thickness : 0.095 in.
Initial a : 0.288 in.

Toughness J

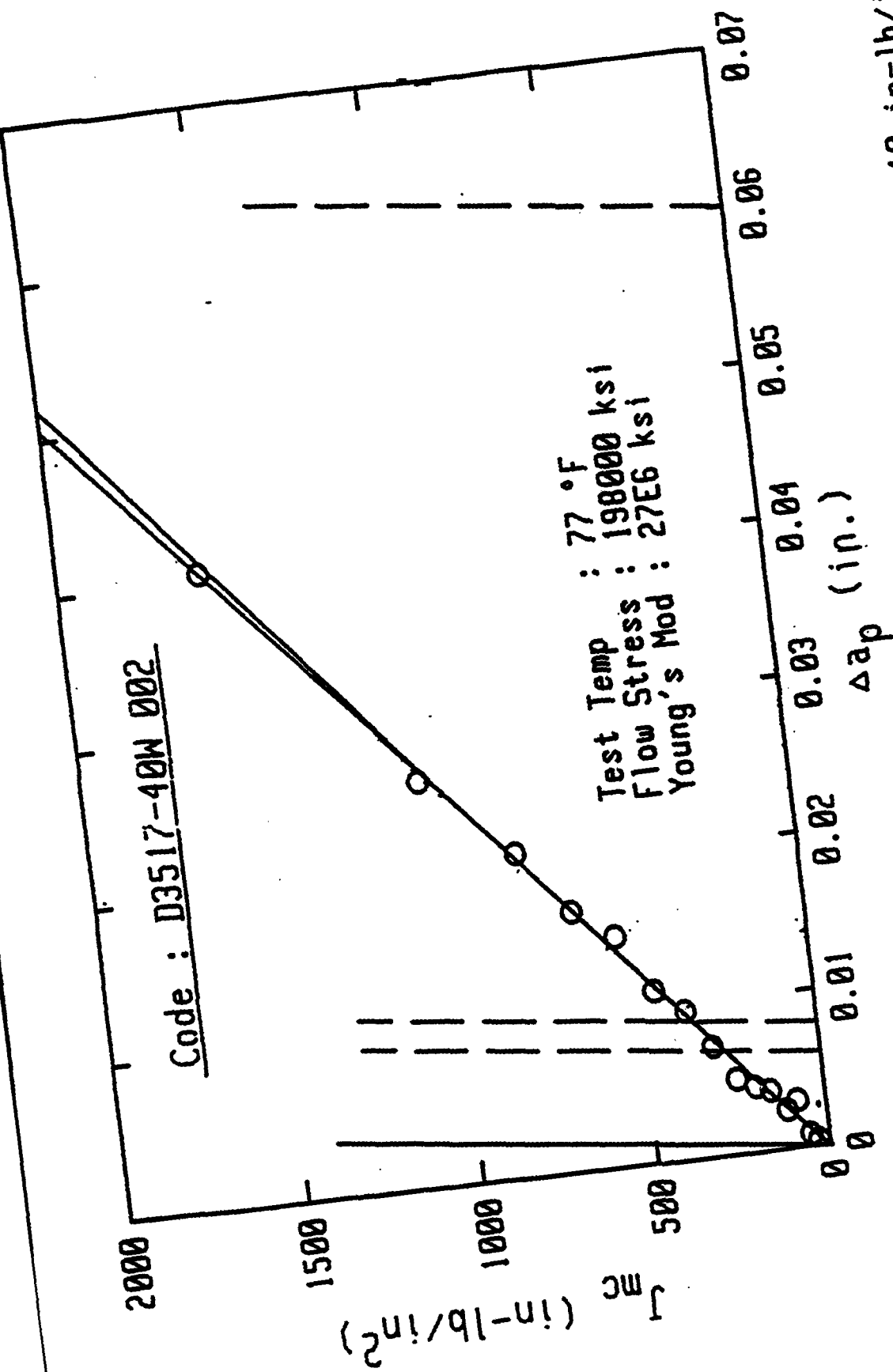
Event	Load lb	Jac in-lb/in ²	Jbt in-lb/in ²	J(Kr) in-lb/in ²	del-ap in.
1	2516	15.5	15.5	37.9	0.0000
2	3543	39.5	18.8	60.9	0.0000
3	4523	72.2	27.5	88.8	0.0013
4	5522	111.2	41.2	122.8	0.0021
5	6467	155.3	59.2	160.5	0.0027
6	7446	207.6	82.9	205.2	0.0042
7	8387	265.5	113.0	255.5	0.0053
8	9320	332.4	151.2	313.8	0.0063
9	10190	407.6	198.2	379.0	0.0083
10	11030	495.0	260.4	457.6	0.0115
11	11835	595.2	337.1	550.0	0.0146
12	12605	715.3	434.8	662.8	0.0178
13	13300	840.5	536.1	782.1	0.0206
14	13964	977.2	665.8	930.8	0.0234
*15	14358	1250.0	912.5	1175.4	0.0287
16	14254	2081.6	1747.7	2044.8	0.0434

Pmax = 14600 (lb)

Net Stress = 213710 (psi)

*K_c determined at this event.

Code : D3517-40W 002



Test Temp : 77 °F
 Flow Stress : 198000 ksi
 Young's Mod : 27E6 ksi

$J_{Ic} = 10 \text{ in-lb/in}^2$
 $K_{Ic} = 16.4 \text{ ksi}\sqrt{\text{in}}$
 $r = 0.9988$

$J_{pl} = 359 \text{ in-lb/in}^2$
 $K_{pl} = 98.5 \text{ ksi}\sqrt{\text{in}}$
 $r = 0.9972$

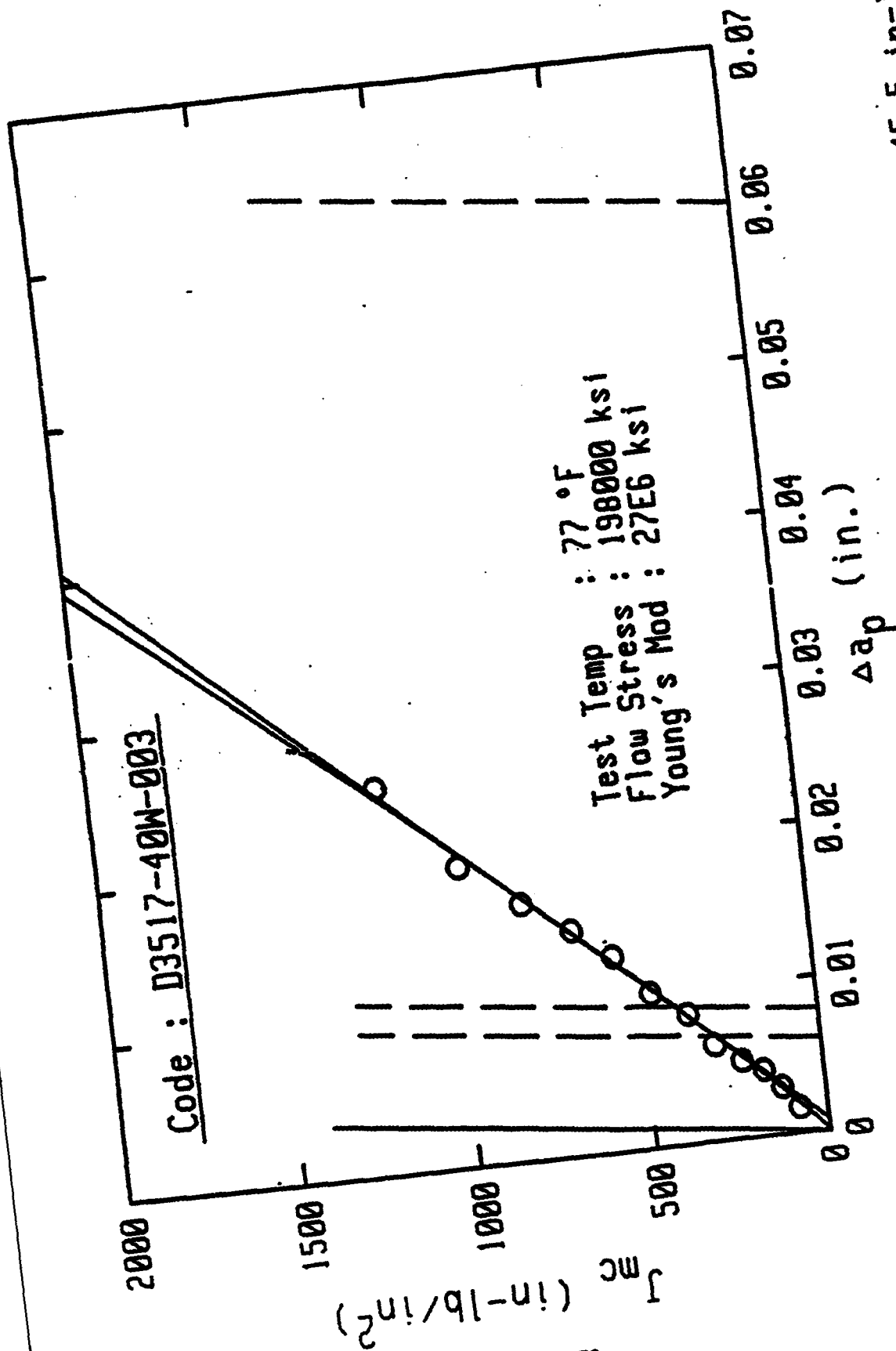
Thickness : 0.093 in.
 Initial a : 0.289 in.

Toughness J

Event	Load lb	Jac in-lb/in ²	Jbt in-lb/in ²	J(Kr) in-lb/in ²	del-ap in.
1	2590	17.2	17.2	39.4	0.0000
2	3459	29.8	19.9	58.2	0.0004
3	4458	50.9	29.1	85.7	0.0008
4	5396	78.4	43.4	117.4	0.0030
5	6316	110.2	62.5	153.9	0.0025
6	7341	152.4	89.7	201.8	0.0038
7	8211	193.5	117.8	246.5	0.0042
8	9163	246.3	154.4	302.7	0.0048
9	10065	306.2	202.8	367.5	0.0070
10	10948	374.0	259.4	441.8	0.0095
11	11797	453.7	329.1	527.6	0.0110
12	12613	546.1	411.8	626.3	0.0146
13	13379	663.2	520.6	748.0	0.0165
14	14066	803.5	651.8	898.9	0.0206
*15	14681	1052.6	898.7	1130.3	0.0258
16	14912	1600.8	1433.1	1666.5	0.0473

Pmax = 15000 (lb)
Net Stress = 222780 (psi)

K_c determined at this event.



C-78

$$J_{p1} = 403.2 \text{ in-lb/in}^2$$

$$K_{p1} = 104.3 \text{ ksi}\sqrt{\text{in}}$$

$$r = 0.9967$$

Thickness : 0.093 in.
Initial a : 0.298 in.

$$J_{Ic} = -45.5 \text{ in-lb/in}^2$$

$$K_{Ic} = 0 \text{ ksi}\sqrt{\text{in}}$$

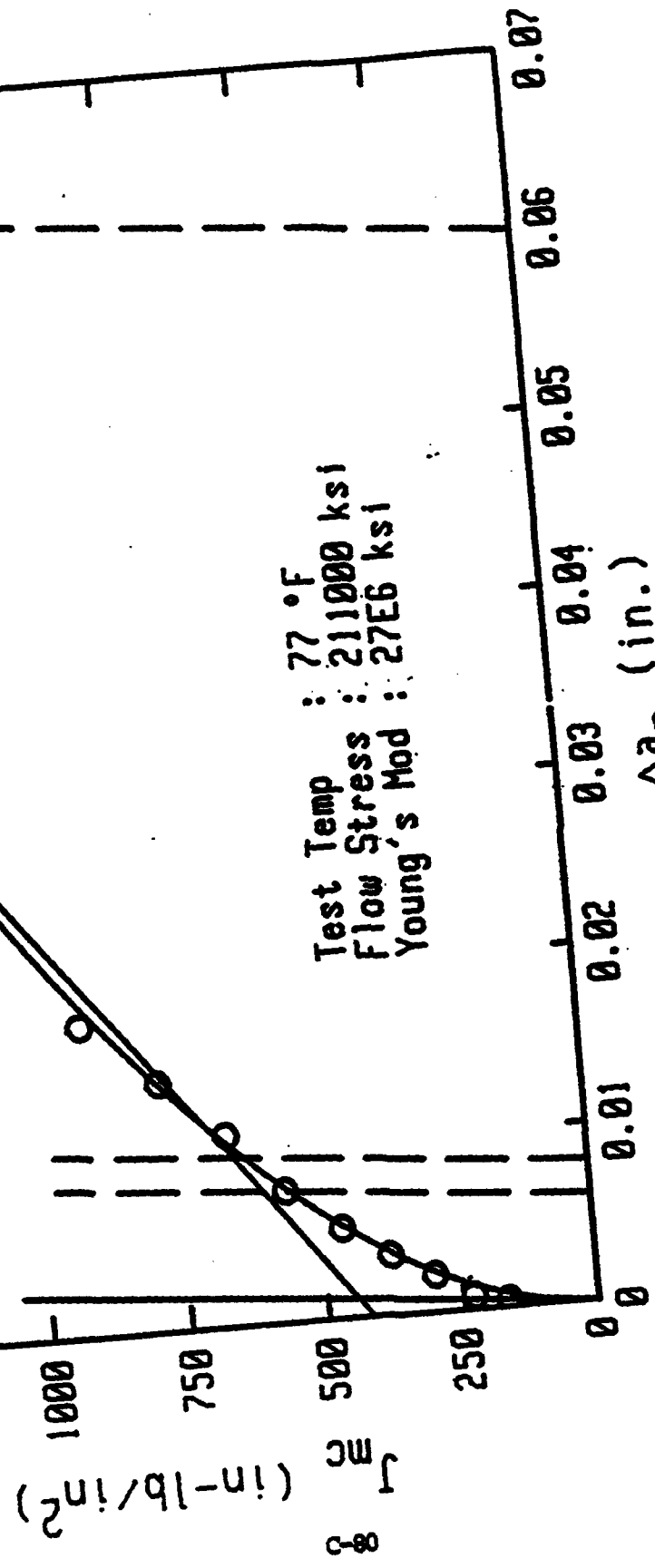
$$r = 0.9959$$

Toughness J

Event	Load lb	Jac in-lb/in ²	Jbt in-lb/in ²	J(Kr) in-lb/in ²	del-ap in.
1	2500	17.0	17.0	40.1	0.0000
2	3560	42.4	22.8	66.6	0.0000
3	4600	78.2	34.4	99.3	0.0016
4	5626	122.5	53.2	139.8	0.0030
5	6600	170.1	75.9	184.4	0.0042
6	7500	229.4	106.8	237.8	0.0050
7	8572	302.8	148.9	303.0	0.0062
8	9300	369.2	191.0	365.4	0.0083
9	10330	470.6	254.4	452.7	0.0099
10	11140	566.4	324.2	544.3	0.0126
11	11933	675.2	407.7	651.6	0.0145
12	12667	808.4	511.7	779.1	0.0166
13	13319	974.0	661.2	949.1	0.0193
14	13856	1182.6	861.5	1172.3	0.0249

Pmax = 14100 (lb)
Net Stress = 206520 (psi)

Code : D3517-40-001



Test Temp : 77 °F
 Flow Stress : 211000 ksi
 Young's Mod : 27E6 ksi

Thickness : 0.092 in.
 Initial a : 0.286 in.

$J_{p1} = 634.4 \text{ in-lb/in}^2$
 $K_{p1} = 130.9 \text{ ksi}\sqrt{\text{in}}$
 $r = 0.9976$

$J_{Ic} = 443 \text{ in-lb/in}^2$
 $K_{Ic} = 109.4 \text{ ksi}\sqrt{\text{in}}$
 $r = 0.9869$

Specimen Code : 33517-48-081

Toughness J

Event	Load lbs	Jac in-lbs/in ²	Jbt in-lbs/in ²	J(Kr) in-lbs/in ²	del-ap in.
1	2513	16.4	16.4	37.0	0.0000
2	4811	57.6	25.4	73.2	0.0000
3	5049	106.2	40.5	107.4	0.0000
4	6891	163.9	60.8	148.0	0.0004
5	7070	227.3	87.8	194.2	0.0008
6	8027	296.4	117.0	244.0	0.0021
7	8966	375.2	154.4	301.5	0.0034
8	9875	461.4	197.6	364.9	0.0050
9	10839	561.0	250.1	446.1	0.0074
10	11693	663.0	323.8	530.7	0.0107
11	12516	776.5	402.2	627.0	0.0139
12	13311	909.4	503.0	746.0	0.0174
13	14025	1066.7	633.3	889.7	0.0241
14	14688	1272.2	821.6	1082.7	0.0357

Pmax = 14700 (lbs)
Net Stress = 216630 (psi)

Code : D3517-40-002

J_{IC} (in-lb/in²)

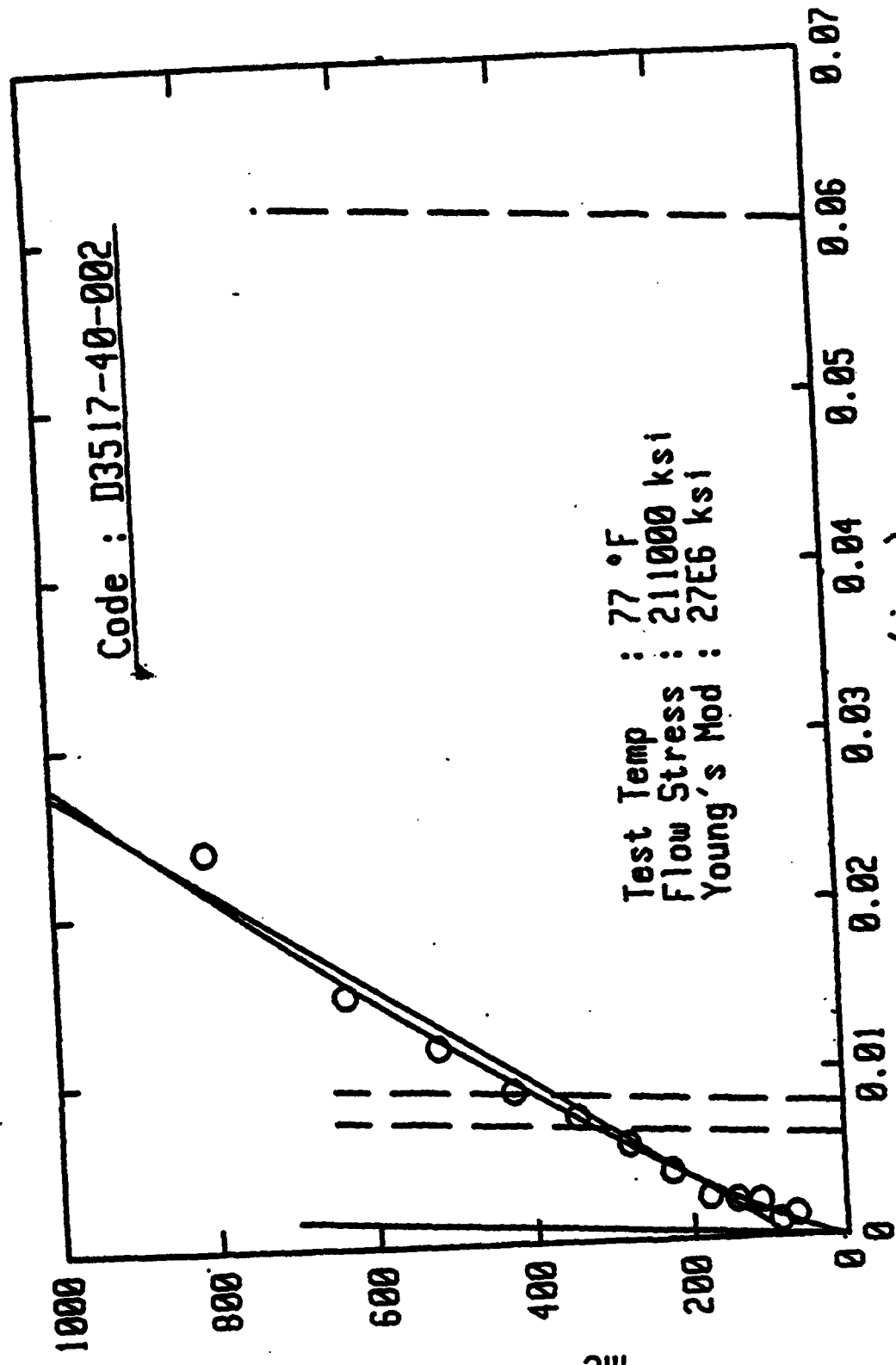
Test Temp : 77 °F
 Flow Stress : 211000 ksi
 Young's Mod : 27E6 ksi

Δa_p (in.)

Thickness : 0.093 in.
 Initial a : 0.298 in.

J_{p1} = 396.7 in-lb/in²
 K_{p1} = 103.5 ksi√in
 r = 0.9836

J_{Ic} = 79.2 in-lb/in²
 K_{Ic} = 46.2 ksi√in
 r = 0.9853



Specimen Code : 03517-48-002

Toughness J

Event	Load lbs	Jac in-lbs/in ²	Jbt in-lbs/in ²	J(Kr) in-lbs/in ²	del-ap in.
1	5262	63.4	41.4	120.2	0.0014
2	6229	85.5	60.2	159.6	0.0010
3	7161	109.6	83.8	203.4	0.0022
4	8101	139.8	113.7	254.0	0.0023
5	9022	175.9	149.6	310.4	0.0025
6	9921	223.5	195.1	374.9	0.0041
7	10790	277.9	248.9	447.0	0.0057
8	11644	342.7	314.9	530.1	0.0074
9	12487	423.3	397.0	628.1	0.0090
10	13274	515.5	491.4	737.1	0.0117
11	14016	631.3	611.4	867.8	0.0150
12	14602	803.4	789.8	1039.0	0.0237

Pmax = 14940 (lbs)
Net Stress = 210100 (psi)

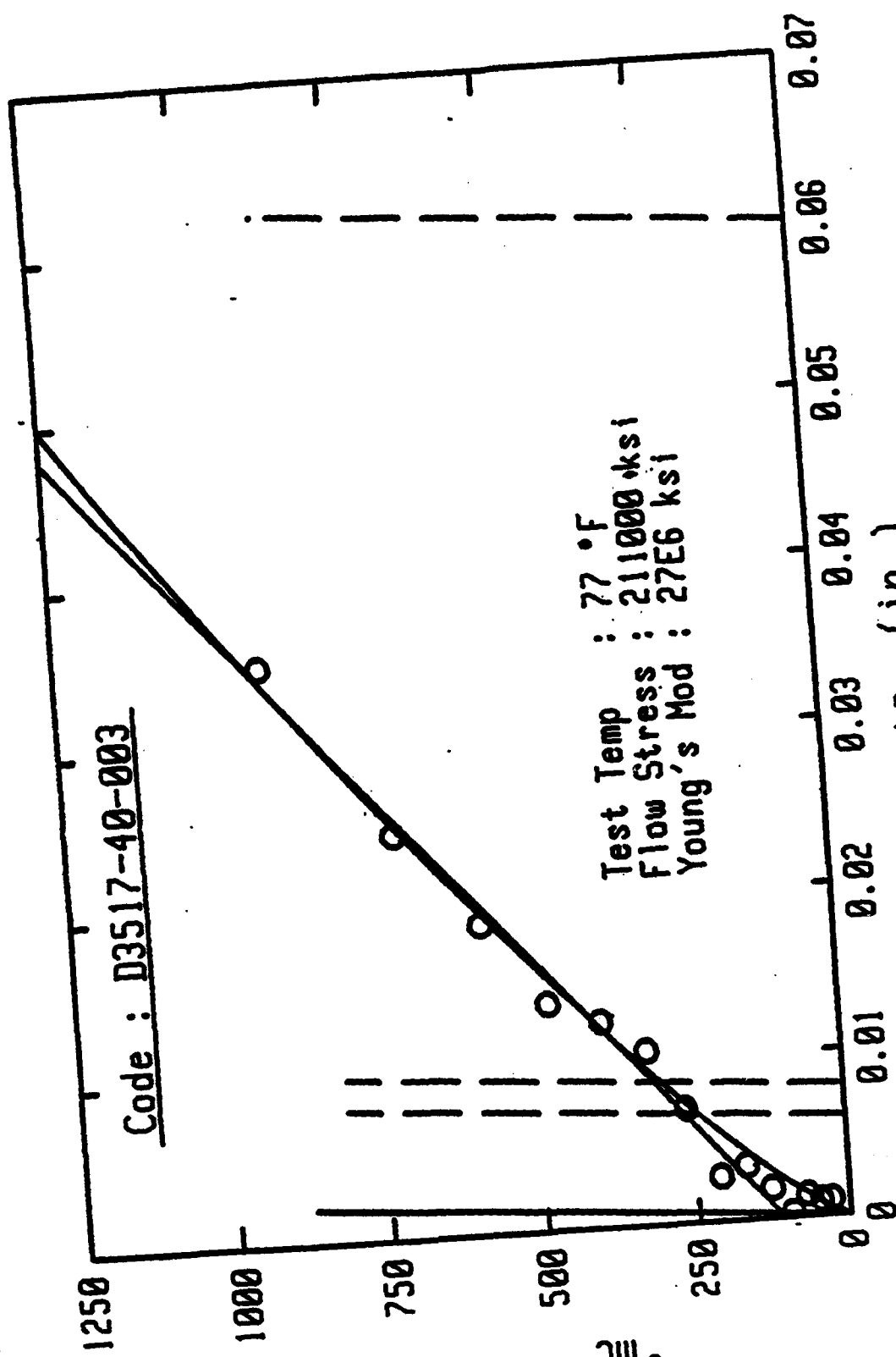
Code : D3517-40-003

J_{IC} (in-lb/in²)

C-84

Test Temp : 77 °F
 Flow Stress : 211000 ksi
 Young's Mod : 27E6 ksi

Δa_p (in.)



Thickness : 0.093 in.
 Initial a : 0.291 in.

$J_{p1} = 300.8$ in-lb/in²
 $K_{p1} = 90.1$ ksi $\sqrt{\text{in}}$
 $r = 0.991$

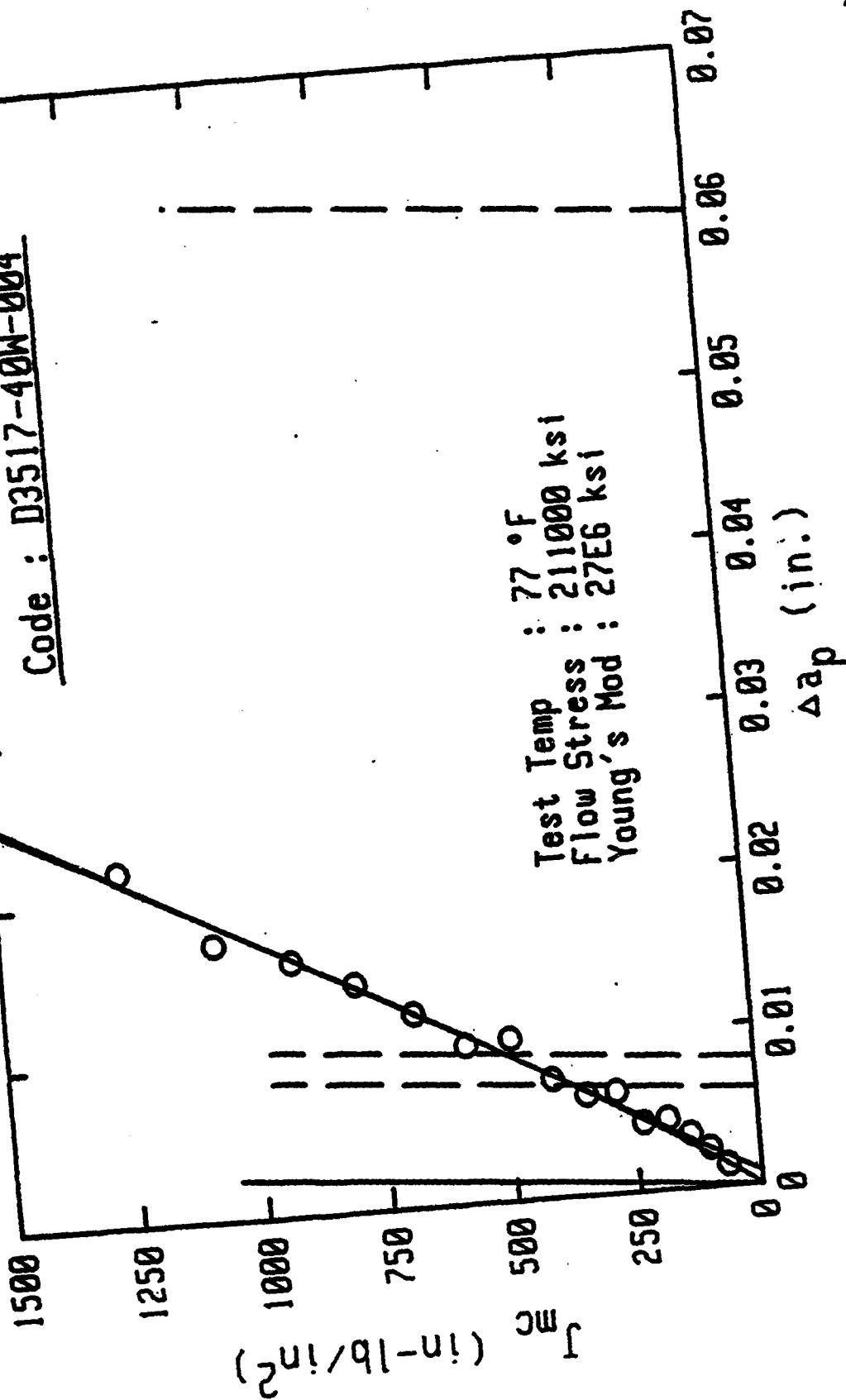
$J_{Ic} = 115.5$ in-lb/in²
 $K_{Ic} = 55.8$ ksi $\sqrt{\text{in}}$
 $r = 0.9913$

Toughness J

Event	Load lbs	Jac in-lbs/in ²	Jbt in-lbs/in ²	J(Kr) in-lbs/in ²	del-ap in.
1	3586	28.7	18.4	61.5	0.0010
2	4547	46.4	26.8	88.2	0.0009
3	5470	67.7	39.3	118.3	0.0013
4	6373	93.4	56.8	152.8	0.0003
5	7253	125.1	79.3	191.7	0.0018
6	8135	165.3	107.8	236.4	0.0033
7	9062	208.3	145.4	290.7	0.0027
8	9958	260.6	192.0	352.5	0.0069
9	10791	320.6	245.1	419.4	0.0105
10	11580	392.8	310.0	495.7	0.0124
11	12421	477.5	390.7	589.4	0.0137
12	13164	578.8	486.5	693.8	0.0187
13	13865	710.6	607.2	820.1	0.0244
14	14328	912.1	816.0	1004.7	0.0349

Pmax = 14440 (lbs)
 Net Stress = 212910 (psi)

Code : D3517-40W-004



Q-86

Thickness : 0.093 in.
Initial a : 0.289 in.

$J_{pl} = 502.4 \text{ in-lb/in}^2$
 $K_{pl} = 116.5 \text{ ksi}\sqrt{\text{in}}$
 $r = 0.9857$

$J_{Ic} = -58.7 \text{ in-lb/in}^2$
 $K_{Ic} = 0 \text{ ksi}\sqrt{\text{in}}$
 $r = 0.9881$

Toughness J

Event	Load lbs	Jac in-lbs/in ²	Jbt in-lbs/in ²	J(Kr) in-lbs/in ²	del-ap in.
1	2530	16.5	16.5	56.6	0.0000
2	3600	37.6	14.8	83.9	0.0000
3	4525	65.2	19.3	114.3	0.0013
4	5418	99.8	27.3	147.6	0.0024
5	6344	137.3	39.7	186.7	0.0034
6	7222	182.2	52.7	225.6	0.0044
7	8136	232.5	74.2	273.4	0.0043
8	8996	283.8	100.3	324.2	0.0063
9	9928	346.6	134.8	385.8	0.0062
10	10736	411.8	167.5	442.6	0.0073
11	11583	492.5	210.5	518.7	0.0100
12	12423	582.4	273.0	595.9	0.0098
13	13173	681.8	331.1	676.9	0.0120
14	13930	793.9	419.2	785.1	0.0148
15	14678	918.5	519.1	908.2	0.0157
16	15330	1078.8	644.9	1053.6	0.0177
17	15911	1253.3	793.5	1223.1	0.0219

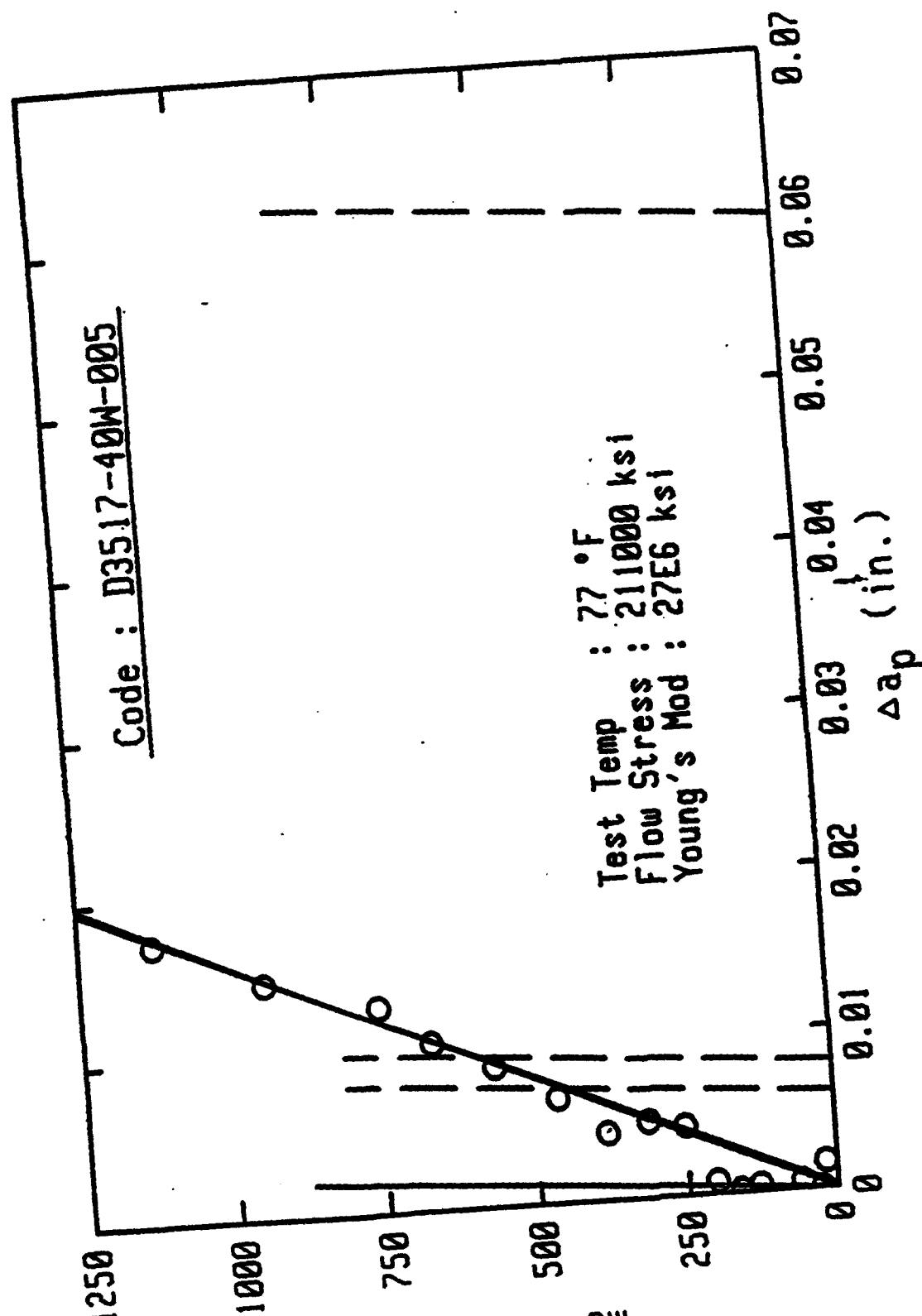
Pmax = 16100 (lbs)
Net Stress = 228020 (psi)

Code : D3517-40W-005

J_{mc} (in-lb/in²)

C-88

Test Temp : 77 °F
Flow Stress : 211000 ksi
Young's Mod : 27E6 ksi



Thickness : 0.093 in.
Initial a : 0.287 in.

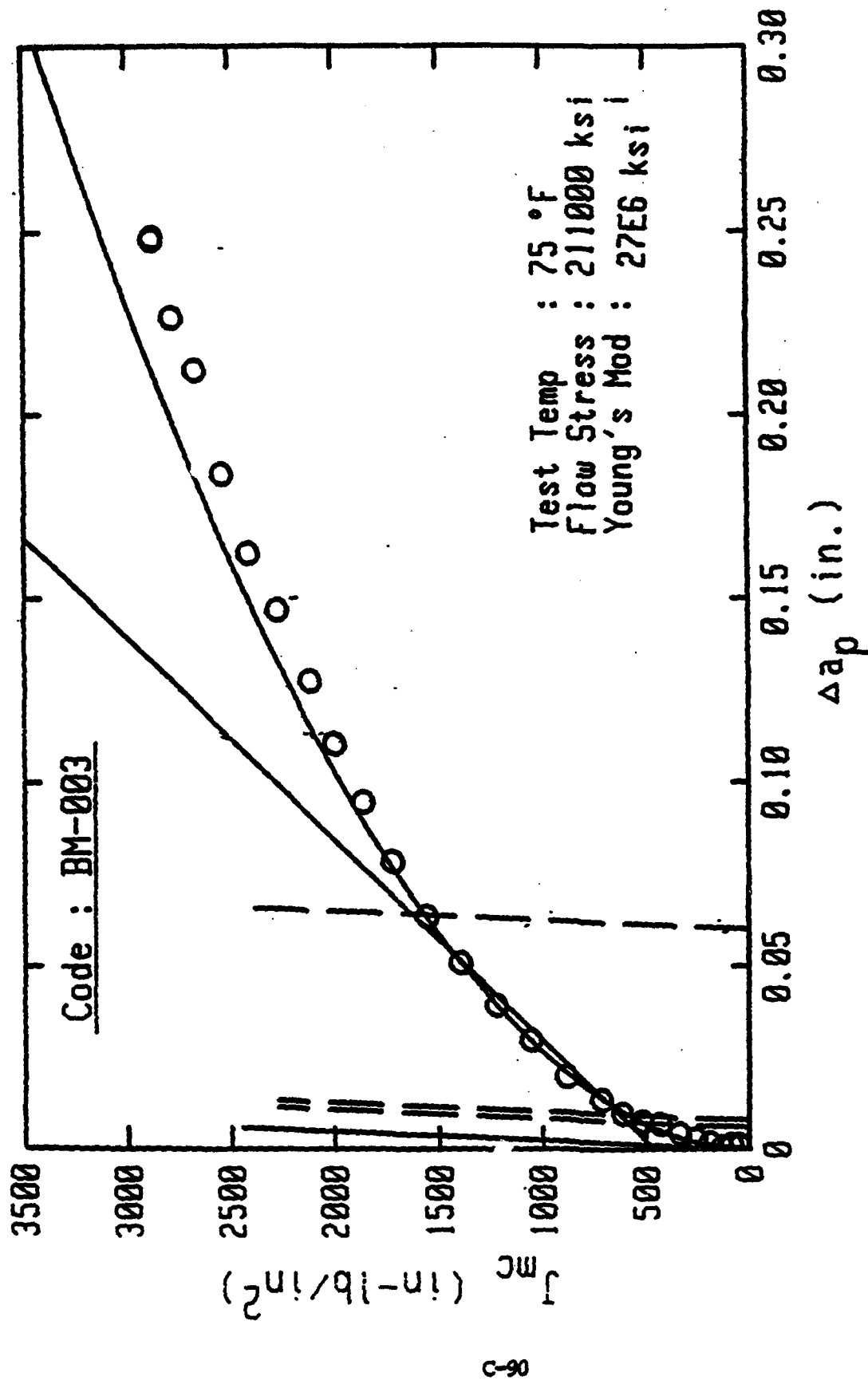
$J_{pl} = 593.6 \text{ in-lb/in}^2$
 $K_{pl} = 126.6 \text{ ksi}\sqrt{\text{in}}$
 $r = 0.9871$

$J_{Ic} = -16.2 \text{ in-lb/in}^2$
 $K_{Ic} = 0 \text{ ksi}\sqrt{\text{in}}$
 $r = 0.988$

Toughness J

Event	Load lbs	Jac in-lbs/in ²	Jbt in-lbs/in ²	J(Kr) in-lbs/in ²	del-ap in.
1	2530	16.3	16.3	39.3	0.0016
2	3470	24.0	18.0	59.6	0.0000
3	4353	41.1	24.1	83.1	0.0000
4	5270	57.3	35.1	112.2	0.0005
5	6215	74.6	51.6	147.3	0.0000
6	7119	97.9	72.7	186.2	0.0000
7	8051	128.0	100.2	232.0	0.0004
8	8968	160.8	132.6	282.7	0.0002
9	9863	201.4	172.6	339.9	0.0008
10	10729	250.5	219.1	402.8	0.0043
11	11624	311.6	279.5	479.1	0.0047
12	12453	380.6	344.4	559.2	0.0042
13	13250	461.8	425.9	652.8	0.0065
14	14035	563.8	525.2	763.1	0.0086
15	14690	664.8	622.6	870.2	0.0103
16	15113	747.9	701.5	953.6	0.0122
17	15657	937.5	895.0	1134.3	0.0145
18	16028	1122.1	1086.5	1313.3	0.0172

max = 16000 (lbs)
Net Stress = 222980 (psi)



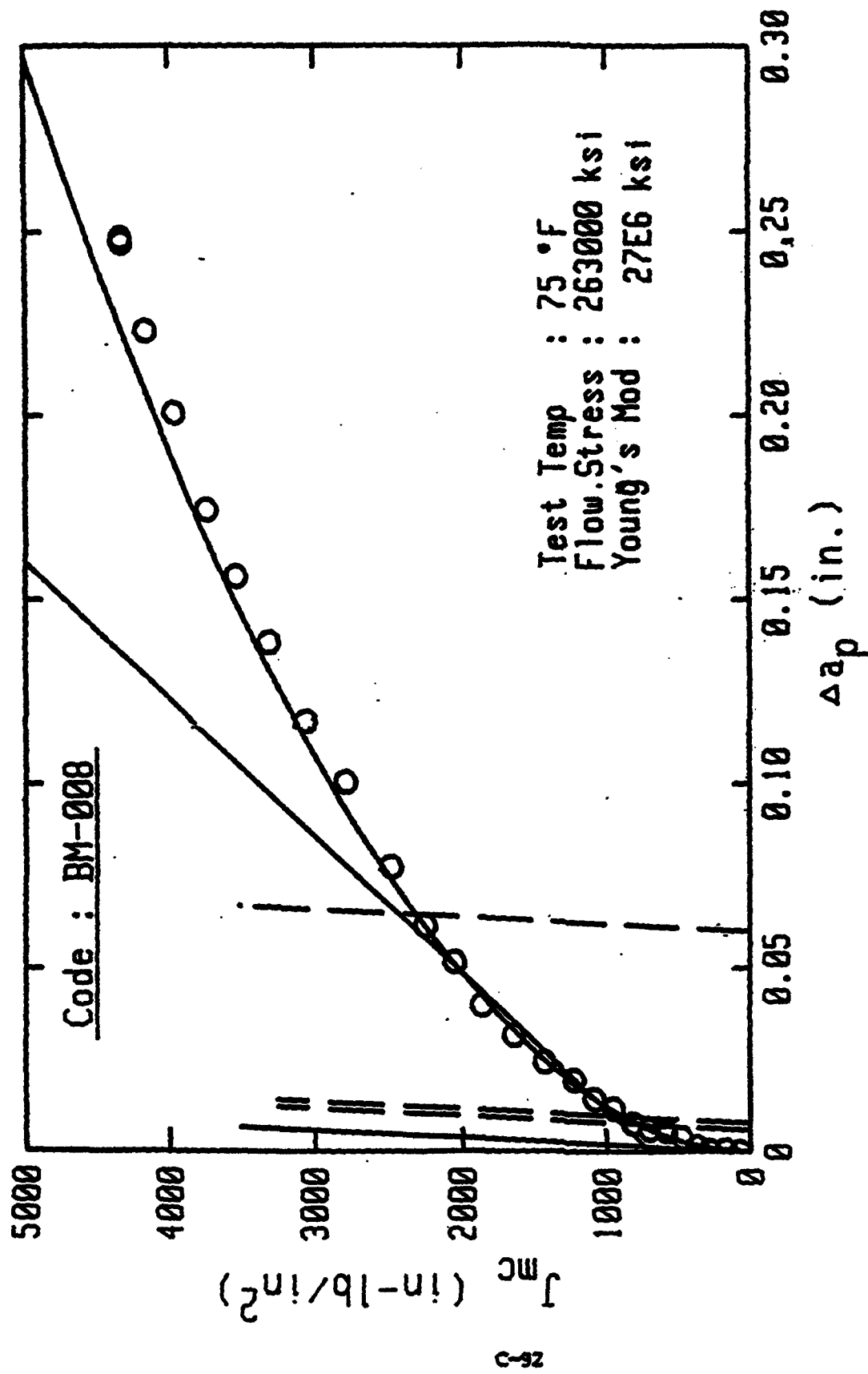
Thickness : 0.09 in. $J_{Ic} = 483.6$ in-lb/in²
Initial a : 0.523 in. $K_{Ic} = 120.2$ ksi√in
 $r = 0.9991$ $r = 0.9897$

Specimen Code : BM-003

Toughness J

Event	Load lb	Jac in-lb/in ²	G in-lb/in ²	Ja in-lb/in ²	del-ap in.
1	295	38.8	43.3	43.7	0.0011
2	415	77.9	85.5	87.6	0.0013
3	517	123.7	132.5	139.8	0.0006
4	621	183.7	192.4	205.2	0.0018
5	712	251.6	255.8	279.5	0.0029
6	794	331.3	319.6	365.6	0.0043
7	865	426.8	385.9	465.6	0.0069
8	926	514.3	444.2	568.6	0.0075
9	988	613.9	584.6	665.8	0.0096
10	1022	715.2	562.1	768.1	0.0134
11	1067	885.1	639.5	939.1	0.0197
12	1085	1056.8	707.5	1103.4	0.0296
13	1079	1222.9	748.9	1263.3	0.0392
14	1063	1394.2	789.9	1425.1	0.0507
15	1014	1554.4	788.2	1572.2	0.0632
16	969	1715.8	887.8	1728.7	0.0781
17	891	1856.3	777.6	1843.6	0.0943
18	832	1992.8	775.4	1969.9	0.1103
19	777	2113.9	787.1	2081.6	0.1274
20	688	2271.6	738.6	2242.4	0.1466
21	634	2489.4	731.6	2397.8	0.1621
22	548	2537.6	684.6	2531.8	0.1837
23	463	2669.9	676.6	2671.5	0.2119
24	398	2782.8	597.5	2826.8	0.2262
25	338	2876.9	549.8	2948.8	0.2481
26	316	2879.8	582.9	2948.9	0.2479
27	315	2879.8	497.8	2958.8	0.2473

P_{max} = 1096 lb



Thickness : 0.09 in.
Initial a : 0.5189 in.

J_{p1} = 882.8 in-lb/in²
 K_{p1} = 162.3 ksi√in
 r = 0.9977

J_{Ic} = 730.9 in-lb/in²
 K_{Ic} = 147.7 ksi√in
 r = 0.9885

Specimen Code : BM-888

Toughness J

Event	Load lb	Jac in-lb/in ²	S in-lb/in ²	J _a in-lb/in ²	del-ap in.
1	292	33.9	48.7	48.7	0.0000
2	396	63.1	75.3	75.6	0.0000
3	586	184.6	122.8	125.1	0.0000
4	619	158.9	185.0	189.5	0.0005
5	784	289.3	238.1	249.3	0.0000
6	797	274.5	385.4	325.5	0.0003
7	896	358.9	389.4	422.8	0.0014
8	992	467.3	485.2	544.3	0.0039
9	1074	576.8	574.7	666.9	0.0056
10	1141	696.6	658.4	799.5	0.0061
11	1199	811.5	725.5	925.1	0.0076
12	1252	945.1	812.8	1045.5	0.0116
13	1299	1077.1	888.9	1206.4	0.0142
14	1332	1216.5	967.1	1347.8	0.0194
15	1371	1421.2	1059.6	1568.7	0.0242
16	1384	1639.8	1133.4	1777.6	0.0315
17	1385	1861.8	1202.1	1996.2	0.0397
18	1331	2046.7	1288.1	2156.1	0.0514
19	1295	2244.1	1228.7	2342.8	0.0612
20	1221	2472.5	1231.9	2544.7	0.0772
21	1188	2776.9	1222.6	2822.1	0.1003
22	1020	3058.8	1198.8	3188.5	0.1167
23	985	3381.8	1134.8	3346.5	0.1381
24	820	3521.6	1183.1	3584.5	0.1568
25	722	3723.3	1028.9	3806.6	0.1741
26	599	3958.9	944.3	4078.5	0.2084
27	581	4168.8	861.5	4348.5	0.2228
28	413	4326.7	797.8	4563.6	0.2467
29	393	4331.9	736.7	4568.5	0.2482
30	391	4332.2	721.6	4561.7	0.2473

P_{max} = 1386 lb

Specimen Code : WM-11

Toughness J

Event	Load lb	Jac in-lb/in ²	S in-lb/in ²	J _a in-lb/in ²	del-ap in.
1	385	42.8	45.5	46.5	0.0000
2	399	73.7	77.9	81.3	0.0000
3	502	121.2	123.8	133.2	0.0000
4	591	179.6	173.5	195.5	0.0022
5	667	245.2	224.7	264.8	0.0049
6	738	319.5	274.2	342.5	0.0075
7	798	397.6	324.8	425.8	0.0098
8	844	481.3	372.8	513.9	0.0098
9	898	576.8	424.2	614.7	0.0109
10	955	729.8	491.2	771.3	0.0146
11	1002	876.5	557.5	921.8	0.0192
12	1031	1087.5	638.2	1138.8	0.0287
13	1022	1388.4	678.7	1346.9	0.0408
14	1006	1514.3	788.5	1558.8	0.0506
15	976	1723.8	717.4	1768.8	0.0550
16	947	1922.2	736.7	1961.9	0.0734
17	877	2111.5	721.8	2145.1	0.0901
18	796	2298.2	697.2	2319.2	0.1091
19	749	2485.8	684.5	2541.8	0.1212
20	661	2676.4	653.7	2746.8	0.1434
21	619	2844.6	665.3	2948.8	0.1585
22	565	2997.7	628.8	3143.5	0.1788
23	488	3135.9	572.8	3387.4	0.1924
24	394	3258.5	589.9	3445.2	0.2164
25	365	3348.6	514.5	3592.2	0.2293
26	338	3439.3	491.3	3741.5	0.2373
27	326	3442.6	453.3	3746.2	0.2369
28	325	3442.5	447.7	3746.4	0.2365

P_{max} = 1035 lb

Code : WM-12

J_{IC}
(in-lb/in²)

Test Temp : 75 °F
Flow Stress : 198000 ksi
Young's Mod : 27E6 ksi

Δa_p (in.)

Thickness : 0.09 in.
Initial a : 0.5262 in.

$J_{pl} = 452 \text{ in-lb/in}^2$
 $K_{pl} = 116.2 \text{ ksi}\sqrt{\text{in}}$
 $r = 0.9838$

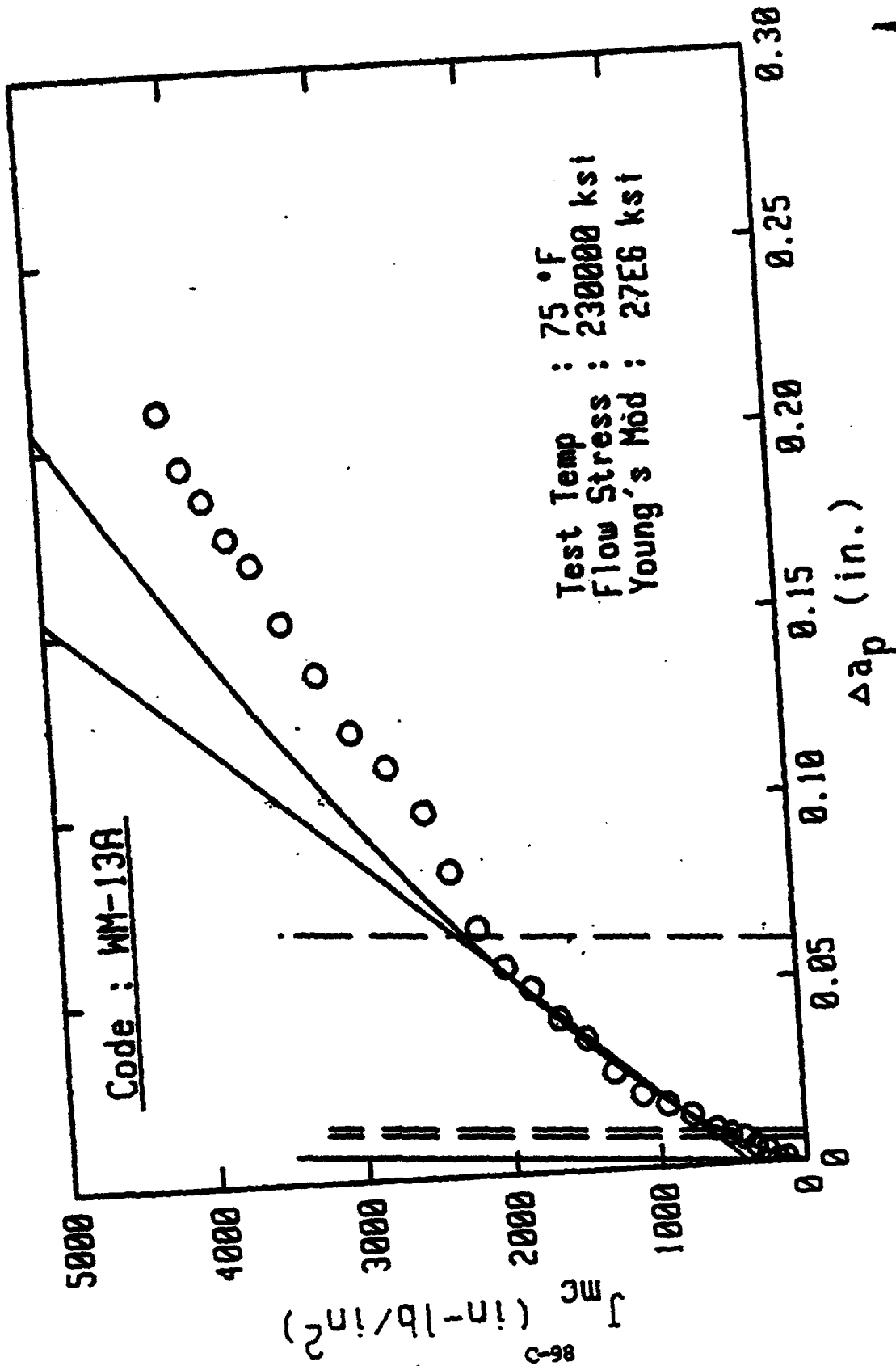
$J_{Ic} = 290.1 \text{ in-lb/in}^2$
 $K_{Ic} = 93.1 \text{ ksi}\sqrt{\text{in}}$
 $r = 0.9825$

Specimen Code : MN-12

Toughness J

Event	Load lb	Jac in-lb/in ²	S in-lb/in ²	Ja in-lb/in ²	del-ap in.
1	382	43.3	46.4	47.6	0.0011
2	387	72.4	75.4	79.5	0.0003
3	478	115.3	115.4	126.8	0.0005
4	572	174.8	167.7	189.2	0.0029
5	644	236.8	214.8	254.1	0.0043
6	711	311.1	267.4	332.3	0.0073
7	771	388.6	316.2	414.8	0.0084
8	822	473.2	361.4	503.1	0.0092
9	868	568.8	488.2	594.8	0.0111
10	909	654.6	452.3	691.6	0.0125
11	952	789.9	586.4	838.2	0.0157
12	997	962.2	576.8	1004.6	0.0212
13	1000	1114.8	616.8	1154.9	0.0277
14	1014	1278.4	655.2	1317.1	0.0347
15	1010	1439.7	693.8	1473.9	0.0437
16	986	1594.8	702.5	1625.7	0.0521
17	982	1758.8	727.7	1787.5	0.0588
18	968	1908.5	746.1	1958.3	0.0649
19	981	2059.7	733.7	2084.9	0.0811
20	877	2193.2	737.8	2226.8	0.0884
21	858	2335.7	745.8	2382.2	0.0952
22	889	2463.5	731.2	2518.4	0.1068
23	751	2786.9	723.8	2785.4	0.1224
24	714	2982.4	715.7	3028.9	0.1321
25	638	3088.8	678.2	3224.2	0.1489
26	585	3248.9	642.8	3422.4	0.1620
27	492	3386.5	576.6	3598.8	0.1843
28	421	3584.4	539.2	3733.9	0.2058
29	383	3688.4	522.7	3885.1	0.2185
30	323	3782.6	487.5	4011.1	0.2392
31	311	3785.2	451.5	4013.8	0.2393
32	310	3785.4	451.1	4012.9	0.2399

Pmax = 1024 lb

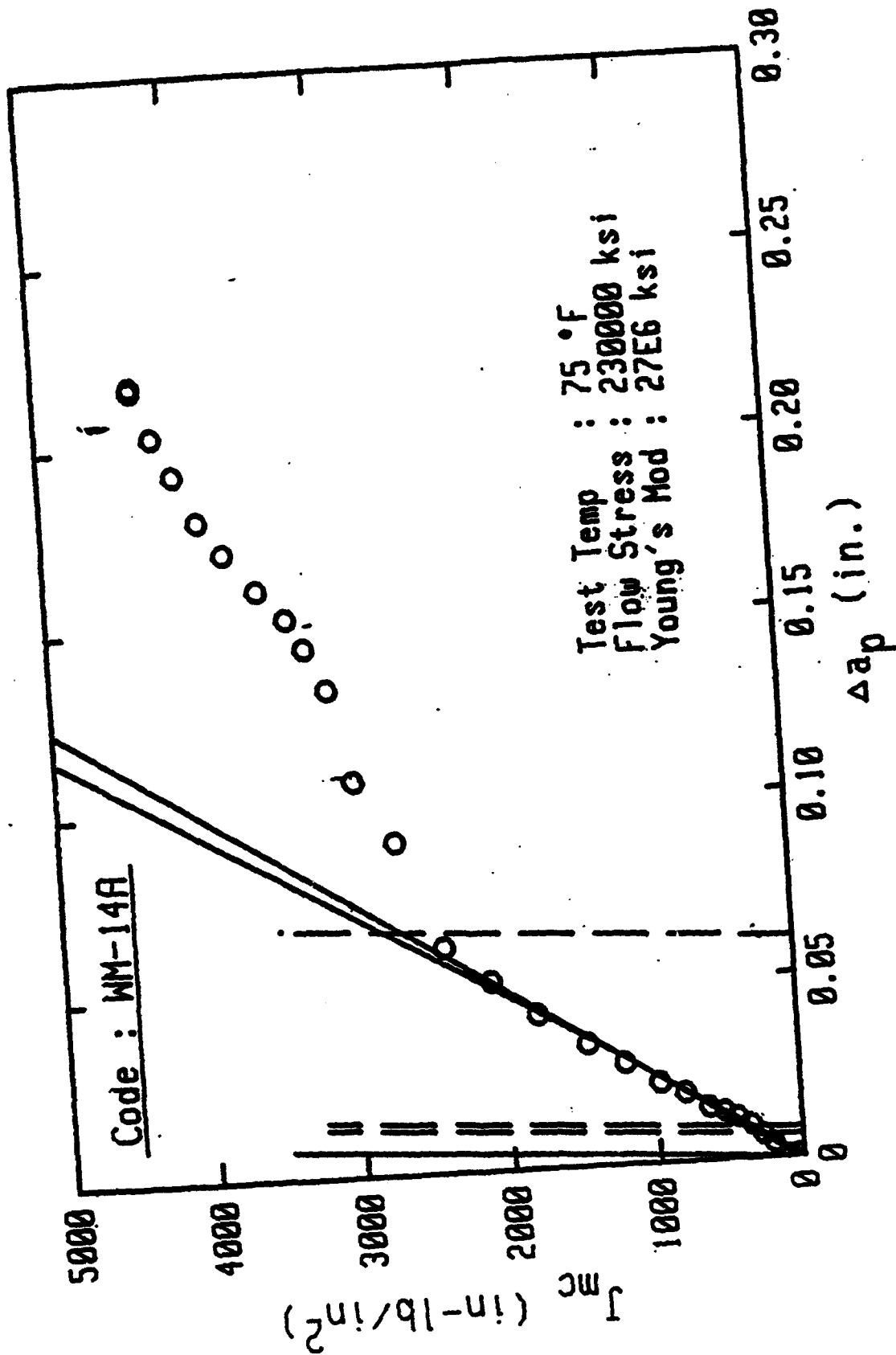


Specimen Code : WH-13A

Toughness J

Event	Load lb	J _{dc} in-lb/in ²	S in-lb/in ²	J _a in-lb/in ²	del-ap in.
1	296	48.6	46.4	47.8	0.0000
2	400	75.5	84.9	87.4	0.0000
3	512	127.6	140.8	146.7	0.0010
4	606	185.9	195.9	213.1	0.0007
5	687	253.8	256.1	287.8	0.0033
6	766	333.2	320.8	375.6	0.0046
7	834	417.3	385.9	467.8	0.0069
8	896	509.8	449.2	567.8	0.0081
9	947	607.2	507.7	672.6	0.0096
10	1016	771.4	600.4	845.9	0.0137
11	1068	934.9	678.5	1018.4	0.0169
12	1108	1106.1	745.5	1198.1	0.0199
13	1128	1291.7	807.6	1384.8	0.0264
14	1127	1472.7	863.5	1559.6	0.0352
15	1125	1650.8	896.3	1739.7	0.0414
16	1101	1831.4	914.6	1916.6	0.0499
17	1077	2004.1	917.8	2091.5	0.0561
18	1040	2174.3	928.2	2254.6	0.0668
19	978	2348.9	914.9	2401.9	0.0823
20	915	2488.8	933.7	2533.5	0.0986
21	863	2727.5	927.8	2796.4	0.1112
22	819	2955.6	913.9	3061.7	0.1210
23	749	3166.9	888.4	3295.6	0.1369
24	683	3388.8	858.7	3538.4	0.1512
25	611	3565.5	805.1	3778.7	0.1672
26	581	3721.0	787.8	3984.5	0.1745
27	538	3871.9	762.8	4187.4	0.1852
28	505	4018.9	744.8	4384.9	0.1942
29	448	4143.7	708.3	4561.7	0.2097
30	435	4146.4	663.3	4562.8	0.2095
31	433	4147.7	660.7	4563.8	0.2099

P_{max} = 1136 lb



C-100

Thickness : 0.09 in.
Initial a : 0.5206 in.

$J_{p1} = 350.1 \text{ in-lb/in}^2$
 $K_{p1} = 102.2 \text{ ksi}\sqrt{\text{in}}$
 $r = 0.996$

$J_{Ic} = 47.1 \text{ in-lb/in}^2$
 $K_{Ic} = 37.5 \text{ ksi}\sqrt{\text{in}}$
 $r = 0.9962$

Toughness J

Event	Load lb	Jac in-lb/in ²	S in-lb/in ²	Ja in-lb/in ²	del-ap in.
1	385	38.8	45.3	45.9	0.0006
2	438	81.6	93.5	96.4	0.0003
3	558	132.4	147.8	155.7	0.0000
4	648	194.3	209.4	225.2	0.0040
5	736	267.8	273.9	307.5	0.0064
6	814	347.6	341.7	396.8	0.0093
7	879	437.7	403.9	495.8	0.0113
8	943	529.3	478.2	596.3	0.0131
9	1082	633.8	535.9	710.5	0.0144
10	1072	796.4	638.7	885.5	0.0187
11	1122	966.7	784.9	1067.1	0.0217
12	1172	1285.8	799.8	1317.7	0.0274
13	1289	1451.9	885.8	1577.1	0.0331
14	1221	1788.3	959.8	1917.1	0.0417
15	1194	2887.4	982.3	2228.2	0.0513
16	1158	2392.4	988.8	2541.4	0.0611
17	1846	2683.8	1017.0	2796.8	0.0982
18	968	2948.6	985.8	3056.2	0.1071
19	989	3884.7	1102.7	3165.1	0.1323
20	777	3221.6	895.5	3291.1	0.1437
21	744	3337.4	889.8	3428.7	0.1528
22	787	3525.7	866.9	3678.5	0.1599
23	653	3741.8	823.5	3953.1	0.1783
24	612	3986.8	797.2	4175.5	0.1795
25	558	4858.5	748.2	4372.4	0.1922
26	511	4197.1	728.3	4567.3	0.2028
27	461	4321.3	693.9	4737.2	0.2171
28	447	4325.9	645.1	4741.4	0.2163
29	446	4326.9	648.8	4743.8	0.2159

Pmax = 1224 lb

APPENDIX IV
EXAMPLE CALIBRATION INFORMATION

Job: 1000
 Personnel:
 Calibration temperature:

LVDT Size: Clip Gage - MTS #77
 Conditioner Serial Number:
 LVDT Serial number

Excit at 0n = 7.40 Volts

Index	Volts	Displacement	Prediction	Difference
1	-1.510	.23500	.23502	.00002
2	-.960	.24000	.24007	.00007
3	-.415	.24500	.24509	.00009
4	.125	.25000	.25005	.00005
5	.671	.25500	.25507	.00007
6	1.215	.26000	.26008	.00008
7	1.751	.26500	.26509	.00009
8	2.305	.27000	.27010	.00010
9	2.847	.27500	.27509	.00009
10	3.387	.28000	.28005	.00005
11	3.926	.28500	.28501	.00001
12	4.462	.29000	.28994	-.00006
13	3.922	.28500	.28497	-.00003
14	3.377	.28000	.27996	-.00004
15	2.832	.27500	.27495	-.00005
16	2.286	.27000	.26993	-.00007
17	1.744	.26500	.26494	-.00006
18	1.200	.26000	.25994	-.00006
19	.655	.25500	.25493	-.00007
20	.109	.25000	.24991	-.00009
21	-.430	.24500	.24495	-.00005
22	-.975	.24000	.23994	-.00006
23	-1.520	.23500	.23492	-.00008

*Secondary
slope*

Displacement = .00919685 * volts + .24890380

Correlation Coefficient = .99999185

Standard deviation: .00000173

Standard error of estimate .00000000

95% Confidence limits--lower: .00919

Upper: .00920

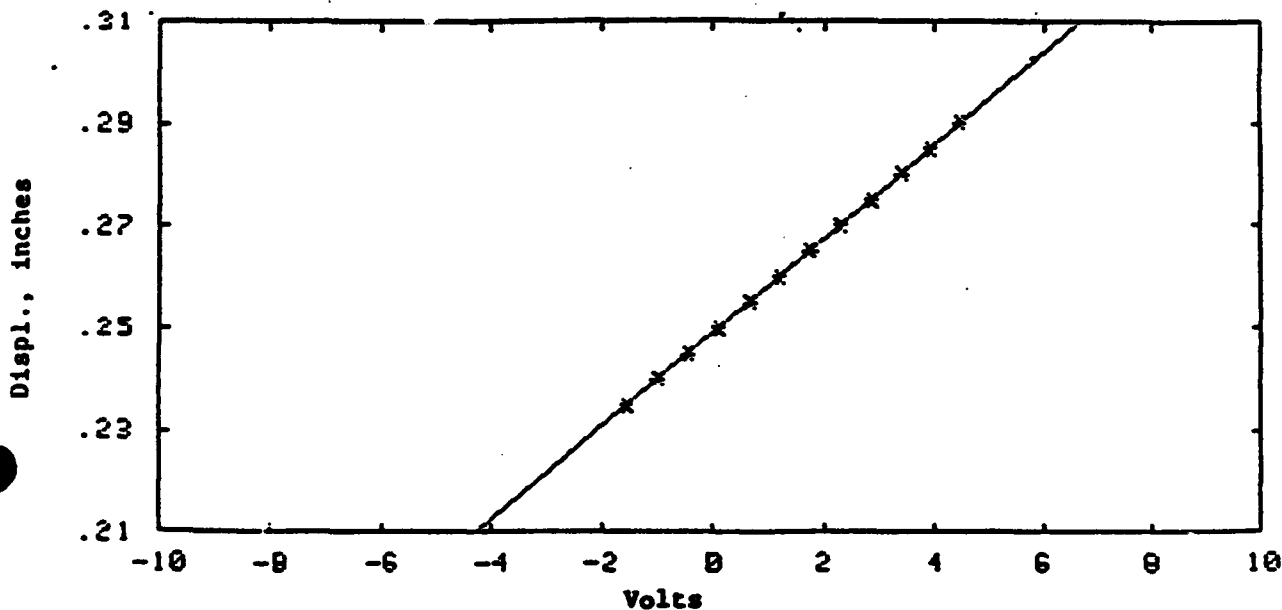
Minimum difference = -.00009

Maximum difference = .00010

Percent minimum error = -1.01932

Percent maximum error = 1.06486

Adj = .009166



Today's date: 3/11/86
Personnel: HANK
Calibration temperature: 78F

LVDT Size: DSST
Conditioner Serial Number: MTS 1183
LVDT Serial number GAGE Y

Index	Volts	Displacement	Prediction	Difference
1	-1.101	0.00000	-.00010	-.00010
2	-.560	.00500	.00499	-.00001
3	-.021	.01000	.01006	.00006
4	.509	.01500	.01504	.00004
5	1.040	.02000	.02003	.00003
6	1.570	.02500	.02501	.00001
7	2.100	.03000	.03000	-.00000
8	2.633	.03500	.03500	.00000
9	3.167	.04000	.04003	.00003
10	3.696	.04500	.04500	-.00000
11	4.220	.05000	.04993	-.00007

Displacement = .00940260 * volts + .01025245

Correlation Coefficient = .99999616

Standard deviation: .00000274

Standard error of estimate .00000000

95% Confidence limits--lower: .00939

Upper: .00941

Minimum difference = -.00010

Maximum difference = .00006

Percent minimum error = -1.01160

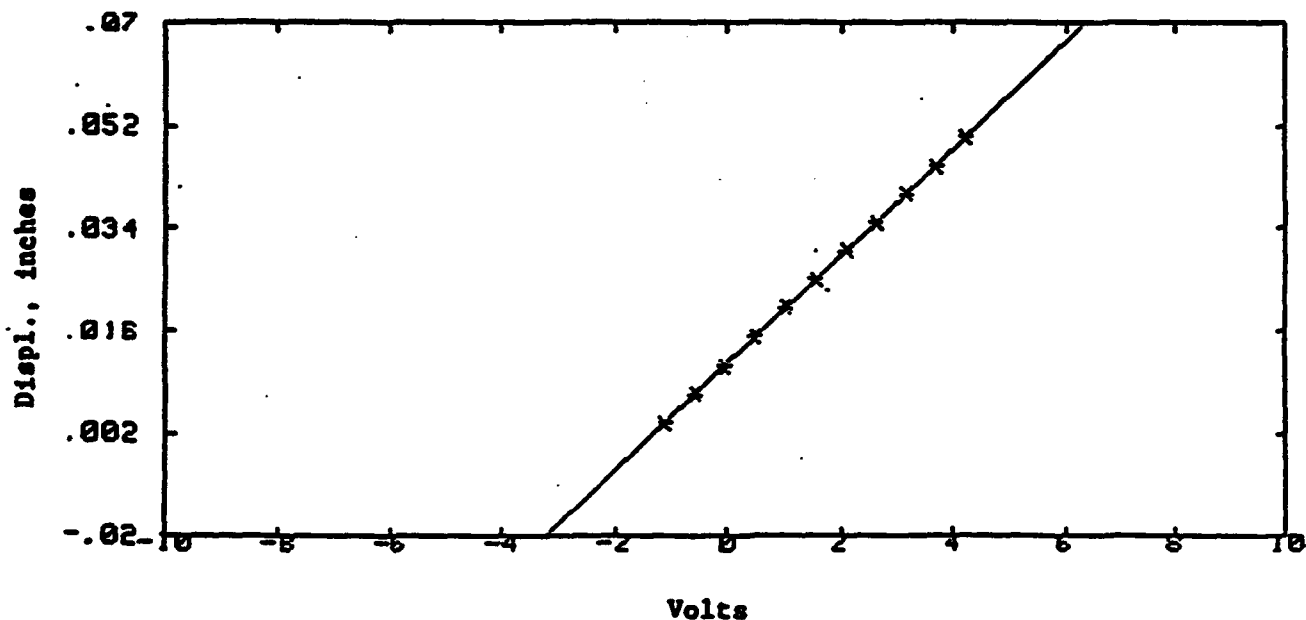
Percent maximum error = .63486

Mean Displacement = .00191798 * Volts + .01973719

Number of runs = 5

Standard deviation of Slope = .01032635

Standard deviation of Zero-intercept = .01865068



CLIP GAGE NUMBER MTS #810

TRIAL NUMBER 1

TODAYS DATE IS 6/27/86

CLIP GAGE MTS #810 VOLTAGE IS READ ON DVM # 702

EXCITATION VOLTAGE FOR CLIP GAGE MTS #810 IS 3.23

INITIAL POINT = .25 STEP SIZE = .005

01137"/V

CLIP GAGE #MTS #810 USED FOR DATA ACQUISITION 6/27/86

LOAD and DEFLECTION VALUES AS ACQUIRED

LOAD = SLOPE x DEFLECTION + CONSTANT

CORRESPONDING SLOPE = 87.9911761991 INVERSE = .011364775915
ALTERNATE METHOD SLOPE = 87.9910047431 INVERSE = .01136479806
THE Y INTERCEPT = -16.3525088379
COEFFICIENT OF DETERMINATION R^2 = .999998051446
CORRELATION COEFFICIENT R = .999999025722
STANDARD ERROR OF ESTIMATE = 2.34753333333E-09
STANDARD DEVIATION OF SLOPE = 7.38066651691E-07
99% CONFIDENCE ON SLOPE IS = 87.9760926572 < SLOPE < 88.0062649125
THE INVERSE SLOPE RANGE IS = 1.13628274191E-02 < SLOPE <
1.13667244111E-02

LOAD and DEFLECTION VALUES INTERCHANGED

(X) = SLOPE x (Y) + Constant

CORRESPONDING SLOPE = .01136479806 INVERSE = 87.9910047431
ALTERNATE METHOD SLOPE = .011364775915 INVERSE = 87.9911761991
THE Y INTERCEPT = .18584297856
COEFFICIENT OF DETERMINATION R^2 = .999998051446
CORRELATION COEFFICIENT R = .999999025722
STANDARD ERROR OF ESTIMATE = 1.81756190476E-05
STANDARD DEVIATION OF SLOPE = 5.71443115329E-03
99% CONFIDENCE ON SLOPE IS = 1.13628498941E-02 < SLOPE <
1.13667468939E-02
THE INVERSE SLOPE RANGE IS = 87.9759186453 < SLOPE < 88.006090E417

POINT #	1	DVM =	5.637500	DEFL =	.250	DIFF =	0.000000	PD =	.24991
POINT #	2	DVM =	5.199100	DEFL =	.245	DIFF =	.438400	PD =	.24493
POINT #	3	DVM =	4.761700	DEFL =	.240	DIFF =	.437400	PD =	.23996
POINT #	4	DVM =	4.323800	DEFL =	.235	DIFF =	.437900	PD =	.23498
POINT #	5	DVM =	3.885300	DEFL =	.230	DIFF =	.438500	PD =	.23000
POINT #	6	DVM =	3.445800	DEFL =	.225	DIFF =	.439500	PD =	.22500
POINT #	7	DVM =	3.006800	DEFL =	.220	DIFF =	.439000	PD =	.22001
POINT #	8	DVM =	2.567930	DEFL =	.215	DIFF =	.438870	PD =	.21503
POINT #	9	DVM =	2.129180	DEFL =	.210	DIFF =	.438750	PD =	.21004
POINT #	10	DVM =	1.690300	DEFL =	.205	DIFF =	.438880	PD =	.20505
POINT #	11	DVM =	1.249980	DEFL =	.200	DIFF =	.440320	PD =	.20005
POINT #	12	DVM =	.810110	DEFL =	.195	DIFF =	.439870	PD =	.19505
POINT #	13	DVM =	.370430	DEFL =	.190	DIFF =	.439680	PD =	.19005
POINT #	14	DVM =	-.069087	DEFL =	.185	DIFF =	.439517	PD =	.18506
POINT #	15	DVM =	-.510590	DEFL =	.180	DIFF =	.441503	PD =	.18004
POINT #	16	DVM =	-.951280	DEFL =	.175	DIFF =	.440690	PD =	.17503
POINT #	17	DVM =	-1.391850	DEFL =	.170	DIFF =	.440570	PD =	.17002
POINT #	18	DVM =	-1.833240	DEFL =	.165	DIFF =	.441390	PD =	.16501
POINT #	19	DVM =	-2.274620	DEFL =	.160	DIFF =	.441380	PD =	.15999
POINT #	20	DVM =	-2.716210	DEFL =	.155	DIFF =	.441590	PD =	.15497
POINT #	21	DVM =	-3.158000	DEFL =	.150	DIFF =	.441790	PD =	.14995
POINT #	22	DVM =	-3.599900	DEFL =	.145	DIFF =	.441900	PD =	.14493
POINT #	23	DVM =	-4.041200	DEFL =	.140	DIFF =	.441300	PD =	.13992

5.2 APPENDIX C-II

LEAK-BEFORE-BURST CRITERIA APPLIED TO CRYOFORMED PRESSURANT TANKS

K. H. Cotter
Fracture Proof Design Corporation
St. Louis, MO

Abstract

A leak-before-burst (LBB) criteria, based on linear-elastic fracture mechanics, was applied to typical pressurant tanks fabricated from cryoformed TP301 stainless steel. The LBB criteria included consideration of sub-critical flaw growth via fatigue and sustained load mechanisms. The analytical results, developed using toughness data obtained from coupons, were verified by full scale pressure vessel tests of two designs. For the verification tests, flaws were introduced into base metal, weld metal and HAZ regions and subsequently pressure cycled to leakage followed by overpressure. It is shown that the margins of safety attainable using a LBB criteria are inversely proportional to the square root of the wall thickness when other parameters are held constant. Because of the method of fabrication, consideration of weld residual stress effects and bending stresses due to misalignment was not necessary. Significant margins based on LBB characteristics were demonstrated for effective crack lengths that were in excess of those expected for in-service conditions and in excess of flaw sizes detectable by normal NDI methods.

Introduction

Background

During 1984 and 1985, the author participated in the review of the integrity of cryoformed stainless steel tanks. It became apparent during those meetings that the true damage tolerance capacity of such tanks and their likely "leak-before-burst" (LBB) character had not been demonstrated by test or by analysis. The lack of a valid analysis stemmed from the fact that no fracture toughness data existed for through-thickness cracks. Accordingly, it was suggested that fracture toughness data and crack growth resistance curves be obtained from coupon tests and a LBB analysis be performed. In view of the potential significance of a LBB demonstration, verification tests were planned in order to verify the leak-before-burst character of typical tanks. In order to obtain verification of the true residual strength of vessels containing cracks, a test program was begun. This paper details the findings from the full scale tests of 11 and 23 inch diameter, cryoformed and aged TP301 stainless steel spherical tanks.

Leak-Before-Burst Concepts

The current design philosophies for "high energy" pressure vessels, in safety related applications, include the consideration of the integrity of the vessel based on fracture mechanics in addition to margins against tensile failure. In addition to providing a measure of the margin of safety for a given detectable or postulated flaw

size, fracture mechanics principles can be used to define inspection and material toughness requirements.

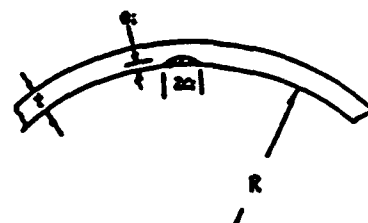
To that end, the leak-before-burst (LBB) concept is a useful measure of the tolerance of the pressure vessel to defects, that is, its damage tolerance. The simple concept begins with the assumption that a crack-like defect exists in the vessel (Figure 1a) and that the crack propagates by a fatigue crack growth (or other) mechanism until it penetrates the wall of the vessel (Figure 1b) which results in a detectable leak (Figure 1c). At break-through, the minimum size of the crack causing the leak is assumed to have a length, $2c$ of twice the wall thickness, $2t$, or longer. Naturally, the larger the crack that can be tolerated, the easier it is to detect the leak and the larger the margin against failure.



c) Assumed Length for Detectable Leak and Stability Calculations ($2c \geq 2t$)



b) At Breakthrough



a) Assumed initial defect

Figure 1. Crack Propagation for LBB

Fabrication, Metallurgy & Fracture Toughness

Fabrication

The procedure for the fabrication of the spherical tanks consisted of hydroforming the hemispheres, machining the hemispheres and then TIG welding. Each tank was next subjected to a detailed inspection sequence followed by solution annealing strengthening by cold work at -320°F ("cryoforming"), aging, and finally, proof-testing

The welds of the tank were not machined after welding which resulted in a slightly larger net section thickness in the weld region than in the base metal. As a result, a strain gradient exists in this region during the cryoforming procedure. Due to strain hardening effects, this thickness differential is less pronounced after the completion of the cryoforming process. Because of the plastic deformation that accompanies the cryoforming procedure, any bending stress component across the girth weld, that might be caused by misalignment during welding, is eliminated. This plastic straining, in addition to the solution anneal, insures that no weld residual stresses remain.

The results of more than 20 burst tests, conducted on similarly fabricated tanks were reviewed. All tanks exhibited fracture surfaces characteristic of tough materials. That is, the fracture surfaces exhibited some 30-40% shear rather than the flat fracture surface indicative of brittle behavior. Even though the running cracks crossed the girth weld, none of the burst test fractures tended to follow the weld metal or heat-affected zone. This behavior is indicative of high toughness at the weld metal and HAZ. The failures all appeared to initiate in the maximum effective stress region, that is, the region near to the transition from the sphere to the boss.

Metallurgy of Cryoformed TP301

The stainless steel alloy formulation used for the cryoforming, was developed in the 1960's as a closely controlled chemistry selected for reproducibility of process and maintainability of toughness and strength. It is a dual phase alloy composed of a very tough austenitic matrix with interlocking platelets of high strength martensite. The combination and distribution of phases results in a unique stainless steel alloy microstructure combining strength with high fracture toughness.

The thermal-mechanical processing technique used ("cryoforming") applies the metallurgical principle that an austenitic alloy, when strained, transforms to martensite. As the transformation to martensite occurs, the microstructure is locally hardened with no resultant local necking or thinning of the wall during the metallurgical transformation reaction. To accelerate the metallurgical reaction with minimum strain, the alloy is stretched at liquid nitrogen temperatures.

Forming of the hemispheres, machining of the bosses and the welding together of the vessel components are completed when the alloy is in the highly ductile austenitic phase. Room temperature deformation resulting from the fabrication leads to some work hardening of the vessel shell and welds. This is subsequently relieved by solution annealing.

Base Metal Microstructures. Straining the alloy at liquid nitrogen temperature significantly alters the initial austenitic microstructure by a shear transformation mechanism to martensite. The transformation occurs along the slip planes in the grains responding to the applied strain. The greater the strain the more complete the transformation. The structure can be visualized as platelets or laths of high strength material wedged in an orderly array to support the applied strain.

As the transformation is strain dependent, only those directions and areas in which (plastic) strain is applied are transformed. The remaining matrix is retained as a highly tough austenite. A typical microstructure at 500x magnification, using an electrolytic oxalic acid etchant, is shown in Figure 2D.

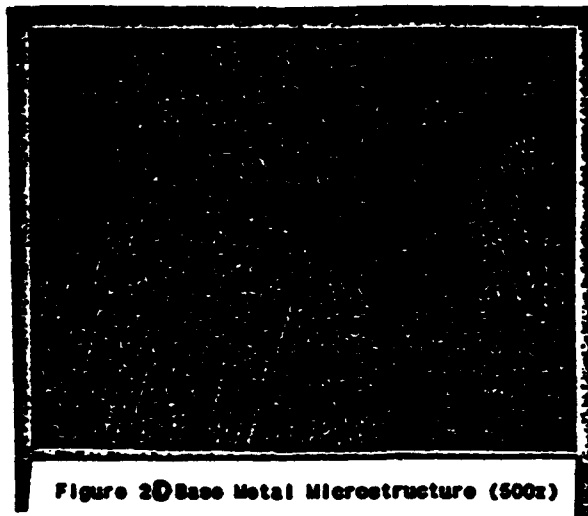


Figure 2D Base Metal Microstructure (500x)

Weld Metal Microstructure. The cast microstructure in the weldment is austenitic plus about a 5% delta ferrite phase principally located in the grain boundaries. The delta ferrite forms when the weld metal cools from the melting point through 1950F. The microstructure may, on occasion, be somewhat strained as the weld metal plastically deforms on cooling to release the thermal residual stresses.

The vessel, after welding, is solution heat treated and water quenched to assure that the microstructure is fully austenitic by redissolving all precipitated chromium carbides. This significantly alters the cast weldment as a major portion of the delta ferrite is converted to austenite. The residual delta ferrite grain boundary precipitates have also been significantly altered during the solution heat treatment and are observed in the microstructure as small isolated white or unetched spheres. The austenitic grain size formed during solution heat treatment is slightly larger than the adjacent wrought shell grain size. The small variations in chemical content inherent in the cast weld metal slightly modifies the amount of strain required to trigger the martensitic shear transformation. The cryostretched weld metal microstructure at 500x magnification is therefore somewhat mottled in appearance but otherwise equivalent to the wrought structure as shown in Figure 3D.

Aging. The low temperature aging heat treatment of cryostretched material increases the ultimate tensile strength by 40 ksi and is accompanied by a small gain in fracture toughness. There is no apparent change in the aged microstructure as viewed optically. At very high magnifications a very fine precipitate is apparent at the martensite laths to austenite matrix boundary. The Cr rich precipitate is quite fine and of insufficient volume to be positively identified by presently available diagnostic techniques.



Figure 3 Weld Metal Microstructure (500x)

Comparison with a Quenched and Tempered Martensitic Structure. A typical medium carbon low alloy steel, such as type 4340, is heated into the austenite range and cooled rapidly to insure that all of the austenite is converted to martensite. After quenching, the material is at its maximum hardness and lowest toughness. This requires that the steel must be subsequently tempered at a lower temperature to increase ductility and toughness with a corresponding lowering of strength. The tempering leads to a fine needle shaped microstructure of a high strength martensite matrix with a identifiable precipitate of carbides and converts a portion of the martensite to ferrite. The longer the tempering cycle, the coarser the carbides and the lower the alloy's hardness and strength.

In contrast, the straining during the thermal-mechanical processing of TP301 stainless steel alloy induces the martensite to form in the areas of applied strain. The former austenitic grains end up as a series of platelets of untransformed austenite and martensite. Aging of the alloy increases its strength as a fine precipitate is formed at the martensite/austenite interface. The microstructure is quite different in appearance from low alloy carbon steels and is a composite of an austenitic matrix with interlocked platelets of high strength martensite.

The two microstructures react quite differently when strained in the presence of a sharp notch. In both microstructures the martensite fractures. The quenched and tempered steels have a long continuous path through the martensitic matrix while the austenite matrix of the cryoformed alloy blunts the fracture and redistributes the strain at the crack tip. This explains why the cryoformed alloy has higher fracture toughness values at equivalent strength levels.

Fracture Toughness

It was found that the majority of toughness values reported in the literature³⁻⁸ for cryoformed TP301 stainless steel range from 85 to 105 ksi/in for weld metal, MAZ and base metal alike. See Table 1. These values were computed from test specimens with part-through thickness crack shapes which are not strictly applicable to the demonstration of LBB characteristics. In order to determine whether LBB conditions exist, it is necessary to have data from specimens containing

through-thickness cracks and from material of similar thickness.

Fracture toughness tests were conducted by Beck and Schwartzberg³ using part-through crack (PTC) specimens to determine the sustained load crack growth threshold, K_{Ih} . After sufficient hold times they cycled the specimens to produce center through-the-thickness crack specimen geometries (CTC) and then loaded the specimens to failure. Based on their data, the first applicable CTC data became available for LBB evaluations. Unfortunately, the material is not truly representative as there was not sufficient cryostraining and the alloy chemistry was not consistent with that currently in use.

The work of Bizier⁸ resulted in the demonstration of the LBB character of tanks tested at -295F. He also demonstrated that the cracks were stable at 72F when the PTC's penetrated the thickness of the specimens to become through-the-thickness cracks (TC's). However, the results⁸ relative to the toughness of TC's is qualitative rather than quantitative.

Recently, McCabe² tested cryoformed material in a number of conditions. He used the CTC specimen geometry for developing resistance curves for aged and unaged base metal and aged MAZ and weld metal. His results are compared with the results of prior studies in Table 1 where it is readily apparent that the cryoformed material exhibits excellent toughness. McCabe² also obtained estimates of the value of the toughness at which crack extension begins, the initiation toughness, K_{Ii} . He found that the values were in the range of 87-122 ksi/in. This range for K_{Ii} is consistent with the results of Forman⁷, Bizier⁸ and others.^{3,4,5,6} Testing by McCabe² also provided data that conclusively showed some stable crack extension prior to instability as shown in the typical R-curve of Figure 4 for aged material.

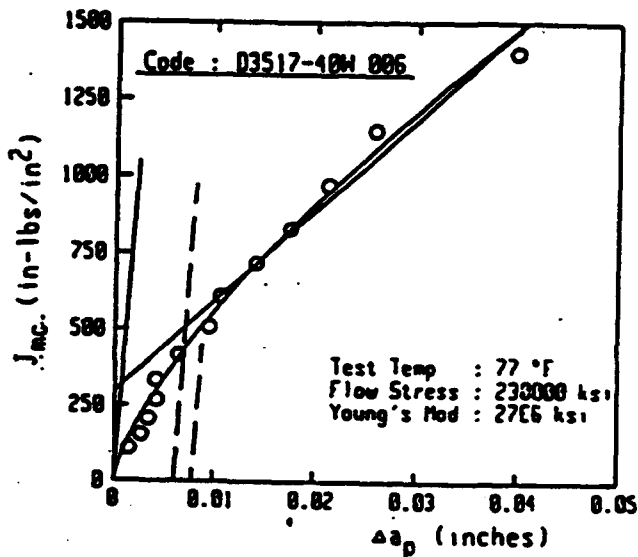


Figure 4 Typical Cryoformed Weld CTC R-Curve, 301 Base Metal/308L Weld Wire

Table 18 Room Temperature Fracture Toughness Data

Material (1)	Weld Wire	Specimen type (2)	Number of tests	Average Toughness (ksi/10)	σ_y (ksi)	σ_u (ksi)	t (in)	Source
BM/A		CTC	3	177.4	281	285	.084	Ref. 2
WM/A	308L	CTC	3	188.4	229	231	.084	
HAZ/A		CTC	3	188.4			.084	
WM/A	308L	CTC	3	183.2	220	231	.084	
BM/UA		CTC	3	158.0	207	215	.084	
BM/UA		PTC/TC	1	158	180	188	.125	Ref. 3
BM/UA		PTC	1	74	180	188	.125	
WM/UA	308L	PTC	1	85			.125	
WM/UA	308L	PTC	1	94			.125	
WM/UA	308L	PTC/TC	1	134			.125	
WM/UA	308L	PTC/TC	1	137			.125	
WM/UA	308L	PTC	1	57			.125	
BM/A		PTC(PV)	1	88.5	~200		.084	Ref. 5
BM/A		PTC	1	102.8	220		~.200	Ref. 6
BM/A		PTC	1	108.8	220		~.200	
WM/A	308L	PTC	1	103.8	219		~.200	
WM/UA	308L	PTC	3	86.8	175		.145	Ref. 7
HAZ/UA		PTC	3	86.8	~205		.145	
BM/UA		PTC	2	86.5	215		.145	
WM/A	308L	PTC	2	93.0	235		.145	
HAZ/A		PTC	2	97.3	~254		.145	
BM/A		PTC	2	102.8	258		.145	
BM/UA		PTC	10	116.5	174	210	(.100	Ref. 8
WM/UA	308L	PTC	7	92.3	181		2.028)	

Note:

.145 should be .063

1) BM= base metal; WM= weld metal; HAZ= heat-affected zone; /A= aged;
and, /UA= unaged

2) CTC= center through-crack; PTC= part-through crack; PTC/TC= PTC became TC
after penetrating thickness; and, CT= compact tension

LBS Analysis

Analytical Approach. The analysis of through-thickness cracks in the spherical tanks (Figure 1c) was based on that due to Sih and Dobrowoff⁹ and Sih and Hagendorf.¹⁰ For the computation of the stress-intensity factor, it is assumed that the crack is short compared with the radius of curvature of the shell and that the loading can be represented by a membrane force or stress, σ . For that condition, the stress intensity factor is given as follows:

$$K_I^2 = F_0(\lambda c) \sigma \sqrt{a_2} \quad (\text{tension}) \quad (1)$$

where the function F_0 is given in Figure 5 in terms of $\lambda c = E_1 c / \sqrt{Rt}$, $E_1 = [12(1-\mu^2)]^{1/2}$ and c , R , and t are as shown in Figure 1d. For the contribution due to the pressure of the fluid acting on the crack surface, the expression

$$K_p = p \sqrt{a_2} \quad (\text{crack surface pressure}) \quad (2)$$

was used where p is the internal pressure (psi) in the sphere. Using the foregoing crack driving force parameters, the total K_{app} can be found by the use of superposition of Equations (1) and (2). The effects of the crack-tip plastic zone correction on K_{app} were included where significant.

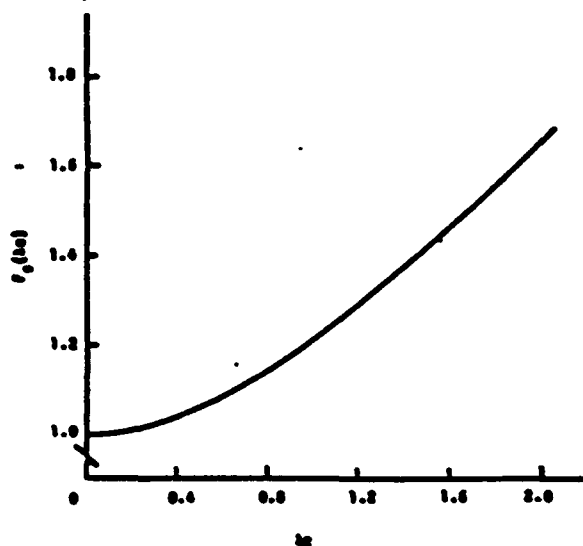


Figure 5 Spherical Shell Correction Factor.
 $F_0(\lambda c)$, Ref. 9 & 10

Crack Stability Calculations. Margins of safety for LBS computed using fracture mechanics methodology rely on the comparison of the crack driving force or stress-intensity factor, K_{app} , with the material's resistance to crack extension or R-curve. Alternately, a toughness criteria, $K_{app} < K_c$, can be used. The values of K_c used for the stability calculations were taken as the maximum values of the R-curves from Ref. 2 and shown in Table 1D.

Three 11 inch diameter spherical tanks and one 23 inch diameter spherical tank were selected for the LBS analyses. Tanks S/N 104 and S/N 105 were 11

inches in diameter with flaws located in the base metal (shell wall). The wall thickness at the flaw location, t_{off} , was nominally 0.080 inches. Tank S/N 003 also had an 11 inch diameter, but had flaws located in the girth weld metal, $t_{off} = 0.121$ inches. The final tank, S/N 113, was 23 inches in diameter with flaws in the girth weld metal, $t_{off} = .314$.

To determine the LBS characteristics of the tanks, K_{app} was computed as a function of the through-thickness crack length, $2c$, in multiples of wall thickness, t . K_{app} was computed for pressures equal to the operating pressure, P_{oper} , and for the overpressure, P_{max} . Because of the shape of the R-curves and the small amounts of crack extension, Δa , prior to failure ($\Delta a \leq .05$ in), it was possible to use the toughness criteria for stability computations. For reference, K_{app} was compared to both K_{I1} and K_c .

The results for tank S/N 104 for $P_{oper} = 3,800$ psi and $P_{max} = 4,060$ psi are shown in Figure 6D. For flaw lengths $2c = 3t$, $K_{app} < K_{I1}$. It is apparent that this tank can tolerate flaws of 7t in length at P_{oper} and still maintain LBS conditions. The value of P_{oper} corresponds to liquid pressurant while that of P_{max} represents an overpressure condition with a gas pressurant. This tank exhibited LBS with large margin.

In tank S/N 105, the results at $P_{oper} = 3,850$ psi are similar to S/N 104 and appear in Figure 7D. At $P_{max} = 6,100$ psi, flaws of length $2c > 1.5t$ in the base metal have values of $K_{app} > K_{I1}$. However, flaws as long as 5t are stable at P_{max} based on $K_{app} < K_c$. Again large margins were evident for LBS.

The flaws were located in the weld metal in tank S/N 003. For $P_{oper} = 4,060$ psi, flaws of length, $2c = 4t$, have $K_{app} < K_{I1}$. See Figure 8. This apparent improvement in tolerance to defects, compared with tanks S/N 104 & 105, is attributed to lower stresses in the weld than in the shell without any degradation in toughness. At $P_{max} = 6,800$ psi, $K_{app} < K_c$ for a flaw of length $2c = 5t$. The margins for LBS were greater than those for flaws in base metal for the reasons noted.

The analysis of the 23 inch tank, S/N 113, also showed excellent margins of integrity based on a LBS criteria. At $P_{oper} = 4,000$ psi, $K_{app} < K_{I1}$ for flaws $2c < 2.5t$ while no instability was apparent at $P_{max} = 4,860$ psi and $2c = 5t$ based on $K_{app} < K_c$. This tank showed slightly lower margins based on K_{I1} than the 11 inch tanks due to the thicker shell and weld sections, but the margins for LBS remained excellent. The results appear in Figure 9.

This analysis was based on coupon data and was without the benefit of full scale verification tests. In the next section, the verification tests are presented and reviewed.

Verification Tests

Full scale demonstration tests were performed on the tanks analyzed in the previous section. The results are evaluated based on fracture mechanics principles. The tanks had 11 and 23 inch diameters with nominal base metal wall thicknesses of 0.080 and 0.220 inches respectively with their flaw locations summarized in Table 2D.

LBB EVALUATION
 COMPARED WITH CRACKLESS STEEL, SPHERICAL TANK
 S/N 104, D = 11 IN., FLOW IN BASE METAL

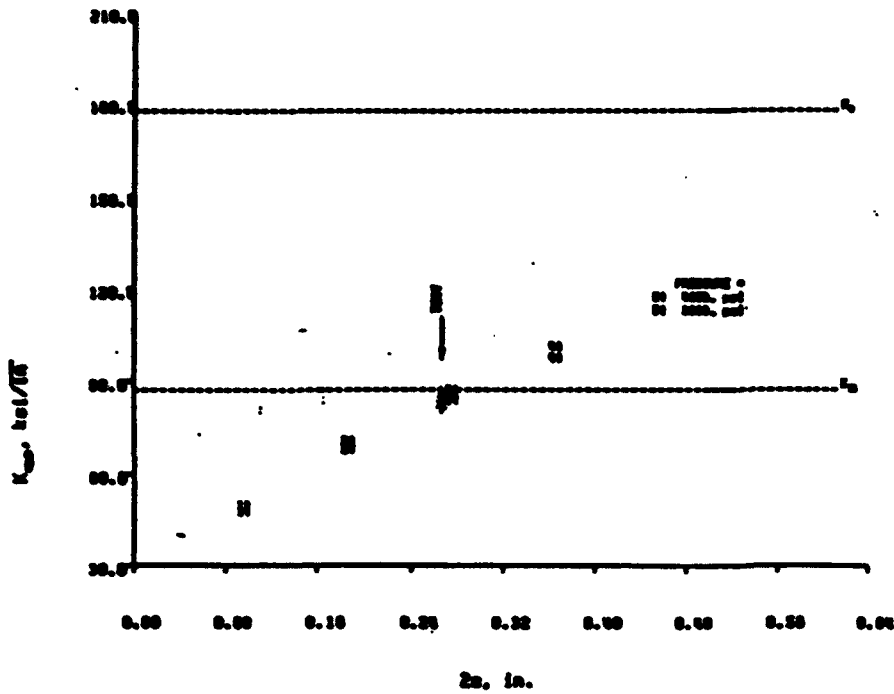


Figure 6D LBB Evaluation for Tank S/N 104,
 D = 11 in., Flow in Base Metal

LBB EVALUATION
 COMPARED WITH CRACKLESS STEEL, SPHERICAL TANK
 S/N 105, D = 11 IN., FLOW IN BASE METAL

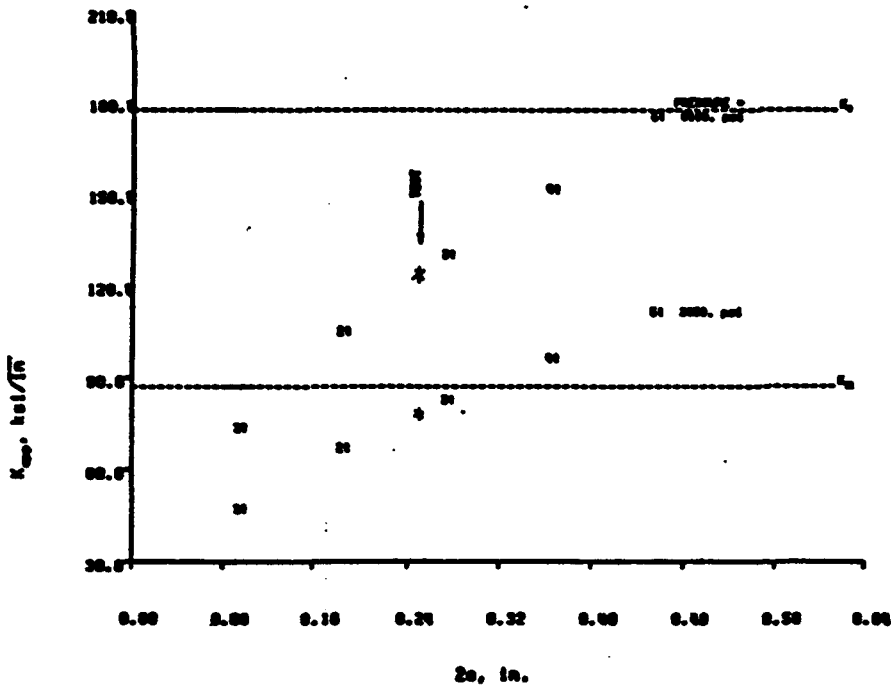




Figure 7D LBB Evaluation for Tank S/N 105,
 D = 11 in., Flow in Base Metal

See  Note
 on Fig. 7 P. 16
 of main text.

See  Note
 on Fig. 7 P. 16
 of main text.

LBS EVALUATION
 COMPARED WITH CRACKED STEEL, SPECIAL TANK
 S/N 003, D = 11 IN., FLAW IN WELD METAL

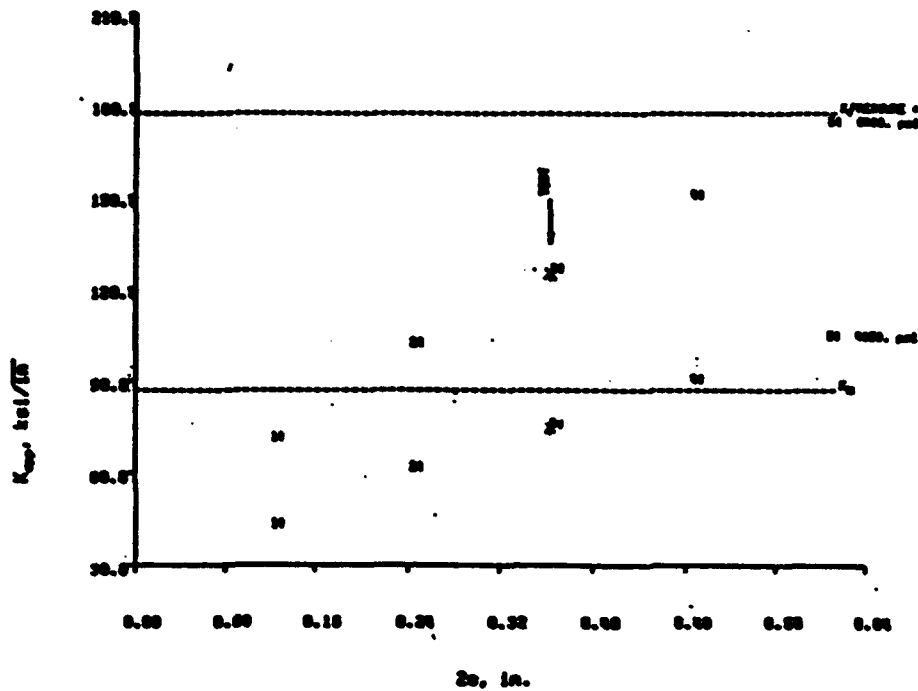


Figure 8D LBS Evaluation for Tank S/N 003,
 D = 11 in., Flaw in Weld Metal

See Note
 on Fig. 7B,
 P. 16 of main
 text.

LBS EVALUATION
 COMPARED WITH CRACKED STEEL, SPECIAL TANK
 S/N 113, D = 23 IN., FLAW IN WELD METAL

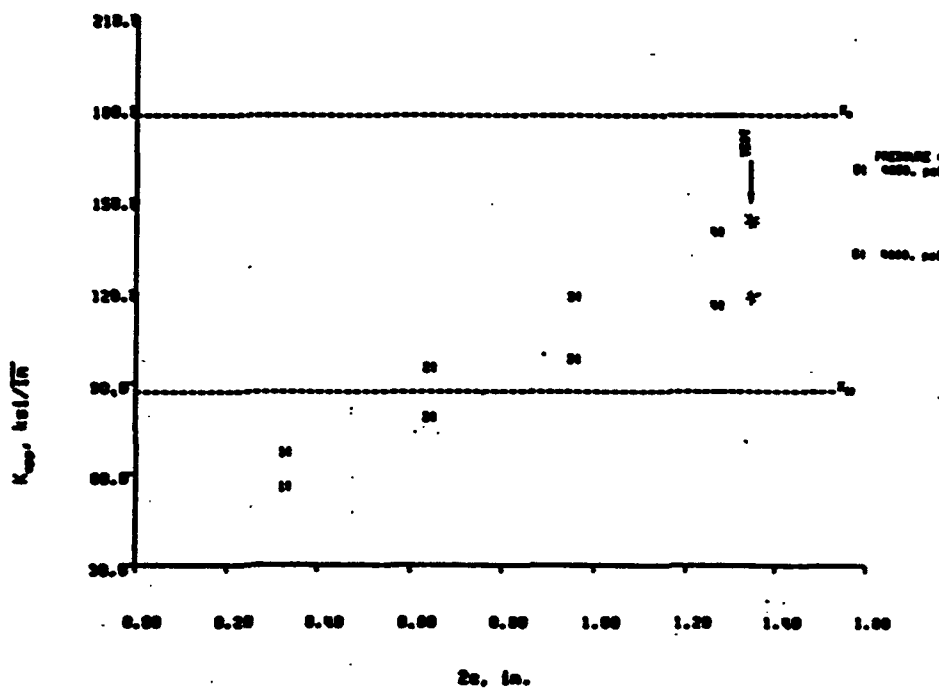


Figure 9D LBS Evaluation for Tank S/N 113,
 D = 23 in., Flaw in Weld Metal

See Note
 on Fig. 7B,
 P. 16 of main
 text.

4.00 Test Parameters

Initial Defects. EDM notches were cut into the vessels in order to initiate fatigue cracks. These notches were all semi-elliptical having the initial aspect ratios, $(a/2c)_i$, given in Table 3D. The aspect ratio was selected to produce fatigue cracks that would be conservative compared with that which might be expected to occur in practice. The notch cut into the 23 inch tank, S/N 113, is shown in Figure 10D.

Load Spectrum. For purposes of propagating the cracks introduced by the EDM notches, the vessels were subjected to pressure cycles (0- P_{oper} -0) where P_{oper} is shown in Table 3D. After, the through-the-thickness crack had developed and a visible leak was noted, 2 of the vessels were subjected to the sustained loads for the durations and pressures, P_{oper} , shown in Table 4D. Finally, attempts to burst the tanks were made at the overpressures, P_{max} , shown in Table 5D. The load cycles to develop fatigue cracks were accomplished using an oil + water mixture to pressurize the tanks. The overpressure was similarly applied except to tank S/N 104 for which the overpressure was with gas.

Crack Stability. Specific computations were made for the effective crack lengths, $2c_{eff}$, for the 4 tanks. The associated values of K_{app} are shown in Figures 6-0D and identified as "TEST." The LBB characteristics of all tanks were verified as shown in Figures 6-0D. The pronounced leak in the 23 inch tank, S/N 113, due to the large crack size, is evident in Figure 11D at $P_{max} = 4,850$ psi.



Figure 10D EDM Crack Starter Notch in Tank S/N 113

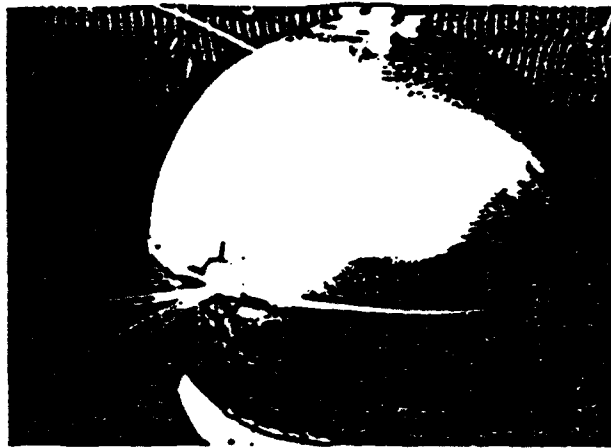


Figure 11D Fluid Leakage at $P_{max} = 4,850$ psi.
Tank S/N 113

Sustained Load Crack Growth

The remaining concern in the evaluation of the integrity of the tanks is that of static or sustained-load crack growth. Two sustained-load crack growth tests were performed as a part of the test program. No crack growth was observed after 75 hours at operating pressure for tank S/N 105. Similarly, none was observed for the 48 hours at operating pressure during the test of tank S/N 003.

The literature⁷ indicates that the value for the threshold for sustained load growth, K_{th} , should be between approximately 80% of the value of initiation toughness, K_{II} . K_{II} is the value of K_{app} at which crack extension begins, but not necessarily the point of instability. The values of K_{app} shown in Table 4D agree with those of Forman.⁷

Metallurgical Evaluation

After the completion of the tests, the vessels were subjected to a metallurgical examination. This consisted of taking SEM photomicrographs of the defect locations after exposing the crack surface. The penetration of the fatigue crack through the inside wall of tank S/N 113 is shown in Figure 12D. The fracture surface for tank S/N 113 is shown in Figure 13D. Note the EDM flaw, the fatigue crack growth and the shear lips, associated with a tough material, that were generated at breakthrough.

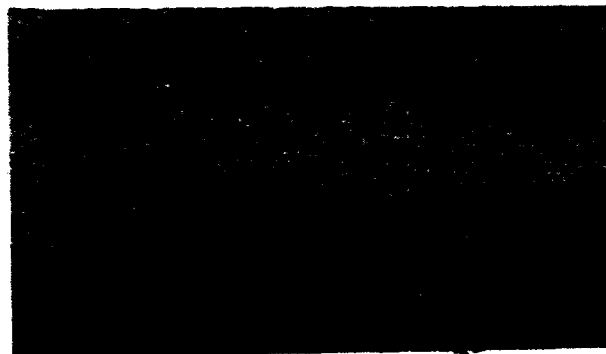


Figure 12D Breakthrough of Crack on ID of
Tank S/N 113

Table 2D Test Parameters

Tank S/N	Condition	Flaw Location	Nominal Diameter (in)
105	Aged	BM	11
003	Aged	WM	11
104	Aged	BM	11
113	Aged	WM	23

Table 3D Cycles to Leak

Tank S/N	P_{oper} (psi)	t_{eff} (in)	$(a/2c)_i$	a_i (in)	N (cycles)
105	4,200	.088	.21	.041	2,580
003	4,000	.121	.24	.074	2,948
104	3,800	.080	.23	.044	2,338
113	4,000	.314	.20	.183	2,877

Table 4D Sustained Load Tests

Tank S/N	Duration (hr)	P_{oper} (psi)	K_{app} (ksi/ \sqrt{in})
105	27	3,475 to 4,130	84.9
105	48	3,850 to 4,000	82.2
003	48	~4,060	71.0

Table 5D LBB Verification

Tank S/N	$2c_{eff}$ (in)	$2c_{eff}$ t_{eff}	P_{max} (psi)	K_{app} (ksi/ \sqrt{in})	K_{II} (ksi/ \sqrt{in})	K_c (ksi/ \sqrt{in})
105	.252	2.83	6,100	131.7	87.0	177.4
003	.363	3.00	6,800	118.2	87.0	177.4
104	.288	2.96	4,050	80.9	108.7	158.0
113	1.350	4.30	4,850	135.9	87.0	177.4



Figure 130 Fracture Surface of Leaking Crack,
Tank S/N 113, EDM Notch on OD

Conclusions

Based on the full scale tests performed, it was found that all of the tanks exhibited leak-before-burst (LBB) characteristics, with large margins, for defects located both in base and weld metal.

LBB characteristics were demonstrated by test for effective crack lengths, $2c_{eff}$, between 2.83 and 4.30 times the wall thickness. This is contrasted with an expected length at breakthrough, for in-service defects, of 2 times the wall thickness.

At the operating pressure selected for the 11 inch tanks, the value of K_{app} was less than K_{II} for cracks having lengths greater than $3t$. Similar behavior was noted for the 23 inch tanks, but due to greater wall thickness, it was limited to cracks having lengths as long as $2.5t$.

Based on coupon test data², no difference in tolerance to defects was noted between the weld metal, base metal or HAZ. It also appears that aged material, with its higher strength, has higher toughness than unaged material. This observation was substantiated by the full scale verification tests.

The analytical results showed that all tanks could tolerate defects having through-thickness lengths greater than $6t$ at operating pressure. Based on the values of overpressure considered, 4,000-6,000 psi, defects up to $5t$ in length would not cause failure of the tanks.

The low fatigue crack growth rate present in the full scale tests translates to additional margins when coupled with the fact that the flaw sizes used for the tests were much larger than that which would be expected in actual service.

From the review of the manufacturing procedures, it was determined that the combined weld procedures plus cryoforming result in weld residual stresses at or very near zero and have eliminated the possibility of local bending stresses at the weld.

References

1. "Standard General Requirements for Safe Design and Operation of Pressurized Missile and Space Systems," USAF MIL-STD-1522A, May 28, 1964.

2. McCabe, D.E., preliminary fracture properties of cryoformed TP301 stainless steel, March 21, 1966, Materials Engineering Associates, Inc., Lanham, MD, to be published.

3. Beck, E.J. & Schwartzberg, F.R., "Fracture Behavior of Cryogenically Stretched 301 Stainless Steel Used in the M-600 Pressure Vessel," Martin Marietta Report MCR-71-63, February 1971, prepared under NASA Contract NAS 9-6339.

4. Private communication with A. Cozowith, Arad, Inc., Mahwah, NJ, March 1966.

5. Campbell, J.E., DMIC Review of Recent Developments - Mechanical Properties of Metals, DMIC, Battelle Memorial Institute, Columbus, OH, February 16, 1968.

6. Tests conducted by Thiekel Chemical Corporation under NASA Contract NAS 9-11977.

7. Forman, R.G., "Environmental Crack Growth Behavior of High-Strength Pressure Vessel Alloys," NASA TN D-7952, April 1975.

8. Bizler, W.D., "Fracture Control Method for Composite Tanks with Load Sharing Liners," NASA CR-134758, July 1975.

9. Sih, G. and Dobroff, P.S., Glasgow Math J., 12, 65, 1971.

10. Sih, G. and Hagendorf, H.C., "Thin-Shell Structures, Theory, Experiment and Design," edited by Y. C. Fung and E. E. Sechler, Prentice-Hall, Englewood Cliffs, NJ, 1974.

11. Escalona, A., "Leak Before Burst and Crack Growth Under Sustained Load Tests of D3912, S/N 105 HT, 88019," Arad Report ARM No. 289, Oct. 4, 1965.

APPENDIX D - Fiber Wrapped Cylinder Pressure/Strain Tests

ARDE Report EG 42001-1, which describes 6" ϕ fiber wrapped cylinder experiments and test data correlation, is presented in this section.

EG 42001-1

Issue Date: Dec. 14, 1984

PRELIMINARY MODEL VERIFICATION TESTS -
6 INCH DIAMETER KEVLAR -49 FIBER
WRAPPED CYLINDER PRESSURE/STRAIN TESTS

Prepared for:


PATRICK AIR FORCE BASE
FLORIDA, 32925

CONTRACT FO8606-84-C-0029

Prepared by:


D. Gleich

Approved by:


Engineering


Program Management

Submitted By:

ARDE, INC.
19 Industrial Avenue
Mahwah, N.J. 07430

CODE IDENT. NO. 05980

TABLE OF CONTENTS

	<u>PAGE</u>
1. Introduction and Summary	D-5
2. Test Description	D-7
2.1 Test Specimen	D-7
2.2 Test Set-Up	D-14
3. Test Results	D-14
4. Appendices	D-22
4.1 Test Data Correlation	D-22
4.2 Strain vs. Pressure Traces	D-28

LIST OF FIGURES

<u>FIGURE</u>		<u>PAGE</u>
2-1 E	6"Ø Cylindrical Fiber Wrapped Vessel	D-8
2-2 E	Photo-Test Set-Up	D-9
2-3 E	Photo - Vessel 030	D-10
2-4 E	Photo - Vessel 030	D-11
2-5 E	Photo - Vessel 028	D-12
2-6 E	Photo - Vessel 028	D-13
2-7 E	Schematic 6"Ø Cylinder Test Set-Up	D-15
3-1 E	Pressure vs. Hoop Strain S/N 030 (Gage C1)	D-17
3-2 E	Pressure vs. Helical Strain S/N 030 (Gage D2)	D-18
3-3 E	Pressure vs. Axial Strain S/N 030 (Gage L1)	D-19
3-4 E	Pressure vs. Hoop Strain S/N 028 (Gage C1, C2)	D-20
4-1 E	Cylinder Fiber Wrap, Stresses, Configuration and Pressure Load	D-24
4-2 E	Pressure vs. Strain Test Traces S/N 030 (Gages C1, C2, L1, L2)	D-30 to D-33
4-3 E	Pressure vs Strain Test Traces S/N 030 (Gages D1, D2)	D-34 to D-37
4-4 E	Pressure vs. Strain Test Traces S/N 028 (Gages C1, C2, L1, L2)	D-38 tp D-39
4-5 E	Pressure vs. Strain Test Traces S/N 028 (Gages D1, D2)	D-40 to D-41

1. Introduction and Summary

This report describes the Preliminary Model Verification Tests performed under Task I, "Develop Prediction Methods," of ARDE Contract F08606-84-C-0029, "Kevlar Overwrap Study". The purpose of the tests was to obtain fiber/resin materials properties data that would aid in the composite vessel failure modeling analysis task, using vessels constructed of the same fiber/resin system. The tests were designed to determine fiber less resin Young's modulus in the fiber directions, fiber ultimate strain and to confirm the strain transformation relations. The testing was performed by Teledyne Engineering Services, Waltham, Mass., under ARDE direction.

Two (2) 6" diameter Kevlar -49/resin fiber wrapped cylinders (S/N 028 and 030) were pressure tested to failure at room temperature using hydraulic oil as the pressurizing fluid. Pressure versus fiber strains were monitored by a pressure transducer and six (6) each strain gages mounted on each vessel. The test pressures and strains were recorded on strip chart recorders.

The test results confirmed fiber material properties and ultimate strain values to be used in the failure modeling analysis:

- (1) Fiber (less resin) Young's Moduli values of 19.5×10^3 ksi were obtained in the fiber direction for both the hoop and helical fibers. This result agrees closely with the 19×10^3 ksi value given by the manufacturer (DuPont), detailed by other investigators in the literature and used in the failure modeling.

- (2) The maximum fiber strain measured by a strain gage at rupture was 1.91%, close to the 2% ultimate strain value to be assumed in the failure modeling study. Hoop fiber stress was 372 ksi, compatible with the 1.91% strain, 19.5×10^3 ksi Young's modulus and the 3100 psig failure pressure.
- (3) Strain gage readings in the hoop, helical and axial directions were consistent. The change in fiber helical strain per change in pressure, $\frac{\Delta \epsilon_x}{\Delta p}$, was found to be about .004 (in/in)/ksi as directly measured, or as computed from measured hoop and axial strains, ϵ_θ and ϵ_x , together with the 24.75° helical fiber angle. This result confirms the classical strain transformation relations which will be utilized in the failure modeling analysis.

Proper installation of strain gages is generally difficult on uneven fiber wrapped surfaces. Although post yield strain gages (3 to 5% ultimate strain) and compatible adhesives, together with appropriate installation techniques were used on the 6" diameter test cylinders, most strain gages failed at strain levels much less than 2%. This result indicates that there is a potential strain gage installation problem with the full scale 16" diameter fiber overwrapped test spheres whose outer fiber surfaces are significantly more

irregular than the outer hoop fiber wrapped surfaces of the 6" diameter test cylinders discussed in this report. It is suggested that consideration be given to checking out the strain gage installation technique by testing suitable fiber wrapped hardware prior to testing the full scale 16" diameter composite spheres at RPL.

2. Test Description

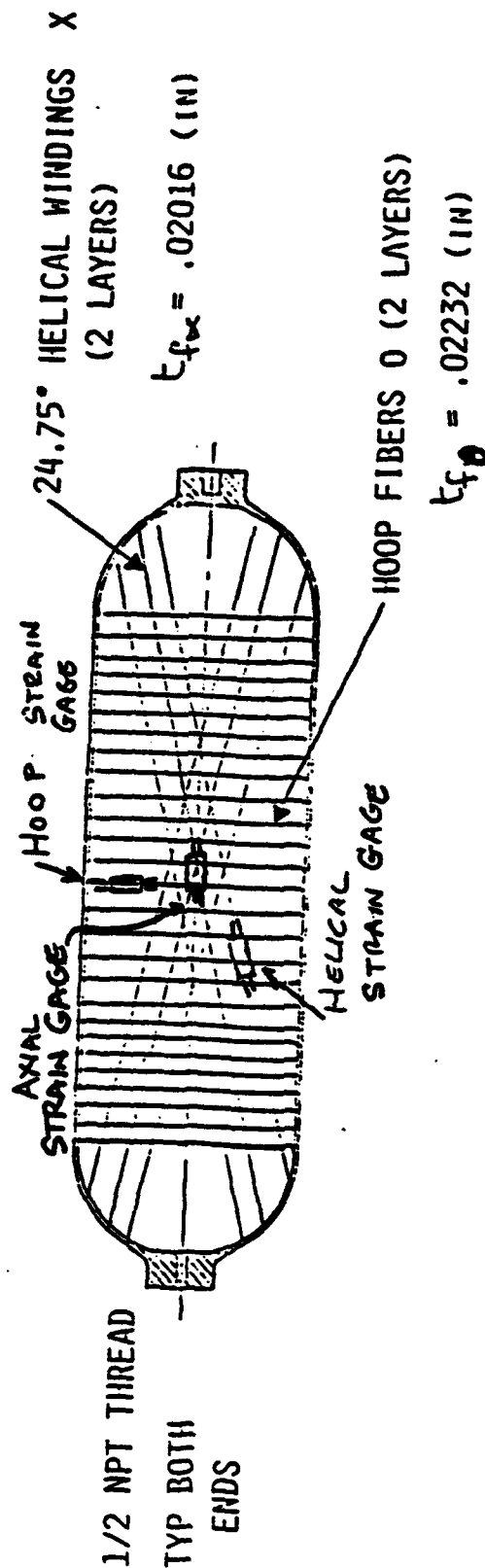
2.1 Test Specimen

The test specimen used is a 6" diameter Kevlar -49 fiber wrapped cylinder as shown on the sketch of Figure 2-1E and the photographs of Figures 2-2E to 2-6E. The fiber wrap pattern consists of two (2) each alternate layers of 24.75° helical and (90°) hoop fibers, with hoop fibers on the outer layer. The fibers are wrapped over a rubber liner supported by an aluminum mandrel. Port bosses and holes in the aluminum mandrel are provided for fiber cylinder fill, pressurization and draining. This construction assures that the fibers alone carry the internal pressure load. Hoop and helical Kevlar-49 fiber (less resin) thicknesses were .02232" and .02016", respectively, as given on Figure 2-1E. These test vessel fiber thicknesses were selected to give a hoop fiber failure mode. The resin system and cure temperature/time cycle for the 6" diameter cylindrical test specimen is the same as that which

• VESSEL

- HERCULES ABL STANDARD 6" NOMINAL I.D. CYLINDRICAL FILAMENT WOUND VESSELS WRAPPED OVER RUBBER COVERED ALUMINUM MANDREL WITH TWO BOSSES ATTACHED

VESSEL DESIGNED TO FAIL IN HOOP SECTION



WRAP PATTERN XOXO

FIGURE 2-1



PHOTO 1 - TEST SET-UP

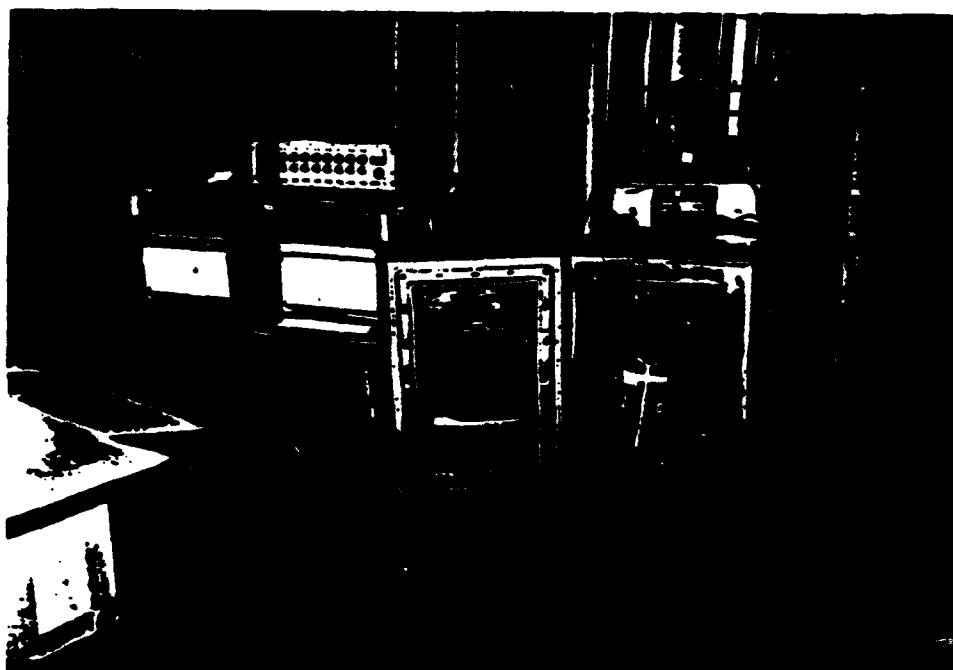


PHOTO 2 - TEST SET-UP

FIG. 2-2E



PHOTO 3 - VESSEL 030 READY FOR TESTING



PHOTO 4 - VESSEL 030

FIG. 2-3E

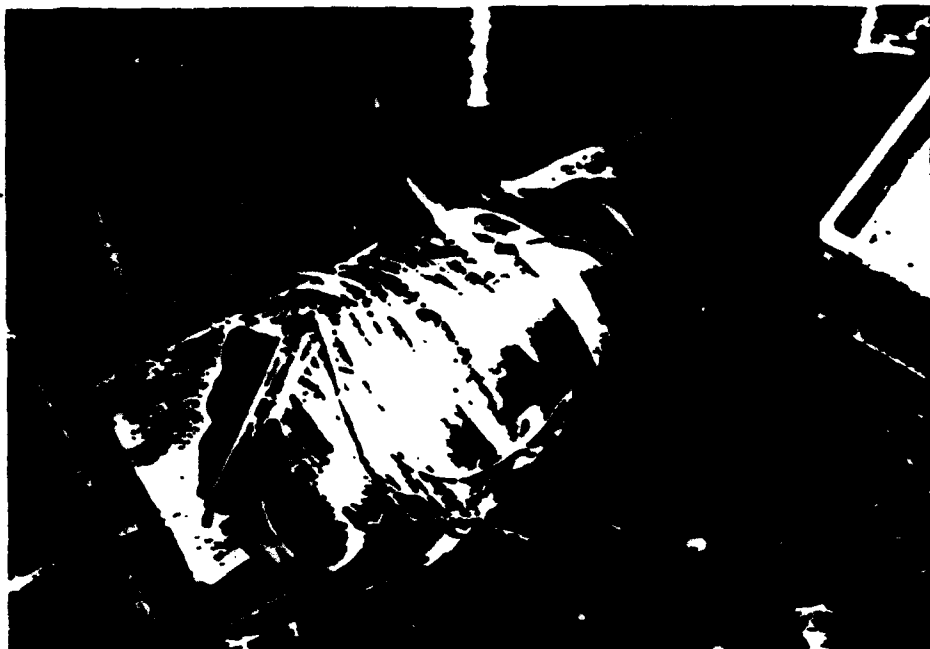


PHOTO 5 - VESSEL 030



PHOTO 6 - VESSEL 030

FIG. 2-4E

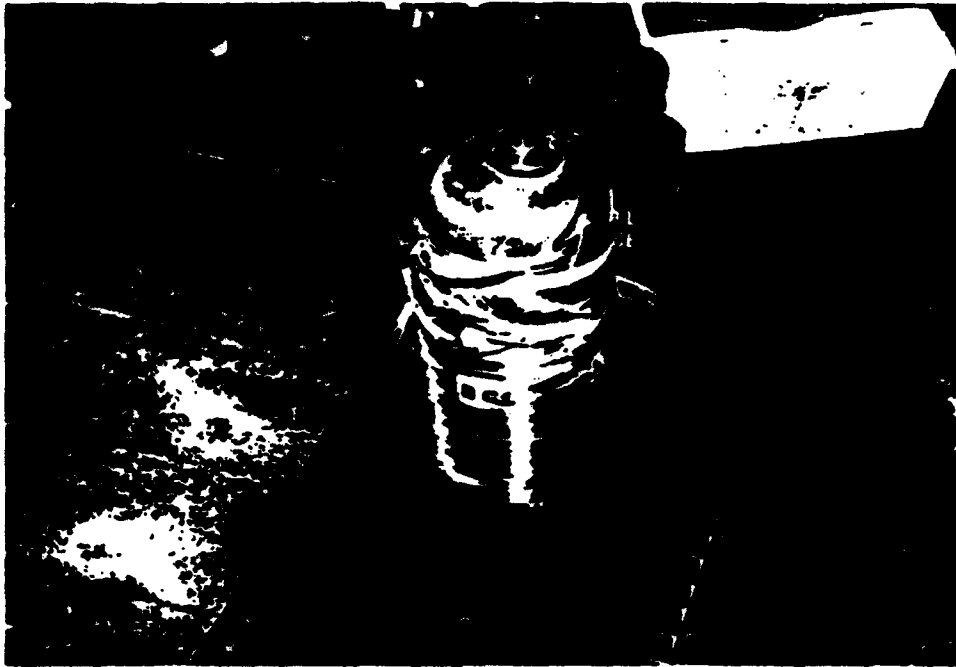


PHOTO 7 - VESSEL 028

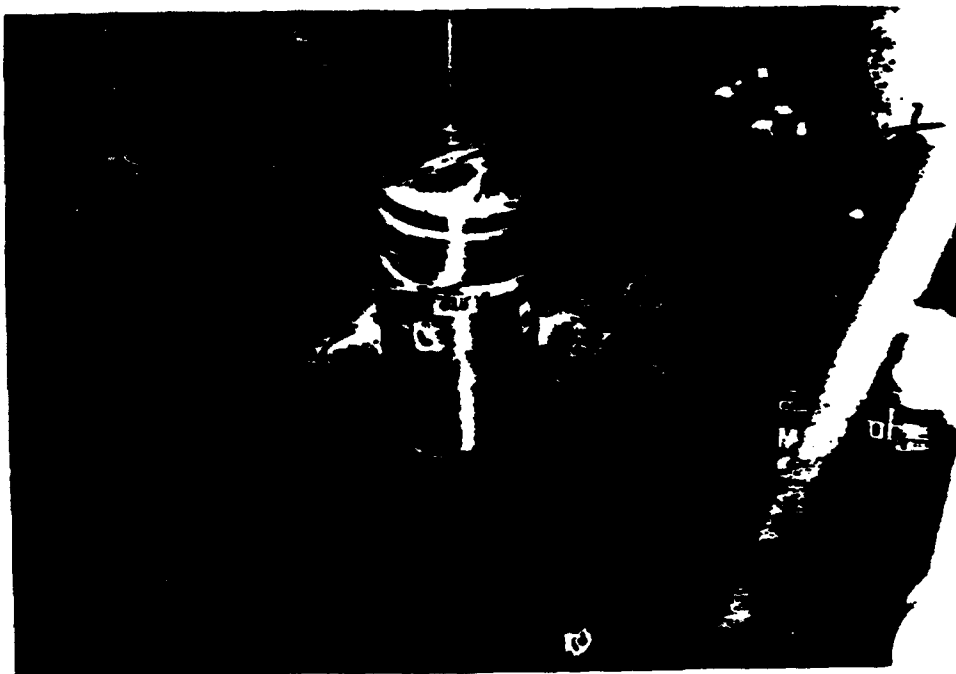


PHOTO 8 - VESSEL 028

FIG. 2-5E

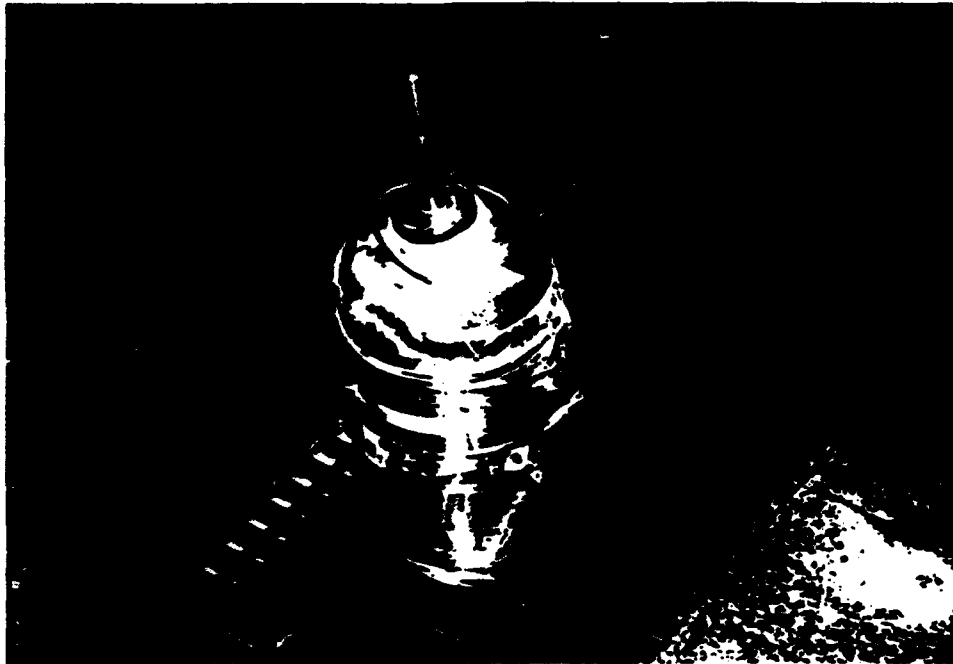


PHOTO 9 - VESSEL 028

FIG. 2-6E

will be used on the 16" diameter full scale composite test spheres. The resin is designated HARF 53 (DER 332/RD-2/TONOX 6040 with distribution in parts by weight of 100/25/29.3) cured 3 hours at 140°F followed by 4 hours at 248°F.

2.2 Test Set-Up

The test set-up is shown on the photographs of Figures 2-2, 2-3 and the schematic of Figure 2-7. The fiber wrapped cylindrical test specimen was instrumented at the cylinder center by hoop, helical and axial strain gages, 3 each at two locations 180° apart, as shown on the sketch of Figure 2-7. Pressure was monitored by a pressure transducer. Strain and pressure were recorded continuously on strip charts. The pressurizing fluid was hydraulic oil pressurized by an oil pump. The test specimen was housed in a metallic box for protection of personnel upon test vessel rupture.

3. Test Results

3.1 Fiber Material Properties and Strains

The actual test strain versus pressure traces for the two (2) test cylinders (S/N 028 and 030) are given on Figures 4-2 to 4-5 of Appendix 4.2. Details of the test data correlation are presented in Appendix 4.1. Figures 3-1 to 3-4 herein are graphs

REPORT NO. _____

JOB NO. _____

PREPARED BY _____

DATE _____

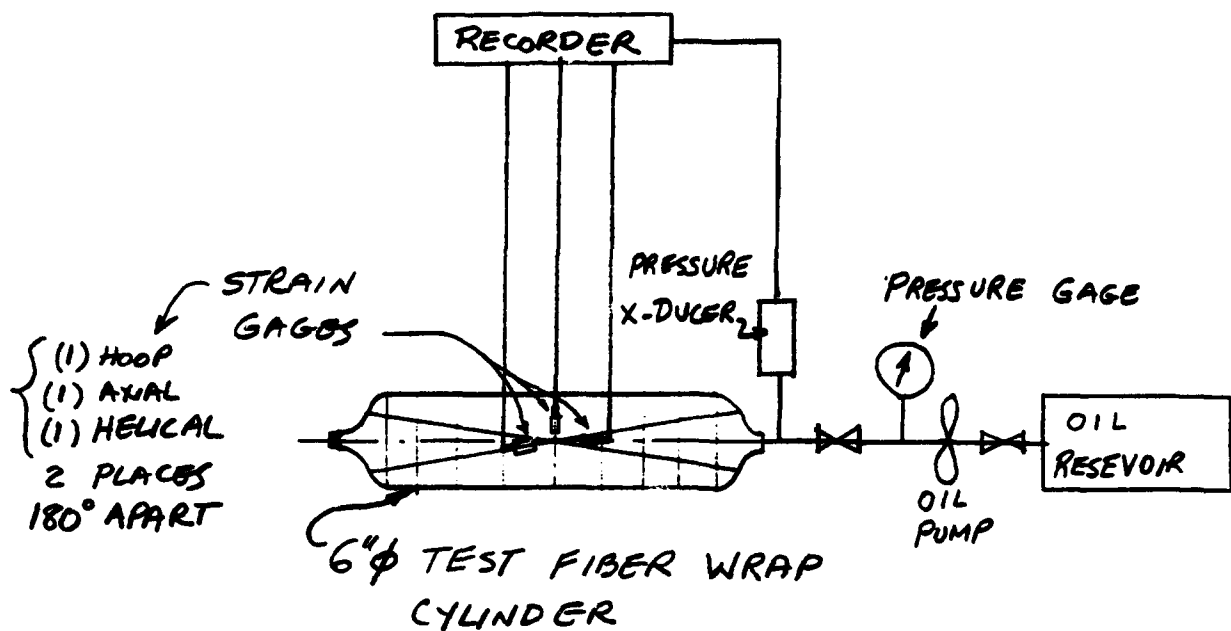
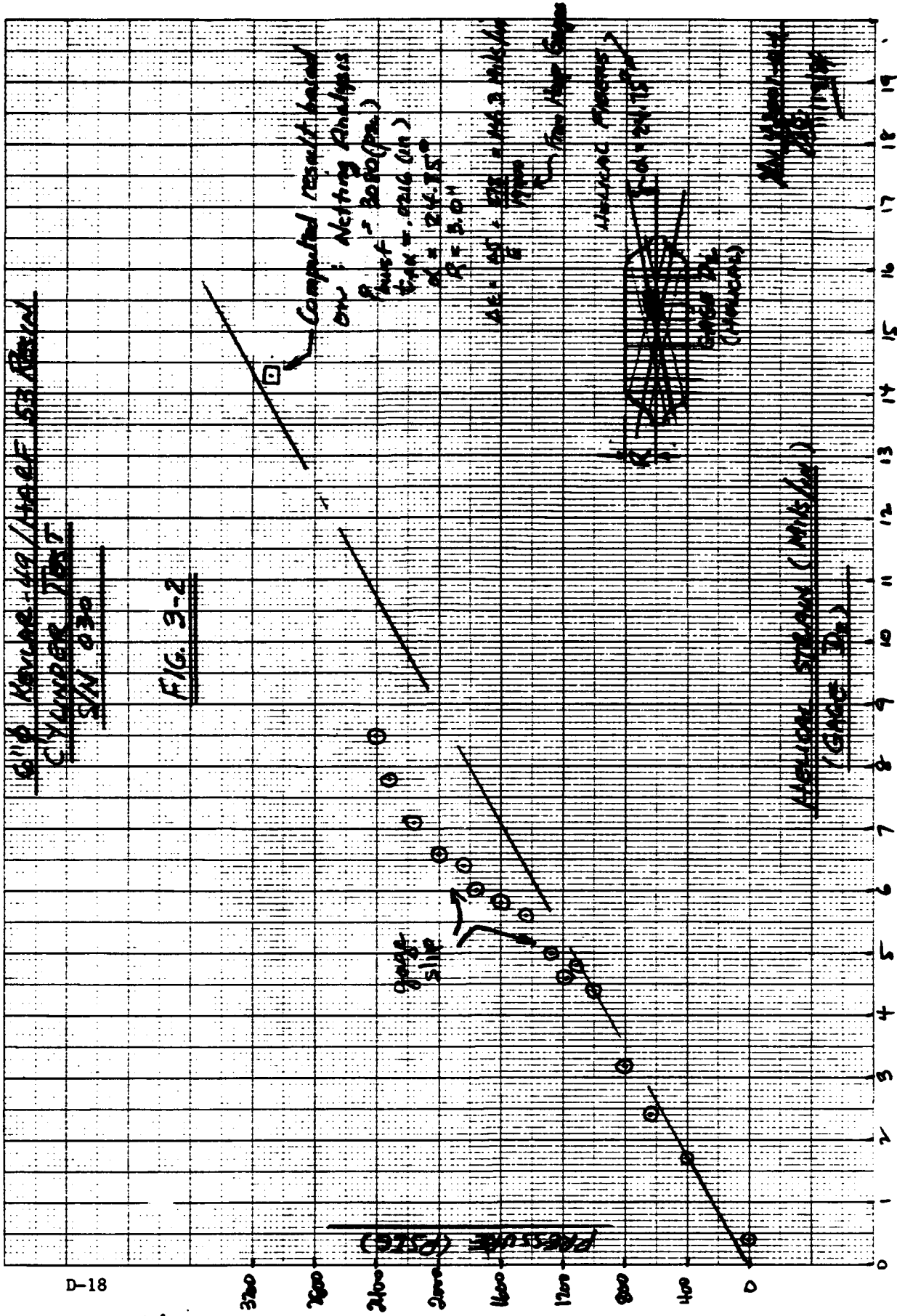


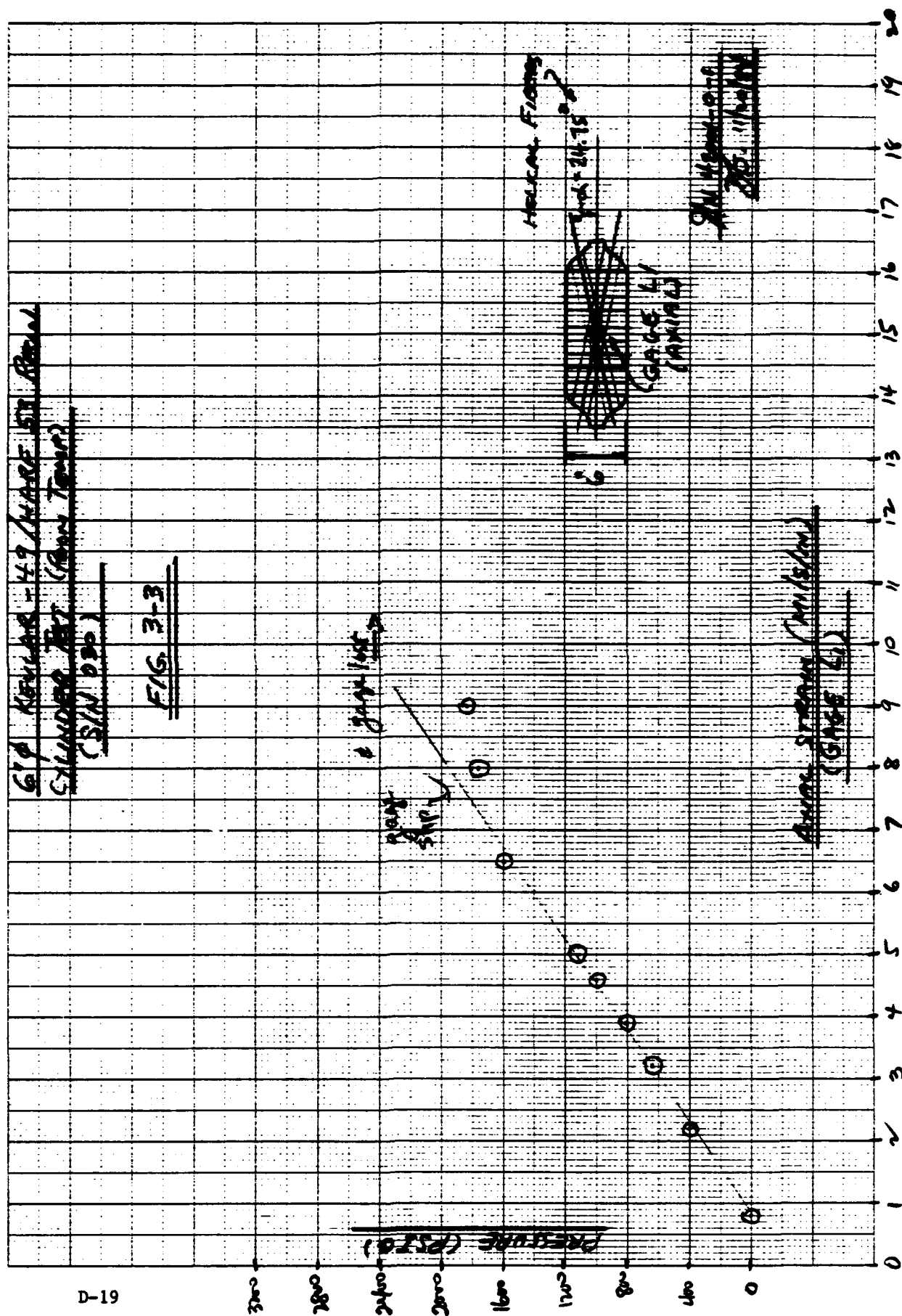
FIG. 2-7 E
SCHEMATIC
6" ϕ CYLINDER TEST
SET UP

of pressure versus strain for selected strain gages derived from the test traces. Figures 3-1 E to 3-3 E give hoop, helical and axial strain versus pressure for test cylinder 030 and Figure 3-4 E presents hoop strain versus pressure for test cylinder 028.

Test data correlation based on an equilibrium netting analysis (fibers only resist load) and measured strains, resulted in fiber less resin Young's Modulus in the fiber directions (hoop and helical) of 19.5×10^3 ksi which agrees closely with the 19×10^3 ksi value given by DuPont and reported in the literature by other investigators. Fiber hoop strain at burst was measured as .0191 in/in (See Figure 3-1 E) which is close to the 2% ultimate strain assumed in the failure modeling analysis. The vessel failure mode was hoop fiber failure, as designed (See Figures 2-3 E to 2-6 E). Burst pressures for the two test cylinders were very close; 3100/3080 psig for S/N 030 and 3040 psig for S/N 028 specimen. Fiber stresses at rupture were 372 ksi hoop and 280 ksi helical for S/N 030 cylinder. The measured hoop, helical and axial strain values were found to be consistent. The change in fiber









helical strain per change in pressure, $\frac{\Delta \epsilon_{\alpha}}{\Delta p}$, was determined to be about .004 (in/in)/ksi as directly measured, or as calculated from measured hoop and axial strains, ϵ_{θ} and ϵ_x , for the 24.75° helical fiber angle. This result verifies the classical strain transformations which will be used in the failure modeling analysis. The effective vessel fiber (less resin) Young's modulus in the non-fiber axial direction derived from this data was 14.1×10^3 ksi.

3.2 Strain Gage Failures

Many strain gages failed well below rupture pressure at strain levels much less than 2%. This is illustrated on the Figures 4-2E through 4-5E pressure traces of Appendix 4.2 and the graphs of Figures 3-2E, 3-3E. The undulating, uneven surface of the fiber wound vessel presents a difficult strain gage installation problem. It is suggested that consideration be given to verifying the adequacy of the strain gage type and installation technique to be used on the full scale 16" diameter composite spherical test vessels by means of tests of suitable fiberwrapped hardware prior to full scale testing at RPL.

4. APPENDICES

4.1 Test Data Correlation

4.1.1 S/N 030 Test Vessel

4.1.1.1 Notation

E = Youngs Modulus

p = Pressure

R = Radius

t = Thickness

α = angle of fiber with cylinder
axis of rotation

Δ = Increment

ϵ = Normal Strain

γ = Shear Strain

ν = Poisson's Ratio

σ = Normal Stress

Subscripts

f = Fiber

α = Inclined angle direction

θ = Hoop direction

X = Axial direction

4.1.1.2 Equilibrium Analysis

Figure 4-1 shows schematically the stresses, fiber directions, pressure load and radius of the test cylindrical vessel. Assuming that the resin does not resist load, hoop and axial equilibrium require that,

$$\sigma_{f\theta} t_{f\theta} + \sigma_{f\alpha} t_{f\alpha} \sin^2 \alpha = pR \quad \text{---(1)}$$

$$\sigma_{f\alpha} t_{f\alpha} \cos^2 \alpha = \frac{pR}{2} \quad \text{---(2)}$$

From (1) and (2) we have,

$$\sigma_{f\theta} = \frac{pR}{t_{f\theta}} \left(1 - \frac{1}{2} \tan^2 \alpha\right) \quad \text{---(3)}$$

For S/N 030 test results, Figures 2-1E, 3-1E,
 $\alpha = 24.75^\circ$, $t_{f\theta} = .02232$, $t_{f\alpha} = .02016$,
 $p_b = 3100$, $R = 30$, $\Delta \epsilon_{f\theta} = .0191$

one obtains from (2) and (3) above the fiber less resin stresses and hoop Young's modulus,

$$\sigma_{f\theta} = \frac{3100 \times 30}{.02232} \left(1 - \frac{1}{2} \tan^2 24.75^\circ\right) = 372 \text{ ksi}$$

$$\sigma_{f\alpha} = \frac{3100 \times 30}{2 \times .02016 \cos^2 24.75^\circ} = 280 \text{ ksi}$$

$$E_\theta = \frac{\Delta \sigma_{f\theta}}{\Delta \epsilon_{f\theta}} = \frac{372}{.0191} = 19.5 \times 10^3 \text{ ksi}$$

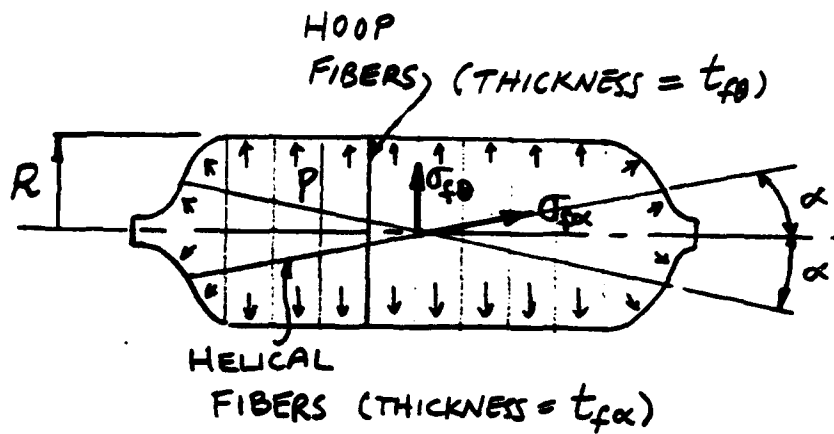


FIG. 4-1 E
CYLINDER
FIBER WRAP
STRESSES, CONFIGURATION
AND PRESSURE LOAD

4.1.1.3 Strain Transformation and Measured Strain Consistency

From Figures 3-1E to 3-3E, we obtain the measured slopes of the pressure versus fiber strain curves as,

$$\frac{\Delta P}{\Delta \epsilon_{\theta}} = \frac{1.2}{.007} = 171.429 \text{ ksi/(in/in)} \text{ (Hoop)}$$

$$\frac{\Delta P}{\Delta \epsilon_x} = \frac{1.4}{.0052} = 269.231 \text{ ksi/(in/in)} \text{ (Axial)}$$

$$\frac{\Delta P}{\Delta \epsilon_{\alpha}} = \frac{1.8}{.008} = 225.0 \text{ ksi/(in/in)} \text{ (Helical)}$$

Using the classical strain transformation relation,*

$$\epsilon_{\alpha} = \epsilon_x \cos^2 \alpha + \epsilon_{\theta} \sin^2 \alpha + \frac{\gamma_{\theta x}}{2} \sin 2\alpha \quad \text{--- (4)}$$

*Stavsky, Y. and Hoff, N.J., "Mechanics of Composite Structures," in "Composite Engineering Laminates," edited by A.G.H. Dietz, MIT Press, 1969.

we find with ($\gamma_{\theta x} = 0$ for hoop and axial principal directions) $\alpha = 24.75^\circ$

and the above numerical values that,

$$\epsilon_{\alpha} = \frac{\Delta p \cos^2(24.75^\circ)}{269.231} + \frac{\Delta p \sin^2(24.75^\circ)}{171.429}$$

or,

$$\frac{\epsilon_{\alpha}}{\Delta p} = .0041 \text{ (in/in)/ksi}$$

This computed value using hoop and axial measured strains agrees very closely with the directly measured helical strain/pressure slope of

$$\frac{\epsilon_{\alpha}}{\Delta p} (\text{measured}) = \frac{1}{225} = .0044 \text{ (in/in)/ksi}$$

The validity of the classical strain transformation and the consistency of the measured strains are therefore verified.

4.1.1.4 Helical Fiber Young's Modulus

We have from (2) and (3) with

$$\alpha = 24.75^\circ, R = 3, t_{f\theta} = .02232, t_{fx} = .02016,$$

$$\sigma_{f\theta} = \frac{3p}{.02232} \left(1 - \frac{1}{2} \tan^2 24.75^\circ\right) = 120.126 p \dots (5)$$

$$\sigma_{fx} = \frac{3p}{2 \times .02016 \times \cos^2 24.75^\circ} = 90.218 p \dots (6)$$

Taking principal directions as hoop and axial, Hooke's Law for the fibers

becomes*

$$\epsilon_x = \frac{\sigma_x}{E_x} - \frac{\nu_{ex} \sigma_{\theta}}{E_{\theta}} \quad \text{--- (7)}$$

Substituting numerical values (5), (6)

in (7) gives with $\alpha = 24.75^\circ$, $\nu_{\theta x} = .25$, $\sigma_x = \epsilon_x \cos^2 \alpha$,

$$\epsilon_x = \frac{90.218 p \cos^2(24.75^\circ)}{E_x} - \frac{.25(120.126 p)}{E_{\theta}}$$

or,

$$E_x = \frac{90.218 \cos^2(24.75^\circ) p}{\epsilon_x + \frac{.25(120.126 p)}{E_{\theta}}} \quad \text{--- (8)}$$

From Figure 3-3E, $\epsilon_x = .0052$ at $p = 1.4$ ksi and taking $E_{\theta} \approx 19 \times 10^3$ ksi, we have from (8) the axial direction Young's modulus,

$$E_x = \frac{90.218 \cos^2(24.75^\circ) \times 1.4}{.0052 + \frac{.25(120.126) \times 1.4}{19 \times 10^3}} = 14.05 \text{ ksi (fiber less resin)}$$

* See footnote on page D-25

For fiber volume ratio = 2/3, the composite axial Young's modulus is,

$$E_x(\text{composite}) = \frac{2}{3} \times 14.05 \times 10^3 = 9.37 \times 10^3 \text{ ksi}$$

4.1.2 S/N 028 Test Vessel

Hoop Young's modulus is given by

$$E_\theta = \frac{\Delta \sigma_{f\theta}}{\Delta \epsilon_\theta} \dots (9)$$

Using (5) and noting from Figure 3-4 that

$$\frac{\Delta p}{\Delta \epsilon_\theta} = \frac{1.2}{.0074}, \text{ we compute from (9)}$$

$$\frac{120.126 \Delta p}{\Delta p \left(\frac{.0074}{1.2} \right)} = 19.5 \times 10^3 \text{ (fiber less resin) ksi}$$

This value agrees with the prior determined S/N 030 vessel result, demonstrating measurement consistency.

4.2 Strain vs. Pressure Traces

Two (2) separate time-coordinated strip chart recorders were used in the test and an individual pressure trace was used on each recorder to maintain accurate pressure versus strain recording.

APPENDIX E - 16" ϕ and 22" ϕ PSC Vessel Tests

This appendix gives detail descriptions of all the 16" ϕ and 22" ϕ full scale composite vessel tests. For ease of reference, the table of contents of this large appendix is given below.

<u>Section</u>	<u>Page</u>
E.1 Full Scale Composite Vessel Tests -	E-1
Instrumentation Requirements/Procedures	
E.2 16" ϕ and 22" ϕ PSC Vessel Test Matrix	E-33
E.3 RV-4 RV-4A Tests (16" ϕ PSC)	E-37
E.4 PV-5 Test (16" ϕ PSC)	E-59
E.5 RV-7 Test (16" ϕ PSC)	E-81
E.6 RV-9 Test (16" ϕ PSC)	E-112
E.7 RV-10 Test (16" ϕ PSC)	E-138
E.8 RV-11 Test (16" ϕ)	E-166
E.9 RV-12 Test (22" ϕ)	E-196
E.10 RV-12A Test (22" ϕ)	E-204
E.11 RV-14 Test (16" ϕ)	E-234
E.12 RV-14A Test (16" ϕ)	E-252

E.1

Full Scale Composite Vessel Tests -
Instrumentation Requirements/Procedures

This section of Appendix E contains ARDE document EG 42001-5 and ARDE letter 42001-KOS-084, which define Kevlar Overwrap Study Composite Vessel Tests Instrumentation Requirements/Procedures and near term experimental system checkout tests, respectively.

February 3, 1986

Mr. Jim Miller
AFRPL/TOAE
Stop 24
Edwards AFB, CA 93523-5000

- Reference:
- (1) Contract F08606-84-C-0029
 - (2) ARDE Document EG42001-8, "Kevlar Overwrap Study Full Scale Composite Sphere Testing Scope of Work"
 - (3) ARDE Document EG42001-5, "Kevlar Overwrap Study Full Scale Composite Vessel Tests Instrumentation Requirements/Procedures"
 - (4) AFRPL Document, AFRPL Project Number 573000RV, "Kevlar Overwrap Study Full Scale Composite Vessel Experimental Plan and Procedure", by Jim Miller, AFRPL/TOAE, Nov. 1985
 - (5) ARDE Letter 52001-KOS-080, "Transmittal of Meeting Minutes for Kevlar Overwrap Study Test Planning Meeting at AFRPL, EAFB, California, 12/10 to 12/12/85."
 - (6) Telephone Discussion, D. Gleich (ARDE) Sgt. J. Day AFRPL, 1/22 and 1/27/86
 - (7) Telephone Discussion, S. Berko (ARDE) and M. Dieckhoff (AFRPL) 1/23/86
 - (8) In Reply Refer to 42001-KOS-084

Gentlemen:

This letter defines revised test sequencing for near term tests to be performed by AFRPL (ref. 1 to 5). The objective of this revised near term test sequencing is to obtain Kevlar overwrap sphere brittle liner failure mode test data and test facility/instrumentation verification at the earliest possible date. The revised test sequencing, effective immediately, has been coordinated with and approved by Mr. Pete Taddie, ESMC/SEM and discussed verbally with AFRPL personnel, ref. 6,7.

An outline of test objectives and compatible test mode brief descriptions is set forth below. Additional data are given on Figure 2 attached, which defines the projected time phasing for the revised near term test sequencing.

TEST OBJECTIVES/TEST MODES1. TEST OBJECTIVES I

- 1.1 Verify tank temperature/pressure control
- 1.2 Verify strain gage installation/monitoring system
- 1.3 Verify readiness of acoustic emission (AE) equipment

TEST MODES I

- 1.4 Mount 24 strain gages on 16"φ composite checkout vessel (P/N E4170 S/N 004) and hook up strain instrumentation to recorder(s). See Figure 16 for strain gage location and orientation. Check out AE equipment with pencil break.
 - 1.4.1 Pressure cycle test to check pressure/temperature control, strain monitoring system and AE equipment. Increase the pressure from 0 to 2000 ± 100 psig in a convenient "slow" time and then increase the pressure from 2000 psig to 5000 + 1 psig ± 100 in 90 seconds or less and hold for 5 - 0 minutes.
+ 100
Vent pressure to 0 - 0 psig. Monitor pressure, temperature, strain and AE instrumentation outputs. Maximum number of cycles is four (4).
 - 1.4.2 Remove P/N E4170 S/N 004 from test stand, retain strain gages and hold tank for later test.

2. TEST OBJECTIVE II

- 2.1 Verify hydrogen embrittlement procedure
- 2.2 Verify temperature/pressure/AE Equipment signals and strain monitoring system
- 2.3 Perform brittle liner "dress rehearsal" test.

TEST MODE II

- 2.4 Same as 1.4
- 2.5 Pressure cycle 0 to 5000 - 0 + 100 psig to 0 - 0 + 100 psig. Monitor pressure, temperature, strain and AE instrumentation to verify instrumentation/test set-up. Maximum number of cycles is two (2).

February 3, 1986

- 2.6 Disassemble tank from test stand and hydrogen embrittle per ARDE Procedure EG42001-6 Rev. A.
- 2.7 Re-install tank in test stand and hook up instrumentation.
- 2.8 Fill vessel to operating GHe pressure (0 to 2000 - 0^{+ 100} psig^{+ 100} in convenient "slow" time and from 2000 - 0^{+ 100} psig to 5000 - 0 psig in 90 seconds or less) and hold 5000 psig pressure level until liner rupture. Monitor instrumentation.

3. TEST OBJECTIVE III

- 3.1 Verify witness panel/overpressure instruments and failure strain monitoring.

TEST MODE III

- 3.2 Re-install P/N E4170 S/N 004 in test set-up and perform gas burst test.

4. TEST OBJECTIVE IV

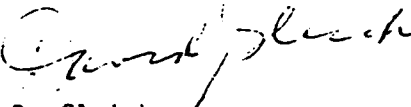
- 4.1 Obtain brittle liner rupture test data on full up 16"φ tank (P/N E4168 S/N 001).

TEST MODE IV

- 4.2 Assuming successful completion of Test Modes I to III, hydrogen embrittle P/N E4168 S/N 001 and perform brittle liner rupture test at operating pressure in accordance with the prior verified test procedures/test set-up.

Very truly yours,

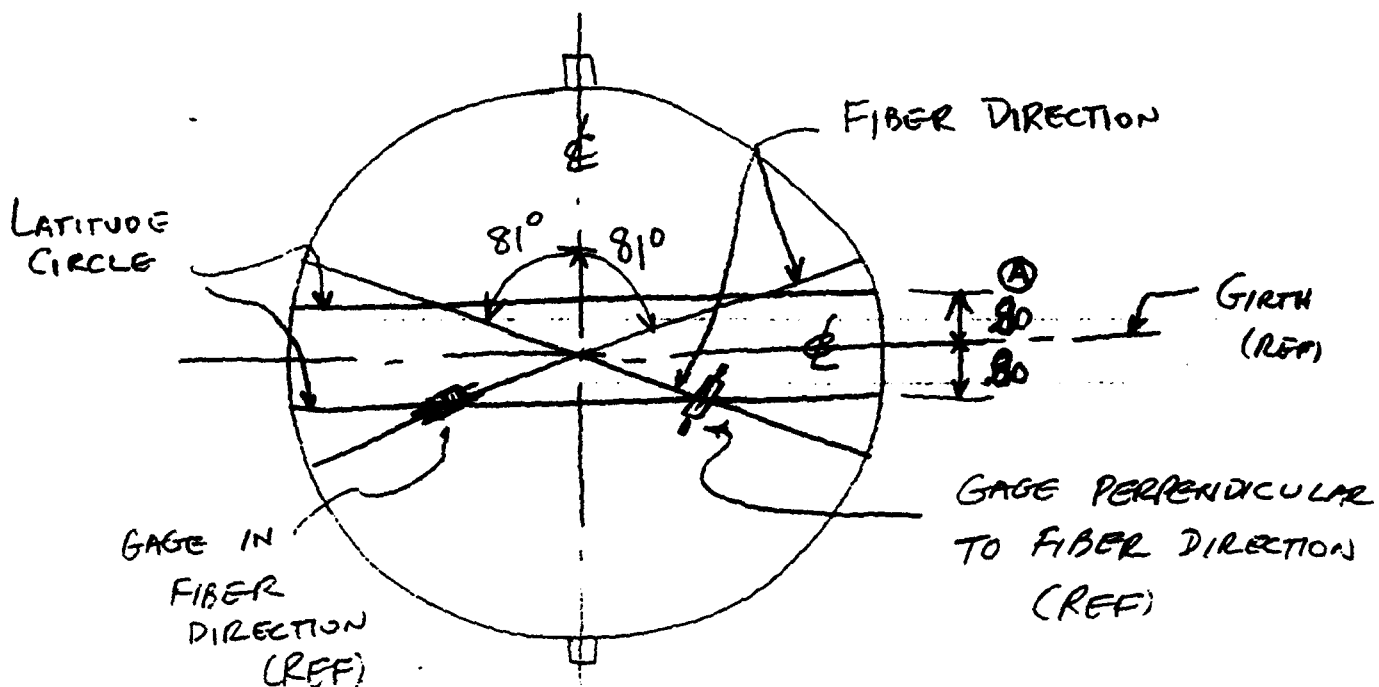
ARDE, INC.



D. Gleich
Principal Investigator

DG:sr

FIG. 1G-
SKETCH, STRAIN GAGE MOUNTING



MOUNT 6 PAIRS OF GAGES (1 EA OF EACH PAIR IN THE OUTER FIBER DIRECTION AND 1 EA PERPENDICULAR TO THE OUTER FIBER DIRECTION ON EACH LATITUDE CIRCLE) EQUALLY SPACED FOR A TOTAL OF 24 GAGES.

ARDE INC.

CONTRACT F08606-84-C-0029

J/N 42001-0-3

(REV A - 80 WAS 90)

 ARDE, INC.

SALES, ENGINEERING AND MANUFACTURING
19 INDUSTRIAL AVENUE, MAHWAH, NEW JERSEY
PHONE (201) 529-3700

May 13, 1985

AFRPL/LKLH
Mr. John Marshall
Stop 24
Edwards AFB, CA 93523-5000

Subject: Transmittal of Arde Document EG 42001-5
"Kevlar Overwrap Study Full Scale Composite Vessel
Tests Instrumentation Requirements/Procedures"

- Reference:
1. Contract F08608-84-C-0029
 2. Arde Letter 42001-KOS-036
 3. Telcon 5/6/85 and 5/7/85 John Marshall and Dick Grove (RPL) and D. Gleich (Arde)
 4. Telcon 5/7/85 D. Gleich (Arde) and Frank Davies (PI)
 5. Letter, John Marshall (RPL) to D. Gleich (Arde) 5/3/85, "Transmittal of Technical Review Comments of Arde Document EG 42001-5, "Kevlar Overwrap Study Full Scale Composite Vessel Tests Instrumentation Requirements/Procedures"
 6. EG 42001-8, "Kevlar Overwrap Study, Full Scale Composite Sphere Testing Scope of Work
 7. In Reply Refer to 42001-KOS-042

Gentlemen:

Subject document has been formerly issued and is transmitted to AFRPL for use in Their testing task defined by reference 6 Scope of work.

The formal issue subject document reflects the comments of ESMC/SEM, AFRPL, Aerospace Corp. and PI as finalized in discussions with Arde, references 3, 4, 5.

Very truly yours,

ARDE, INC.




David Gleich
Principal Investigator

DG:sr
p.c. See separate distribution
list

KEVLAR OVERWRAP STUDY
FULL SCALE COMPOSITE VESSEL TESTS
INSTRUMENTATION REQUIREMENTS/PROCEDURES

PATRICK AIR FORCE BASE
Contract No. FO 8606-84-C-0029

Prepared By:


D. Gleich

Approved By:


S. Beyko


A. Cozewith

ARDE, INC.
19 Industrial Avenue
Mahwah, N.J. 07430

TABLE OF CONTENTS

	<u>TITLE</u>	<u>PAGE</u>
1.0	SCOPE	E-11
2.0	APPLICABLE DOCUMENTS	E-11
3.0	TEST CONDITIONS	E-11
	3.1 Atmospheric Conditions	E-11
	3.2 Test Measurement Tolerances	E-12
	3.3 Accuracy of Test Equipment	E-12
4.0	MEASUREMENTS REQUIRED	E-12
	4.1 Pre-Test Processing/Checkout	E-12
	4.1.1 Hydrogen Embrittlement/Strain Gage Installation Check/Acoustic Emission Applicability	E-12
	4.1.1.1 Pre-Pressurization	E-12
	4.1.1.2 Pressurization Mode	E-13
	4.1.1.3 Post Test	E-13
	4.1.2 System Checkout Tests	E-13
	4.2 Full up Composite Sphere Tests Measurements	E-14
	4.2.1 Hydrogen Embrittlement Liner Test Mode	E-14
	4.2.2 Leak Before Burst (LBB) Liner Test Mode	E-14
	4.3 Data Recording	E-14
5.0	INSTRUMENTATION DETAILS/REQUIREMENTS	E-15
	5.1 Overview	E-15
	5.2 Instrumentation Details	E-15
	5.2.1 Kevlar 49 Fiber Strain Monitoring Requirements	E-15
	5.2.2 Kevlar Shell Displacement	E-23
	5.2.3 Temperature Measurement Requirements	E-25
	5.2.4 Tank Pressure Measurement Requirements	E-27
	5.2.5 Valve Closure Requirements	E-29
	5.2.6 Timing, Firing and Monitor Requirements	E-30
	5.2.7 Air Blast Measurement Requirements	E-31
	5.2.8 Fragment Velocity Measurement Requirements	E-32

LIST OF FIGURES

<u>FIGURE NO.</u>	<u>TITLE</u>	<u>PAGE</u>
1 F	Schematic Test Tank Instrumentation	E-17
2 F	Strain Gage Mounting Requirements	E-19
3 F	Basic Strain Gage Recording System	E-21
4 F	Mechanical Measurement Instrumentation System	E-22
5 F	Fotonic Fiberoptic Non-Contact Sensor	E-24
6 F	Temperature Measurement System	E-26
7 F	Piezo Electric Pressure Measurement System	E-28

1.0

SCOPE

This document defines the instrumentation requirements/procedures to be used in the testing of prestressed composite Kevlar 49 overwrapped cryoformed 301 CRES spheres (typified by 2.4, 2.5 & 2.6) under Patrick AFB Contract No F08606-84-C-0029. The testing is to be performed per 2.2 work scope and 2.3 test plan and procedures by AFRPL, who will furnish all necessary manpower, facilities, equipment and instrumentation.

2.0

APPLICABLE DOCUMENTS

- 2.1 Patrick Air Force Base Contract No. F08606-84-C-0029, "Kevlar Overwrap Study".
- 2.2 EG 42001-8, "Kevlar Overwrap Study, Full Scale Composite Sphere Testing Scope of Work".
- 2.3 EG 42001-4, "Kevlar Overwrap Study Full Scale Composite Vessel Test Plan and Procedure "TBD".
- 2.4 Arde Drawing E4168, "Pressurant Tank Composite"
- 2.5 Arde Drawing E4171, "Pressurant Tank Composite - Ductile Mode Wrap"
- 2.6 Arde Drawing E4170, "Test Set-Up Pressurant Tank Composite - Patrick AFB".
- 2.7 EG 42001-6, "Liner Hydrogen Embrittlement"
- 2.8 EG 42001-7, "Machining Defects in Metal Tank Wall by EDM Process"
- 2.9 MIL-STD-45662, 5 January 1983, "Calibration System Requirements"

3.0

TEST CONDITONS

3.1

Atmospheric Conditions

Unless otherwise specified in 2.3, testing shall be conducted at external ambient conditions existing at AFRPL. Sun shading shall be provided, wherever practical, to minimize the temperature rise in the test article, lines, plumbing and pressurant gas.

3.2 Test Measurement Tolerances

Unless otherwise specified, the maximum allowable tolerance of test conditions (exclusive of instrument accuracy) during the testing of the vessels (2.4, 2.5 & 2.6) shall be as follows:

a) current	5%
b) deflection	5%
c) flow rate	10%
d) frequency	2%
e) pressure, barometric	5%
f) pressure, fluid	2%
g) strain	500×10^{-6} (in/in)
h) temperature	5 degrees F
i) time	5%
j) velocity	10%
k) voltage	5%
l) weight	5%

3.3 Accuracy of Test Equipment

A calibration system conforming to MIL-STD-45662 (2.9) shall be utilized to control the accuracy of instruments and facility type test equipment used to monitor and control test parameters. The accuracy of special test equipment used to control and monitor test parameters shall be validated periodically and the validation period shall be less than the calibration period of any instrument contained with it. All instruments and test equipment used in conducting tests shall conform to laboratory standards whose calibration is traceable to the prime standards at U.S. Bureau of Standards. The instrumentation used to monitor pressure, strain, displacement, temperature, time and acoustic emission signals shall be calibrated immediately prior to the start of testing.

4.0 MEASUREMENTS REQUIRED

Measurements required are defined for each test mode, i.e., pre-test processing/checkout experiments and full up test modes (brittle liner failure and leak before burst ductile liner failure modes). Instrumentation details/requirements to obtain this measurement data are given in Section 5.0 herein.

4.1 Pre-Test Processing/Checkout Experiments Measurements

4.1.1 Hydrogen Embrittlement/Strain Gage Installation Check/Acoustic Emission Applicability (Ref. 2.2 and 2.7).

4.1.1.1 Pre-Pressurization

- a) acid solution composition
- b) depth and volume of acid solution fill
- c) charging current and voltage
- d) time versus events (charging and hold)
- e) photographic coverage

4.1.1.2 Pressurization Mode

As function of time with common time base:

- a) pressure (gas)
- b) fiber strain
- c) temperatures (gas, tank, strain gages)
- d) acoustic emission signals
- e) fragment velocity and overpressure (if fibers rupture)
- f) ambient conditions (pressure, temperature, humidity)
- g) photographic coverage

4.1.1.3 Post Test

- a) post test inspection
 - 1) visual inspection of outside and inside surfaces (boroscope, if applicable) and note condition of specimen and type of failure; describe fragments (if applicable).
 - 2) pack and ship test specimen (all parts) to Arde for further inspection/evaluation
- b) data documentation
 - 1) document post test inspection results (including sketches and photos)
 - 2) review and update test logs and data
 - 3) transmit test reports and data to Arde (see 2.2 Scope of Work)
- c) photographic coverage
 - 1) sufficient 3" X 5" or larger black and white photographs to adequately describe post test specimen condition; three (3) photographs minimum
 - 2) Provide title/legend as part of photograph

4.1.2 System Checkout Tests (Ref. 2.2)

As function of time with common time base:

- a) GN2 parameters (pressure, temperature and flow for system and tank)
- b) heat exchanger characteristics (temperature and pressure drop, flow)
- c) tank (fiber strain, metal, strain gage and fiber temperature, GN2 parameters)
- d) valve and pressure regulator settings/sequencing
- e) ambient conditions (temperature, pressure, humidity)
- f) photographic coverage

4.2 Full Up Composite Sphere Tests Measurements

4.2.1 Hydrogen Embrittled Liner Test Mode

As function of time with common time base:

- a) Tank Input Parameters
 - 1. GN2 internal pressure, temperature
 - 2. metal, fiber and strain gage temperatures
 - 3. ambient (temperature, pressure, humidity)
- b) Tank Response Parameters
 - 1. fiber strain
 - 2. fiber displacement
 - 3. acoustic emission signals (if applicable)
 - 4. fragment velocity and overpressure (if fibers rupture).
- c) System Parameters
 - 1. GN2 pressure, temperature, flow rate
 - 2. heat exchanger characteristics (temperature and pressure drop, flow rate)
 - 3. valve and pressure regulator settings/sequencing
- d) Post Test
 - 1. post test inspection
 - 2. data/documentation
- e) Photographic Coverage

Still and motion picture coverage as applicable, from pre-test through post test modes.

4.2.2 Leak Before Burst (LBB) Liner Test Mode

Same as 4.2.1 except:

- a) valving, plumbing and tank pressure measuring instrumentation shall facilitate isolating the tank from the rest of the system and permit the monitoring, during hold at operating pressure, of any pressure decay to indicate a tank leak, as set forth in detail in 2.3 test plan and procedure.
- b) the pressure cycling spectrum, including holds at operating pressure, shall be as defined in 2.3.

4.3 Data Recording

All measured data as applicable during pre-test, calibration and test modes shall be recorded with a common time base. The recorded data, together with test logs, shall be presented in a form convenient for analysis by PISCES 2D ELK computer program.

5.0 INSTRUMENTATION DETAILS/REQUIREMENTS

5.1 Overview

A schematic of test tank instrumentation indicating the type of tank measurements required is sketched on Figure 1F. Recording instruments, acoustic emission monitoring equipment, blast overpressure and fragment velocity monitoring devices are not shown on Figure 1F. Specific instrumentation details/requirements are discussed in 5.2 following:

5.2 Instrumentation Details

5.2.1 Kevlar 49 Fiber Strain Monitoring (See Figures 1, 2, 3, 4)
Requirements: F F F F

Maximum Strain 2%
Bandwidth 80 KHZ

Instrumentation System:

- a) Sensor:
 - 1) Micromeasurement (Type EA06)
 - 2) Four element bridge; dummy gage mounted close to active element
- b) Cables:
 - 1) RG 58/RG 62 coaxial cable to tape machine and Twinax to preamplifier
- c) Signal Conditioning:
 - 1) Pre-amplifier 100/80 KHZ
 - 2) Calibration System: Relay switching system to provide end to end calibration by insertion of appropriate resistors.
- d) Recording System:
 - Wideband Group II FM tape recorder or
 - Wideband Group I direct record tape recorder
 - Wideband Group I FM (80 KHZ)
- e) Temperature measurement at active and dummy elements

Number of Channels:

Brittle liner failure 24 channels.

Twelve (12) bi-axial gages equispaced on two (2) great circles ten degrees from equator.

Ductile liner failure 8 channels.

Four (4) bi-axial gages, 1/2" from flaw, spaced 90 degrees apart.

Data Processing:

Strain-time history plots. Digitized data on a VAX compatible tape (1600 BPI, 9 track ASCII character set with record length block set and number of files specified).

NOTE: AFRPL to send PI tape with signal on it for PI comment.

Strain Gage Procurement: Gages from one (1) lot

Strain Gage Mounting Requirements:

Use separate support posts for connectors to isolate them from shock and vibration (See Figure 1).

KEY

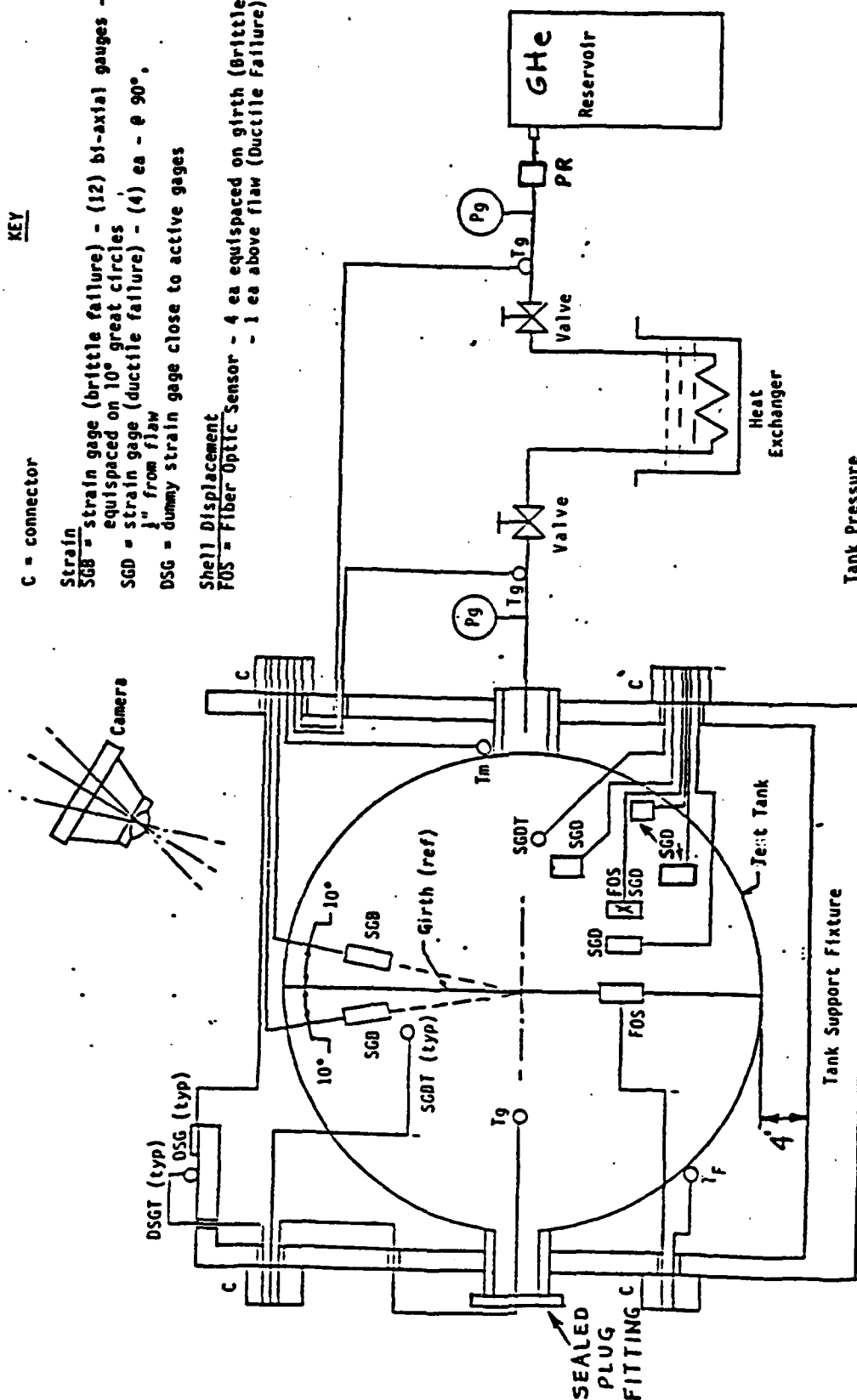
C = connector

Strain

SG8 = strain gage (brittle failure) - (12) bi-axial gauges -
equispaced on 10° great circles
SGD = strain gage (ductile failure) - (4) ea - @ 90°,
1" from flaw
DSG = dummy strain gage close to active gages

Shell Displacement

FOS = Fiber Optic Sensor - 4 ea equispaced on girth (Brittle Failure)
- 1 ea above flaw (Ductile Failure)



Tank Pressure
Pg = Pressure gauge (Piezo - resistive)
PR = Pressure Regulator

Temperatures (Thermocouples)

Tg = gas temp
Tm = tank metal temp
Tf = fiber temperature
SGBT = strain gage (brittle failure) temp
SGDT = strain gage (ductile failure) temp
DSGT = dummy strain gage temp

Valves

Valve closures identified and sensed (microswitches)

FIG. 1 F

SCHEMATIC
TEST TANK INSTRUMENTATION

Data Processing:

Strain-time history plots. Digitized data on a VAX compatible tape (1600 BPI, 9 track ASCII character set with record length block set and number of files specified).

NOTE: AFRPL to send PI tape with signal on it for PI comment.

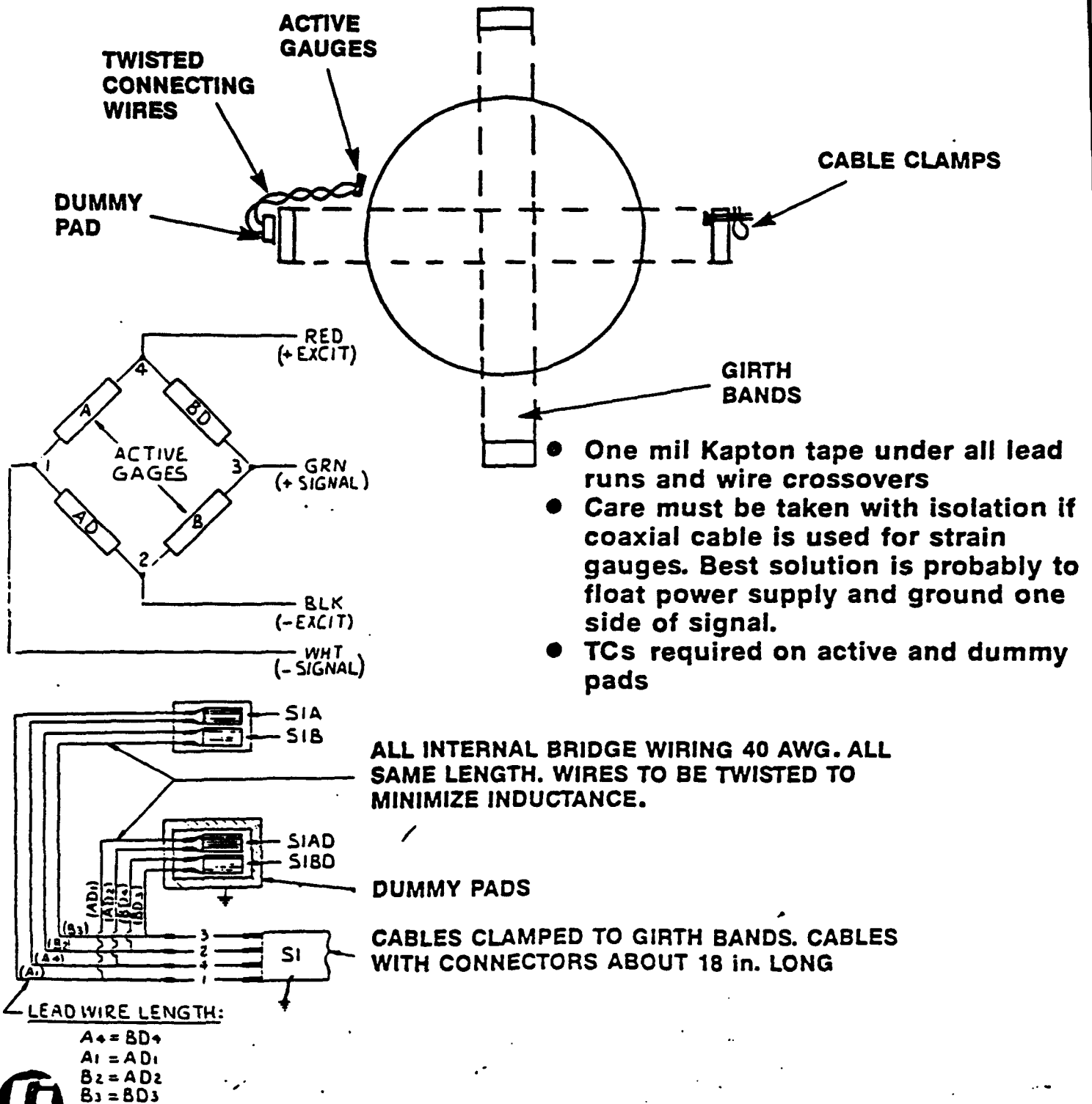
Strain Gage Procurement: Gages from one (1) lot

Strain Gage Mounting Requirements:

Use separate support posts for connectors to isolate them from shock and vibration (See Figure 1).

FIGURE 2F

Strain Gauge Mounting Requirements



Strain Gauge Bonding Requirements

Strain gauge bonding procedures:

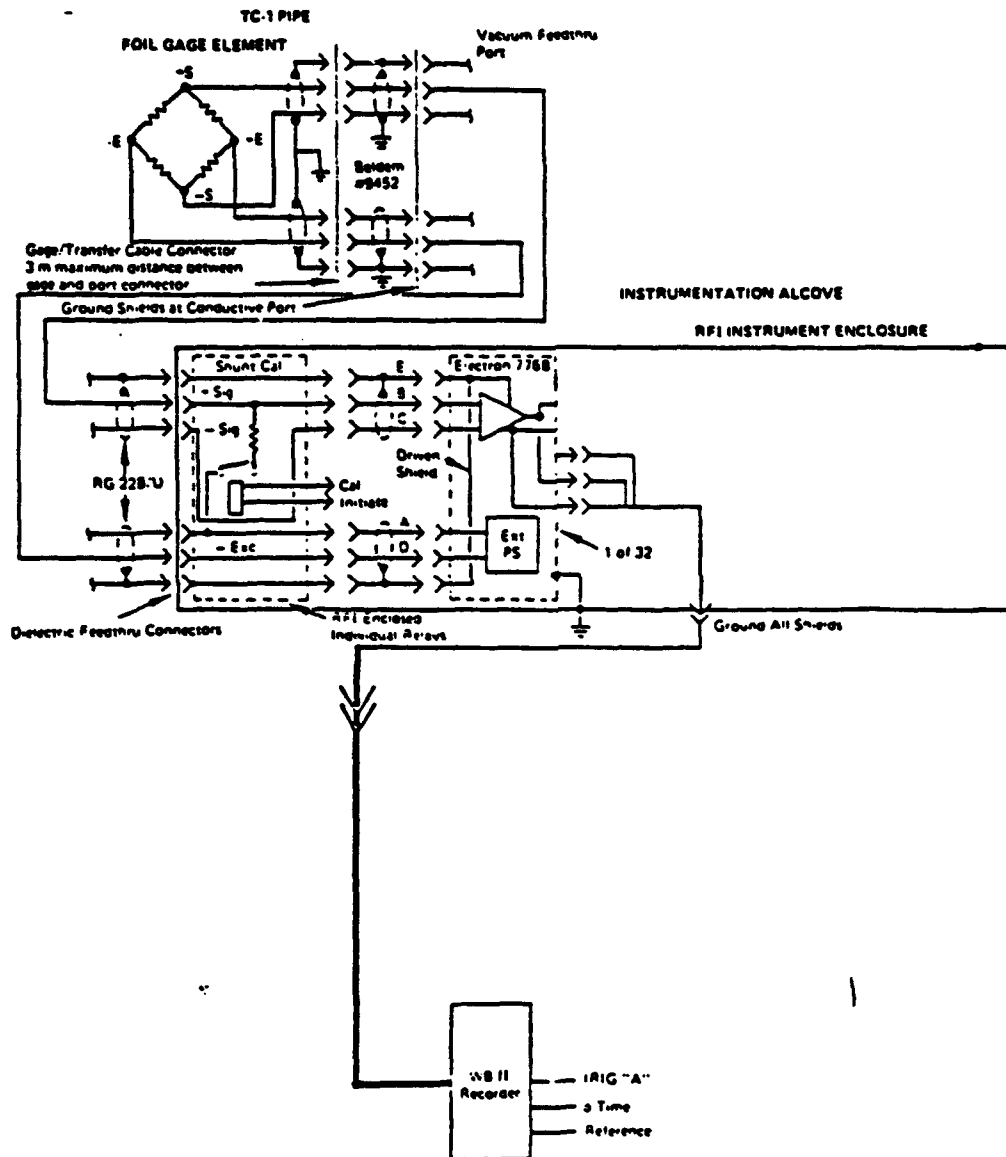
- Bond under pressure using room temperature cured epoxies
 - Instruction Bulletin B-129-2, surface preparation for strain gauge bonding
 - Instruction Bulletin B-137-8, strain gauge applications with M Bond AE-10/18 and M Bond and GA-2 adhesive systems
 - Instruction Bulletin B-141-2, application of M coat G and GL protective coatings
- Must minimize mass of solder connection and lead wire
 - Manufacturer applied solder dot only
 - 40 AWG Belden magnet wire (type 8046)



85 02-104

FIGURE 3F

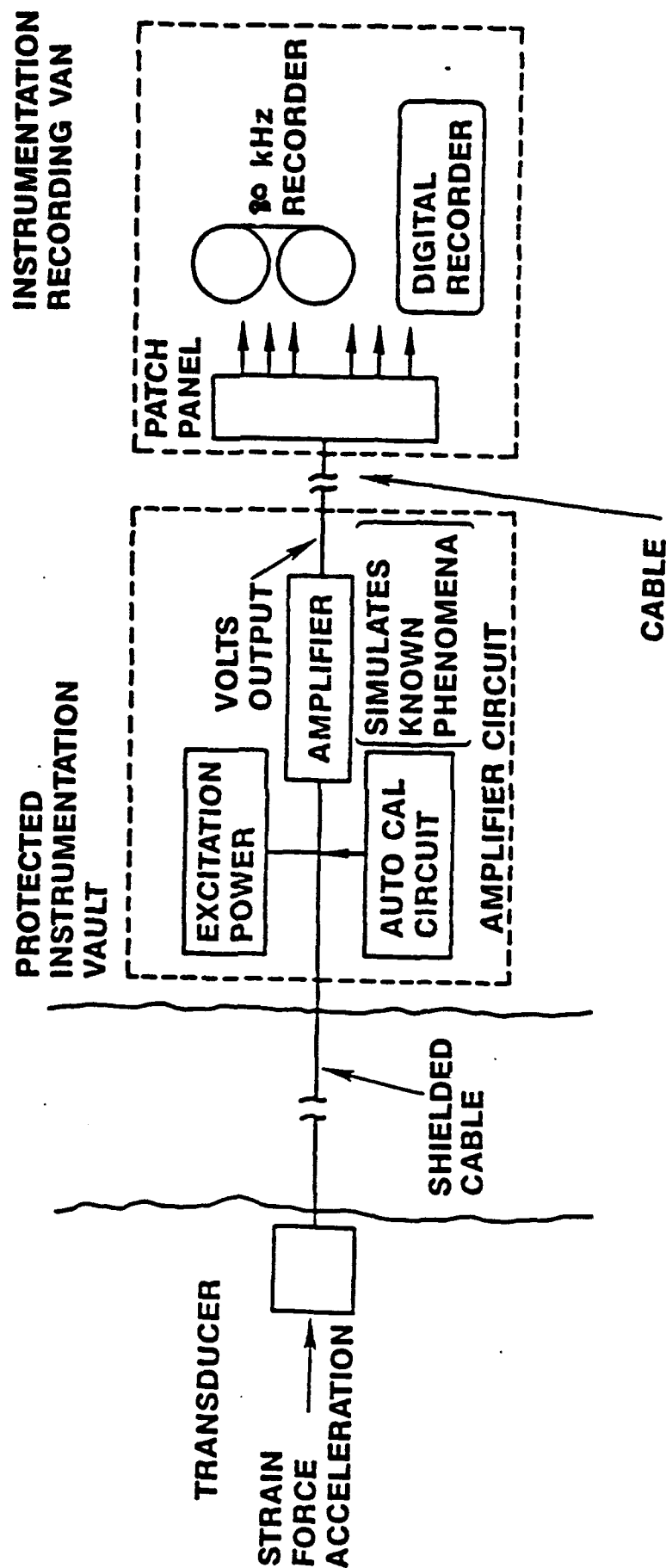
Basic Strain Gauge Recording System



85-02-114

FIGURE 4 F

Mechanical Measurement Instrumentation System



Shell Displacement Measurement Requirements (See Figure 1, 5)

Mounting:

Rigidly mount sensor heads to define their reference positions

Requirements:

Maximum displacement - $\sim 1/2$ cms.

Resolution - 0.05 cms, 10 μ sec.

Bandwidth - 70 KHz

Instrumentation System:

a) Sensor

i) Fatonic KDC4SL/KT-245HF. Fiberoptic noncontact sensor.

b) Cables

(i) RG 213 coaxial cable or Twinax.

e) Signal conditioning

i) KD-245 signal conditioner located in forward bunker. Fiber optic cable from KD-245 to sensor head.

d) Recording System

Wideband Group I FM tape recorder or equivalent.

Number of Channels:

Brittle Liner Failure: Four sensors equispaced around the equator.

Ductile Liner Failure: Single sensor located immediately above flaw.

Data Processing:

Plotted displacement time histories, digital data print outs, digitized data on VAX compatible tape.



Fotonic Fiberoptic Noncontact Sensor

- Bifurcated fiberoptic probe transmits and receives light

Typical Probe Tip

○ Transmit ● Receive

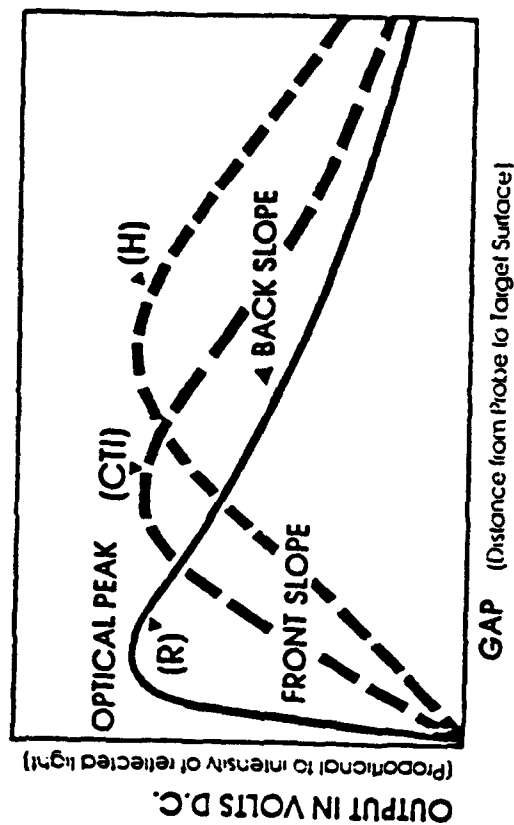
Hemispherical Fiber Distribution (H)



Concentric Transmit Inside (CTI)



Random Fiber Distribution (R)



Plug-In Cartridge	Probe Model KDP —	Probe Tip Diameter Total Active	Frequency Response (-3db)	FRONT SLOPE CHARACTERISTICS						BACK SLOPE CHARACTERISTICS						Optical Peak (mils)	
				Output Signal Ripple (Mv.p-p)	Dynamic Resolution' (μ in)	Static Resolution' (μ in)	Sensitivity (μ in /mv)	Linear Range* (mils)	Standoff Ctr. of Range (mils)	Dynamic Resolution' (μ in)	Static Resolution' (μ in)	Sensitivity (μ in /mv)	Linear Range* (mils)	Standoff Ctr. of Range (mils)	Mid Range* Point ±5%	100	
KT	245 HF	0.245" 0.230"	750 kHz	8	320	1000	40	70	35	2400	6000	300	300	300	150	100	



85-02-138

Temperature Measurement Requirements

(See Figures 1, 6)
F F

Requirements:

150°F

Bandwidth > 1 KHz

Instrumentation System:

a) Sensor

Chromel/Alumel thermocouples with reference junction.

b) Cables

Twisted Shielded Pairs

c) Signal Conditioning

i) Preamplifier

ii) Calibration (end to end) by use of known voltage sources.

d) Recording System

Datalogger.

Number of Channels:

Brittle Liner Failures

Strain gauge temperatures	24
Gas temperatures	4

Ductile Liner Failure

Strain gauge temperature	16
Gas temperatures	4

Thermocouples used to detect gas temperatures must have fast response, i.e., low thermal capacity.

Data Processing:

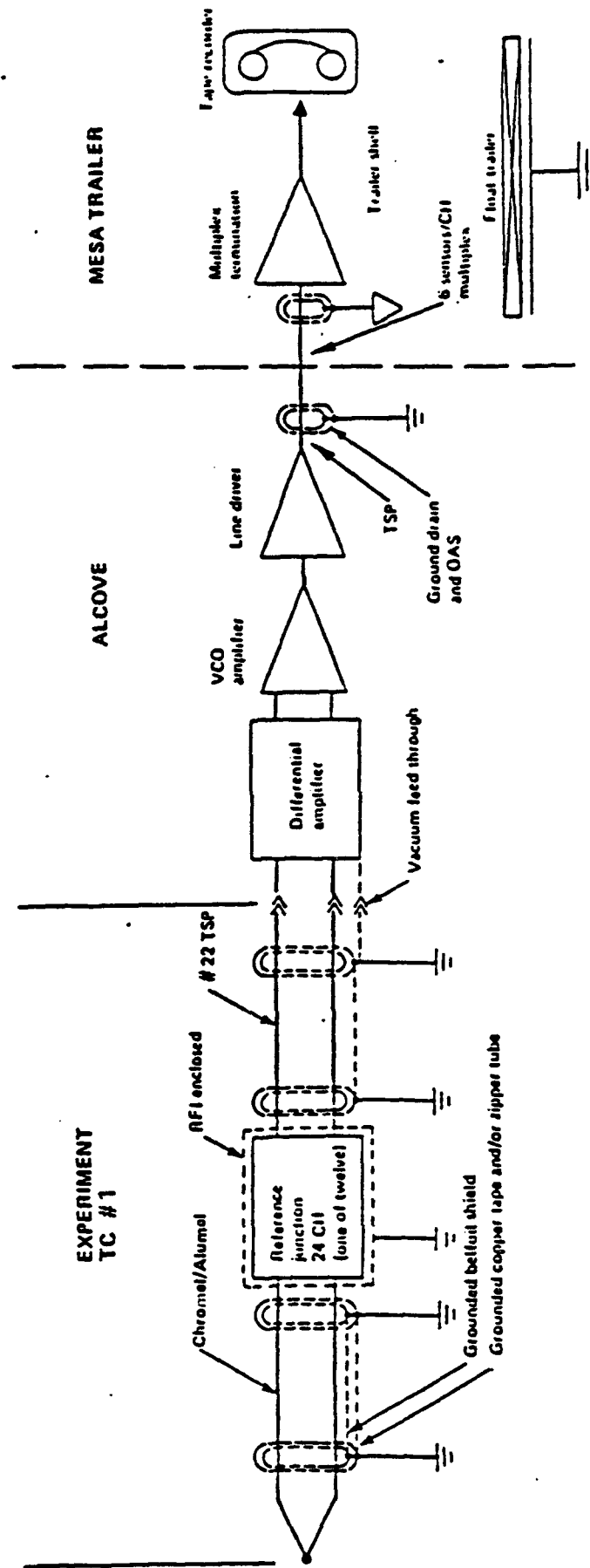
Temperature time history plots, digitized data print out, VAX compatible magnetic tape file.



85-02-097

FIGURE 6 F

Temperature Measurement System



Tank Pressure Measurement Requirements

(See Figures 1,7)

F F

Requirements:

5000 psi

Bandwidth - > 1KHz.

Instrumentation System:

a) Sensor

Piezo-resistive pressure gauges.

b) Cables

Twisted Shielded Pair

c) Signal Conditioning

i) Preamplifier

ii) Calibration system

d) Recording system

Datalogger

Number of Channels: 4

Monitor pressures at vessel and reservoirs.

Data Processing:

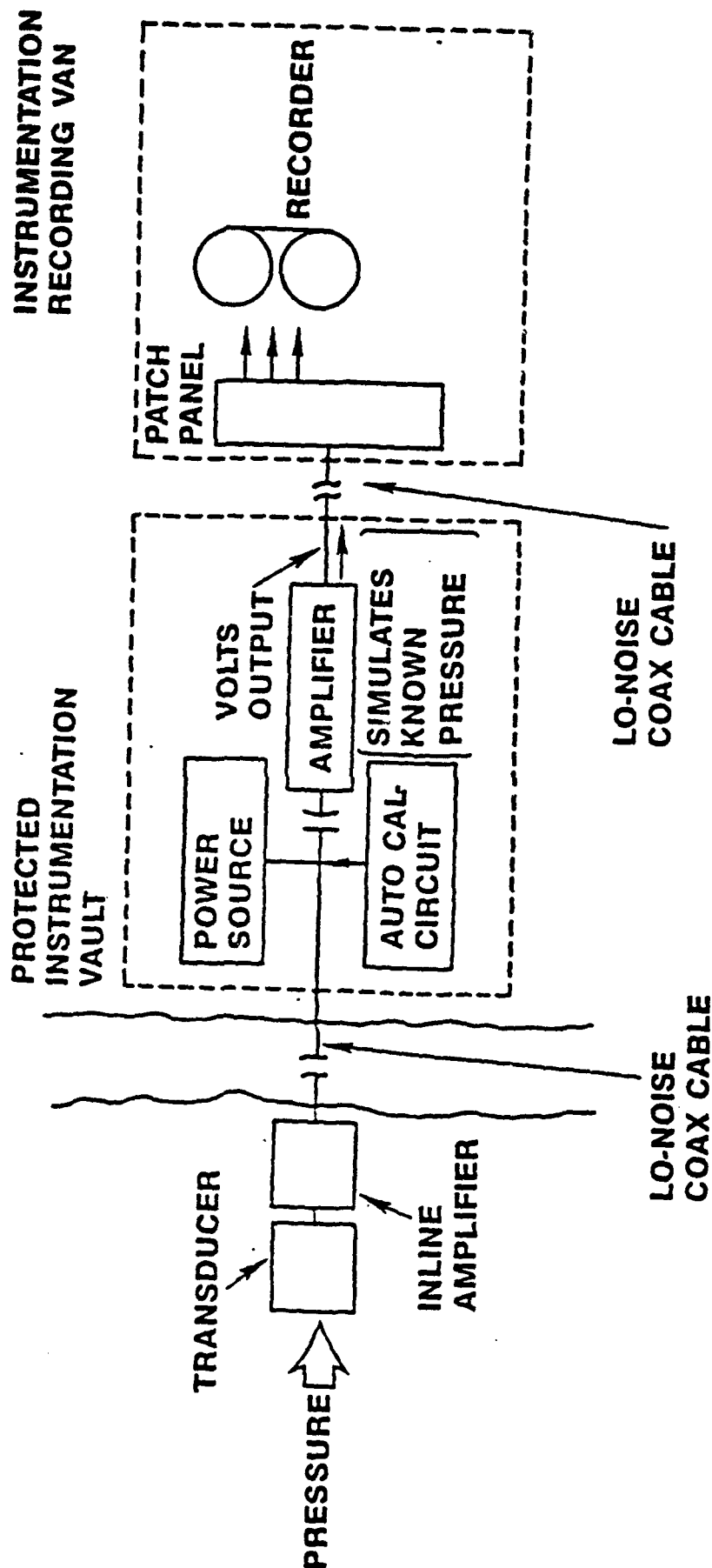
Plots of pressure time histories and digitized data print out.



85-02-096

FIGURE 7F

Piezoelectric Pressure Measurement System



Valve Closure Requirements

Requirements:

Valve positions unambiguously identified.

Bandwidth - > 1 KHz

Instrumentation System:

- a) Sensor: Microswitches
- b) Cables: Twisted Shielded Pairs
- c) Signal Conditioning
- d) Recording System: Datalogger.

Number of Channels: 5

Data Processing:

Print out defining times of valve position changes.



85-02-091

Timing, Firing and Monitor Requirements

Requirements:

Time correlation of all measurements

Instrumentation System:

IRIG time on all tape recorders and data loggers.

Data Processing:

History of time of all events such as tape starts and camera activation.



85-02-099

Airblast Measurement Requirements

REQUIREMENTS:

1—10 psi overpressure and stagnation pressure
80 kHz bandwidth

INSTRUMENTATION SYSTEM:

(a) Sensor	(X-DUCER)	Piezoelectric pressure gauges (1-50 PSI)
(b) Cables		RG 213 coaxial cable
(c) Signal conditioning		Liner drivers
(d) Recording system		Wide-band group one FM tape (80 KHz)
(e) TANK 4' ABOVE GROUND (POINT X-DUCERS TO TANK CENTER)		

NUMBERS OF CHANNELS:

Three radials with overpressure measurements at four ranges (2', 6', 10', 14')
i.e., total of 12 plus stagnation pressures at closest and mid-range (6 measurements)

Radials spaced 120 degrees apart

DATA PROCESSING:

Plots of pressure time histories, digitized data printout,
digitized data on VAX compatible tape

Fragment Velocity Measurement Requirements

Requirements:

Maximum velocity - 20 meters/sec.

360° coverage

Instrumentation System:

a) Sensors

- i) High speed cameras - $\frac{2000}{5000}$ fps Hycam or Fastex
1 Kc Timing
- ii) Witness panels - (foam, plywood, or celetex)

Number of channels:

- i) Cameras - 2 split image.
- ii) Witness panels - 8 ranges on 4 radials. Provide 360 degree coverage on a single range for brittle rupture. For LBB only need local zone in region of flay

Data Processing:

Developed film.

Photographic documentation of witness panels before recovery.



85-02-098

E.2

16" ϕ and 22" ϕ PSC Vessel Test Matrix

Table E-1 herein contains the 16" ϕ and 22" ϕ PSC Vessel Test Matrix and brief descriptions of test specimens employed, test objectives and key test results. Additional details for each test are given in following sections E.3 to E.12.

TABLE E-1 16" ϕ AND 22" PSC VESSEL TEST MATRIX

TEST TYPE	OBJECTIVE	TEST SPECIMEN DESCRIPTION	TEST RESULTS
(RV-4, 4A) high pressure GHe test 5600/5000 psig (16" ϕ PSC)	Demonstrate "fail safe" mode and define structural response	16 " ϕ sphere Olympus configuration Kevlar overwrapped 301 cryo CRES Global embrittlement (100% fiber thickness)	Demonstrated "fail safe" mode at operating pressure. "Static" structural response behavior observed. Need for increased hydrogen concentration at tip of cracks for enhanced brittle liner failure indicated.
(RV-5) high pressure GHe test 4900 psig (16" ϕ PSC)	Demonstrate "fail safe" mode and define structural response. Determines effect of increased H_2 charging time, pickling and N_AO_2 additive on brittle failure	Same as RV-4, 4A except increased H_2 charge time liner I.D. pickle and N_AO_2 solution additive.	Demonstrated "fail safe" mode at operating pressure with "static structural response. Enhanced brittle liner failure observed: Broke in short time at 4900 psig on way up to 5000 psig.
(RV-7) high pressure GHe test 3800 psig (16" ϕ PSC)	Demonstrate "fail safe" mode for local girth embrittlement (worst case structural) (model) Define structural response.	Same as RV-5 except local girth embrittlement and increased H_2 charge current density.	Demonstrated "fail safe" mode. Large dynamic fiber strain spikes observed. Liner broke in short time on way up to pressure (effect of increased charge current density). Liner separated in two halves at girth simulating worst case structural model, Fiber shell intact.

TABLE E-1 16" ϕ AND 22" PSC VESSEL TEST MATRIX

(CONTINUED)

RV-9 high pressure GHe test 3700 psig (16" ϕ PSC)	Demonstrate fail safe mode for local girth embrittle- ment. Define structural response. Get higher metal liner operating stress at failure.	Same as RV-7 except H ₂ charge current density reduced by 50%.	Repeat of RV-7. Demonstrated fail safe mode; observed large dynamic fiber strains; liner separated in two halves as as intended. Did not achieve achieve higher liner failure stress. Need still lower H ₂ charge current density.
RV-10 high pressure GHe test 3260 psig (sure fail test) (16" ϕ PSC)	Demonstrate brittle liner & fiber both fail mode for local girth embrittled liner. Determine structural response. Get higher metal liner operating stress at failure. Obtain fragment & over pressure data	Same as RV-7 except (fiber thickness reduced 50%) and H ₂ charge current density reduced still further to RV-4 & RV-5 test level.	All test objectives achieved. Demonstrated as designed intended "catastrophic" brittle liner & fiber both fail mode. Predicted liner separation/fragments & large fiber strain spikes observed. Obtained desired magnitude of metal liner operating stress at failure. Obtained fragmentation and over pressure data.
RV-11 high pressure GHe test 3600 psig margin test (16" ϕ PSC)	Demonstrate fail safe mode margin for local girth embrittlement. Define structural response.	Same as RV-10 except fiber thickness was nominally 83% of baseline.	Both fibers and embrittled liner liner failed very close to pre- dicted pressure. Anticipated large fiber strain spikes observed. Over pressure and fragmentation data obtained. Strain gage data indicates fibers came very close to remaining intact per no failure prediction.

TABLE E-1 16" O AND 22" PSC VESSEL TEST MATRIX

(CONTINUED)

RV-12 high pressure GHe test 2500 psig (22" ϕ PSC)	Demonstrate fail safe mode and define structural response for local boss/head weld hydrogen embrittlement	22" ϕ Shuttle Centaur PSC sphere Kevlar overwrapped 301 cryo CRES. Local boss/head weld weld embrittlement (100% design fiber thickness, .192")	Demonstrated "fail safe mode" at low (2500 psig) liner failure pressure. Too much hydrogen at tip of crack (effect of new tank geometry). Need for decrease in hydrogen embrittlement charging current indicated to raise liner failure pressure.
RV-12A high pressure GHe test 3750 psig (22" ϕ PSC)	Demonstrate fail safe mode and define structural response for local boss/head weld hydrogen embrittlement	22" ϕ Shuttle Centaur PSC sphere Kevlar overwrapped 301 Cryo CRES. Local boss/head weld embrittlement 100% design fiber thickness, .192	Demonstrated "fail safe" mode at operating pressure. Reduced hydrogen embrittlement charging current density raised liner operating failure pressure to 3750 psig. No boss separation; boss still attached to liner head.
RV-14 pressure GHe test 3914/3788 psig (16" ϕ PSC)	Demonstrate fail safe mode margin for local girth weld embrittlement	Same as RV-10 except Kevlar fiber thickness was nominally 90% of baseline	No liner failure at operating high pressure \approx 3900 psig. Test aborted after FM tape ran out. Too little hydrogen at tip of crack. Need to increase hydrogen embrittlement charging current density indicated in order to achieve desired liner failure at operating pressure.
RV-14A high pressure GHe test 3112 psig (16" ϕ PSC)	Demonstrate fail safe mode for local girth weld embrittlement	Same tank as RV-14 except hydrogen embrittlement charging current increased by 10% and hold time decreased to 3 hours instead of 3-1/2 hours compared to RV-14 test.	Fail Safe mode demonstrated by benign leak mode.

E.3

RV-4, RV-4A Tests (16" ϕ PSC)

There was no liner failure in test RV-4.

The vessel was then re-embrittled and
repressurized in test RV-4A.

E.3.1

Test Vessel Description

- P/N E4170, S/N 002 (Kevlar Overwrapped 301 Cryo
CRES Composite Sphere)
- Kevlar Fiber (less resin) thickness = .154" (100%
Baseline Thickness)
- Metal Thickness = .05 nominal
- Inside Radius = 7.66"
- Hydrogen Embrittlement Mode = Global
- Electrolyte Solution =
$$\frac{20 \text{ cc H}_2\text{SO}_4 + 980 \text{ cc Tap H}_2\text{O}}{1000 \text{ cc solution}}$$
- Solution Additive = none
- Sensitize liner inside surface = No
- Charging Current Density = .005 amps/in² of
surface to be embrittled
- Charging Time = 60 hours (RV-4), 72 hours (RV-4A)
- Hold Time Before Test = 12 hour (RV-4), 2-1/2
hours (RV-4A)
- Adcoat AC818T liquid maskant on areas not to be
embrittled

Recd 9/27/88 S.M.B.
Dist DG, KP
Eng 42001

INSTRUMENTATION OBSERVATIONS. (By AFAL Instrumentation Eng)

E.3.2.1

KEVLAR TEST 004, 25FEB86. Project number 573000RV.

EXPERIMENTAL PROCEDURE. The vessel was pressurized from 2000 psig to 5000 psig in slightly less than 60 seconds, and pressure was maintained for about another 8 minutes. Pressurization was preceded by a 150 second purge for cool down from the initial ambient condition; the tank vent was closed, and pressure was increased to 2000 psig for a 30 second hold before starting the final pressure increase to 5000 psig. No leak was observed. Frost appeared on the vessel and remained for at least 30 minutes. The vessel did not rupture. Reembrittlement and retesting were scheduled. Vessel S/N 002, which was hydrogen embrittled, was tested in a horizontal configuration.

IMPRESSIONS FROM THE DIGITIZED FM DATA.

Data analyst's comments. The ITT data analyst's comments follow: "SG5/7105, SG6/7106, SG18/7118, SG19/7119, SG22/7122 were not amplified - (or) recorded; SG9/7109, SG13/7113, SG21/7121 bad - not able to calibrate; SG20/7120 goes bad at 267 seconds."

Delta strain measurement. The data graphs from the FM do not show the initial condition strain because the pressurization was started prior to starting the FM tape. Measuring the initial strain level is a contractor requirement because delta strain measurement is a key parameter. This is an action item requiring a modification to future testing procedures.

IRIG time code. IRIG time code format was satisfactory.

Graphs. Three copies of data were made for TOA. The initial graphs were filtered at 100 Hz, and the digitized sample rate was 1024 samples per second; data were plotted at one point every 400 milliseconds. The graphs contained a few spikes. Time expansion of some of the spikes revealed their shapes are similar; the strain drops rapidly in a single dip from the initial condition at an abrupt inflection, reverses direction rapidly at the bottom of the dip and rapidly ascends to a point slightly past the initial condition where it changes direction in a single slow overshoot that recovers in an overdamped profile that settles without major oscillation at the initial condition. Additional analysis of the spikes at a much higher sample rate may uncover their true shapes without the filter distortion present on the initial graphs, which were required to identify the spikes exact time locations for subsequent analysis. The spikes may represent fiber snapping, debonding, or crack noise; on this test 18 gages had completely debonded, and the remaining 6 were partially debonded after the test; a decision was made to improve the mounting technique by sanding, etc. Visual inspection of the Kevlar surface after the test revealed small fractures in the

moisture barrier. Trace identifiers are periodic and are also automatically generated on excessively large data excursions.

QUALITY CONTROL CHECK. A quality control check of the strain parameter was done; the resistance RCAL in the bridge completion circuit indicated a plus 2.3mv shift; physically placing the RCAL resistor across the active gage also caused a similar shift, which confirms the established arbitrary polarity convention for compression is plus and for tension is minus.

IMPRESSIONS FROM THE QUICK-LOOK AND DIGITAL DATA ACQUISITION SYSTEM DATA. Immediately after the test, three quick-look plots were compared: item 1901, Tank Pressure; item 7123, Strain Gage #23; and item 2208, Vessel Temperature #12. Comparing graphs indicate better correlation probably exists between the strain gage and tank pressure than between the strain gage and tank temperature. This was determined by laying down the strain gage graph face up on a light box and turning over the tank pressure graph and laying it face down over the strain gage graph (to correct for the opposite polarity); if the major points of inflection are observed, an impressive correlation is apparent; note how most of the inflection events occur slightly ahead in time on the strain gage graph, which is consistent with the strain gage channel's higher frequency response; also note how the small tank pressure variations, which are caused by cycling the pressurization valve during the steady-state condition, are reflected in the strain channel. Later it was confirmed that the tank temperature #12 had a polarity reversal, and this data is not correct; it is similar to the family of curves generated by adjacent thermocouples, however; but, it just can't be flipped over to correct for the reversal because of nonlinearities in the mv-to-F transform; we will not request that this problem be resolved by the data analyst unless it is established that the work would be worth the effort. Strain gage #11 can be used in place of strain gage #12, for strain gage #11 is only 4 inches away from strain gage #12.

REQUEST FOR CORRELATION ANALYSIS. A rigorous step-wise regression correlation analysis has been requested, and this will be provided by the data analyst. Briefly, the strain gage will be correlated with the tank pressure to find the residuals; the residuals will be correlated with the temperature, and the results will be evaluated by a mathematician and discussed in a short report.

ACOUSTIC EMISSION IMPRESSIONS. Supplied to ARDE directly by AET.

AIR PRESSURE SENSORS did not produce any significant data because the tank did not rupture.

SUMMARY. As the tank was pressurized to about 5000 psig, the strain gages responded with a tension strain of about 4800

microinches/inch. During pressurization, all of the tank temperatures decreased; the temperatures near the strain gages started out between 95 to 130 degrees F, rose about 5 F degrees above the initial condition, and then dropped rapidly 25 to 35 F degrees below the initial condition during steady pressurization before settling out to their final smooth behavior profiles after steady-state tank pressure was reached. Boss and gas temperatures behaved similarly except prominent undershoots are evident just prior to steady pressurization; the undershoots are consistent with the rapid vessel cooling experienced during the purging associated with the cool down phase and the location of the sensors.

REVISION RECORD. Initial issue: 4MAR86. Filename: testrv4. Revision A: 18MAR86; added paragraph on impressions from the digitized FM data. Revision B: 7APR86; added text to the summary and consolidated the quick-look impressions. Added text to the digitized FM data to clarify sample rate, etc. Revision C: 8APR86; corrected S/N from 004 to 002. Experimental procedure paragraph expanded. Improved spike description in digitized FM data. Acoustic emission impressions and air pressure paragraphs added.

DESCRIPTION OF THE EMBRITTLEMENT PROCEDURE. The embrittlement procedure was started at 1130 PST 15FEB86. Arde procedure EG 42001-6 Rev A was followed. Sixty hours of embrittlement was completed at 2330 on 17FEB86; the tank was drained, flushed and purged. The tank was placed in Bldg 9665 for a 12 hour hold; at 0900 the tank was placed on the test stand, and instrumentation was hooked up; at 1120 on 18FEB86 the test was started.

DISTRIBUTION: ITT, ARDE, AFRPL.

INSTRUMENTATION OBSERVATIONS. (By APAL Instrumentation Eng.)

KEVLAR TEST 004A, 17MAR86. Project number 573000RV.

EXPERIMENTAL PROCEDURE.

Cool Down and Initial Pressurization Cycle. Pressurization was preceded by a 60 second purge for cool down from the initial ambient condition; the tank vent was closed, and pressure was increased to 2000 psig for a short hold before starting the final pressure increase to 5000 psig. No leak was observed during the hold period.

Final Pressurization Ramp. The vessel was pressurized with a steady ramp from 2000 psig to 5000 psig in about 27 seconds, and pressure was maintained near 5100 psig for a 150 second hold period with some minor pressure readjustments. There were no major leaks. Following the hold period, pressure was maintained within a 5000 to 5600 psig bandwidth by the following three distinctly separate pressurization adjustments.

First Repressurization Cycle. The pressure was raised from about 5100 psig to 5500 psig and the vessel started to leak. Pressurization was stopped. The pressure loss profile that followed was smooth and almost linear. The loss rate was small, 1.5 psi/sec.

Second Repressurization Cycle. Repressurization continued when the pressure dropped to 5300 psig, and it was stopped at 5540 psig. The vessel continued to leak. The pressure loss profile that followed was smooth and almost linear. The loss rate increased slightly to 1.7 psi/sec.

Third Repressurization Cycle. Repressurization continued when the pressure dropped to 5450 psig, and it was stopped at 5640 psig. The vessel continued to leak. The pressure loss profile that followed was again smooth and almost linear. The loss rate increased slightly again to 2.5 psi/sec.

Pressure Decay Cycle. As pressure decay continued, the rate of decay remained almost linear; when the pressure reached 4940 psig, the tank was vented in one step to zero psig.

Post Test Observations. The vessel retained its shape; no pieces separated from the vessel. The vessel was checked (before/after borescoping) for leaks at 2000 psig with yellow sea dye and tap water, which readily oozed through many pinholes in the Kevlar overwrap.

Other Details. Vessel S/N 002, which was hydrogen embrittled, was tested in a vertical configuration. Because the vessel leaked, reembrittlement and retesting was not done. The vessel was borescoped and hair line cracks were detected.

The vessel was returned to ARDE by AFRPL where it was cut in half and a large crack, approximately two-thirds around the girth, was noted along with numerous hair line cracks.

IMPRESSIONS FROM THE QUICK-LOOK DATA. No quick-look data was generated for immediate post-run evaluation.

IMPRESSIONS FROM THE DIGITAL DATA ACQUISITION SYSTEM. To conserve record time, the data systems were started after the 2000 psig point was reached, and the initial condition data values are missing from the data cut but are available from the calibration zero cut. This condition will be corrected on subsequent tests.

Chamber Pressure Graphs. The PC1/1901 and PVSOUT/1904 graphs were essentially identical. The PC1/1901 graph indicates after the pressure was stabilized at 2000 psig, it remained steady with less than a 5 psig drop for 2 minutes. Then the pressure was adjusted upward three times followed by three periods of pressure loss; the slopes of the loss rates progressively increased after each pressure readjustment. Similiar loss slopes exist on the TBALL gas temperature thermocouple. Speculation as to the cause is reserved, except to note the ball started to leak at 5500 psig.

Strain Gage Graph. The only S/G on the DACS, SG2143/7124, operated satisfactorily. The S/G profile was almost an exact duplicate of the PC1 profile, except for scaling and polarity differences. No major spikes appeared.

Temperature Graphs. All of the T/Cs worked satisfactorily.

Strain Gage T/Cs: During pressurization, after the 2000 psig point, all S/G T/Cs increased about 15 to 25 F degrees above their 53 to 70 degrees F initial condition. Each S/G T/C was within a family of curves with a reasonably smooth increasing tendency modulated with explainable inflections, moderate magnitude excursions and slopes consistent with system time constants, sensor locations and heating rates.

Other T/Cs: The behavior of the boss, ball and heat exchanger temperatures was within normal limits. While probably not of importance, it is noted the boss outlet temperature was lower than the boss inlet temperature, and this is the reverse of what was observed on the first test; the boss outlet temperature was more sensitive to temperature changes caused by the tank pressure adjustments than the inlet temperature, which doesn't reflect the adjustments or, for that matter, temperature decays as it had a consistent slow rate of climb; the differences may be related to the following facts: This vessel had thicker bosses than the first vessel; more cool gas was used than in the first test because the vessel leaked. The test configuration was vertical with the inlet at the top and exposed to the sun while the outlet was shaded by the vessel.

IRIG Time Code Format. The IRIG data was within normal limits. It was not decoded, but the code was of sufficient quality to allow decoding.

DESCRIPTION OF THE EMBRITTLEMENT PROCEDURE. ARDE embrittlement procedure dated 7-15-85 was followed; embrittlement was started at 0700 hours on 4APR86. Seventy-two hours of embrittlement were completed at 0815 hours on 7APR86; the tank was immediately moved from the shop embrittlement area to the test site, instrumented, hooked up and tested at 1045 hours on 17MAR86.

IMPRESSIONS FROM THE DIGITIZED FM DATA.

Data analyst's comments, first data pass. "SG14/7114 goes out at 29.0 seconds."

Graphs. The initial graphs were filtered at 100 Hz, and the digitized sample rate was 1024 samples per second; data were plotted at one point every 400 milliseconds. A couple of spikes appeared on the S/G graphs; these spikes will be analyzed at a higher sample rate.

Data analyst's comments, second data pass. "(data) rerun with correct time reference and cal cuts for zero strain to determine delta strain."

Graphs. The graphs on the second data pass confirms the magnitudes of strain on the graphs from the first data pass are correctly referenced to the initial strain conditions; to verify this, the time axis was started at -150 seconds; the initial conditions are shown near this time. The graphs from both passes are identical except for the differences already noted.

ACOUSTIC EMISSION IMPRESSIONS. Acoustic emission data were not taken.

AIR PRESSURE SENSORS did not produce any significant data because the tank did not rupture in a catastrophic failure mode.

REVISION RECORD. Initial issue: 9APR86. Filename: TESTRV4A.
Revision A: 16APR86; major text corrections, and additions.
Revision B: 17APR86; major text additions, time & date corrections in embrittlement paragraph. Revision C: 25APR86; corrected acoustic emission impressions text. Revision D: 12May86; FM S/G data rerun to include initial condition values so strain deltas can be confirmed; comments added to impressions from the digitized FM data.

E.3.3

Pressure and Strain Versus Time Plots

Figures E-1 to E-12 give pressure versus time and fiber strain versus time plots for tests RV-4 and RV-4A. Tensile strain is negative. A total of twenty four (24) strain gages were installed on the fiber outer surface, twelve (12) each above and below the girth at $\pm .80$ height on the outer last 81° fiber wrap, as sketched on Figure 1G. Even numbered gages are parallel to the fibers and odd numbered gages are perpendicular to the fibers.

Fig. E-1
KEVLAR VESSEL TEST RV-4 - P/N E4170. S/N 002 25 FEB 1986

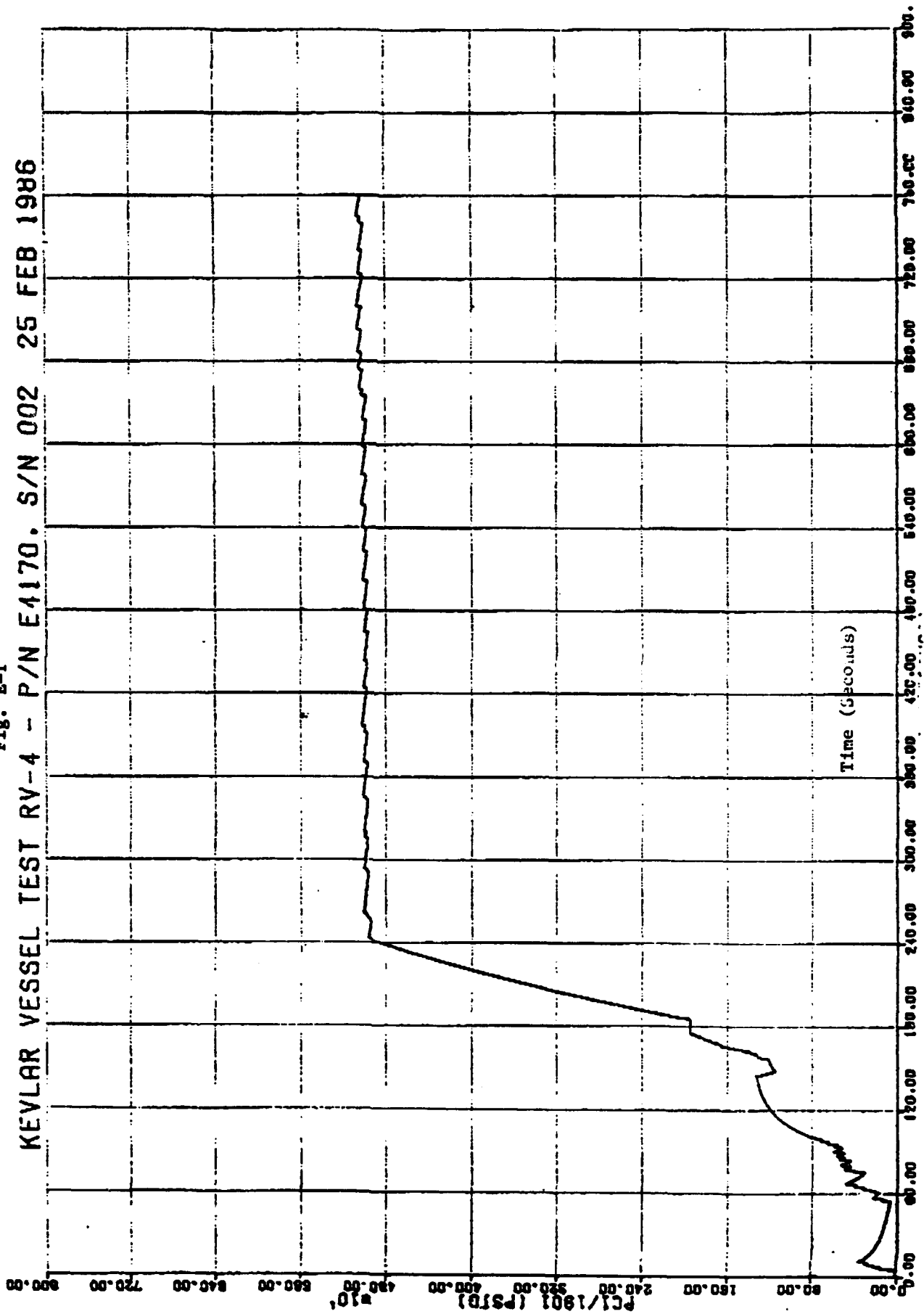


Fig. E-2

KEVLAR VESSEL TEST RV-4 - P/N E4170. S/N 002 25 FEB 1986

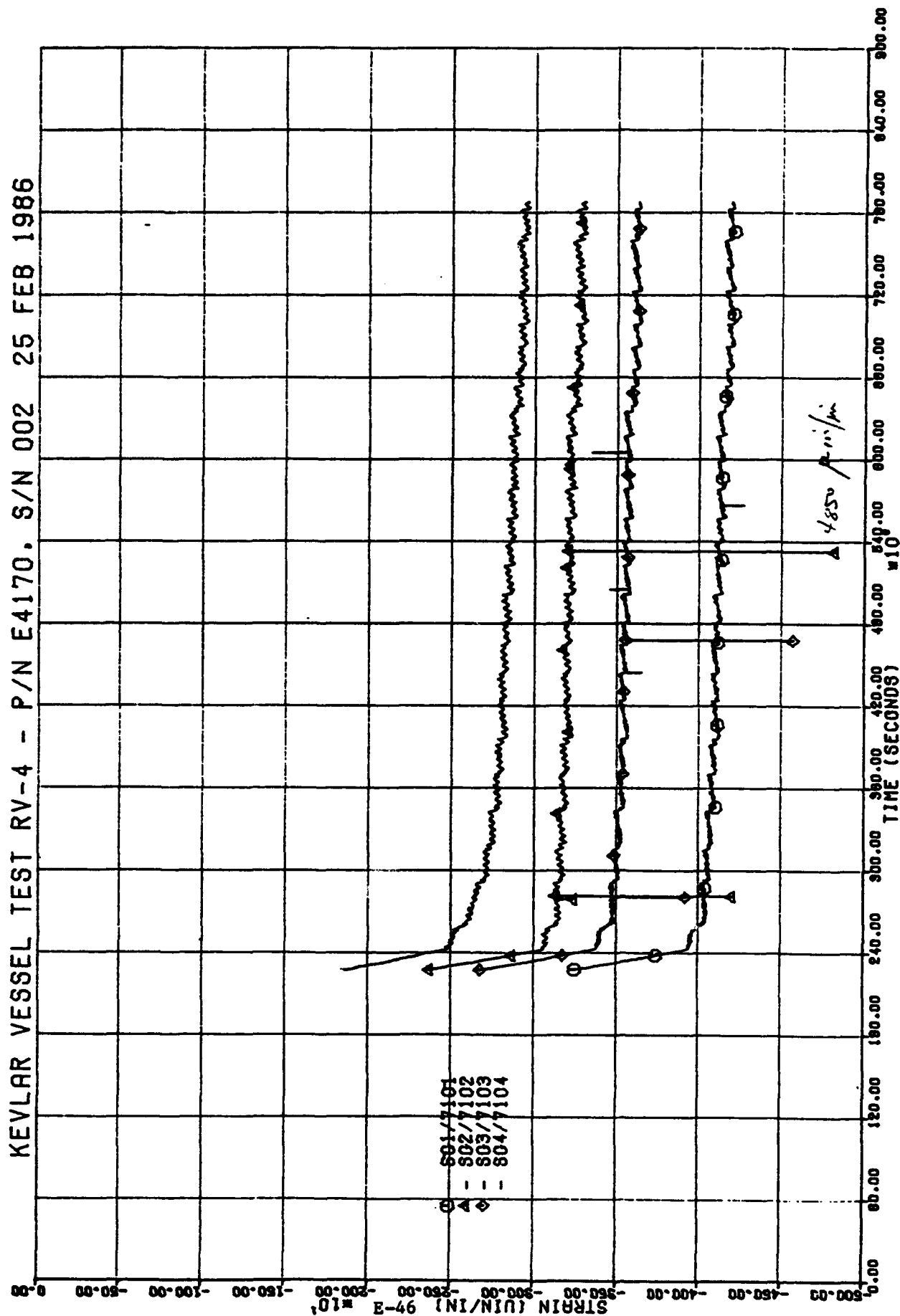


Fig. E-3
KEVLAR VESSEL TEST RV-4 - P/N E4170, S/N 002 25 FEB 1986

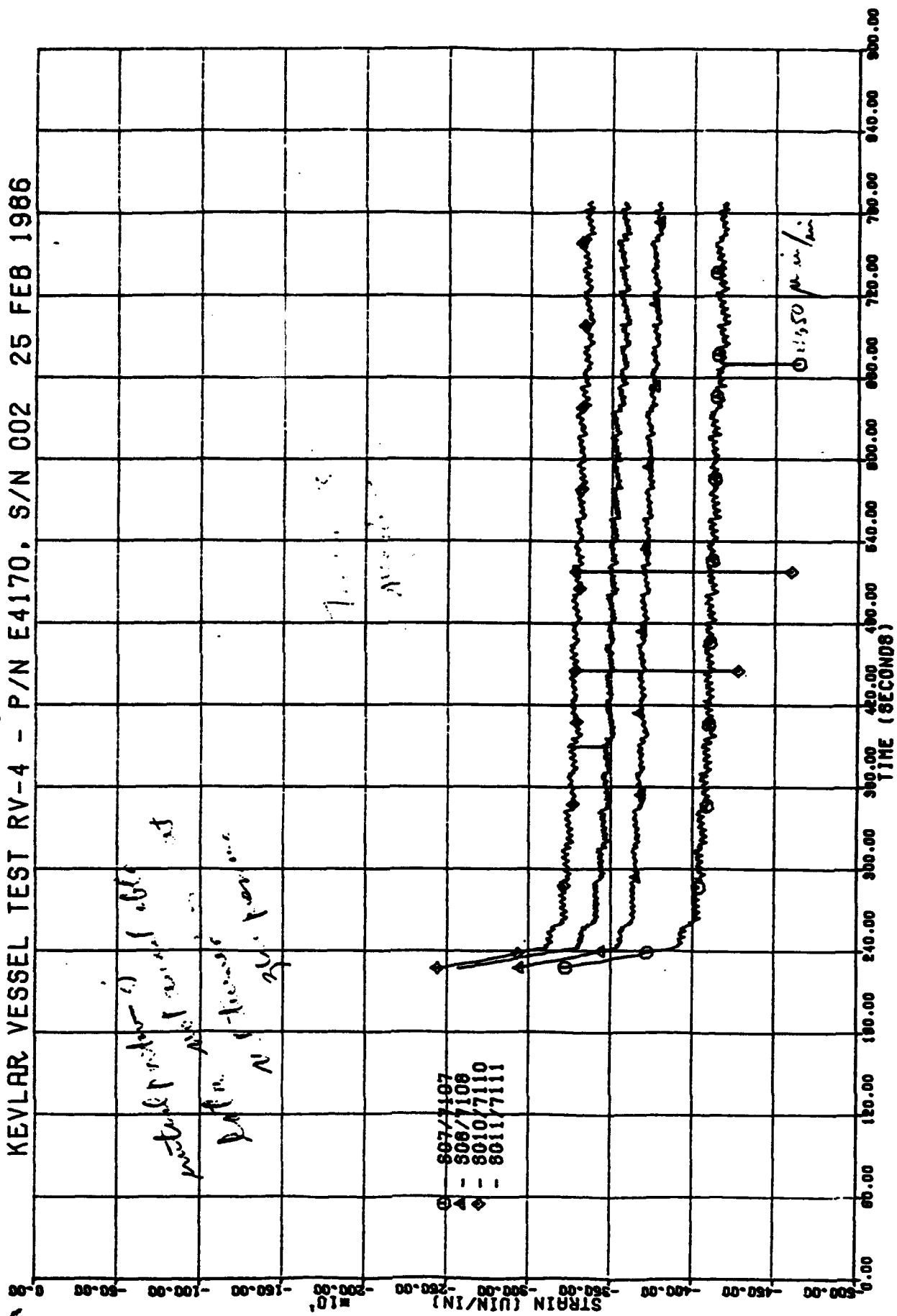


Fig. E-4

KEVLAR VESSEL TEST RV-4 - P/N E4170, S/N 002 25 FEB 1986

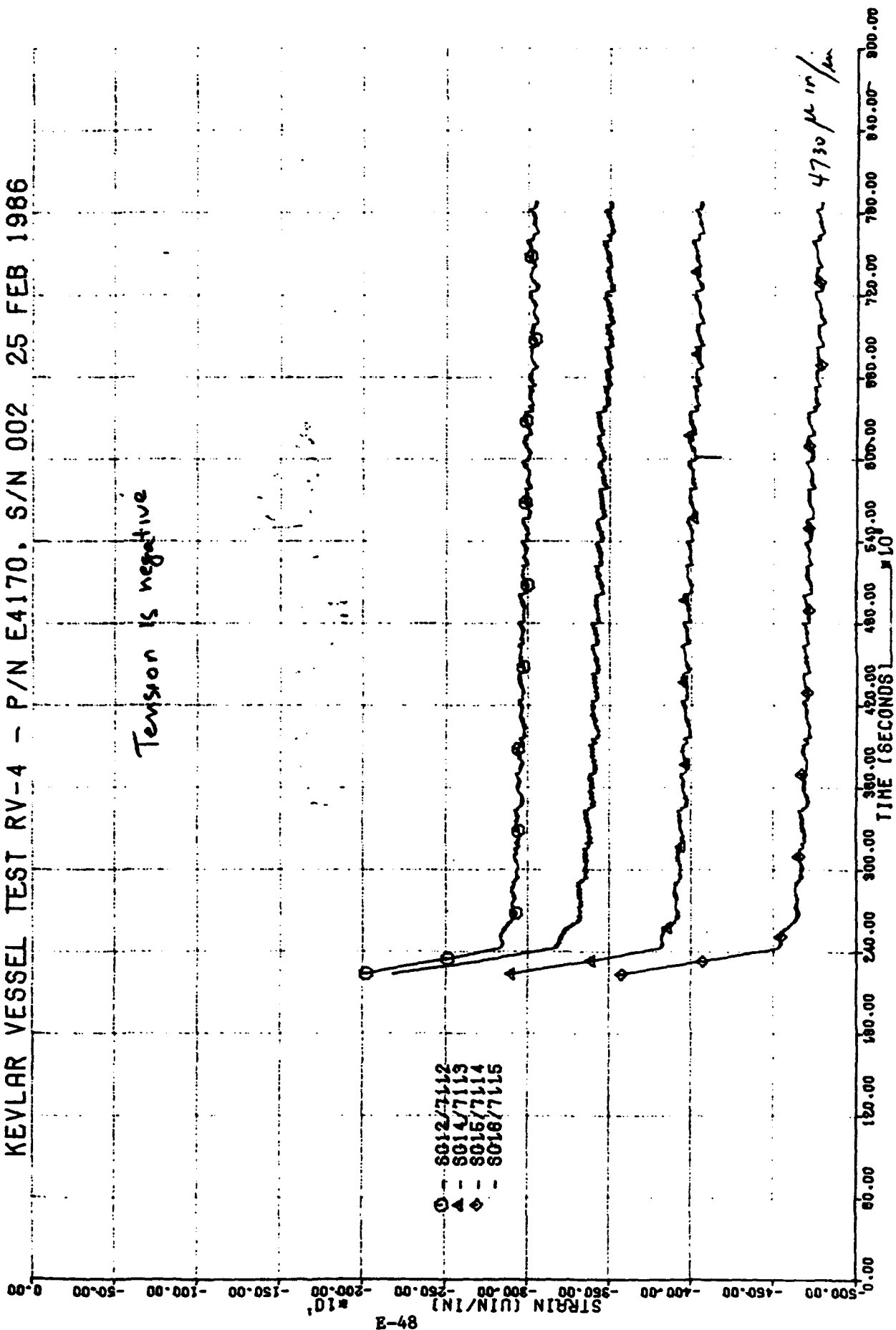
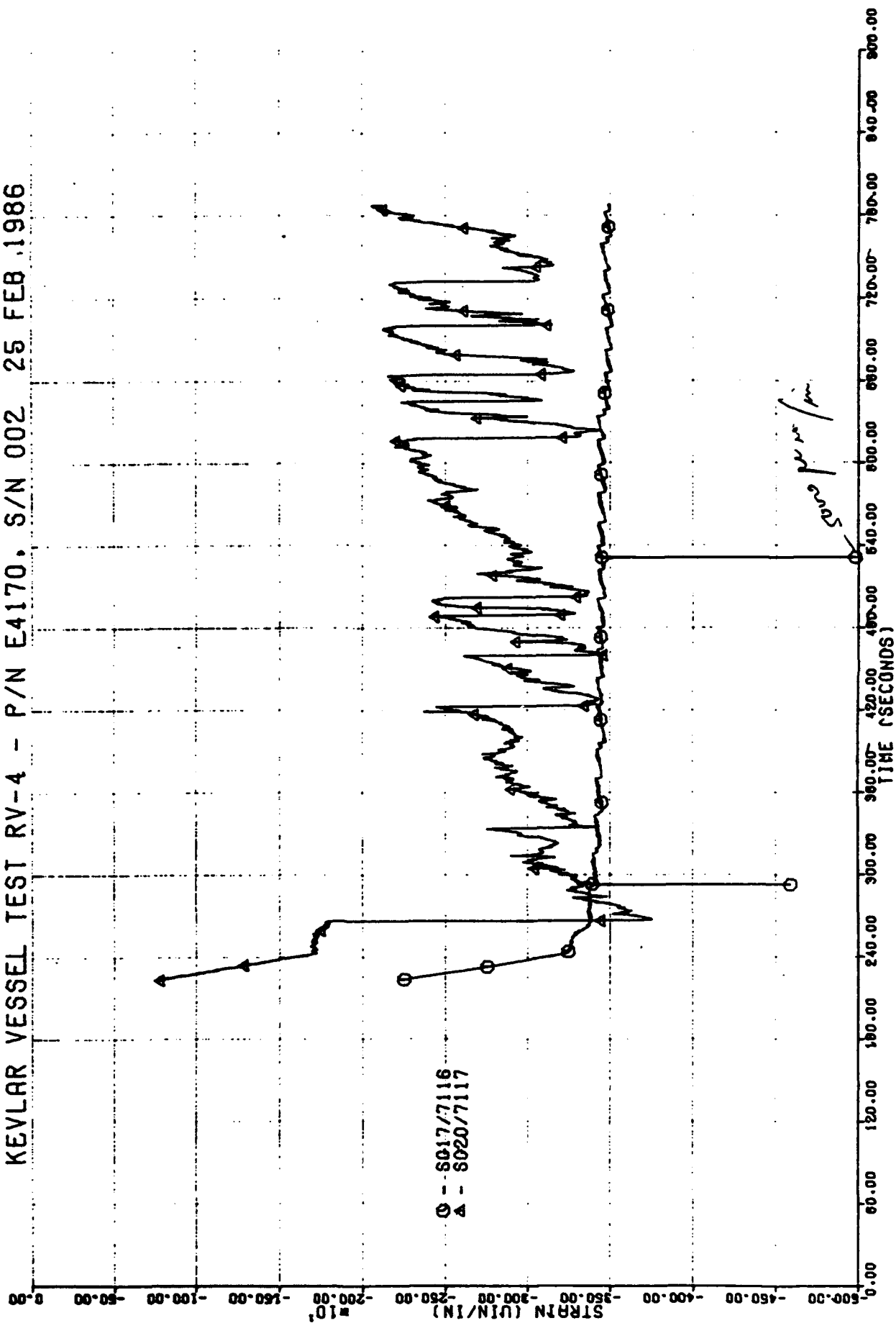
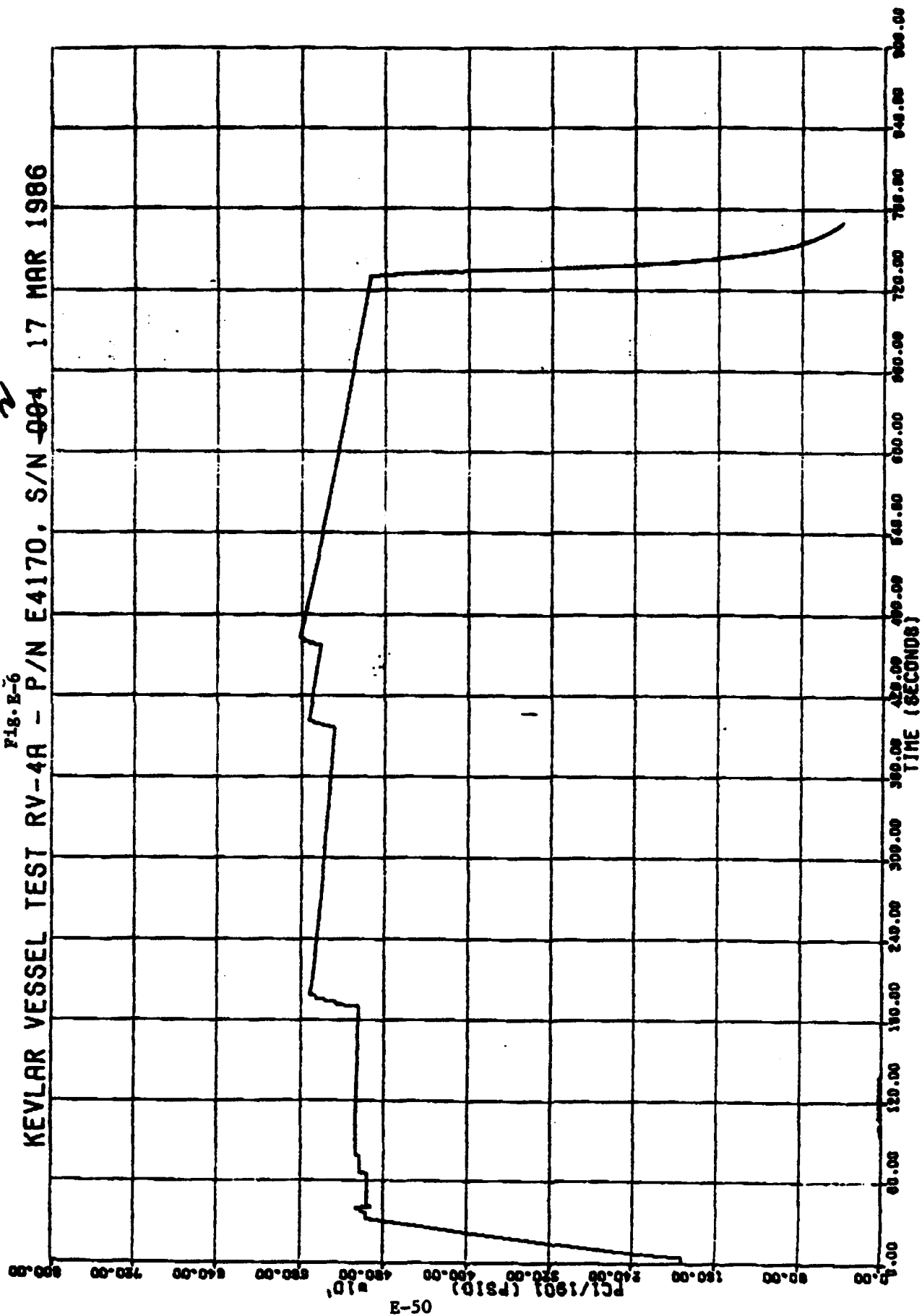


Fig. E-5
KEVLAR VESSEL TEST RV-4 - P/N E4170, S/N 002 25 FEB 1986



2
 KEVLAR VESSEL TEST RV-4R - P/N E4170, S/N 004 17 MAR 1986

Fig. E-6



E-50

FILED IN E-50

10:23

04/11/00

Data from 2ND H₂ Embrittlement Experiment on this tank
 Note: 100 Hz F.1 Kering/1024 samples/sec digitized Data plot every 400 ms.

Fig. E-7

002

KEVLAR VESSEL TEST RV-4A - P/N E4170. S/N 004 17 MAR 1986

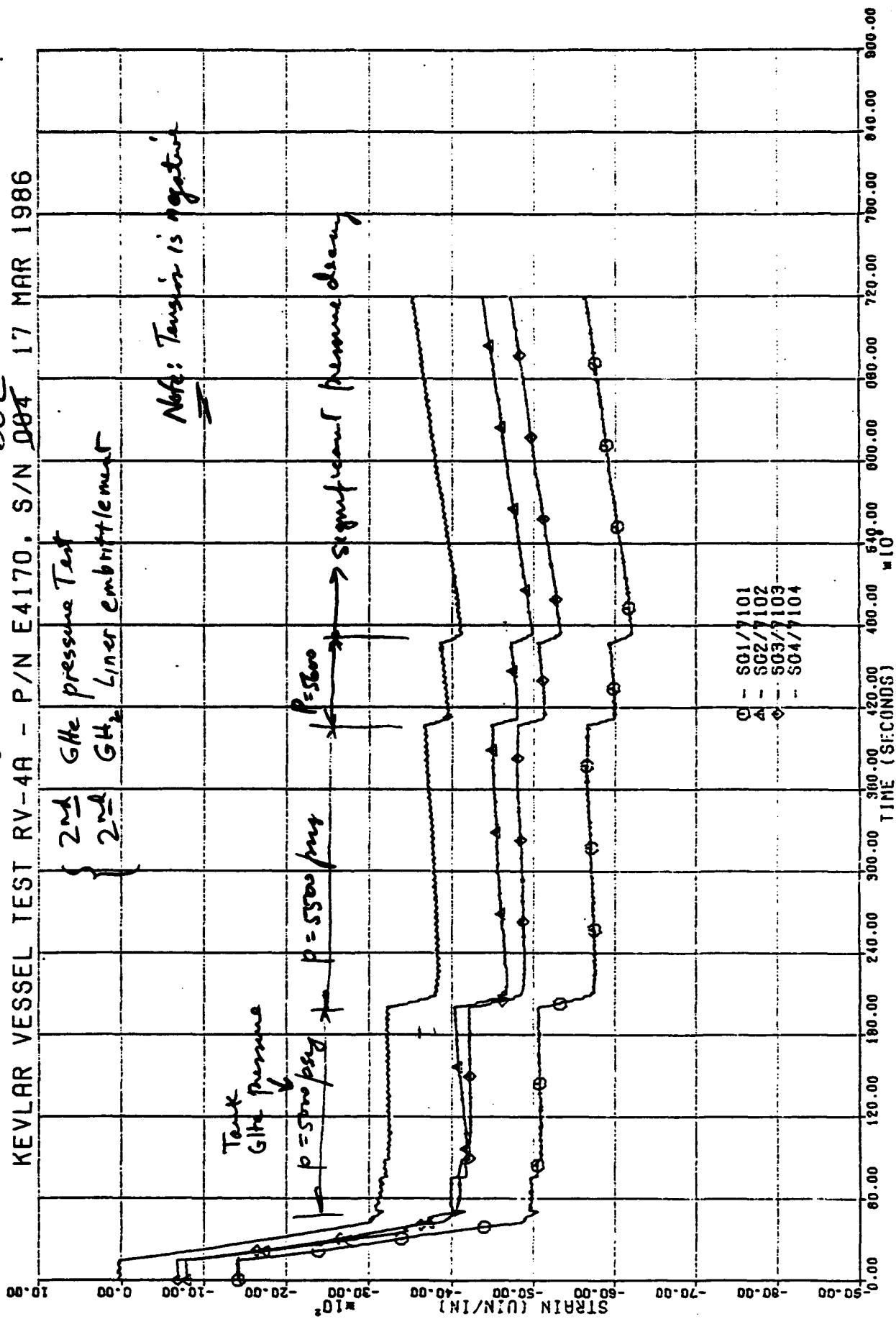


Fig. E-8

KEVLAR VESSEL TEST RV-4A - P/N E4170. S/N ~~004~~ 002 17 MAR 1986

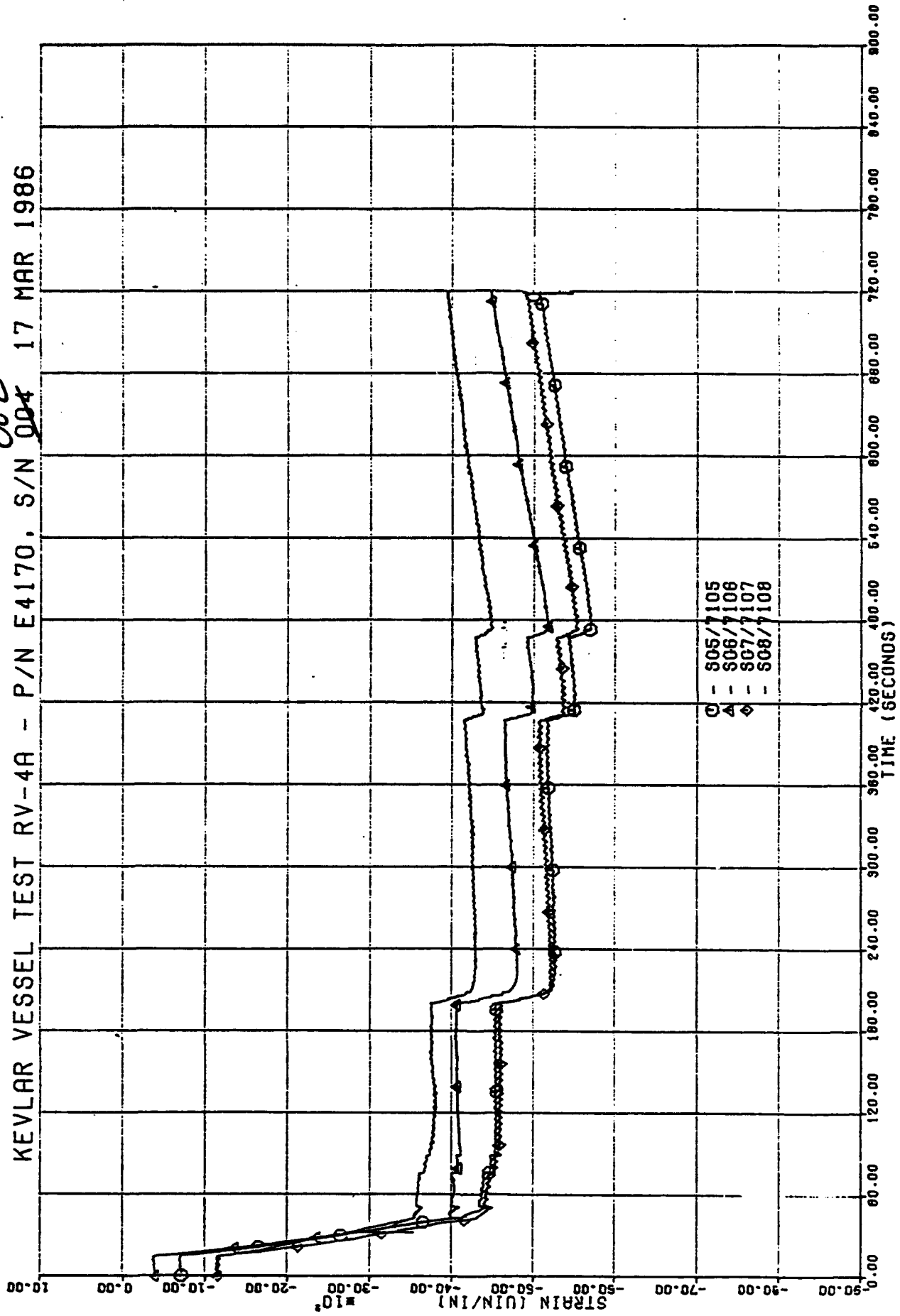


Fig. E-9
KEVLAR VESSEL TEST RV-4A - P/N E4170, S/N 004 17 MAR 1986

002

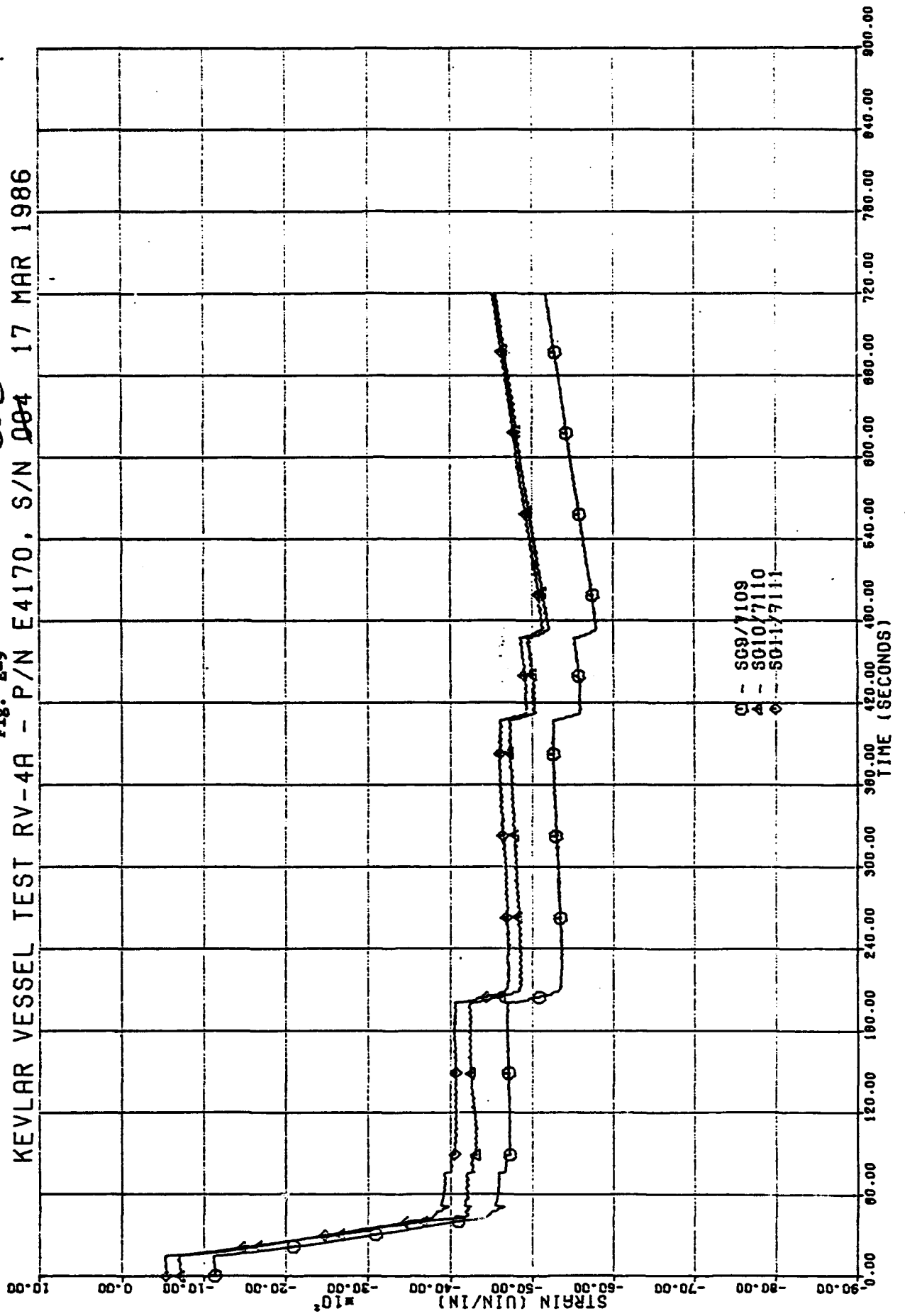


Fig. E-10 KEVLAR VESSEL TEST RV-4A - P/N E4170. S/N 004 17 MAR 1986

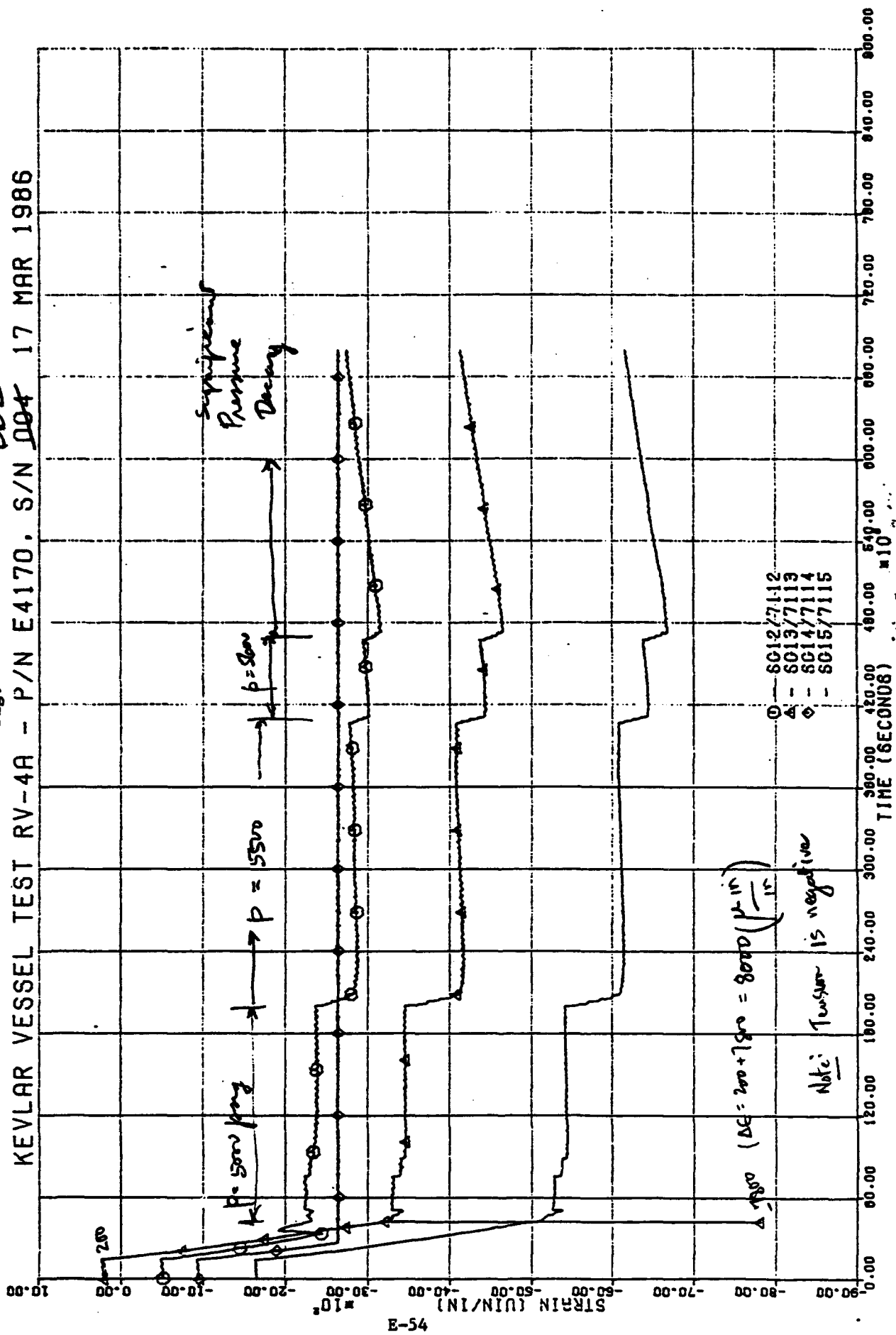
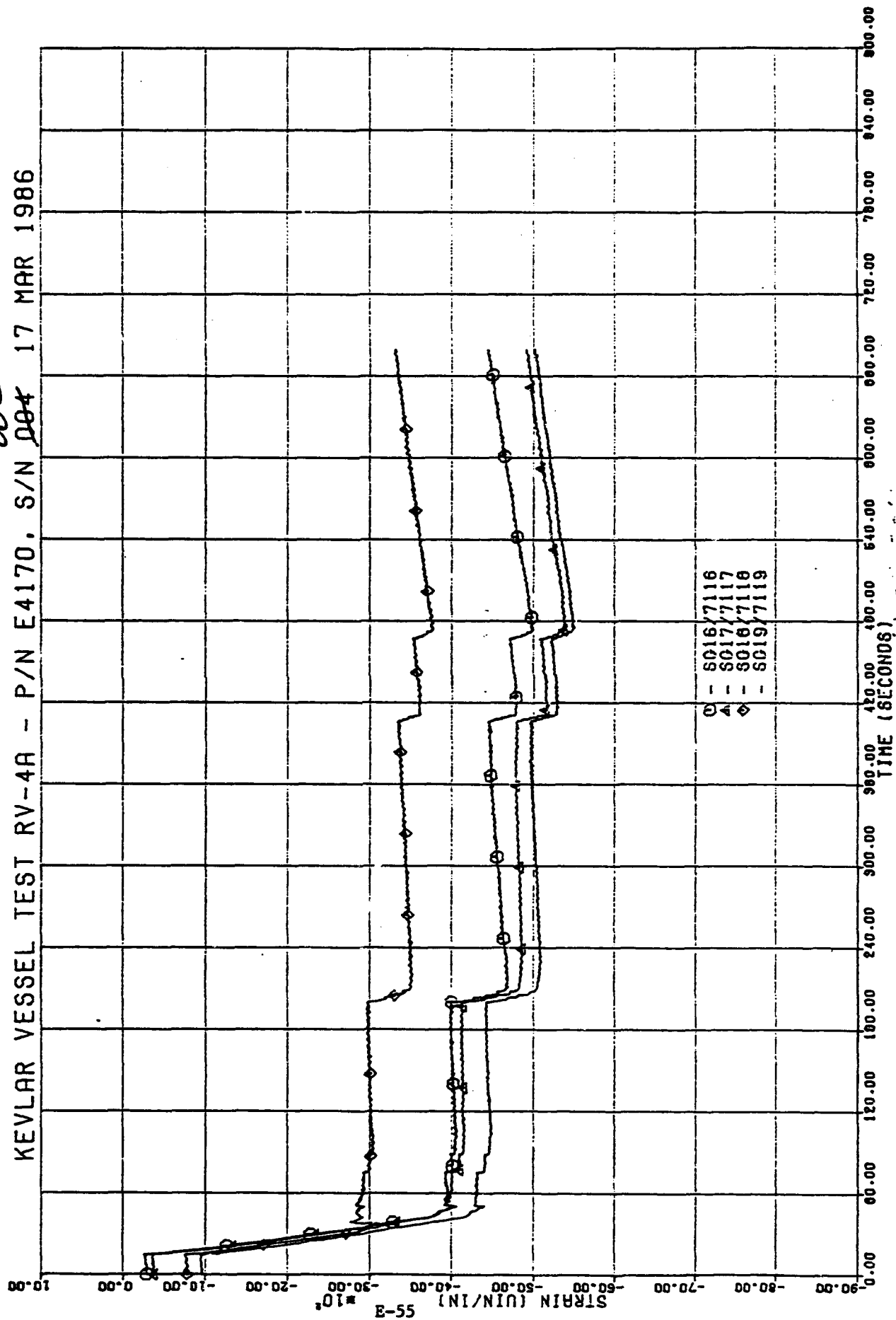


Fig. E-11

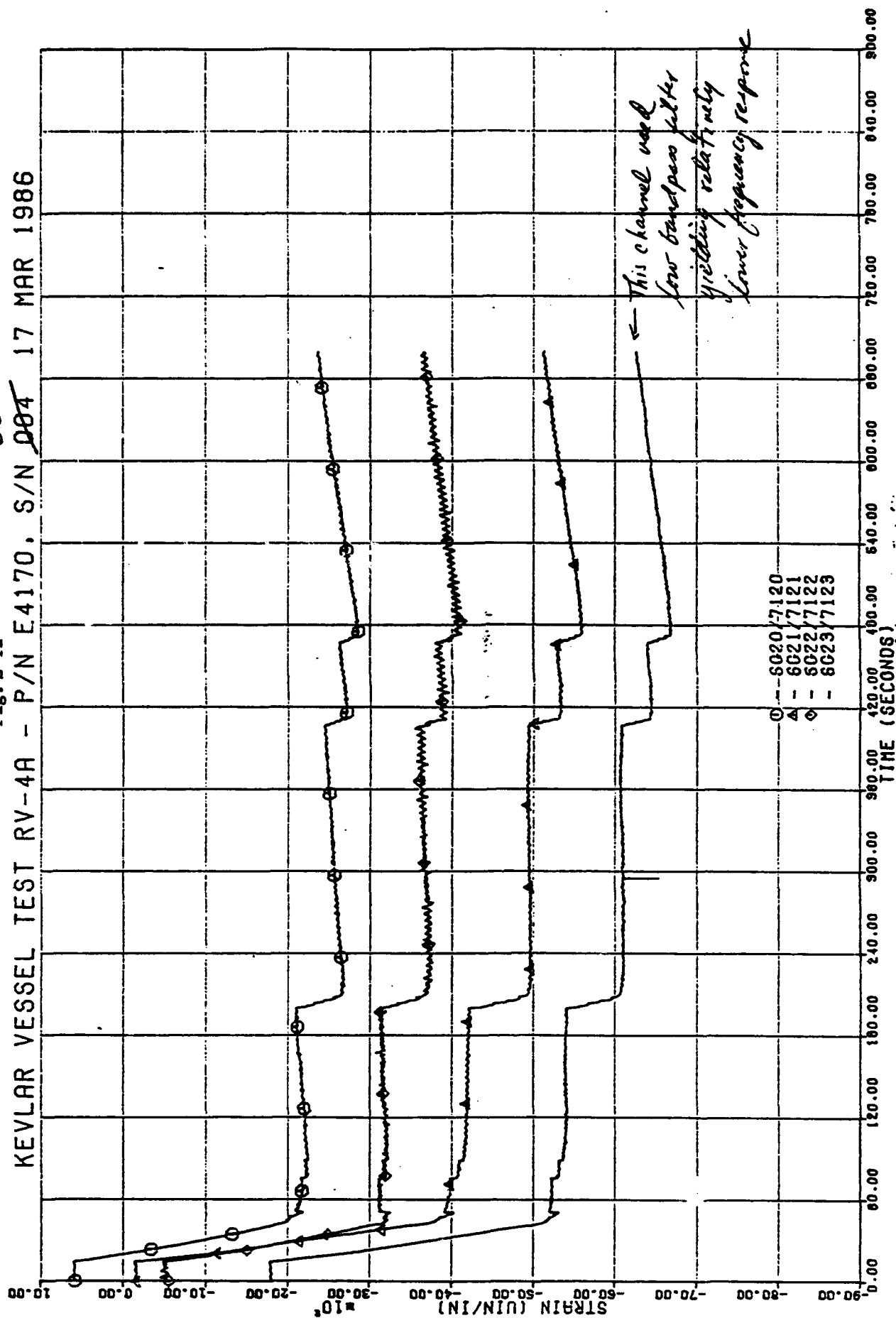
KEVLAR VESSEL TEST RV-4A - P/N E4170. S/N ~~004~~ 002 17 MAR 1986



KEVLAR VESSEL TEST RV-4A - P/N E4170. S/N 004 17 MAR 1986

Fig. E-12

002



E.3.4

Acoustic Emission Monitoring

Acoustic emission (AE) probes were mounted on each metal boss for the RV-4 test. During testing, the AE signals were masked by high noise level coming from the tank outlet boss region which indicated a leaking fitting. No AE data was taken for RV-4A experiment.

E.3.5

Post Test Inspection

E.3.5.1

RV-4 Test

Borescopic examination of the pre-compressed intact vessel liner inside surface at AFAL revealed many hairline type cracks in the metal, indicating that the CH_2 embrittlement process was working. A tank leak check verified a leaky outlet fitting (bad seal). This demonstrated the effectiveness of the AE monitoring.

E.3.5.2

RV-4A Test

A post-test elevated pressure water/yellow die leak check performed on the vessel at AFAL showed pronounced leakage. Additional post test examination of the tank was performed at ARDE. The composite vessel was parted at the girth for viewing/die penetrant of the tank's metal liner to assess the extent and type of liner cracking.

A fine network of matrix-type cracking was observed in the liner's inside surface and a large, fairly wide continuous crack was also seen. This large crack traversed approximately 28 surface inches and had some branching. Figure 2-4 is a photograph of the die penetrant-enhanced cracked liner inside surface.

E.4 RV-5 Test (16" ϕ PSC)

E.4.1 Test Vessel Description

- P/N E4170, S/N 004 (Kevlar Overwrapped Cryo Cres Composite Sphere)
- Kevlar Fiber (less resin) Average Thickness = .154" (100% Baseline Thickness)
- Metal Thickness = .05" nominal
- Inside Radius = 7.66"
- Hydrogen Embrittlement Mode = Global
- Electrolyte Solution -
$$\frac{20 \text{ cc H}_2\text{SO}_4 + 980 \text{ cc Tap H}_2\text{O}}{1000 \text{ cc Solution}}$$
- Solution Additive = 500 mg Sodium Arsenite
- Sensitize liner inside surface (cold pickle, 70°F-90°F)
 - a. Nitric acid A.C.S Technical Grade, 70 weight percent, 2% by volume.
 - b. Hydrofluoric acid A.C.S. Technical Grade, 55 weight percent, 2% by volume.
 - c. Potable tap water - remainder. The same solution used on all applicable test tanks.
- Charging Current Density = .005 amps/in² of surface to be embrittled

- Charging Time - 72 hours
- Hold Time Before Test - 2-1/2 hours
- Adcoat AC818T liquid maskant on areas not to be embrittled.

The photographs of Figures E-13 and E-14 show the entrance to the AFAL test area with the camera tower in the background and an upper view of the test stand and tower showing the motion picture camera installations. Figures E-15 to E-17 are photographs of the tank in the test fixture and closeups of strain gages on the test tank. Installation and checkout of Acoustic Emission (AE) probes on the test tank metal bosses is shown in the photograph of Figure E-18. A view of the tank mounted in the test stand together with pole mounted Bikini blast over pressure gages and fragment catching witness panels in the background is given on Figure E-19.

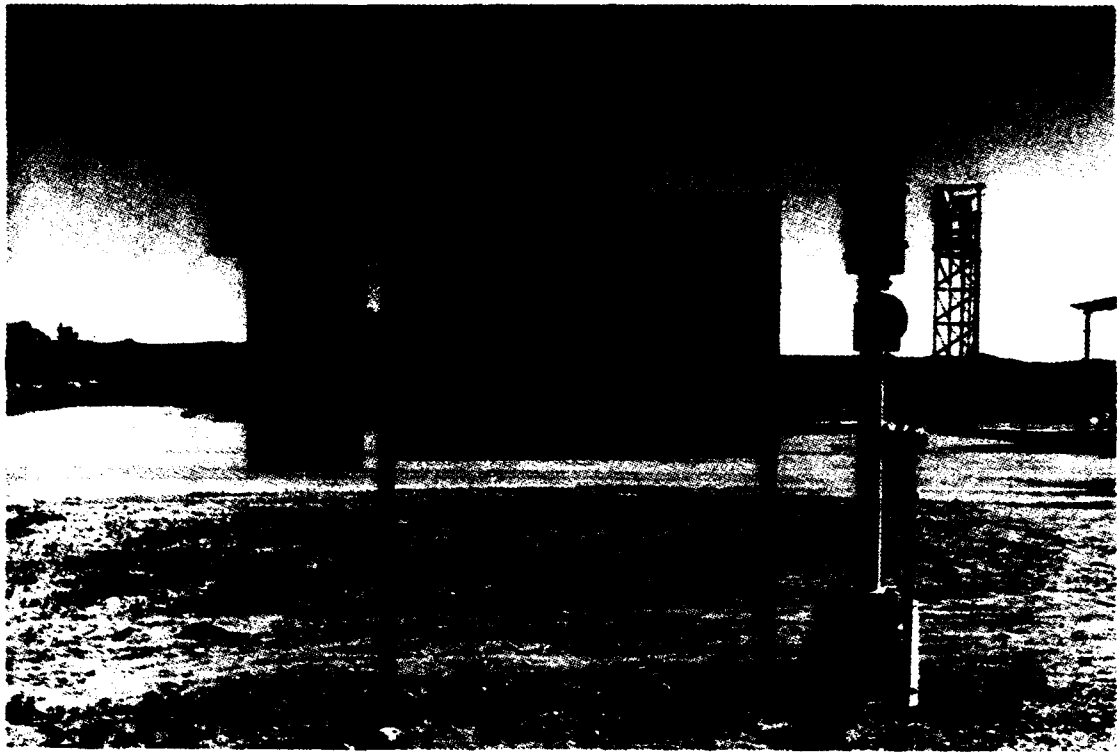


Fig. E-13

AFAL TEST AREA 1-52



Fig. E-14

TEST TOWER CAMERA INSTALLATION



Fig. E-15

TANK MOUNTED IN TEST FIXTURE



Fig. E-16

TEST TANK STRAIN GAGE INSTRUMENTATION



Fig. E-17
STRAIN GAGE CLOSE UP VIEW



Fig. E-18
ACOUSTIC EMISSION PROBE INSTALLATION AND
CHECK OUT

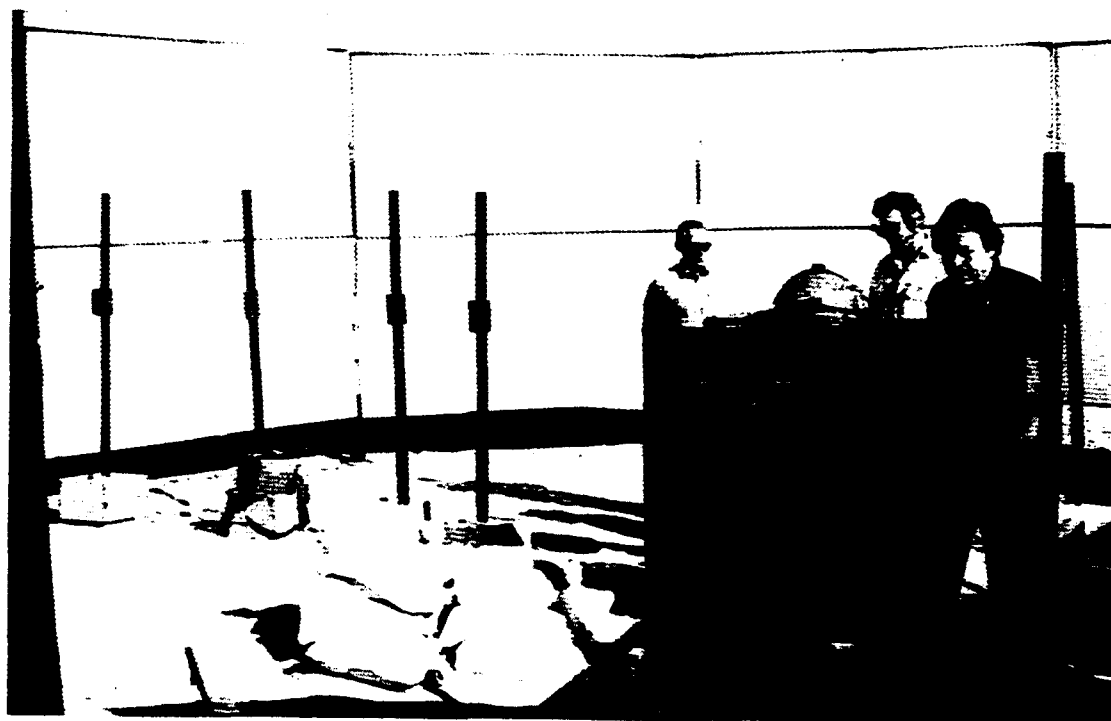


Fig. E-19
VIEW OF TEST TANK, BIKINI GAGES AND WITNESS PANELS

INSTRUMENTATION OBSERVATIONS (by AFAL Instrumentation Engineer)

1211 4/2/86
DIST DC, KP
- 1 -

KEVLAR TEST 005, 7APR86. Project number 573000RV.

EXPERIMENTAL PROCEDURE.

Cool Down and Initial Pressurization Cycle. Pressurization was preceded by a 150 second purge for cool down from the initial ambient condition; the tank vent was closed, and pressure was increased to 2000 psig for a 15 second hold before starting the final pressure increase to 5000 psig. No leak was observed during the hold period.

Final Pressurization Ramp. The vessel was pressurized with a steady ramp from 2005 psig to 5000 psig in 32 seconds, but pressure could not be maintained; pressure loss started as soon as pressurization was stopped at 5000 psig; the pressure loss was sharply demarcated and followed a profile that was smooth, nonlinear and rapid. The loss rate was 13.2 psi/sec.

First Repressurization Cycle. Repressurization was requested by ARDE when the tank pressure failed to hold at 5000 psig and dropped to 3500 psig. Pressurization was attempted but it couldn't be maintained much past 4730 psig and was stopped; the pressure loss profile that followed remained smooth and nonlinear but was much more rapid than the loss following the final pressurization ramp. The loss rate increased to 86.9 psi/sec.

Second Repressurization Cycle. Repressurization continued when the pressure dropped to 4300 psig, but it couldn't be maintained past 4600 psig and was stopped; the pressure loss profile that followed was again smooth and nonlinear but had a changing slope magnitude that started at 125 psi/sec and ended up approaching zero before the pressure decay cycle was started. Frost started to appear during this cycle and remained for at least 30 minutes.

Pressure Decay Cycle. As pressure decay continued, the rate of decay decreased; when the pressure started to level out near 1000 psig, the tank was intentionally vented in one step to zero psig. PC1 shows a two step vent profile, but this is due to pressure lockup caused by line icing, and the graph in this region isn't correct; PVSOUT displays the correct pressure-time history.

Post Test Observations. The vessel retained its shape; no pieces separated from the vessel. The source of the leaks was not obvious until the vessel was separated at its girth weld by an AFRPL machinist. A cleaner, dye penetrant and developer were used to enhance the apparent fine cracks, pits and bumps, which were moderately spaced and randomly concentrated in a wide field between the girth weld and end bosses.

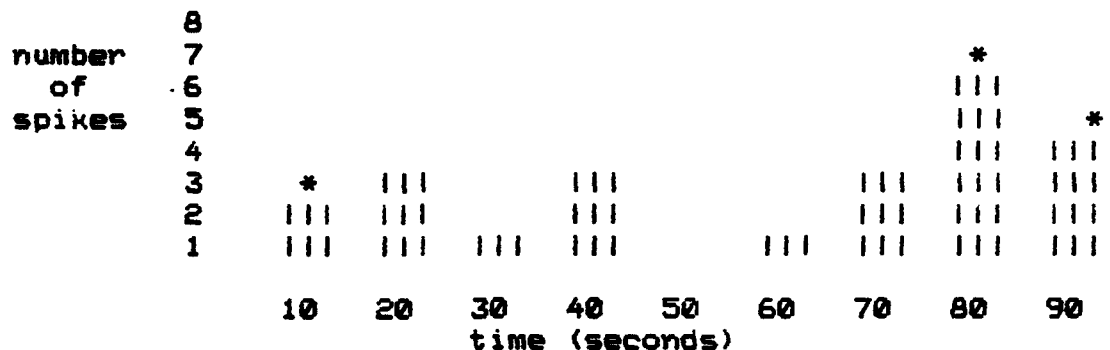
Other Details. Vessel S/N 004, which was hydrogen embrittled, was tested in a vertical configuration. Because the vessel leaked, reembrittlement and retesting was not done. The vessel's halves were returned to ARDE by ARDE via air freight.

IMPRESSIONS FROM THE DIGITIZED FM DATA.

Data Analyst's Comments. Richard Thomsen, ITT, noted "SG1/7101 and SG7/37103 (is bad and) SG7/7107 is (noisy)." Also, he continues, "several data anomalies were noted: SG1/7101 zero and 50% cal were the same. SG3/7103 too noisy to calibrate. SG4/7104 three shifts and return on two of these. SG6/7106 shows the smallest tension delta strain. SG7/7107 extremely noisy. SG14/7114 shows a step at 70 seconds. SG16/7116 has alot of what I would call noise spikes. SG20/7120 shows a prominate step at 205 seconds. SG22/7122 low frequency noise."

Additional data passes were made for the purpose of evaluating the spikes, and the analyst's comments continue with the following:

"4AUG86. Plots of RV-5 (70PR86) strain gage 16, digitized FM at 80,000 SPS (10,000 Hz filter). (This set of graphs shows) data from 7-98 seconds (which) was first plotted at 10,000 SPS to detect spikes. These show many barely detectable spikes (<150 microstrain), some bigger ones (150 to 300 microstrain) and a few large ones (>300 microstrain). The frequency (of distribution, or histogram,) of spikes of all sizes, for time intervals of ten seconds, are shown (below).



The regions with large spikes are marked with a *. To be selected, a spike had to be an abrupt increase and decrease in tension, above the noise bands. This eliminated possible data drop outs that show up as a single spike in one direction only. This method did not select all of the spikes as there are some within the noise band."

The comments for the second set of graphs follow:

"Several spikes (on SG16) were plotted at the full 80,000 SPS rate to study their shape. At 75.371 seconds is an example of (a) single downward pointing spike. Many of these spikes showed up on the 1024 SPS pass, but only a few (showed up) at this high (80,000 SPS) sample rate. Also, the rise time is the minimum allowable by the filter, in this case 50 microseconds. For these reasons, I would consider them noise (generated during data

reduction).

Spikes at 67.354, 71.211, 72.988, 76.699, 77.300, 82.054, 83.206, 83.734 and 92.460 seconds were also plotted. These show a consistent pulse shape with a gradual increase in tension, a quick release and then a gradual return to the same level as before. The rise time of the release averages 250 microseconds, well within the limits of the 10K Hz filter. I suggest these are due to resin cracking, the Kevlar wrap snapping, or liner cracking.

Plots at full sample rate were also made for 300 milliseconds during the maximum tension strain, but no new spikes were noted.

Plots of the 1024 SPS SG16 data are also included for comparison purposes.

These (two) sets of plots (SG16/711 SPIKE ANALYSIS, sample rate 80,000 SPS, filter frequency 10,000 Hz, full sample rate plot from 75.36 to 77.010 seconds; and SG16/7116 Spike Analysis, 10K SPS plots) should be used rather than those (plots) previously sent, due to a (small) time reference error on those (plots) first sent (to the agencies listed on the distribution list)."

Spike theory #1 speculates the spikes represent the natural resonant frequency of the composite structure; the resonance is alleged to be 10,000 Hz, which would have a period of 100 microseconds and a rise time of 33 microseconds (using $rt=1/3(f)$ method). The frequency seen at the 72.98800 second spike is about 2440 Hz (period=72.98885-72.98844 seconds=410 microseconds); the other spikes have similar periods. Recognizing that the error in estimating the period from the graphs is considerable, and, in practice, acknowledging the disrupting influence of the broken liner on the composite resonance, it would be expected to have a resonant frequency, particularly a lower resonance frequency, other than that which was predicted. In fact, half an order of magnitude isn't too bad considering the complications. However, note the damping characteristic of the spike; it is close to being critically damped, for there is no major overshoot or evident period of resonance, characteristic of underdamping, or prominent slow approach to the peak, characteristic of overdamping. In nature and with artifacts, critical damping is rare and is usually obtained through modification or design not pure circumstance. For this reason, suspicion is cast on this theory; and it should be more thoroughly explored.

Graphs. The initial graphs were filtered at 100 Hz, and the digitized sample rate was 1024 samples per second; data were plotted at one point every 400 milliseconds. Several spikes appeared on the S/G graphs; these spikes will be analyzed at a higher sample rate. Except as noted elsewhere, the parameters' noise floors did not include major transverse or common-mode minus $L(di/dt)$ transients, artifacts, crosstalk, atmospherics,

noticeable RFI, intermodulation, spurious parasites, or sibilants. However, latent noise or data manifestations may be obscured in some parameters, and digital signal processing may be needed for signal enhancement. In general, the data appeared to be unbiased, precise and accurate.

Strain Gage Graphs. Except for the problems already mentioned, the strain data from the 20 good strain gages were within normal limits.

Fourteen (70%) of the strain gages had final values slightly higher than their initial conditions; the remaining six (30%) had values slightly lower than their initial conditions. At the end of the test, ninety percent (18) of all the gages (20) were within about 300 uin/in of their initial conditions.

Speculation as to the cause of this general trend of higher final strain values on a very large percentage of the gages is important particularly if it shows temperature is involved. Temperature induced apparent strain error is an unwanted data contributor in this experiment, and the investigators remain alert for any data that would confirm its expected influence or for any data that would overwhelm and distort valid data. Unfortunately, the reason for the differences in static strain levels before and after the test is not immediately obvious.

It may be an erroneous oversimplification to assume the general trend for higher final strain values is a simple intrinsic erratic experimental error caused only by vessel frosting and how it influences the gages, Kevlar fiber, metal liner and resin. As temperature decreases, the -08 STC gages generate a tension (expansion) correction, the Kevlar fiber expands, the metal liner contracts and the resin contracts. The gages parallel to the fiber and the fiber respond synergistically with one another and this is probably the major contributor; the liner may be out of the picture at this point (it is broken or weakened, has a complicated preload characteristic and may not necessarily be touching the overwrap uniformly although the gages track the pressure rather well, which may contradict this theory!); the potential for compliant resin behavior in the parallel direction is overpowered by the stiffer, more influential fiber (In other special Kevlar sample tests, as the sample heated to equilibrium, the total absolute strain change in the perpendicular direction was about 37% of the total absolute strain change in the parallel direction; the polarity wasn't the same, however. The strain parallel to the fibers went into an obvious compression, and the perpendicular direction went into a general tension trend. For cooling, it is assumed, the strain parallel to the fibers would go into significant tension and the perpendicular direction would go into not so significant compression). Anyway, the strain graphs that end up with the most amount of deviation from their initial condition have the least amount of temperature change over the same time period, and this information would appear to be exciting, except that the strain directions have opposite

polarity.

IMPRESSIONS FROM THE QUICK-LOOK AND DIGITAL DATA ACQUISITION SYSTEM DATA. Immediately after the test, the tank pressure graph, 1901, and the strain gage graph, 7124, were generated and compared. Both data parameters were satisfactory and were practically identical except for known scaling differences, expected opposite polarity and two interesting locations on the strain gage graph that exhibited unexpected behavior profiles. Remaining unexplained, after reviewing the digital data graphs, is a small but very obvious dip in the strain gage graph at 65 seconds, which occurs between 64 to 76% of the final pressurization ramp duration; surprisingly, the dip doesn't show in either tank pressure graph; and the dip doesn't appear to be a clear function of the temperatures; although most T/Cs are changing only slightly during this period, suspicion could start with TT9/2205, TT10/2206 or TBSIN/2209 because they exhibit small but conspicuous inflections as they undergo noticeable rates of change near this time period. Also, there remains an unexplained slow strain inflection during the pressure decay following the second repressurization cycle, at 400 to 500 seconds; the inflection isn't an obvious function of the tank pressure or tank gas temperature, TBALL; temperature relationships again are under suspicion, as TT1, 2, 4, 8, 9, 10, & 12, continue to exhibit small but conspicuous inflections as they undergo noticeable rates of change at the onset of this slow strain inflection. Implicated also in this manifestation may be the other tank pressure transducer, PVSOUT, which shows some unexplained trace widening between 400 and 450 seconds; this transducer is in the valve box and is subject to less icing risk than PC1. The trace widening is consistent with undesirable noise or may represent valid data.

ACOUSTIC EMISSION IMPRESSIONS. From Jim Leaird, AET: "...I believe that the onset of AE activity at time 47 seconds (my test time) represents the onset of catastrophic cracking/failure. This is well indicated on the 2nd pass. AE data where I filtered on the basis of AE to valid had to be >2RDC>4000 (eliminates electronic signals & 90% leak type noise) & greater than 47 dB peak amplitude to indicate fracture type AE. Please note that this is first pass at AE analysis." A number of graphs indicate the AE events vs time that were recorded. RDC = ring down counts, which are acoustic emissions or sound pulses that travel from a discontinuity or an origin and correspond to a microscopic deformation event such as the sudden forward movement of a crack.

AIR PRESSURE SENSORS did not produce any significant data because the tank did not rupture in a catastrophic failure mode.

DESCRIPTION OF THE EMBRITTLEMENT PROCEDURE. ARDE embrittlement procedure dated 3-27-86 was followed; embrittlement was started at 0815 hours on 4APR86. Seventy-two hours of embrittlement were completed at 0815 hours on 7APR86; the tank was immediately moved

from the shop embrittlement area to the test site, instrumented, hooked up and tested a 1045 hours on 7APR86. The electrolyte was sulphuric acid; sodium arsenite was added as an enhancer. The liner inside surface was pickled for 10 minutes immediately prior to the embrittlement.

ADMINISTRATIVE INFORMATION.

Revision Record. Initial issue: 7APR86. Filename: Testrv5. Revision A: 17APR86; text updated and corrected; made minor text revisions. Revision B: 23APR86; grammatical errors corrected; FM impressions added; data analyst comments added. Revision C: 23May86; pickling procedure added to embrittlement discussion; 32 second ramp was 45 seconds in second paragraph. Revision D: 14AUG86; data analyst comments expanded to include comments on spike analysis; administrative paragraph clarified. Revision E: ; clarified text in IMPRESSIONS FROM THE DIGITIZED FM DATA paragraph.

Filename. testrv5.

Distribution. ARDE, Steve Berko, Dave Gleich
PI, Dr. Pius Chih Hsu Chao
Aerospace Corp., Dr. Yen Pan
AFRPL, Jim Miller, Mike Dieckhoff, Dick Grove,
MSgt Jim Day, John Marshall
ITT, Richard Thomsen
PAFB, Pete Taddie

Office of Primary Responsibility. USAF/AFRPL/TOAE/Edwards CA 93523.

E.4.3

Pressure and Strain Versus Time Plots

Figures E-20 to E-26 give measured test tank pressure versus time and fiber strain versus time plots. Data anomalies were noted for strain gages 4, 6, 14, 16, 20, 22. Tensile strain is negative. Location of strain gages is given on Figure E-27.

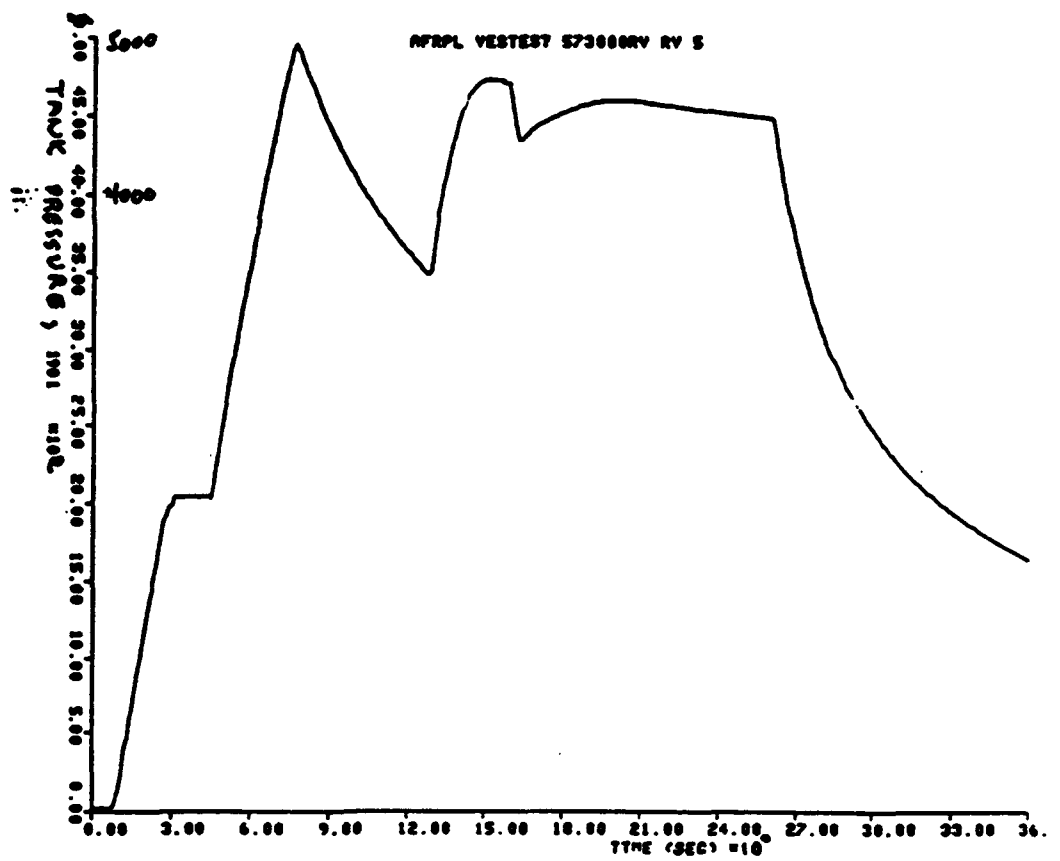
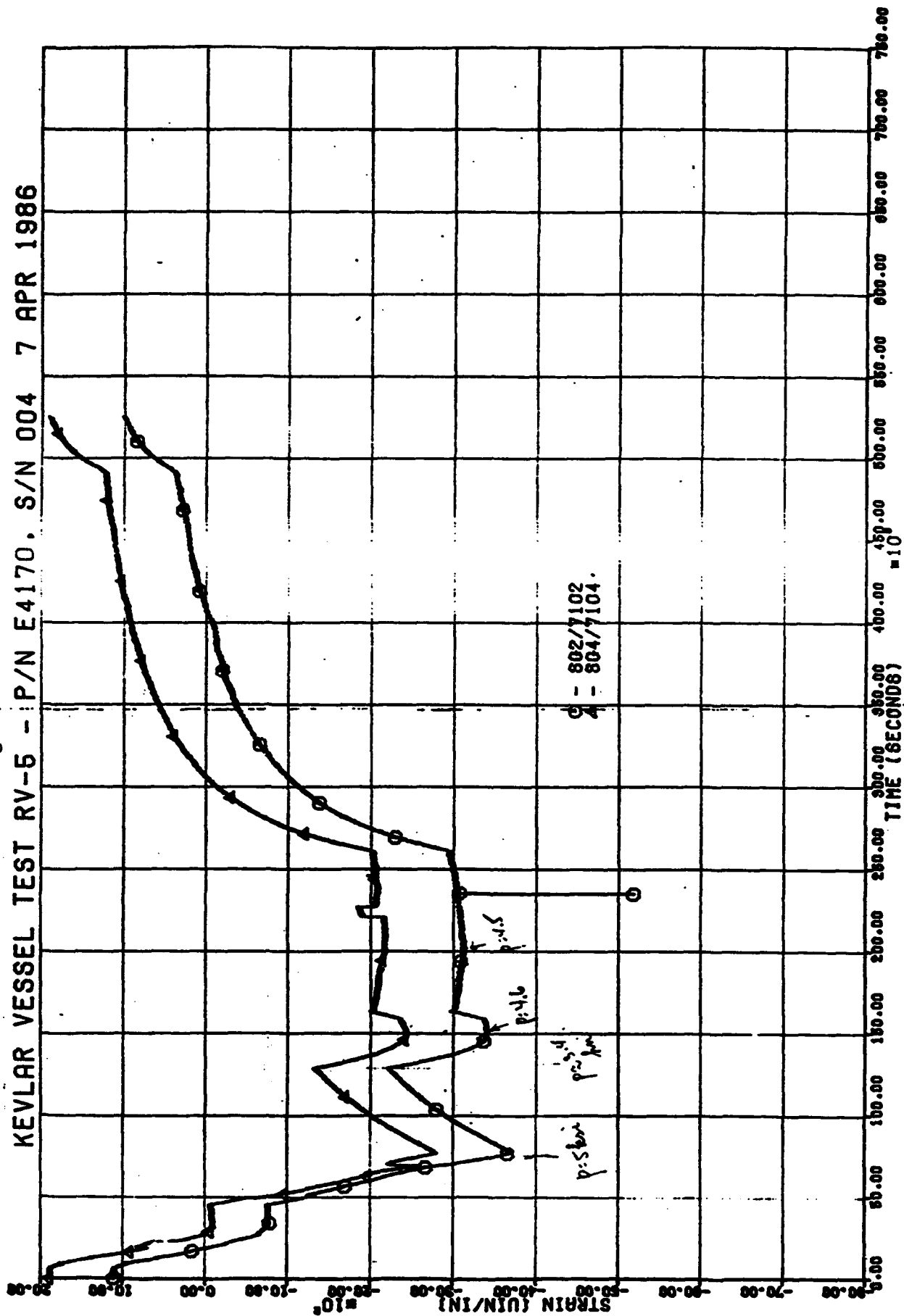
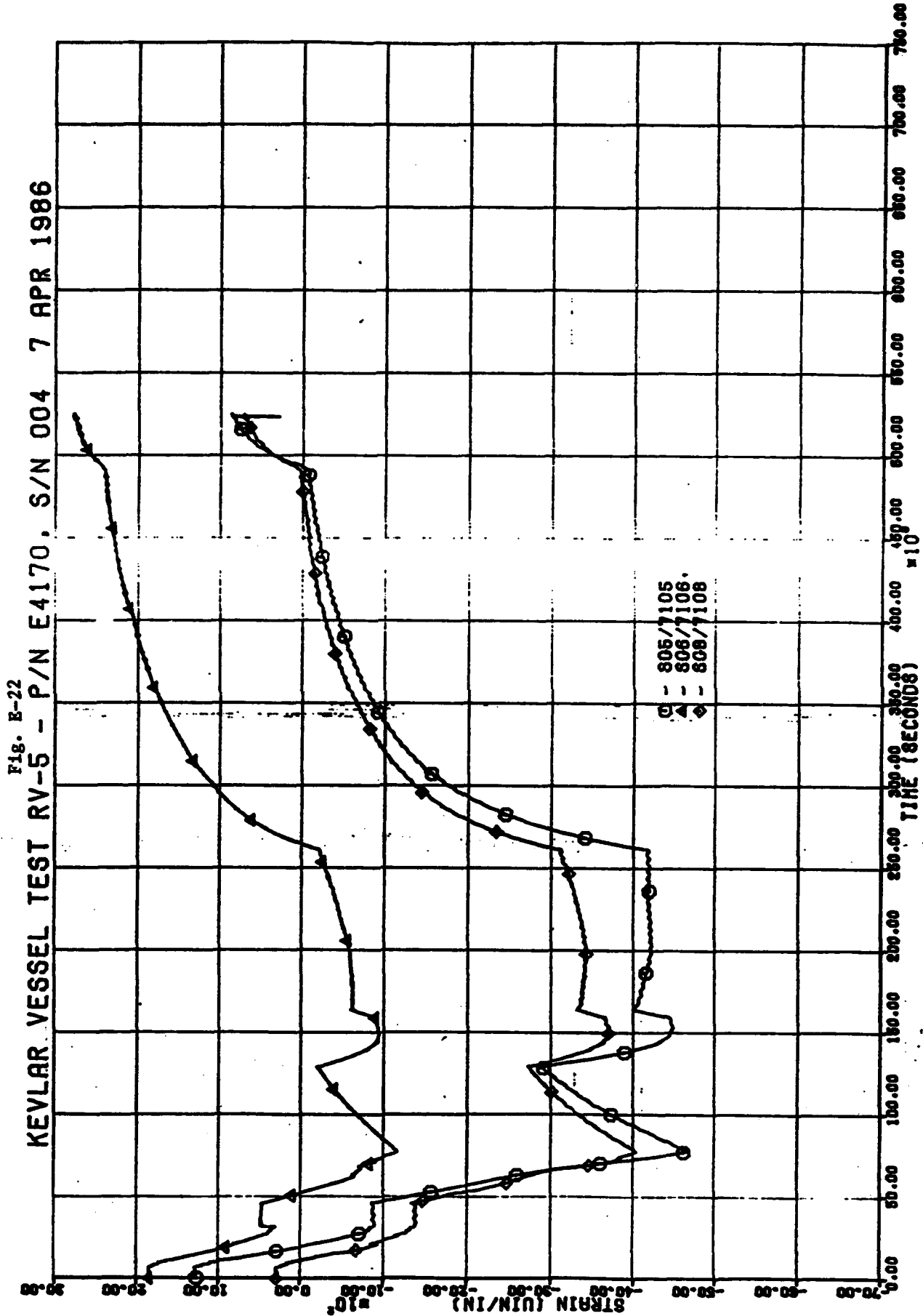


Fig. E-20

Fig. E-21

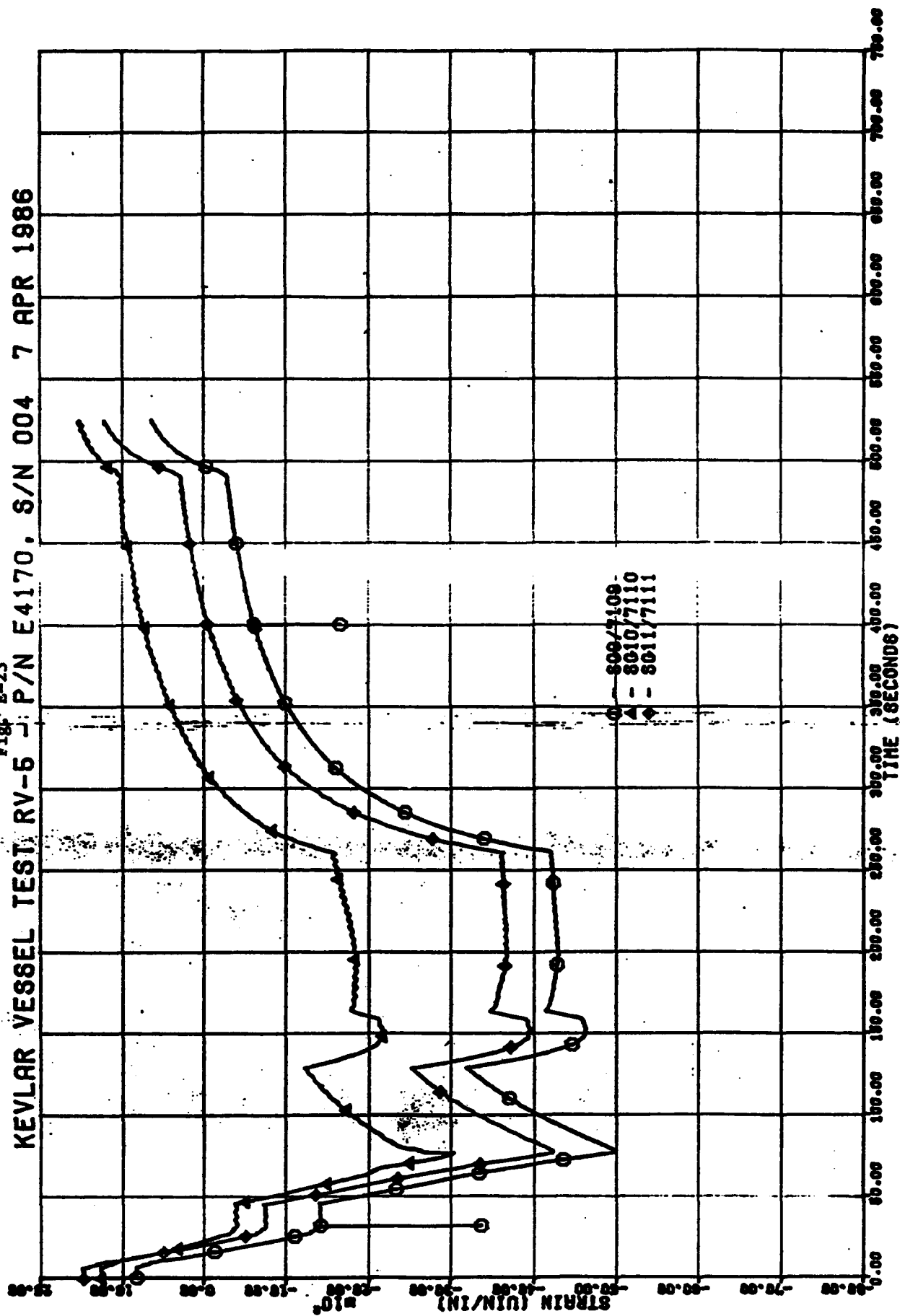
KEVLAR VESSEL TEST RV-5 - P/N E4170. S/N 004 7 APR 1986





KEVLAR VESSEL TEST, RV-5 - P/N E4170, S/N 004 7 APR 1986

Fig. E-23



KEVLAR VESSEL TEST RV-5 - P/N E4170, S/N 004 7 APR 1986

Fig. E-24

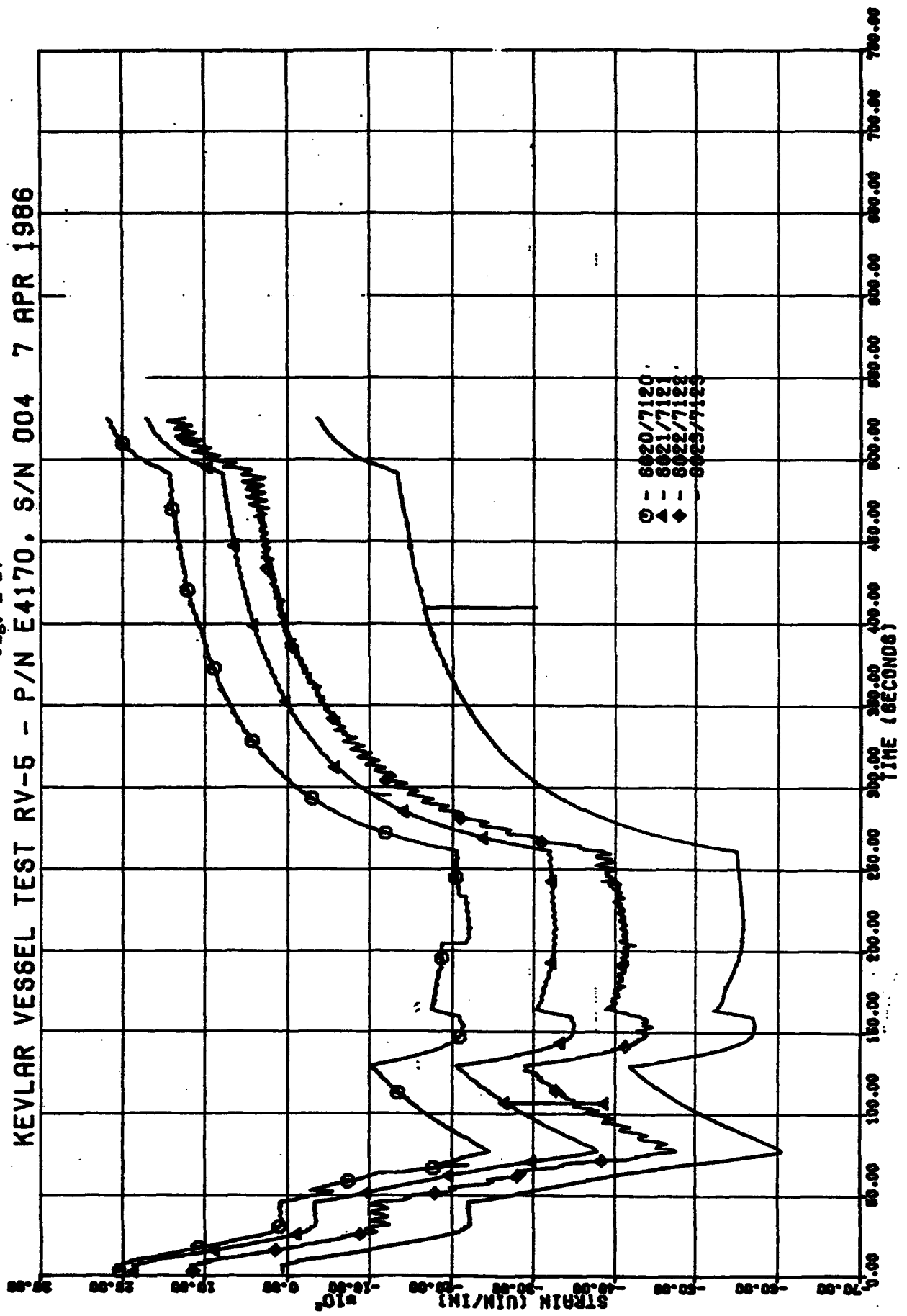


Fig. E-25

KEVLAR VESSEL TEST RV-5 - P/N E4170. S/N 004 7 APR 1986

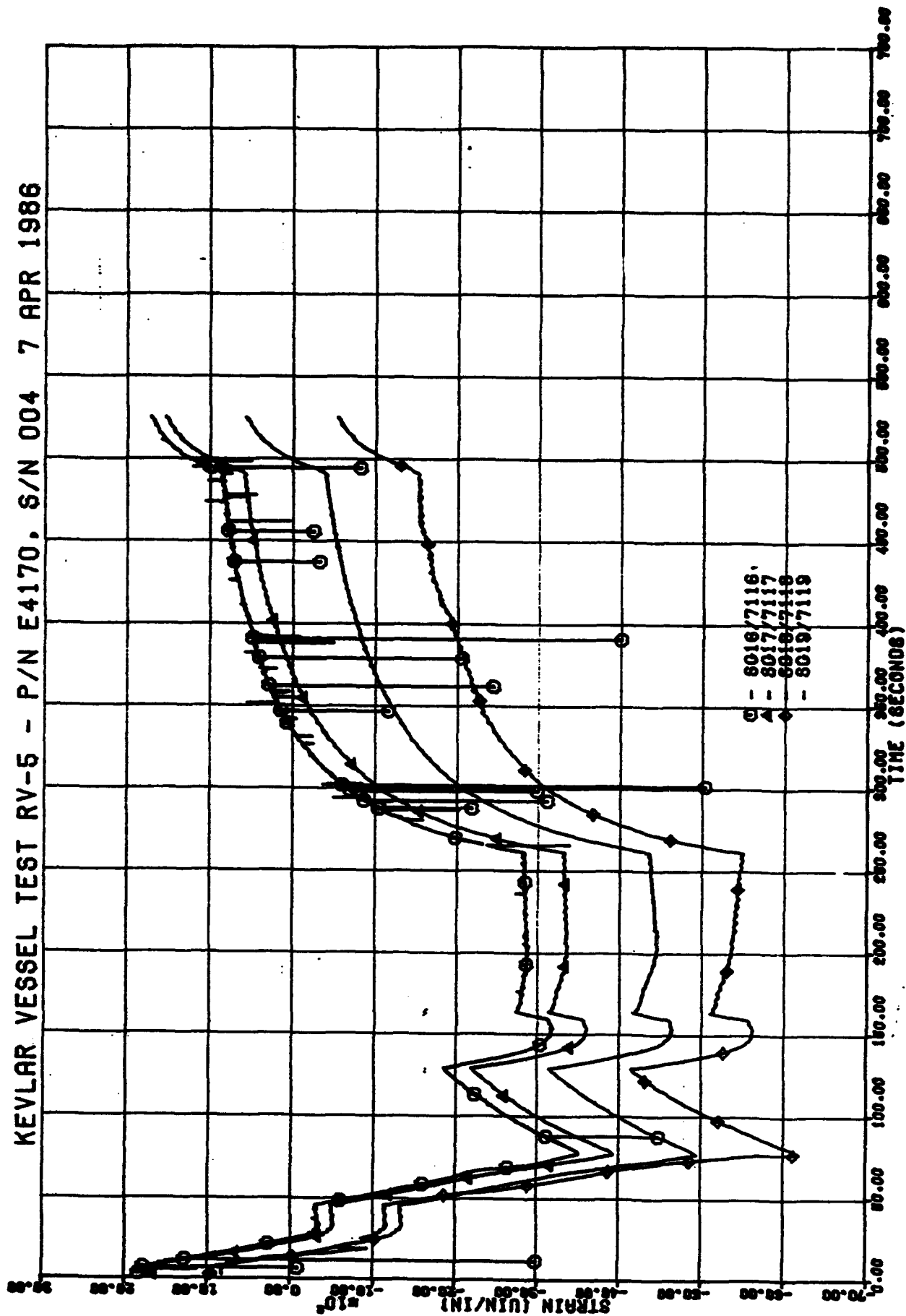


Fig. E-26
KEVLAR VESSEL TEST RV-5 - P/N E4170, S/N 004 7 APR 1986

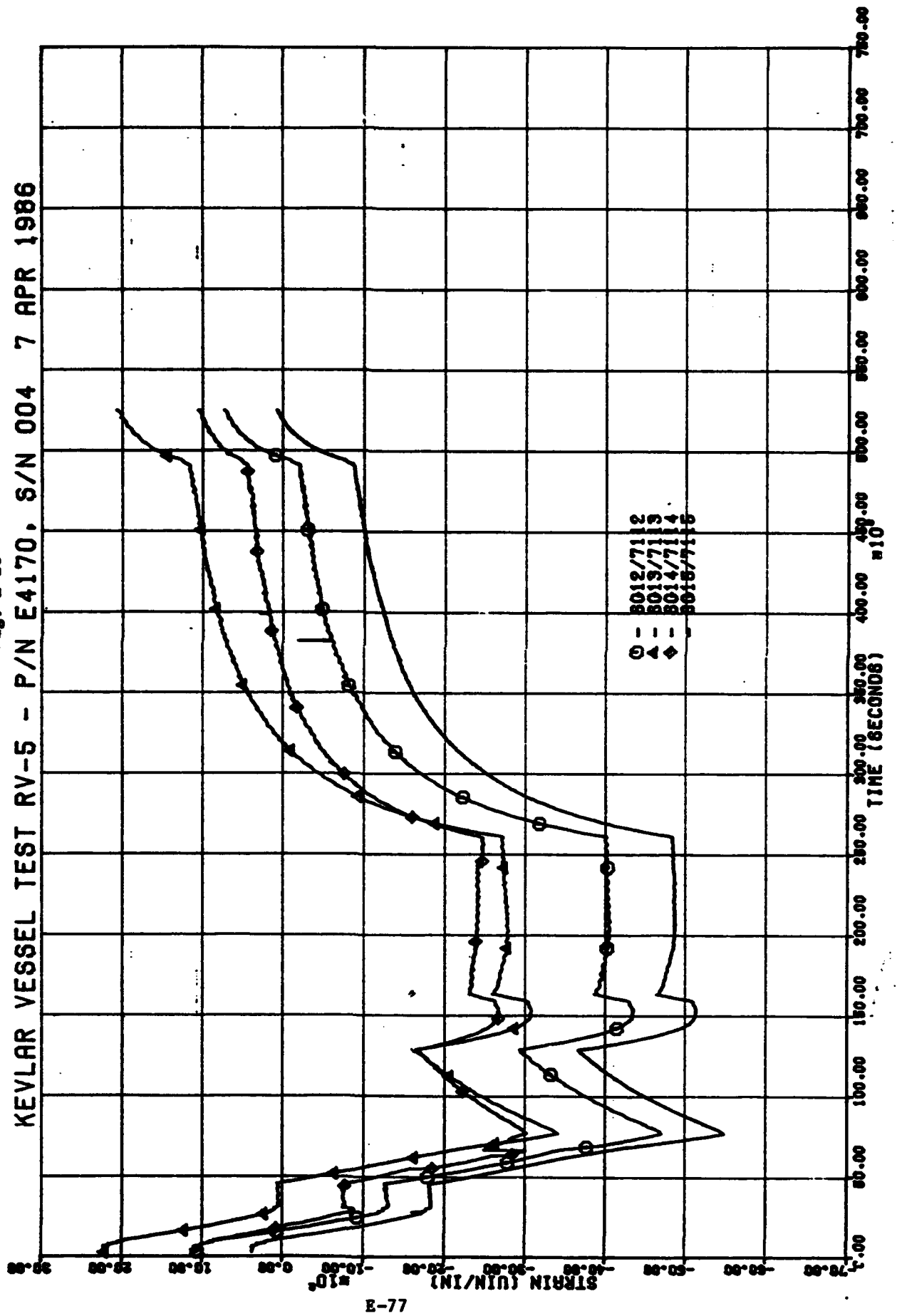
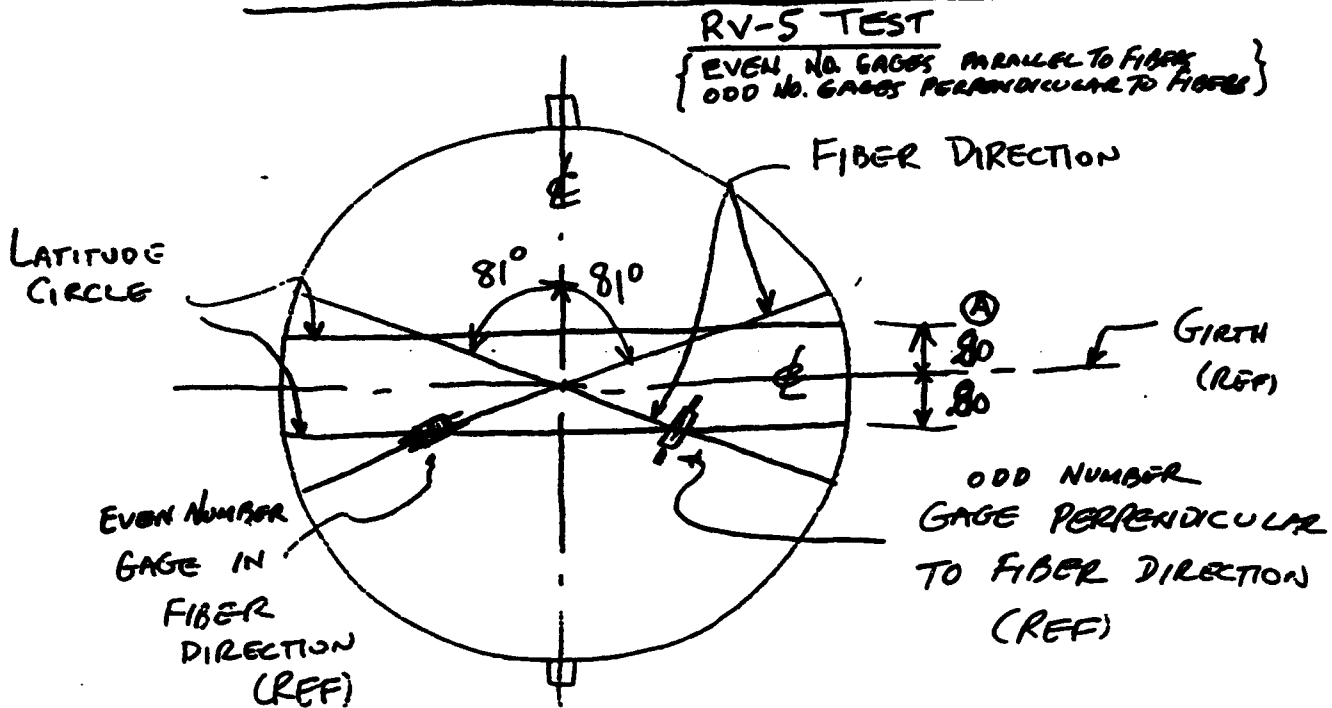


FIG. B-27
SKETCH, STRAIN GAGE MOUNTING



MOUNT 6 PAIRS OF GAGES (1 EA OF EACH PAIR IN THE OUTER FIBER DIRECTION AND 1EA PERPENDICULAR TO THE OUTER FIBER DIRECTION ON EACH LATITUDE CIRCLE) EQUALLY SPACED FOR A TOTAL OF 24 GAGES.

ARDE INC.

CONTRACT F08606-84-C-0029

J/N 42001-0-3

(REV A - .80 WAS .90)

E.4.4

Post Test Inspection

The post test tank was intact in its spherical shape with no visible exterior fiber damage. The vessel was cut at the girth and die check was applied to the liner inside surface. Multitudes of interconnected radial and tangential cracks outlining the grain boundaries were visible in the hydrogen embrittled zone between the girth and the boss region as shown on the photographs of Figures E-28 and E-29.

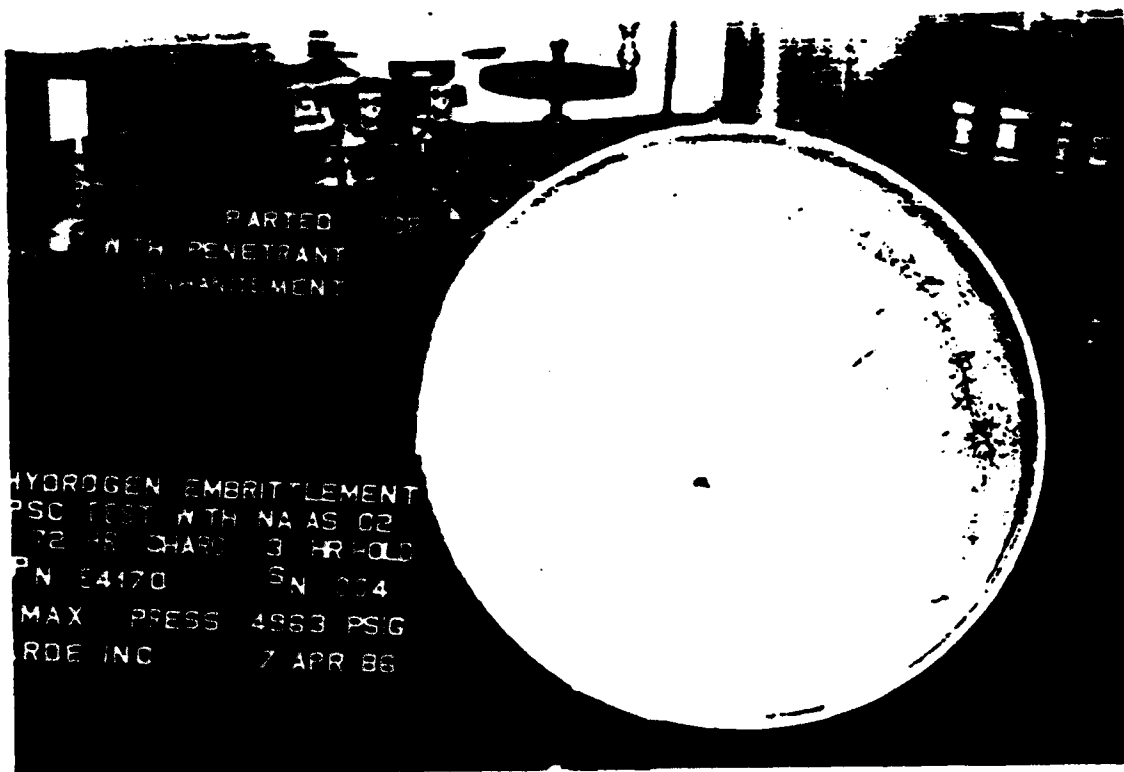


Fig. E-28
TEST RV-5, POST TEST HYDROGEN EMBRITTLED LINER
- CRACKS, DIE PENETRANT ENHANCED

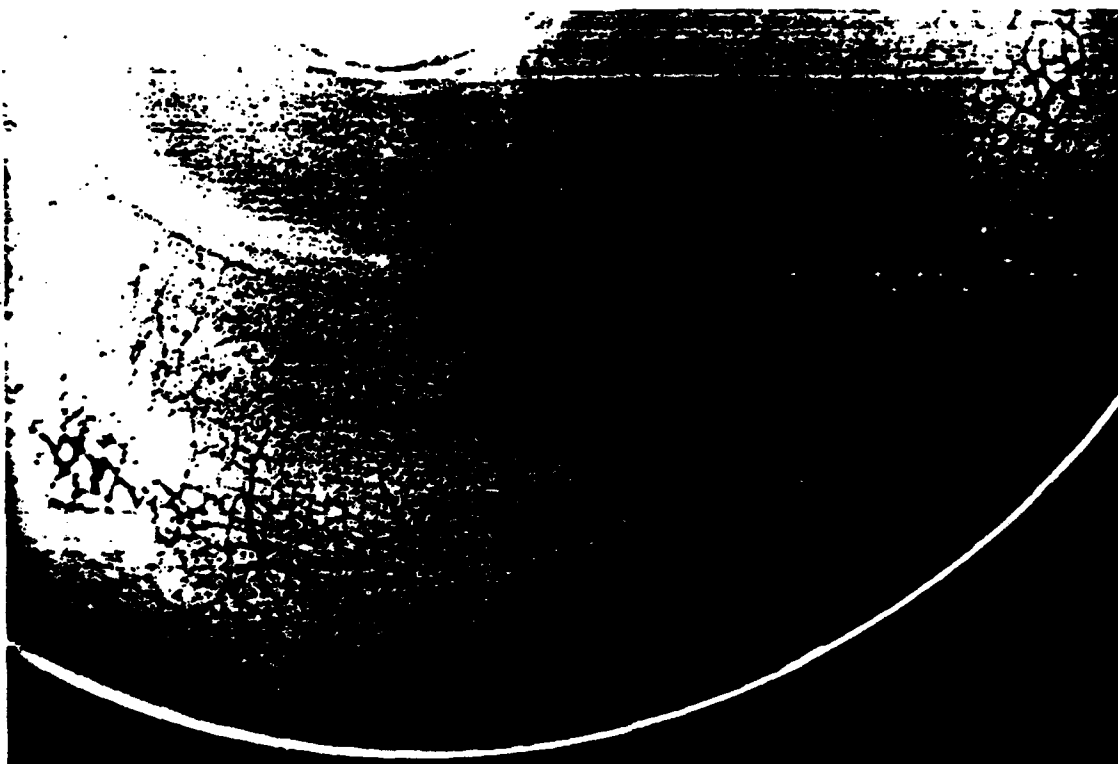


Fig. E-29
TEST RV-5, CLOSE UP OF POST TEST LINER DIE

E.5 RV-7 Test (16" ϕ PSC

E.5.1 Test Vessel Description

- P/N E4168, S/N 001 Kevlar Overwrapped 301 Cryo CRES (Composite Sphere)
- Kevlar Fiber (less resin) Average Thickness = .154" (100% Baseline Thickness)
- Metal Thickness = .054/.048"
- Inside Radius = 7.66"
- Hydrogen Embrittlement Mode = Local Girth Weld Region
- Electrolyte Solution =
$$\frac{20 \text{ cc H}_2\text{SO}_4 + 980 \text{ cc Tap H}_2\text{O}}{1000 \text{ cc Solution}}$$
- Solution Additive ~ 500 mg Sodium Arsenite
- Sensitize liner inside surface (cold pickle)
- Charging Current Density = .042 amps/in² of surface to be embrittled.
- Charging Time = 72 hours
- Hold Time Before Test = 3-1/2 hours
- Adcoat AC818T liquid maskant on areas not to be embrittled.

A photograph of the instrumented tank on the test stand at AFAL is shown on Figure E-30 herein.



Fig. E-30

TEST RV-7, INSTRUMENTED TANK MOUNTED IN TEST STAND

SMB

E.5.2

INSTRUMENTATION OBSERVATIONS (by AFAL Instrumentation Engineer) Dist to DG all originals incl digital data

KEVLAR TEST 007, 26JUN86. Project number 573000RV.

EXPERIMENTAL OBSERVATIONS.

Introduction. Vessel S/N 004 was tested. It was a 16 inch diameter stainless steel sphere and had a Kevlar overwrap. The vessel was hydrogen embrittled about the girth for about a 1 inch width. This vessel was the first vessel in the test matrix with a girth embrittlement; all previous embrittlements were global. It was tested in a vertical configuration. Briefly, the tank pressure was increased with pressure pulses and ramps until liner cracking occurred. More specifically, the tank pressure graph displays a locus consisting of the polarization and depolarization components representing the moderately complex pressurization and depressurization histories, which are discussed elsewhere. Furthermore, the pressure locus morphology is impressively reflected in the strain gage loci, and the similarities are emphasized in the text.

Pressurization Ramp. The vessel was pressurized with cool helium gas. Initially, the pressure was increased from ambient pressure to about 640 psig (most figures were estimated from the graphs) during a cool-down period, which took about 2 minutes. During the next 24.5 seconds (28.0-3.5 seconds), pressure was increased with a salvo of 17 small pulses and steps to a plateau, which stabilized at 2080 psig during a 17 second (45-28 seconds) pause. After a rapid but small 120 psig pressure increase, pressurization continued in a classical linear ramp from 2200 psig to 3850 psig in 20.3 seconds (65.3-45.0 seconds), which is a pressurization rate of 189.7 psig/sec. The vessel cracked following 20.3 seconds of ramp time at 63.3 seconds. The crack generated a sharply demarcated depressurization profile. The profile followed an exponential decay, which was distorted by a failed repressurization episode at 76 seconds, and ended in an asymptotic approach to zero pressure. Total pressurization time above 640 psig was 61.8 seconds (24.5+17.0+20.3 seconds). Initially, the depressurization rate was 7700 psig/second $[(3850-0 \text{ psig})/(65.8-65.3 \text{ seconds})]$, from the graph, or 1,275.6 psig/second $[(3804-2529 \text{ psig})/(64999.836-65999.352 \text{ milliseconds})]$, from the tabular data.

Inner
Should be 65 sec
JG

Catastrophic Burst. ^{Should be 65 sec} The vessel ^{Inner} cracked at the end of the 20.3 second ramp time at 63.3 seconds with subsequent rapid pressure loss; during depressurization, a repressurization attempt failed, and depressurization continued to zero pressure; as zero pressure was approached, prominent Kevlar fiber pinging, within the audio spectrum, became noticeable and continued for about 6 minutes. The Kevlar fiber remained intact, in general; but some fiber fraying was concentrated on the ends of the vessel near the bosses. In particular, fiber wrap 1 had no fraying; wraps 2-8 had moderate fraying; and wrap 9-to-the-girth had no fraying.

Post-run Inspection. After the test, the vessel was cut open by AFRPL; the cut was made away from the girth weld; seen was the location of one small (3/8") missing triangular metal piece, which was probably lost through one of the fittings, and the fractures outlining another small, potentially loose, metal piece. At ARDE, another cut was made creating a ring of liner and overwrap; the overwrap was severed, and the ring separated into two rings at a continuous, circumferential crack adjacent to the girth weld; there were accompanying fractures.

Other Details. After the Post-run Inspection, the parts were shipped to ARDE. Acoustic emission and overpressure data were not taken.

IMPRESSIONS FROM THE DIGITIZED FM DATA.

Strain Gages. The gages were mounted on the 81 degree wrap angle, which is the last fiber layer; they were equally distributed and were 8 degrees off the girth. The polarity convention for increasing strain is negative. Except where indicated, the following comments are based on the initial data pass, which generated graphs with a sample rate of 1024 SPS, filter frequency of 100 Hz and plot rate of 80 SPS.

Data Analyst's Comments. ITT, Richard M. Thomsen, states

"Strain gauges: 1,2,7,10 and 19-21 were bad. SG6 went out when the vessel burst. SG14 did not detect the burst and has no data under -5000 microstrain.

Two ranges were calculated for the good strain gauges. The difference between zero and the hold at 2000 psig, and that between the strain just before the spike at rupture and the minimum value of the spike. These follow:

Strain Gage #	Microstrain 0 to 2000 psig	Microstrain Burst Spike size
3	-1540	-2700
4	-1470	-7100
5	-1510	-3500
6	-1450	-8300
8	-1950	-2000
9	-1570	-3400
11	-1554	-3400
12	-1820	-8100
13	-1540	-2500
14	-1360	-----
15	-1580	-3600
16	-1730	-5500
17	-1490	-2400
18	-1510	-2200
22	-1350	-4000
23	-1580	-3000" (End of ITT text)

Observations. Strain gages parallel to the fibers have odd numbers, and strain gages perpendicular to the fibers have even numbers. The arithmetic mean (average) for the eight odd gages parallel to the fiber is 3060 microinches/inch; the average for the seven gages perpendicular to the fiber is 5314 microinches/inch. This 2254 microinches/inch differential is consistent with the characteristic stiffness parallel to the fiber and the excessive compliancy perpendicular to the fiber. Noteworthy are the irregularities seen during the pressurization ramp on the even gages perpendicular to the fibers. In most cases, there are no spikes; major distortions present as slope changes at inflection points, transient offsets, and complex nonlinear transitions, etc. Such distortions are conspicuously absent in the gages parallel to the fibers; the ramp on these gages is linear and smooth except for a few spikes. Some of the distortions continue into the decay portion of the profile in several of the perpendicular gages. The parallel gages remain distortion free during the decay, except for the repressurization attempt discussed elsewhere. The observed dynamic strain performance (increasing strain) is not the same as the predicted model (implosion - decreasing strain prior to increasing strain).

Speculations. Changes in slope represent changes in stiffness.

General Comments.

Except for the bad gages discussed above, and item 7114, the strain gage data appeared to be unbiased, precise and accurate. Item 7114 exhibited bizarre behavior. The noise floors were within normal limits, except for item 7123.

Item 7123.

Item 7123 had excessive noise randomly modulating the strain data; the rate of occurrence was particularly high near the beginning and end of the test period where it is directly proportional to the lower dynamic conditions - a very unusual performance characteristic. The alleged noise was predominantly unipolar, clearly nonperiodic and contained random magnitudes. The etiology shows the following: The zero and calibration cuts were satisfactory. The noise can probably be blamed on a bad connection somewhere in the strain gage circuit. Strain gage crazing cannot be ruled out.

Item 7114.

Item 7114 had a bizarre response to the Kevlar strain. The channel saturated during the ramp; it stayed saturated during and for a short time after the rupture. The data are probably not valid. Channel overload has been eliminated as a cause. The probable cause is gage debonding or an amplifier problem. The calibration information follows:

	Counts	MV	microstrain
0 cal	1380	-2.7	-1205
50 cal	3802	----	-----
75 cal	5023	0.9	402
data limit	-7186	-11.2	-5000

The FM input was set for 1 volt full scale input, which was adequate to capture the -11.2 mv ($\times 50 = 0.55V$ after the amplifier) signal and the -2.7 mv ($\times 50 = 0.135V$ after the amplifier) offset without overload.

Spikes.

Occasional legitimate spikes on the remaining strain parameters are consistent with Kevlar fiber noises created by breaking, stretching and settling. Note the polarity direction trend (same direction as increasing strain), magnitude (usually 1/3 to 1/2 of total strain seen on the channel), phase (not unique, unless time disparities can be related to location by subsequent spike analysis), and frequency of occurrence (not too often). On the initial 80 SPS plot rate graphs, no discernible spike time differences were noted, or expected.

Correlations.

In general, the strain gage profiles were directly proportional to the tank pressure profile, and excellent correlation exists between the strain gages and tank pressure. The systemic inflections, modulations, plateaus, slopes and decays are impressively similar. The only major exception is the large, single spike paroxysm, at rupture, seen on each strain gage parameter; the spike is not on the tank pressure parameter.

Theory #1: This theory speculates the spike represents the natural resonant frequency of the composite structure; the resonance is alleged to be 10,000 Hz, which would have a period of 100 microseconds and a rise time of 33 microseconds (using $rt=1/3(f)$ method). This theory is discussed in more detail in file TESTRV5.

Theory #2: The spike may be due to the metal tank halves slamming into the fiber overwrap at rupture. Of course, this is an oversimplification, for the metal is probably touching the overwrap many places at the higher pressures seen prior to rupture.

Theory #3: This speculation admits the spike may represent the energy released at rupture, and the two rapidly separating halves cause the spike by just pushing very quickly against the overwrap they already are contacting when the integrity of the metal liner is lost.

Theory #4: Much less probable as a possible cause is the pressurization of the Kevlar overwrap: the overwrap has open ends

and cannot hold much pressure, and this theory isn't much of a contender.

IMPRESSIONS FROM THE QUICK-LOOK AND DIGITAL DATA ACQUISITION SYSTEM DATA. All data appeared to be unbiased, precise and accurate. The noise floors were within normal limits.

Tank Pressure. The tank pressure functioned as described under the Pressurization Ramp paragraph. All the pressure parameters were within normal limits.

Temperatures.

Tank Temperatures. The tank temperatures, TT1-TT12, were within normal limits. The graphs were clean and smooth; in general, they formed a family of broadly separated curves representing valid behavior profiles. The graphs started with stable initial conditions, around 86.3-91.6 degrees F (@ 60 seconds); the curves continue with a very small (about 2 F degrees) increase immediately following rupture. Following the small increase, the graphs plunge smoothly, at different rates, to their lowest values where they reverse direction and heat, at different rates, to about half their initial conditions, or they remain almost level or return to near the initial condition; some modulate slowly after they plunge to their lowest values. The lowest temperatures ranged from -1.0 degrees F (TT4) to -105.2 degrees F (TT5). Intentionally remaining unexplained are the causes of the modulations, inflections and rates of changes not already discussed, and the final values; for the values and variations seen are considered normal and consistent with sensor locations, depressurization, and sensor specifications, etc. However, these behavior variations and profiles may be important in subsequent analyses.

Temperatures, Other. The remaining temperatures, TBSIN, TBSOUT, TBALL, THXIN and THXO were within normal limits. The trend performances, however, were not evaluated, and speculations on the behavior of these parameters are reserved.

IMPRESSIONS CONCERNING THE DISPLACEMENT SENSORS.

Displacement Sensors. The ITT data analyst, Richard Thomsen reports in his "DATA ANALYST COMMENTS 20JUN85 TEST RV-7 26JUN86 (AN) OSCILLOGRAPH TRACE OF SG15, SG17, SG23, DP1(-), DP2(+) AND IRIG B (was made.)

The strip chart shows the upper band edge, the center frequency and the lower band edge. The cal cuts from the analog tape are next. Immediately the signal from DP2 becomes very noisy and remains so for the rest of the data. DP1 shows a good zero cal, but shifts to the upper band edge for the RC1 and RC2 cals. On the digital output this shows up as noise (possibly 60 Hz) making this channel impossible to calibrate.

Suorizingly (sic) DP1 again appears at the beginning of the run. It is modulated by a 60 Hz signal, but well below the band edges. (The numbers penciled in on the edge of the strip chart are the approximate time in seconds.) At 65.5 seconds the burst occurs as shown by the strain gauges. DP1 records this event well. Why this channel should show up as noise on the digital output is not known.

In reference to the strain gauge spikes, the ones that show up on the strip chart for SG15 also show up on the plots of the digitized data. It is not known why the many spikes that show up on the plots for SG23 do not show up on the strip chart..."

DESCRIPTION OF THE EMBRITTLEMENT PROCEDURE. ARDE embrittlement procedure dated 18JUN86 was followed; only the girth area for a width of about 1 inch was embrittled. Embrittlement was inhibited, where required, with a maskant. Embrittlement was started at 0800 hours on 23JUN86. Seventy-two hours of embrittlement were completed at 0800 hours on 26JUN86; the tank was immediately moved from the shop embrittlement area to the test site, instrumented, hooked up and tested at 1130 hours on 26JUN86. The electrolyte was sulphuric acid; sodium arsenite was added as an enhancer.

ADMINISTRATIVE INFORMATION.

Revision Record. Initial Issue: 23JUL86. Revision B: 19UG86; changed text in item 7114 and 7123 paragraphs. Milliseconds was seconds in Pressurization Ramp paragraph. Added text to Strain Gage paragraph. Added Displacement Sensor paragraph. Revision C: 17SEP86; expanded Displacement Sensor paragraph. Revision D: 17OCT86; S/N corrected from 007 to 004; added text to Catastrophic Burst paragraph; many was many in Displacement Sensors paragraph; expanded distribution list; added text to Introduction paragraph. Revision E: 6NOV86; added text to Introduction paragraph.

Filename: testrv7.

Distribution.

ARDE, Steve Berko, Dave Gleich
PI, Dr. Pius Chih Hsu Chao
Aerospace Corp., Dr. Yen Pan
AFRPL, Jim Miller, Mike Dieckhoff, Dick Grove,
MSgt Jim Day, John Marshall, Capt
Seidemann
ITT, Richard Thomsen, Dr. Tae-Woo Park
PAFB, Pete Taddie

Office of Primary Responsibility. USAF/AFRPL/TOAE/Edwards CA 93523.

E.5.3 Pressure and Strain Versus Time Plots

Measured test GHe tank pressure vs. time and fiber strain vs. time plots for key strain gages are given on Figures E-31 to E-43. Data for both 100 Hz filter frequency, 1024 samples/scc (SPS) and 20,000 Hz, 160,000 SPS are given for each strain gage. The higher filter frequency and sample rates (20,000 Hz and 160,000 SPS, respectively) show greater detail on the strain spike amplitudes at liner failure.

Tensile strain is negative and even numbered strain gages are perpendicular to the fibers and odd numbered strain gages are parallel to the fibers. The strain gages were evenly distributed and were mounted at .80" height above and below the girth on the outer last 810 fiber wrap. Figure E-44 is a sketch of the strain gage locations.

VESTEST 573000RV TEST 7

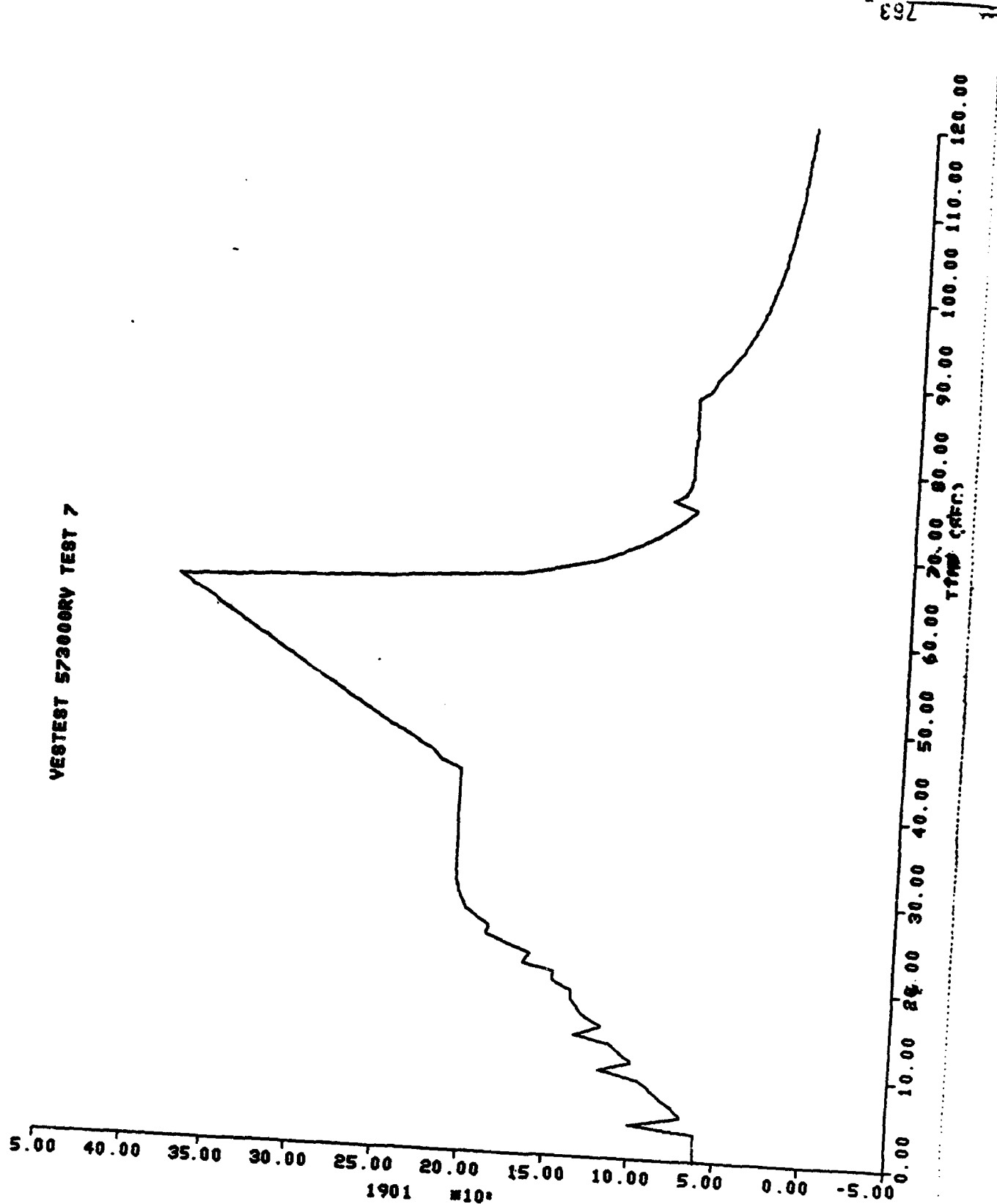


Fig. E-31

E-90

Fig. E-32 468 001
KEVLAR VESSEL TEST RV-7 - P/N E4170, S/N 004 26 JUN 1986

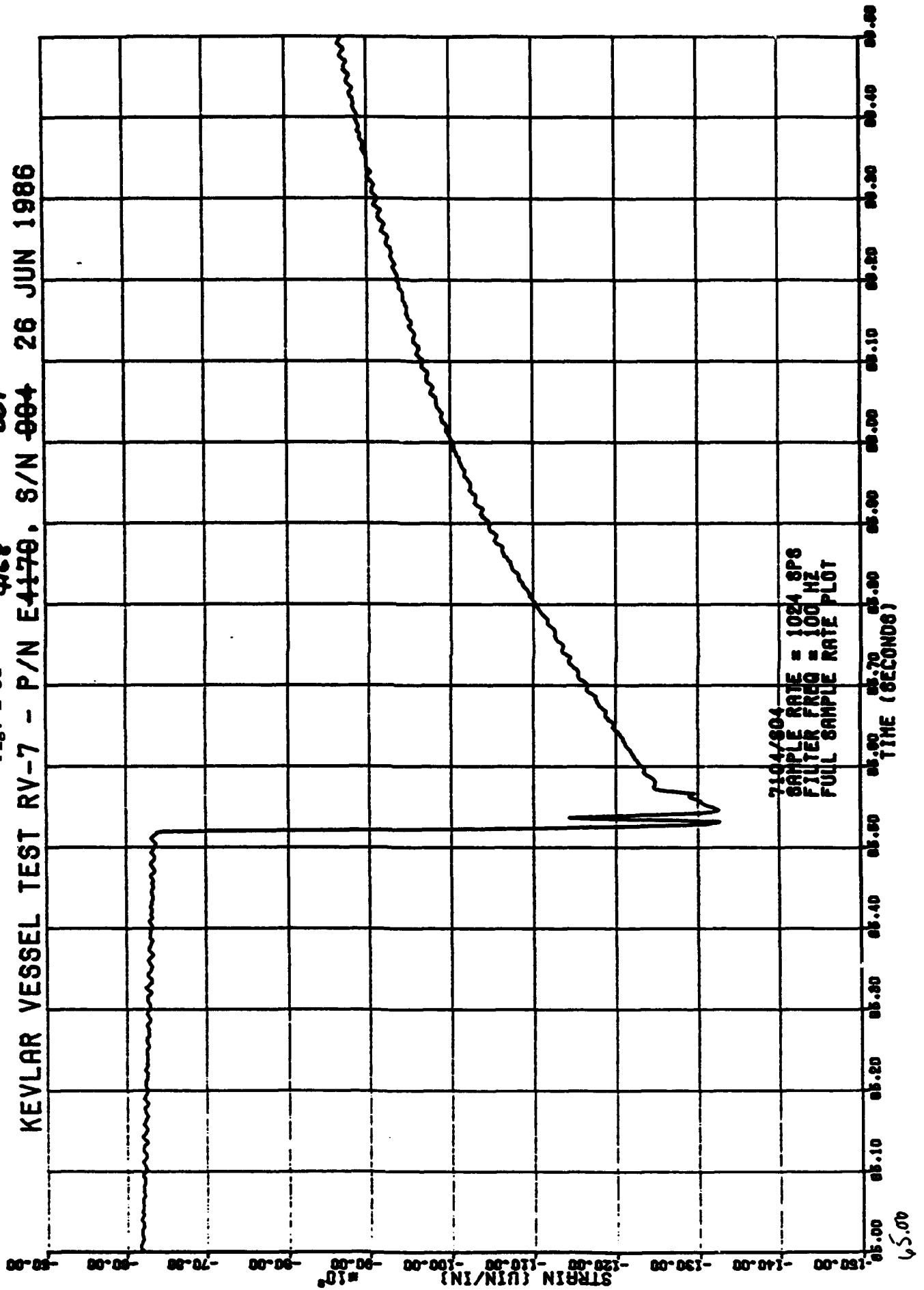


Fig. E-33

KEVLAR VESSEL TEST RV-7 P/N 4170, S/N 004, 26 JUN 86

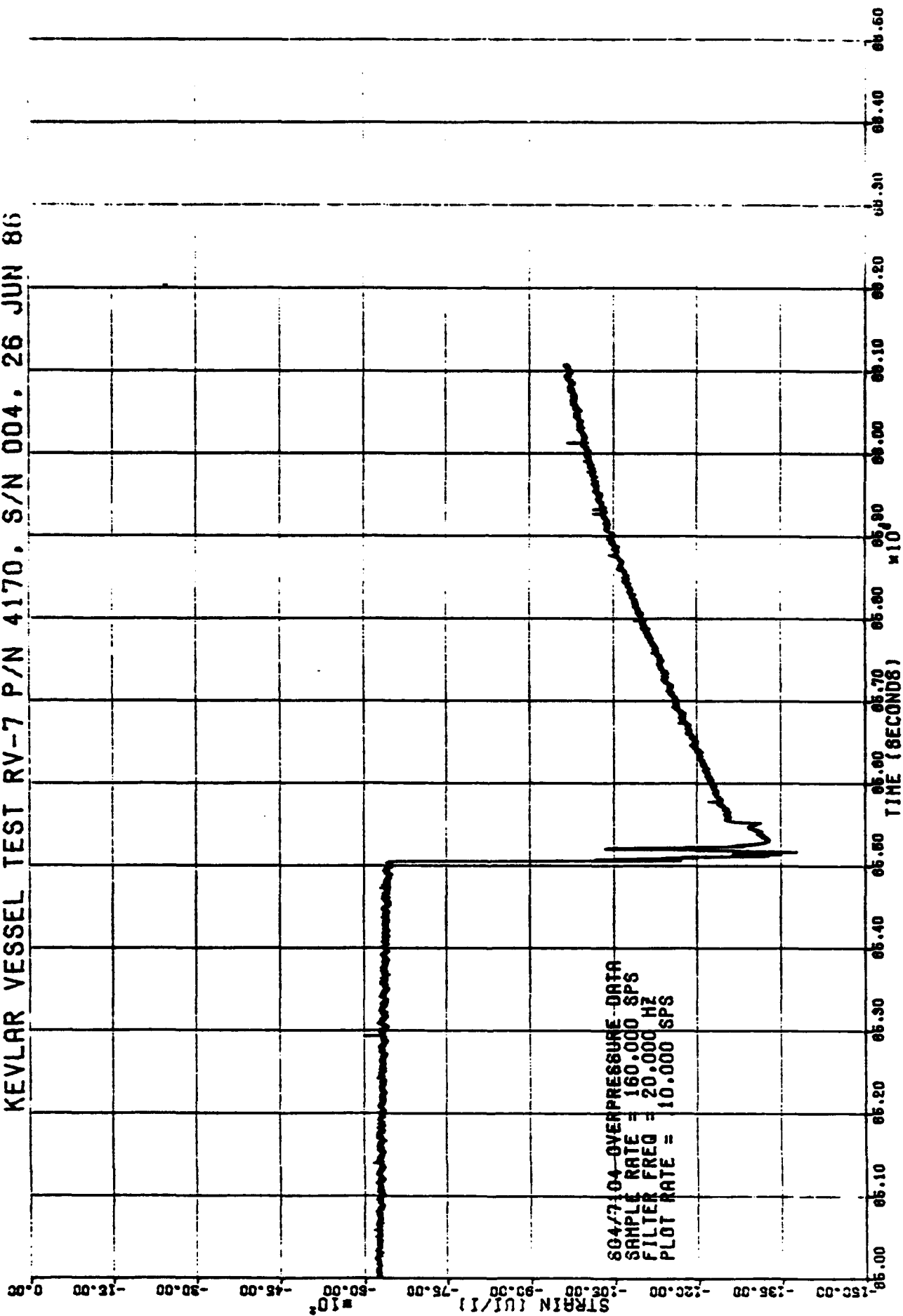


Fig. E-34

KEVLAR VESSEL TEST RV-7 P/N 4170. S/N 004. 26 JUN 86

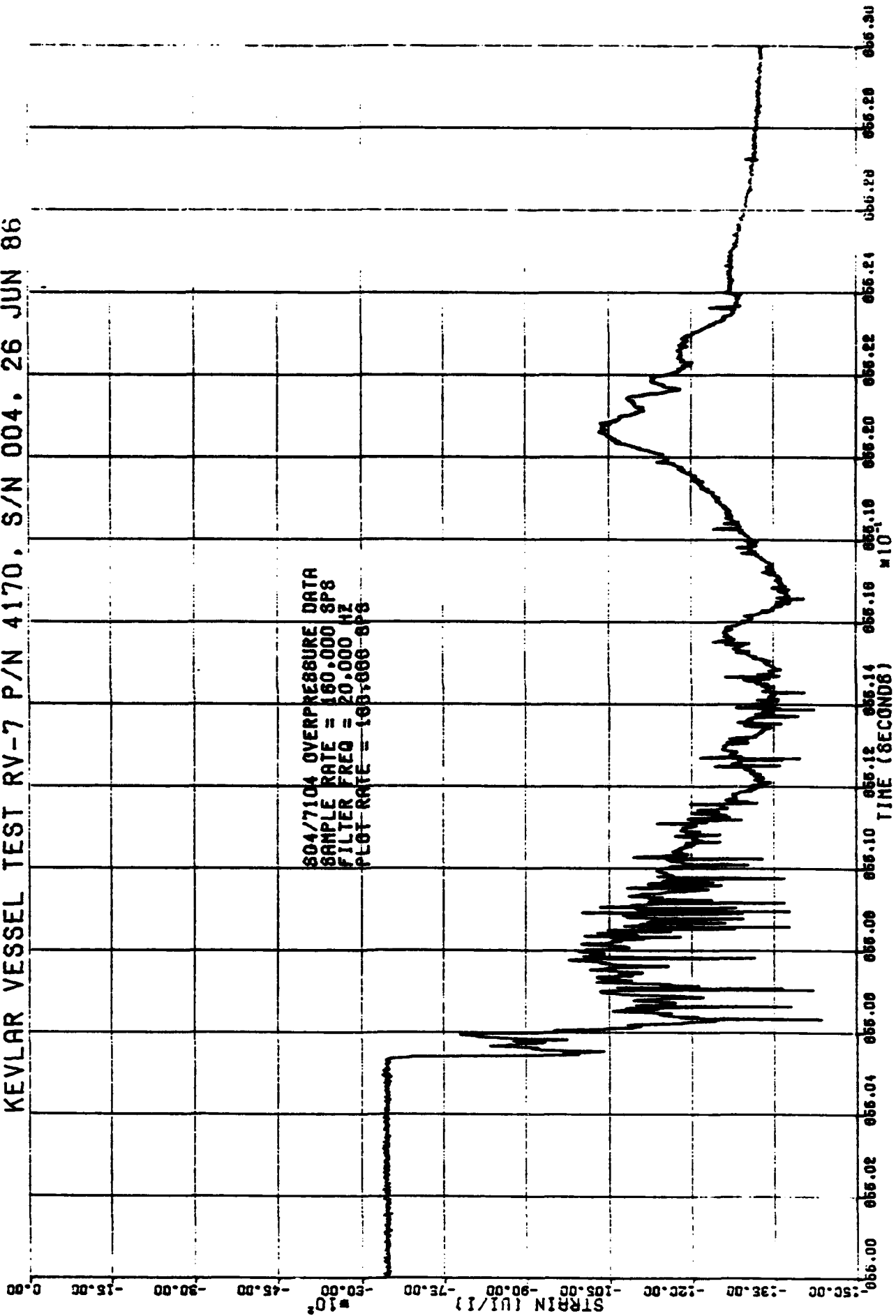
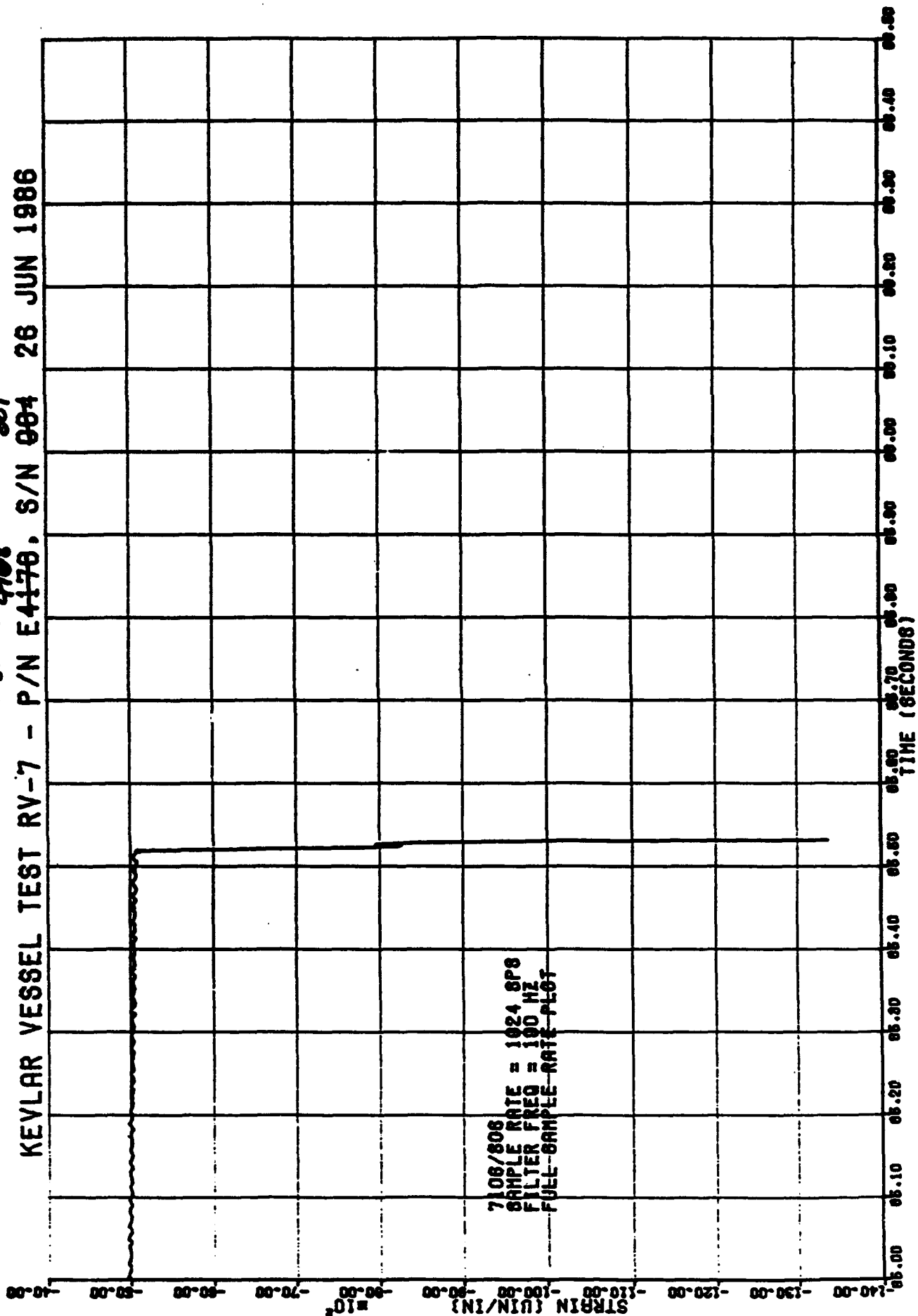


Fig. E-35 ⁰⁰¹ 468
 KEVLAR VESSEL TEST RV-7 - P/N E4170, S/N 004 26 JUN 1986



KEVLAR VESSEL TEST RV-7 P/N 4170. S/N 004. 26 JUN 86

Fig. E-36

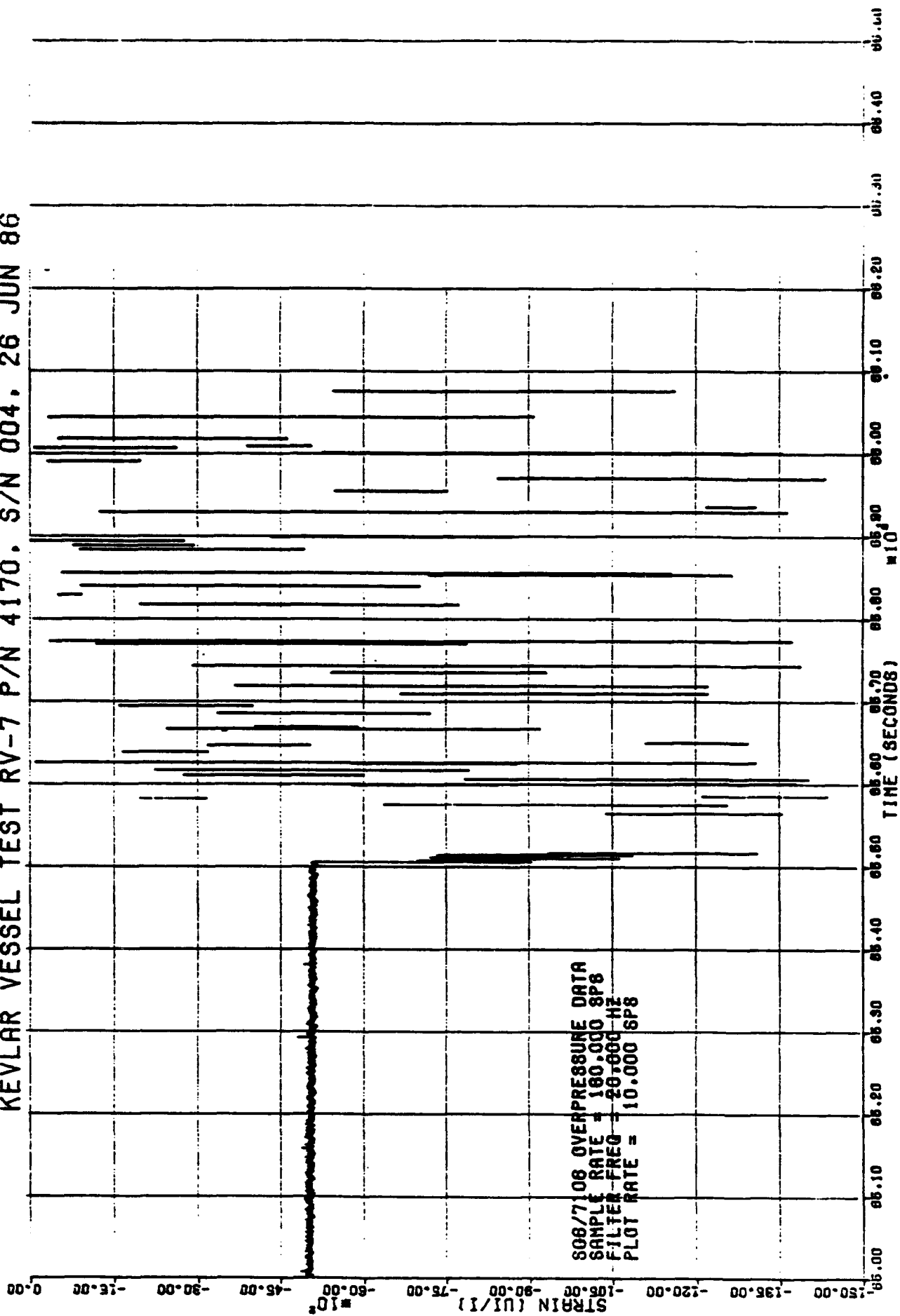


Fig. E-37

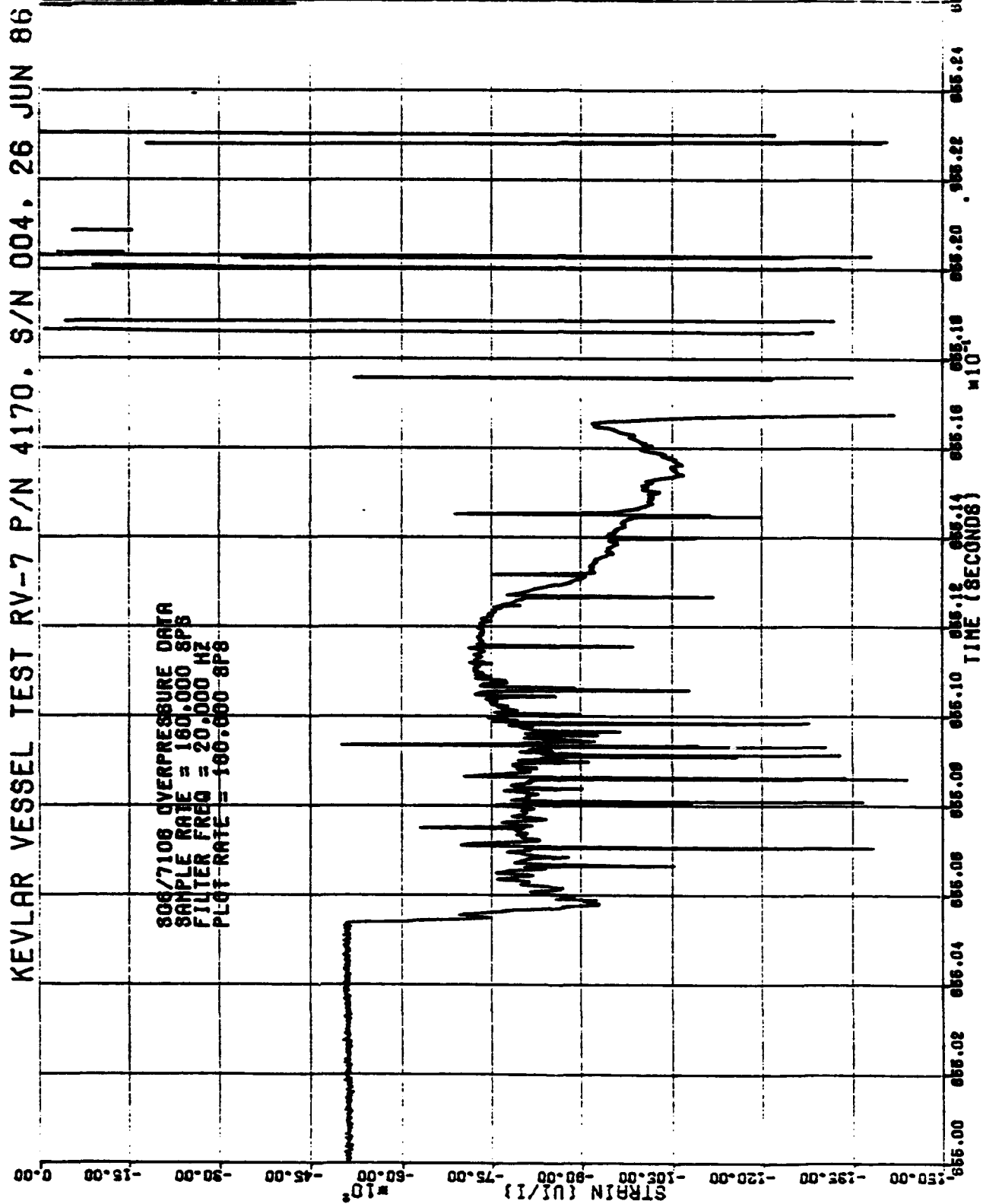


Fig. E-38 468 001
KEVLAR VESSEL TEST RV-7 - P/N E4170. S/N 004 26 JUN 1986

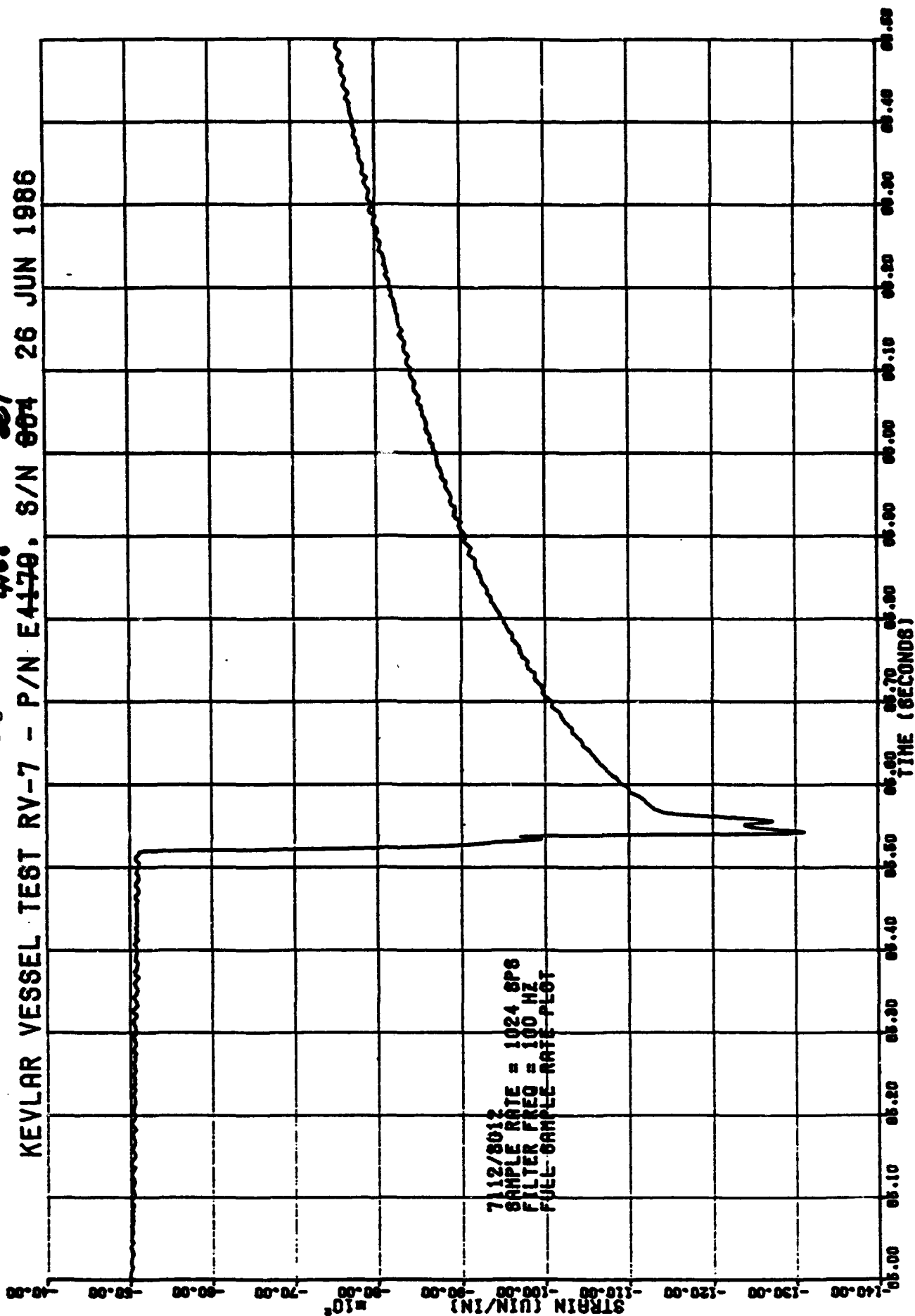


Fig. E-39

KEVLAR VESSEL TEST RV-7 P/N 4170. S/N 004. 26 JUN 86

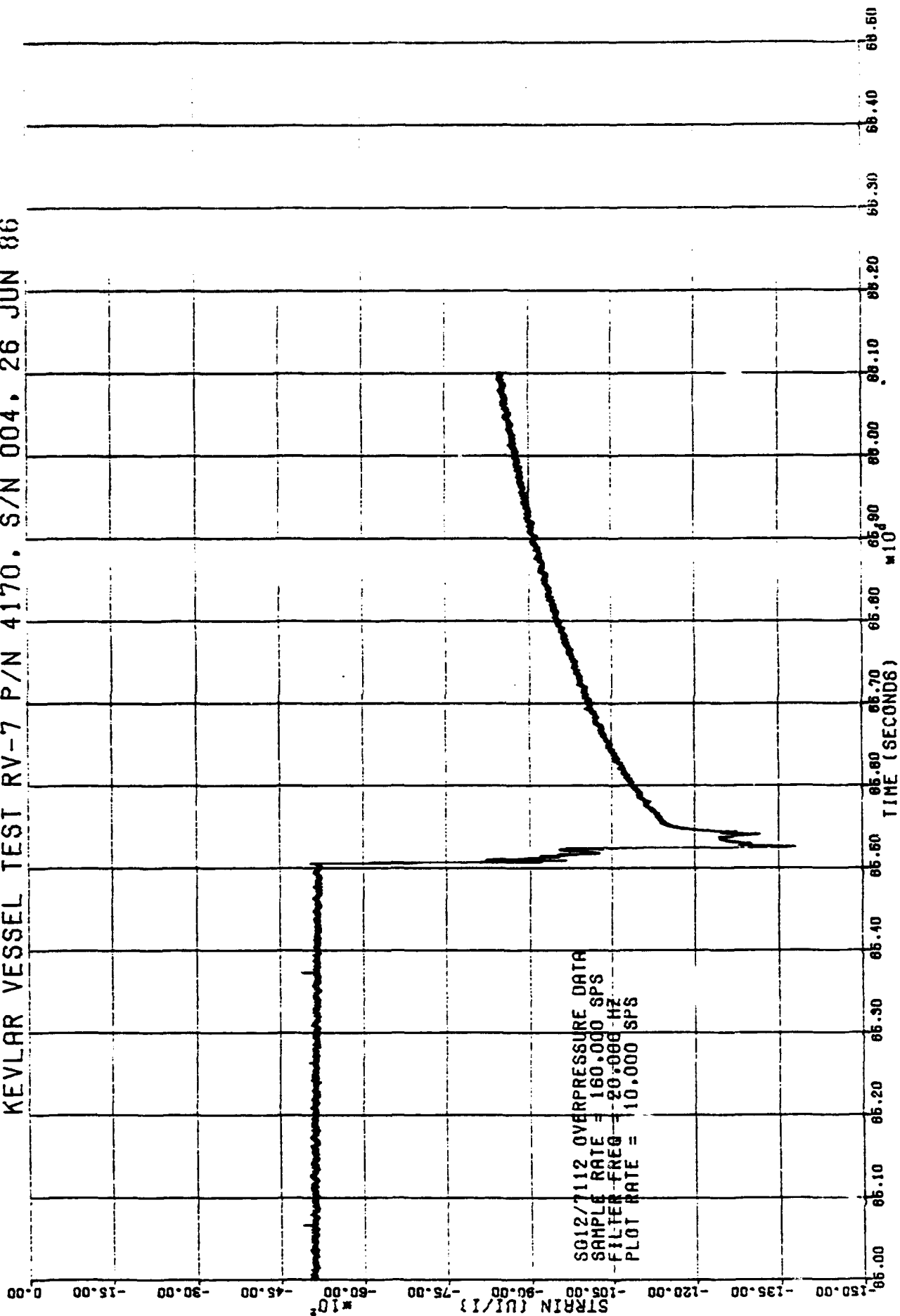


Fig. E-40
KEVLAR VESSEL TEST RV-7 P/N 4170. S/N 004. 26 JUN 86

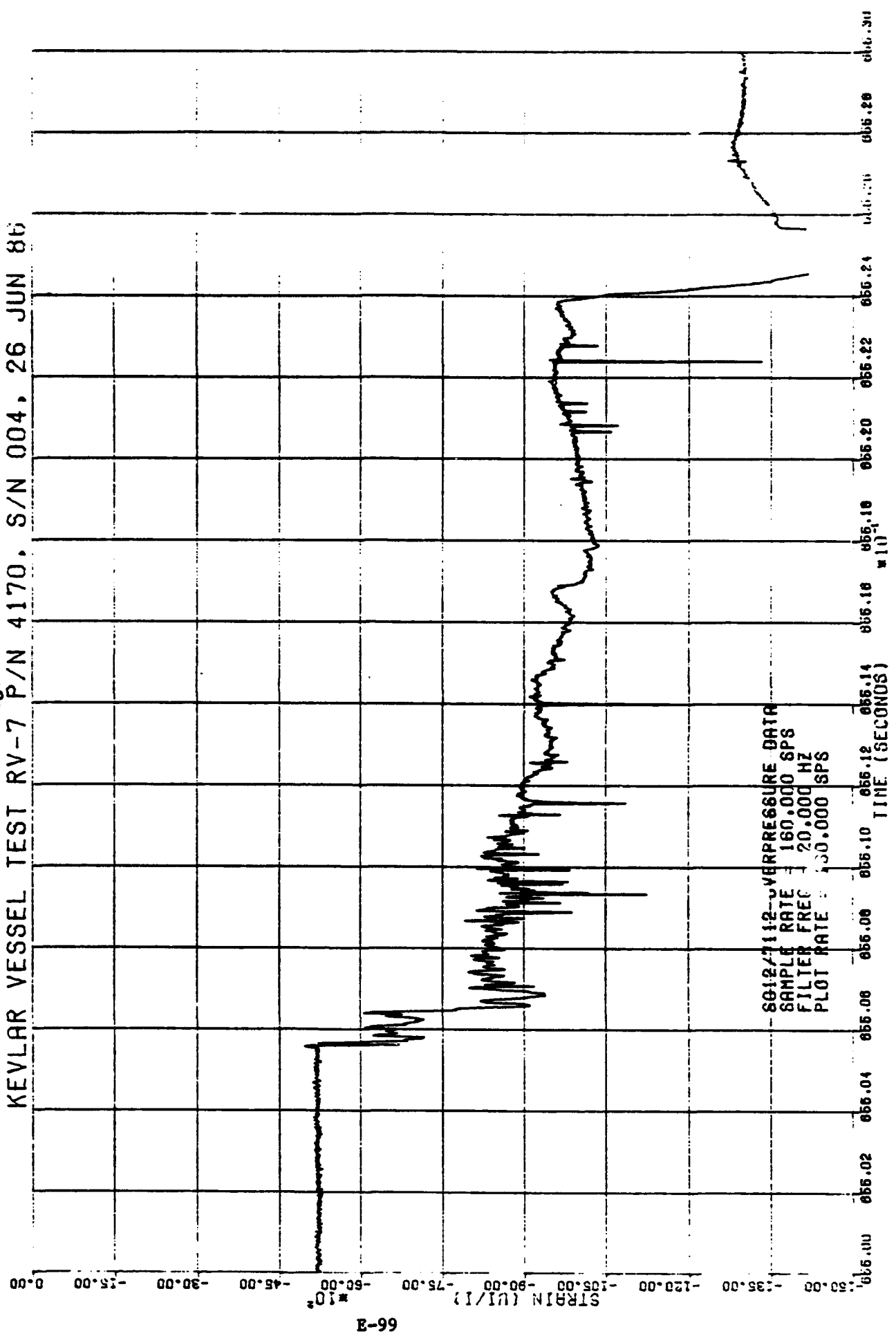


Fig. E-414168 001
KEVLAR VESSEL TEST RV-7 - P/N E4170. S/N 004 26 JUN 1986

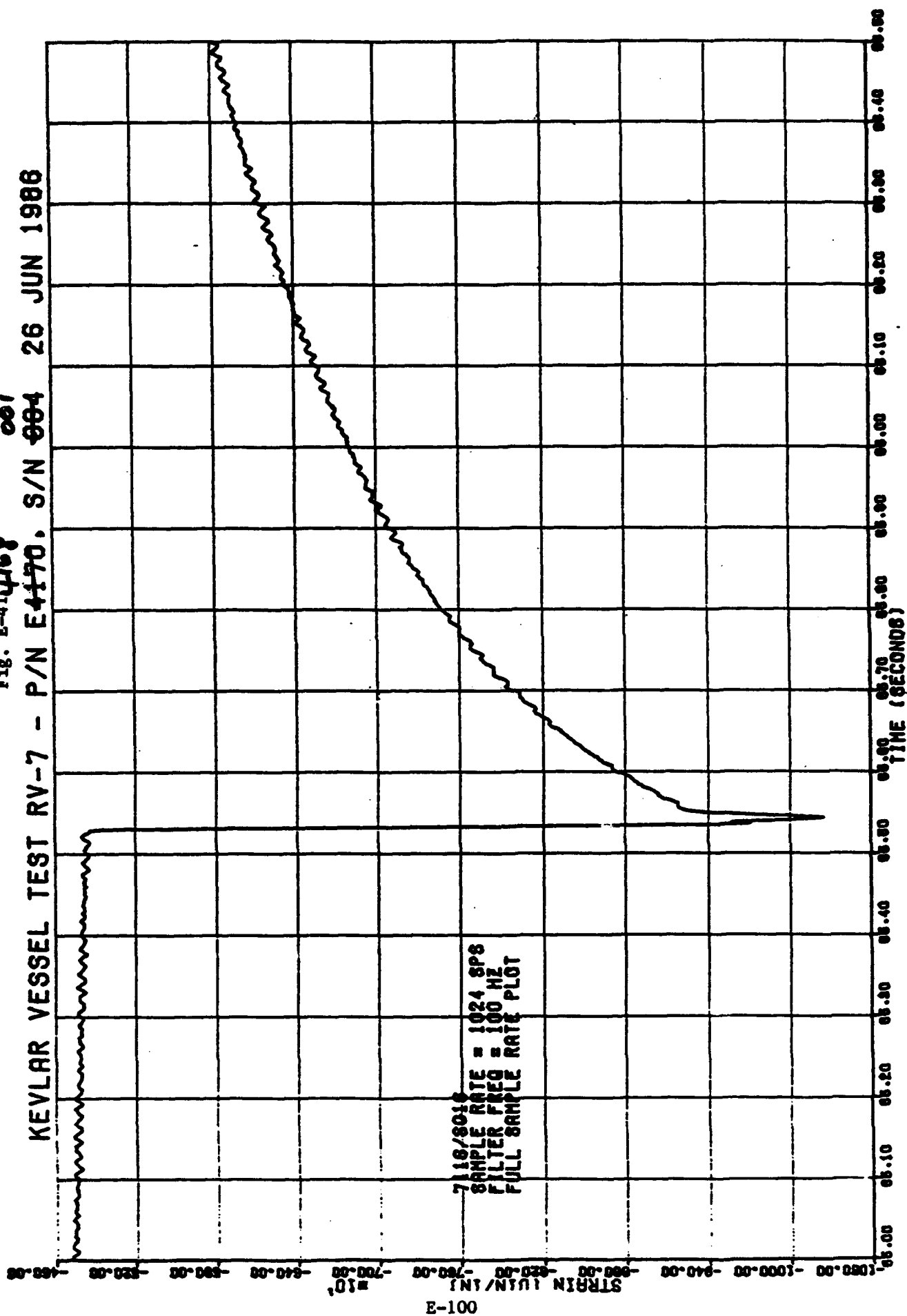
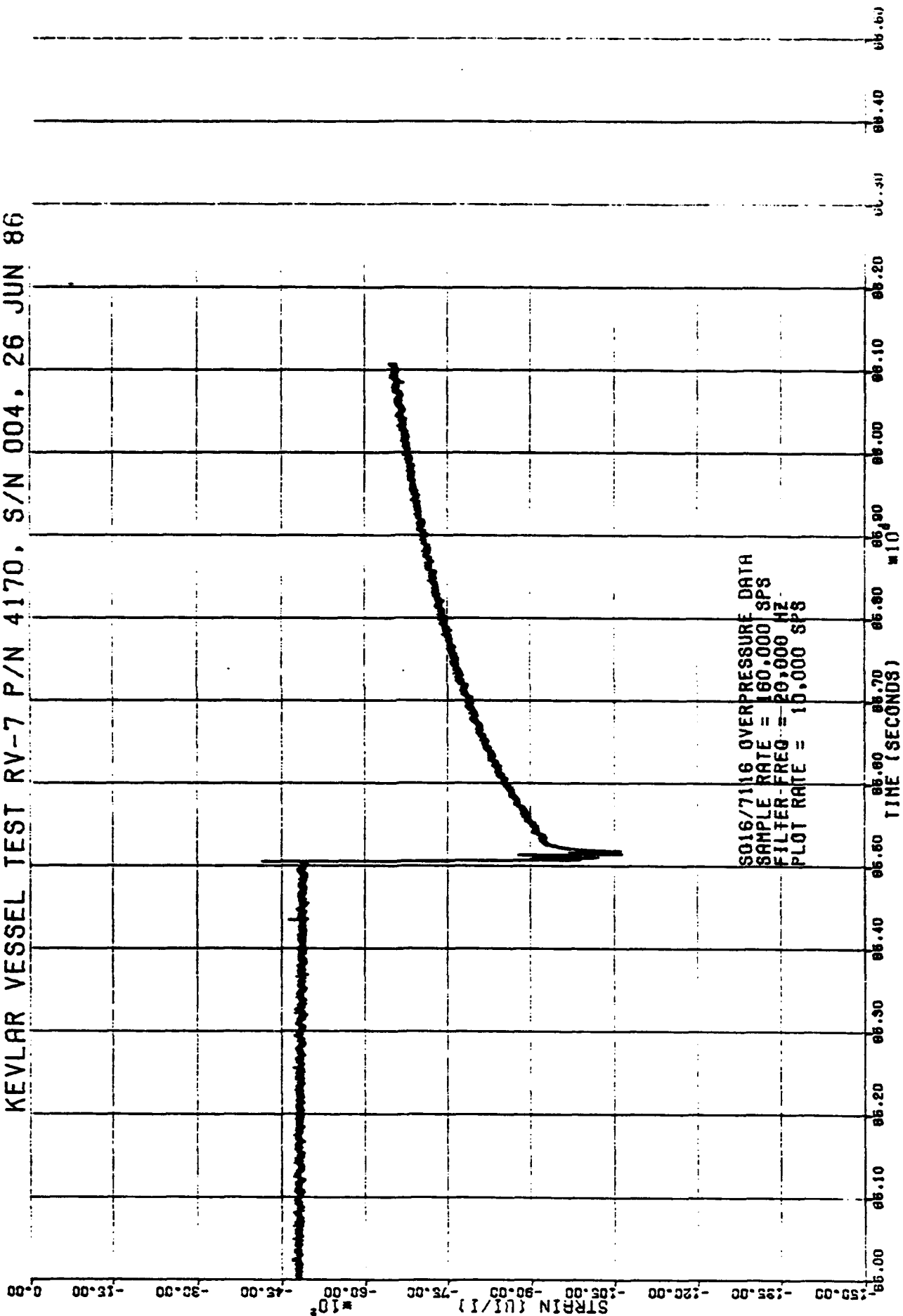


Fig. E-42
KEVLAR VESSEL TEST RV-7 P/N 4170, S/N 004, 26 JUN 86



KEVLAR VESSEL TEST RV-7 P/N 4170. S/N 004. 26 JUN 86

FIG. E-43

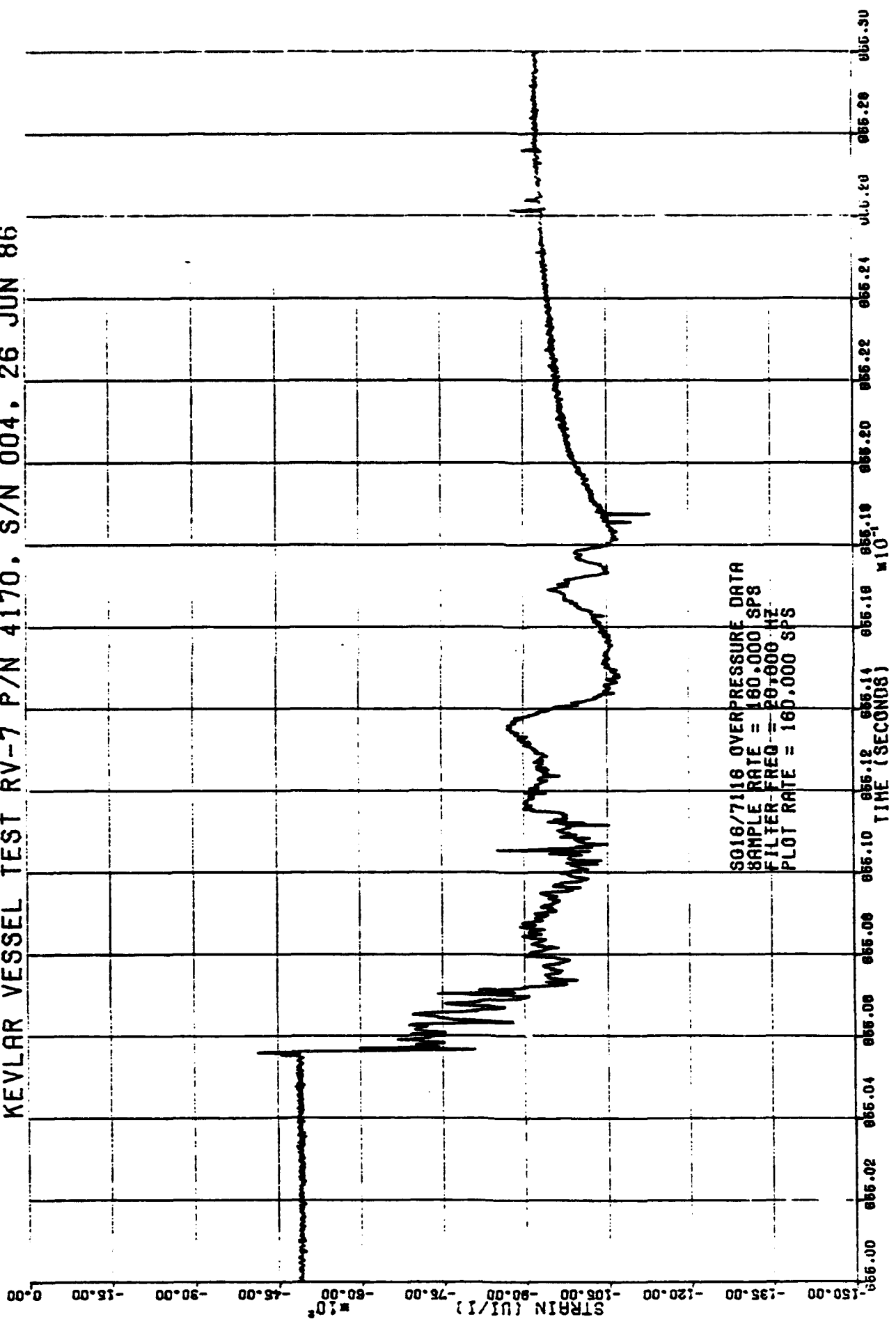
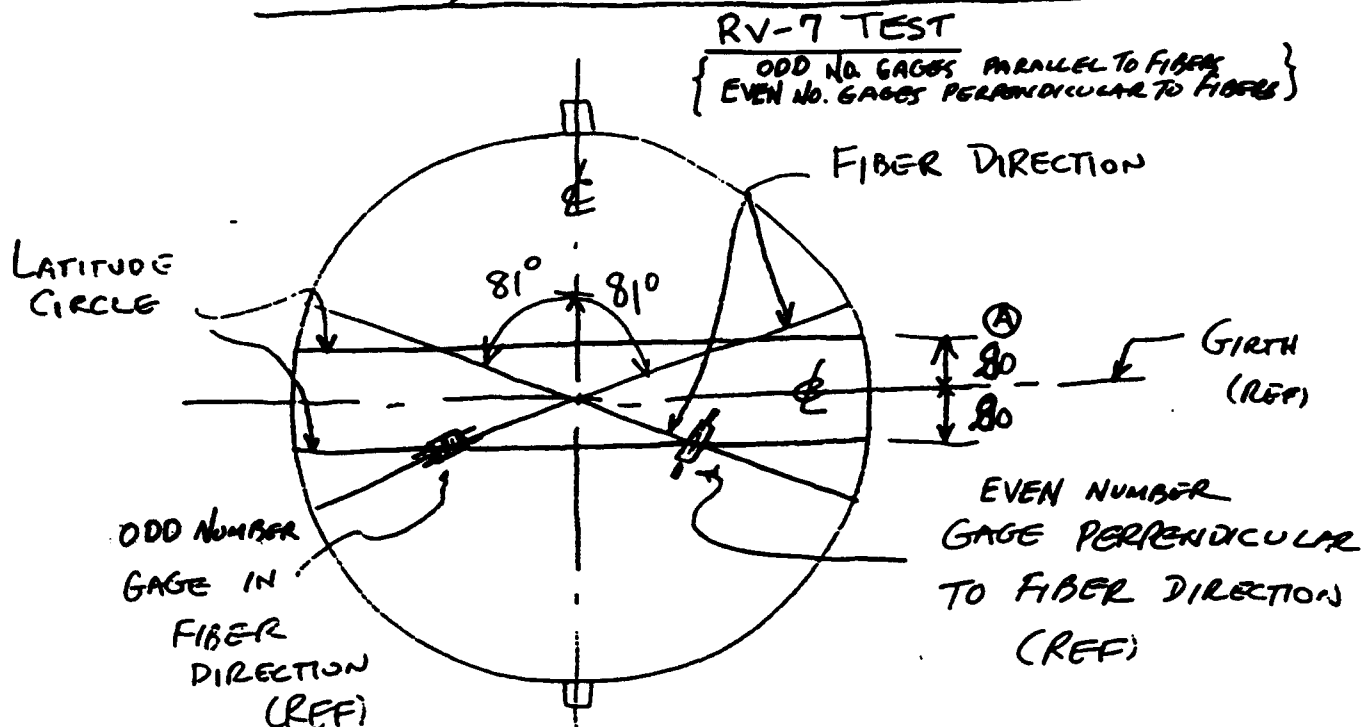


FIG. E-44
SKETCH, STRAIN GAGE MOUNTING



MOUNT 6 PAIRS OF GAGES (1 EA OF EACH PAIR IN THE OUTER FIBER DIRECTION AND 1 EA PERPENDICULAR TO THE OUTER FIBER DIRECTION ON EACH LATITUDE CIRCLE) EQUALLY SPACED FOR A TOTAL OF 24 GAGES.

ARDE INC.

CONTRACT FO 8606-84-C-0029

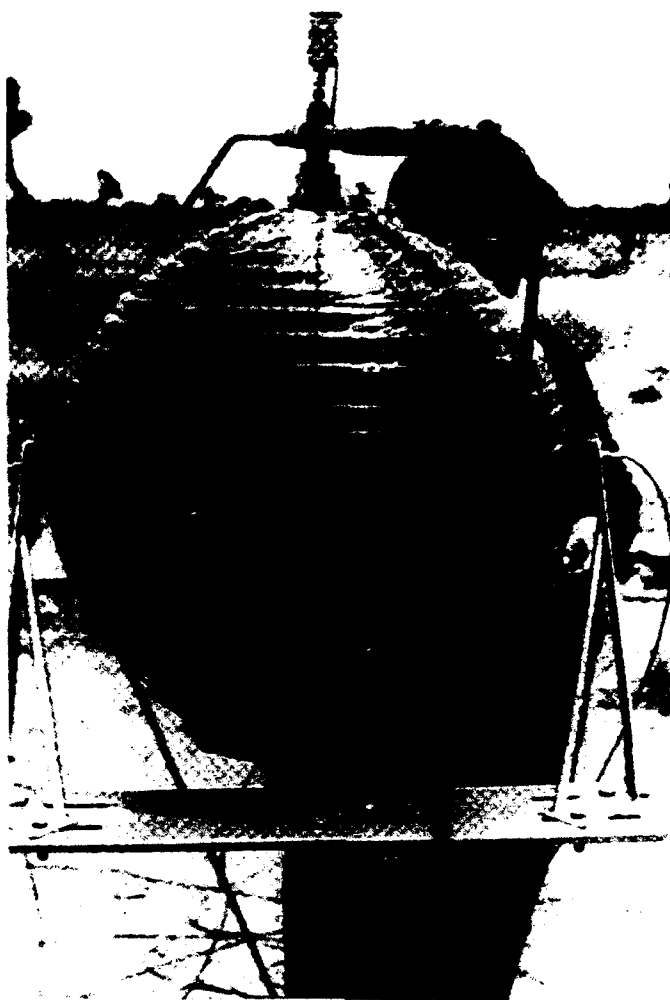
J/N 42001-0-3

(REV A - 80 WAS 90)

E.5.4 Post Test Inspection

After the test, the tank was first inspected when it was still attached to the test stand/instrumentation. The outer fiber shell of the tank was completely intact with no evidence of any metal liner pieces exterior to the tank. Some outer surface fiber damage was observed as seen in the post test photo of Figure E-45. The vessel was removed from the test stand and cut open away from and parallel to the girth weld by AFAL. Continuous liner fracture around the girth weld region was noted and one small (3/8") triangular metal piece was missing, probably lost through one of the fittings during the cutting operation. The test tank was shipped to ARDE for further inspection, where the liner inside surface was die checked and another girth region cut made parallel to the girth, producing a ring of liner and fiber overwrap. The ring overwrap was then severed, releasing its hoop restraint and the metal liner ring separated into two rings

at the continuous circumferential crack adjacent to the girth weld. The remaining portions of the liner heads were then readily removed from the fiber overwrap. The liner and fiber overwrap pieces were photographed in detail.



TEST RV-7, POST TEST VIEW OF TANK ON TEST STAND

Fig. E-45

Figures E-46 and E-47 show views of the continuous through girth cracks highlighted by die check of the cut tank inner liner surface as received from AFAL, prior to additional ring cut and fiber removal. Details of the continuously girth cracked liner ring and a view of the separated metal liner ring and heads are given on the photographs E-48, E-49, E-50 and E-51, respectively. The liner failure mode included a small loose girth ring fragment in addition to the two halves split at the girth. Views of the small fragment are shown on Figure E-55. Photographs of the removed fiber ring and head pieces are shown on Figures E-52 and E-53 which provide overall views of fiber damage. Whatever bonding that existed on the liner fiber interface was broken when the intentionally embrittled liner broke into two pieces, as evidenced by the ready removal of the overwrap and the photograph of the fiber wrap pieces inside surfaces as shown in E-54, as well as the smooth outer surfaces of the metal heads and ring (Figures E-49 to E-51).

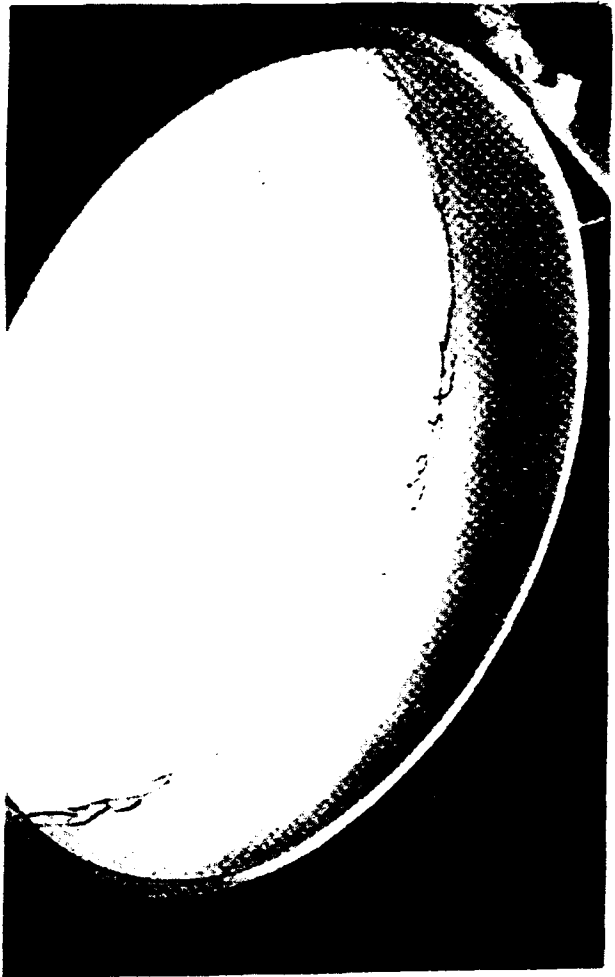


FIG. E-46 TEST RV-7, CONTINUOUS GIRTH CRACKS HIGHLIGHTED

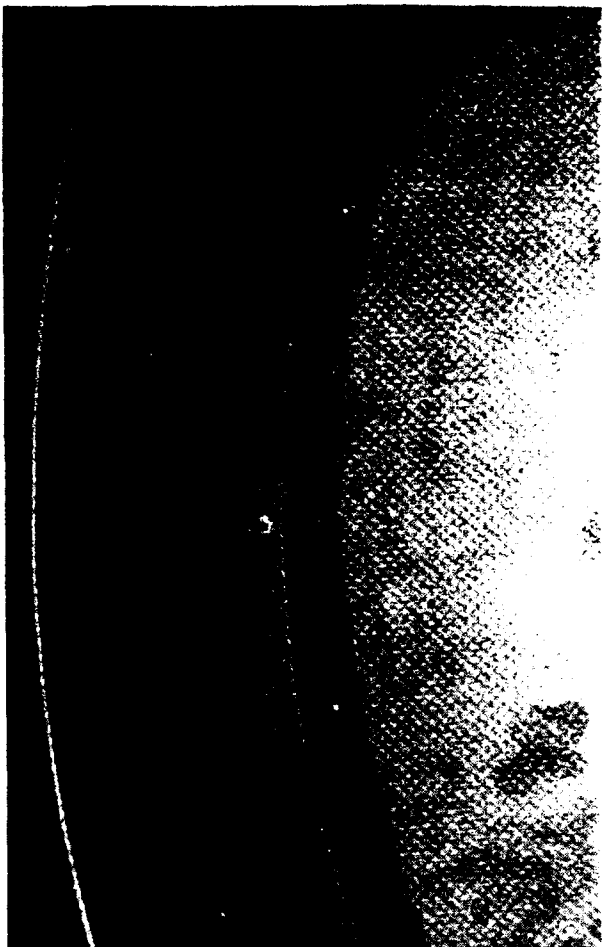


FIG. E-47 TEST RV-7, CLOSE UP OF CONTINUOUS GIRTH CRACKS HIGHLIGHTED BY DIE CHECK

E-108



FIG. E-48 TEST RV-7, CONTINUOUSLY CRACKED EXERTITLED GIRTH RING

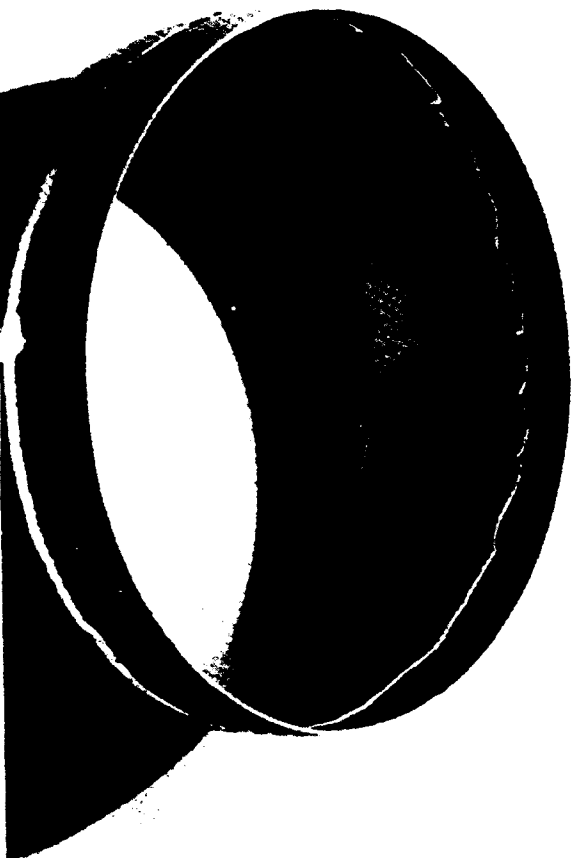


FIG. E-49 TEST RV-7, CONTINUOUSLY CRACKED EXERTITLED GIRTH RING



FIG. E-50 TEST RV-7 SEPARATED METAL RING



FIG. E-51 TEST RV-7, SEPARATED METAL RING AND HEADS



FIG. E-52 TEST RV-7, REMOVED FIBER GIRTH RING AND

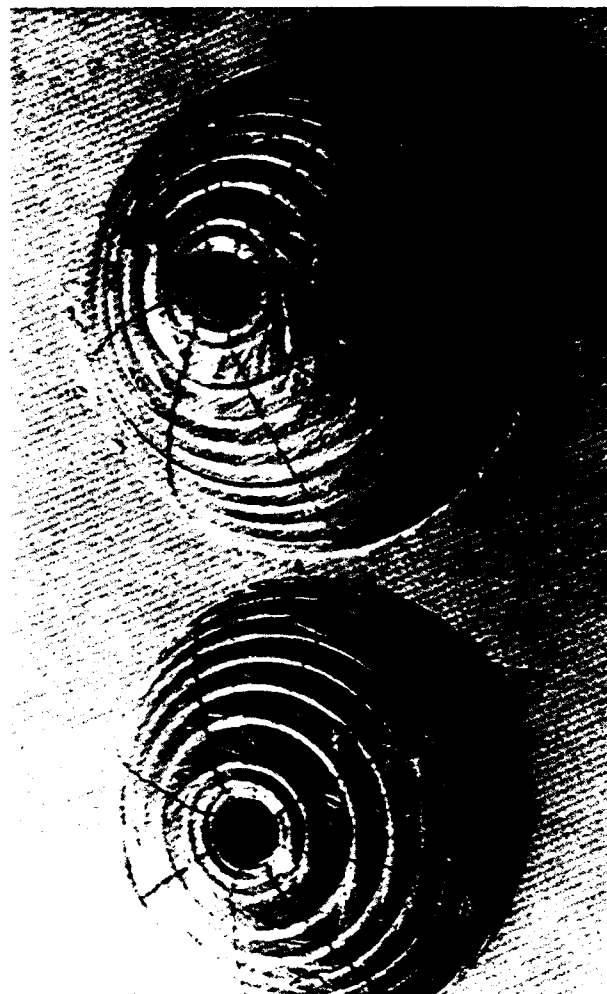


FIG. E-53 FIBER HEAD PIECES TEST RV-7, REMOVED FIBER HEADS

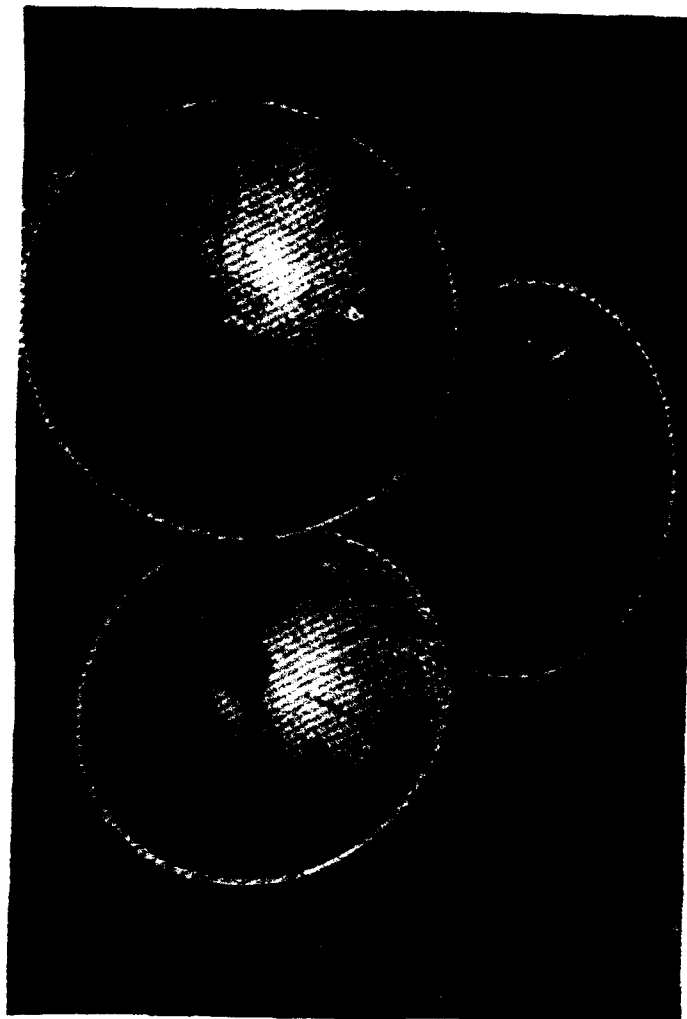


Fig. E-54 TEST RV-7, INSIDE VIEW, REMOVED FIBER HEADS
AND GIRTH RING

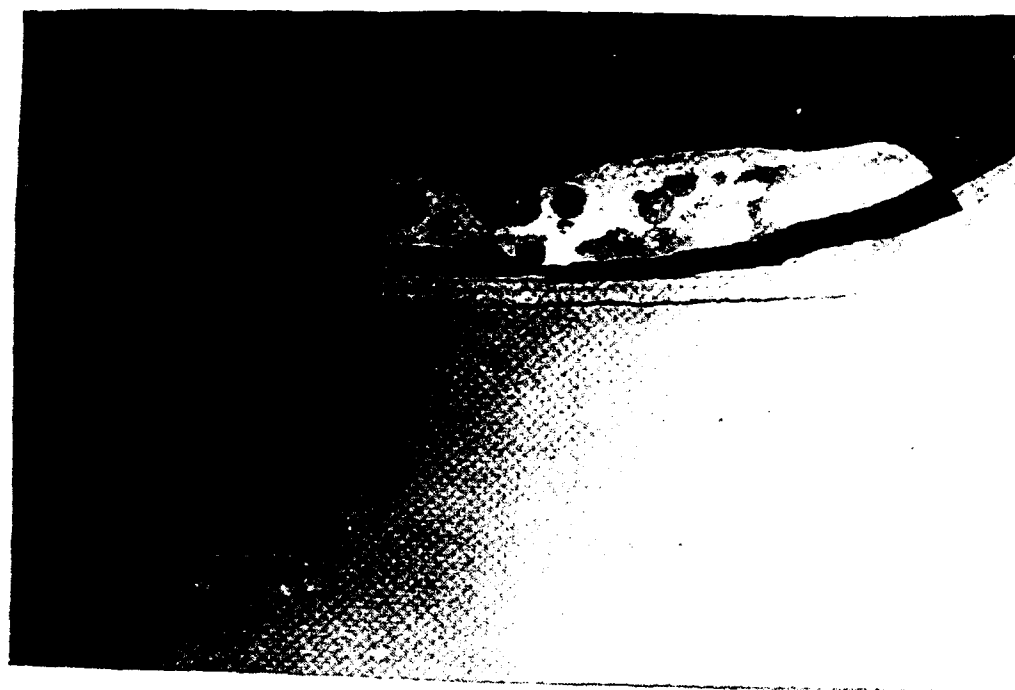


Fig. E-55 SMALL LOOSE LINER FRAGMENT

E.6 RV-9 Test (16" ϕ PSC)

E.6.1 Test Vessel Description

- P/N E4171, S/N 002 (Kevlar Overwrapped 301 CRYO CRES Composite Spheres)
- Kevlar Fiber (less resin) Average thickness - .154 (100% baseline thickness)
- Metal Thickness - .057/.050
- Inside Radius - 7.64
- Hydrogen Embrittlement Mode - Local Girth Weld Region
- Electrolyte Solution -
$$\frac{20 \text{ cc H}_2\text{S)}_4 + 980 \text{ cc Tap H}_2\text{O}}{1000 \text{ cc Solution}}$$
- Solution Additive - 500 mg Sodium Arsenite
- Sensitize Liner Inside Surface (cold pickle)
- Charging Current Density - .021 amps/in² of surface to be embrittled
- Charging Time - 72 hours
- Hold Time Before Test - 3 hours
- Adcoat AC818T liquid maskant on areas not to be embrittled.

Prior test photographs of the instrumented tank in the wooden handling stand and a close up of strain gages 11, 12, 13, 14 are shown on Figures E-56 and E-57 of this section



Fig. E-56

TEST RV-9, INSTRUMENTED TANK IN WOODEN HANDLING
STAND



Fig. E-57

E-113 TEST RV-9, CLOSE UP OF STRAIN GAUGES 12 TO 14

E.6.2

INSTRUMENTATION OBSERVATIONS (by AFAL Instr. Eng)

KEVLAR TEST 009, 9OCT86. Project number 573000RV.

EXPERIMENTAL OBSERVATIONS.

Introduction. Vessel S/N 002, P/N E4171, was tested. It was a 16 inch diameter stainless steel sphere and had a Kevlar overwrap. The vessel was hydrogen embrittled about the girth for about a 1 inch width. It was tested in a vertical configuration. The tank pressure was increased with pressure pulses and ramps until liner cracking occurred.

Pressurization Ramp. The vessel was pressurized with cool helium gas. Initially, the pressure was increased from ambient pressure to about 200 psig during a cool-down period, which took about 2 minutes. During the next 32.3 seconds, pressure was increased with a salvo of 19 small pulses and steps to a plateau, with an average value of 1956 psig. The plateau pressure was not maintained; it started at 1973 psig and decayed slightly to 1940 psig over a period of 33 seconds. After a 1.099 second long pressure transient, pressurization continued in a classical linear ramp from 2244 psig to 3752 psig in 17.6 seconds (89.699226-72.099138 seconds), which is a pressurization rate of 85.7 psig/second. The vessel cracked following 17.6 seconds of ramp time at 89.7 seconds. The crack generated a sharply demarcated depressurization profile. The profile followed an exponential decay, which was not distorted until one repressurization episode was attempted at 23.2699452 seconds; repressurization failed, and pressure could not be maintained above 1951 psig. Total cool-down and pressurization time was 203.999 seconds (120.000 + 32.300 + 33.000 + 1.099 + 17.600 seconds). Initial depressurization rate was 1515 psig/second $[(2236-3752 \text{ psig})/(90.699720-89.699226 \text{ seconds})]$.

Catastrophic Burst. The vessel cracked at the end of the 17.6 second ramp time at 89.7 seconds with subsequent rapid pressure loss; during depressurization, one repressurization episode was attempted. During depressurization, prominent Kevlar fiber pinging, within the audio spectrum, became noticeable, but the pinging only lasted for about 2 minutes. The Kevlar fiber remained intact, in general; but some fiber fraying was concentrated on the ends of the vessel near the bosses.

Post-run Inspection. After the test, the vessel was cut open by AFRPL; the cut was made 3 inches away from the girth weld; seen was a jagged, circumferential crack near the girth weld. Dye penetration was not done at this time to identify any accompanying fractures. A more detailed examination was done in DEC86 at ARDE.

Other Details. After the post-run inspection, the parts were shipped to ARDE. Acoustic emission was not used.

IMPRESSIONS FROM THE DIGITIZED FM DATA.

Strain Gages.

Location. The strain gages were located IAW ARDE drawing dated 29AUG86. The locations were concentrated near the bosses and the 4th wrap, although some were near the girth and the 13th wrap.

Evaluation of the Graphs.

Of the 23 strain gages recorded, the activities before, during and after the burst for 21 gages were compared; not compared were SG7, which opened immediately following burst and SG10, which was noisy. All 21 graphs started from reasonable noise floors (SG3 and SG23 were the slightly noisy), and each of 10 graphs (SG1, 2, 8, 9, 13, 15, 16, 17, 18, 21) progressed into a steady but short period of prominent oscillation, without offset, before making the transition to tension strain activity. The remaining 11 graphs made almost immediate transitions to tension strain, but some did so abruptly (SG4, 6, 14, 20, 22); and some did so with a little oscillatory activity modulating a noticeable slope (SG3, 5, 11, 12, 23) or smooth curve (SG19). The distribution of the nominal differential strain magnitudes is interesting; twelve of the 21 gages are close together between 2100 (SG12) and 3300 (SG2) microinches/inch; the other 9 gages are much more widely distributed between 3860 (SG17) and 7800 (SG9) microinches/inch; the 7800 value for SG9 is isolated and considerably higher than the other gages. These categories are subjective calls, and exhibit considerable variance because of interpretation; the trends, however, are apparent. Of unknown significance is the observation of just how the 10 oscillatory graphs started their oscillations; seven of the 10 started in the positive (compression) direction, and 3 of the 10 started in the negative (tension) direction. The oscillation is most clear on SG16, and the frequency is about 7000 Hz [7 cycles/(89.782-89.781 second)], which is close to the estimated 10,000 Hz resonance frequency of the composite structure discussed in test 5, Spike Theory #1.

The distribution of the 9 gages (SG 1, 4, 6, 9, 14, 15, 16, 17, 22) with the higher nominal differential strain values is biased as to location. Seven of the 9 gages are on the half of the vessel containing sections 1, 2, 3, 4, which are outlined by the grid lines used to locate the positions of the sensors. Also, out of 6 girth gages (SG4, 6, 12, 14, 20, 22) mounted perpendicular to the fiber (the weakest direction), 4 gages (SG4, 6, 14, 22) are in the high strain category; out of 6 boss gages (SG1, 7, 9, 15, 17, 23) mounted parallel to the fiber (the strongest direction), 4 gages (SG1, 9, 15, 17) are in the high strain category. Simply stated, the exiting gas at the girth failure could provide uniform stress to the girth area resulting in more strain in the weak direction, and the two vessel halves slamming into the wrap near the end bosses could provide nonuniform strain in the Kevlar with more strain in the fibers

trying to keep the end bosses together. Other speculations exist.

The activity on all channels starts between 44% to 66% of the time between 89.780 and 89.782 seconds. After activity following burst, 3 of the functioning graphs (SG2, 16, 18) return to above the initial condition, and the remaining 10 graphs (SG3, 5, 8, 9, 12, 13, 15, 17, 19, 21) stay below the initial condition.

An interesting paroxysm, appearing most prominent on SG18 between 89.788 and 89.790 seconds, may be related to inflection activity in the same time period on SG6, 8, 12, 16, 17, 20, 23. The phase shifts in time are probably related to gage location. The width relationships remain undefined and vague, and there may not be a correlation.

All gages had spikes.

Displacement Sensors.

Both displacement sensors worked. They remained noise free. DP1/8001 shows a displacement of about 87 mils and DP2/8002 shows a displacement of 127 mils. The start of activity correlated well with the strain gages. The 7000 Hz oscillation seen on the strain gages was not seen on the displacement gages. Much lower frequencies were seen on the displacement sensors, and the frequencies were not the same; DP1 had about 300 Hz and DP2 was noticeably lower - about 200 Hz. Good correlation exists between both graphs for the first 0.015 seconds following vessel fracture. After that, the frequencies are not the same, but the nominal trends are similar. Only a couple of spikes were noticed on DP1.

Data Analyst's Comments. ITT, Richard M. Thomsen, 20NOV86, states:

DATUM ANOMALIES

Item PC1/1901 shows pressure spiking unlike previous tests. Item PVSOUT/1904 may show a better pressure trace.

Item SG24/7124 has four strain shifts during the pressure ramp prior to burst.

FM ANOMALIES

No IRIG-B was recorded on the analog tape. The burst pulse recorded on SG1/7101 was used to synchronize the times of these gauges with the burst pulse recorded by the datum system for SG24/7124.

The recording started 42 seconds into the test.

SG7/7107 was noisy (sic). SG23/7123 looks bad until 72 seconds. SG13, 14 and 16/7113, 14 and 16 show a spike at approximately 89 seconds. Several strain gauges showed strain level shifts during the pressure ramp prior to burst. SG 1,4,6,10,20,22 and 23/7101,04,06,10,20,22 and 23 went out completely at the burst. SG2 and 14/7102 and 14 went out after the burst. SG8 and 11/7108 and 11 overranged during the burst spike."

FM HIGH FREQUENCY PROCESSING. ITT continues with comments dated 17DEC86.

"DIGITIZING PROCESS

Digitizing was done at 160,000 samples per second using a 20,000 Hz filter. SG1 was recorded with each of the other items and used as the time reference to sync the FM time scales. This time scale was referenced to that recorded by the DATUM system, synchronizing the burts recorded (sic) for SG1 on the FM and SG24 on the DATUM (89.78301).

DATA ANOMALIES

Most of the strain gauges show spiking at the burst. Some of the spikes occur at the same time on different gauges. Note the spikes at 89.7861 and 89.7892 seconds for SG1 and 2. SG3 has periodic noise spikes every millisecond. SG7 has a complex noise signal with a frequency of 120 Hz. SG8 overranges at the burst. The following items go out at [following] the burst: SG1, 4, 6, 10, 11, 14, 20, 22 and 23." End of ITT text.

IMPRESSIONS FROM THE QUICK-LOOK AND DIGITAL DATA ACQUISITION SYSTEM DATA.

Tank Pressure. The tank pressure functioned as described under the Pressurization Ramp paragraph.

PVSOUT/1904 is the vessel output pressure, but it is located near the vent valve about 15 feet from the vessel. This parameter's behavior is smoother than 1901, which is subject to interference from the line pressurization activity as discussed in TESTRV8. Note the differences between 1904 and 1901; the pulses do not reach 1904, the 1.099 second long transient at 70.999866 seconds on 1901 doesn't appear on 1904, and neither does the transient at the beginning of the repressurization effort at 232.699452 seconds. In some respects, 1904 may be more interesting than 1901 because it is 94 psig higher than 1901 at rupture, although some of this difference is probably due to transducer error; 1901 could be in error by 37.5 psig (.5%X7500 psig) and 1904 could be in error by 60 psig (0.5%X12000 psig), but it is unlikely both errors would compound one another in the opposite direction at the same time.

DESCRIPTION OF THE EMBRITTLEMENT PROCEDURE. An undated ARDE embrittlement procedure was followed; only the girth area for a width of about 1 inch was embrittled. Embrittlement was inhibited, where required, with a maskant. Embrittlement was started at 0915 hours on 6OCT86. The current level was 0.65 amperes. Seventy-two hours of embrittlement were completed at 0915 hours on 9OCT86; the tank was immediately moved from the shop embrittlement area to the test site, instrumented, hooked up and tested at 1210 hours on 9OCT86. The electrolyte was sulphuric acid; sodium arsenite was added as an enhancer.

ADMINISTRATIVE INFORMATION.

Revision Record. Initial Issue: 17SEP86. Revision A: 2DEC86; Pressurization ramp description and embrittlement procedure completed. Revision B: 14JAN87; text added: Evaluation of the Graphs, Displacement Sensors, Data Analyst's Comments.

Filename: testrv9.

Distribution. ARDE, Steve Berko, Dave Gleich
PI, Dr. Pius Chih Hsu Chao
Aerospace Corp., Dr. Yen Pan
AFRPL, Jim Miller, Mike Dieckhoff, Dick Grove
MSGT Jim Day, John Marshall, Capt
Seidemann
ITT, Richard Thomsen, Dr. Tae-Woo Park
PAFB, Pete Tadie

Office of Primary Responsibility. USAF/AFRPL/TOAE/Edwards CA
93523.

E.6.3 Pressure and Strain Versus Time Plots

Figures E-58 and E-59 give test pressure versus time graphs. Key strain versus time plots are given on Figures E-60 to E-69 for sample rates of 1000 and 160,000 SPS, filter frequencies of 100 and 160,000 Hz and plot rates of 1000, 80,000 and 160,000 SPS. Strain gages were located in the apex and girth regions on the 23° and 81° fiber wraps as detailed in Figures E-70 and E-71. Odd number gages were parallel to the fibers and even numbered gages were perpendicular to the fibers.

RUN RV 9

Fig. E-58

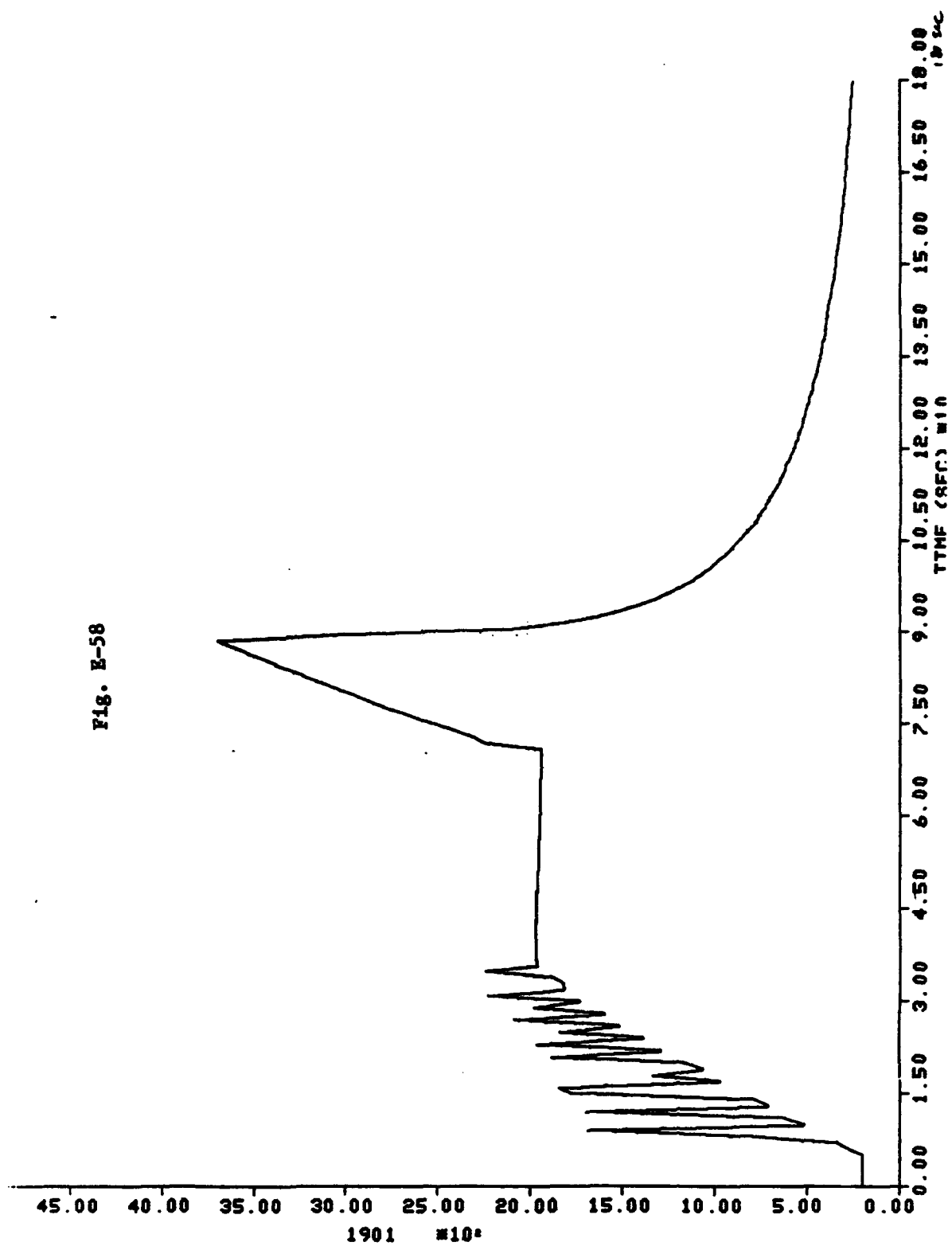


Fig. E-59

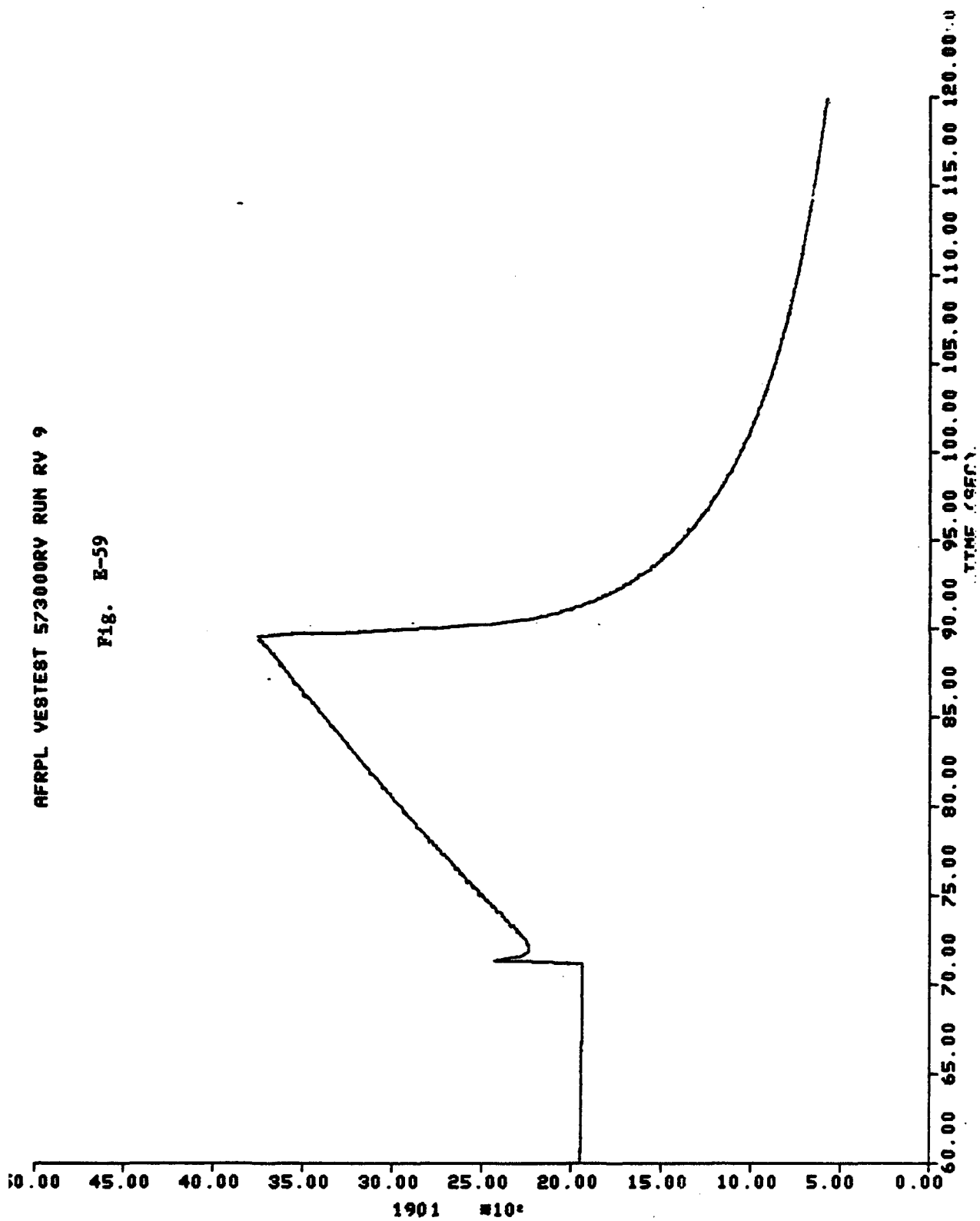


Fig. E-60

KEVLAR VESSEL TEST RV-9 - P/N E4171. S/N 002 9 OCT 1986

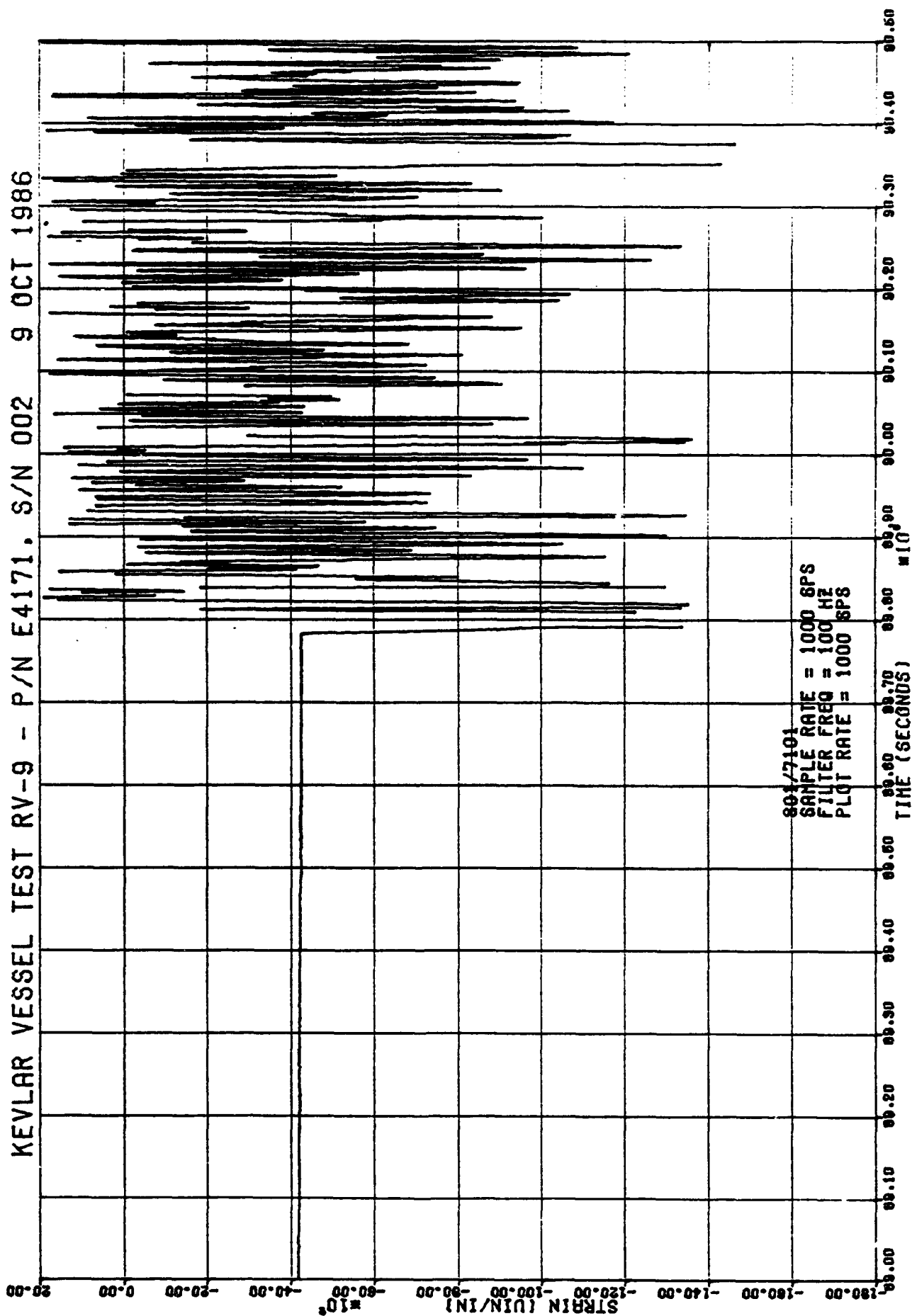


Fig. E-61

KEVLAR VESSEL TEST RV-9 - P/N E4171, S/N 002 9 OCT 1986

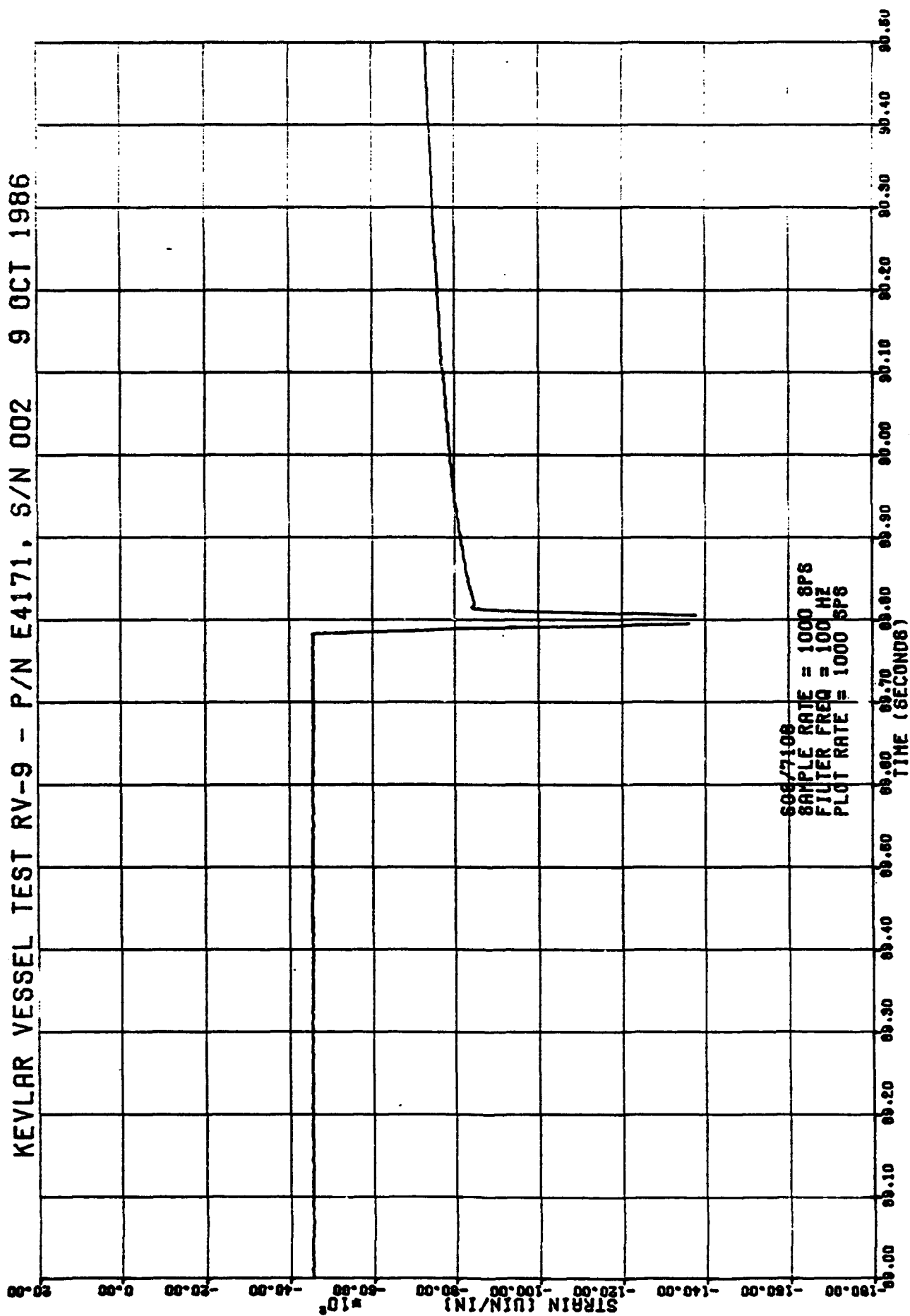


Fig. E-62

KEVLAR VESSEL TEST RV-9. P/N 4171. S/N 002. 9 OCT 86

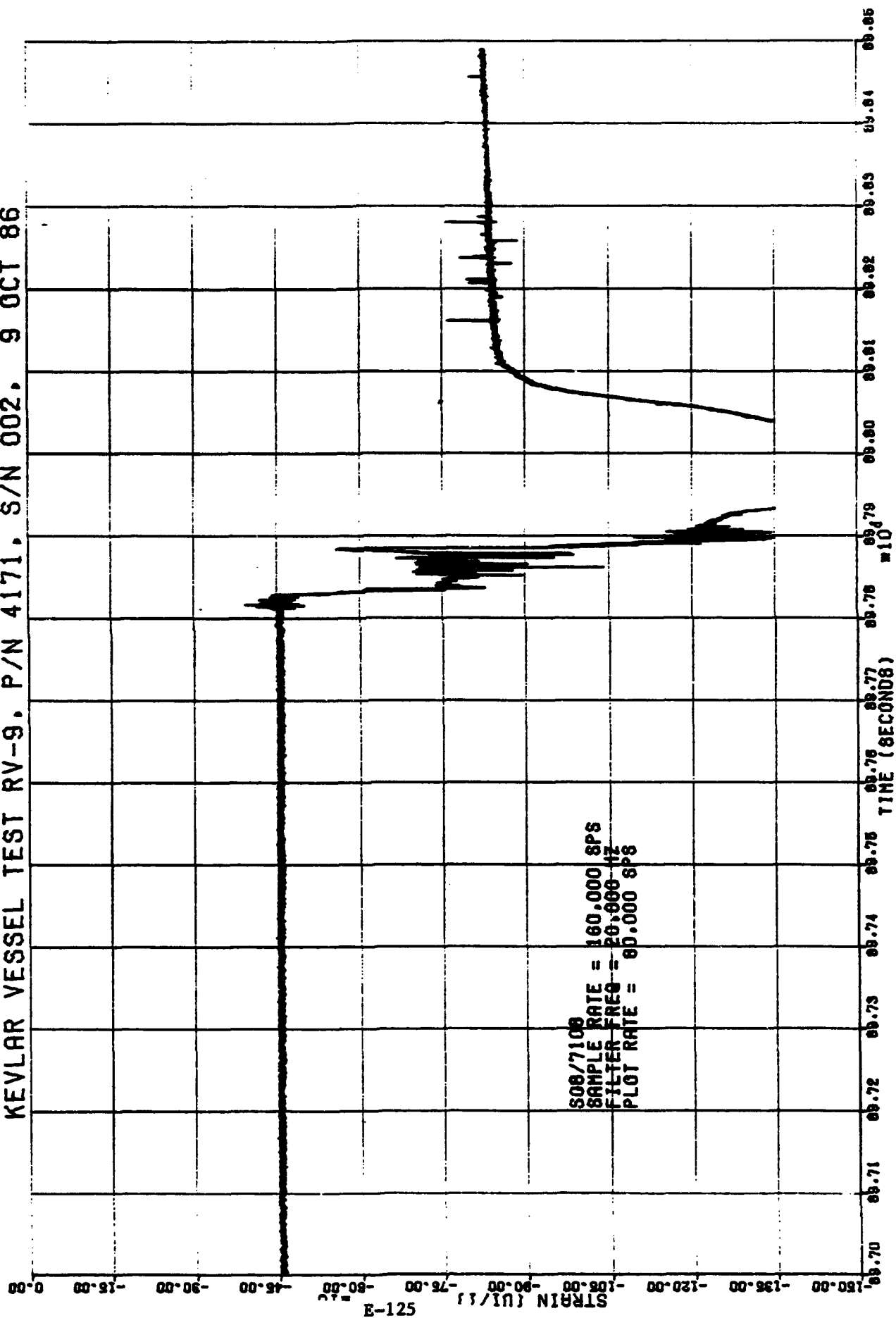
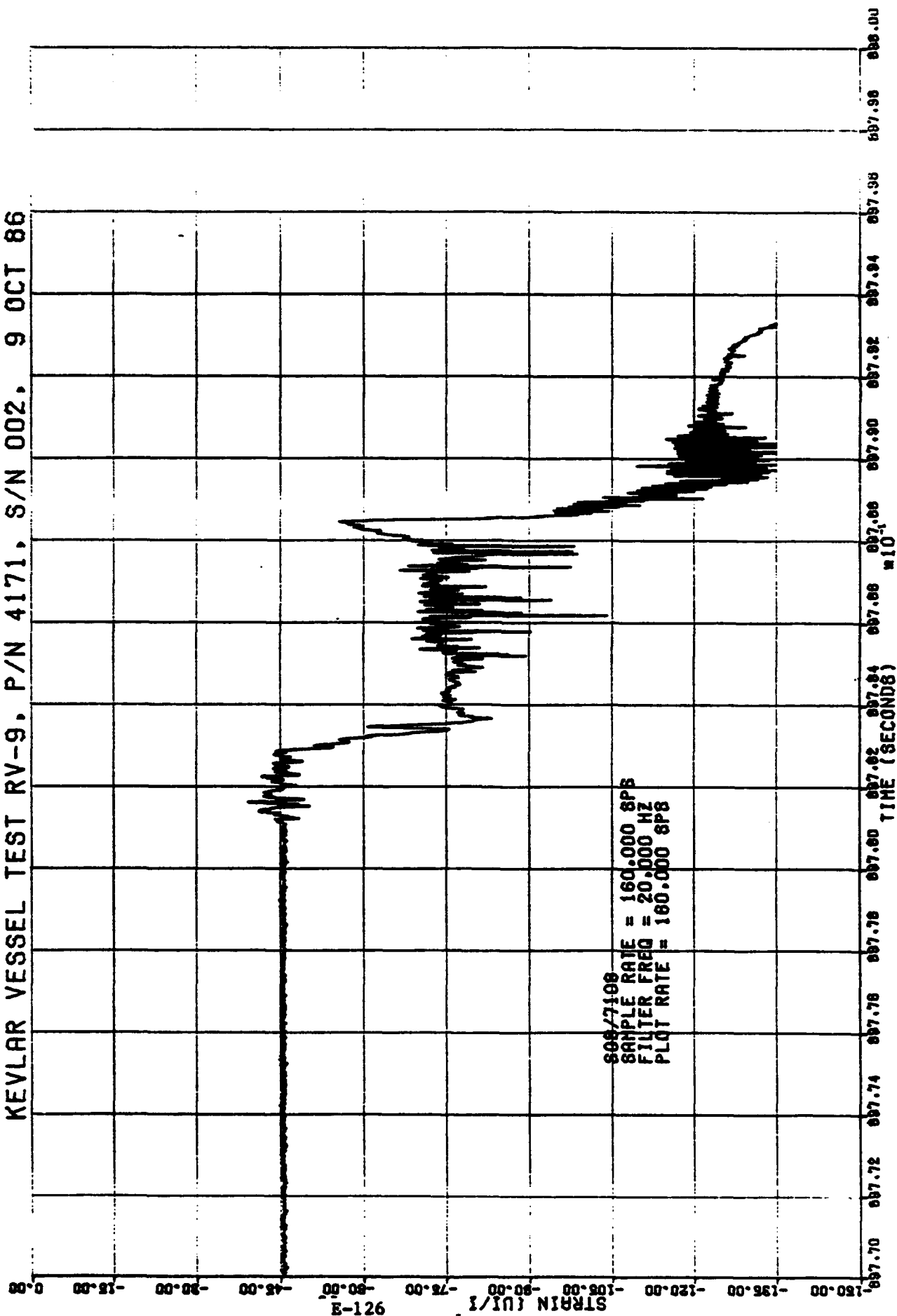


FIG. E-63

KEVLAR VESSEL TEST RV-9, P/N 4171, S/N 002, 9 OCT 86



KEVLAR VESSEL TEST RV-9 - P/N E4171, S/N 002 9 OCT 1986

Fig. E-64

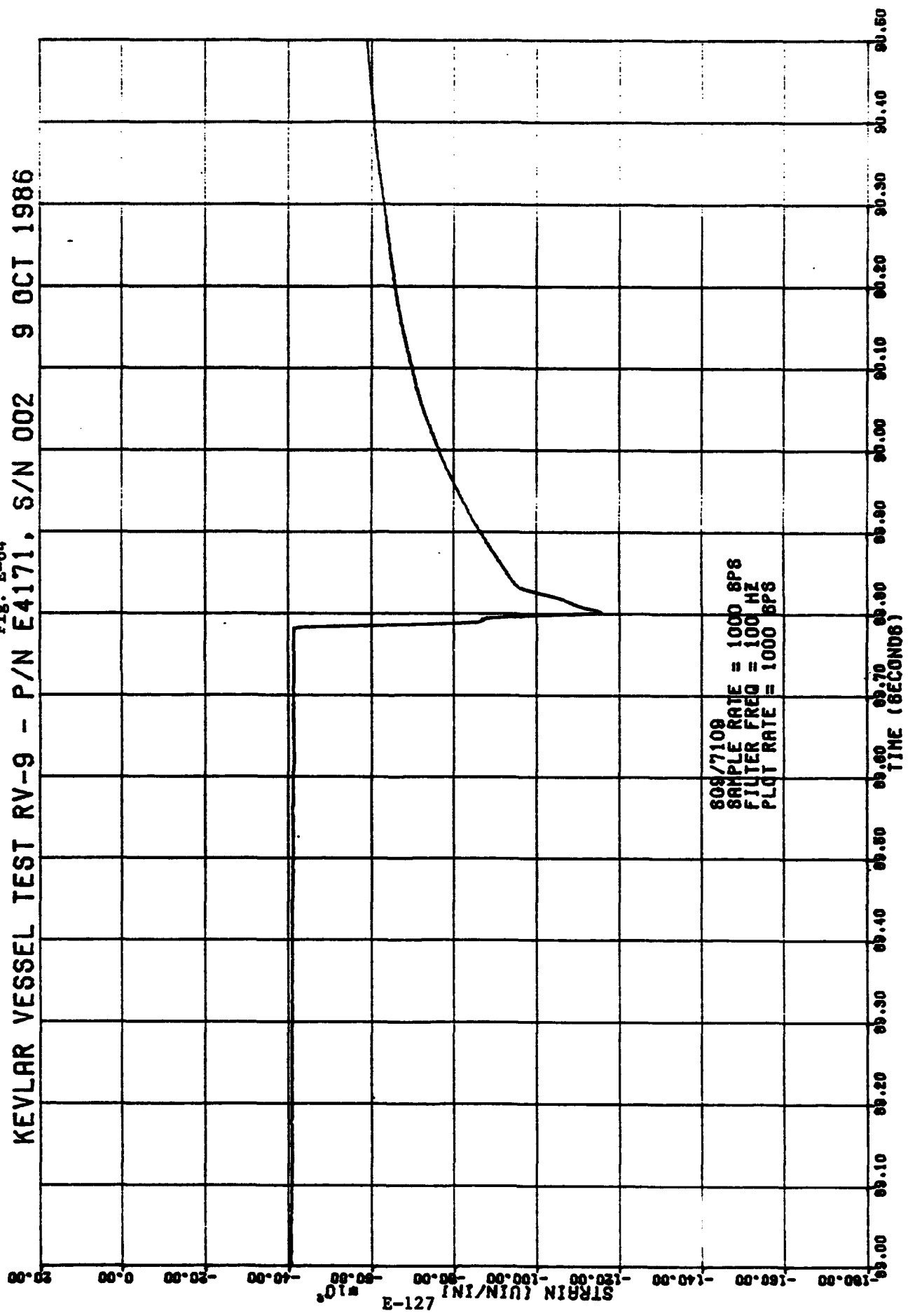


Fig. E-65

KEVLAR VESSEL TEST RV-9, P/N 4171, S/N 002, 9 OCT 86

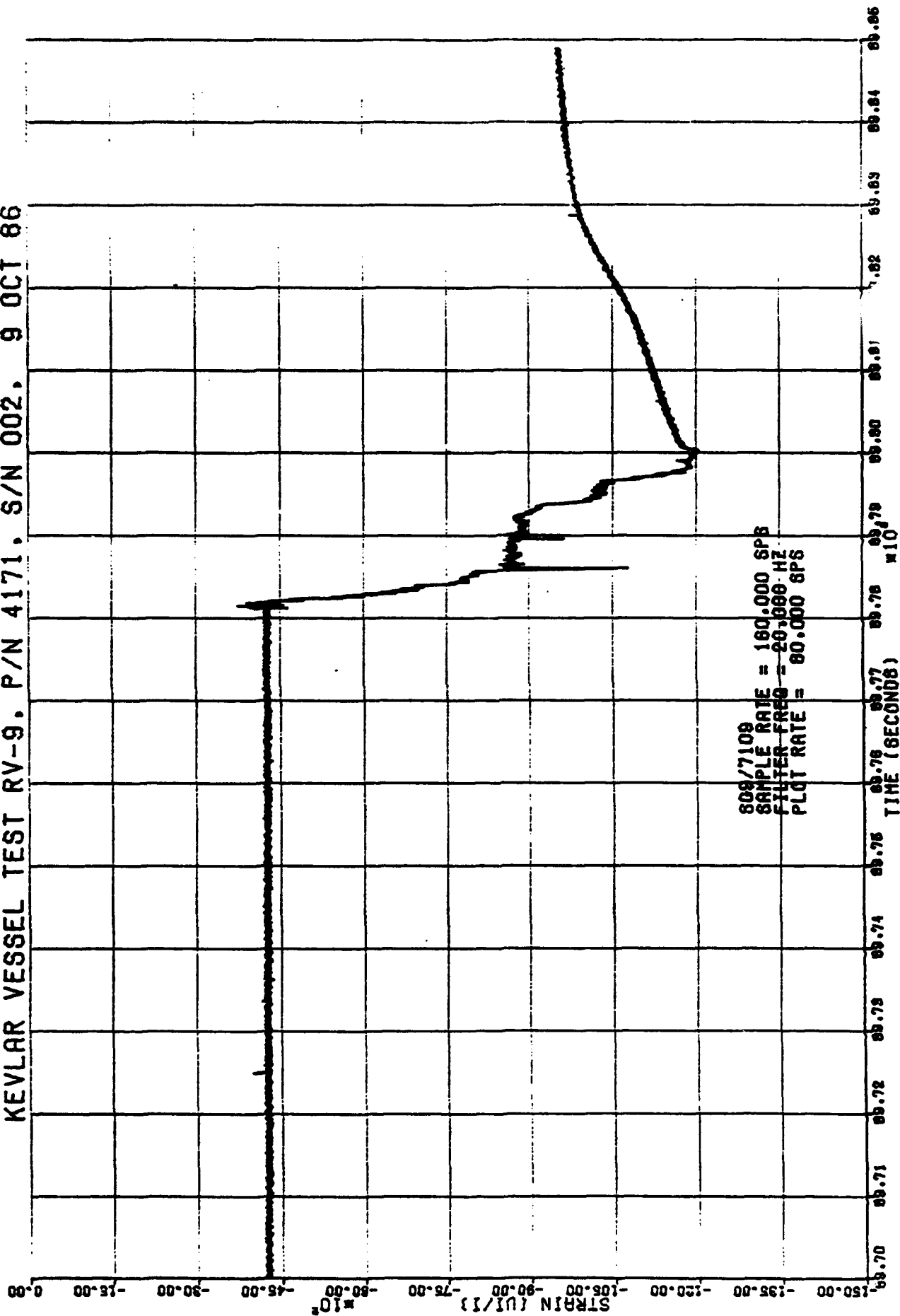


Fig. E-66

KEVLAR VESSEL TEST RV-9, P/N 4171, S/N 002, 9 OCT 86

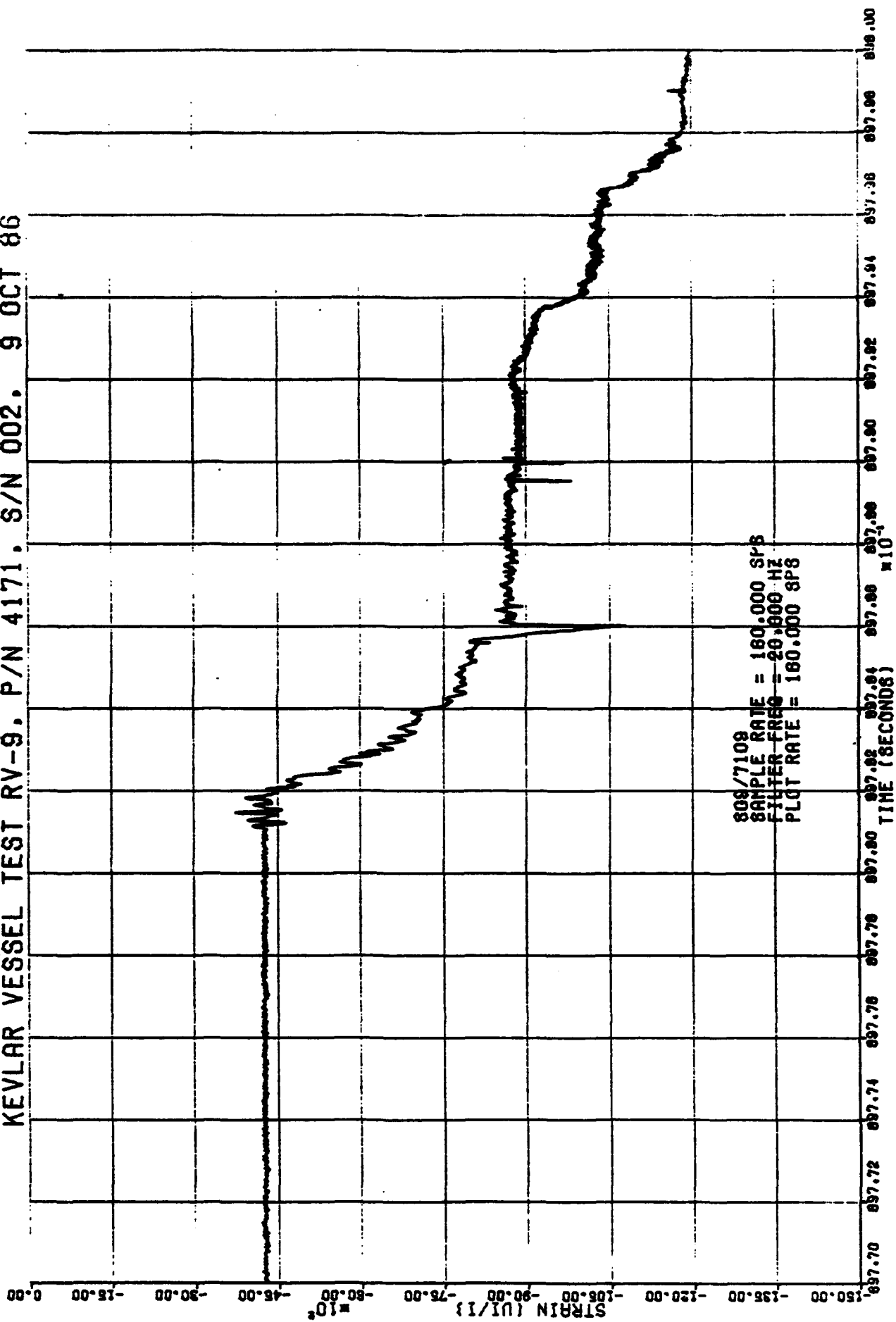


Fig. E-67

KEVLAR VESSEL TEST RV-9 - P/N E4171, S/N 002 9 OCT 1986

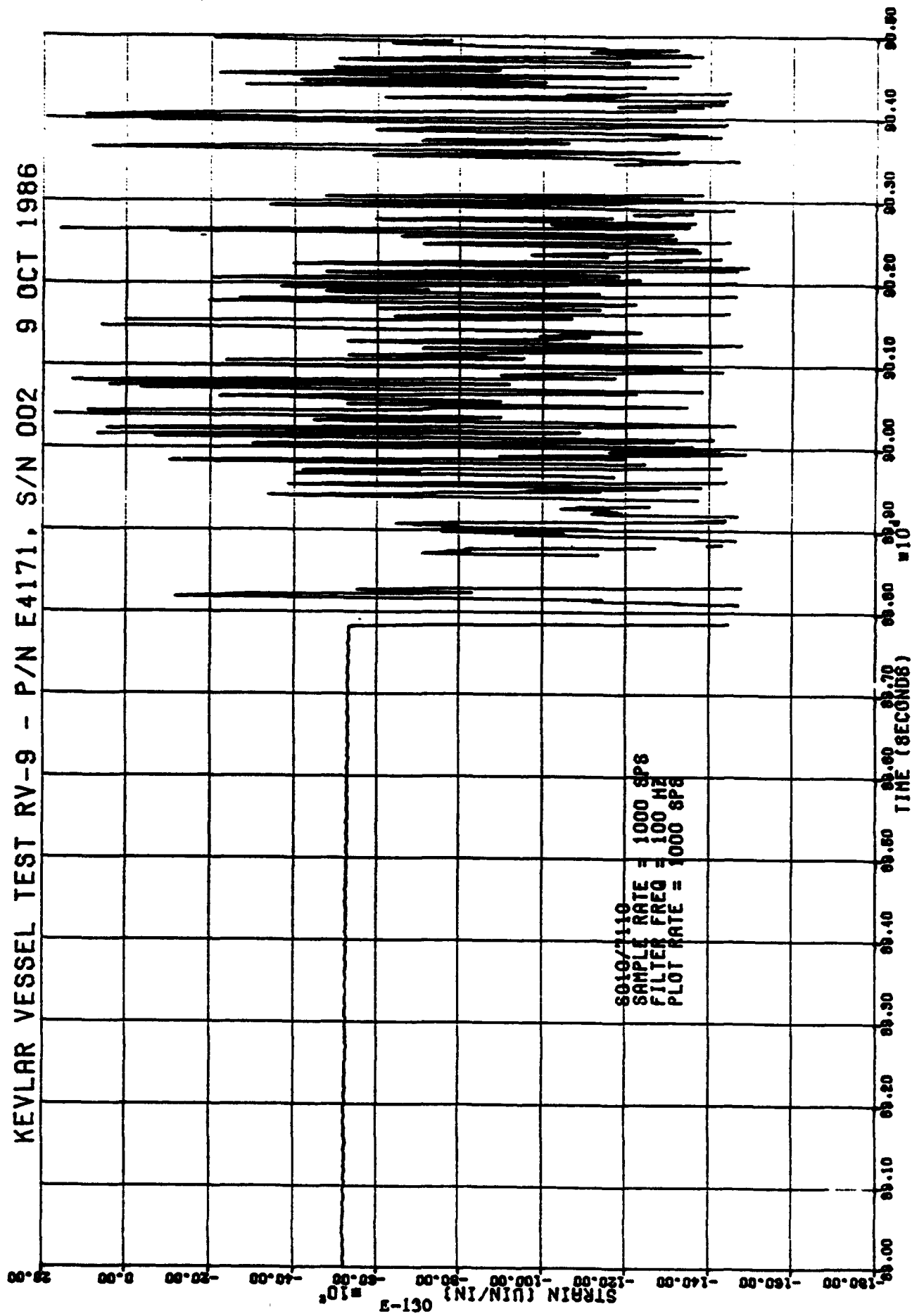


Fig. E-68

KEVLAR VESSEL TEST RV-9. P/N 4171. S/N 002. 9 OCT 86

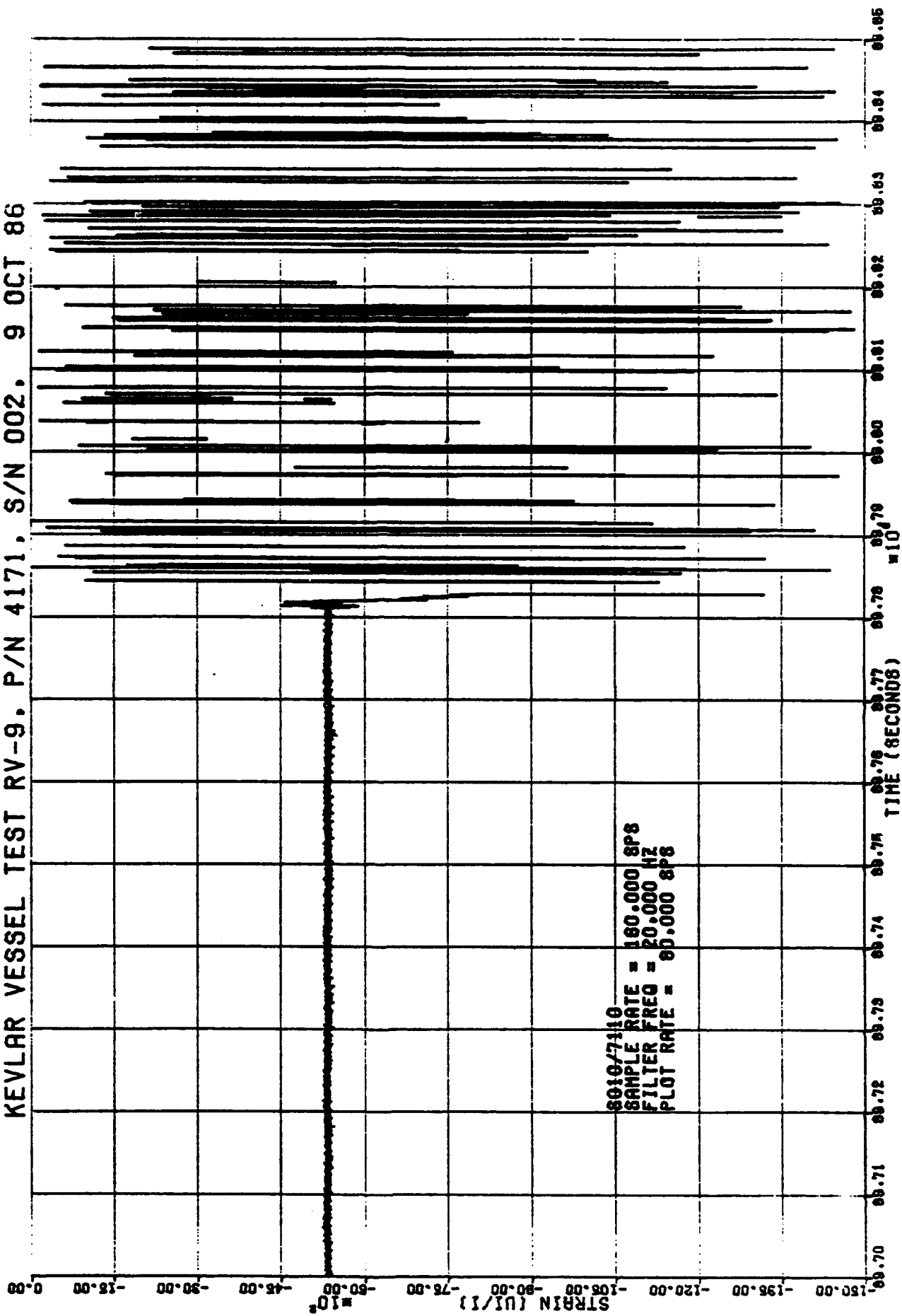
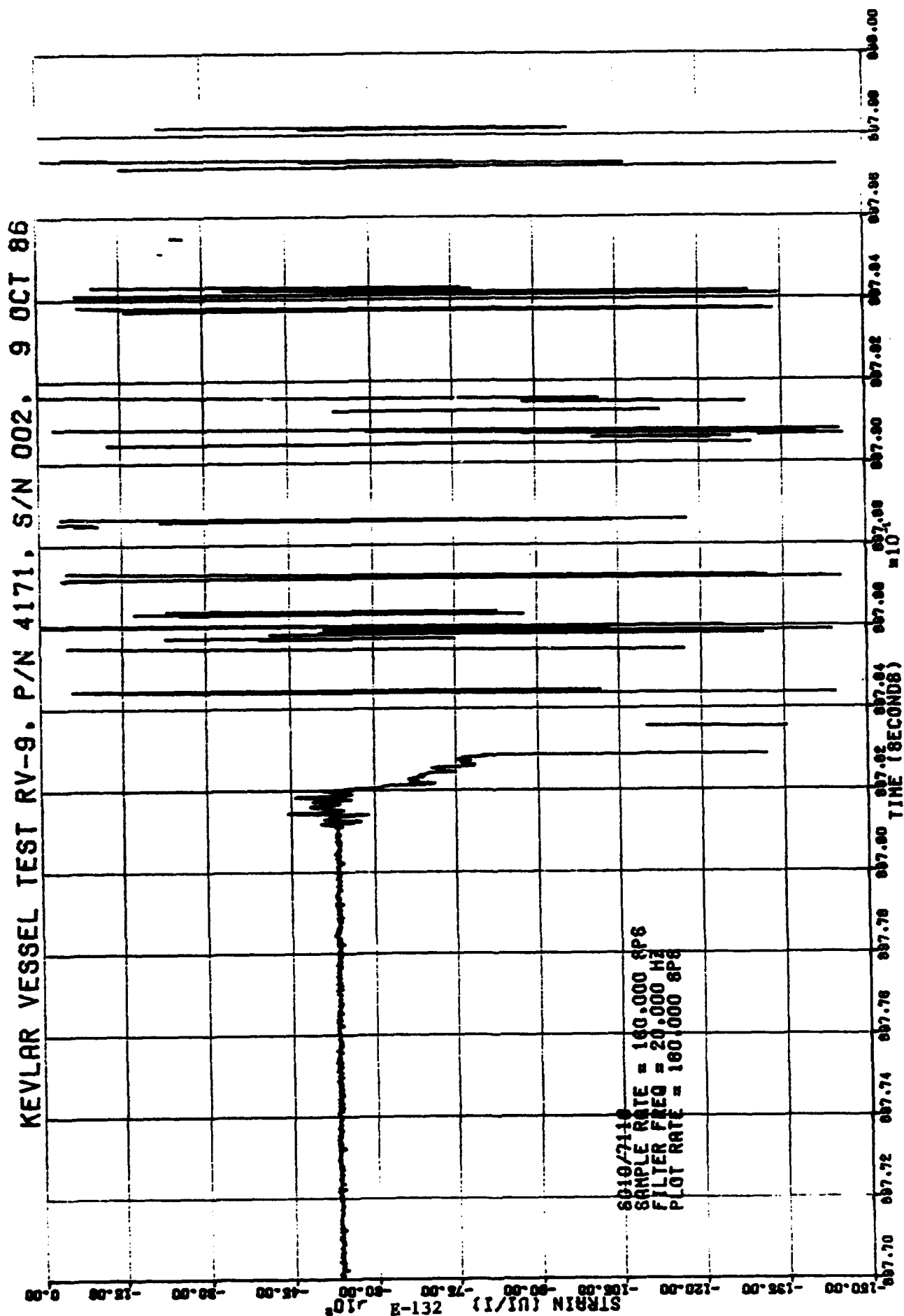


Fig. E-69



REPORT NO. _____

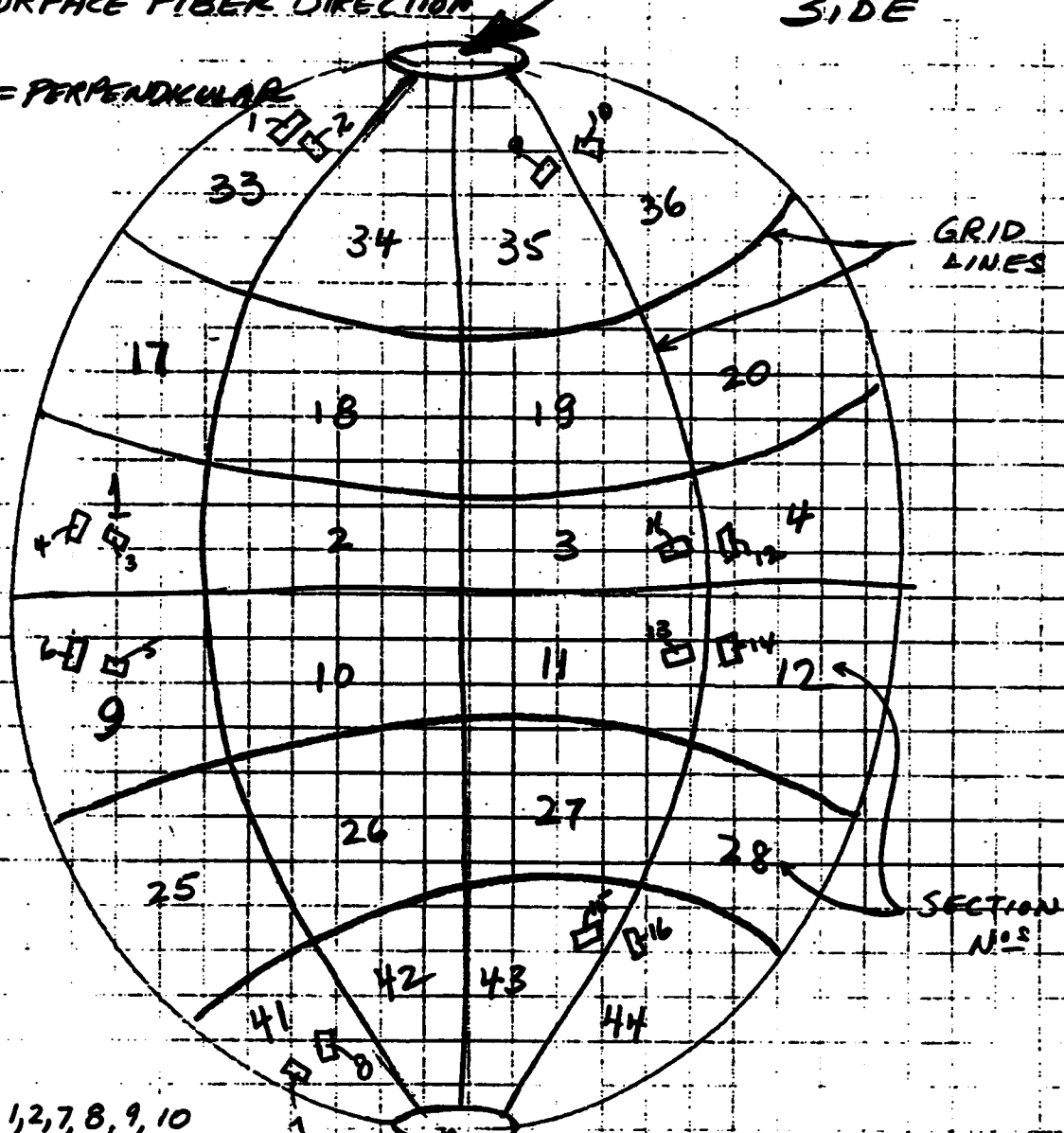
JOB NO. 42001

PREPARED BY: SMB

DATE 29 Aug 86

P/N E4171 S/N 002 STRAIN GAGE LOCATIONSODD GAUGE NOS = PARALLEL
TO SURFACE FIBER DIRECTIONMS33649-8
SIDE

EVEN = PERPENDICULAR



GAUGES 1, 2, 7, 8, 9, 10

15, 16, 17, 18, 23, 24

ON 4TH WRAP (23.55°)

GAUGES 3, 4, 5, 6, 11, 12

13, 14, 19, 20, 21, 22 ON 13TH (FINAL) GIRTH WRAP NEAR EDGES
(81°)MS33649-6
SIDE

FIGURE E-70

REPORT NO. _____

JOB NO. 42001

PREPARED BY smf

DATE 29 Aug 86

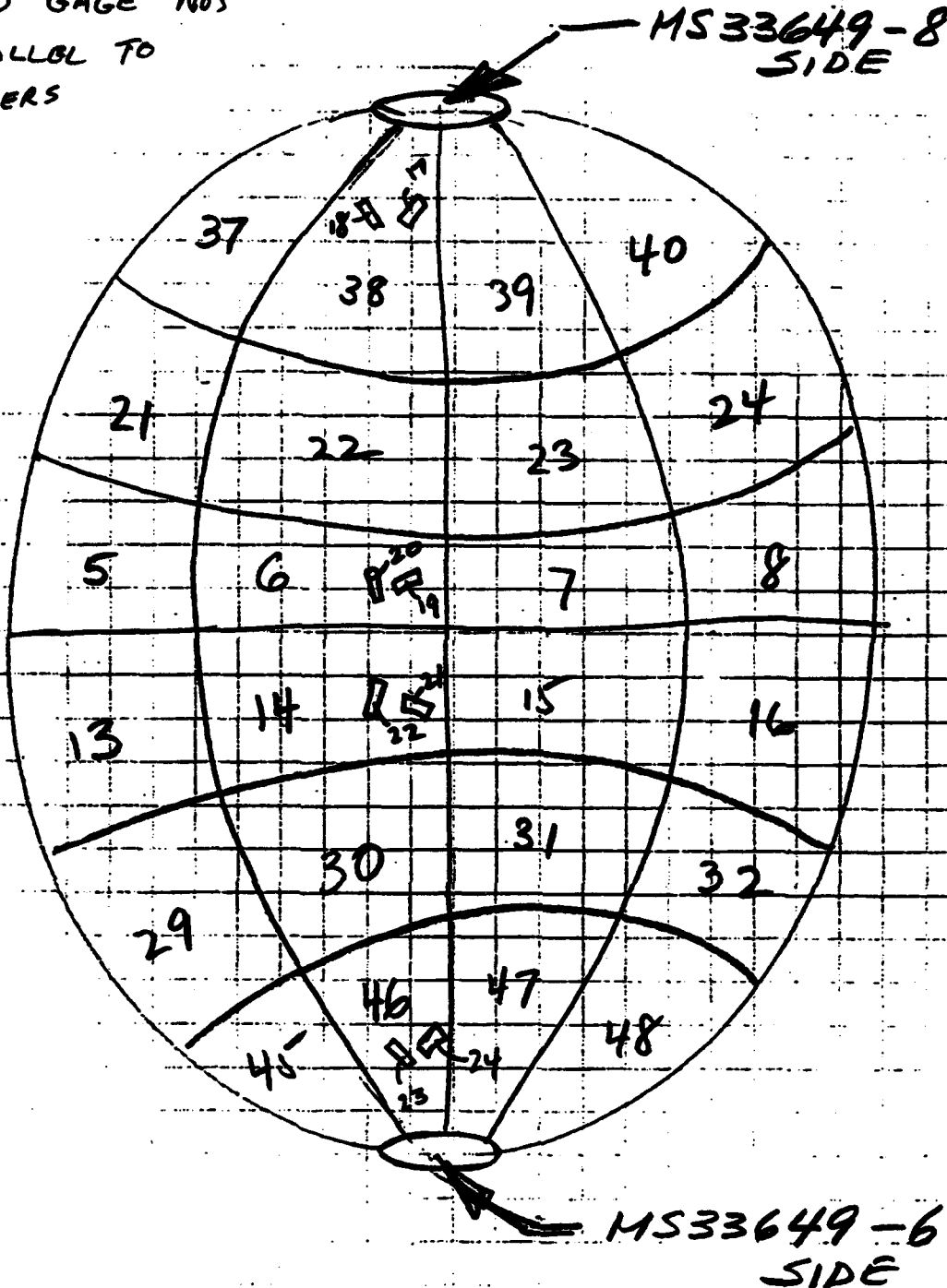
P/N E4171 S/N 002 STRAIN GAGE LOCATIONSODD GAGE NOS
PARALLEL TO
FIBERS

FIGURE E-71

E.6.4 Post Test Inspection

The tank was post-test inspected on the test stand. The outer fiber shell was intact. Some slight fiber damage was observed in the region between the apex and about 45°, similar in nature to RV-7 test result. The vessel was then cut open by AFAL parallel to and 3" away from the girth weld. A jagged circumferential crack around the girth near the girth weld was seen. The vessel was shipped to ARDE for further inspection. The inside liner surface was die checked, the fiber shells removed and photographs were taken at ARDE. The liner failure mode was similar to the RV-7 test result. Complete liner separation at the girth was again verified and there was no bonding between the metal/fiber interface surface. Figures E-72 and E-73 show the girth crack highlighted by die check colorization. Exterior photographic views of the cut fiber shell (Figures E-74, E-75) depict the slight fiber damage regions. The fiber/metal interface of the cut fiber and metal shells are shown on the photograph of Figure E-76. The lack of bond between fiber and metal is evident by the smooth clean and undisturbed interface surfaces.

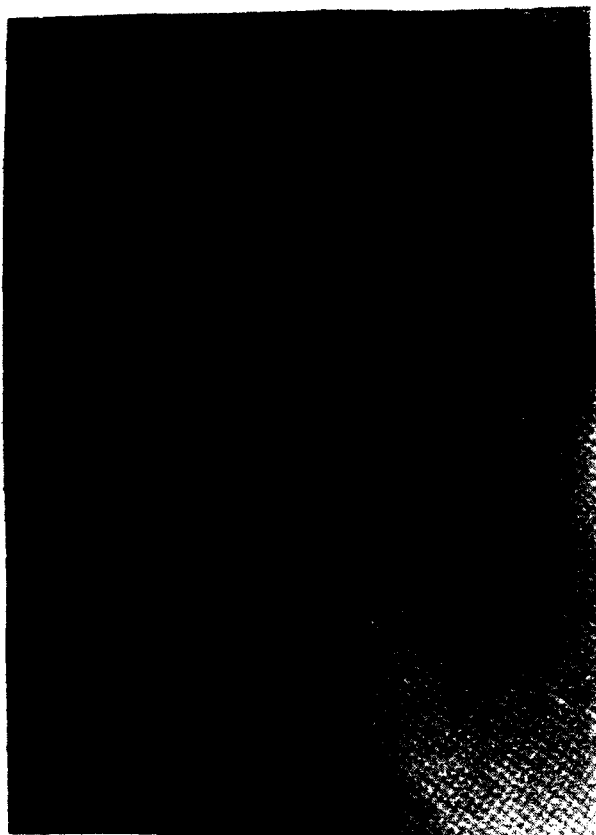


Fig. E-72

TEST RV-9, GIRTH CRACK, DIE CHECK ENHANCED

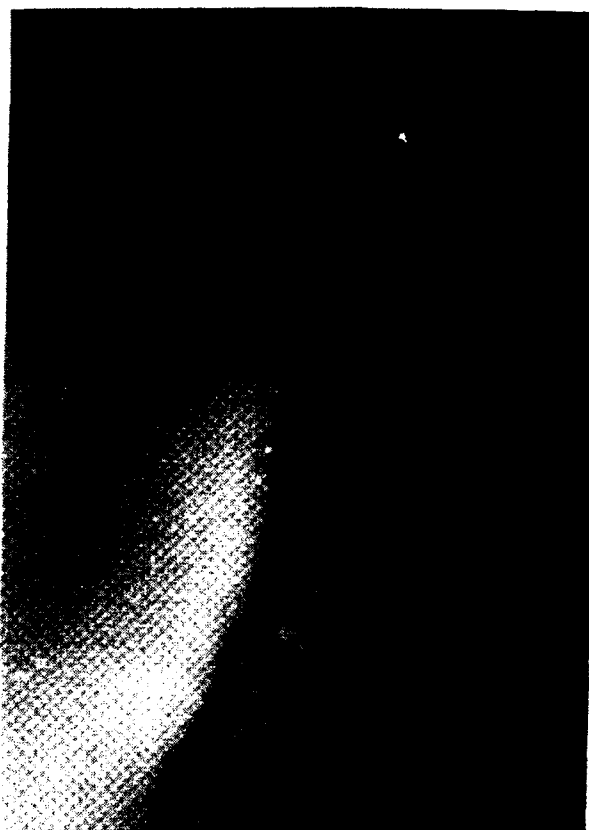


Fig. E-73

TEST RV-9, GIRTH CRACK, DIE CHECK ENHANCED

Fig. E-74



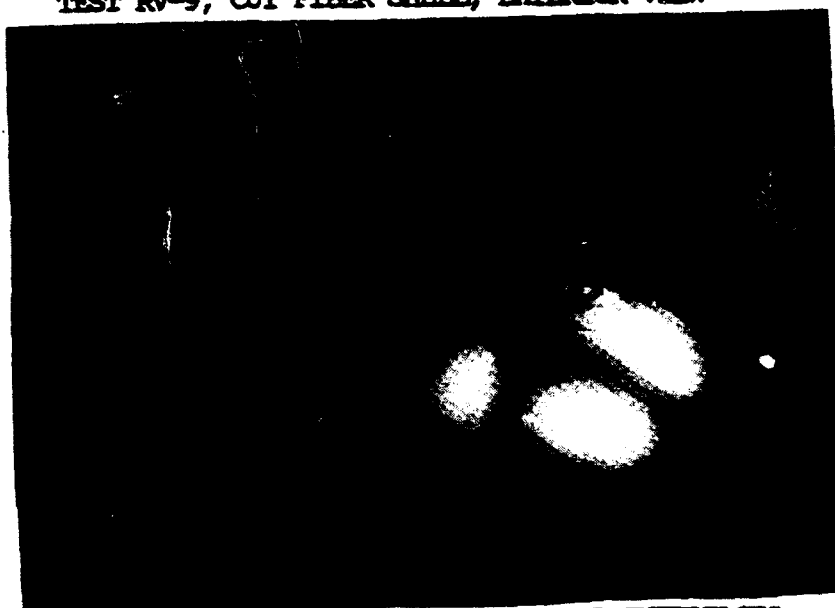
TEST RV-9, CUT FIBER SHELL, EXTERIOR VIEW

Fig. E-75



TEST RV-9, CUT FIBER SHELL, EXTERIOR VIEW

Fig. E-76



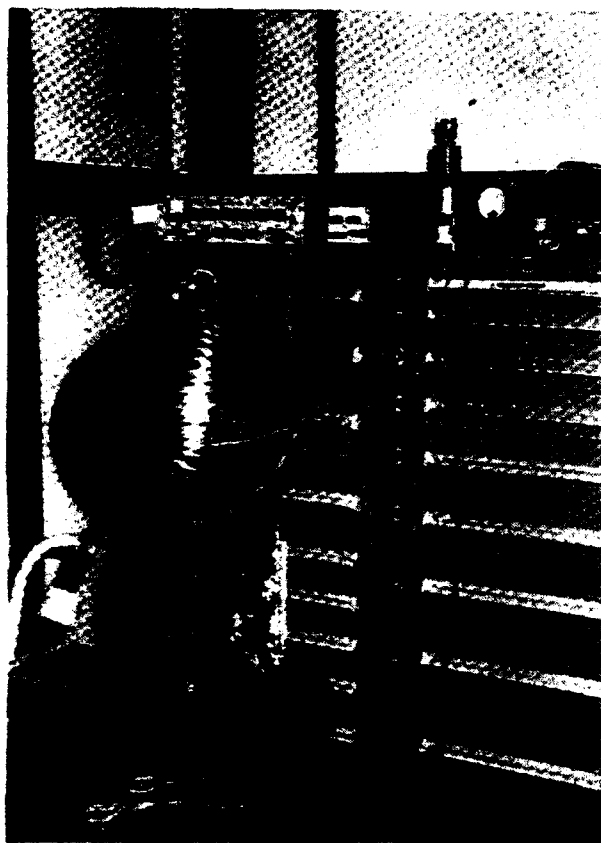
TEST RV-9, CUT SHELLS, FIBER/METAL INTERFACES

E.7 RV-10 Test (16 ø PSC

E.7.1 Test Vessel Description

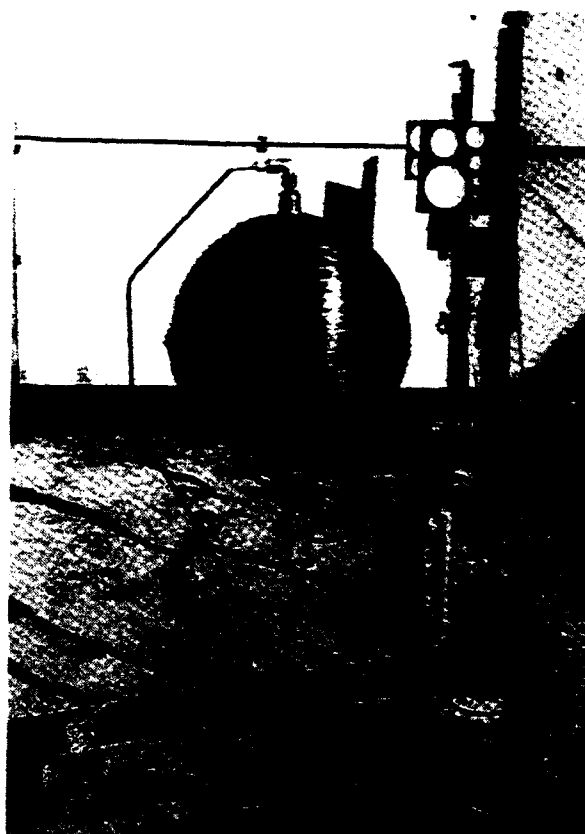
- P/N E4168, S/N 003 (Kevlar Overwrapped 301
Cryo CRES Composite Sphere.
- Kevlar Fiber (less resin) average thickness =
.077 (50% baseline thickness)
- Metal Thickness = .054/.051
- Inside Radius = 7.64
- Hydrogen Embrittlement Mode = Local Girth Weld
- Region Electrolyte Solution =
$$\frac{20 \text{ cc H}_2\text{SO}_4 + 980 \text{ cc Tap H}_2\text{O}}{1000 \text{ cc solution}}$$
- Solution Additive = 500 mg Sodium Arsenite
- Sensitize Liner Inside Surface (cold pickle)
- Charging Current Density = .006 amps/in² of
surface to be embrittled
- Charging Time = 72 hours
- Hold Time Before Test = 2.5 hours
- Adcoat AC818T liquid maskant on areas not to be
embrittled

Figure E-77 is a photograph of the RV-10 test tank during the hydrogen embrittlement mode prior to pressure testing. The composite vessel metal liner is used as the cathode and a lead anode is immersed in the $\text{H}_2\text{SO}_4/\text{H}_2\text{O}$ electrolyte solution inside the tank as prior detailed in section 2.4. A controlled power source completes the circuit, providing the charging current in the electrolyte needed to generate the hydrogen embrittling gas on the liner inside surface. Figures E-78, E-79 show prior test photographs of the tank on the test stand with the Bikini gages, overpressure transducers and witness panels. A close up photographic view of strain gage and thermocouple installation of the fiber wrap outer surface is given on Figure E-80.



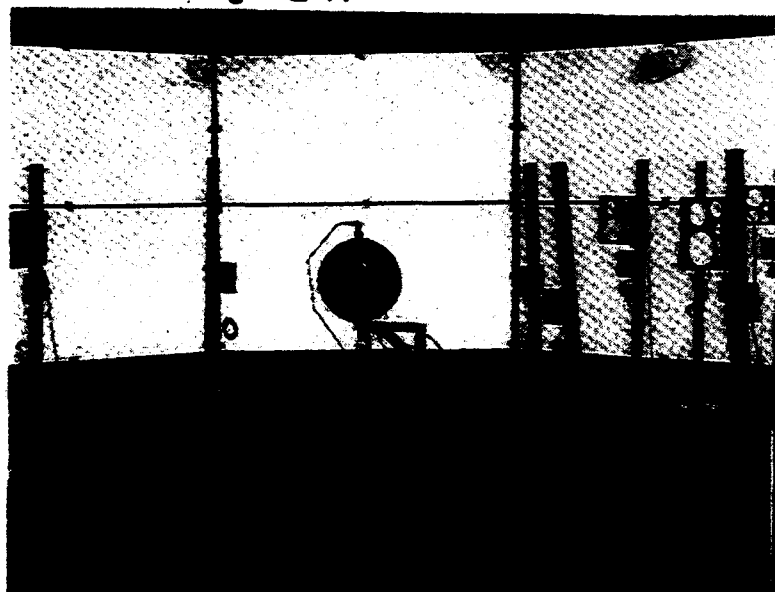
TEST RV-10, PRIOR TEST HYDROGEN
EMBRITTLEMENT MODE

Fig. E-77



TEST RV-10, CLOSE UP, VESSEL
ON TEST STAND

Fig. E-78



TEST RV-10, VESSEL ON TEST STAND, BIKINI
GAUGES, OVERPRESSURE TRANSDUCERS AND WITNESS
PANELS

Fig. E-79



TEST RV-10, CLOSE UP OF STRAIN GAUGE
AND THERMOCOUPLE INSTALLATION

Fig. E-80

Rec'd from AFAL
5/15/87
SMB

INSTRUMENTATION OBSERVATIONS (by AFAL Instr. Eng.)

KEVLAR TEST 010, 18DEC87. Project number 573000RV.

EXPERIMENTAL OBSERVATIONS.

Introduction. Vessel S/N 003 was tested. It was a 16 inch diameter stainless steel sphere and had a thinned Kevlar overwrap. The vessel was hydrogen embrittled about the girth for about a 1 inch width. It was tested in a vertical configuration. The tank pressure was increased with pressure pulses and ramps until catastrophic rupture of the liner and overwrap rapidly occurred.

Pressurization Ramp and Catastrophic Rupture. The vessel was pressurized with cool helium gas. Initially, the pressure was increased from ambient pressure to about 200 psig during a cooldown period, which took about 2 minutes. The tank was vented. The data system was started, and the tank pressure was kept at ambient pressure for 16.399104 seconds before pressure was increased with a salvo of 30 small pulses and steps to the beginning of a 3.3999302 second wide plateau, with a nominal value of 2215 psig. One additional small pulse raised the plateau to a nominal value of 2276 psig. A steady ramp of pressure was started at 55.999302 seconds from a pressure of 2277 psig. The pressurization rate was 92.606 psig/second (3269-2277 psig)/(66.7113366-55.999302 seconds). The first significant change in data as measured by the following sensors occurred at the time indicated for the time between samples specified:

	delta t
	0.001 sec
PTANK/1901 TANK PRESSURE	66.711336
PVSQUT/1904	66.720138
SG24	66.708402
SG1-9	66.709600

From this data, burst was definitely no later than the PTANK time and probably before the SG1-9 (as this value is the time these items go offscale - not the time of oscillation onset, which is somewhere near or between 66.70920 and 66.709300 - depending on the particular SG of interest). The data analyst determined the burst time to be 66.7097 seconds (S/G34/7124) or 66.7093 seconds (S/G21 or 7121); see the Data Analyst's Comments below.

Post-run Inspection. Witness panels, 4'X8'X1" Celotex sheets backed with 1/16" thick aluminum, were used to collect fragments. Some fragments penetrated the panel. Photographs were taken, and the locations of the major fragments were recorded elsewhere.

Other details. ARDE collected some of the broken pieces, and the pieces were returned to ARDE. Acoustic emission was not used.

IMPRESSIONS FROM THE DIGITIZED FM DATA.

Strain Gages.

Location.

The strain gages were located IAW ARDE drawing dated 13NOV86. The locations were concentrated in the same areas as testrv9, but some of the gages were repositioned slightly. For this test, even numbers are parallel with the grain and odd numbers are perpendicular with the grain. The previous test, testrv9, had the opposite assignments.

Evaluation of the Graphs.

Of the 23 strain gages recorded, the activities before, during and after the burst for 20 gages were compared; not compared were strain gages 7, 13, and 23 because of the reasons discussed in the Data Analyst's Comments below. All 20 graphs started from better than reasonable noise floors, and most graphs progressed into a steady but short period of prominent undamped oscillation prior to rupture. However, the exact trends for duration and offset for, say, 0.01 seconds, for comparison to testrv9, cannot be determined by using the first high frequency data pass time scale; the time scale for testrv9 was 0.002 sec/div and for test10 was 0.0001 sec/div. A second high frequency data pass will be made. The oscillation's first few cycles are clearly undamped, and the damped or almost critically damped gage performances seen in testrv9 changed to undamped performances in testrv10; the differences are probably due to the thinner Kevlar wrap in testrv10. A question now arises about the onset of the oscillation. Did it start before, during or after the cracking? The metal cracking or the Kevlar failing is probably the source of excitation, for the oscillation probably didn't occur during the abrupt pressure changes and gas flows experienced during the pressure salvos (TBD). Other speculations can be expressed. One interpretation favors burst after the oscillation; this interpretation is based on observing that most SG graphs first enter into oscillation with a small compression excursion; they reverse direction and continue with a tension ramp, modulated by the oscillation, to burst.

Clinical confirmation of the theoretical prediction of SG compression behavior prior to burst may be obscured by the undamped oscillation, however.

The observed compression excursion at the beginning of the oscillation is probably incidental to the theoretical prediction and is most likely oscillation related. However, the compression mentioned in the prediction may be a latent data manifestation obscured in some data parameters, and digital signal processing may be needed for signal enhancement, identification and recovery.

Data Analyst's Comments. ITT, Richard M. Thomsen, states:

DIGITAL DATA

All channels recorded data correctly. The IRIG signal shows the burst occurring at 21:06:30.786 (66.7097 seconds from the time recording began).

The only anomaly noticed is a sudden decrease in tension strain recorded by SG24/7124 at 62.9 seconds.

FM STRAIN GAUGE DATA.

The first pass was digitized at 1000 samples per second (SPS) using an (sic) 100 HZ filter. Recording began at 24 seconds and continued through the burst. SG7 and SG13 were noisy and SG23 had bad calibration data. SG1, 3, 4, 5, 6, 7, 9, 11, 12, 14, 15, 17, 19, 20 and 21 show jumps in strain prior to burst. SG11 has a severe drop in tension strain at 58.4 seconds, then shows decreasing strain during the pressure ramp until burst.

The high frequency pass was digitized at 160,000 SPS using a 20,000 Hz filter. The IRIG time signal was used to sync the FM data to plus or minus 0.02 milliseconds and to reference it to the digital data time scale. SG7, 13 and 23 were not included for the reasons stated above. SG1, 10, 15 and 17 show large swings in strain at the burst, with a frequency of about 8000 Hz." End of ITT text.

IMPRESSIONS FROM THE QUICK-LOOK AND DIGITAL DATA ACQUISITION SYSTEM DATA.

Tank Pressure. The tank pressure functioned as described under the Pressurization Ramp paragraph.

For this test, the tank pressure sensor, PTANK/1901, was moved to the bottom of the tank where it would not be sensitive to interference from the line pressurization activity, which was observed on the previous tests. The profiles of PTANK/1901 and PVSOUT/1904 are now practically identical, and the irritating pressure spikes seen previously during the pressure salvos are gone.

Other Parameters. The performance of the other parameters was within normal limits; this was determined by a quick review of the graphs for items PHXIN/1902, PHXOUT/1900, PTRAIL/1903, THXIN/2100, TBALL/2211, TBSOUT/2210, TBSIN/2209, THXOUT/2101, TT1/2102, TT2/2103, TT3/2104, TT4/2105, TT5/2201, TT6/2202, TT7/2203, TT8/2204 and TT9/2205.

IMPRESSIONS FROM THE OVERPRESSURE SENSORS.

Bikini Gages. A Bikini gage is one piece of bond paper compressed between two metal plates containing different sized round holes. The gages are aligned so the paper is perpendicular

to the pressure source. Discrete pressure data can be obtained and is a function of the location of the damaged paper diaphragms. The approximate calibration is as follows for the indicated hole size using bond paper:

HOLE #	PSIG	SIZE
1	7.3	5/8
2	5.2	7/8
3	3.7	1-1/4
4	2.7	1-7/8
5	1.9	2-3/4
6	1.4	3-3/4
7	1.0	5-3/8

The results of this test broke some of the diaphragms and left others intact at the 6 and 14 foot diameters where the gages were deployed.

	2 o'clock	6 o'clock	10 o'clock
2 ft	-	-	-
6 ft	all torn	all torn	1 left
10 ft	-	-	-
14 ft	1,2,3 left	1,2,3 left	1,2 torn 3,4 left 5,6,7 torn

Comparing the above Bikini data with the data from the overpressure sensors (in parenthesis) shows an excellent agreement. The Bikini data is discrete in nature, and only gives information best expressed as "at least XX psig." The 6 ft diameter experienced at least 7.3 psig (12.02 psig) overpressure for the 2 o'clock and at least 7.3 psig (15.84 psig) overpressure for the 6 o'clock stations and at least 5.2 psig (17.68 psig) for the 10 o'clock stations. The 14 ft diameter experienced at least 2.7 psig (4.92 psig) overpressure for the 2 o'clock and 2.7 psig (2.53 psig) overpressure for the 6 o'clock stations. The 10 o'clock station experienced some inconsistencies, which are discussed below.

The inconsistencies can be seen if the pressures are drawn on a polar diagram. The 6 foot pressure line is biased away from the 10 o'clock leg (hole # 1 is left). Conversely, if the 14 foot pressure line is drawn, it is biased away from the 2 and 6 o'clock legs (holes 1, 2, 3 are left). Overlaying the two, the peculiar eccentricity becomes apparent. One would think the two pressure lines would at least be biased in the same direction.

A simple explanation would involve assuming the 1,2 hole locations torn on the 10 o'clock leg are incorrect. Perhaps they were torn by fragments. This speculation biases the low pressure isobar away from the 10 o'clock leg (1,2 assumed left; 3,4 left) and makes it consistent with the bias of the high pressure

isobar.

Piezoelectric Sensors.

OVERPRESSURE SENSORS. Ideally, each overpressure sensor located to measure pressure should respond to a passing pressure pulse with a characteristic graph. The graph's curve should have a prominent leading edge rising from a stable initial condition. The typical leading edge should polarize positively and rise to the curve's maximum peak pressure over a smooth and almost linear path. At the peak pressure, the curve should inflect, and, at this reversal, enter into a characteristic depolarization decay consisting of an almost linear but slightly distorted return to below the initial condition with an undershoot, more fully described below, representing rarefaction and the start of the refractory period.

More often than not, the linear decay should gradually change into a sluggish curve containing one prominent inflection, forcing the plot into the opposite direction, but staying below the initial condition. Eventually, the pressure rarefaction should deteriorate completely, and the plot should return smoothly to the initial condition, ending the refractory period.

Modulations and variations in behavior are caused by sensor placement (parallel or perpendicular to the flow direction), reflections, pressure wave distortions, time constants, frequency response, particulate impingement, insulation resistance, short circuits, open circuits and gas cloud geometry, etc.

For this test, 9 of the 11 sensors recorded exhibited profiles as described above. The exceptions were items 1809 and 1810, which were on the 10 o'clock leg at 2 and 6 feet.

The overpressure item numbers and peak values for the overpressure sensors are shown below along with the times in seconds (in parenthesis):

	2 ft	6 ft	10 ft	14 ft
	1801	1802	1803	1804
2	30.62 psig	12.02	7.57	4.92
o'clock	(66.710350)	(66.712563)	(66.714869)	(66.718351)
	1805	1806	1807	1808
6	46.52	15.84	5.78	2.53
o'clock	(66.710526)	(66.712306)	(66.715076)	(66.718419)
	1809	1810	1811	
10	17.68	3.54	4.62	----
o'clock	(66.710707)	(66.712544)	(66.715938)	----

To easily visualize when the pressure peak passed each station

and in what order, draw circles around each of the above 11 data groups and connect the circles in sequence according to time, starting with the 2 o'clock 2 ft sensor. Note the pressure peak always passed the stations in a 2, 6 and 10 o'clock order except for the 6 foot stations where the order was 6, 10 and 2 o'clock. This observation may indicate rupture activity favored the 2 and 6 o'clock positions more than the 10 o'clock position. Also, the pressure magnitudes are larger for the 2 and 6 o'clock positions.

The pressure magnitudes on the 2 and 6 o'clock legs behaved as expected. The pressure wave decreased in size as the wavefront passed each station.

But, the pressure magnitudes on the 10 o'clock leg behaved in a peculiar manner. The first station's response included a negative pressure, and the remaining two stations recorded increasing positive pressure! There was no 14 foot station. Note there was also peculiar behavior reported for the Bikini gages located on the 10 o'clock leg. The behavior of the 10 o'clock overpressure data includes pressure profiles with oscillatory tendencies for the first and third stations and the sluggish negative pressure at the first station. These behavioral characteristics are probably more attributable to actual performance than to errors in the instrumentation system. For example, simple signal polarity reversal can be easily achieved with the amplifier's polarity switch, but the steepness of the slope of the leading edge would not be changed, and we see in item 1809 a slowness in the rarefaction not seen in any other parameter (the adjacent station, 1810, is slightly slow compared to the others). Also, scattered about are small positive precursory artifacts on one-half the parameters (including 1809). If 1809 had been reversed, its artifact would be reversed, and it isn't. All of this notwithstanding, it still isn't too difficult to believe 1809 is a reversed channel, particularly when the graph is turned over and viewed through the paper from the reverse side (the rarefaction exhibits a slow leading edge, peak, linear decay, undershoot and a modulated recovery). The calibration polarity was checked to settle this controversy once and for all. The calibration polarity was the same as all the other channels. Therefore, the channel is not reversed. Looking at the profile again, the analyst suggested that the part of the graph that crosses 66.7108 seconds is the actual leading edge followed by a heavily modulated peak and linear decay. This observation is probably the speculation of choice as the wave arrival times for the other two 2 foot stations are within reasonable agreement with this graph's wave arrival time; and, more importantly, the slopes on the leading edges of the wavefronts recorded by items 1809 and 1810 are almost identical and are remarkably slower than the slopes on all the other overpressures. In other words, the heavy modulations seen on 1809 just about obscures the classic profile and makes it difficult to see that the slope crossing 66.7108 seconds is probably the passing of the desired wavefront.

The ITT data analyst, Richard M. Thomsen states:

"FM OVERPRESSURES. The overpressures were digitized at 160,000 samples per second with a 20,000 Hz filter. Each was digitized with the IRIG timing signal to sync the time scales to plus or minus 0.025 milliseconds (1 sigma). The time was then referenced to the start of the test with the burst occurring at 66.7097 seconds (SG24/7124) or 66.7093 (SG21/7121).

Two of the gauges were calibrated using the peak-to-peak AC calibration. Both had a bad R4 resistor calibration; on PV2/1802 it was the same as the R0 resistor calibration and on PV8/1808 it was maximum counts (Actually, cal resistors are not used; the calibrations are full scale voltage substitutions). The AC calibration peak-to-peak maximum and minimum counts over 20 cycles for these gauges was used with that of th PV1/1801 to determine the calibration coefficients.

Most of the overpressures show a small shift in pressure at the time of the burst, then one to nine milliseconds later the shock wave hits, with another following 0.5 to 4.5 milliseconds later. I cannot determine why there is a shift at the time of the burst, but on PV1 it is surprizingly strong. I would take this to be the shock wave except (1) it occurs too soon and (2) the shape is wrong. Usually the shock wave rises quite sharply and drops off more slowly, but this pulse does the opposite. I think the pulse at 66.7104 seconds is the one that travels out to the other gauges.

The secondary shock wave may be a reflection from the test stand (fragment panels). The wild swings in pressure may be particles hitting the gauges." End of ITT text.

DESCRIPTION OF THE EMBRITTLEMENT PROCEDURE. An undated ARDE embrittlement procedure was followed; only the girth area for a width of about 1 inch was embrittled. Embrittlement was inhibited, where required, with a maskant. Embrittlement was started at ____ hours on _____. The current level was ____ amperes. Seventy-two hours of embrittlement were completed at ____ hours on ____; the tank was immediately moved from the shop embrittlement area to the test site, instrumented, hooked up and tested at ____ hours on 18DEC86. The electrolyte was sulphuric acid; sodium arsenite was added as an enhancer.

ADMINISTRATIVE INFORMATION.

Revision Record. Initial Issue: 16JAN87. Revision A: 6MAY87:
overpressure information added.

Filename: testrv10

Distribution. ARDE, Steve Berko, Dave Gleich
PI, Dr. Pius Chih Hsu Chao
Aerospace Corp., Dr. Yen Pan
AFRPL, Jim Miller, Mike Dieckhoff, Dick Grove
MSgt Jim Day, John Marshall, Capt
Seidemann
ITT, Richard Thomsen, Dr. Tae-Woo Park
PAFB, Pete Tadie

Office of Primary Responsibility. USAF/AFRPL/TOAE/Edwards CA
93523.

E.7.3 Pressure and Strain Versus Time Plots

Tank pressure and selected fiber strain versus time graphs are presented on Figures E-81 to E-86. A 20,000 Hz filter frequency and sampling and plot rate of 160,000 SPS were used to adequately define the strain spikes. Strain gages were located in the apex and girth regions on the 23° and 81° fiber wraps as sketched on Figures E-87, E-88. Even numbered gages were oriented parallel to the fibers and odd numbered gages were perpendicular to the fibers.

E.7.4 Blast Overpressure Data

Blast overpressure summary data has been given in prior section E.7.2. Figures E-89 to E-92 show plots of overpressure versus time for some key sensors using a 20,000 Hz filter and 160,000 samples per second (SPS). The center of the test tank is zero feet and "clock" coordinates are used to define the angular location of the sensors. Maximum measured peak overpressures were 46.52 psig at 2 foot radius, decreasing to 7.57 psig at 10 foot radius, indicating severe personnel damage potential.

Fig. E-81

KEVLAR VESSEL TEST RV-10, P/N E4168, S/N 003, 18 DEC 86

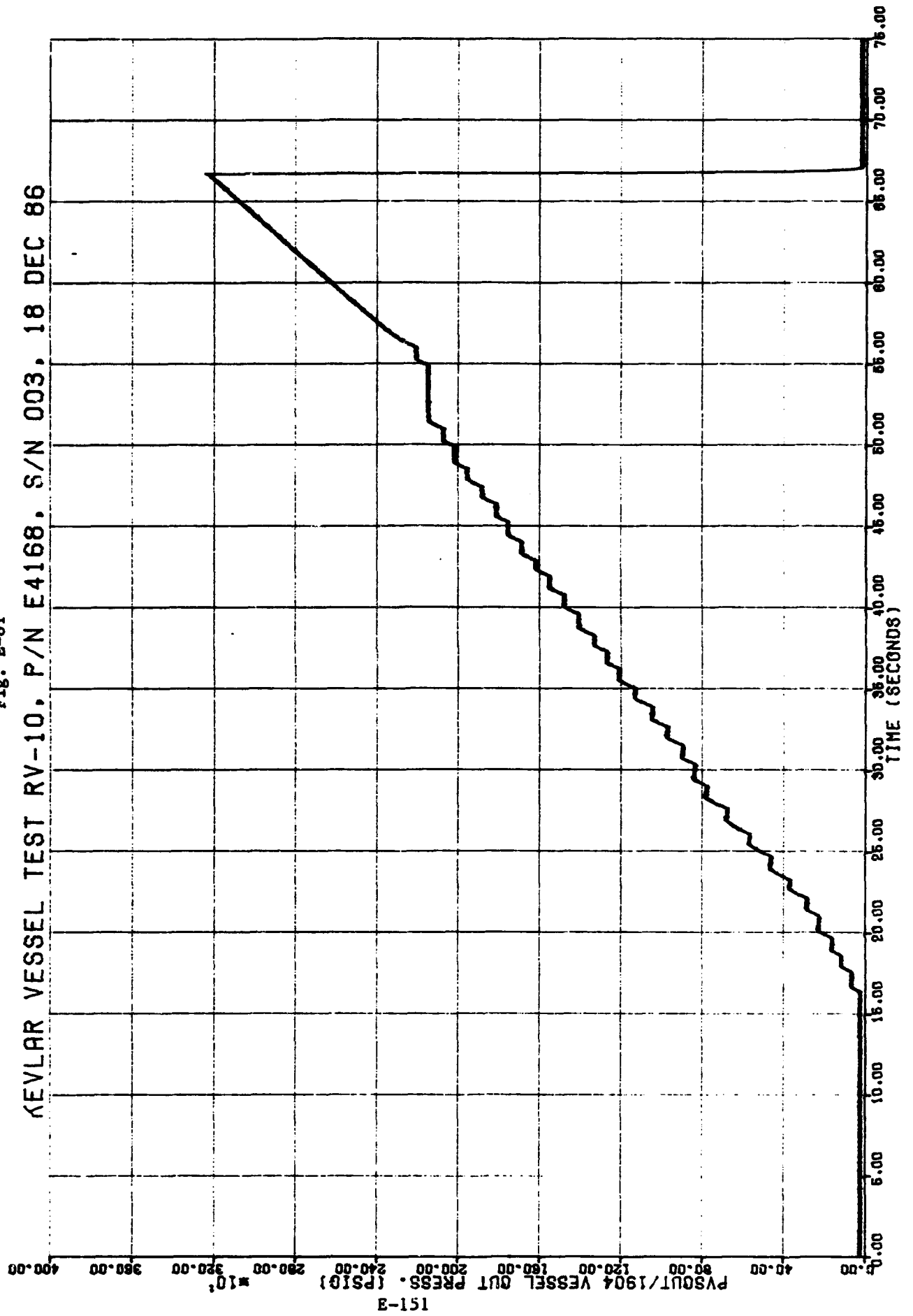


Fig. E-82

KEVLAR VESSEL TEST RV-10, P/N E4168, S/N 003, 18 DEC 86

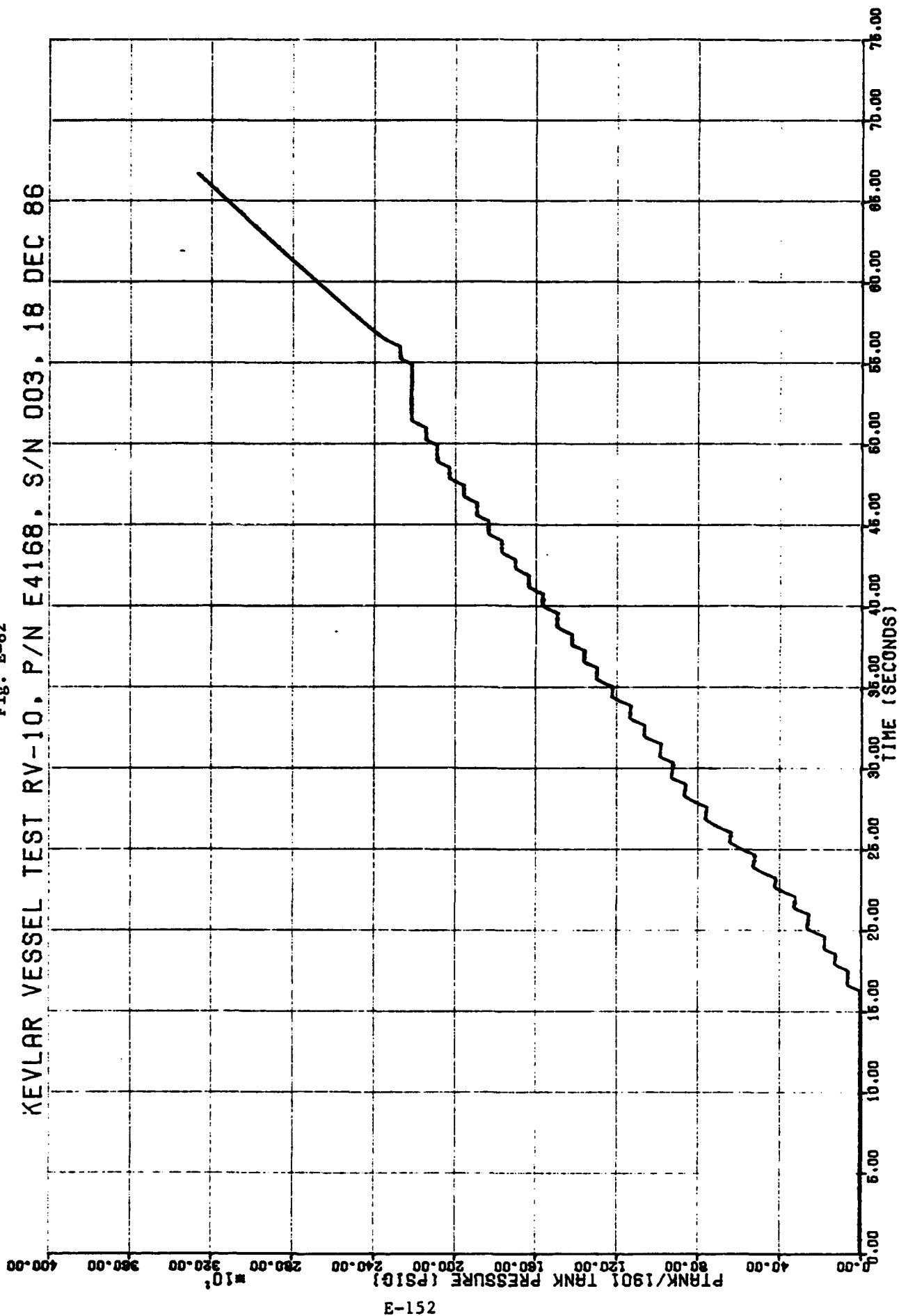


Fig. E-83

KEVLAR VESSEL TEST RV-10, P/N 4168, S/N 003, 18 DEC 86

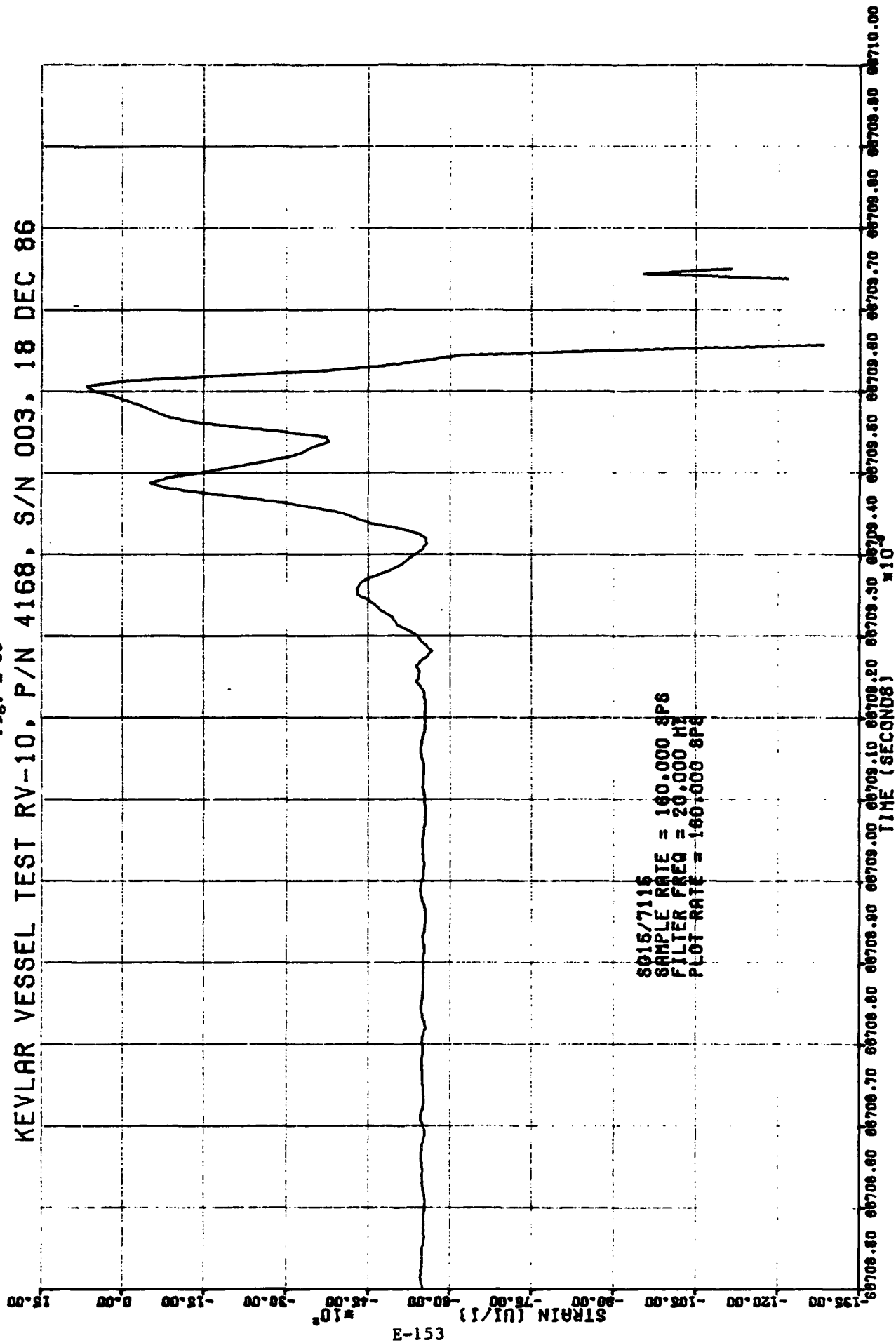


Fig. E-84

KEVLAR VESSEL TEST RV-10, P/N 4168, S/N 003, 18 DEC 86

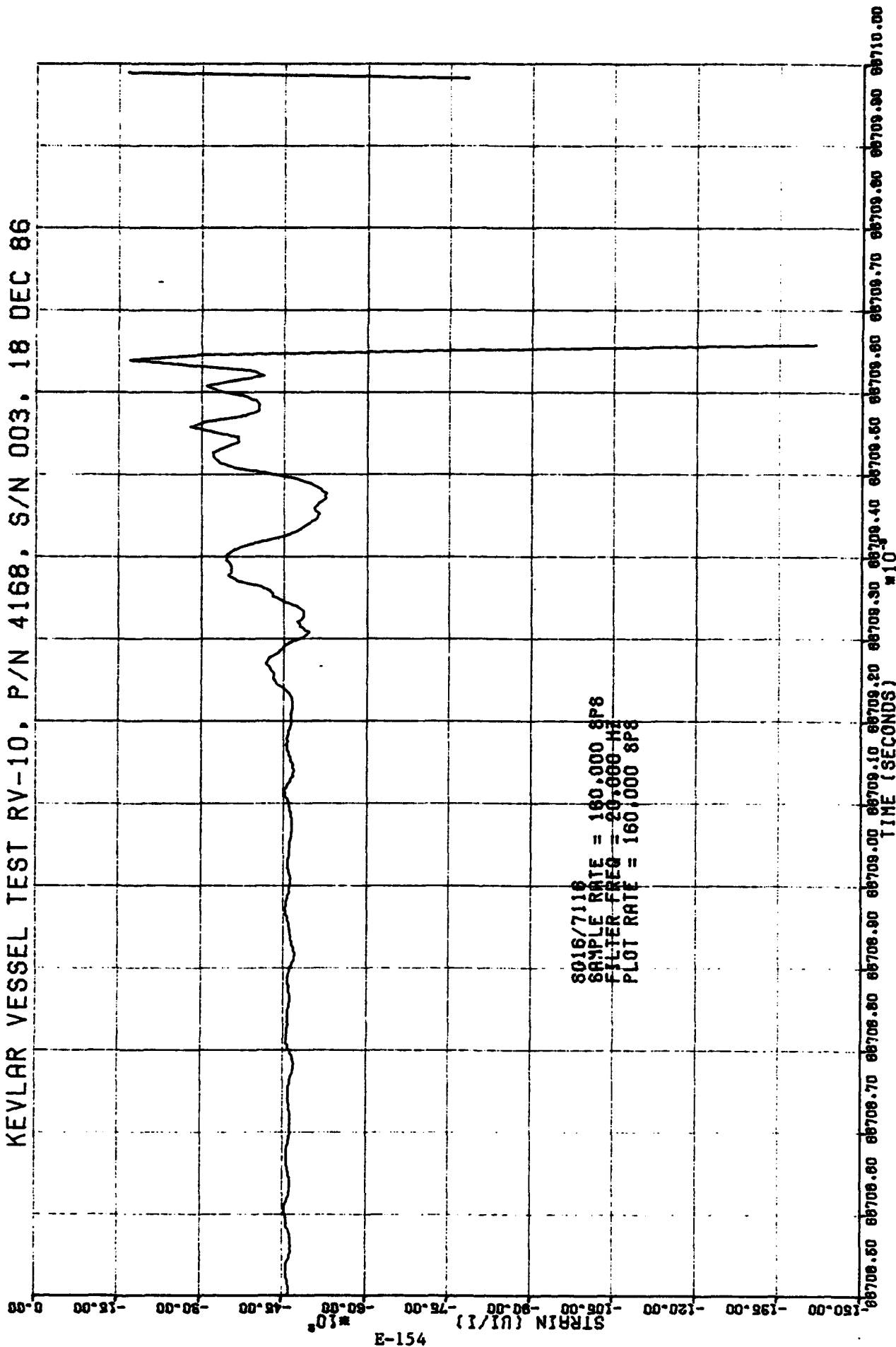


Fig. E-85

KEVLAR VESSEL TEST RV-10, P/N 4168, S/N 003, 18 DEC 86

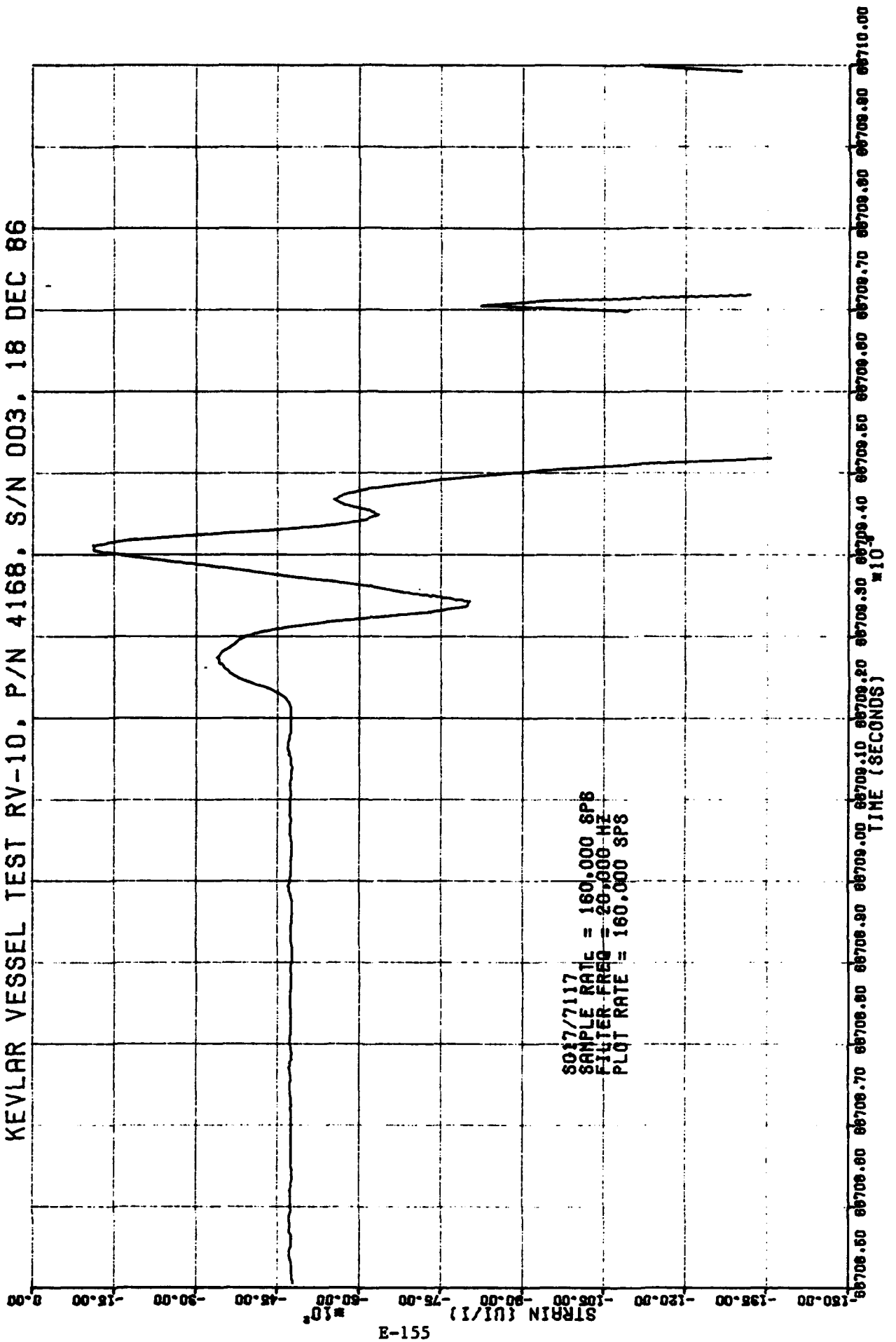
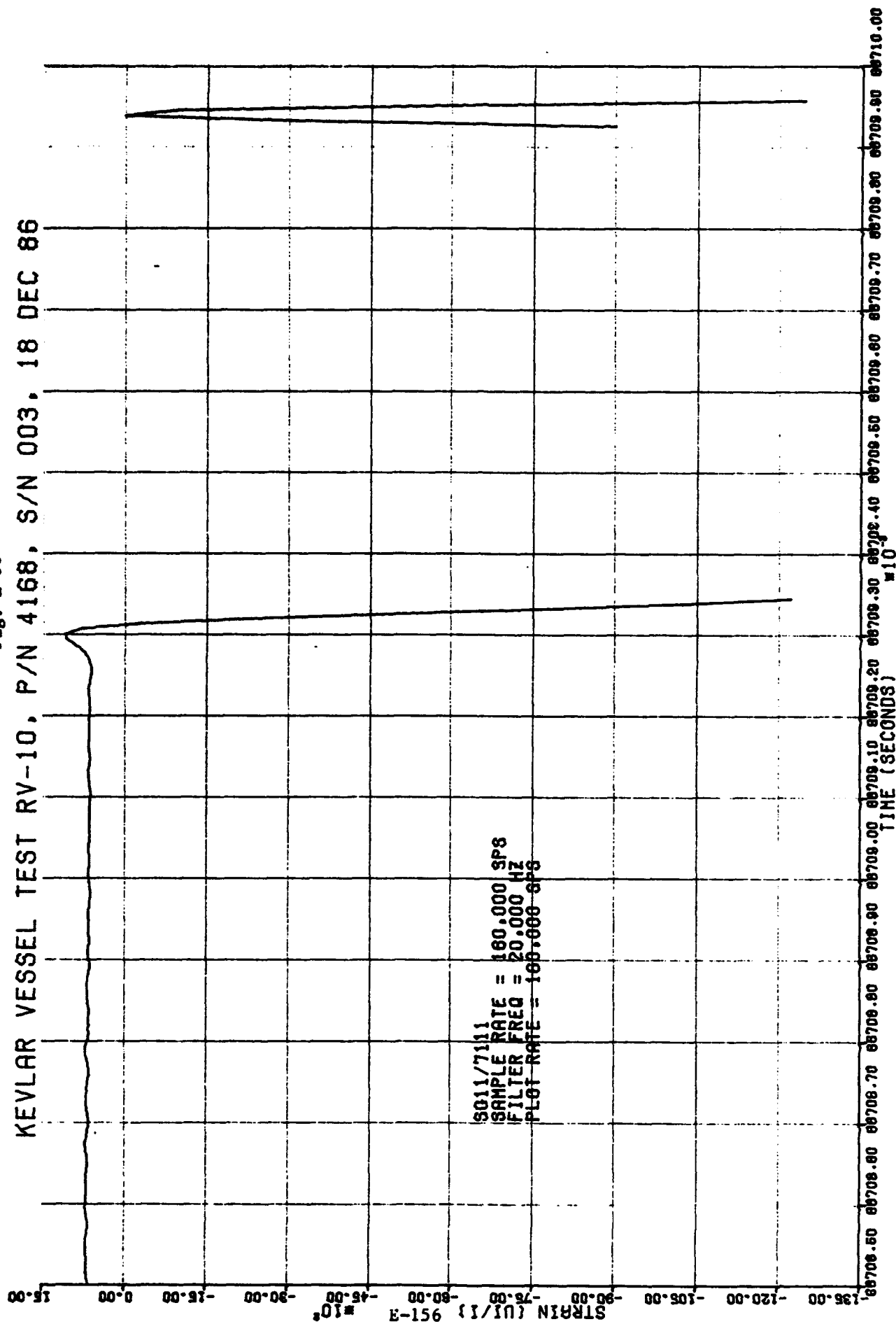


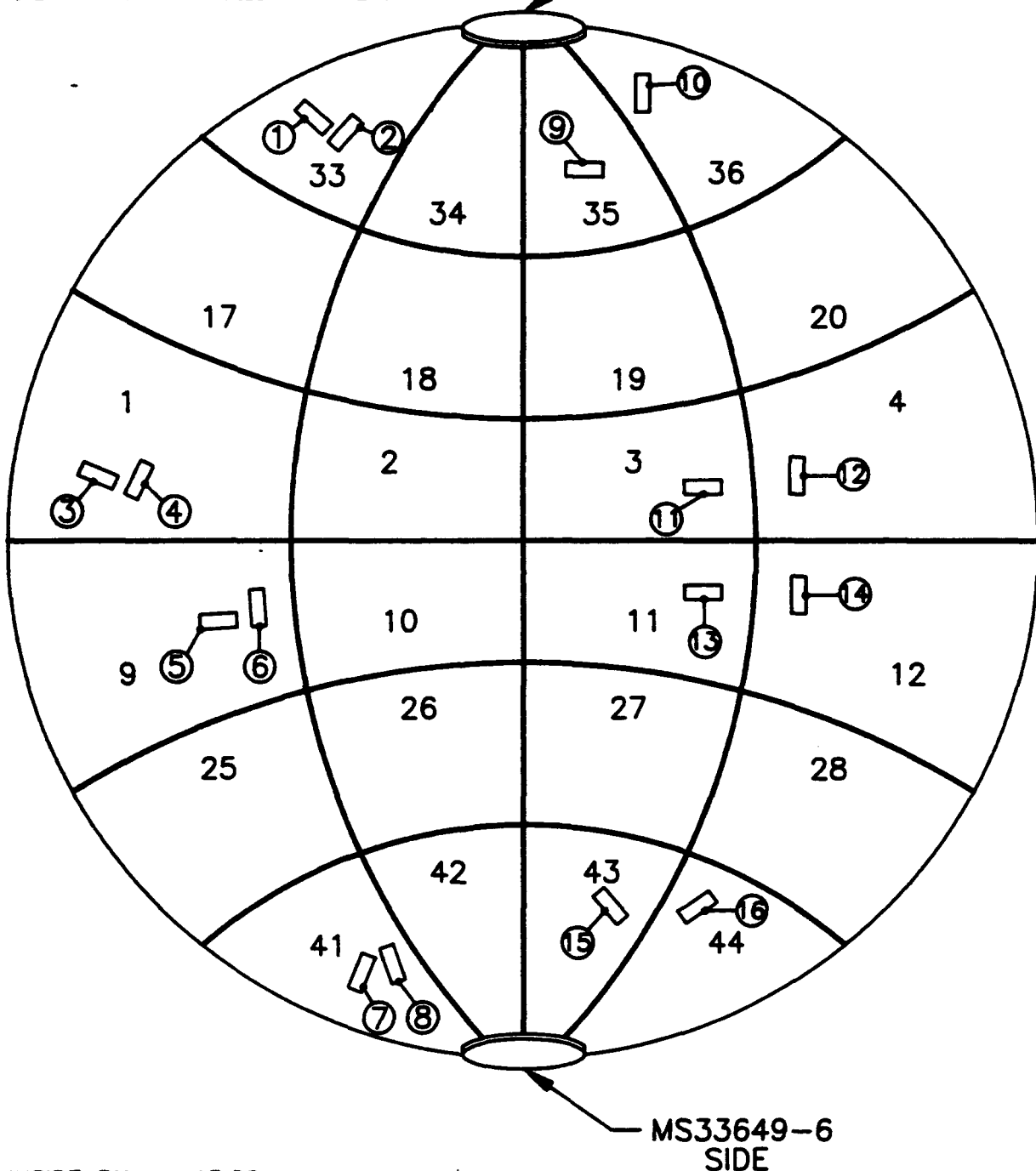
Fig. E-86

KEVLAR VESSEL TEST RV-10, P/N 4168, S/N 003, 18 DEC 86



1/2 KEVLAR THICKNESS

MS33649-8
SIDE



FIBER THICKNESS = .078 (1/2 THE THICKNESS OF RV-7 TEST)

 = STRAIN GAGE

Fig. E-87
E-157

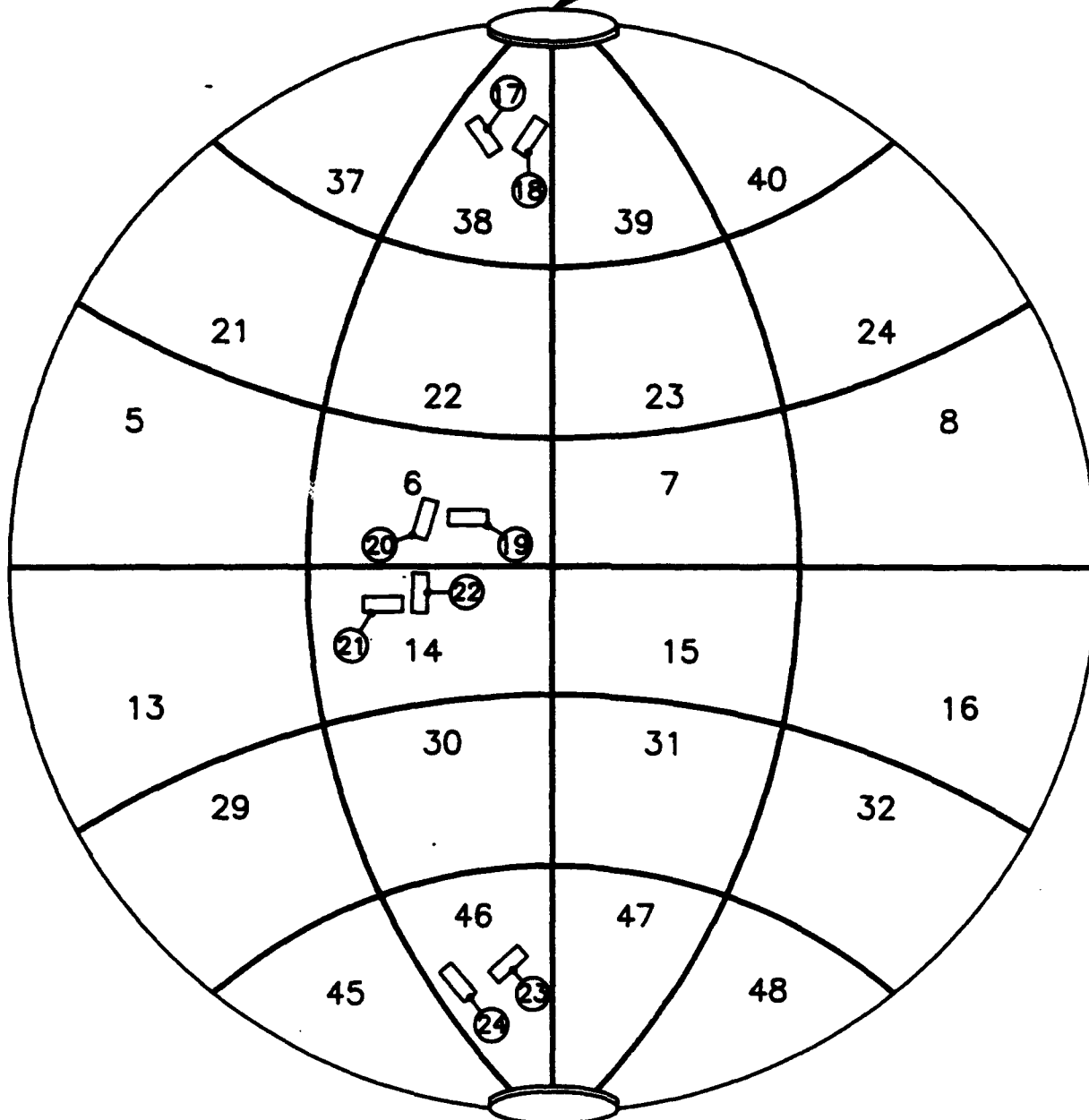
RV-10

P/N E4168 S/N 003 STRAIN GAGE LOCATIONS

1/2 KEVLAR THICKNESS

EVEN GAGES = PARALLEL TO FIBERS

MS33649-8
SIDE



MS33649-6
SIDE

#1-48-SECTOR #'S
①-②④=STRAIN GAGE #'S
□ — =STRAIN GAGE

Fig. E-88
E-158

Fig. E-89

KEVLAR VESSEL TEST RV-10, P/N 4168, S/N 003, 18 DEC 86

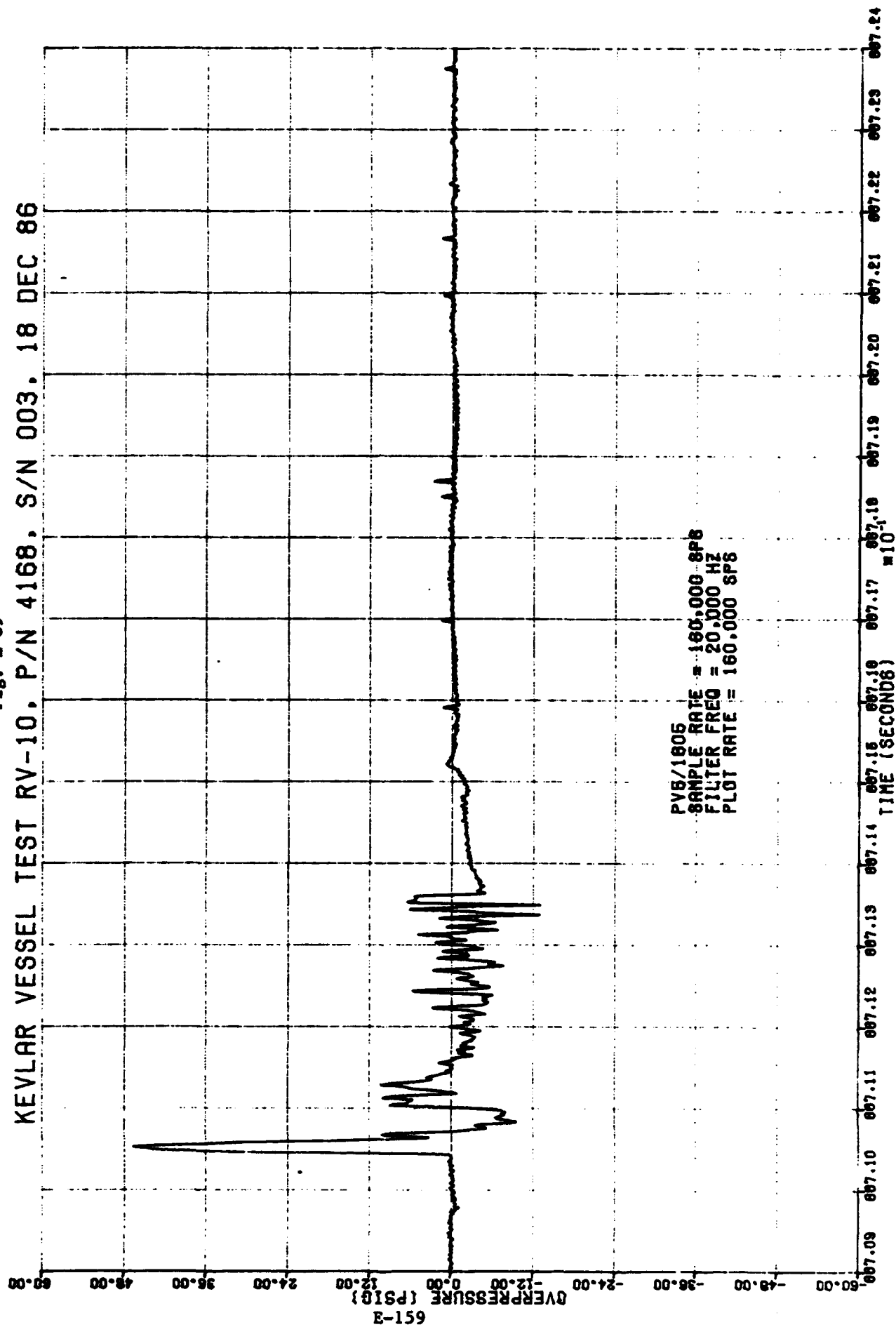


Fig. E-90

KEVLAR VESSEL TEST RV-10, P/N 4168, S/N 003, 18 DEC 86

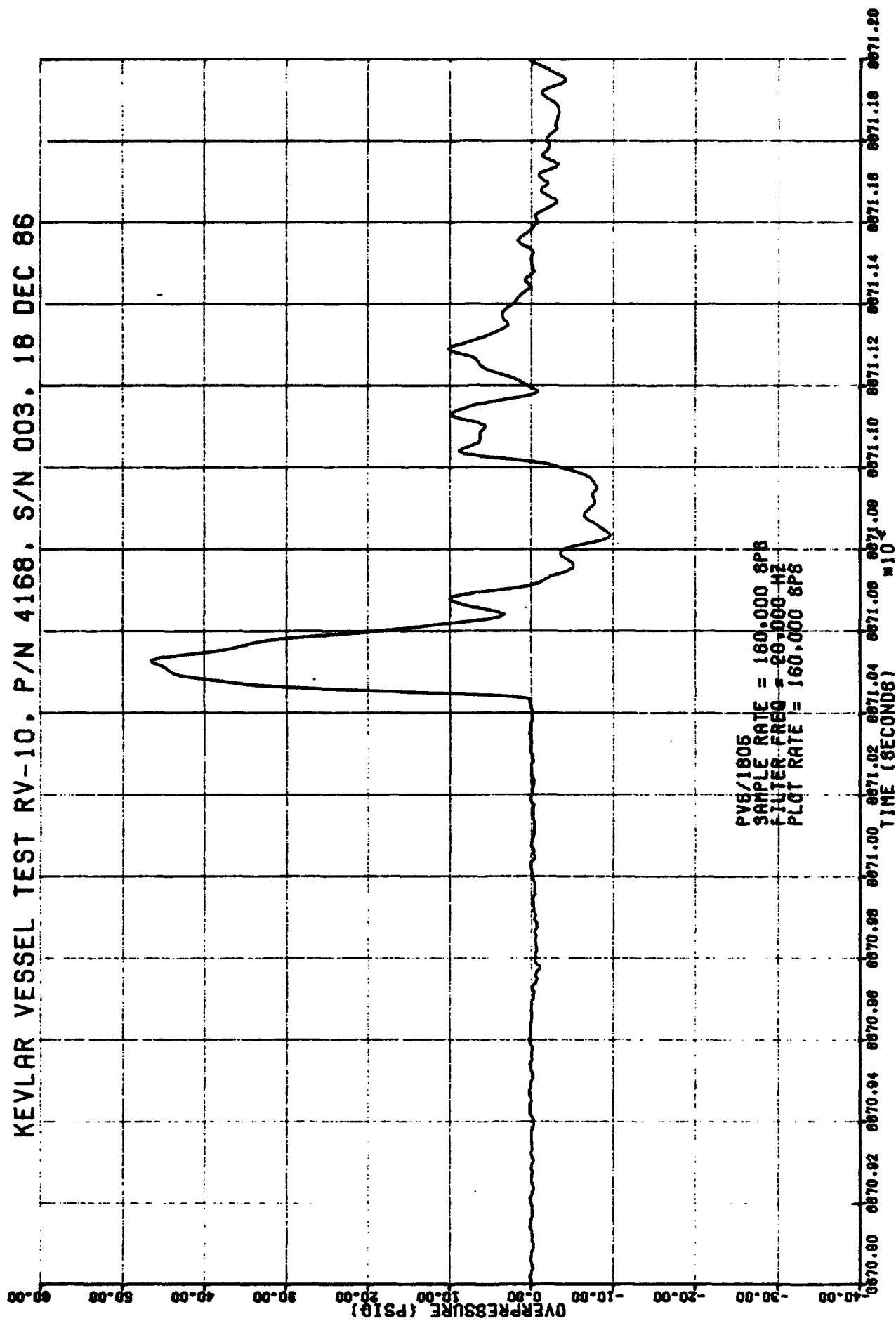


Fig. E-91

KEVLAR VESSEL TEST RV-10, P/N 4168, S/N 003, 18 DEC 86

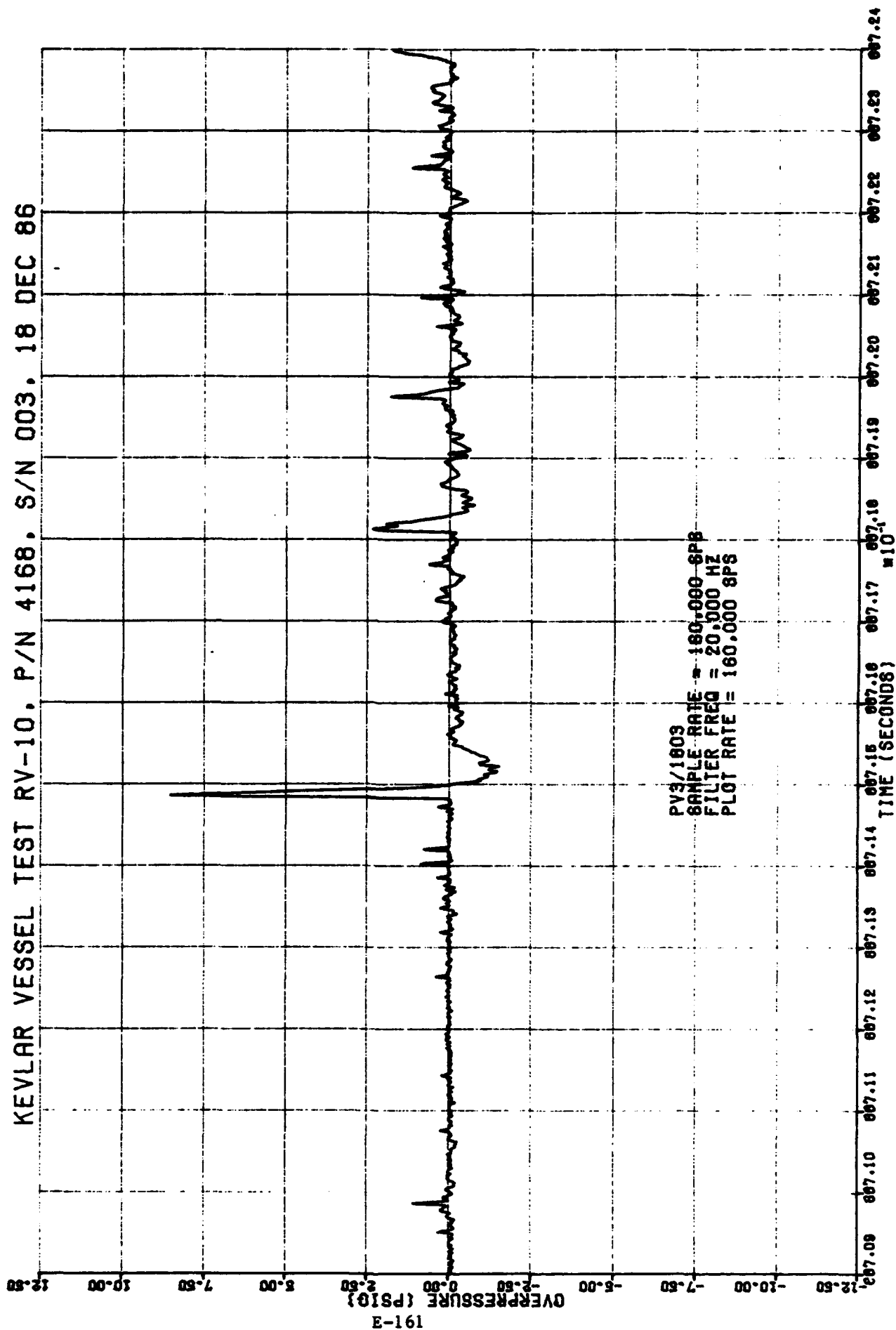
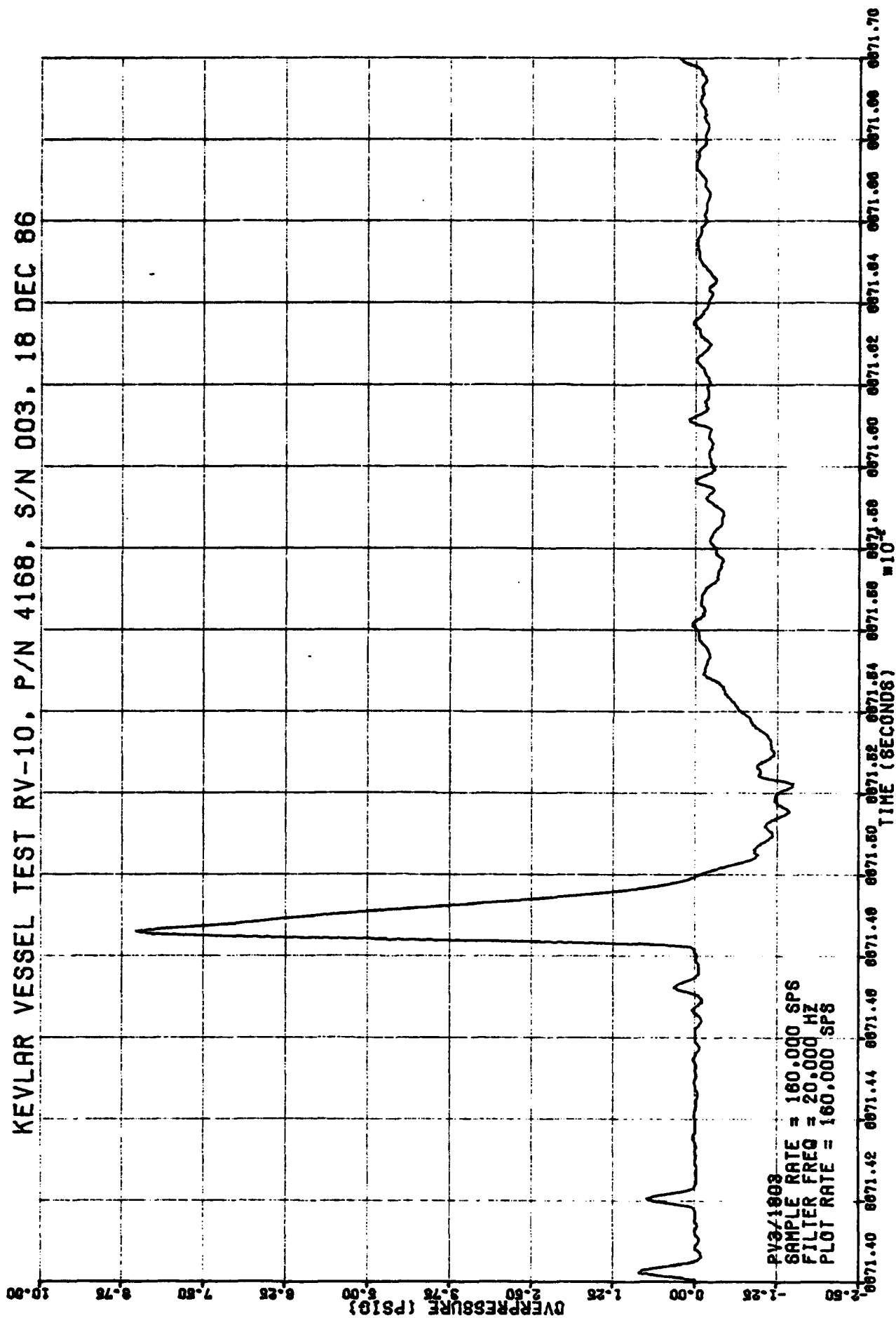


Fig. E-92

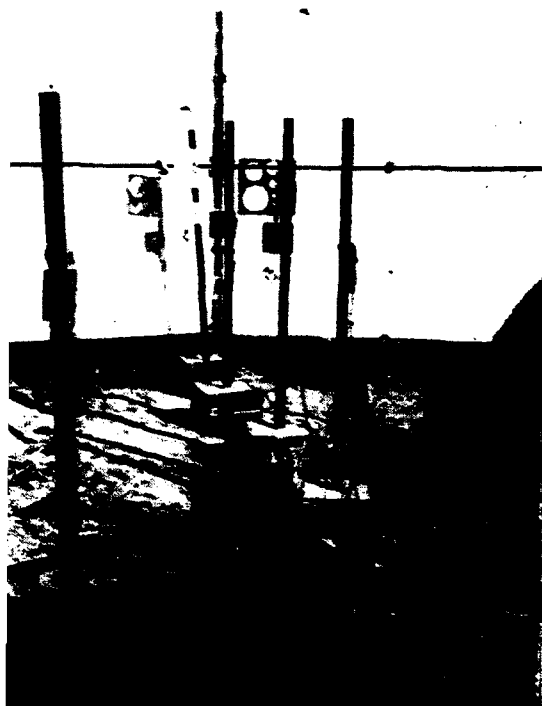


E.7.5 Post Test Inspection

The bikini gages and witness panels (used to collect fragments) were inspected. Some fragments penetrated the panels. The test stand was severely damaged. Test tank fragment locations in the test area were noted. Metal fragments were found as far as 500 feet from the test stand. This demonstrates the severe damage potential for total catastrophic failure of high pressure gas tanks. Photographs were taken.

Figures E-93, E-94 show photo views of the damaged test stand, Bikini gages, overpressure transducers, witness panels and fiber fragments. Photographs of typical metal fragments are given on Figures 2-13 and E-98. A typical fiber wrap fragment is shown on Figure E-95 and Figure E-96 shows a fragment embedded in a witness panel fifteen feet away from the test stand. Post test liner fragment debris are depicted on the photograph of Figure E-97.

Fig. E-93



TEST RV-10, POST TEST VIEW OF DAMAGED TEST
STAND, BIKINI GAUGES, OVERPRESSURE
TRANSDUCERS AND WITNESS PANELS



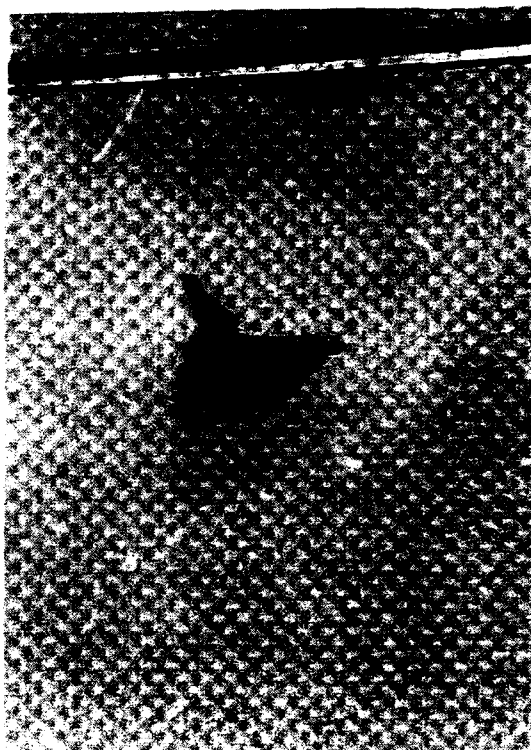
TEST RV-10, FIBER OVERWRAP FRAGMENT

Fig. E-94



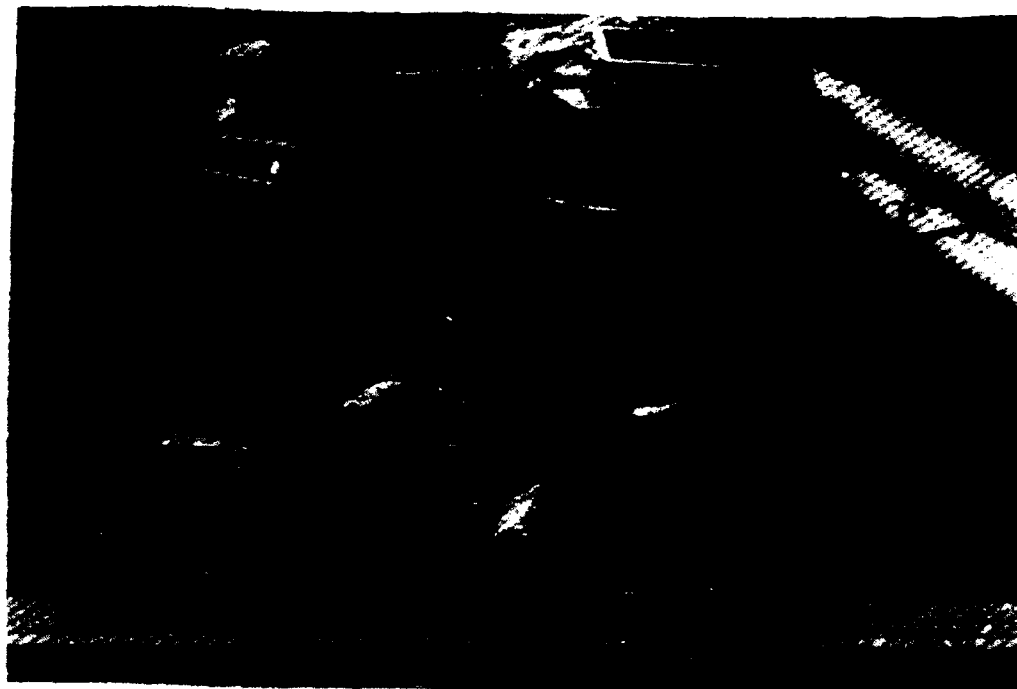
TEST RV-10, POST TEST CLOSE UP VIEW OF
DAMAGED TEST STAND AND FIBER OVERWRAP
FRAGMENTS

Fig.
E-95



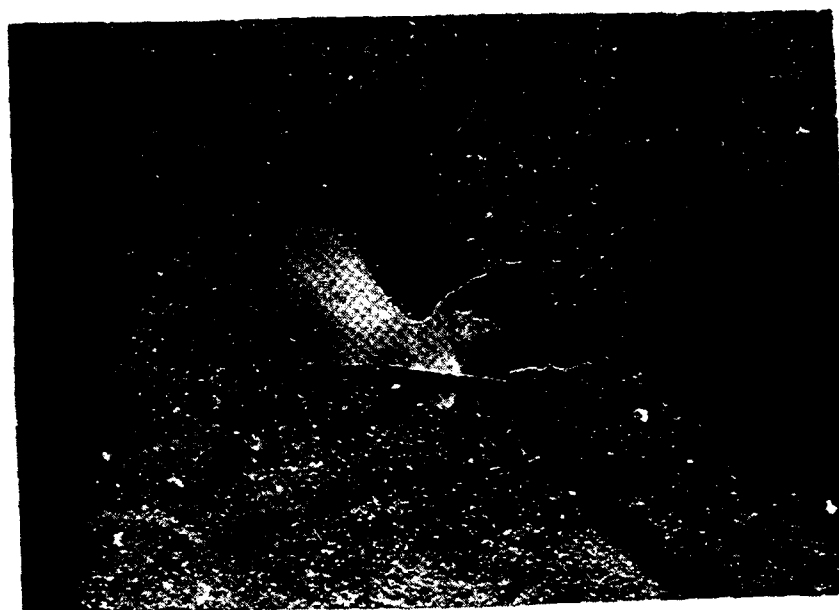
TEST RV-10, FRAGMENT EMBEDDED IN WITNESS PANEL

Fig. E-96



TEST RV-10, POST TEST LINER FRAGMENT DEBRIS

Fig. E-97



TEST RV-10, LINER FRAGMENT

Fig. E98

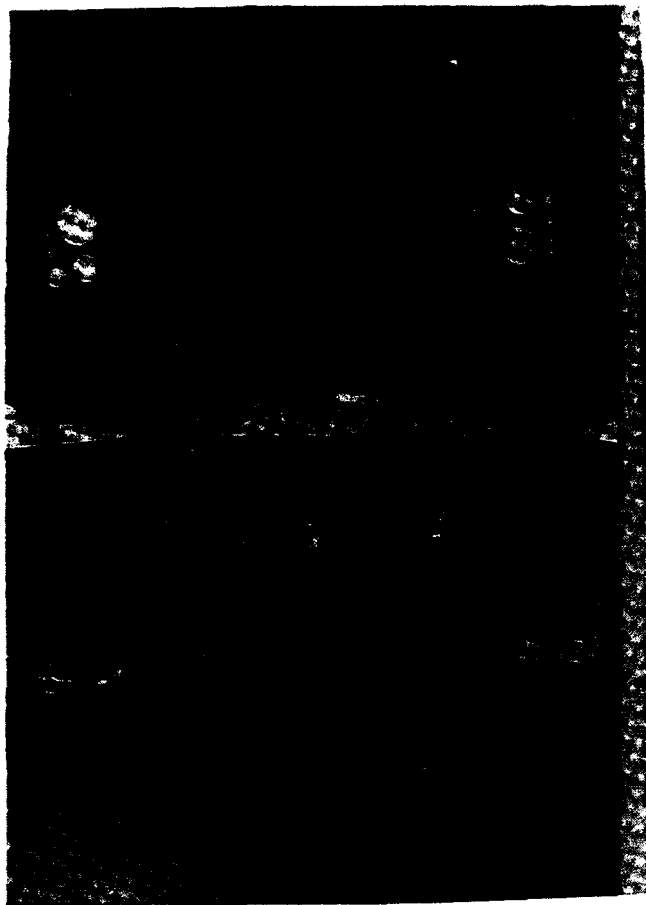
E.8 RV-11 Test (16" d)

E.8.1 Test Vessel Description

- P/N E4168, S/N 004 Kevlar Overwrapped 301 Cryo CRES Composite Sphere Kevlar Fiber (less resin) Average Thickness = .130 (83% of Baseline Thickness)
- Metal Thickness = .049
- Inside Radius = 7.64"
- Hydrogen Embrittlement Mode = Local Girth Weld Region
- Electrolyte Solution =
$$\frac{20 \text{ cc H}_2\text{SO}_4 + 980 \text{ cc Tap H}_2\text{O}}{1000 \text{ cc solution}}$$
- Solution Additive = 500 mg Sodium Arsenite
- Sensitize Liner Inside Surface (cold pickle)
- Charging Current Density = .006 amps/in² of surface to be embrittled
- Charging Time = 72 hours
- Hold Time Before Test = 2-1/2 hours
- Adcoat AC818T liquid maskant on areas not to be embrittled

Figure E-99 is a photograph of the instrumented composite tank mounted in the test stand. Strain gage, displacement gage, overpressure transducer and bikini gage instrumentation can be seen and readily identified in the photograph. Close up views of typical strain gage and thermocouple installations on the tank are shown in Figures E-100 and E-101.

Fig. E-99



TEST RV-11, COMPOSITE TANK MOUNTED IN TEST STAND

Fig. E-100



E-168 TEST RV-11, STRAIN GAGE INSTALLATION



TEST RV-11, STRAIN GAGE INSTALLATION

Fig. E-101

INSTRUMENTATION OBSERVATIONS (by Instr. Eng)

Rec'd 12/31/87
 Dist; DG KP RW
 J/N 42001

KEVLAR TREST 011, 10CT87. Project number 573000RV.

EXPERIMENTAL OBSERVATIONS.

Introduction. Vessel S/N 004, P/N E4168, was tested. It was a 16 inch diameter stainless steel sphere and had an 83% thinned Kevlar overwrap. The vessel was hydrogen embrittled for about 1/2 inch about the girth. It was tested in a vertical configuration. The tank pressure was increased with pressure pulses, held for a while, then ramped up until catastrophic rupture of the liner and overwrap rapidly occurred. Rupture of the tank generated a debris field with considerable content centered around the 6 o'clock leg; piezoelectric overpressure sensors and bikini gages registered a pressure bias toward the 2 o'clock leg.

Pressurization Ramp and Catastrophic Rupture. The vessel was pressurized with cool helium gas. Initially, the pressure was increased from ambient pressure to about 200 psig during a cool-down period, which took about 2 minutes. The tank was vented. The digital data system was started, and the tank pressure was kept at ambient pressure for 1.699764 seconds before pressure was increased with a series of 3 short pressure bursts, 1 long pressure burst, and another series of 7 short pressure bursts to the beginning of an 18.800094 second wide plateau, with a nominal value of 1401 psig. At the end of the pressure plateau, a steady ramp of pressure was started at 41.599230 seconds, and the high frequency data system was started. For the most part, the ramp of pressure was linear and progressed at a rate of 72.599637 psig/second (3274-2548 psig)/(65.099.592-55.099542 seconds). The tank ruptured, and the main tank pressure transducer, PTANK/1901, failed at 69.399858 seconds. Failure of the other tank parameters quickly followed.

at = 3600 psig,

PTANK/1401 = 3647 psig.

Post-run Inspection. Witness panels and acoustic emission technology were not used. Scattered about were remains of the vessel, including many metal fragments and loose Kevlar fibers. One Kevlar piece was found about 40 feet from the test site; it was a large piece - about 25% of the vessel. This large piece did not degenerate into loose fibers, and the resin was still intact. Some metal fragments were found about 500 feet from the site. A fragment distribution map was not made, but there seemed to be more pieces on the blacktop area near the adjacent C-D test complex and shop area, which is south-west of the test site, than in the desert area on the north side. Extensive damage to the vessel's instrumentation wiring and pressurization plumbing was observed. The two displacement sensors used on this test were not recovered. The sensors' 3" diameter reference disks were mounted on the vessel. The disks were aluminum, and these disks were found 200 feet from the test site. They were no longer flat, but had been bent around the sensors into a cup shape that even had the impression of the front of the sensor imbedded in the bottom of the cup. The sensor support arms were found near the

mechanics' shop, which is 500 ft from the site. The over pressure sensors are discussed elsewhere.

IMPRESSIONS FROM THE DIGITIZED FM DATA.

Strain Gages.

Strain Gage Locations. The strain gages were located IAW ARDE drawing dated 9/2/87 J/N 42001-0-14, page 1 & 2. The even strain gages are perpendicular to the wrap, and the odd strain gages are parallel to the wrap. The previous test, testrv10, had the opposite assignments.

Strain Gage Temperature. Not shown on this print are the thermocouple locations. Their locations are shown by the following sequence: Field #/Thermocouple #/Nearest strain gage pair. 33/1/1,2; 9/2/5,6; 41/3/7,8; 36/4/9,10; 4/5/11,12; 44/6/15,16 (from page 1); 38/7/17,18; 6/8/19,20; 46/9/23,24 (from page 2). The 9 thermocouple loci form a family of curves with almost identical profiles. Collectively, the gages measured temperature behavior over a span between 78 and 119 degrees F, approximately. However, each gage didn't change much. The typical temperature variation didn't exceed 5 F degrees and reached its minimum temperature at the bottom of a very slowly formed single depression near the center of the locus. Of the 9 gages, 5 (55.5%) were measuring temperatures grouped between 78 and 87 degrees F, and 4 (44.4%) were measuring temperatures grouped between 94 and 119 degrees. Six (66.6%) finished above their initial conditions; two (22.2%) finished below their initial conditions; and one (11.1%) finished very near its initial condition. All had a slight depression in the middle of the graph. The vessel's temperature behavior is considered to be within normal limits.

Performance Summary. There were 23 strain gages recorded. All were functioning, and, during the initial conditions, had much better than reasonable noise floors. The noise floors are discussed elsewhere under Noise Floors. All gages were destroyed as the tank ruptured.

Sign Convention. Positive strain gage polarity represents compression, and negative strain gage polarity represents tension.

Noise Floors. Except as noted elsewhere, the strain gage and other parameters' noise floors did not include major transverse or common-mode minus $L(di/dt)$ transients, artifacts, crosstalk, atmospherics, noticeable RFI, intermodulation, spurious parasites, or sibilants. However, latent noise or data manifestations may be obscured in some parameters, and digital signal processing may be needed for signal enhancement. In general, the data appeared to be unbiased, precise and accurate. SG08/7108 had the noisiest initial condition, but it only amounted to about 4.5% of the channel's range

(.4X3000=1200; (1200/26666) X100%=4.5%).

Performance Exceptions. Strain gage behavior was within normal limits with only two exceptions. SG17/7117 failed, at tank rupture, in the same manner as all the other strain gages; but it did not show any change in strain when all the others changed at 6.93870 milliseconds, which is the start of rupture. Its performance may be related to its location as it was located in field 38 at the top of the vessel, and it was parallel to the wrap. SG04/7104 failed almost immediately following the start of rupture.

Strain Direction. Disregarding the two exceptions, the remaining 21 gages exhibited similar activity at the start of rupture. The activity showed tension (negative polarity) strain by 19 of the gages and compression strain (positive polarity) by 2 of the gages before all gages are lost about 7 milliseconds after the start of rupture. The arithmetic mean of the net change in strain for the 19 gages indicating tension amounted to about 3800 microinches/inch; the minimum change was about 2300 microinches/inch for gage 10 and the maximum change was about 6000 for gage 8. For comparison, it is interesting to note that the strain gages for testrv9 also exhibited tension (negative) strain activity, and the changes were similar to those changes in testrv10, between 2100 and 7800 microinches/inch. The general trend of the tension strain is interesting and is discussed under Profile Categories. The net change in strain for the 2 gages registering compression was only +500 to +600 microinches/inch.

Dynamic Performance. All the loci had dynamic activity, which presented as complex, small magnitude, damped oscillations. Damping was completed within 5 milliseconds of the 7 millisecond period preceeding rupture. This behavior is considerably different than that which was observed in testrv10. In testrv10, "...most (strain gage) graphs progressed into a steady but short period of prominent undamped oscillation prior to rupture."

Profile Categories. Based on their shape, the loci can be fit, with considerable imagination, into either of two categories: the slope-plateau (SP) category or the plateau-slope-plateau (PSP) category. Of the 19 gages sensing tension strain, 7 (36%) were SP and 12 (63%) were PSP. This behavior is different than that which was observed in testrv10. In testrv10, the strain gage "...graphs enter into oscillation with a small compression excursion; they reverse direction and continue with a tension ramp, with modulations by the oscillation, to burst." Although there were oscillations in testrv11, they were damped and not nearly as great as in testrv10.

Strain Polarization. Of the 19 gages, 11 are odd numbered (parallel with the wrap) and 8 are even numbered (perpendicular with the wrap). Of the 11 parallel gages, 8 (72%) polarize negatively at the start of rupture, and only 3 (27%) polarize positively. Of the 8 perpendicular gages, only 3 (37.5%)

polarize negatively at the start of rupture, but 5 (62.5%) polarize positively. At the start of rupture, this makes a total of 11 (58%) polarizing negatively and 8 (42%) polarizing positively. At rupture, 7 milliseconds later, only 7 (37%) polarize negatively, and 12 (63%) polarize positively. Speculations on the causes of this behavior are reserved. By comparison, testrv9 had 66% of the gages registering tension, which is slightly more than the 58% registering tension for testrv11 at the start of rupture.

Statistical Analysis. Valid speculations about strain gage behavior may involve biserial correlation of certain dichotomies (positive or negative polarization) to assess their associations (with wrap direction, etc.). For truly dichotomous distributions, the phi coefficient can be used. Because some of these dichotomous variables are really continuous (the magnitude or duration of polarization, and the degree of wrap thickness, location & direction, etc.) and normally distributed, tetrachoric correlation may be involved. An expert statistician should be approached with a clear statement of which variables and associations are important if valid conclusions about some of these data are to be obtained. An accurate evaluation of which variables are really dichotomies and which are proportionally continuous would also have to be prepared and passed to the statistician.

Data Analyst's Comments. ITT, Richard M. Thomsen, states:

"Digital Data.

The data for SG24/7124 shows the burst occurring at 69.390 seconds (20:43:27.160 IRIG). The spike occurring at 69.408 seconds is only one data point and I would question its validity. The strain gauge also shows a large shift at 54 seconds.

FM Low Frequency Data.

Four digitizing passes were done. Two Strain gauges on each of the first three passes did not register, so the fourth picked these up. All values should be aligned to the nearest tenth of a millisecond. (For the first pass,) data was digitized at 1000 samples per second using a 100 Hz filter. SG03/7103 shows three spikes several seconds before the burst. I have seen these same type spikes on unrelated digitized FM data and would probably say they are tape dropouts. SG04/7104 shows non-pressure related stress changes starting at 64 seconds. SG08/7108 has several shifts in strain. SG10/7110 has 60 Hz hum. So does SG17/7117, DP01/8001 and DP02/8002. SG12/7112, SG14/7114, SG16/7116, and DP02/8002 have sudden increases prior to the burst. SG15/7115 has an unusual downward, decreasing spike prior to the burst. SG20/7120 has stress changes similiar to those of SG04/7104 prior to burst.

FM High Frequency Strain and Displacement.

The sample rate restriction on the Lark drive limited the frequency response to 16 kHz. The roll-off characteristic of the Datum 1 kHz filters may be slow enough that higher frequencies come through. In fact, SG07/7101 shows a frequency of 21 kHz for a millisecond at 69.392 seconds.

The start of the burst occurred at 69.387 seconds (20:43:27.15743 IRI6) and ended with sharp changes in strain and displacement about 7.5 milliseconds later. Each item was aligned using the IRI6 signal to the nearest hundredth of a millisecond."

Displacement Sensors.

General Behavior. Both displacement sensors worked very well, and they remained noise free. DP2/8002 started with an initial condition near 220 mils, went positive to near 238 mils, and then dropped to about 230 mils. DP1/8001 made a much larger excursion. It started with an initial condition near 217 mils and finally ended up near 112 mils. In other words, the gap sensed by DP2 had a net increase of about 10 mils, and the gap sensed by DP1 had a net decrease of about 105 mils. The start and end of the displacement sensors' activity correlates well with the strain gages.

The expansion of the vessel is best represented by DP12, Total (vessel horizontal diameter) Displacement, which is the sum of the two (girth) displacement sensors. The sum reflects both graphs' initial conditions, slopes, inflections and plateaus, etc., and must be used for correct interpretation of the total vessel displacement performance.

Noted in the loci sum is moderate smoothing of the dynamic constituents seen more prominently in the individual graphs. For example, the 250 Hz modulations are noticeably suppressed, and phase distortion is evident during the 3000 Hz modulations. Furthermore, the mean slope characterizing the prevailing decreasing trend increases about 31% over the mean slope seen in DP01/8001.

The dynamic variations seen by both displacement sensors between 69.3930 and 69.3940 seconds are phased in such a manner that the sum displays suppressed magnitude variations. The mean slope increases just prior to the onset of the variations and then decreases after the variation. The variation is probably valid, as it is about 3/4 the way through the 7 millisecond period of primary interest. Also, there is nothing to indicate the apparent mean slope changes are invalid. Destruction of the vessel is obvious and agrees with the PTANK/1901 graph.

Calibration Information. The zero and 0.250" calibration cuts are shown on the page just prior to the digital printout of the run data. The polarity is positive for the 0.250" calibration displacement. After the calibration, the sensors were not moved, and their initial conditions remain, as expected, near 0.250".

Description of Expected Performance. As the tank expands, the gaps get less, and the readings should decrease. The general trend for testrv9, and for testrv11, followed this logic, except for the variations discussed. The general trends of the data from the two sensors will not necessarily match.

Description of Actual Performance. For testrv11, DP01/8001 had a prevailing decreasing trend in the form of a negative slope with prominent modulations. The slope is slowly modulated by a 250 Hz damped oscillation, which deteriorates after several cycles. Riding on top of this carrier is another damped oscillation, seen more clearly by the other position sensor, that is oscillating near 3000 Hz and damps out after 6 cycles or 0.002 seconds.

Surprisingly, DP02/8002 increased slightly, after a very slight delay which contained no major modulations, and stayed above its initial condition in a rough plateau containing the heavily damped 3000 Hz frequency.

The frequency oscillations seen on the two graphs may be mutually related, but they are not necessarily in phase. The same frequency of oscillation is seen on both displacement sensors, and it is about 3000 Hz (3 cycles/0.001 seconds). This frequency may also be a component in the strain gage data, but it isn't immediately obvious on the graphs because of the complex nature of the frequency domain. Both displacement gages were lost when the tank ruptured and were not recovered, although the reference disks were found as discussed elsewhere. Not confirmed is the speculation DP01/8001 was located on the tank half nearest the black top. The still photos show excessive debris in this debris field, and this may be related to the fact DP01/8001 had a slope profile while DP02/8002 had a plateau profile.

IMPRESSIONS FROM THE QUICK-LOOK AND DIGITAL DATA ACQUISITION SYSTEM DATA.

Tank Pressure. PTANK/1901 was located on the top of the tank in the vent line. PVSOUT/1904 was also in the vent line, but it was located at the valve box about 15 feet from the tank. PTANK/1901 functioned as described under the Pressurization Ramp... paragraph.

The locations of the transducers was the same as test 10.

PVSOUT/1904 had readings that started about 10% higher than PTANK/1901, but changed quickly to about 20% lower for the remainder of the test. This graph's inspissated locus is due to a small amount of continuous noise, and there are numerous small magnitude bipolar spikes appearing about 1.2 seconds apart throughout the graph; the noise origins were not investigated as they do not appear to be insidious. The noise is probably not associated with the test item; it is most likely a systemic artifact recorded during data acquisition, although there is a small possibility it may be related to the data reduction process. The phase performance of PVSOUT/1904 was slightly

behind PTANK/1901 which is consistent with the distant location of PVSOUT/1904. The general trends of both graphs agree, however.

It is interesting to note that when the tank failed, the data from the two transducers went in opposite directions. When the transducer at the tank was torn from the instrumentation line, its data abruptly went to positive full-scale overload following a very rapid rate of change. The PVSOUT/1904 transducer in the box wasn't damaged and reflects legitimate pressure loss in the line as it smoothly underwent a rate of change and progressed towards zero where it made a slight undershoot, inflected and quickly recovered without oscillation to its initial condition, which was slightly above the abscissa. This behavior is easily seen in the expanded graphs, but doesn't have much significance except to confirm the vessel's clinical performance and to verify the sensor locations.

SG24.

General Comments. The performance of SG24 is very interesting. This strain gage duplicated the tank pressure behavior, PTANK/1901, but there were some deviations particularly during the final pressurizing ramp prior to failure.

Phase Behavior and Frequency Response. Noted also is the phase behavior; the two graphs were very close together in the time domain although the sharp corners seen in the pressure graph were rounded in the strain gage graph and much less defined.

Behavior During the Final Pressure Ramp. The deviation during the final pressure ramp manifests itself in gross magnitude and slope changes. Several abrupt magnitude shifts are obvious. More obscure are the subtle changes in slope between the magnitude shifts. With a straight edge, follow the four or five slopes and note how the slopes get gradually less and less as the vessel weakens. The abrupt magnitude and slope behavior might be used in an alarm circuit to warn of impending failure of overwrapped vessels instead of more complicated non destructive methods such as acoustic emission. Unfortunately not all gages show this behavioral pattern. The pattern may be due to gage debonding, but it probably represents a weakening vessel.

Graph Expansion at Rupture. The 0 to 75 second plot was blown up between 69 and 70.5 seconds for a better look at the rupture point. A very small glitch was seen, and another graph blow up was made between 693 and 694.5E-1 seconds to look at the glitch. This graph has a locus progressing from a noise free initial condition to tension strain (negative polarity). The progression follows one smooth cycle of a 54.64 Hz oscillation distressed by the glitch seen as one negative paroxysm followed by an insipid minor variation. The glitch's magnitude is about 264 microinches/inch and represents only 0.099% of the full-scale range (26666 microinches/inch). As ITT indicated, it is only one data point wide and probably isn't significant although it occurs

at the point of maximum interest.

Other Parameters. The performance of the other parameters was within normal limits; this was determined by a quick review of the graphs for items PHXIN/1902, PHXOUT/1900, PTRAIL/1903, THXIN/2100, TBALL/2211, TBSOUT/2210, TBSIN/2209, THXOUT/2101, TT1/2102, TT2/2103, TT3/2104, TT4/2105, TT5/2201, TT6/2202, TT7/2203, TT8/2204 and TT9/2205. The time code parameter, IRIG/3808, recorded satisfactorily.

IMPRESSIONS FROM THE OVERPRESSURE SENSORS.

Bikini Gages. A Bikini gage is one piece of bond paper compressed between two metal plates containing different sized round holes. The gages are aligned so the paper is perpendicular to the pressure source. Discrete pressure data can be obtained and is a function of the location of the damaged paper diaphragms. The approximate calibration is as follows for the indicated hole size using bond paper:

	HOLE #	PSIG	SIZE
	1	7.3	5/8
	2	5.2	7/8
	3	3.7	1-1/4
	4	2.7	1-7/8
	5	1.9	2-3/4
	6	1.4	3-3/4
	7	1.0	5-3/8
	2 o'clock	6 o'clock	10 o'clock
2'	all gone	all gone*	all gone
6'	all gone*	all gone	all gone*
10'	all gone	1 left	1,2,3 left
14'	1,2,3,4 left	1,2,3 left	1,2,3,4 left

* denotes those locations whose supports were tipped over by the overpressure blast.

From the above data, the 2 o'clock leg experienced greater than 7.3 psig at the 2, 6 & 10' locations and less than 2.7 psig at the 14' location. The 6 o'clock leg experienced greater than 7.3 psig at the 2 & 6' locations; less than 7.3 psig at the 10' location; and less than 3.7 psig at the 14' location. The 10 o'clock leg experienced greater than 7.3 psig at the 2 & 6 o'clock locations; less than 3.7 psig at the 10' location; and less than 2.7 psig at the 14' location.

The pressure bias for the 14' pressure data favors the 6 o'clock leg, and the bias for the 10' pressure data favors the 2 o'clock

leg and, to a lesser degree, the 6 o'clock leg. These biases indicate there was an unequal pressure expansion at rupture, and the expansion favored the 6 and 2 o'clock positions. The 6 o'clock leg is the leg pointing towards the blacktop. This finding is consistent with the density and distribution of the debris field, discussed elsewhere.

Reconciliation of the bikini overpressures and bias observations using the results from the piezoelectric overpressure sensors reveals the overpressures were higher at four of the stations than the bikini gages indicated. The bias observations are similar - both conclude there was excessive pressure near the 2 o'clock leg. The actual values measured were 4.28, 4.08, 7.83 & 15.50 psig for the preceding 2.7, 3.7, 3.7 & 2.7 psig bikini entries in the comments following the bikini data.

It is not too suprising the bikini gages don't match the piezoelectric sensors. The calibrations listed above are not traceable. In fact, the source of calibration is unknown. The calibrations will vary depending on the type of paper (bond, vellum, carbon, rag, linen, etc.) and its thickness and water content, etc.

Piezoelectric Sensors. Ideally, each overpressure sensor located to measure pressure should respond to a passing pressure pulse with a characteristic graph. The graph's curve should have a prominent leading edge rising from a stable initial condition. The typical leading edge should polarize positively and rise to the curve's maximum peak pressure over a smooth and almost linear path. At the peak pressure, the curve should inflect, and, at this reversal, enter into a characteristic depolarization decay consisting of an almost linear component followed by a distorted exponential component that returns to below the initial condition with an undershoot, more fully described below, representing rarefaction and the start of the refractory period.

More often than not, the linear decay should gradually change into a sluggish curve containing one prominent inflection, forcing the plot into the opposite direction, but staying below the initial condition. Eventually, the pressure rarefaction should deteriorate completely, and the plot should return smoothly to the initial condition, ending the refractory period.

Modulations and variations in behavior are caused by sensor placement (parallel or perpendicular to the flow direction), reflections, pressure wave distortions, time constants, frequency response, particulate impingement, insulation resistance, short circuits, open circuits and gas cloud geometry, etc.

For this test, 12 sensors were recorded. Two sensor circuits were defective because of noise and were not evaluated, and they are discussed below (1803 & 1807). Of the 10 operating sensors, all exhibited profiles as described above with the following variations. Three had prominent peak distortion (1804, 1805 & 1812); four finished above their initial conditions (1802, 1804,

1809 & 1811); three had a small amount of preliminary undershoot (1801, 1805 & 1806); four had moderate amounts of noise throughout the experiment (1802, 1805, 1806, 1808 & 1812); one had a moderate amount of noise, but the noise appeared only after the pressure pulse occurred (1809); one had a non-exponential decay (1801); and one had reduced rise time (1801). Except for the noise, these variations are, for the most part, within normal limits and can be justified as valid data.

Shown in the table below are the:

Overpressure sensor item number
Peak values, psig
Time in seconds (in parenthesis)
Delta time, same leg, in seconds [in brackets]
Velocity, same leg, in ft/sec {in braces}

Note, the pressure values shown are the maximum pressures experienced, which is not necessarily the first peak measured; three items measured smaller peaks prior to the maximum peak; they were 1804 (0.99 psig @ 69.394756), 1810 (0.56 psig @ 69.394819) and 1811 (1.39 psig @ 69.394795):

	2 ft	6 ft	10 ft	14 ft
	1801	1802	1803	1804
2	123.33	15.65	----	4.28
o'clock	(69.395106)	(69.396294)	----	(69.403787)
	[0.001188]	[0.007493]	----	----
	{3367}	{1067}	----	----
	1805	1806	1807	1808
6	37.03	22.11	----	4.08
o'clock	(69.394800)	(69.396050)	----	(69.403174)
	[0.001250]	[0.007124]	----	----
	{3200}	{1123}	----	----
	1809	1810	1811	1812
10	30.99	18.07	.83	15.50
o'clock	(69.394219)	(69.396038)	(69.398900)	(69.401837)
	[0.001819]	[0.002862]	[0.002937]	----
	{2199}	{1398}	{1362}	

To easily visualize when the pressure peak passed each station and in what order, draw circles around each of the above 10 data groups and connect the circles in sequence according to time, starting with the 10 o'clock 2 foot sensor. The pattern progresses through the above data groups from bottom to top and through the 2, 6, 10 and 14 foot diameters in a left to right order. Note the maximum pressure peak always passed the stations in a 10, 6 and 2 o'clock order with no exceptions. If the order of arrival of the peak pressure is shown on a plan view of the facility (draw 4 concentric circles for the 2, 6, 10 & 14 ft diameters overlayed on a wye representing the 2, 10 and 6 o'clock legs), a reverse helix is formed; the helix winds its way outward in a counterclockwise direction through each station (skipping the 2 missing stations) in the 10, 6, 2 o'clock order already mentioned. The smaller pressure peaks seen on the three sensors discussed earlier do not enter into this reconciliation of maximum peak pressure.

Using this behavior as a premise to support the conclusion a major pressure release occurred whose location was biased away from the exact center of the vessel is one option. The

center of the bias would be somewhere between the 10 and 6 o'clock legs. The helix propagation pattern and debris field contents support this conclusion.

Another option would be a vessel spin mode, but this is unlikely from a mechanical standpoint, and the motion picture films don't back up this idea either; also, multiple pulses with decreasing magnitudes would be seen by all the stations, and such a pattern wasn't recorded.

Returning to the first option, a check on the velocities of propagation of the wave front as it sequentially passed the sensors on each leg indicates the peak pressure's velocity decreased as the propagation progressed. The following graph shows the velocities, but they are plotted as if they were measured halfway between the stations; for example, the table shows the 10 o'clock, 2 ft velocity is 2199 ft/sec, but it is graphed as being at 4 ft, which is halfway between 2 and 6 ft. The graph isn't very accurate because it was fabricated using Wordstar, and a curve in the 2-point 2 and 6 o'clock locus is assumed because the 3-point 10 o'clock locus is curved. Draw the graph using a French curve.

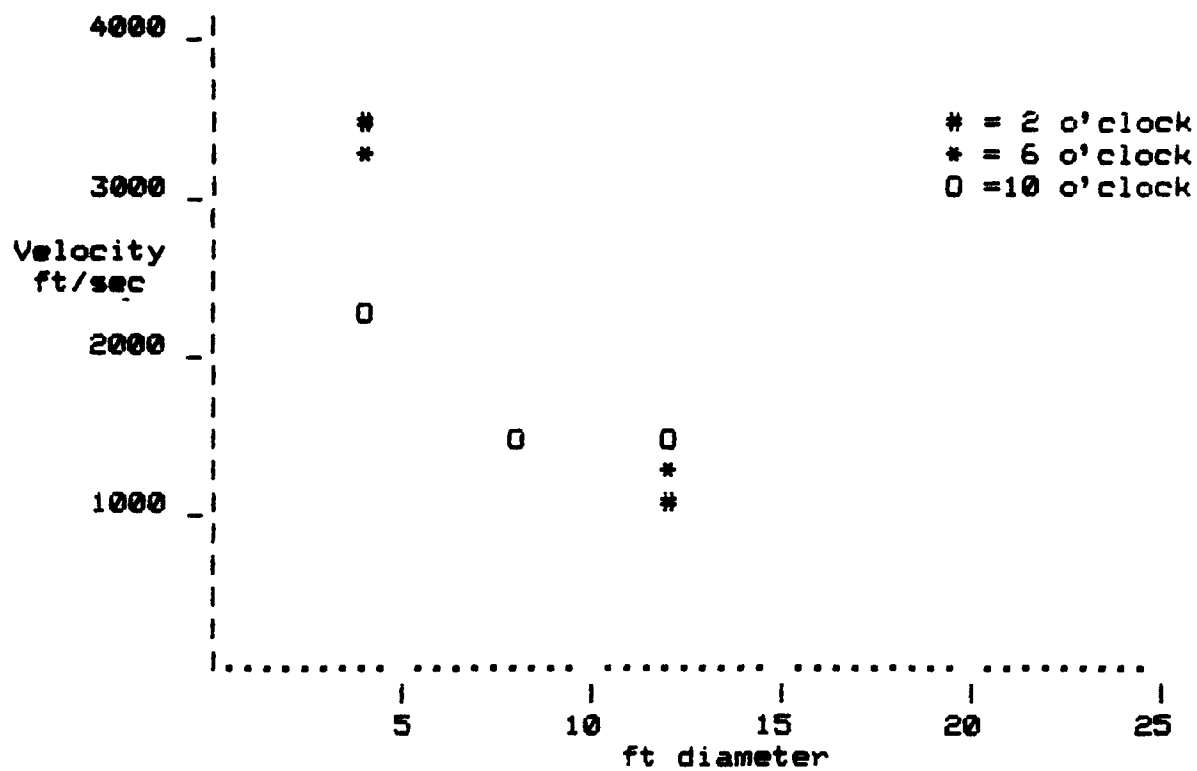
The ITT data analyst, Richard M. Thomsen states:

EM High Frequency Overpressures

The digitizing was done using a 16 kHz filter. The 20 kHz AC calibration signal shows a rolloff of 14 db [$(\log 50)^2 - \log(10)^2 \times 10$] for PV01/1801. Timing was aligned using the IRIG signal to the nearest tenth of a millisecond.

PV03/1803 was so noisy that the pulse was completely obscured. The spikes at 69.4025 and 69.4035 arrive too late and are the wrong direction, so I would not consider them as the pressure pulse. PV07/1807 was too noisy to calibrate.

A table of position vs overpressure (psig) is presented [... elsewhere] for comparison to the bikini gauges."



DESCRIPTION OF THE EMBRITTLEMENT PROCEDURE.

Summary. An undated ARDE embrittlement procedure was followed; only the girth area for a width of about 1/2 inch was embrittled. Embrittlement was inhibited, where required, with a maskant. Embrittlement was started at 1130 hours on 28SEP87. The current level was 0.16 amperes. Seventy-two hours of embrittlement were completed at 1130 hours on 10OCT87; the tank was immediately moved from the shop embrittlement area to the test site, instrumented, hooked up and tested at 1315 hours on 10OCT87. The electrolyte was sulphuric acid; sodium arsenite was added as an enhancer.

Details. Tsgt Dan Hinkle reports "The vessel, ARDE P/N E4168, S/N 004, was pickled with a mixture of Nitric Acid (22% by volume), Hydrofluoric Acid (2% by volume), and potable tap water to equal one liter of total volume. Interior coverage was insured by rotating and tilting the vessel for a period of 10 minutes, including drain time. The vessel was rinsed with tap water, then alcohol, and dried with a slow purge of GN2 from 25 SEP87 to 28SEP87.

On 28SEP87 the vessel's interior was masked with Adcoat AC818T liquid maskant to just above the girth weld. The ARDE technical representative (Steve Berko) insured this level by using a boroscope. The vessel was dried with GN2 for one hour, then filled to 1/2 inch above the maskant with an electrolyte solution (20 ml of 97.3% sulphuric acid in water to equal 1000 ml total volume, with 500 mg per liter of sodium arsenite). The electrolyte was charged by 0.16 amps for a period of 72 hours. The vessel was drained, rinsed with water, then alcohol, and dried with GN2 for one hour prior to installation on the test stand. The vessel was installed and all instrumentation hook-ups were completed at 1315 hours.

The vessel's interior and boss temperatures were cooled with LN2 chilled gaseous helium with a maximum pressure of 250 psig by cycling the pressurization valve and the test article vent valves. When the interior gas and boss temperatures were reduced to 20 degrees F and 60 degrees F, respectively, a ramp up in pressure to 1400 psig was completed. During a short hold, the temperatures were checked to insure both temperature readings were within the 140 degree F called for in the test directive. The interior temperature had risen to 128 degrees F, and the boss temperature had risen to 77 degrees - both well within the parameter restrictions. A ramp up to 3700 psig was initiated whereupon the vessel burst at 3575 psig. At failure, the interior gas temperature was 30 degrees F, and the tank boss temperature was 67 degrees F."

ADMINISTRATIVE INFORMATION.

Revision Record. Initial Issue: 28OCT87. Revision A: 13NOV87; added text here and there. Revision B: 4DEC87; errors fixed: 0.16 amperes was 1.6 amperes; text added to paragraphs: PVSOUT/1904; Displacement Sensors. Revision C: 15DEC87; text added to paragraph Piezoelectric Sensors; other minor changes.

Filename: testrv11

Distribution:

ARDE, Steve Berko, Dave Gleich
PI, Dr. Pius Chih Hsu Chao
Aerospace Corp., Dr. Yen Pan
AFAL, Jim Miller, Dick Grove, John Marshall,
Dr. Tae-Woo Park
ITT, Richard Thomsen
PAFB, Pete Tadie

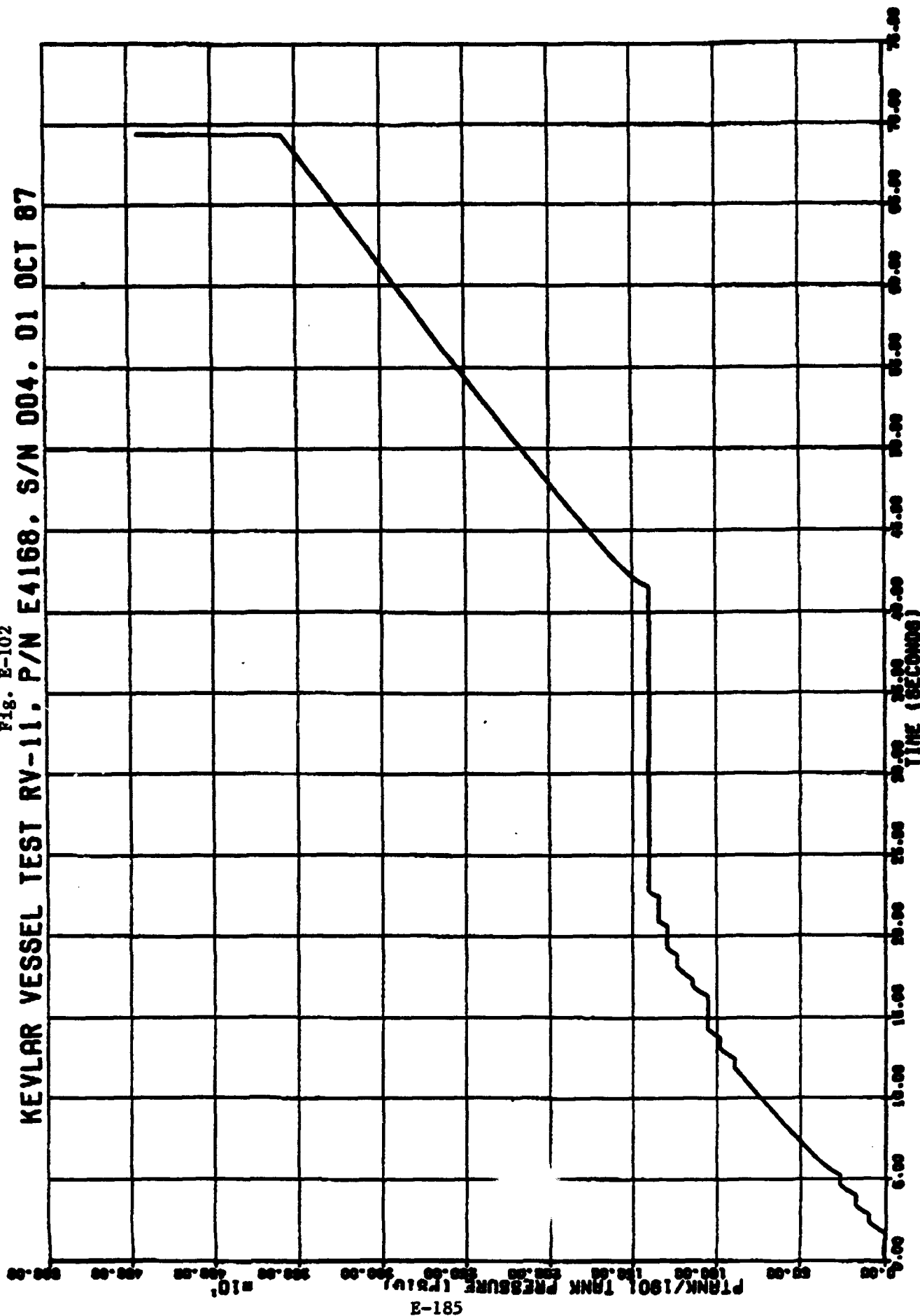
Office of Primary Responsibility. USAF/AFAL/TOAE/Dick
Grove/Edwards CA 93534.

E.8.3 Pressure and Strain Versus Time Plots

Figures E-101 to E-107 are selected measured pressure and fiber strain versus time plots. Digital data are given on Figure E-108, Strain gage locations are shown on Figure E-109. Odd numbered strain gages were parallel to the fiber wrap and even numbered strain gages were perpendicular to the fiber wrap.

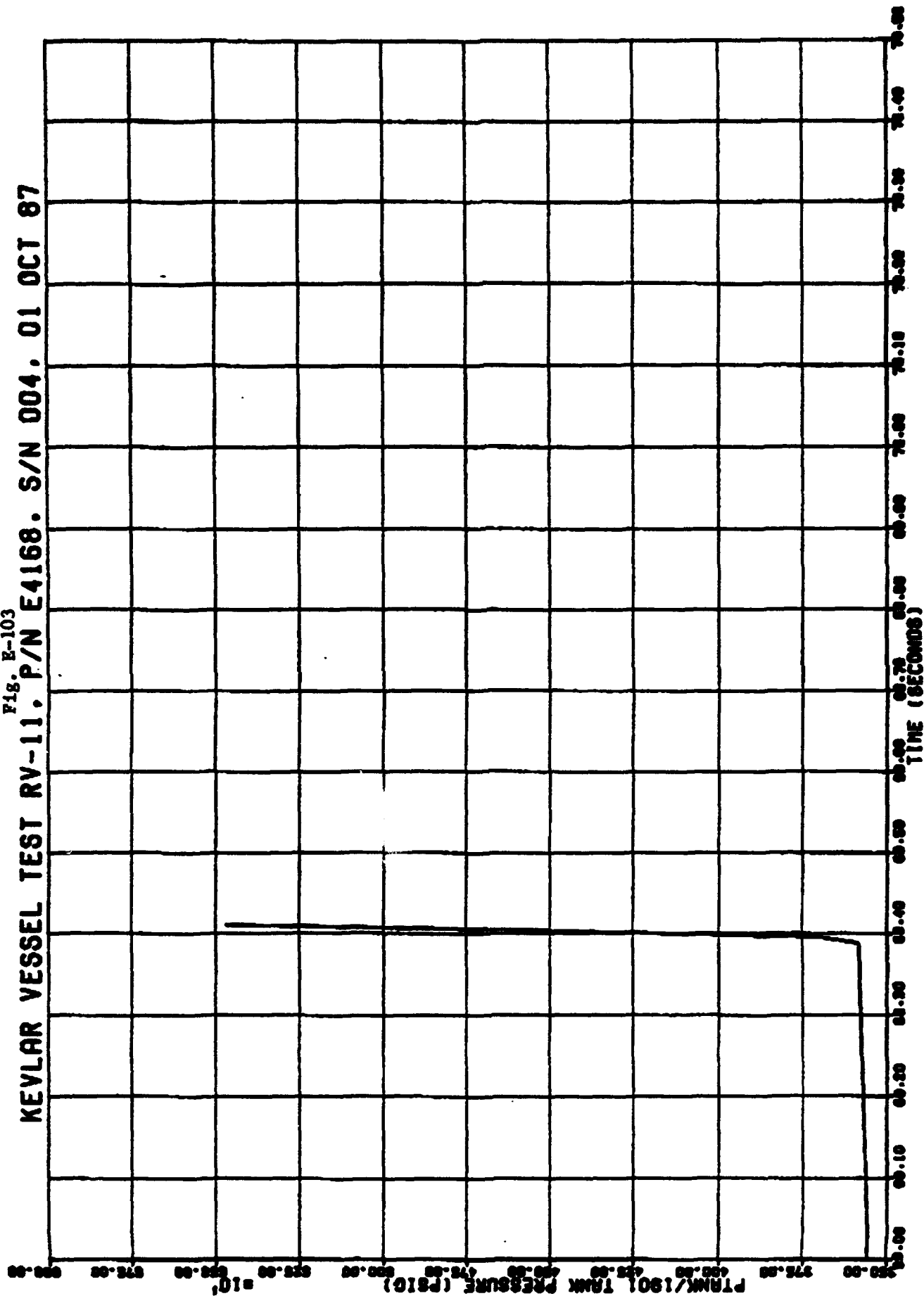
KEVLAR VESSEL TEST RV-11, P/N E4168, S/N 004, 01 OCT 87

Fig. E-102



KEVLAR VESSEL TEST RV-11, P/N E4168, S/N 004, 01 OCT 87

Fig. E-103



E-186

REFL/DH EFB CA

NO. 002

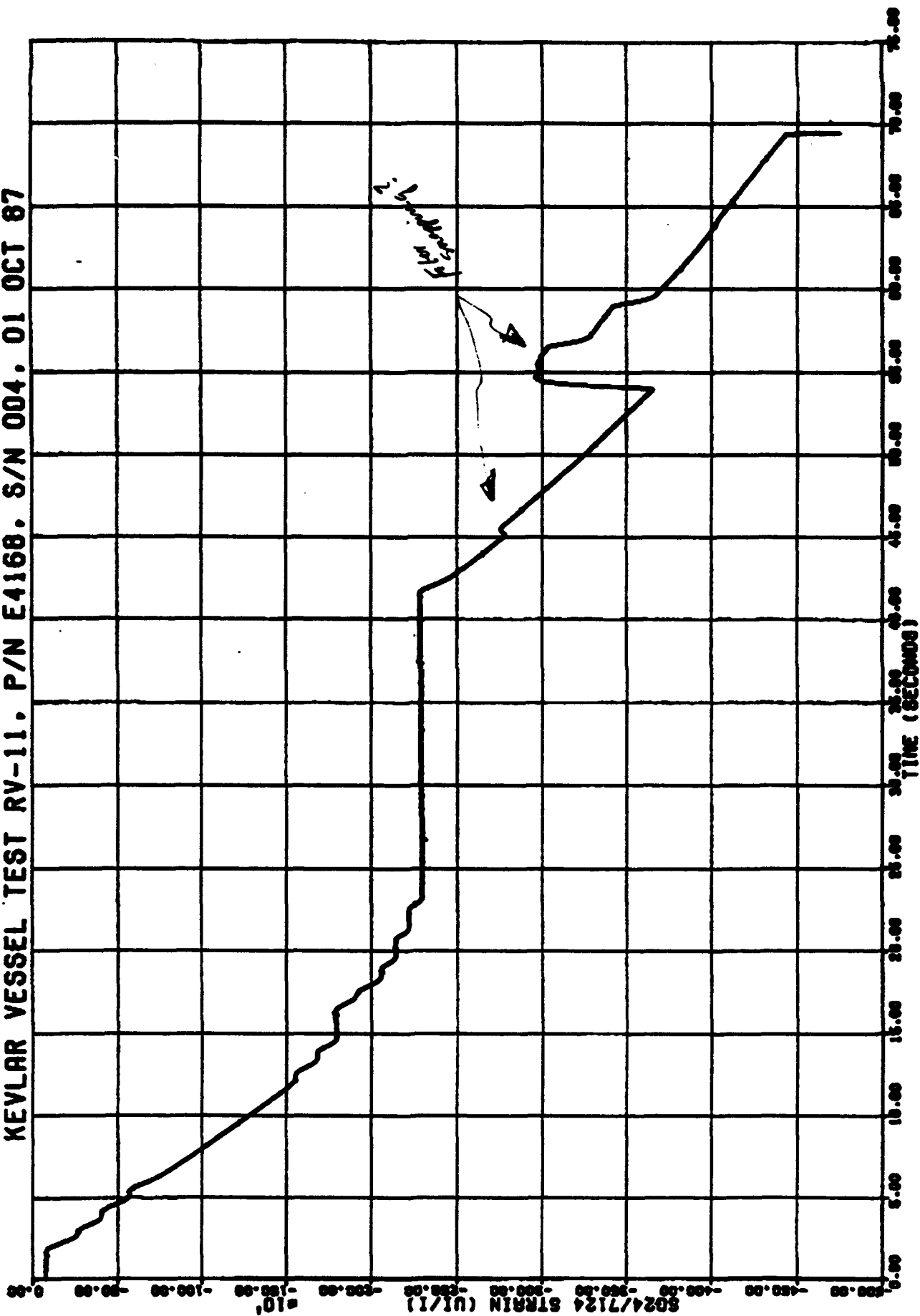
003

09:05

10/06/87

Fig. E-104

KEVLAR VESSEL TEST RV-11. P/N E4168. S/N 004. 01 OCT 87



KEVLAR VESSEL TEST RV-11. P/N E4168. S/N 004. 01 OCT 1987

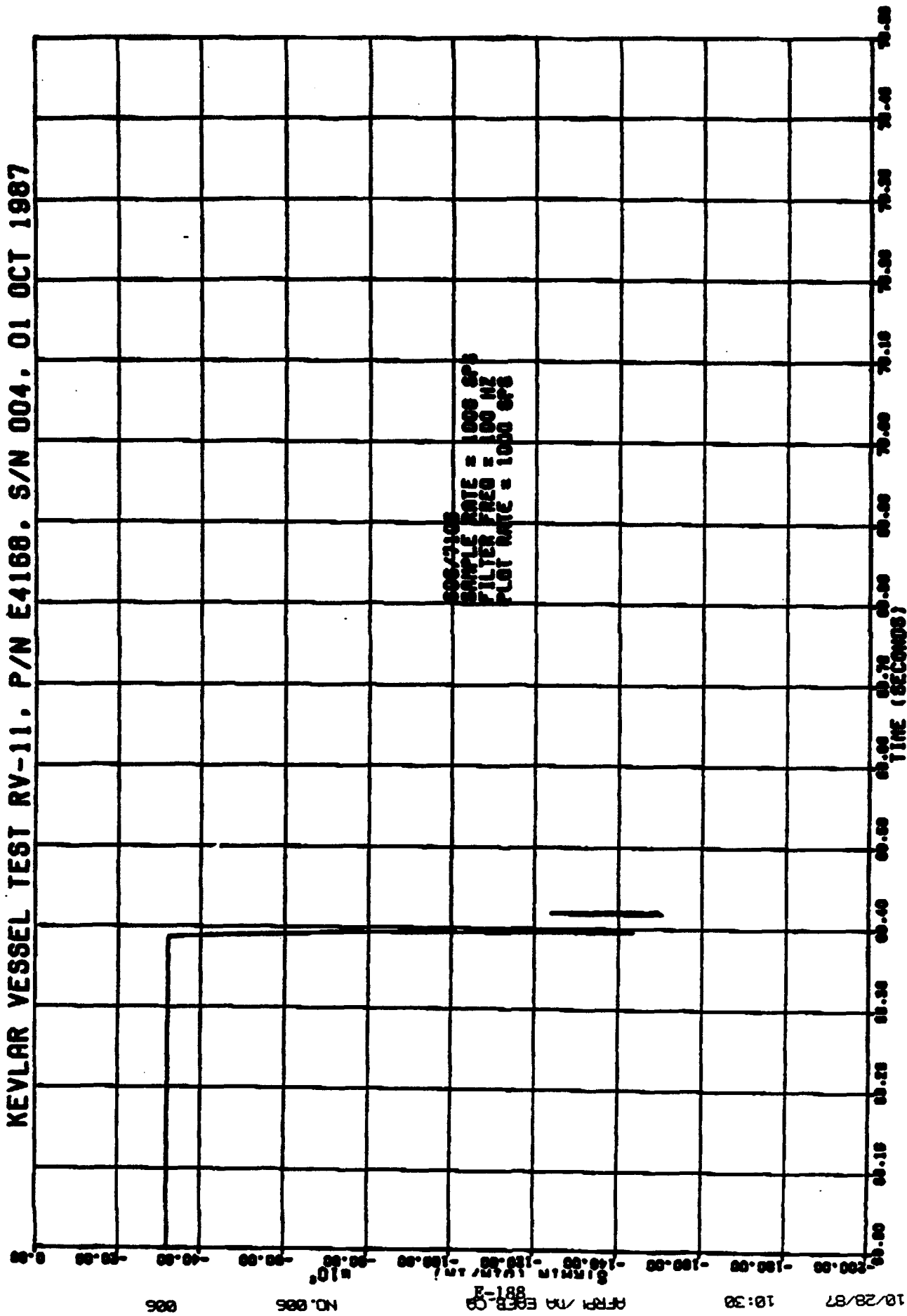
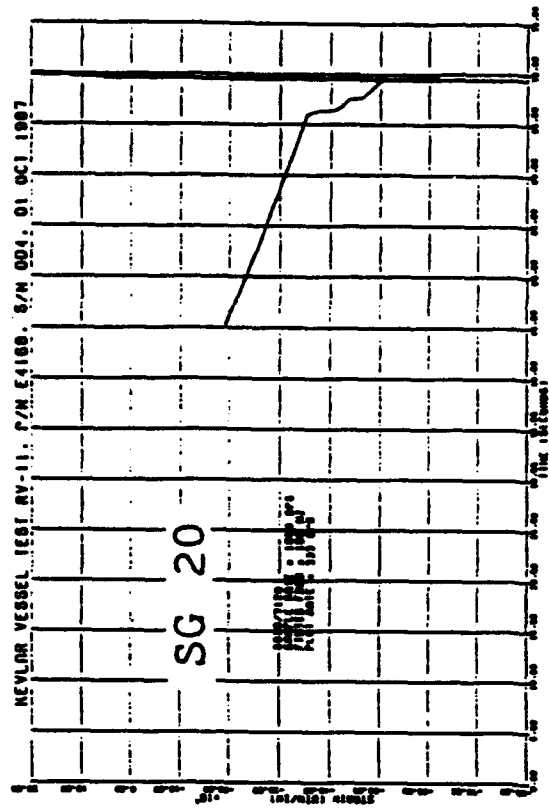
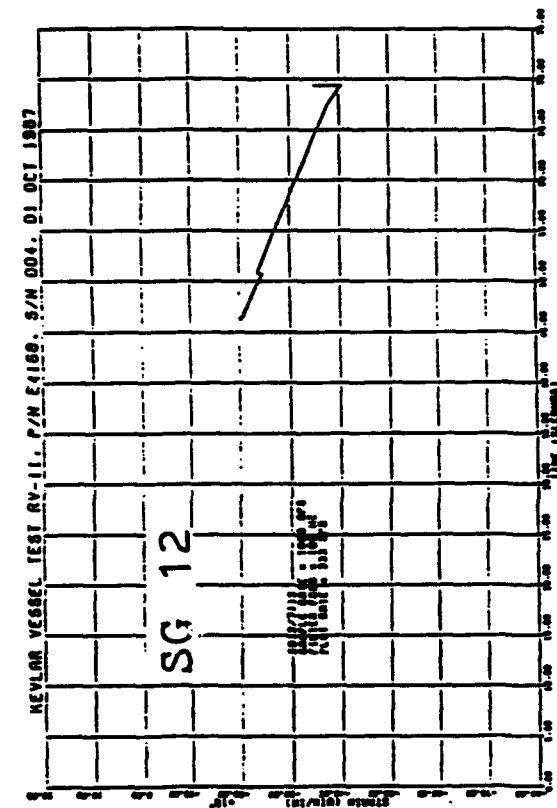
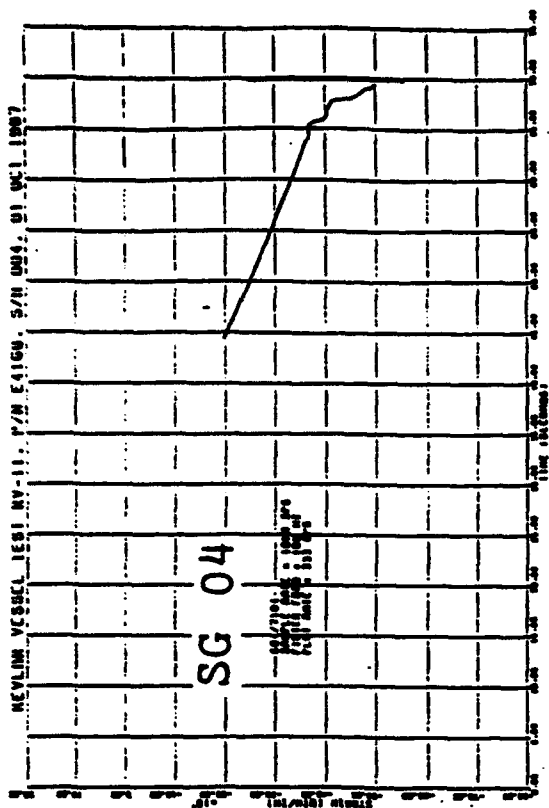


Fig. E-105

Fig. E-106

TEST RV-11, SG 4, 12, 20

N Equator Meridional

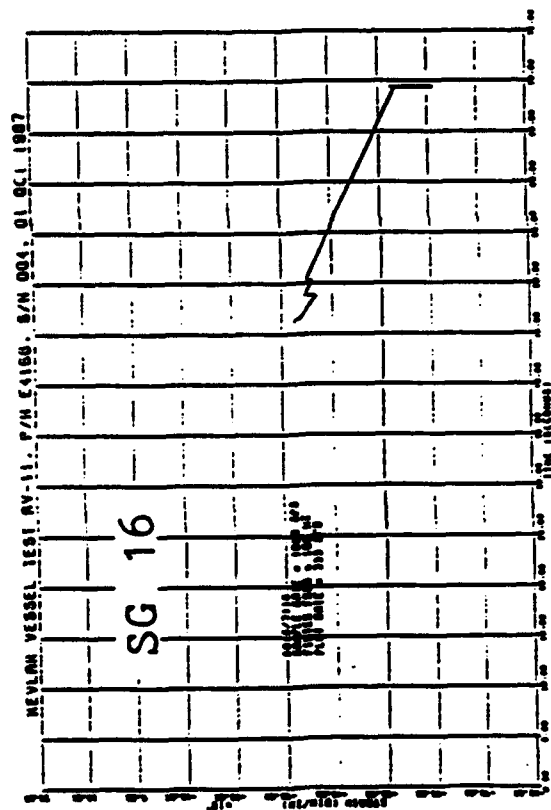
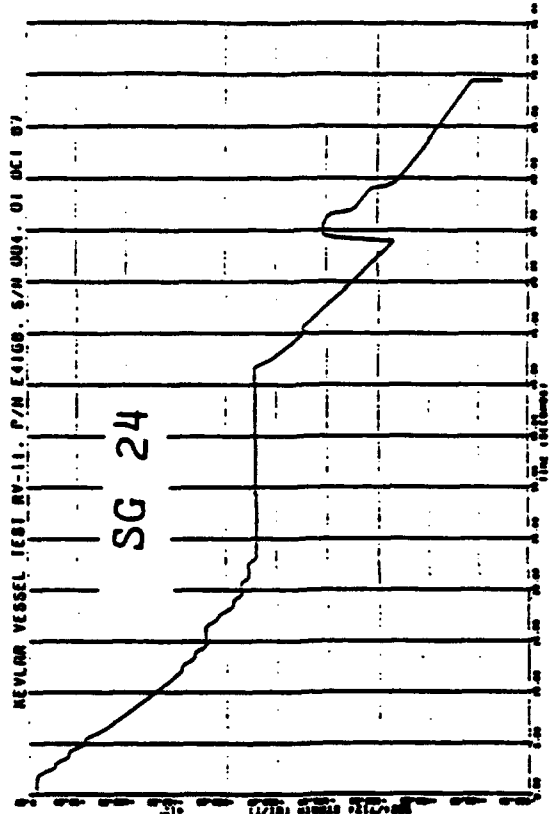
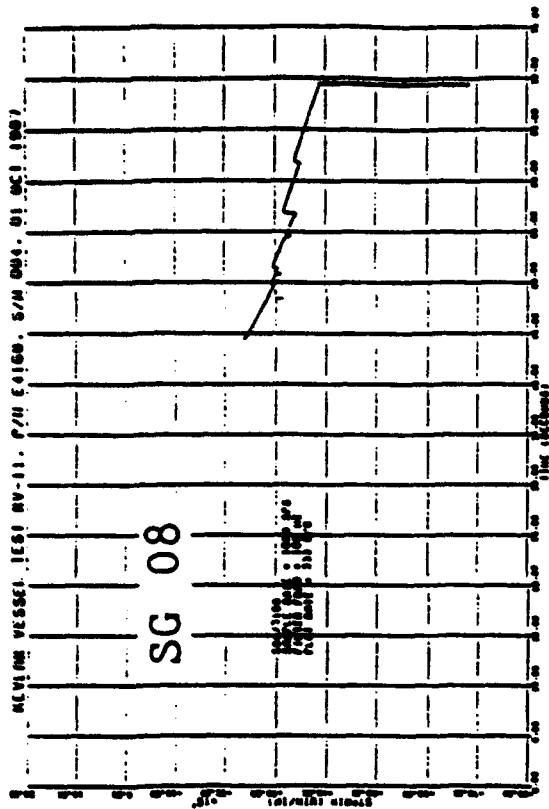


N Equator Meridional gages during pressure ramp-up.

Fig. E-107

TEST RV-11, SG 8, 16, 24

S Pole Meridional



S Pole Meridional gages during pressure ramp-up.

E-191

RV-11
P/N E4168 S/N 004
83% KEVLAR THICKNESS

EVEN GAGES = PARALLEL TO FIBERS

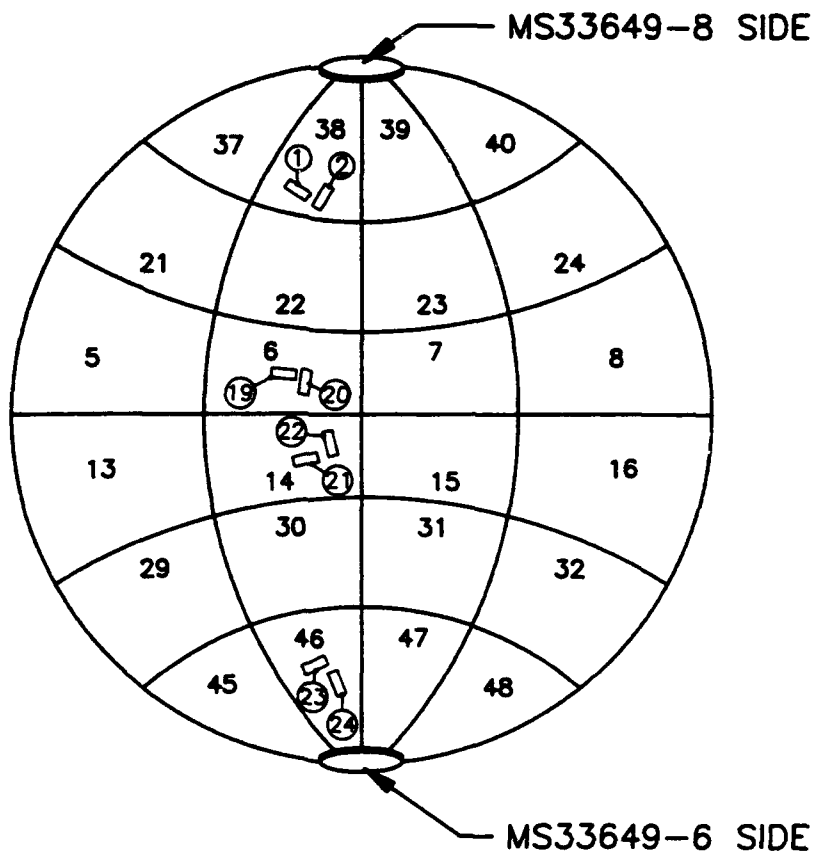
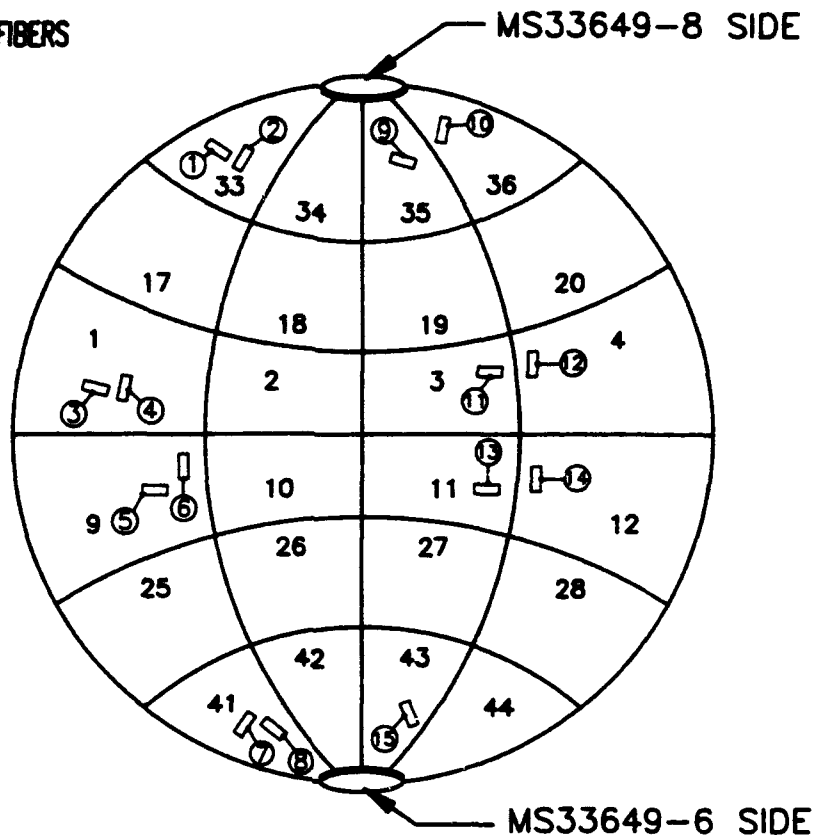


FIGURE E-109 STRAIN GAGE LOCATIONS FOR TEST RV-11.
E-192

E.8.4 Blast Overpressure Data

Blast overpressure data have been given in section E.8.2 as part of "Instrumentation Observations". The maximum pressure measured by the piezoelectric sensors was 123.33 psig at the 2 foot radius for the 2 o'clock position. At 14 foot radius, the peak overpressure measured was still 4.28 psig at the 2 o'clock position and 15.50 at the 10 o'clock position. The pressure distribution was non-symmetrical due to non-symmetrical tank rupture, test rig and ground interference and reflected waves. Radii are measured from the tank center and clock coordinates define the angular position of sensors.

E.8.5 Post Test Inspection

The test stand and surrounding terrain were inspected for damage and tank fragments. Photographs were taken. The test stand was severely damaged and vessel remains (metal fragments and loose Kevlar fibers) were scattered over a considerable distance. Some metal fragments were found about 500 feet from the test

stand. Figure E-110 shows a close up photograph of the post test damaged test stand and a partial view of fragment distribution about the test site is given on the photograph of Figure E-111. The large number of fragments and their distribution over a large area extending far from the blast initiation site, coupled with the high blast overpressure discussed in E.8.4, demonstrates once again the high damage capacity of catastrophically failed high pressure gas tanks.

Fig. E-110



TEST RV-11, POST TEST VIEW OF DAMAGED TEST
STAND

Fig. E-111



TEST RV-11, FRAGMENT DISTRIBUTION

E.9 RV-12 TEST (22" ϕ)

E.9.1 Test Vessel Description

- P/N E4089-2 (Kevlar Overwrapped 301 Cryo CRES Composite Sphere)
- Kevlar Fiber (less resin) Average Thickness - .192
- Metal Thickness - .044
- Inside Radius - 10.3
- Hydrogen Embrittlement Mode - Local Boss/Head Weld Region
- Electrolytic Solution -
20 cc H_2SO_4 + 980 cc Tap H_2O
1000 cc Solution
- Solution additive - 500 mg Sodium Arsenite
- Sensitize Liner Inside Surface (cold pickle)
- Charging Current Density - .0068 amps/in² of surface to be embrittled
- Charging Time - 72 hours
- Hold Time Before Test - 3 hours
- Adcoat AC818T liquid maskant on areas not to be embrittled

A pre-test photograph of the instrumented tank mounted in the test stand is shown on Figure E-112.

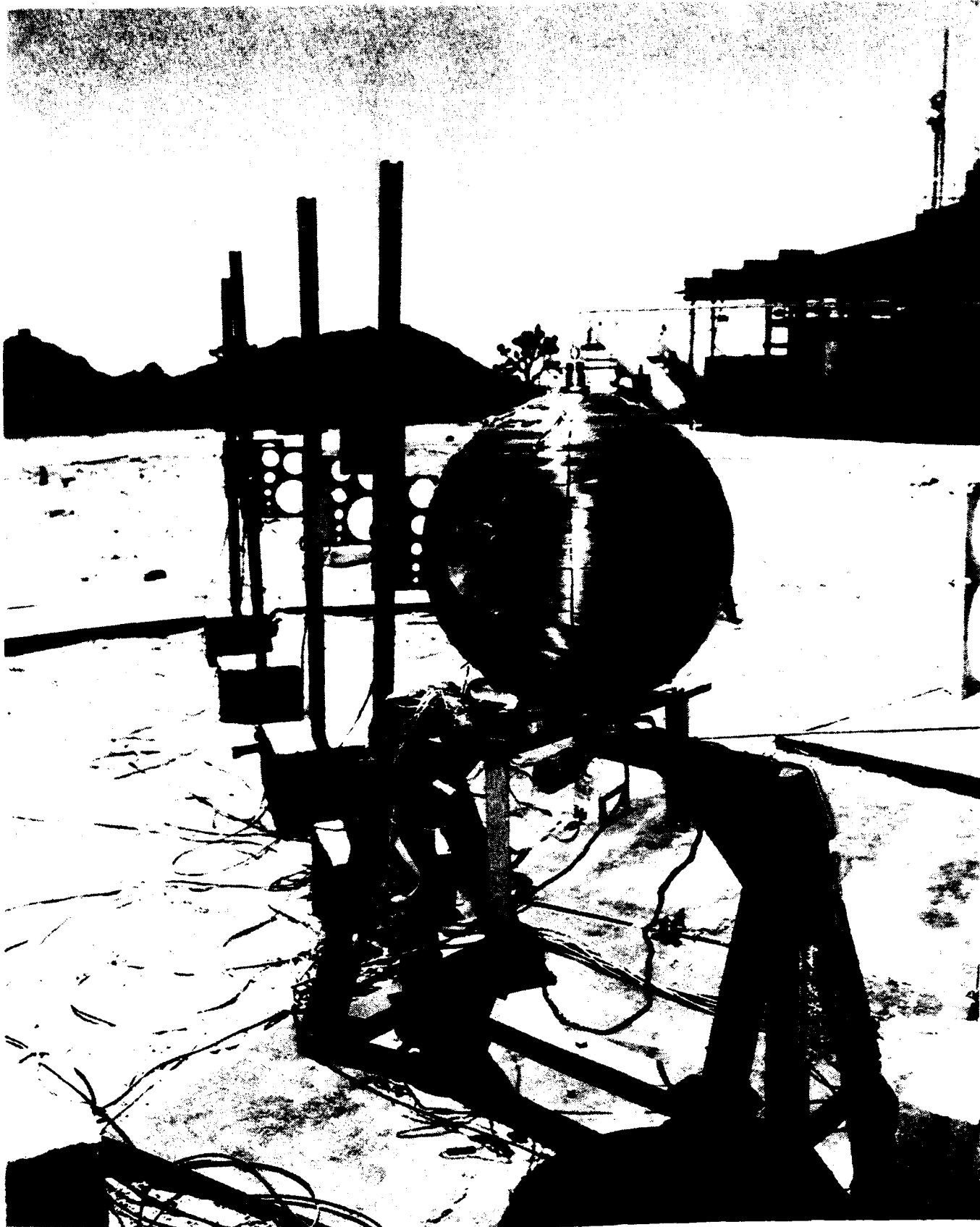


Fig. E-112 TEST RV-12, INSTRUMENTED TANK MOUNTED IN
TEST STAND

E.9.2 Test Discussion

Experiment RV-12 (boss/head weld hydrogen embrittlement mode) demonstrated again a benign, stable, leak tank failure type. Liner failure pressure was low (2500 psig). This test was a first time hydrogen embrittlement experiment with the new larger tank/boss size/geometry and resulted in too much hydrogen gas at the defect (crack) tips leading to too low liner failure pressure. No pressure fiber strain data was obtained because the data acquisition system was not operative at/near the 2500 psig liner failure pressure as detailed in the AFAL letter and AFAL Instrumentation observations of E.9.2.1.

The liner failure was verified by a post test leak check at AFAL and further proven/defined by viewing the multitude of cracks on the die check enhanced inside liner surface of the subsequently cut apart tank at ARDE. The embrittled boss region was still attached to the liner head - no boss/head separation occurred. Figure E-113 shows a post-test close up view of the tank on the test stand at AFAL. A small local external fiber wrap damage in the boss/head



Fig. E-113 TEST RV-12, POST TEST CLOSE UP VIEW OF TANK

weld region can readily be seen. An overall view of the liner tangential and radial through cracks in the boss/head weld HAZ and a close-up view of the largest through crack (outlined by a black rectangular marking) are given on the photographs of Figure E-114. It is to be noted that the radial cracks are soon arrested by the ductile liner material outboard of the boss/head weld HAZ.

The local boss/head weld HAZ liner hydrogen embrittlement mode was investigated again in experiment RV-12A, discussed next. A lower liner hydrogen embrittlement current density was used to provide the desired higher liner failure pressure.

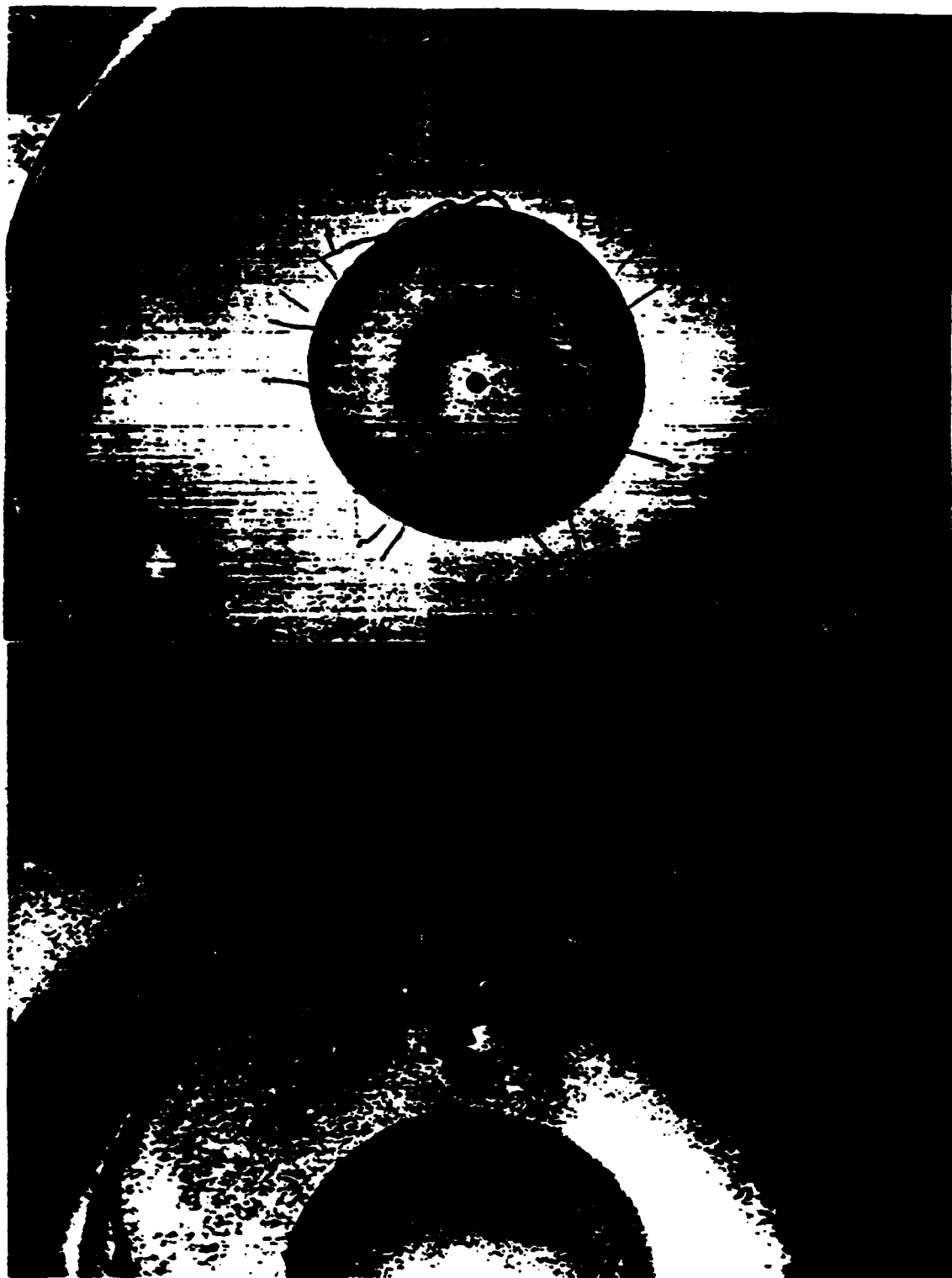


Fig. E-114 TEST RV-12, POST TEST EMBRITTLED LINER BOSS
REGION CRACKS

E.9.2.1

INSTRUMENTATION OBSERVATIONS (by Instrumentation Eng.)

KEVLAR TEST 012, 26MAY88. Project number 573000RV.

EXPERIMENTAL OBSERVATIONS.

Introduction. Vessel S/N 029. P/N E4089. was tested. It was a 22 inch diameter stainless steel sphere. The Kevlar overwrap was 100%. The vessel was hydrogen embrittled at the inlet boss. It was tested in a vertical configuration.

There were problems with this test. It was necessary to conduct an extended cool-down period because of an intermittent fast vent valve. Witnesses allege the tank unexpectedly leaked during the hold period when critical data was not being acquired. Fracture verification could not be confirmed visually with the boroscope, but a post-test leak check at 500 psig proved the vessel had definitely fractured. Damage to the Kevlar was limited; one fiber bundle was frayed for about an inch long near the embrittled flange; some resin debonding was evident near the flange.

Pressurization Procedure. The line was pressurized, vented and a data Z-cal at zero line pressure obtained. The data system was started. During cool-down, the fast vent valve was intermittent and pressurization was very slow as the vessel gas temperature had to be kept below 140 degrees F. Cool-down took about one hour until the vent valve problem cleared spontaneously; pressure was increased to 2500 psig. The data file had filled to capacity, and a new data file was requested. As soon as the new data file started, the tank pressure had dropped to about 1200 psig, and attempts to repressurize failed. Data acquisition was halted during a 3 minute discussion about what had happened and what should be done. It was decided not to repressurize again. The data file was started again to capture the remainder of the pressure decay. It has not been determined how much data was obtained with the FM tape data.

EMBRITTELEMENT PROCEDURE. The ARDE embrittlement procedure dated 4MAY89 was followed. The 22" diameter vessel was boss embrittled. Embrittlement was inhibited, where required, with a maskant. Embrittlement was started at 0800 hours on 16MAY88. The current level was 0.160 amperes. Seventy-two hours of embrittlement was completed at 1115 hours on 19MAY88. The tank was immediately moved from the shop embrittlement area to the test site, instrumented, hooked up, checked and pressure tested at 1305 hours on 19MAY88. The electrolyte was sulphuric acid. Sodium arsenite was added as an enhancer. The maskant was just below the boss weld.

ADMINISTRATIVE INFORMATION.

Revision Record. Initial issue: 25MAY88. Revision A: 29AUG89: Embrittlement Procedure added. The word "leaked" was "ruptured."



DEPARTMENT OF THE AIR FORCE

AIR FORCE ASTRONAUTICS LABORATORY (AFSC)
EDWARDS AIR FORCE BASE, CALIFORNIA 93523-8000

REPLY TO
ATTN OF:

TOAE

SUBJECT:

Kevlar Test 012, 26 May 88 Project Number: 573000RV

TO:

ARDE Inc.
500 Walnut St
Norwood, New Jersey 07648

Att: Mr Dave Gleich

EXPERIMENTAL OBSERVATIONS.

Introduction. S/N 029. P/N E4089, was tested. It was a 22 inch diameter stainless steel sphere. The Kevlar Overwrap was 100 percent. The vessel was hydrogen embrittled at the inlet boss. It was tested in a vertical configuration.

There were problems with this test. It was necessary to conduct an extended cool-down period because of an intermittent fast vent valve. Witnesses allege the tank unexpectedly fractured during the hold period when critical data was not being acquired. Fracture verification could not be confirmed visually with the boroscope, but a post-test leak check at 500 psig proved the vessel had definitely fractured. Damage to the Kevlar was limited; one fiber bundle was frayed for about an inch long near the embrittled flange; some resin debonding was evident near the flange.

Pressurization Procedure. The line was pressurized, vented, and a data Z-cal at zero line pressure obtained. The data system was started. During cool-down, the fast vent valve was intermittent and pressurization was very slow as the vessel gas temperature had to be kept below 140 degrees F. Cool-down took about one hour until the vent valve problem cleared spontaneously; pressure was increased to 2500 psig. The data file had filled to capacity, and a new data file was requested. As soon as the new data file started, the tank pressure had dropped to about 1200 psig, and attempts to repressurize failed. Data acquisition was halted during a 3 minute discussion about what had happened and what should be done. It was decided not to repressurize again. The data file was started again to capture the remainder of the pressure decay. It has not been determined how much data was obtained with the FM tape data.

JIM MILLER, Project Manager

DICK GROVE, Instrumentation Engineer

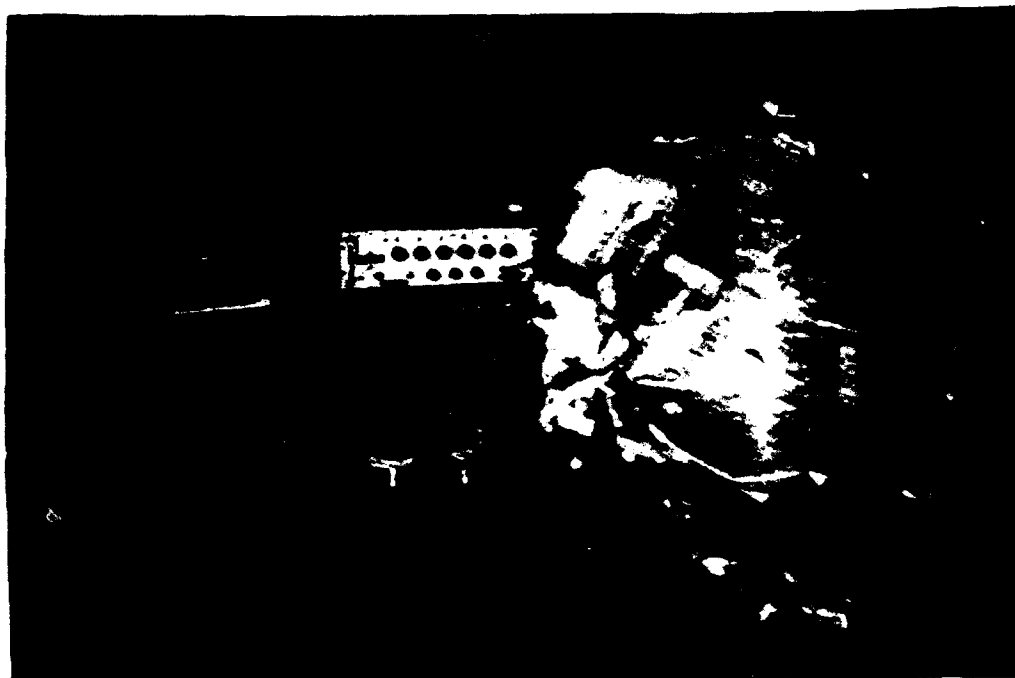
E.10 RV-12A (22" ϕ)

E.10.1 Test Vessel Description

- P/N E4089-2, S/N 034 (Kevlar Overwrapped 301 Cryo CRES Composite Sphere)
- Kevlar Fiber (less resin) Average Thickness -
.192
- Metal Thickness - .044
- Inside Radius - 10.3
- Hydrogen Embrittlement Mode - Local Boss/Head Weld Region
- Electrolytic Solution -
$$\frac{20 \text{ cc H}_2\text{SO}_4 + 980 \text{ cc Tap H}_2\text{O}}{1000 \text{ cc Solution}}$$
- Solution Additive - 500 mg Sodium Arsenite
- Sensitize Liner Inside Surface (cold pickle)
- Charging Current Density - $.0042 \text{ ma/in}^2$ of surface to be embrittled
- Charging Time - 72 hours
- Hold Time Before Test - 2-3/4 hours
- Adcoat AC818T liquid maskant on areas not to be embrittled

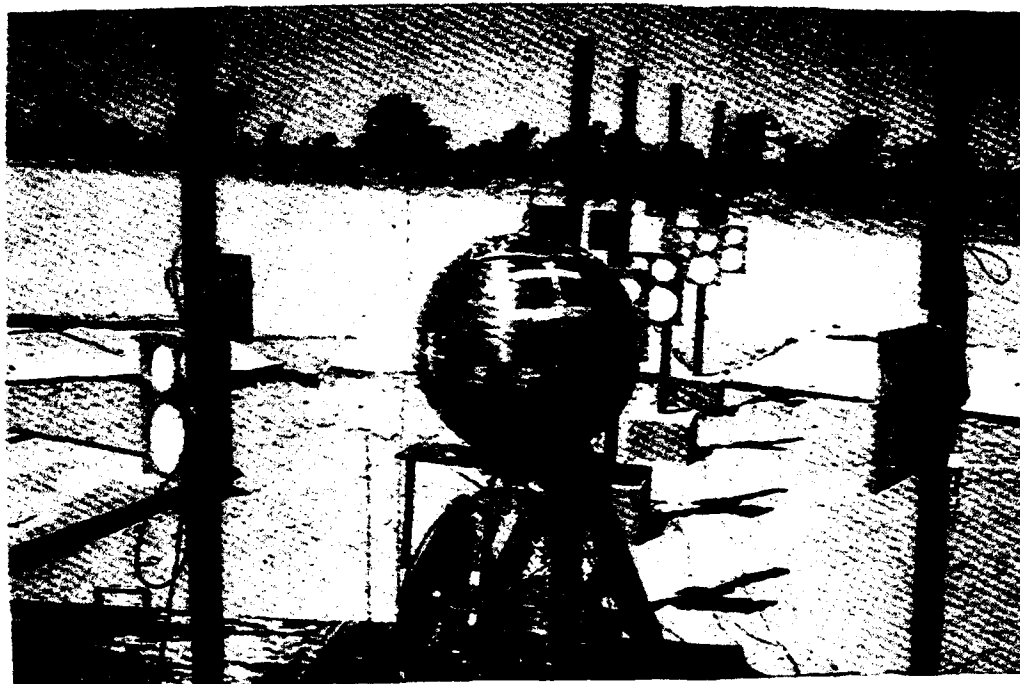
A photograph of the test tank being charged with hydrogen gas during the pre-test hydrogen embrittlement mode is shown on Figure E- 115. Figure E-116 is a pre-test photograph of the test tank mounted in the test stand, showing strain gage, bikini gage and blast overpressure sensor instrumentation. A view of Area 1-52D test pad showing the motion picture camera tower stations is given on the photograph of Figure E-117.

Fig. E-115



TEST RV-12A, PRE-TEST LINER HYDROGEN
EMERITTLEMENT MODE

Fig. E-116



TEST RV-12A, INSTRUMENTED TANK MOUNTED IN
TEST STAND



Fig. E-117 TEST RV-12A, TEST AREA WITH CAMERA TOWER

Strain Gages.

Strain Gage Locations. The strain gages were located IAW ARDE drawing dated 3/6/89, Revision A. The even strain gages are perpendicular to the wrap, and the odd strain gages are parallel to the wrap.

Strain Gage Temperature. Not shown on this print are the thermocouple locations. See the Instrumentation Specification Sheet for the locations and item numbers. The 5 thermocouple loci form a family of curves with almost identical plateau profiles. Collectively, the gages measured temperature behavior over a span between ____ and ____ degrees F, approximately. However, each gage didn't change much during the plateau, and the typical plateau temperature variation didn't exceed about 5 F degrees. This small variation was also seen on test 11. Two thermocouples, TT3/2104 and TT4/2105 dropped rapidly at leak. Thermocouple TT5/2201 dropped slightly at leak, and the others remained steady. The vessel's temperature behavior is considered to be within normal limits, and it wasn't investigated with further detail.

Performance Summary. There were 23 strain gages recorded, and 21 functioned, although several had little activity and some had noise spikes. During the initial conditions, all gages had much better than reasonable noise floors. The noise floors are discussed elsewhere under Noise Floors. None of the strain gages were destroyed at tank leak. Two data passes were made. The first was done at 1000 SPS with a 100 Hz filter. The second was done at 128,000 SPS with a 20,000 Hz filter.

Sign Convention. Positive strain gage polarity represents compression, and negative strain gage polarity represents tension.

Noise Floors. Except as noted elsewhere, the strain gage and other parameters' noise floors did not include major transverse or common-mode minus $L(di/dt)$ transients, artifacts, crosstalk, atmospherics, noticeable RFI, intermodulation, spurious parasites, or sibilants. However, latent noise or data manifestations may be obscured in some parameters, and digital signal processing may be needed for signal enhancement. In general, the data appeared to be unbiased, precise and accurate. SG16 was the noisiest but this is a judgement call as several others had some noise also.

Performance Exceptions. Strain gage behavior was within normal limits.

Dynamic Performance, Profile Categories, Strain Polarization. The general trend for the active strain gages was a tension strain polarization pattern proportional to vessel pressure. SG behavior was similar to previous tests. High frequency dynamic data included oscillations at leak noted by the analyst on SG01, 08 and 13.

maximum SG Values and Performance Trends. The following codes are used below:

NWNL noise within normal limits

GRZ good return to zero

ARZ approximate return to zero

NRZ no return to zero

C compression strain

T tension strain

NTE not to exceed

OSC oscillation (See ITT text for frequency)

Unipolar: data predominately in one direction.

Bipolar: data in both directions but not necessarily evenly balanced between polarities. In most cases, the data carrier was unipolar in tension but contained bipolar compression excursions.

Units for strain values are in microinches/inch

SG01 Unipolar, T NTE 12,500; NWNL, OSC.

SG02 Bipolar, minor C, T not to exceed 6000, NWNL prior to leak.

SG03 -

SG04 Bipolar, major C NTE 5200, T NTE 3000, NWNL prior to leak.

SG05 Unipolar, T only NTE 3000, NWNL but some spikes, NRZ.

SG06 Unipolar, all T NTE 7500, NWNL prior to opening up, NRZ.

SG07 Unipolar, all T NTE 5000, NWNL but some spikes, NRZ.

SG08 Bipolar, major C NTE 2500, T NTE 5000, NWNL but some spikes, NRZ, OSC.

SG09 Unipolar, all T NTE 7500, NWNL, NRZ, OSC.

SG10 Bipolar, major C NTE 3700, minor T, NWNL, GRZ.

SG11 Bipolar, minor C, T NTE 1/3 of 2500, NWNL, NRZ.

SG12 Bipolar, minor C, T NTE 1/3 of 2500, NWNL, NRZ.

SG13 Bipolar, minor C, T NTE 3/4 of 2500, NWNL, NRZ.

SG14 Bipolar, minor C, T 7500, NWNL, NRZ, OSC.

SG15 Unipolar, minor T bump of short duration NTE 1/3 of 2500, NWNL, ARZ.

SG16 No change. NWNL except for major noise spikes.

SG17 No change. NWNL.

SG18 No change. NWNL.

SG19 Bipolar, minor C, T NTE 5000, NWNL, NRZ.

SG20 Bipolar, major C&T excursions NTE 7500 ok-to-ok. NWNL, GRZ.

SG21 No change, NWNL.

SG22 -

SG23 Unipolar, T less than 2500, NWNL, ARZ.

Performance Summary: Seven of the 23 channels (30%) recorded unipolar data. Ten of the 23 channels (43%) recorded bipolar data. Three of the 23 (13%) recorded no change. The maximum unipolar strain was recorded by SG01 as tension, not to exceed 12,500 microinches/inch. The maximum bipolar strain was recorded by SG14, about 7500 microinches per inch, although it

was mostly unipolar in nature. SG20/7120 could be considered as somewhat representative of typical strain gage performance: it tracked the vessel pressure, contained compression data as well as the predominate tension data, returned to the initial condition zero value, and did not have any oscillations, noise spikes or drop outs. Phase information correlates well for some items such as SG15 & SG11. Phase information on other parameters is shifted, such as SG19 & 20, where polarity is reversed on one excursion as well, making the observer wonder if such graphs are phase related at all. The above information was determined by inspecting the graphs and may contain subjective errors.

Statistical Analysis. Valid speculations about strain gage behavior may involve biserial correlation of certain dichotomies (positive or negative polarization) to assess their associations (with wrap direction, etc.). For truly dichotomous distributions, the phi coefficient can be used. Because some of these dichotomous variables are really continuous (the magnitude or duration of polarization, and the degree of wrap thickness, location & direction, etc.) and normally distributed, tetrachoric correlation may be involved. An expert statistician should be approached with a clear statement of which variables and associations are important if valid conclusions about some of these data are to be obtained. An accurate evaluation of which variables are really dichotomies and which are proportionally continuous would also have to be prepared and passed to the statistician.

Data Analyst's Comments.

"[ITT] 15MAY89 DATA ANALYST [Richard Thomsen] COMMENTS. The FM strain gauge data was digitized at 1000 SPS, using an 100 Hz filter. The IRIG time signal was used to align the time scale to within 0.00025 seconds.

Almost all of the plots show spikes that are probably tape drop-outs.

SG03/7103 and SG22/7122 were bad for the whole test.

SG09/7109 was bad until 184 seconds.

SG18/7118 was bad from 159.4 to 166.7 seconds.

SG08/7108, SG12/7112, SG14/7114 and SG16/7116 showed shifts in strain level prior to the burst.

Several of the gauges showed ringing after the burst."

"[ITT] 25JUL89 DATA ANALYST [Richard Thomsen] COMMENTS. The IRIG time signal was used to align the data to the nearest 10 microseconds. This was due to the distorted shape of the IRIG signal with very sharp spikes.

Strain gauges SG03/7103 and SG22/7122 were bad [no graphs].

SG01 goes bad at 286.887 seconds.

SG02 goes bad at 286.888 seconds.

SG06 goes bad at 286.887 seconds.

SG16 has noise spikes.

SG01 has an interesting 19kHz ring.

SG08 has an interesting 25kHz ring.

SG13 has an interesting 22kHz ring.

SG16, 17, 18, and 21 show little change.

The overpressures PV01/8901 and PV12/8912 had no change so processing was only done on PV12, as it may show electrostatic discharge."

End of ITT text.

IMPRESSIONS FROM THE QUICK-LOOK AND DIGITAL DATA ACQUISITION SYSTEM DATA.

Tank Pressure. PTANK/1901 was located on the top of the tank in the vent line. PVSOUT/1904 was also in the vent line, but it was located at the valve box about 15 feet from the tank. PTANK/1901 functioned as described under the Pressurization Ramp... paragraph.

The locations of the transducers was the same as test 10.

PVSOUT/1904 data were similar to PTANK/190 except for the reduced frequency response because of the long pressurization line.

SG24. SG24 tracked the vessel pressure profile with corrections for polarity, etc. This parameter, as in the previous tests, was only recorded on the DACS for quick-look purposes.

General Comments. The performance of SG24 is very interesting. This strain gage duplicated the tank pressure behavior, PTANK/1901, but there were some deviations particularly during the final pressurizing ramp just prior to failure.

Phase Behavior and Frequency Response. Noted is the phase behavior; the two graphs were very close together in the time domain.

The graphs were expanded at leak to enhance the details at leak. SG24 at leak shows about a cycle and a half of oscillation, which is not seen on the tank pressure graph.

Other Parameters. The performance of the other parameters was within normal limits; this was determined by a quick review of the graphs for items PHXIN/1902, PHXOUT/1900, PTRAIL/1903, THXIN/2100, TBALL/2211, TBSOUT/2210, TBSIN/2209. The IRIG Time Code, IRIG/3808 TIMING, recorded satisfactorily and can be referenced to the motion picture data.

IMPRESSIONS FROM THE OVERPRESSURE SENSORS.

Bikini Gages. A Bikini gage is one piece of bond paper

compressed between two metal plates containing different sized round holes. The gages are aligned so the paper is perpendicular to the pressure source. Discrete pressure data can be obtained and is a function of the location of the damaged paper diaphragms. The approximate calibration is as follows for the indicated hole size using bond paper:

HOLE #	PSIG*	SIZE	PSIG**
1	7.3	5/8	4.4
2	5.2	7/8	3.3
3	3.7	1-1/4	2.4
4	2.7	1-7/8	1.7
5	1.9	2-3/4	1.25
6	1.4	3-3/4	----
7	1.0	5-3/8	----

*The source for this calibration data is unknown, but these data have been used since at least 1964 by the Astronautics Laboratory. ***The source for these calibration data is from a report THEORY, CALIBRATION, AND USE OF DIAPHRAGM BLAST METERS by W. T. Read, Division 2 National Defense Research Committee of the Office of Scientific Research and Development, NRDC Report No. A-392, OSRD Report No. 6463, Figure 18, Page 27, DEC45; this report was obtained from the Naval Surface Weapons Center, Silver Springs MD and was referenced in footnote (2) on page 3 of another report, OPERATION SANDSTONE JOINT TASK FORCE SEVEN TASK GROUP 7.1 BLAST MEASUREMENT SECTION, LAJ-8, PART II, Chapter 5.1, USE OF FOILMETERS ON OPERATION SANDSTONE, prepared by J. J. Meszaros and J. F. Moulton, Jr., 7JUN48, Fort Shafter, Oahu, T. H. This report indicates "For a considerable number of years air blast pressure measurements were made with the Aberdeen paper meter. The measurements obtained gave some indication of the peak pressure present. Early in the war Princeton University, under the auspices of NDRC, conducted an extensive experimental study. The primary results of these basic experimental studies..." [are shown in footnote (2) discussed above]. It is not clear when the terms Bikini and Aberdeen were first used to designate diaphragm overpressure sensors. Nevertheless, the gages were used at Bikini [atoll in the N Pacific, Marshall Islands] in the 1946 atomic bomb tests (Crossroads Project) and again at Eniwetok in 1948 (Sandstone Project) and again in 1951 (Greenhouse Project). Most of the above information came from the DoD Nuclear Information and Analysis Center (DASIAC) on 12MAY88 and is the result of a lead provided by HQ/BSO/MYEB/Lt Col Don Gage to AL/TOAE/Dick Grove in FEB88. [Editor's Note: HQ/BSO was HQ/BMO prior to 21APR89 and AL was AFAL prior to 21APR89 and AFRPL prior to 22MAR87].

Reconciliation of the bikini overpressures and bias observations using the results from the piezoelectric overpressure sensors reveals overpressures sufficient to burst the paper diaphragms

were not reached. All of the paper diaphragms were intact.

Piezoelectric Sensors.

There was no overpressure pulse. Overpressure channel PVI2 was temporarily assigned to record any electrostatic discharge (ESD) on the exterior of the Kevlar case, but the channel contained no noticeable ESD data. This crude, point contact measurement was done to rule out Kevlar as an ESD generator. In an unrelated experiment, significant ESD was seen by a similar parameter during rapid pressurization of a Peacekeeper case, and the Kevlar was only one of several possible unidentified contributors. The observation of no ESD is probably correct in this experiment, but should be investigated further, for ESD is a major problem in the [rocket] inventory.

As indicated in earlier experiments, the overpressure sensors, if used, would have behaved as follows:

Ideally, each overpressure sensor located to measure pressure should respond to a passing pressure pulse with a characteristic graph. The graph's curve should have a prominent leading edge rising from a stable initial condition. The typical leading edge should polarize positively and rise to the curve's maximum peak pressure over a smooth and almost linear path. At the peak pressure, the curve should inflect, and, at this reversal, enter into a characteristic depolarization decay consisting of an almost linear component followed by a distorted exponential component that returns to below the initial condition with an undershoot, more fully described below, representing rarefaction and the start of the refractory period.

More often than not, the linear decay should gradually change into a sluggish curve containing one prominent inflection, forcing the plot into the opposite direction, but staying below the initial condition. Eventually, the pressure rarefaction should deteriorate completely, and the plot should return smoothly to the initial condition, ending the refractory period.

Modulations and variations in behavior are caused by sensor placement (parallel or perpendicular to the flow direction), reflections, pressure wave distortions, time constants, frequency response, particulate impingement, insulation resistance, short circuits, open circuits and gas cloud geometry, etc.

DESCRIPTION OF THE EMBRITTLEMENT PROCEDURE. The ARDE embrittlement procedure dated 21MAR89 was followed. The 22" diameter vessel was boss embrittled. Embrittlement was inhibited, where required, with a maskant. Embrittlement was started at 0800 hours on 3APR89. The current level was 0.055 amperes, a significant decrease from the 0.160 amperes used on test 12. Seventy-two hours of embrittlement were completed at 1110 hours on 6APR89. The tank was immediately moved from the shop embrittlement area to the test site, instrumented, hooked up, checked and pressure tested at 1235 hours on 6APR89. The

electrolyte was sulphuric acid. Sodium arsenite was added as an enhancer. The maskant was just below the boss weld.

ADMINISTRATIVE INFORMATION.

Revision Record. Initial Issue: 28OCT87. Revision A: 13NOV87: added text here and there. Revision B: 4DEC87: errors fixed: 0.15 amperes was 1.5 amperes; text added to paragraphs: PVSDUT/1904; Displacement Sensors. Revision C: 15DEC87: text added to paragraph Piezoelectric Sensors; other minor changes. Revision D: 3May88: minor changes. Revision E: 29AUG89: minor changes and some additions; embrittlement procedure added; current level added. ITT comments added. Distribution List changed.

Filename: testrv13

Distribution: ARDE, Aris Escolona, Dave Gleich
PI. Dr. Pius Chih Hsu Chao
Aerospace Corp., Dr. Yen Pan
AFAL, Jim Miller, Dick Grove,
Dr. Tae-Woo Park
ITT, Richard Thomsen
PAFB, Pete Tadie
HQ/BSD/MYEB/Lt Col Don Gage

Office of Primary Responsibility. USAF/AFAL/TOAE/Dick
Grove/Edwards CA 93534.

E.10.3 Pressure and Strain Versus Time Plots

Figures E-118 to E-129 give pressure versus time and selected strain versus time plots.

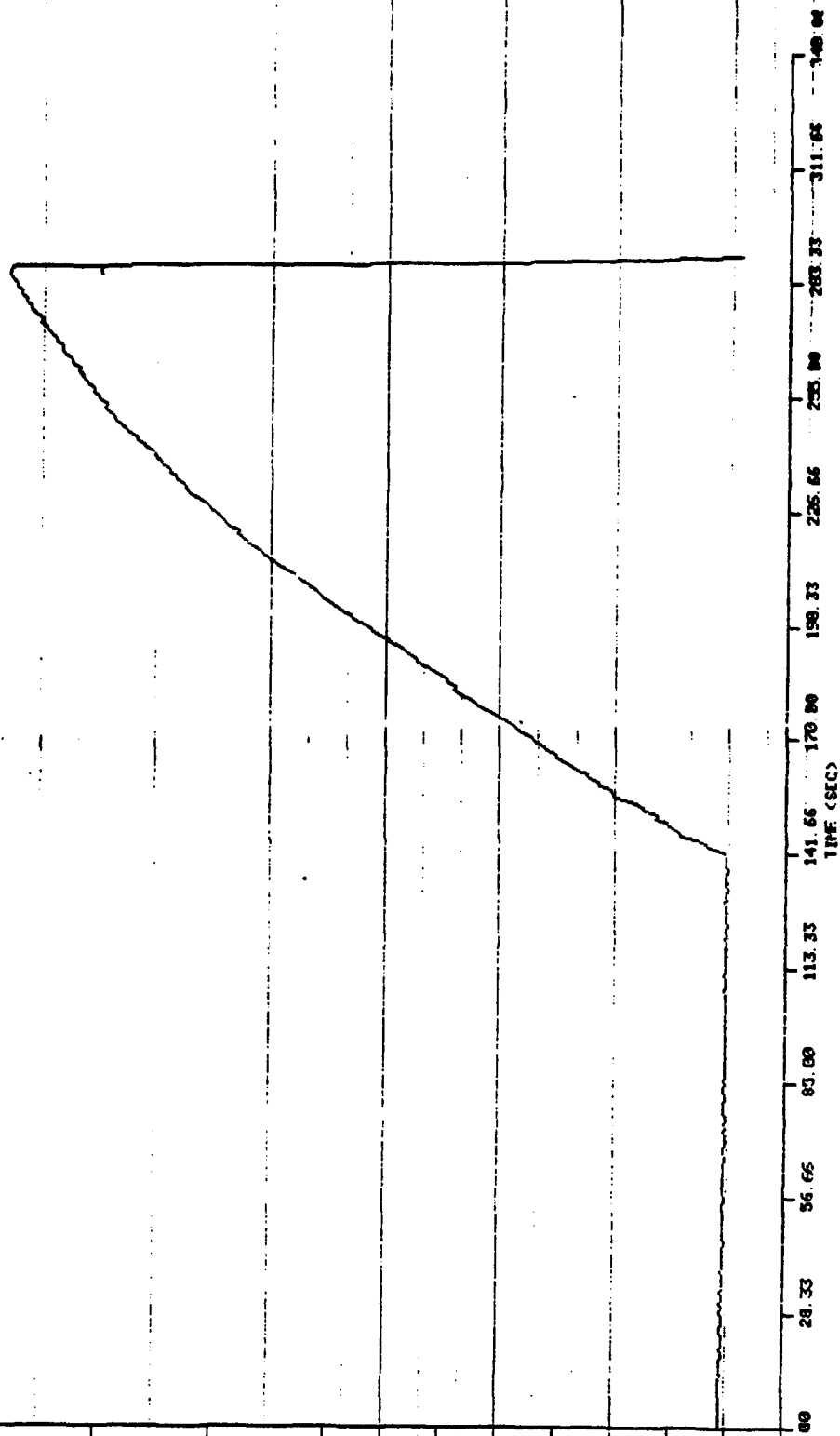
Strain gage locations are sketched on Figures E-130. Odd numbered gages are parallel to the fiber wrap and even numbered gages are perpendicular to the fiber wrap. The photograph of Figure E-132 shows test control console activity in the test control building during the test.

E.10.4 Post Test Inspection

The tank was first inspected on the test stand immediately after the test. The tank fiber shell was intact. Some exterior fiber damage in the vicinity of the hydrogen embrittled boss and to a lesser extent near the other boss, were observed as shown in the photographs of Figures E-133 and E-134. Liner failure was verified by a leak check. The test tank was shipped to ARDE where it was cut apart and the liner inside surface was die checked and photographed. The E-216 liner was in one piece. The tangential

130.00	166.00	202.00	220.00	274.00	310.00	346.00	382.00	410.00	454.50	490.00
--------	--------	--------	--------	--------	--------	--------	--------	--------	--------	--------

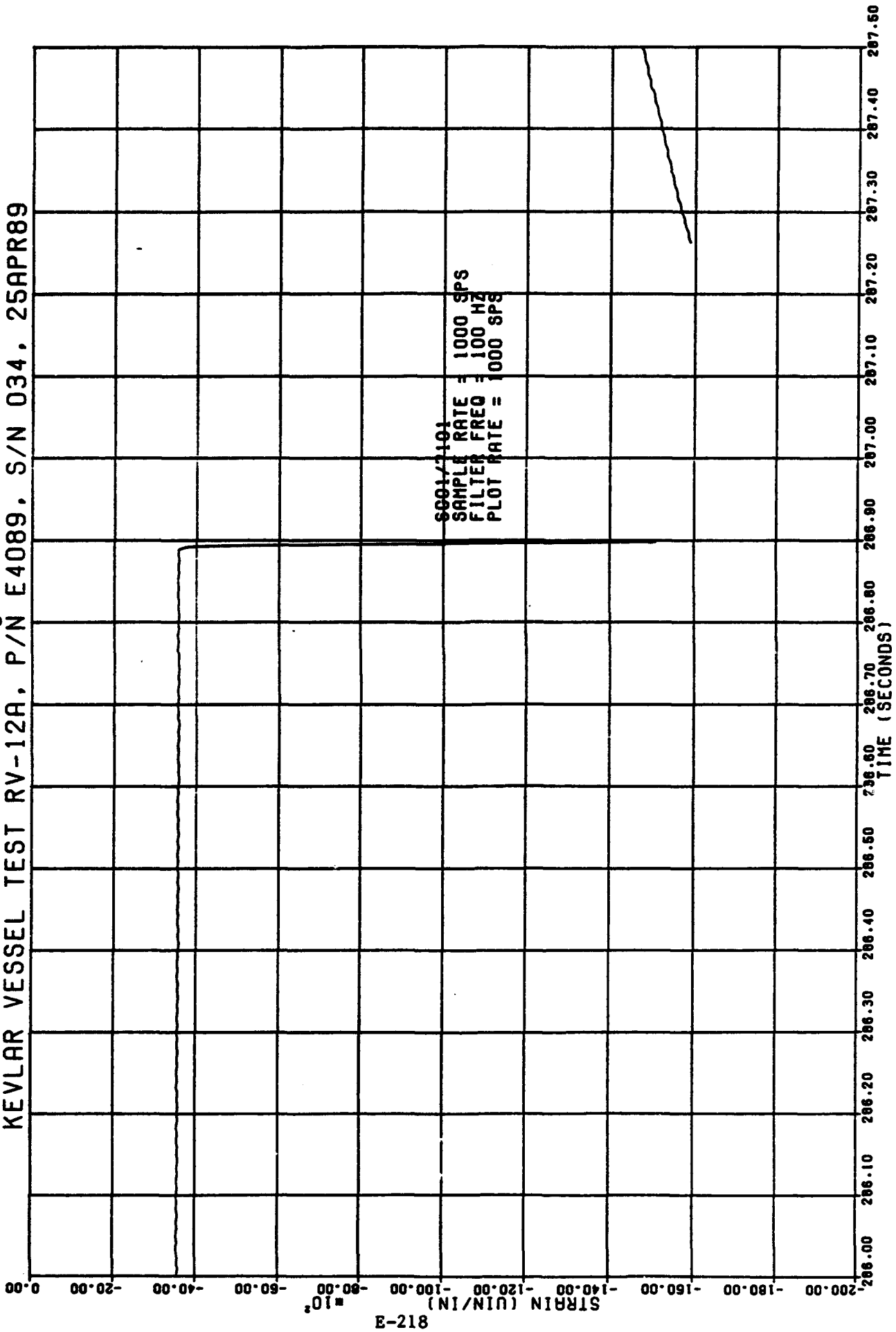
Tank pressure
Test 12A



E-217

KEVLAR VESSEL TEST RV-12A, P/N E4089, S/N 034, 25APR89

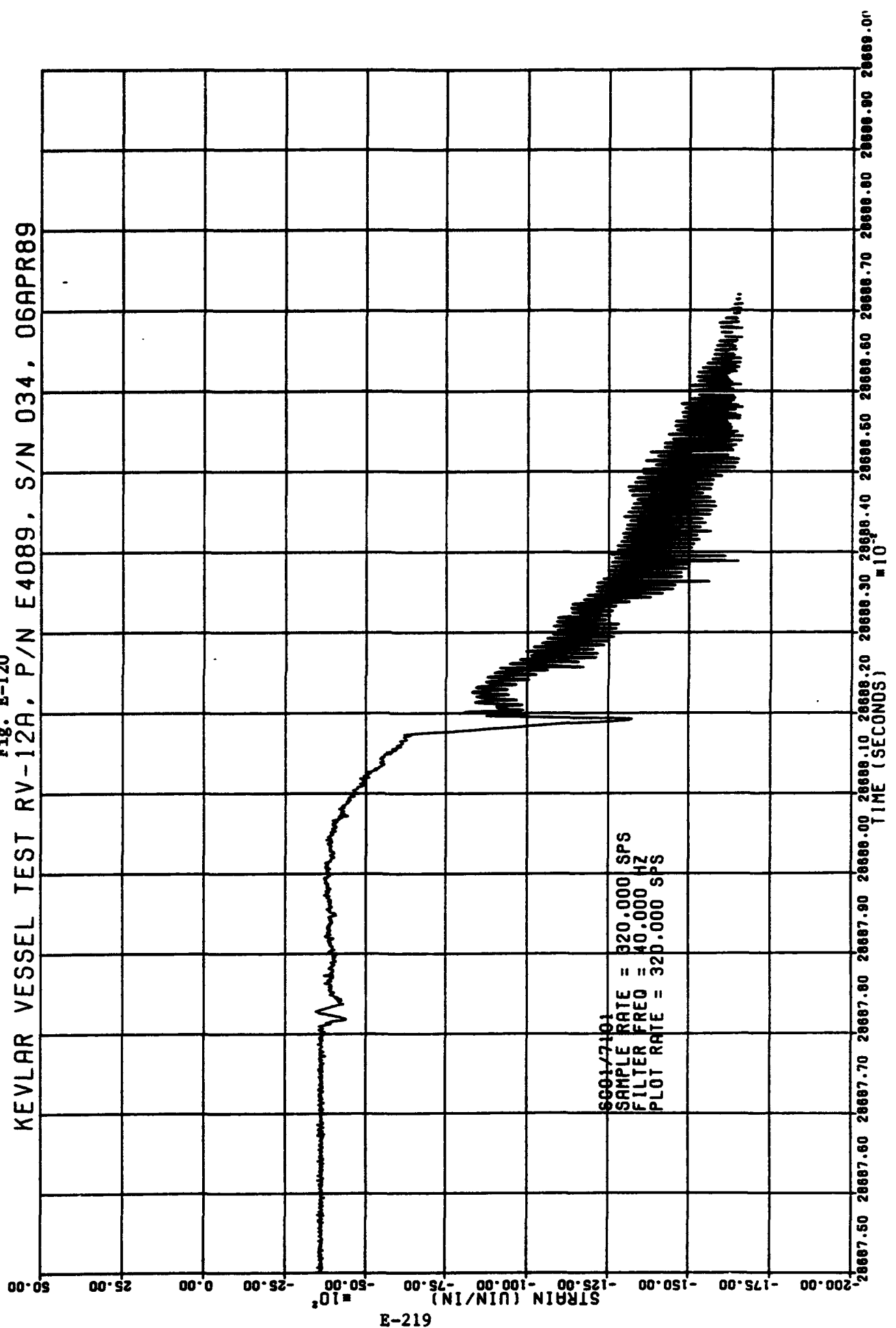
Fig. E-119



E-218

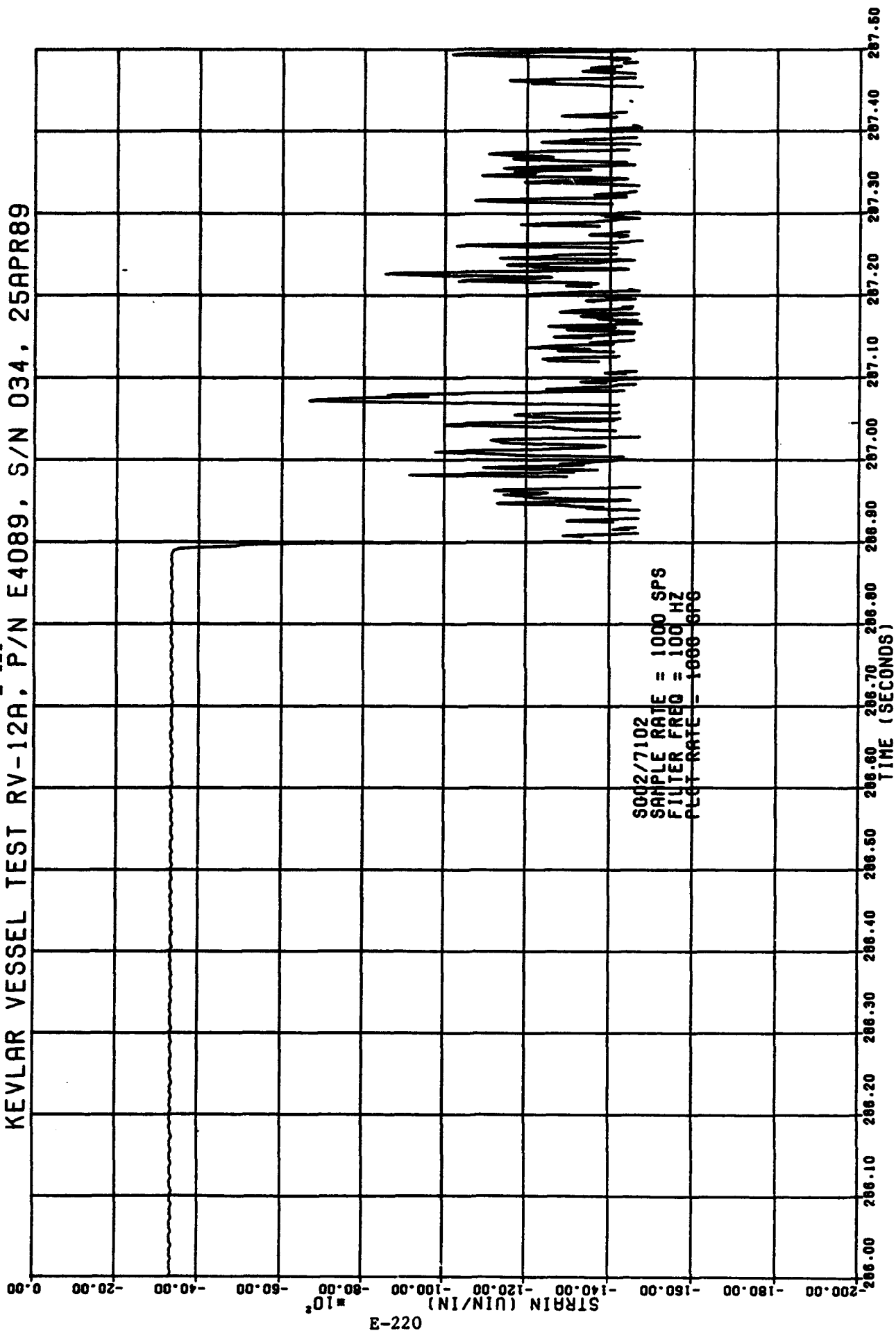
KEVLAR VESSEL TEST RV-12A, P/N E4089, S/N 034, 06APR89

Fig. E-120



KEVLAR VESSEL TEST RV-12A, P/N E4089, S/N 034, 25APR89

E-121



E-220

KEVLAR VESSEL TEST RV-12A, P/N E4089, S/N 034, 06APR89

Fig. E-122

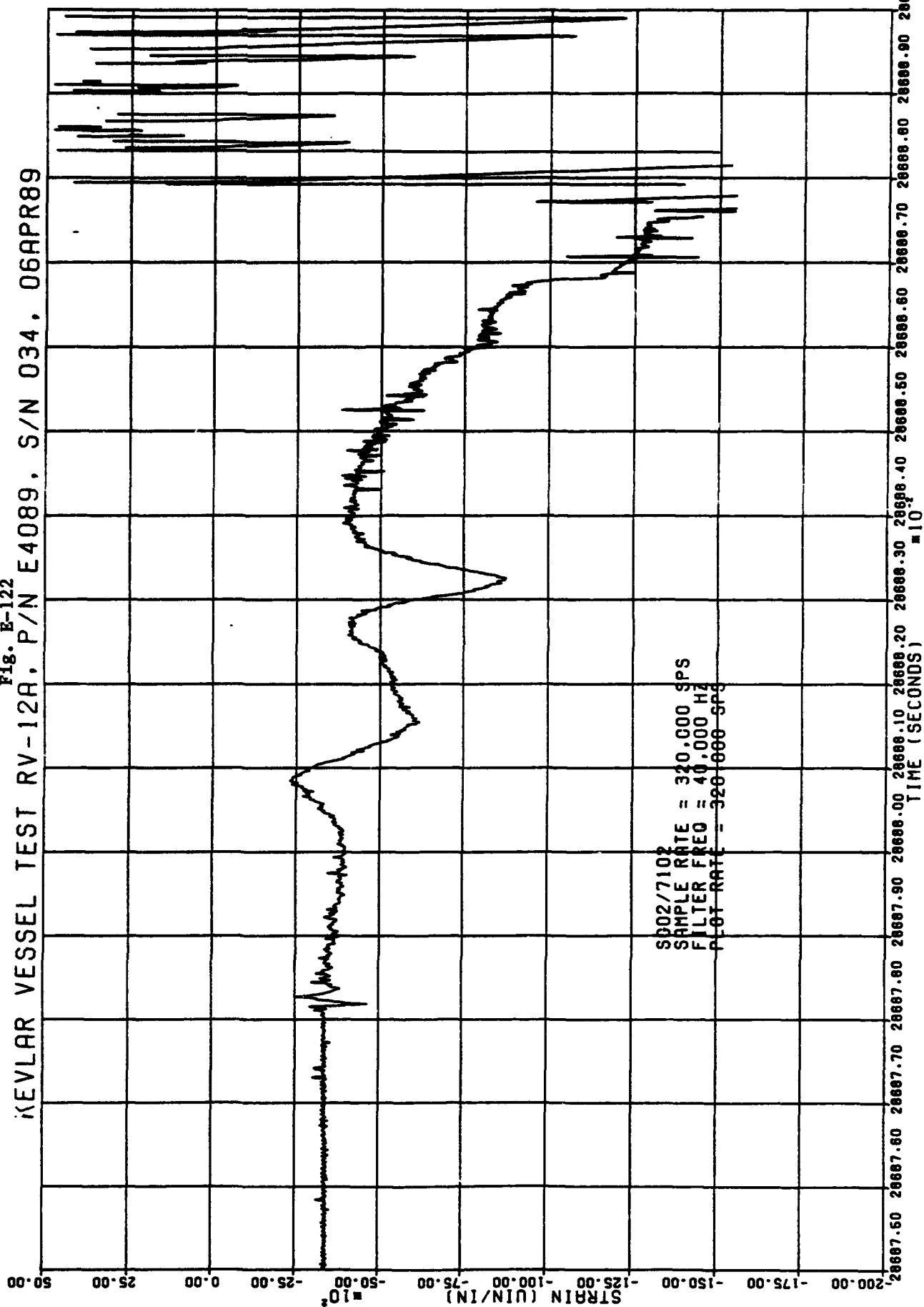
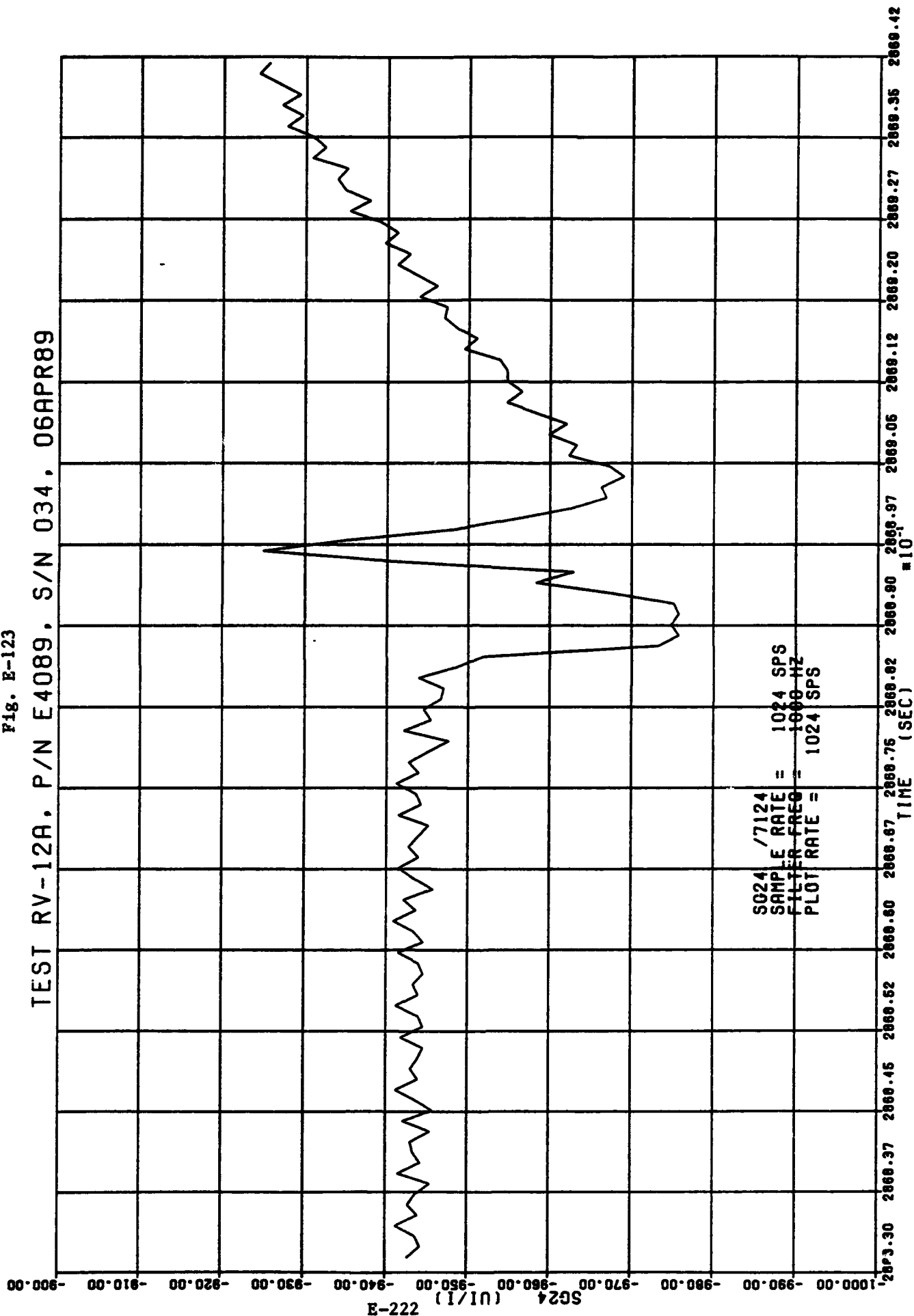


Fig. E-123

TEST RV-12A, P/N E4089, S/N 034, 06APR89



KEVLAR VESSEL TEST RV-12A, P/N E4089, S/N 034, 06APR89

Fig. E-124

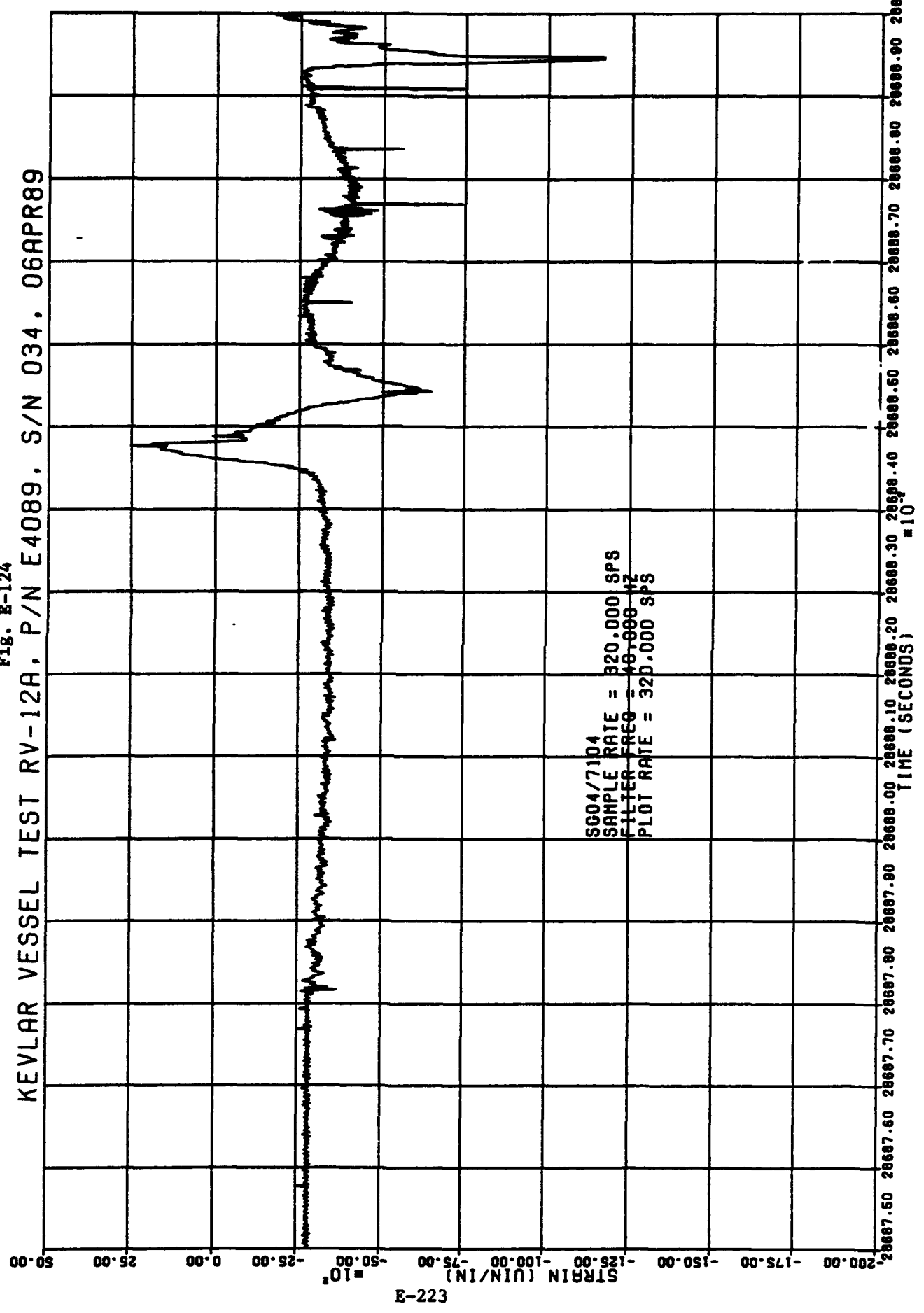
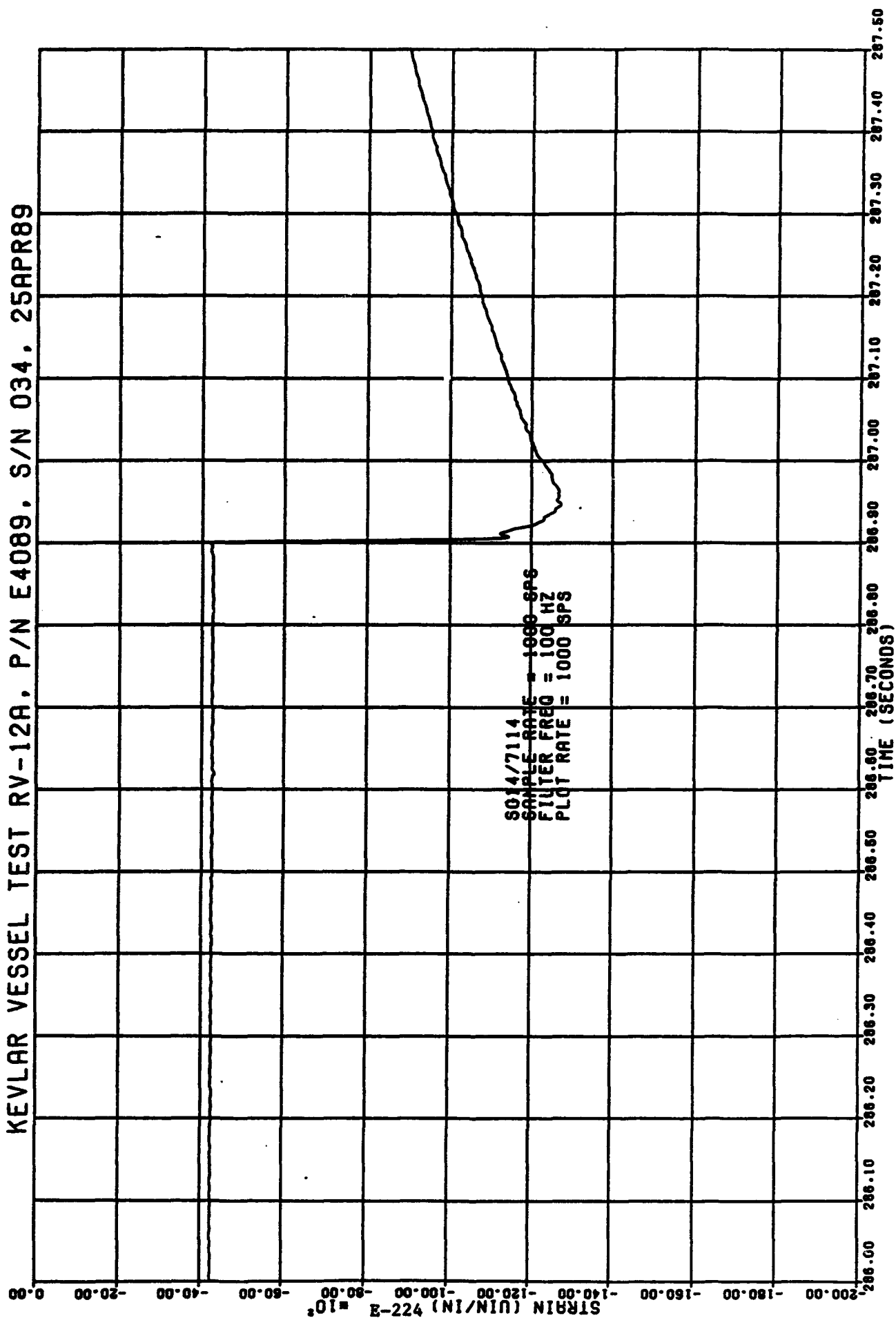


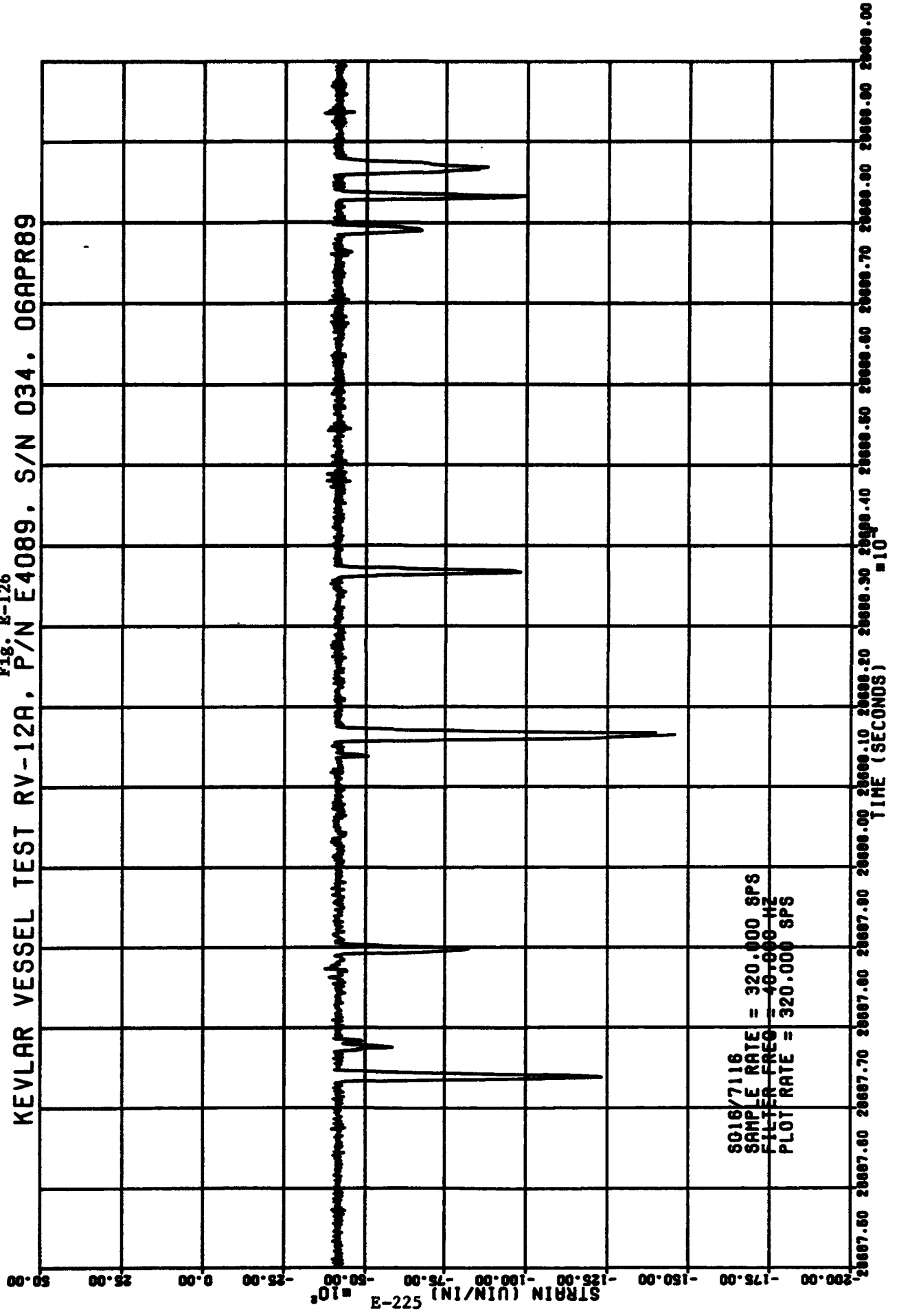
Fig. E-125

KEVLAR VESSEL TEST RV-12A, P/N E4089, S/N 034, 25APR89



KEVLAR VESSEL TEST RV-12A. P/N E4089. S/N 034. 06APR89

Fig. E-126



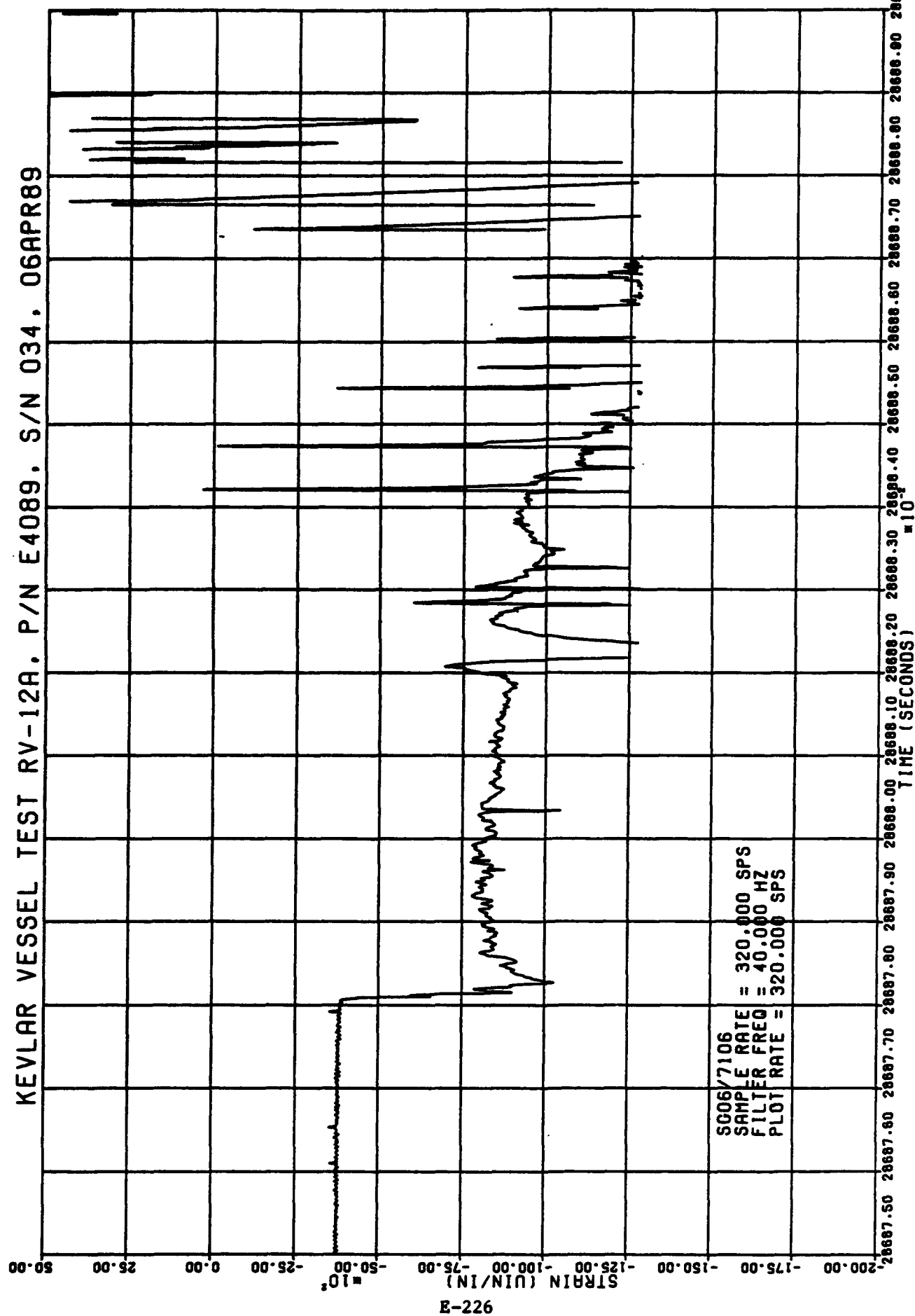


Fig. E-127

Fig. E-128

KEVLAR VESSEL TEST RV-12A, P/N E4089, S/N 034, 06APR89

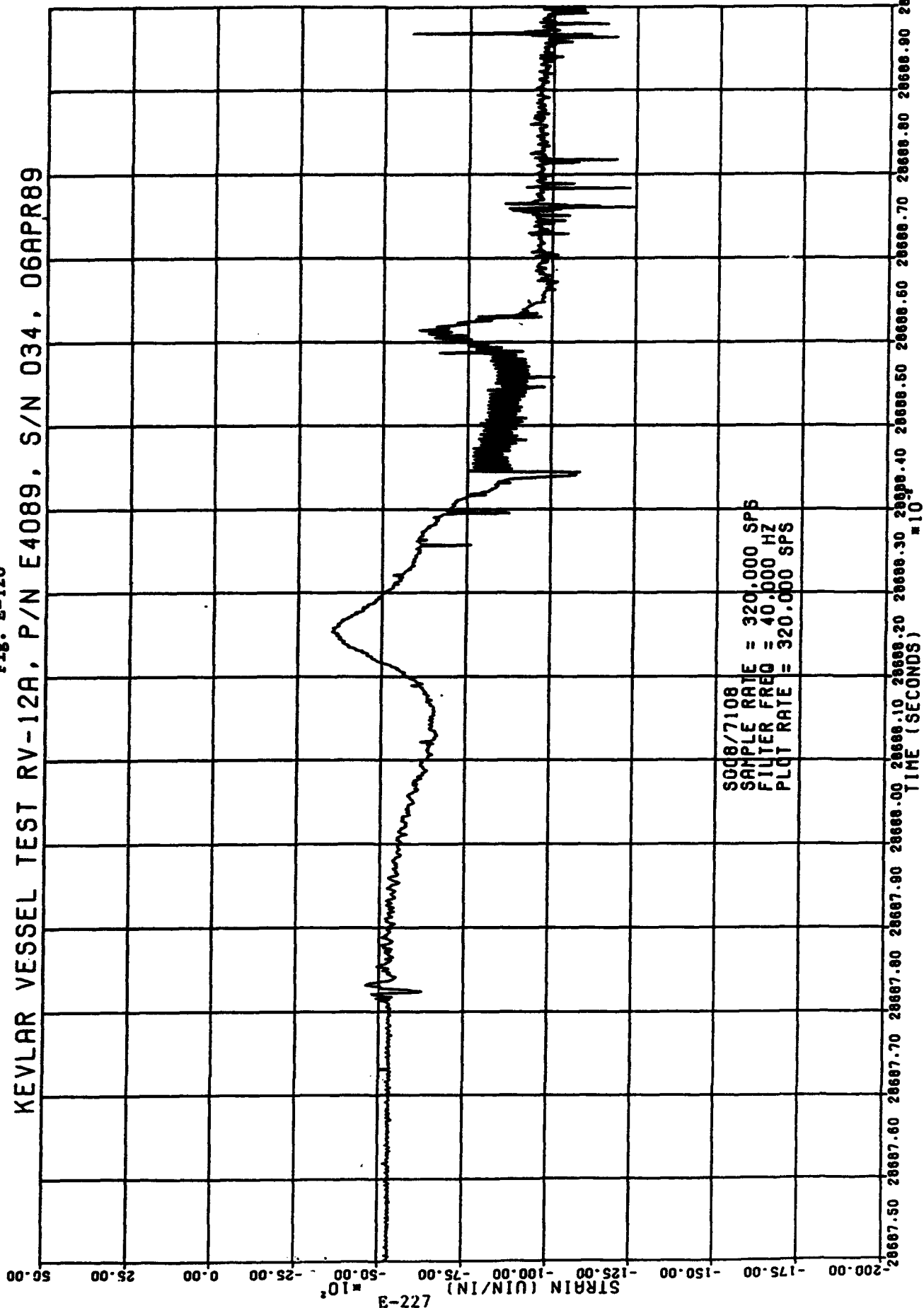


Fig. E-129

KEVLAR VESSEL TEST RV-12A, P/N E4089, S/N 034, 06APR89

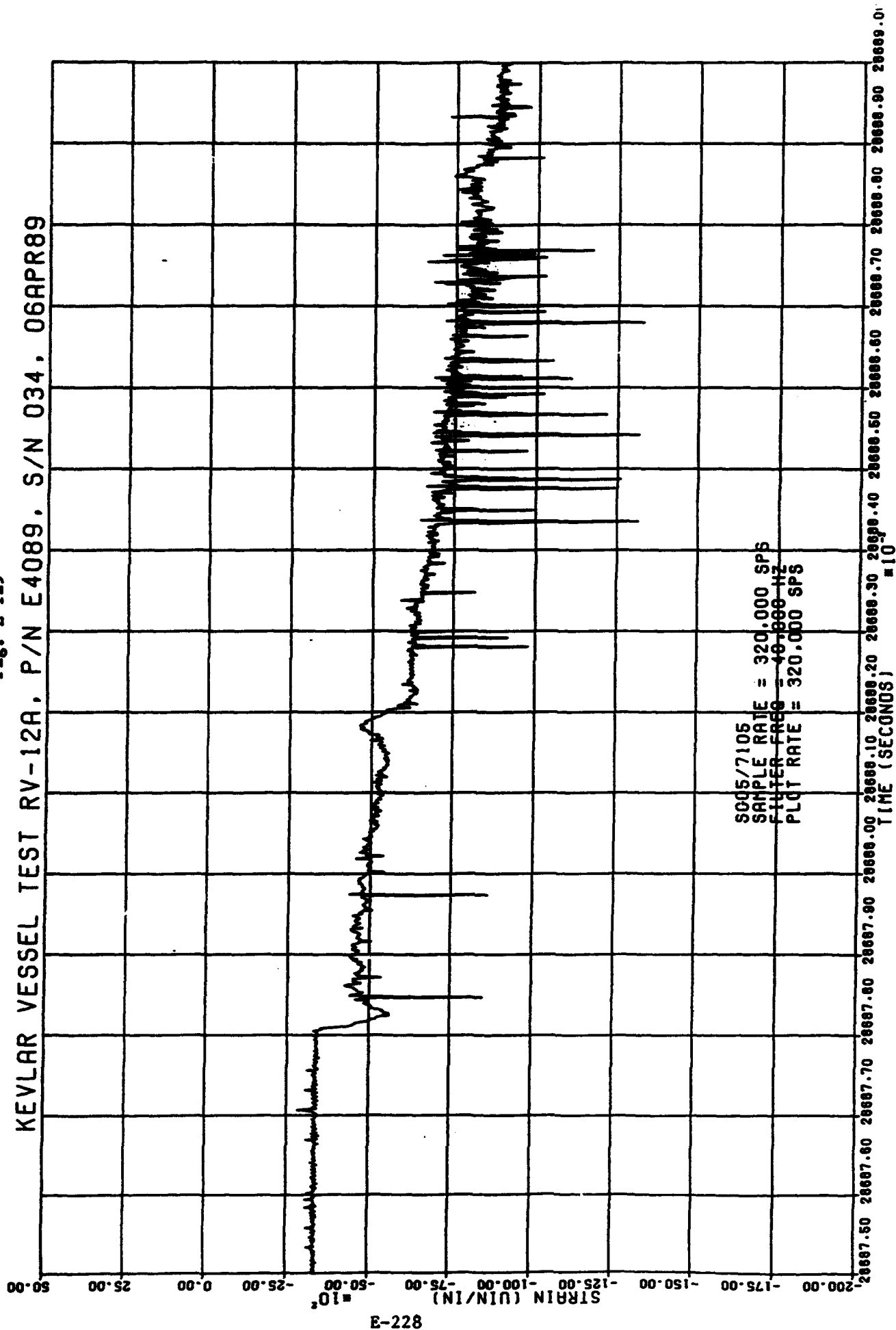
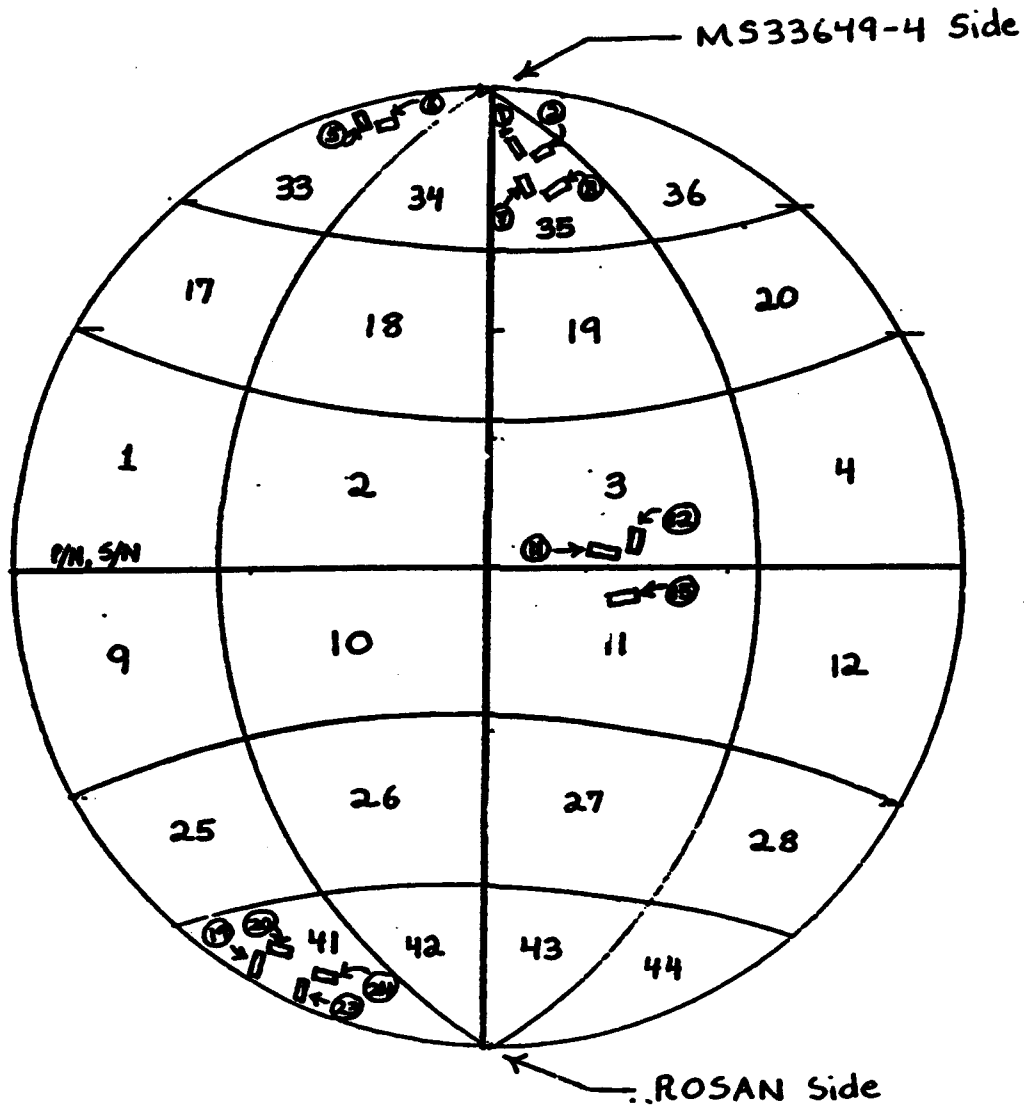


Fig. E-130

3/7/84 (Rev A) *Y/S*
 3/21/88 *Y/S*
 J/N 42001-0-19 ^(A)

P/N E4089-2, S/N 029 ^(A)
 Experiment RV-12A ^(A)



Rev A : RV-12A WAS RV-12
 42001-0-19 WAS 42001-0-17

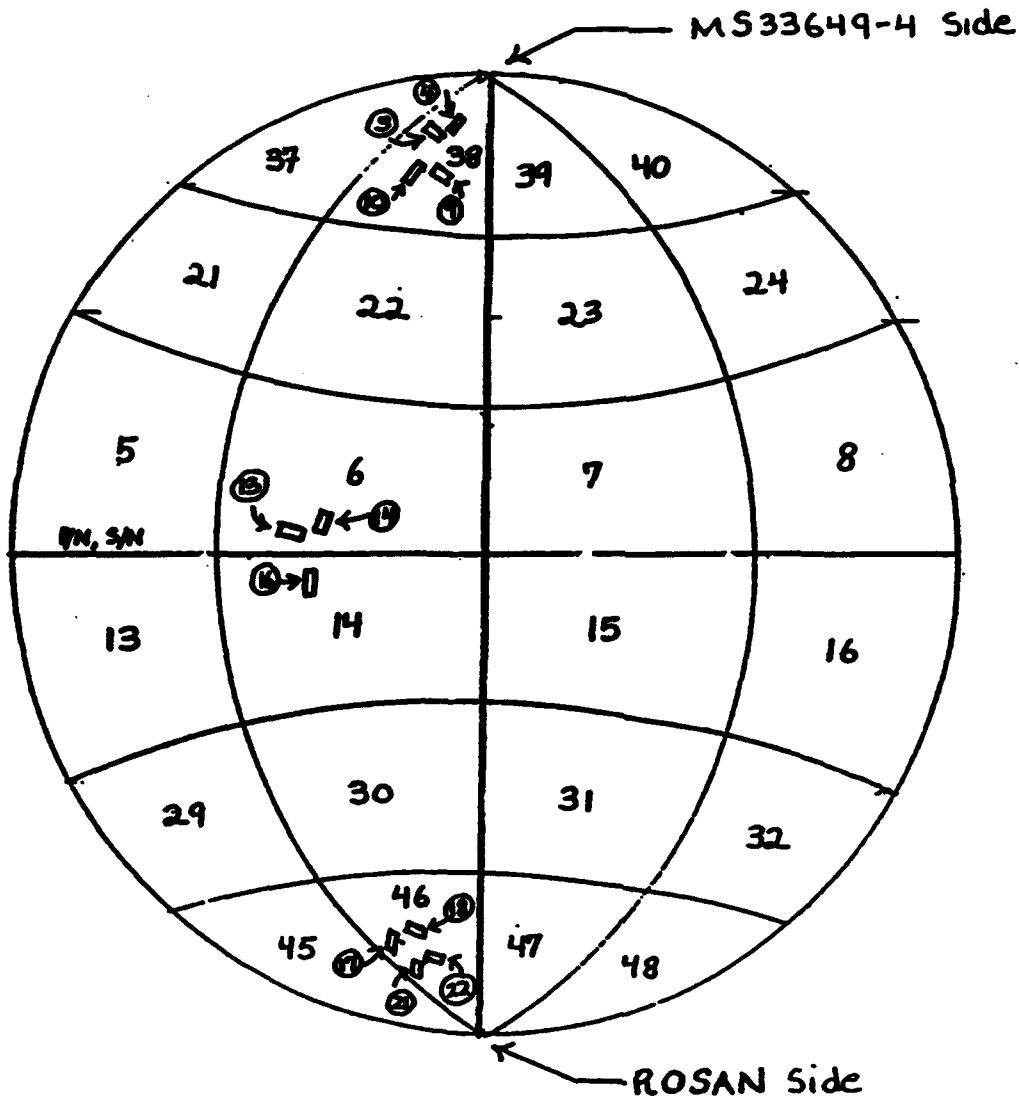
E-229

#1-#48 - Sector #'s.
 #1-#24 - Strain Gage #'s
 [rectangle with arrow] - Strain Gage
 (longitudinal axis of rectangle
 is longitudinal axis of
 strain gage)

Fig. E-131

3/6/84 Rev. A *JS*
 3/21/88 Pg. 2
 J/N 42001-0-19 ^(A)

P/N E4089-2, S/N 029
 Experiment RV-12A ^(B)



Rev. A - RV-12A WAS RV-12
 J/N 42001-0-19 WAS
 J/N 42001-0-17

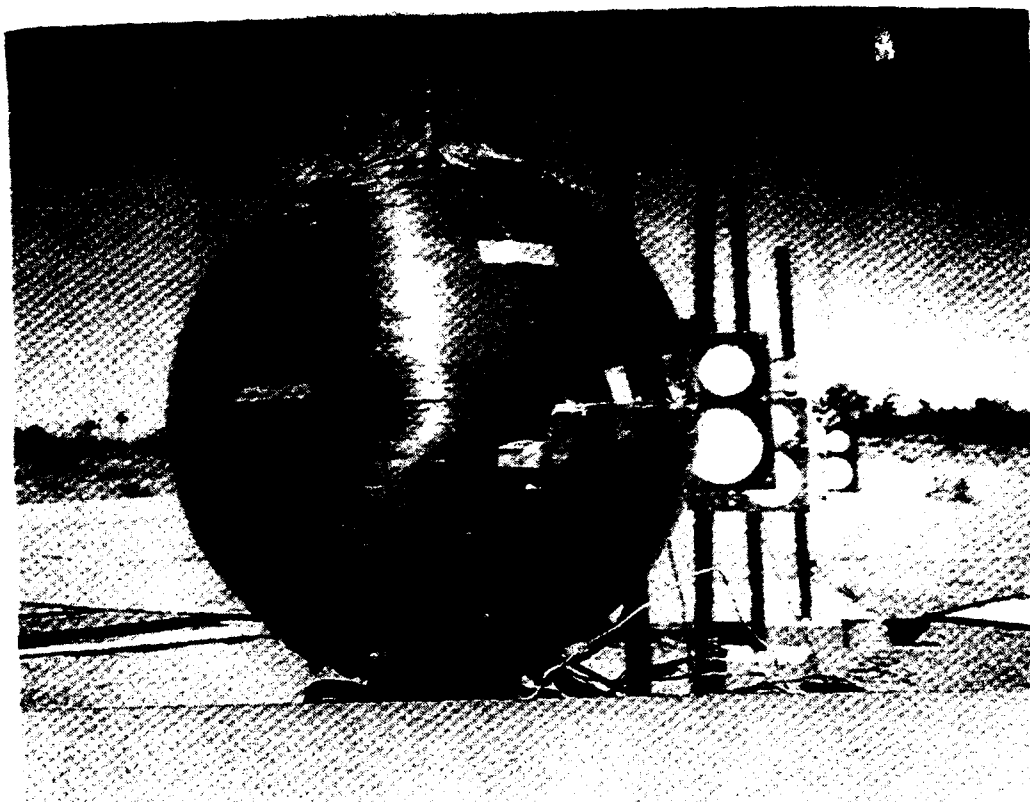
(See Pg. 1)

Fig. E-132



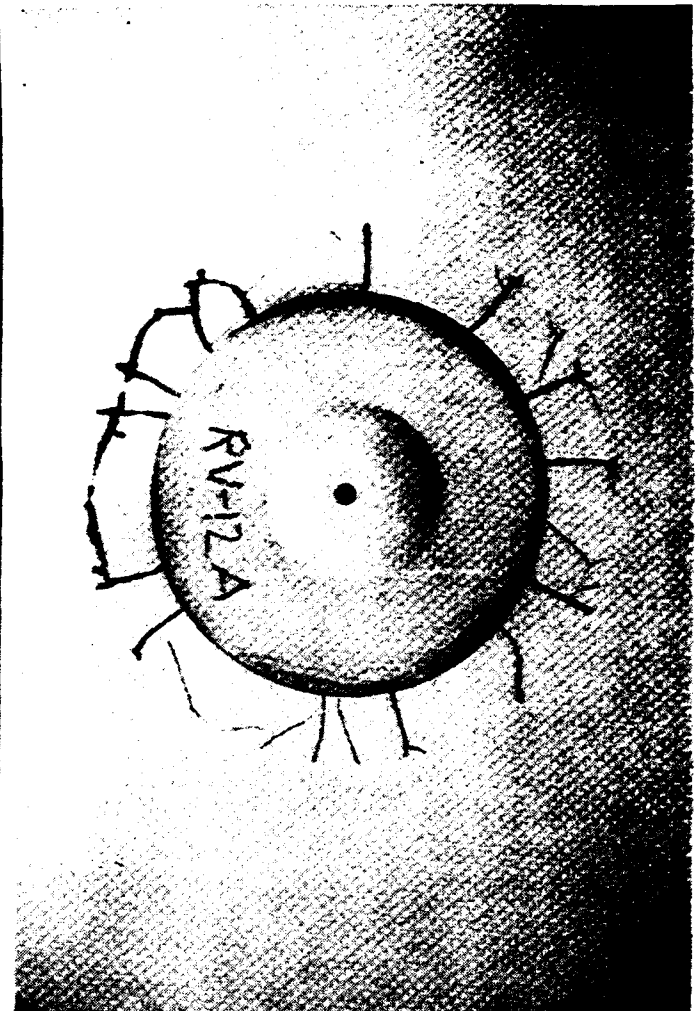
TEST RV-12A, TEST CONSOLE ACTIVITY

Fig. E-133



TEST RV-12A, POST TEST VIEW OF FIBER DAMAGE

through cracks in the embrittled boss/head weld HAZ did not run completely around the entire circumference. Discrete radial cracks running outboard from the HAZ were also found as shown on the photographs of Figures E-135 and E-136. It is to be noted that the radial cracks were arrested by the adjacent ductile liner material outboard of the embrittled boss/head weld region.



TEST RV-12A, POST TEST CLOSE UP VIEW OF FIBER
DAMAGE

TEST RV-12A, CLOSE UP OF EMBRITTLED BOSS HAZ
LINER CRACKS

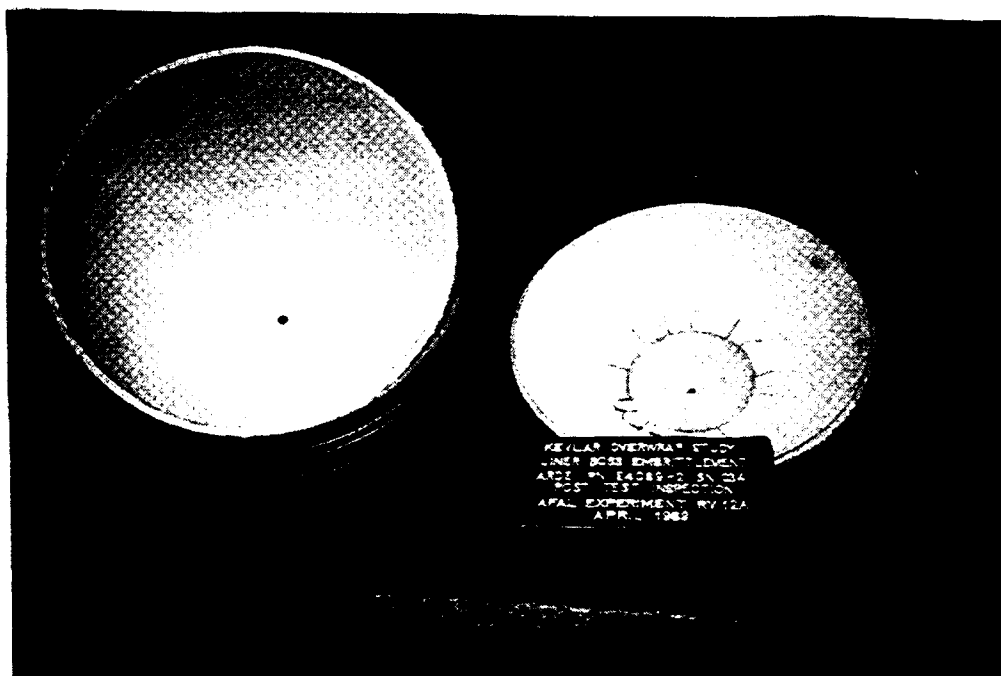


Fig. E-135

TEST RV-12A, EMBRITTLED BOSS HAZ LINER CRACKS

E.11 RV-14 Test (16" ϕ)

E.11.1 Test Vessel Description

- P/N E4168, S/N 006 (Kevlar Overwrapped 301 Cryo CRES Composite Sphere)
- Kevlar Fiber (less resin) Average Thickness - .143
- Metal Thickness - .052"
- Inside Radius - 7.66"
- Hydrogen Embrittlement Mode - Local Girth Weld Region
- Electrolytic Solution -
$$\frac{20 \text{ cc H}_2\text{SO}_4 + 980 \text{ cc Tap H}_2\text{O}}{1000 \text{ cc Solution}}$$
- Solution Additive - 500 mg Sodium Arsenite
- Sensitize Liner Inside Surface (cold pickle)
- Charging Current Density - .006 ma/in² of surface to be embrittled
- Charging Time - 72 hours
- Hold Time Before Test - 3-1/2 hours
- Adcoat AC818T liquid maskant on area not to be embrittled

E.11.2 Test Discussion and Instrumentation Observations

As detailed in the memorandum on the following page, and the instrumentation engineers observations herein, the liner inside surface was pickled to sensitize it and the local girth weld HAZ region was hydrogen embrittled. The tank was internally pressurized with helium gas to 3800 psig operating pressure. The test pressure was increased to 3900 psig operating pressure. The test pressure was increased to 3900 psig when no liner failure was noted at 3800 psig after about six (6) minutes from pressurization start. The 3900 psig pressure was vented after eight (8) minutes when all recording tape was expended. No liner failure occurred as confirmed by post-test inspection and test record review.

MEMORANDUM

Date: June 26, 1989
To: D. Gleich / S. Berko pc: RW/KP/RK
From: A. Escalona
Subject: J/N 42001-0-18 - RV-14 Experiment: 90% Kevlar Wrap
Thickness, Margin Fiber Fail Article

Test Date: Hydrogen Embrittlement - June 19th to 22nd 1989
Pressurization - June 22nd 1989
Test Facility: EAFAL, Edwards AFB, California
Test Procedure: Described in ARDE Letter #42001-KOS-174

- a) Strain gages -24 OK
- b) Pickled OK
- c) Rinsed with water, 2 volumes. OK
- d) IPA rinsed & N2 dry OK
- e) Maskant 9.31" from boss top OK
- f) Drained & N2 dried (1 hr) OK
- g) Electrolyte 8.75" from top. OK
- h) Charged 160 ma for 72 hrs OK
- i) Drained, rinsed with water, 2 vol OK
- j) IPA rinsed & N2 dried OK
- k) Tested in 3.5 hrs
Chilled at 1400 to 1500 psi
Ramped to 3800 psi - held for 4 min. - no leak
Raised to 3900 psi - held for 2 min. - no leak

Note: Test was aborted just prior to FM tape ran out.
Total test time was 9.7 MIN.

AES:sr

A. Escalona /s/

INSTRUMENTATION OBSERVATIONS (by Instrumentation Engineer)

KEVLAR TEST 014. Date: 22JUN89. Project Number 573000RV.

EXPERIMENTAL OBSERVATIONS.

Introduction. vessel S/N 006. P/N 24168 was tested. It was a 16 inch diameter stainless steel sphere and had a 90% Kevlar overwrap. The vessel was hydrogen embrittled about the birth. It was tested in a vertical configuration. The tank pressure was increased with pressure pulses, held for a while at 1500 psig, then ramped up to a plateau that was maintained between 3832 psig and 3788 psig over a time duration extending from 175.099164 to 421.799664 seconds. Plateau pressure was maintained with five short pressure bursts which were scattered throughout the plateau. A second pressure ramp was started at 421.799664 seconds, and this short ramp ended after only 13 seconds at 434.899974 seconds and 3914 psig. The new plateau, starting at the end of the second ramp, ended at 3881 psig and 534.119148 seconds. The new plateau contained only one pressure correction. The vessel did not leak, and tank pressure was vented at the end of the new plateau.

Venting was done with the vent valve. The vent profile was clearly demarcated, almost linear, done at a rate of approximately -170.66 psig per second, not recorded near the end, not stopped for repressurization attempts, unremarkable and within normal limits.

As in previous tests, SG24 and the other strain gages were impressive mirror images of the pressure profile. Case strain in composite cases can be detected and is proportional to case pressure, but a calibration factor must be determined. The SG performance profiles will be slightly noisier than the vessel pressure parameter and retain the risk of SG debonding.

Post-run inspection. witness panels, displacement gages and acoustic emission technology were not used. Extensive damage to the vessel's instrumentation wiring and pressurization plumbing was not observed. The over pressure sensor data showed no change and are discussed elsewhere. No Kevlar damage was observed and fraying was not obvious near either boss. The Kevlar remained intact. No major damage to the resin was observed.

IMPRESSIONS FROM THE DIGITIZED FM DATA.

Strain Gages.

Strain Gage Locations. The strain gages were located IAW ARDE drawing dated 3/7/89, Revision A dated 21MAR89, accompanying a 21MAR89 cover letter. The even strain gages are perpendicular to the wrap, and the odd strain gages are parallel to the wrap.

Strain Gage Temperature. Not shown on this print are the thermocouple locations. See the Instrumentation Specification.

Sheet for the locations and item numbers. The 9 thermocouple locs form a family of curves with almost identical profiles. Collectively, the gages measured temperature behavior over a span between 115 degrees F and 153 degrees F, approximately. However, each gage didn't change much during the plateau, and the typical plateau temperature variation didn't exceed about 8 F degrees. A similar small variation was also seen on test 11. One thermocouple, TT2/2102, had a very steady rise rate. Other thermocouples, TT3/2104, TT9/2205, for example, had major temperature decreases modulating the rise rate in the last one third of the first plateau. All temperature profiles contained small bipolar modulations, some noise near the start and finish of the profile and reasonable noise floors. The vessel's SG temperature behavior is considered to be within normal limits, and it wasn't investigated with further detail.

Performance Summary. There were 23 strain gages recorded on the FM tape recorder, and 21 functioned. Most plots had substantial activity, and most plots had 6 to 12 noise spikes. During the initial conditions, all gages had much better than reasonable noise floors. The noise floors are discussed elsewhere under Noise Floors. None of the strain gages were destroyed by tank depressurization.

Sign Convention. Positive strain gage polarity represents compression, and negative strain gage polarity represents tension.

Noise Floors. Except as noted elsewhere, the strain gage and other parameters' noise floors did not include major transverse or common-mode minus L(d1/dt) transients, artifacts, crosstalk, atmospherics, noticeable RFI, intermodulation, spurious parasites, or signals. However, latent noise or data manifestations may be obscured in some parameters, and digital signal processing may be needed for signal enhancement. In general, the data appeared to be unbiased, precise and accurate. There was no particular SG that could be identified as the noisiest but this is a judgement call. SG10 through SG17 and SG18 through SG23 had noise during venting.

Performance Exceptions. Strain gage behavior was within normal limits, except as noted. The following comments are based on interpretations of the 100 Hz data pass.

In general, strain gage behavior was similar to previous tests. The general trend for the active strain gages was a tension strain polarization pattern proportional to tank pressure with corrections for glitches, polarity, shifts and some possible debonding, etc. The dynamic performance did not include major oscillations. All graphs had noise floors within normal limits. Most graphs had a few glitches. Plots for SG10 through SG17 and plots for SG18 through SG23 had noise during the vent operation. Plots for SG01 through SG09 did not plot data much past 440 seconds, but the columnar data is present up to 599.99810 seconds.

maximum SG Values and Performance Trends. The following codes are used below:

NWNL noise within normal limits

GRZ good return to zero

ARZ approximate return to zero

NRZ no return to zero

C compression strain

T tension strain

NTE not to exceed

OSC oscillation

unipolar: data predominately in one direction.

Bipolar: data in both directions but not necessarily evenly balanced between polarities. In some cases, the data carrier was unipolar in tension but contained bipolar compression excursions.

Units for strain values are in microinches/inch

SG01 Unipolar, T, no data past 155 seconds.

SG02 Unipolar, T

SG03 bad

SG04 Bipolar, T & C, compare with SG11.

SG05 Unipolar, T

SG06 Unipolar, T

SG07 Unipolar, T

SG08 Unipolar, T

SG09 Unipolar, T

SG10 Unipolar, T but the plateau is suspiciously too flat.

SG11 bad

SG12 Bipolar, T & C, compare with SG04.

SG13 Unipolar, T

SG14 Unipolar, T

SG15 Unipolar, T, Exhibited the maximum net tension strain change

SG16 Unipolar, T

SG17 Unipolar, T, Represents a most typical profile

SG18 Unipolar, T

SG19 Unipolar, T

SG20 Bipolar, T & minimal C

SG21 Unipolar, T

SG22 Unipolar, T

SG23 unipolar, T

SG24 Unipolar, T, Recorded on the DACS only. Not on FM.

Performance Summary:

All channels included codes: T and NRZ. Out of the 23 SG channels recorded on the FM tape recorder, two channels were bad. Twenty channels had unipolar tension behavior. Three channels

had bipolar strain activity, probably due to debonding or legitimate abrupt changes in strain.

The maximum strain change was seen on SG13, which started out with a strain of 1584 $\mu\text{in/in}$ at 60.79981 seconds at the 1500 psig pressure plateau and decreased to a -2545 $\mu\text{in/in}$ tension value at 441.79981 seconds at the 3914 psig pressure plateau, which is a net change in tension of $1584 - (-2545) = 4129 \mu\text{in/in}$. This channel was reported to have noisy cal data although the plot during the run was within normal noise limits; therefore, the run data might be considered questionable.

More typically, most strain gages underwent a net tension strain of only 2000 $\mu\text{in/in}$. SG17 is representative of a typical SG.

Important to note is the sensitivity of the SG channels to the pressurization maintenance pulses, which is the basis for discarding SG10 data as not valid because of the excessively flat plateau. Practically all of the SG plots reflect the pressure maintenance pulses.

Note also that some some plots don't track the slope of the pressure plateau very well. In a couple of plots the slope is minimal or flat, as in SG15 and SG16. While others the slope is more prominent as in SG 13 and SG17.

If the higher frequency data pass contains information not indicated by the 100 Hz data pass, a revision will be issued and those differences will be discussed.

The above information was determined by inspecting the graphs and may contain subjective errors.

Statistical Analysis. Valid speculations about strain gage behavior may involve biserial correlation of certain dichotomies (positive or negative polarization) to assess their associations (with wrap direction, etc.). For truly dichotomous distributions, the phi coefficient can be used. Because some of these dichotomous variables are really continuous (the magnitude or duration of polarization, and the degree of wrap thickness, location & direction, etc.) and normally distributed, tetrachoric correlation may be involved. An expert statistician should be approached with a clear statement of which variables and associations are important if valid conclusions about some of these data are to be obtained. An accurate evaluation of which variables are really dichotomies and which are proportionally continuous would also have to be prepared and passed to the statistician.

Data Analyst's Comments.

The ITT Data Analyst, Richard Thomsen, indicated on the front sheets of the three 100 Hz passes "No data on DP01, DP02, DP12" and "SG01/7101 goes bad at 155 seconds. SG03/7103 is bad. No IRIG timing signal" and "SG15/7115 noisy cal data. SG11/7111 is

bad. No IRIG timing signal."

IMPRESSIONS FROM THE QUICK-LOOK AND DIGITAL DATA ACQUISITION SYSTEM DATA.

Tank Pressure. PTANK/1901 was located on the top of the tank in the vent line. PVSOUT/1904 was also in the vent line, but it was located at the valve box about 15 feet from the tank. PTANK/1901 functioned as described under the Pressurization Ramp... paragraph.

The locations of the transducers was the same as test 10.

PVSOUT/1904 data were similar to PTANK/190 except for the reduced frequency response because of the long pressurization line.

SG24. SG24 tracked the vessel pressure profile with corrections for polarity, etc. This parameter, as in the previous tests, was only recorded on the DACS for quick-look purposes.

Phase Behavior and Frequency Response. Noted is the phase behavior; the two gauges were very close together in the time domain.

Other Parameters. The performance of the other parameters was within normal limits, except as noted below; this was determined by a quick review of the gauges for items PHXIN/1902, PHXOUT/1900, PTRAIL/1903, THXIN/2100, TBALL/2211, TBSOUT/2210, TBSIN/2209, THXOUT/2101. Heat Exchanger Output shows 6 major spikes with noticeable decay times. The spikes are apparently due to minus $L(di/dt)$ transients from the pressurization efforts needed to maintain a pressure plateau with the pressurization valve. Suppression with a diode at the valve solenoid is required to stop the problem, or the spikes may be disregarded. The spikes appear as glitches on pressure parameters such as PHXIN/1902, PHXOUT/1900, PTRAIL/1903 and as very small deflections on temperature parameter THXIN/2100.

The IRIG Time Code. IRIG/3808 TIMING, did not record satisfactorily on the FM.

IMPRESSIONS FROM THE OVERPRESSURE SENSORS.

The vessel did not leak. There was no overpressure pulse. Overpressure data was not reduced.

The following text applies to overpressure sensors and is retained for reference.

Bikini Gages. A Bikini gage is one piece of bond paper compressed between two metal plates containing different sized round holes. The gages are aligned so the paper is perpendicular to the pressure source. Discrete pressure data can be obtained

and is a function of the location of the damaged paper diaphragms. The approximate calibration is as follows for the indicated hole size using bond paper:

HOLE #	PSIG*	SIZE	PSIG**
1	7.3	5/8	4.4
2	5.2	7/8	3.3
3	3.7	1-1/4	2.4
4	2.7	1-7/8	1.7
5	1.9	2-3/4	1.25
6	1.4	3-3/4	----
7	1.0	5-3/8	----

*The source for this calibration data is unknown, but these data have been used since at least 1964 by the Astronautics Laboratory. ***The source for these calibration data is from a report THEORY, CALIBRATION, AND USE OF DIAPHRAGM BLAST METERS by W. T. Read, Division 2 National Defense Research Committee of the Office of Scientific Research and Development, NRDC Report No. A-392, DSRD Report No. 6463, Figure 18, Page 27, DEC45; this report was obtained from the Naval Surface Weapons Center, Silver Springs MD and was referenced in footnote (2) on page 3 of another report, OPERATION SANDSTONE JOINT TASK FORCE SEVEN TASK GROUP 7.1 BLAST MEASUREMENT SECTION, LAJ-8, PART II, Chapter 5.1, USE OF FOILMETERS ON OPERATION SANDSTONE, prepared by J. J. Meszaros and J. F. Moulton, Jr., 7JUN48, Fort Shafter, Danu, T. H. This report indicates "For a considerable number of years air blast pressure measurements were made with the Aberdeen paper meter. The measurements obtained gave some indication of the peak pressure present. Early in the war Princeton University, under the auspices of NDRC, conducted an extensive experimental study. The primary results of these basic experimental studies..." (are shown in footnote (2) discussed above). It is not clear when the terms Bikini and Aberdeen were first used to designate diaphragm overpressure sensors. Nevertheless, the gages were used at Bikini [atoll in the N Pacific, Marshall Islands] in the 1946 atomic bomb tests (Crossroads Project) and again at Eniwetok in 1948 (Sandstone Project) and again in 1951 (Greenhouse Project). Most of the above information came from the DoD Nuclear Information and Analysis Center (DASIAC) on 12MAY88 and is the result of a lead provided by HQ/BSO/MYEB/Lt Col Don Gage to AL/TOAE/Dick Grove in FEB88. [OPR's Note: HQ/BSO was HQ/BMO prior to 21APR89 and AL was AFAL prior to 21APR89 and AFRPL prior to 22MAR87].

Reconciliation of the bikini overpressures and bias observations was not done as there was no overpressure pulse. All of the paper diaphragms were intact.

Piezoelectric Sensors.

There was no overpressure pulse.

As indicated in earlier experiments, the overpressure sensors, if used, would have behaved as follows:

Ideally, each overpressure sensor located to measure pressure should respond to a passing pressure pulse with a characteristic graph. The graph's curve should have a prominent leading edge rising from a stable initial condition. The typical leading edge should polarize positively and rise to the curve's maximum peak pressure over a smooth and almost linear path. At the peak pressure, the curve should inflect, and, at this reversal, enter into a characteristic depolarization decay consisting of an almost linear component followed by a distorted exponential component that returns to below the initial condition with an undershoot, more fully described below, representing rarefaction and the start of the refractory period.

More often than not, the linear decay should gradually change into a sluggish curve containing one prominent inflection, forcing the plot into the opposite direction, but staying below the initial condition. Eventually, the pressure rarefaction should deteriorate completely, and the plot should return smoothly to the initial condition, ending the refractory period.

Modulations and variations in behavior are caused by sensor placement (parallel or perpendicular to the flow direction), reflections, pressure wave distortions, time constants, frequency response, particulate impingement, insulation resistance, short circuits, open circuits and gas cloud geometry, etc.

DESCRIPTION OF THE EMBRITTLEMENT PROCEDURE. The ARDE embrittlement procedure dated 21MAR89 was followed. The 16" diameter vessel was girth embrittled. Embrittlement was inhibited, where required, with a maskant. Embrittlement was started on 19JUN89. The current level was 0.160 amperes. Seventy-two hours of embrittlement were completed at 22JUN89. The tank was immediately moved from the shop embrittlement area to the test site, instrumented, hooked up, checked and pressure tested on 22JUN89. The electrolyte was sulphuric acid. Sodium arsenite was added as an enhancer.

ADMINISTRATIVE INFORMATION.

Revision Record. Initial Issue: 8SEP89. Distribution changed.
Revision A: 19SEP89. Removed Draft Status from document. Made
major corrections per ARDE request. 16", 19JUN89, girth, 0.016
and 22JUN89 were 22", 3APR89. 0.055 and 6APR89. Added 100 Hz SG
data pass information to Maximum SG Values and Performance
Trends.

Filename: testrv14

Distribution: ARDE, Aris Escolona, Dave Gleich
PI, Dr. Pius Chih Hsu Chao
Aerospace Corp., Dr. Yen Pan
AFAL, Jim Miller, Dick Grove,
Dr. Tae-Woo Park
ITT, Richard Thomsen
PAFB, Pete Tadie
HQ/BSD/MYEB/Lt Col Don Gage

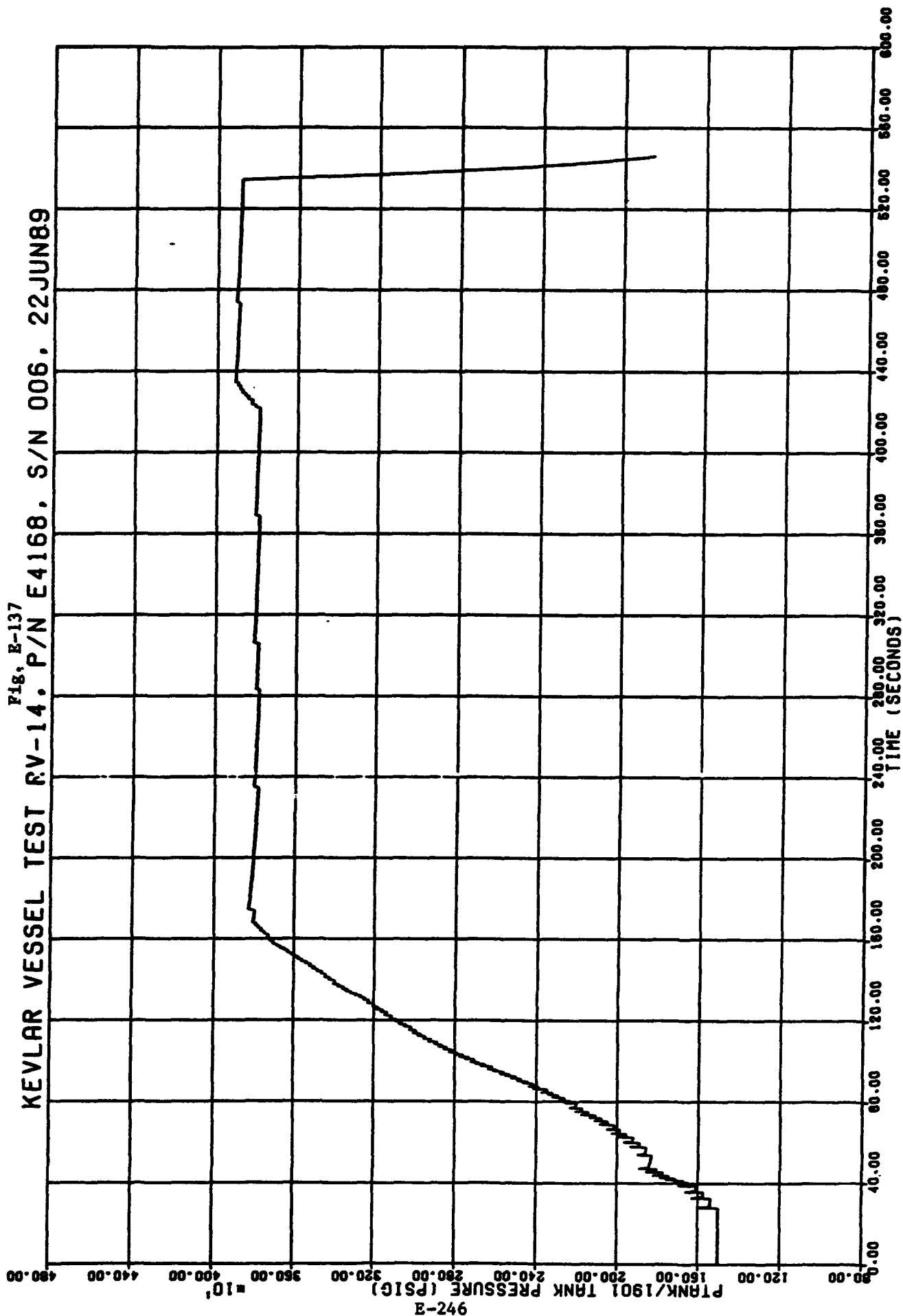
Office of Primary Responsibility. USAF/AFAL/TOAE/Dick
Grove/Edwards CA 93534.

E.11.3 Pressure and Strain Versus Time Plots

Pressure and selected strain versus time plots are shown on Figures E-137 to E-139. Odd numbered strain gages are parallel to the wrap and even numbered gages are perpendicular to the fiber wrap. Strain gage locations are indicated on Figures E-140 and E-141.

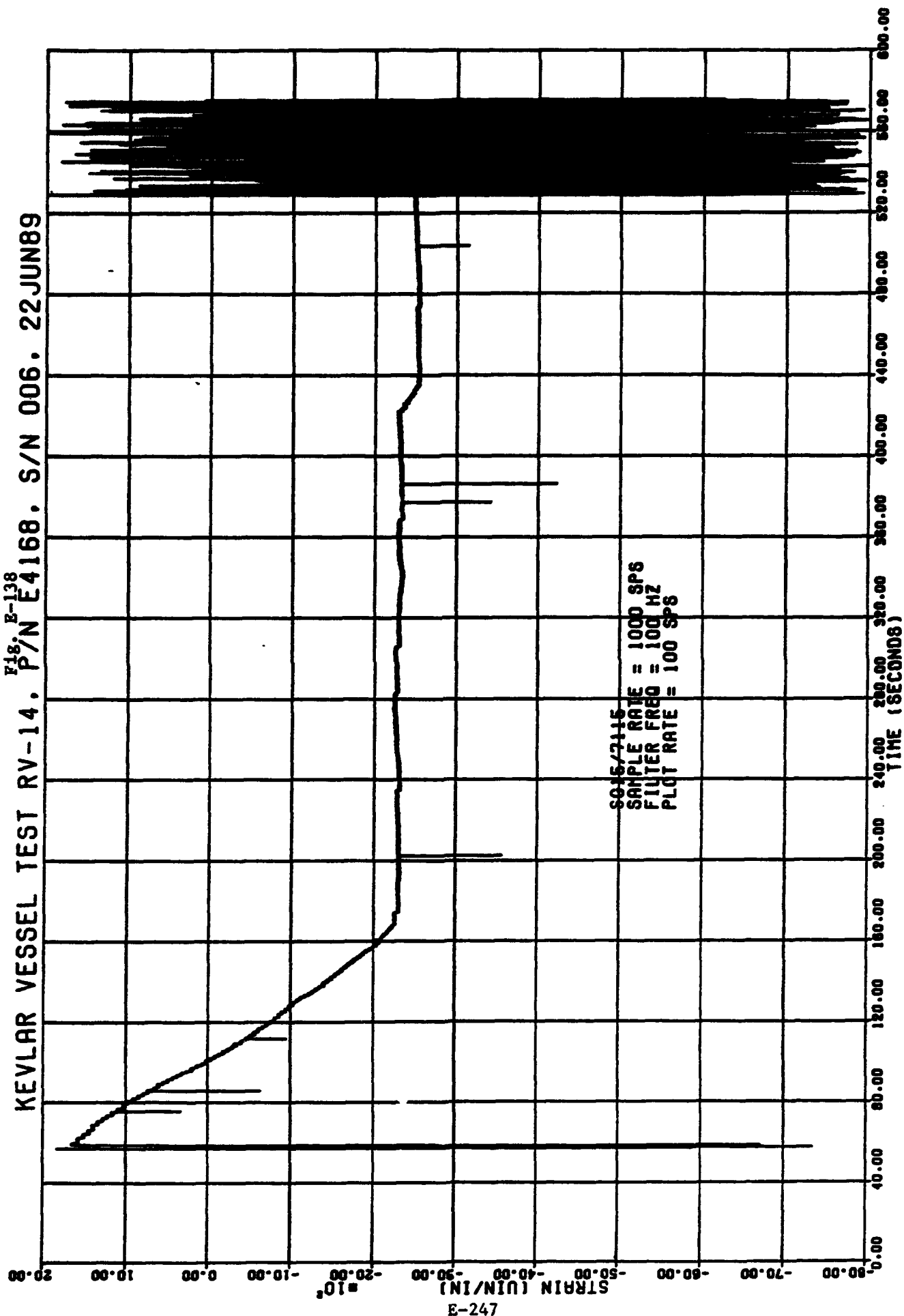
KEVLAR VESSEL TEST RV-14. P/N E4168. S/N 006. 22JUN89

Fig. E-137



KEVLAR VESSEL TEST RV-14. P/N E4168. S/N 006. 22JUN89

Fig. E-138



KEVLAR VESSEL TEST RV-14: P/N E4168. S/N 006. 22JUN89

Fig. E-139

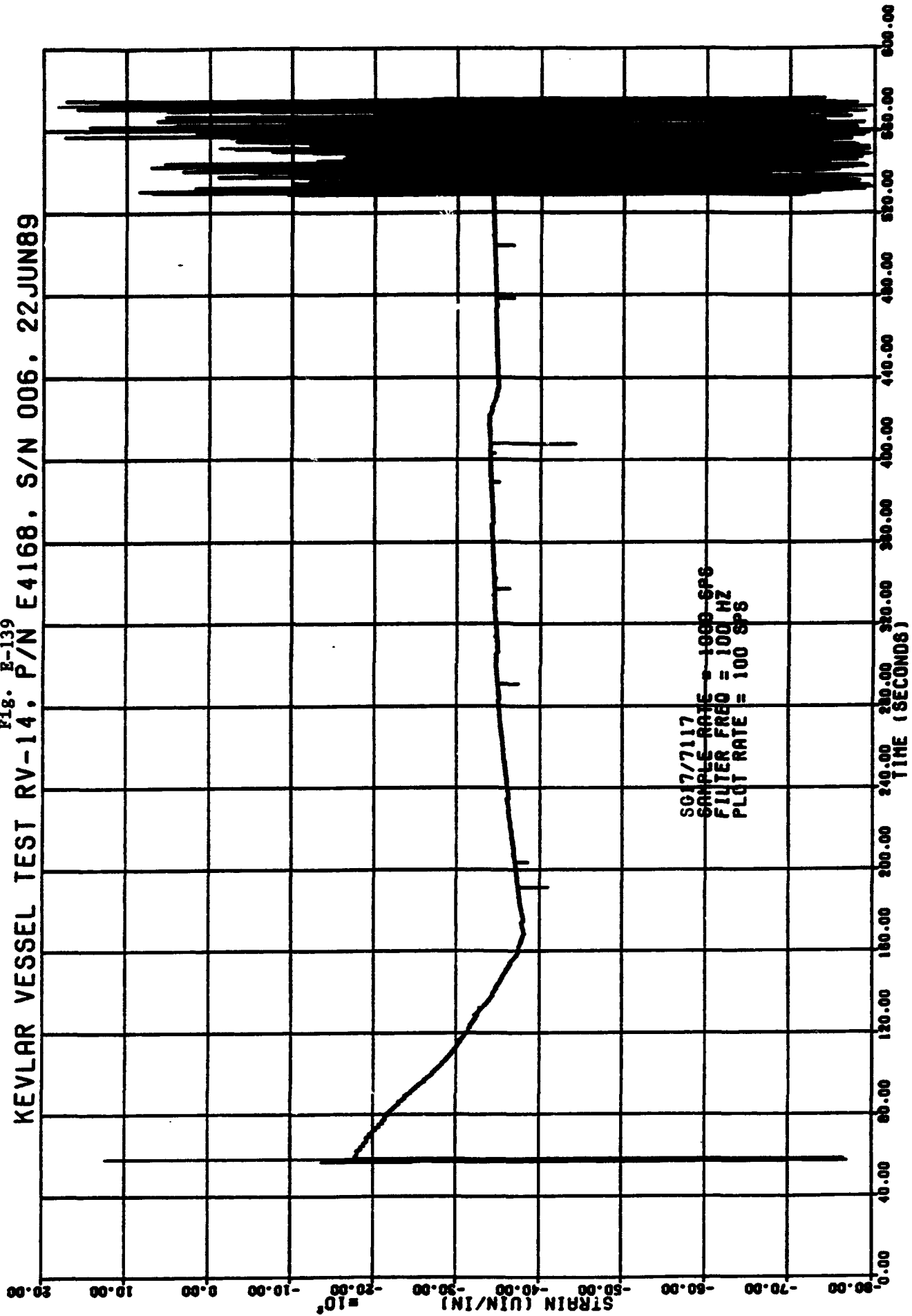
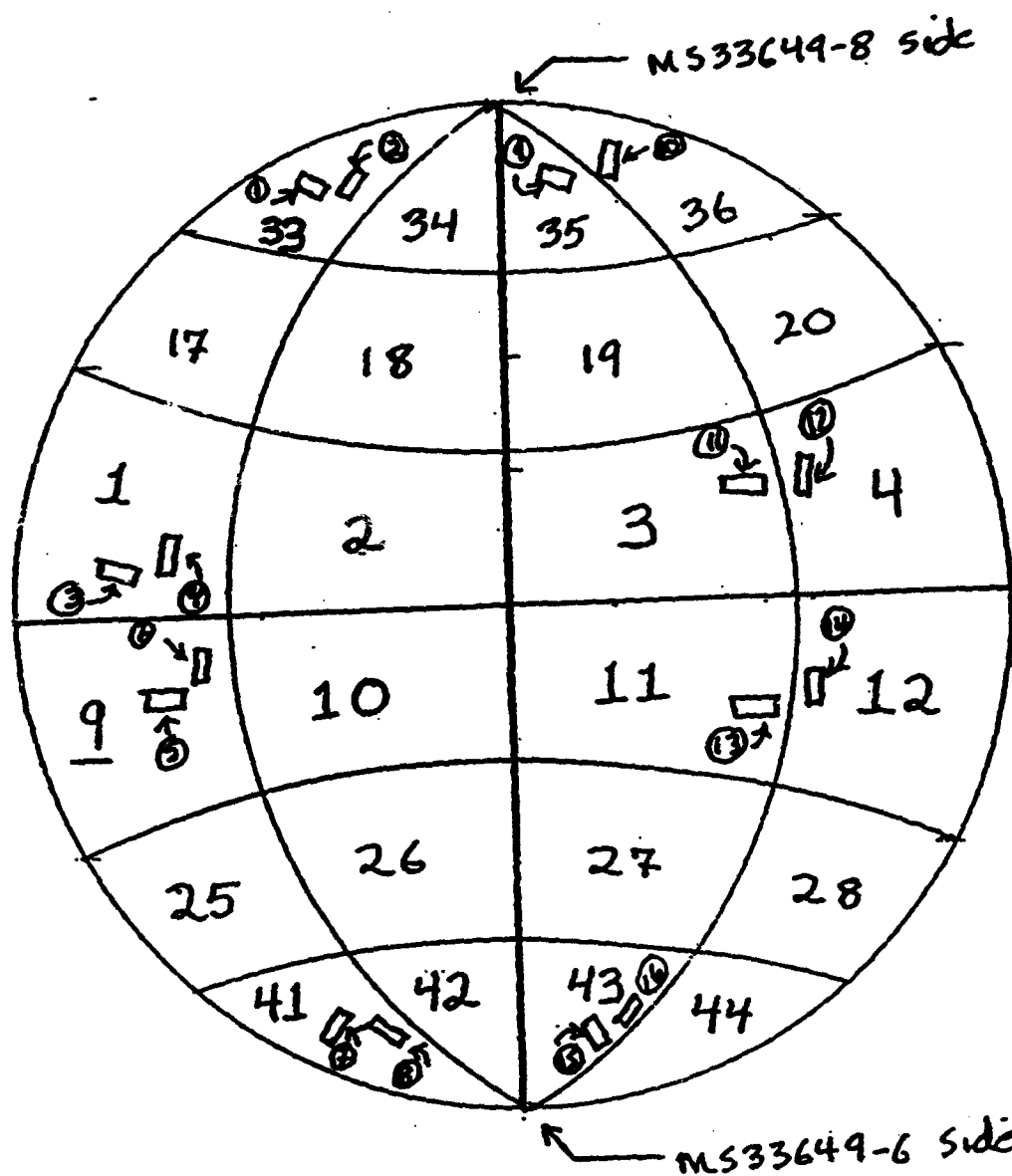


Fig. E-140

RV = 14
 P/N E4168, S/N 006
 90 % Kevlar Thickness



* Longitudinal axis.
 rectangle || longitu-
 axis of strain gage

(page 1)

#1-#48 - Section
 *①-④ - strain Gage
 □ - strain Gage

RV-14
P/N E4168 S/N 006
90% KEVLAR THICKNESS

EVEN GAGES = PARALLEL TO FIBERS

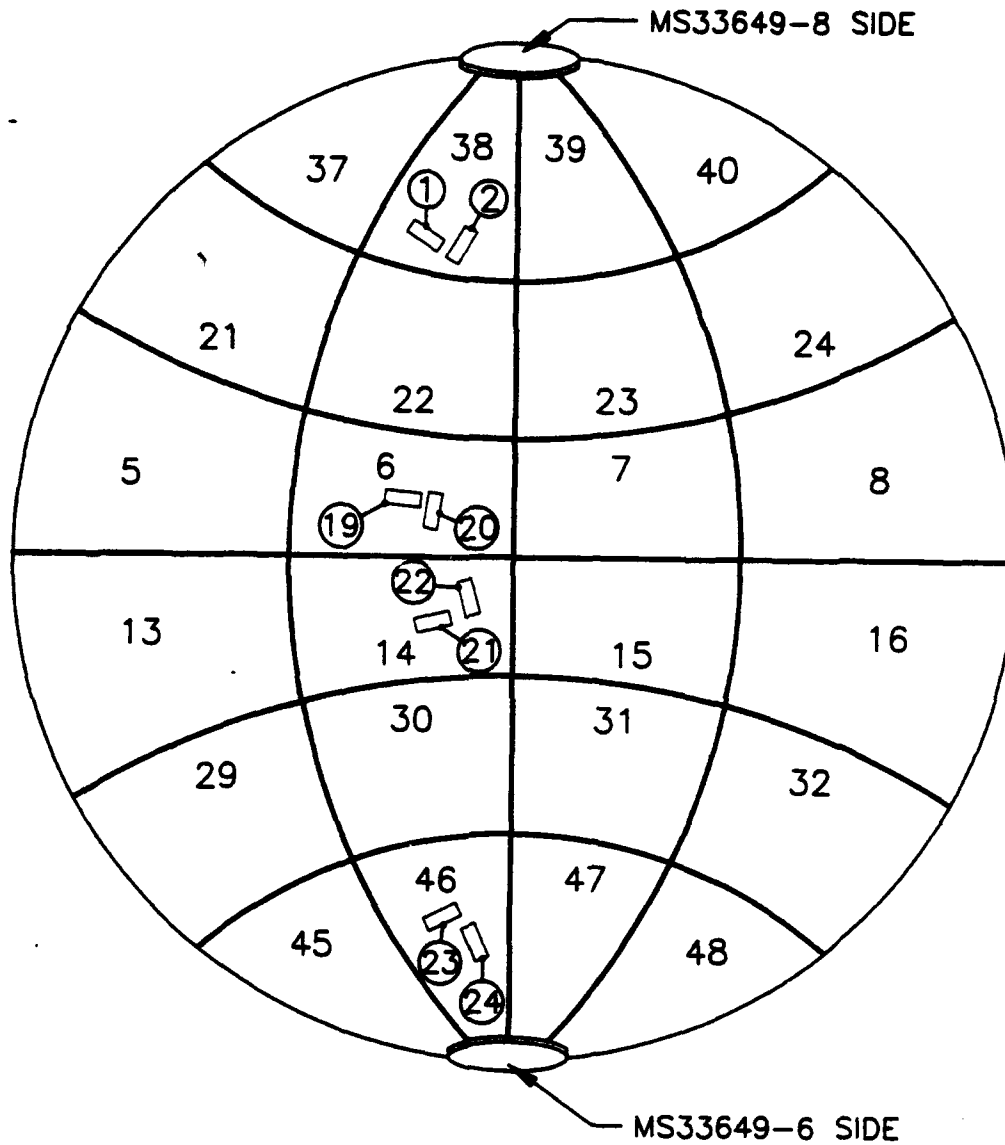


FIGURE E-141 STRAIN GAGE LOCATIONS FOR TEST RV-14.
E-250

E.11.4 Post Test Inspection

The vessel was intact and no Kevlar damage was observed. Leak checking confirmed that the metal liner was undamaged and intact.

E.12 RV-14A Test (16" ϕ)

E.12.1 Test Vessel Description

Same as RV-14 test except:

- (a) Prior test (RV-14)
- (b) Charging Current Density = $.0066 \text{ ma/in}^2$
(10% increase over RV-14 test)
- (c) Hold Time Before Test = 3 hours

INSTRUMENTATION OBSERVATIONS (By Instrumentation Engineer)

14A
KEVLAR TEST 015. Date: 20JUL89. Project Number 573000RV.

EXPERIMENTAL OBSERVATIONS.

Introduction. Vessel S/N 006. P/N E4168 was tested. It was a 16 inch diameter stainless steel sphere and had a 90% Kevlar overwrap. This experiment was a repeat of the previous test, which did not leak. The vessel was hydrogen embrittled about the girth. It was tested in a vertical configuration. Tank pressure increases were ramps created with salvos of short pressure pulses. The tank pressure was increased from a steady state pressure of 1452 psig to about 1802 psig with five pressure pulses. The tank pressure was held for about five seconds near 1802 psig. The tank pressure was increased at 58509.280 milliseconds with eleven more pulses and held for about five seconds near 2224 psig. At 81509.884 milliseconds the tank pressure was increased with twenty more pulses to exactly 3112 psig. At this pressure the tank began an immediate leak at 112.209 seconds.

At leak, the tank pressure decreased following a smooth but abrupt knee in the rising tank pressure profile caused by the twentieth pulse. The pressure decreased over a linear depressurization rate that terminated in an exponential decay. The exponential pressure decay decreased to below the 1500 psig initial condition and abruptly changed slope below 80 psig when venting was started. The pressure approached an assumed final zero asymptote. Noted in the pressure decay profile is the lack of ringing, and lack of prominent periodic modulations, major asperities, data dropouts and major glitches. Two moderate glitches mar the smoothness of the exponential decay, but the cause of these modulations remains unexplored.

The expanded plots show the SG behavior around the leak between 112.0 and 113.5 seconds. The expanded SG plots at leak show interesting variations from the typical plot. SG05 has been selected to represent typical SG behavior about the leak. Activity deviations from the typical plot includes almost no activity, SG23, to very active, SG06. These selections are judgemental, and other interpretations and speculations may also be valid.

Venting was done with the vent valve. The vent profile started after 80 psig, and it was clearly demarcated, almost linear, done at a rate of approximately -46.29 psig per second, not recorded near the end, not stopped for repressurization attempts, unremarkable and within normal limits.

As in previous tests, SG24 and the other strain gages were impressive mirror images of the pressure profile. Case strain in composite cases can be detected and is proportional to case pressure, but a calibration factor must be determined. The SG performance profiles will be slightly noisier than the vessel

pressure parameter and retain the risk of SG debonding.

Information For Test Personnel: Instrumentation technicians, engineers, supervisors and panel operators must note the data loss near 50 to 58 seconds was due to encountering acquisition control file number 1, according to the Data Center printout (apparently the file was exited & reentered for some reason; or another explanation may explain the loss as there is no loss on the quick look print out for tank pressure plot immediately after the test). Also note the FM tape was started too late to capture the start of the test. There is about 8 minutes of tape time, and the start of the final ramping is important to capture, for the net strain change during ramping is required. The tape recorder should be started just prior to the start of the pressure salvos after the pause at the initial pressure condition is completed. The pause at 1452 psig was done to check for leaks and to establish thermal and pressure equilibrium near 1500 psig. Advise electricians to place a spark suppression diode in pressurization solenoid circuit to stop the minus L(di/dt) noise problem seen on PHXOUT/1900, etc. Refer to the discussion on the previous test for details.

Post-run Inspection. Witness panels, displacement gages and acoustic emission technology were not used. Extensive damage to the vessel's instrumentation wiring and pressurization plumbing was not observed. The over pressure sensor data showed no change and are discussed elsewhere. No Kevlar damage was observed and fraying was not obvious near either boss. The Kevlar remained intact. No major damage to the resin was observed.

IMPRESSIONS FROM THE DIGITIZED FM DATA.

Strain Gages.

Strain Gage Locations. The strain gages were located IAW ARDE drawing dated 3/7/89, Revision A dated 21MAR89, accompanying a 21MAR89 cover letter. The even strain gages are perpendicular to the wrap, and the odd strain gages are parallel to the wrap.

Strain Gage Temperature. Not shown on this print are the thermocouple locations. See the Instrumentation Specification Sheet for the locations and item numbers. The 7 thermocouple loci form a family of curves with almost identical profiles. Collectively, the gages measured temperature behavior over a span between 103 degrees F and 125 degrees F, approximately. For example, TT5 ranged from 117.1 to 123.4 degrees F, and TT7 ranged from 103 to 110 degrees F. TT3 read the highest temperature: 125.6 degrees F. All temperature profiles contained reasonable noise floors. The vessel's SG temperature behavior is considered to be within normal limits, and it wasn't investigated with further detail.

Performance Summary. There were 23 strain gages recorded on the FM tape recorder, and 20 functioned. Most plots had valid activity, and most plots had no noise spikes. During the initial

conditions, it is assumed all pages had much better than normal noise floors as most plots were very clean up to leak although data recording was delayed and was not started until after 80 seconds. The noise floors are discussed elsewhere under Noise Floors. None of the strain gages were destroyed by tank depressurization although two (SG1 & SG2) didn't follow the family profile of mirroring the tank pressure profile. SG1 went very flat at leak, and SG2 rapidly changed at leak and finished with a exceptionally flat exponential curve.

Sign Convention. Positive strain gage polarity represents compression, and negative strain gage polarity represents tension.

Noise Floors. Except as noted elsewhere, the strain gage and other parameters' noise floors did not include major transverse or common-mode minus $L(di/dt)$ transients, artifacts, crosstalk, atmospherics, noticeable RFI, intermodulation, spurious parasites, or sibilants. However, latent noise or data manifestations may be obscured in some parameters, and digital signal processing may be needed for signal enhancement. In general, the data appeared to be unbiased, precise and accurate. SG1 was clearly the noisiest in the group. Again, most plots were very clean.

Performance Exceptions. Strain gage behavior was within normal limits, except as noted. The following comments are based on interpretations of the 100 Hz and 1000 Hz data passes.

In general, strain gage behavior was similar to previous tests. The general trend for the active strain gages was a tension strain polarization pattern proportional to tank pressure with corrections for glitches, polarity, shifts and some possible debonding, etc. The dynamic performance did not include major oscillations, except for SG01. Except as noted, all graphs had noise floors within normal limits. Only a few graphs had glitches. There was no noise on the SG plots during the vent operation.

Maximum SG Values and Performance Trends. The following codes are used below:

- NWNL noise within normal limits
- GRZ good return to zero
- ARZ approximate return to zero
- NRZ no return to zero
- C compression strain
- T tension strain
- NTE not to exceed
- OSC oscillation
- EXP exponential decay

Unipolar: data predominately in one direction.

Bipolar: data in both directions but not necessarily evenly balanced between polarities. In some cases, the data carrier was unipolar in tension but contained bipolar compression excursions.

Units for strain values are in microinches/inch

SG01 Unipolar, T,
many noise spikes. flat following burst, OSC @ 28.000 Hz
seen on high frequency data pass for 5 msec duration.

SG02 Unipolar, T, clean, but has rapid decay

SG03 Unipolar, T, EXP, 3 noise spikes,

SG04 bad on 100 and 1000 Hz passes

SG05 Unipolar, T, EXP, 2 noise spikes

SG06 Unipolar, T, EXP, 3 noise spikes

SG07 Unipolar, T, EXP

SG08 Unipolar, T, EXP

SG09 Unipolar, T, EXP

SG10 Unipolar, T, EXP

SG11 Unipolar, T, EXP, 1 noise spike

SG12 Unipolar, T, EXP. Overload due to bad cal cut on 100 & 1000
Hz passes

SG13 Unipolar, T, EXP, 1 noise spike

SG14 Unipolar, T, EXP

SG15 Unipolar, T, EXP, 1 noise spike

SG16 Unipolar, T, EXP, 1 noise spike

SG17 Unipolar, T, EXP, 1 noise spike, bad on 1000 Hz pass

SG18 Unipolar, T, EXP, 1 noise spike

SG19 Unipolar, T, EXP

SG20 bad on 100 Hz pass

SG21 bad on 100 Hz pass

SG22 Unipolar, T, EXP, 1 noise spike

SG23 Unipolar, T, EXP, 2 noise spikes

SG24 Unipolar, T, EXP, Recorded on the DACS only. Not on FM.
Quick-look showed no data interrupts, but Data Center data had
interrupts which are discussed elsewhere.

Performance Summary:

All channels included codes: T, NWNL. Out of the 23 SG channels recorded on the FM tape recorder, three channels were bad. All channels had unipolar tension behavior. Two channels had abnormal bipolar strain activity, probably due to debonding (SG2 & SG3).

Because data recording did not start until after the 1500 psig initial condition, net maximum strain change during the pressure ramp was estimated as shown below.

A typical strain gage underwent a net tension strain of only 2000 unin/in. SG18 is representative of a typical SG. The strain at the initial 1500 psig condition was determined by estimating the strain after drawing in the missing profile by extending the graph using the slope shown in the plot and the critical time

points on the tank pressure plot. In this case the strain at 1500 psip was estimated 1000 uin/in. and the plot peaked at 3000 unin/in.

If the higher frequency data pass contains information not indicated by the 100 Hz data pass, a revision will be issued and those differences will be discussed. Refer to the ITT Analyst's comments for information on the higher frequency data pass.

The above information was determined by inspecting the graphs and may contain subjective errors.

Statistical Analysis. Valid speculations about strain gage behavior may involve biserial correlation of certain dichotomies (positive or negative polarization) to assess their associations (with wrap direction, etc.). For truly dichotomous distributions, the phi coefficient can be used. Because some of these dichotomous variables are really continuous (the magnitude or duration of polarization, and the degree of wrap thickness, location & direction, etc.) and normally distributed, tetrachoric correlation may be involved. An expert statistician should be approached with a clear statement of which variables and associations are important if valid conclusions about some of these data are to be obtained. An accurate evaluation of which variables are really dichotomies and which are proportionally continuous would also have to be prepared and passed to the statistician.

Data Analyst's Comments.

14A

The ITT Data Analyst, Richard Thomsen, reports: "Kevlar Test 15. Low Sample Rate FM Strain Gauges. The data were aligned to the nearest millisecond. The burst occurred at 112.197 seconds (20:02:57.623 IRIG-B). Bad calibration cuts prevented processing of SG04/7104, SG17/7117, SG20/7120 and SG21/7121. There was also a cyclic noise on these channels. The noise appeared to clear up after the cal cuts on SG12/7112, so this channel was plotted, even though the cal cuts were bad, for qualitative purposes only. Some channels had noise spikes that are probably tape drop-outs. Channels SG01/1701 and SG16/7116 overranged after burst."

The ITT analyst continues with the following comments on the high frequency data pass: "Kevlar Test 15.^{MA} High Frequency FM Strain Gages. The FM strain gage data was digitized at 160,000 SPS using a 20,000 Hz filter. All channels were aligned to the nearest tenth of a millisecond. The vessel ruptured [leaked] at 112.197 seconds (20:02:57.620 IRIG-B). SG04/7104, SG12/7112, SG17/7117 had bad calibration values. Processing was completed for SG12 for qualitative purposes only. Almost all channels showed noise beginning at 112.197 seconds, ending at 112.201 seconds. SG01 showed an 20,000 Hz vibration beginning at 112.204 seconds and increasing until it ends at 112.209 seconds."

IMPRESSIONS FROM THE QUICK-LOOK AND DIGITAL DATA ACQUISITION SYSTEM DATA.

Tank Pressure. PTANK/1901 was located on the top of the tank in the vent line. PVSOUT/1904 was also in the vent line, but it was located at the valve box about 15 feet from the tank. PTANK/1901 functioned as described under the Pressurization Ramp... paragraph.

The locations of the transducers was the same as test 10.

PVSOUT/1904 data were similiar to PTANK/190 except for the reduced frequency reponse because of the long pressurization line.

SG24. SG24 tracked the vessel pressure profile with corrections for polarity, etc. This parameter, as in the previous tests, was only recorded on the DACS for quick-look purposes. Note the comment elsewhere concerning skipped data near 50-58 seconds for the Data Center data, although the quick-look did not have any skipped data.

Phase Behavior and Frequency Response. Noted is the phase behavior; the two graphs were very close together in the time domain.

Other Parameters. The performance of the other parameters was within normal limits, except as noted below; this was determined by a quick review of the graphs for items PHXIN/1902, PHXOUT/1900, PTRAIL/1903, THXIN/2100, TBALL/2211, TBSOUT/2210, TBSIN/2209. THXOUT/2101 Heat Exchanger Output shows major spikes without noticeable decay times, as seen on the previous test. The spikes are apparently due to minus $L(di/dt)$ transients from the pressurization efforts needed to increase tank pressure with the pressurization valve. Suppression with a diode at the valve solenoid is required to stoo the problem, or the spikes may be disregarded. The spikes appear as glitches on pressure parameters such as PHXIN/1902, PHXOUT/1900, PTRAIL/1903 and as very small deflections on temperature parameter THXIN/2100.

The IRIG Time Code, IRIG/3808 TIMING, did record satisfactorily on the FM.

IMPRESSIONS FROM THE OVERPRESSURE SENSORS.

The vessel only leaked, and did not burst. There was no overpressure pulse. Overpressure data was not reduced.

The following text applies to overpressure sensors and is retained for reference.

Bikini Gages. A Bikini gage is one piece of bond paper comressed between two metal plates containing different sized round holes. The gages are aligned so the paper is perpendicular to the pressure source. Discrete pressure data can be obtained

and is a function of the location of the damaged paper diaphragms. The approximate calibration is as follows for the indicated hole size using bond paper:

HOLE #	PSIG*	SIZE	PSIG**
1	7.3	5/8	4.4
2	5.2	7/8	3.3
3	3.7	1-1/4	2.4
4	2.7	1-7/8	1.7
5	1.9	2-3/4	1.25
6	1.4	3-3/4	----
7	1.0	5-3/8	----

*The source for this calibration data is unknown, but these data have been used since at least 1964 by the Astronautics Laboratory. ***The source for these calibration data is from a report THEORY, CALIBRATION, AND USE OF DIAPHRAGM BLAST METERS by W. T. Read, Division 2 National Defense Research Committee of the Office of Scientific Research and Development, NRDC Report No. A-392, OSRD Report No. 6463, Figure 18, Page 27, DEC45; this report was obtained from the Naval Surface Weapons Center, Silver Springs MD and was referenced in footnote (2) on page 3 of another report, OPERATION SANDSTONE JOINT TASK FORCE SEVEN TASK GROUP 7.1 BLAST MEASUREMENT SECTION, LAJ-8, PART II, Chapter 5.1, USE OF FOILMETERS ON OPERATION SANDSTONE, prepared by J. J. Meszaros and J. F. Moulton, Jr., 7JUN48, Fort Shafter, Oahu, T. H. This report indicates "For a considerable number of years air blast pressure measurements were made with the Aberdeen paper meter. The measurements obtained gave some indication of the peak pressure present. Early in the war Princeton University, under the auspices of NDRC, conducted an extensive experimental study. The primary results of these basic experimental studies..." [are shown in footnote (2) discussed above]. It is not clear when the terms Bikini and Aberdeen were first used to designate diaphragm overpressure sensors. Nevertheless, the gages were used at Bikini [atoll in the N Pacific, Marshall Islands] in the 1946 atomic bomb tests (Crossroads Project) and again at Eniwetok in 1948 (Sandstone Project) and again in 1951 (Greenhouse Project). Most of the above information came from the DoD Nuclear Information and Analysis Center (DASIAC) on 12MAY88 and is the result of a lead provided by HQ/BSD/MYEB/Lt Col Don Gage to AL/TOAE/Dick Grove in FEB88. [OPR's Note: HQ/BSD was HQ/BMO prior to 21APR89 and AL was AFAL prior to 21APR89 and AFRPL prior to 22MAR87].

Reconciliation of the bikini overpressures and bias observations was not done as there was no overpressure pulse. All of the paper diaphragms were intact.

Piezoelectric Sensors.

There was no overpressure pulse.

As indicated in earlier experiments, the overpressure sensors, if used, would have behaved as follows:

Ideally, each overpressure sensor located to measure pressure should respond to a passing pressure pulse with a characteristic graph. The graph's curve should have a prominent leading edge rising from a stable initial condition. The typical leading edge should polarize positively and rise to the curve's maximum peak pressure over a smooth and almost linear path. At the peak pressure, the curve should inflect, and, at this reversal, enter into a characteristic depolarization decay consisting of an almost linear component followed by a distorted exponential component that returns to below the initial condition with an undershoot, more fully described below, representing rarefaction and the start of the refractory period.

More often than not, the linear decay should gradually change into a sluggish curve containing one prominent inflection, forcing the plot into the opposite direction, but staying below the initial condition. Eventually, the pressure rarefaction should deteriorate completely, and the plot should return smoothly to the initial condition, ending the refractory period.

Modulations and variations in behavior are caused by sensor placement (parallel or perpendicular to the flow direction), reflections, pressure wave distortions, time constants, frequency response, particulate impingement, insulation resistance, short circuits, open circuits and gas cloud geometry, etc.

DESCRIPTION OF THE EMBRITTLEMENT PROCEDURE. The ARDE embrittlement procedure dated 21MAR89 was followed. The 16" diameter vessel was girth embrittled. Embrittlement was inhibited, where required, with a maskant. Embrittlement was started on 17JUL89. The current level was 0.176 amperes. Seventy-two hours of embrittlement were completed at 20JUL89. The tank was immediately moved from the shop embrittlement area to the test site, instrumented, hooked up, checked and pressure tested on 20JUL89. The electrolyte was sulphuric acid. Sodium arsenite was added as an enhancer.

ADMINISTRATIVE INFORMATION.

Revision Record. Initial Issue: 3NOV89. Note significant delays were encountered in data reduction following the 20JUL89 experiment. The FM passes were finally provided on 3NOV89. Test RV15 is the same as RV14A. The 15 designator is used because of limits on the filename size.

Filename: testrv15^{14A}

Distribution: ARDE, Aris Escolona, Dave Gleich
PI, Dr. Pius Chih Hsu Chao
Aerospace Corp., Dr. Yen Pan
AFAL, Jim Miller, Dick Grove,
Dr. Tae-Woo Park
ITT, Richard Thomsen
PAFB, Pete Tadie

Office of Primary Responsibility. USAF/AL/TOAE/Dick
Grove/Edwards CA 93534.

E.12.3 Pressure and Strain Versus Time Plots

Figures E-142 to E-148 give pressure versus time and selected strain versus time plots.

Figures E-140 and E-141 are sketches showing strain gage locations. Even numbered strain gages are perpendicular to the Kevlar wrap and odd numbered strain gages are parallel to the wrap.

E.12.4 Post Test Inspection

The Kevlar shell was intact after the test with no fiber damage noted upon inspection with the tank still attached to the test stand. A leak check confirmed liner leakage. The tank was cut apart, photographed and inspected visually at AFAL. Figures E-149 and E-150 show the cut apart tank. Girth cracks in the local girth embrittled zone were visually observed. The cut apart tank was shipped to ARDE for further inspection. At ARDE, the cut apart tank liner was die checked to enhance the visibility of the cracks and then photographed. Figures E-151 and E-152 show photographs of portions of the cracked liner inside surface. Continuous connected hoop cracks run around the entire girth in the local embrittled area.

KEVLAR VESSEL TEST RV-15, P/N E4168, S/N 006, 20JUL89

Fig. E-142

14A

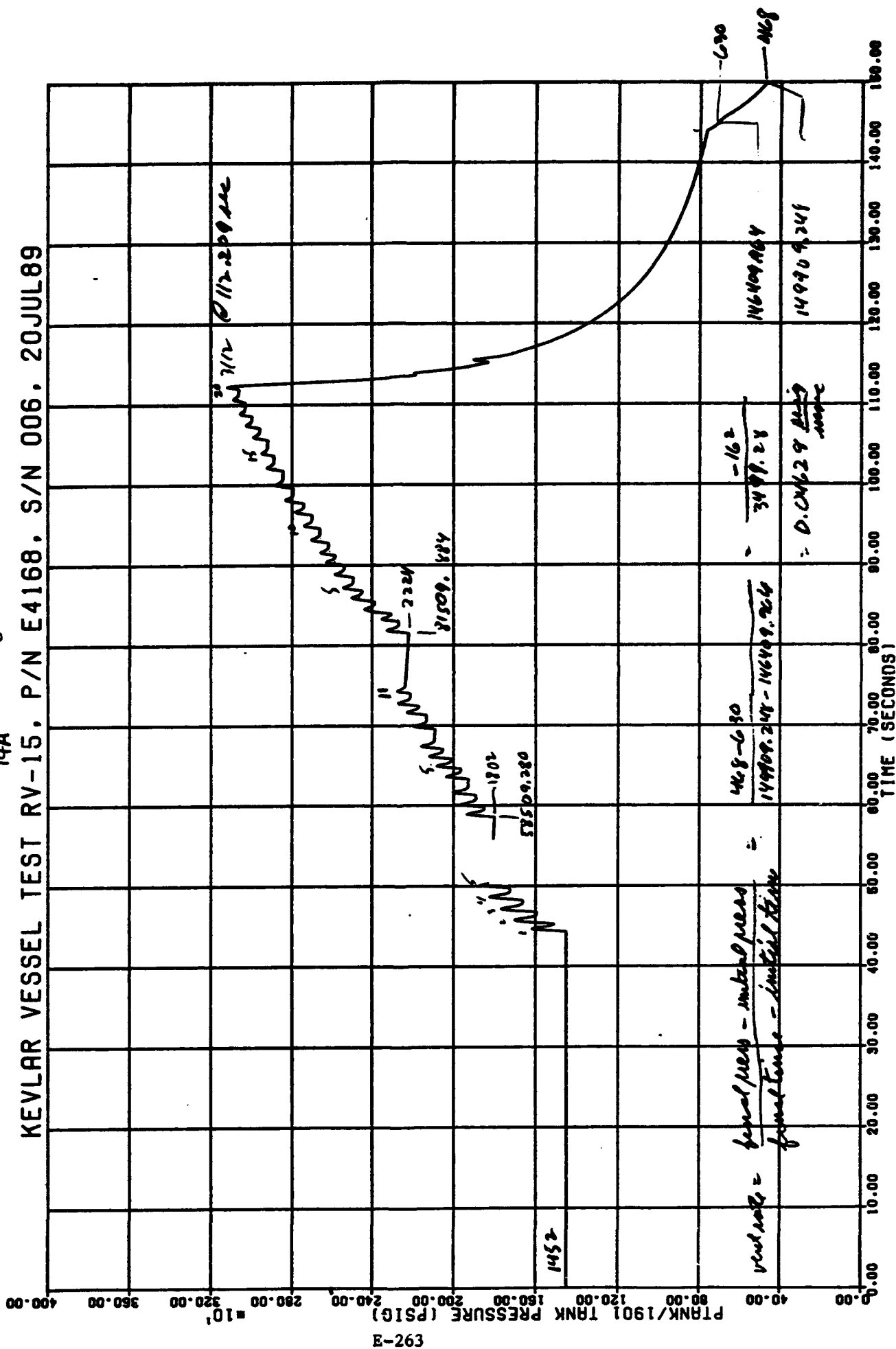


Fig. E-143

KEVLAR VESSEL TEST RV-15. P/N E4168. S/N 006. 20JUL89

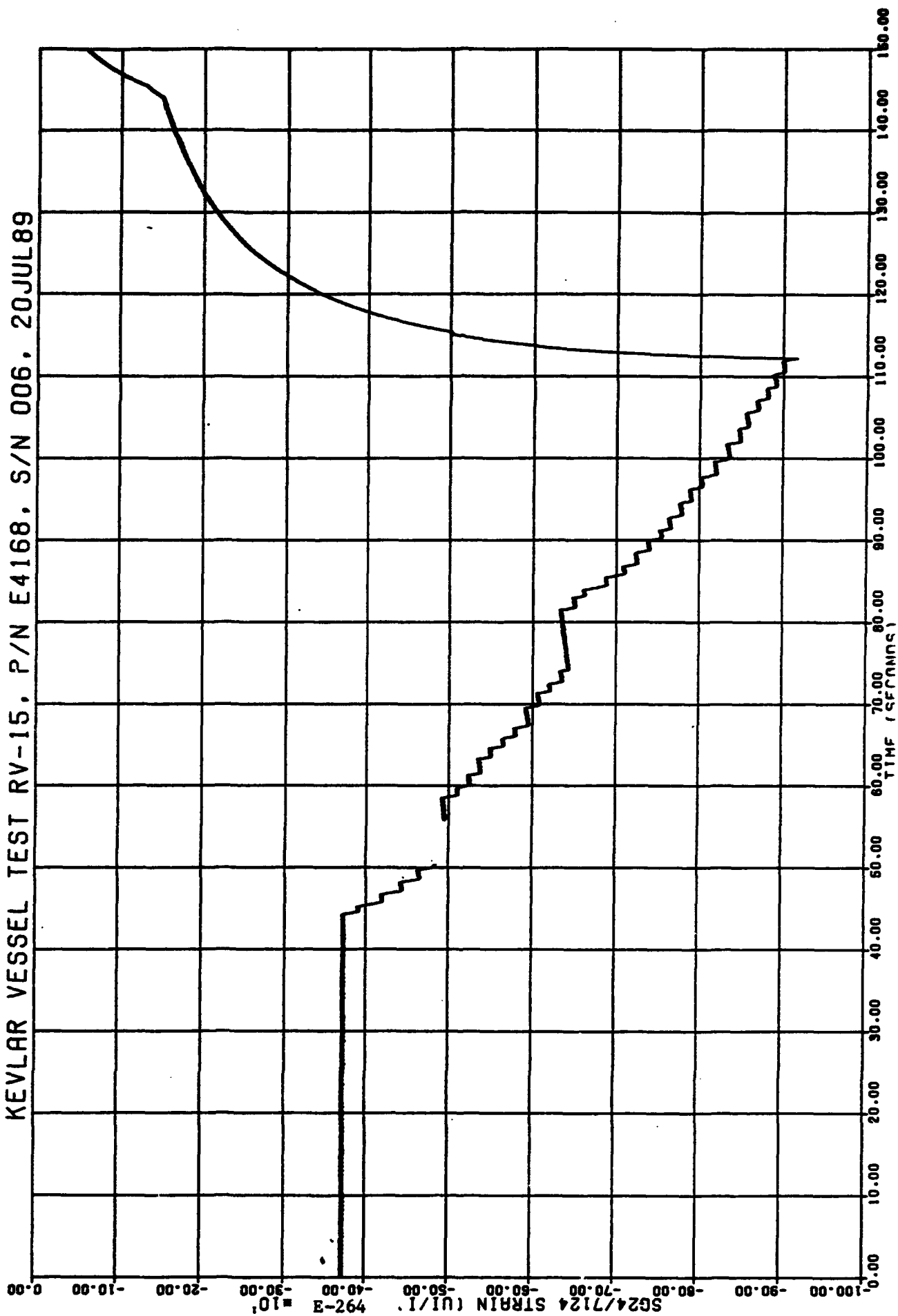
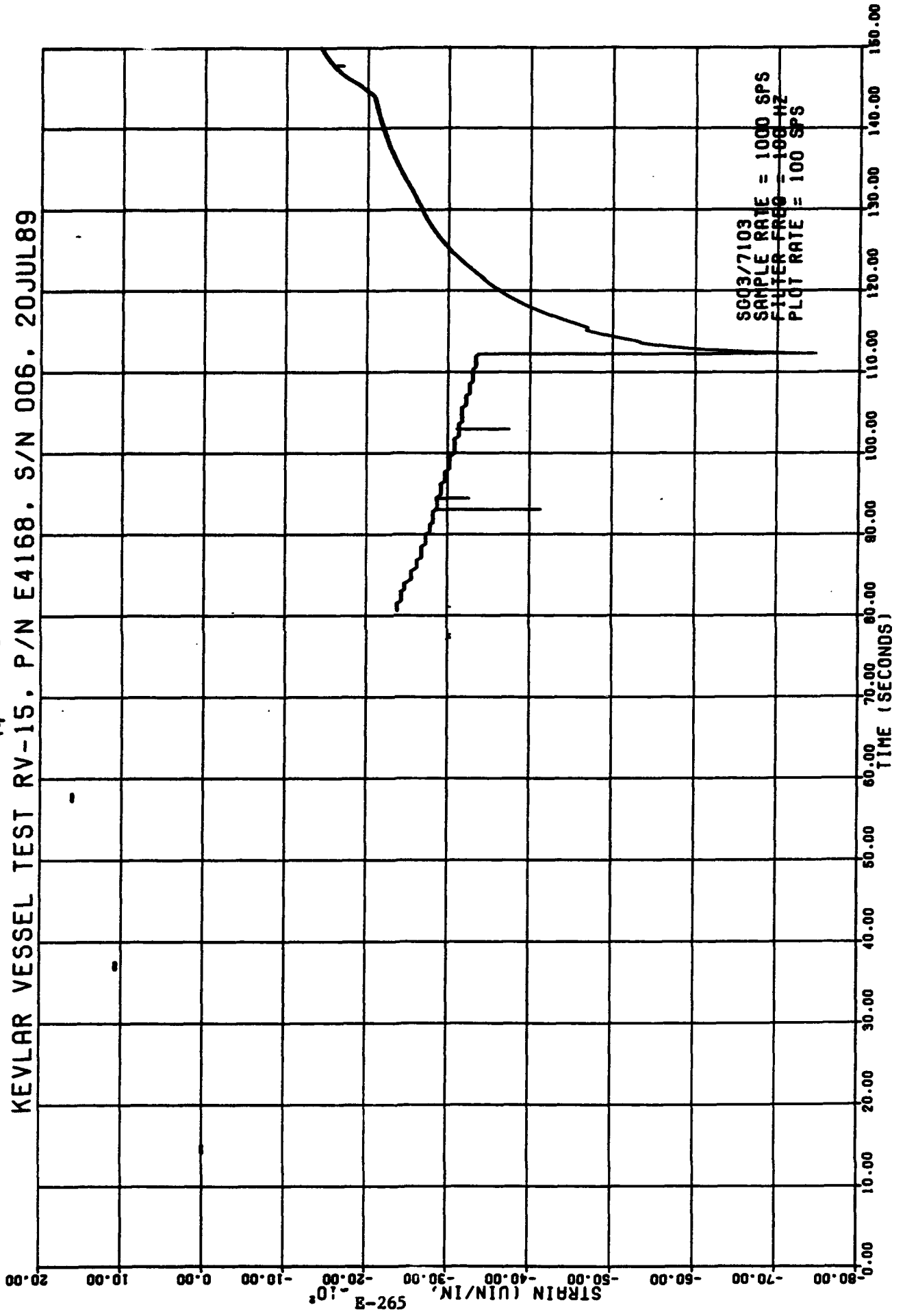


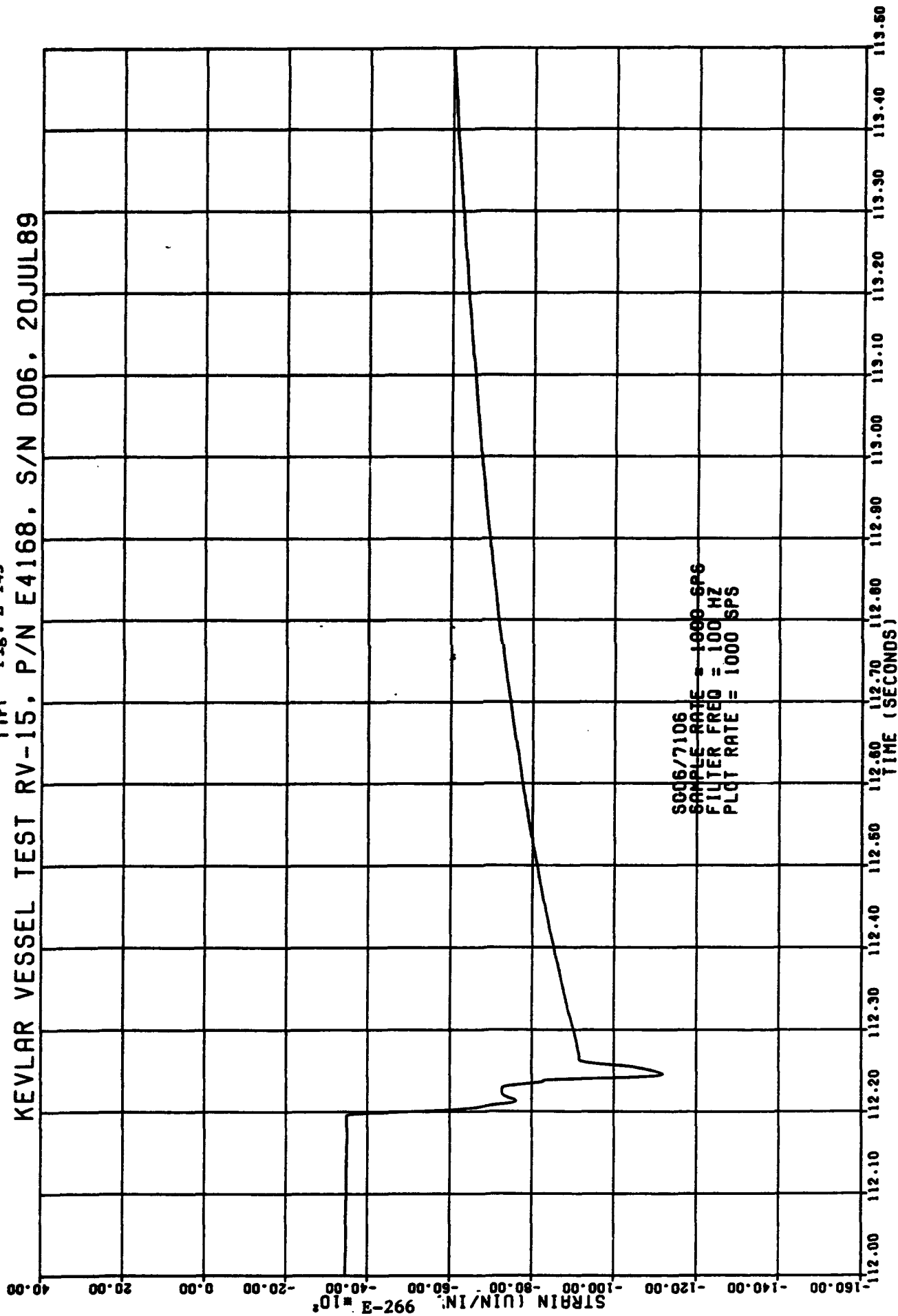
Fig. E-144

KEVLAR VESSEL TEST RV-15. P/N E4168. S/N 006. 20JUL89

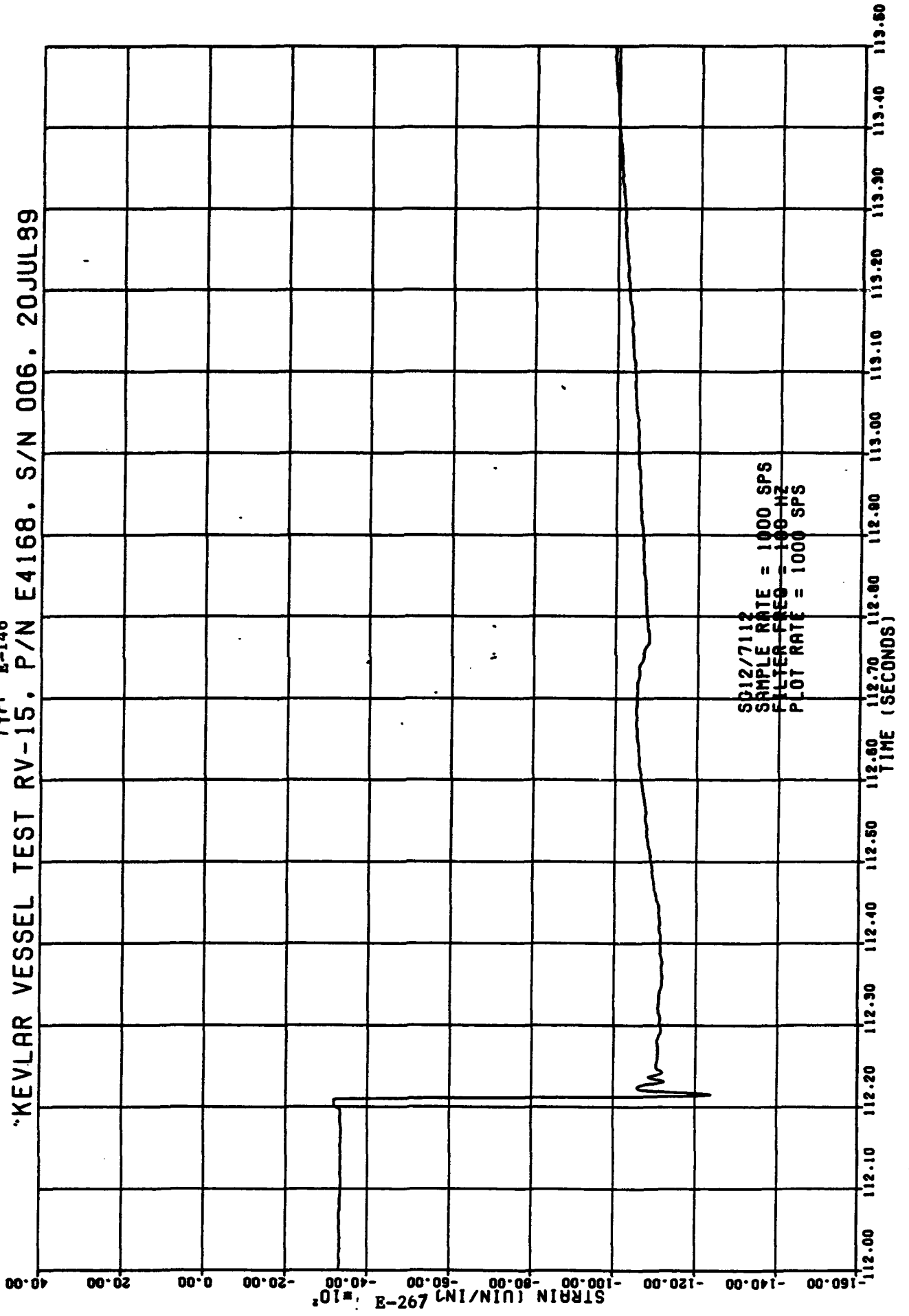


14A Fig. E-145

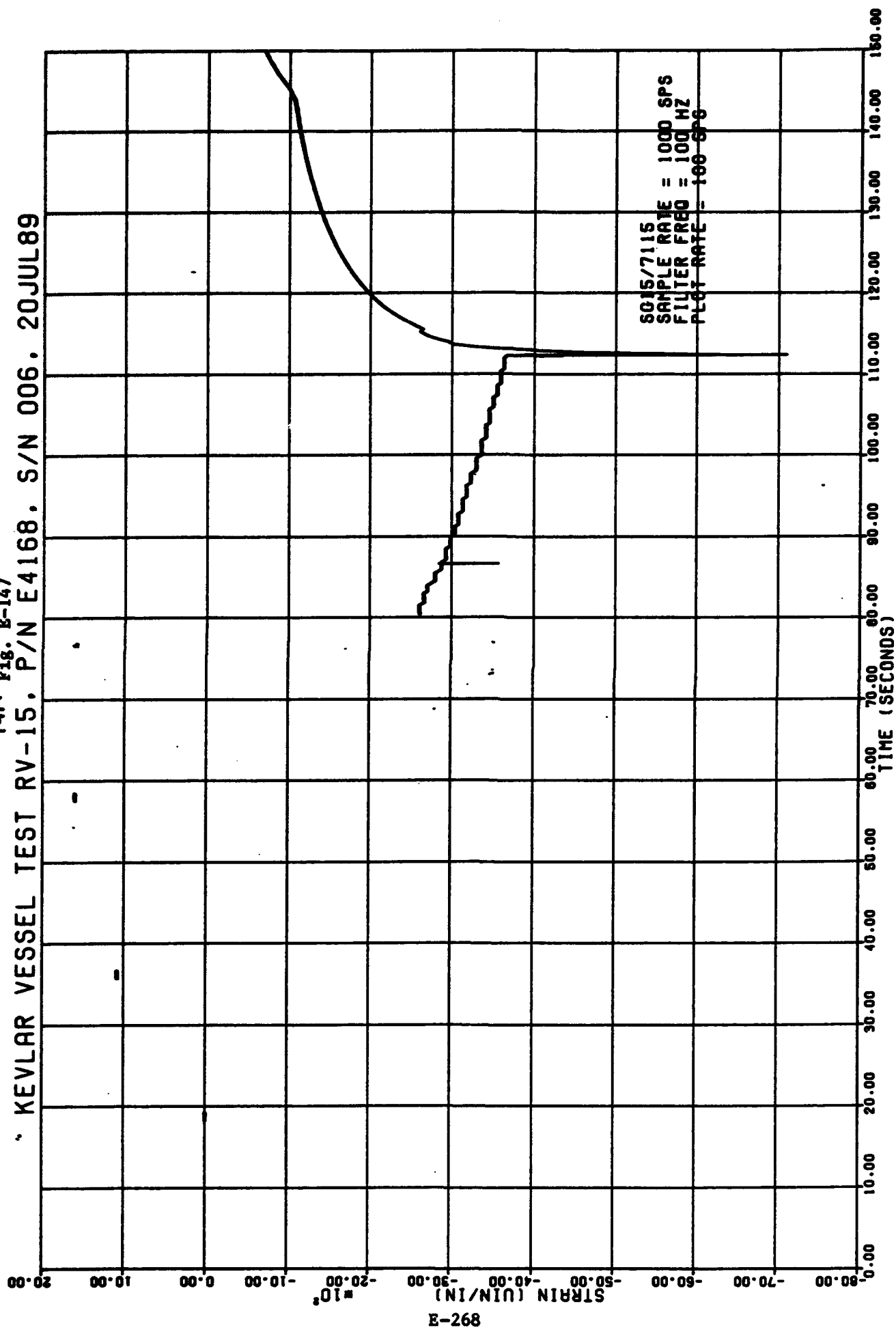
KEVLAR VESSEL TEST RV-15. P/N E4168. S/N 006. 20JUL89



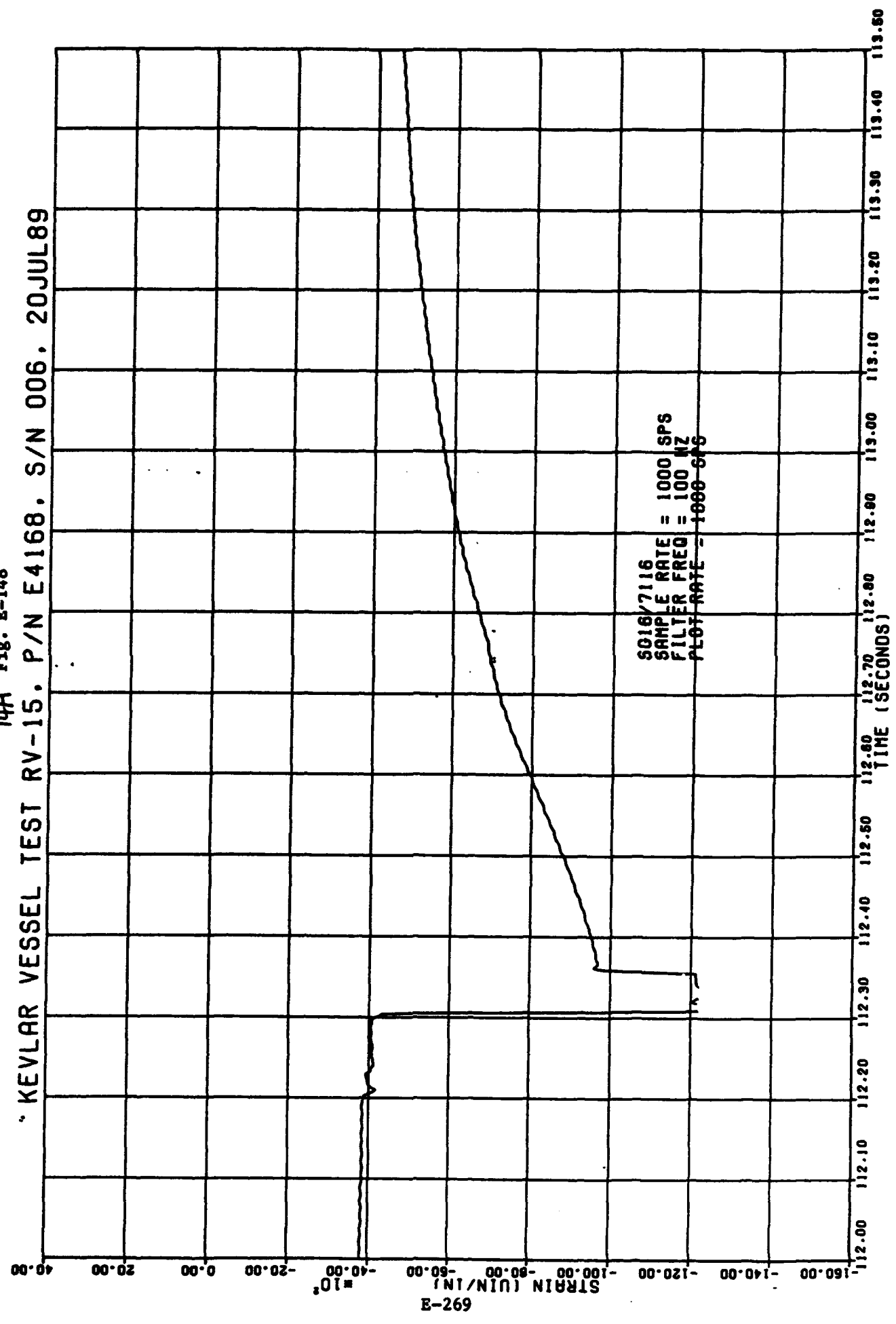
14A E-146
KEVLAR VESSEL TEST RV-15, P/N E4168, S/N 006, 20JUL99

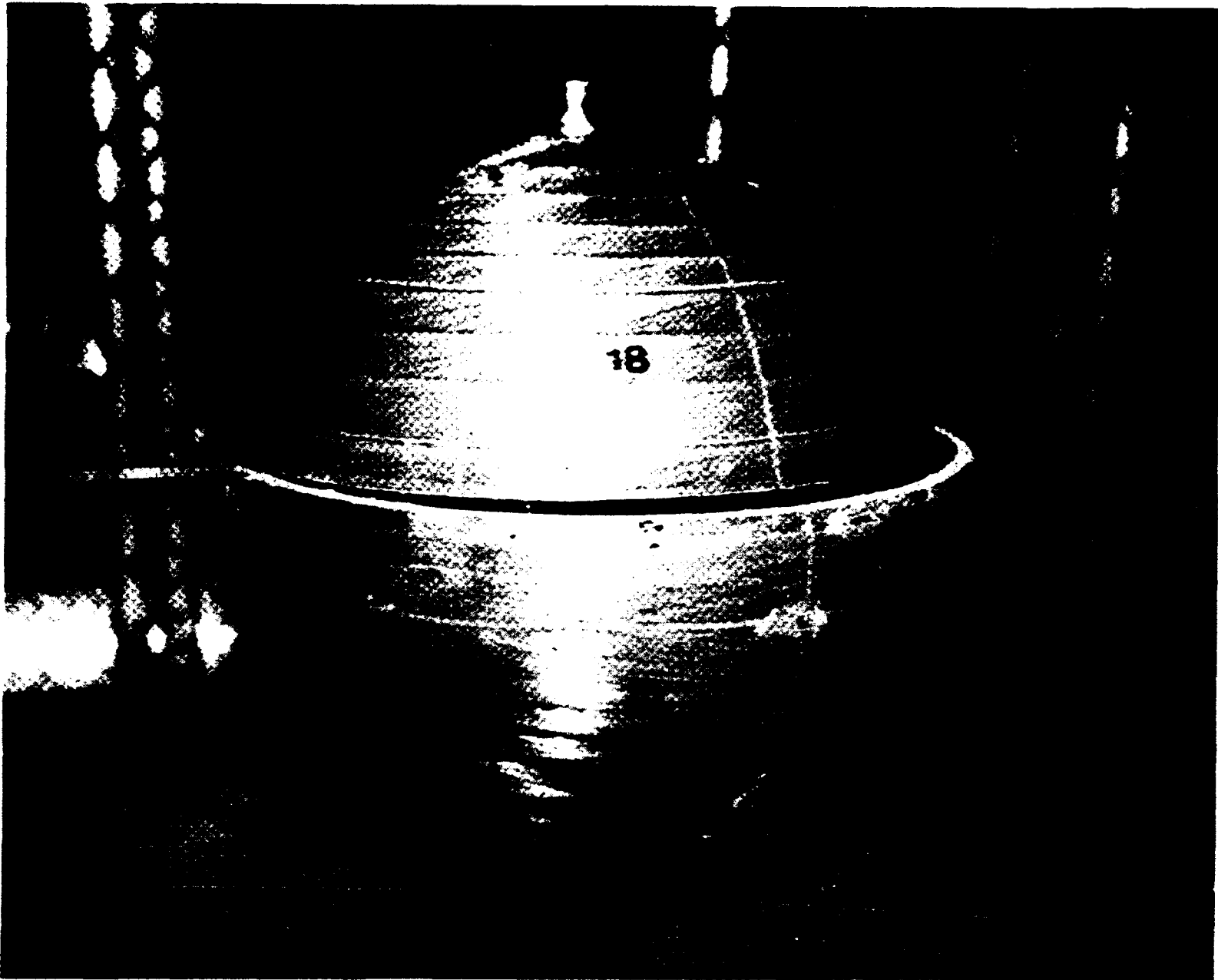


14A Fig. B-147
KEVLAR VESSEL TEST RV-15, P/N E4168, S/N 006, 20JUL89



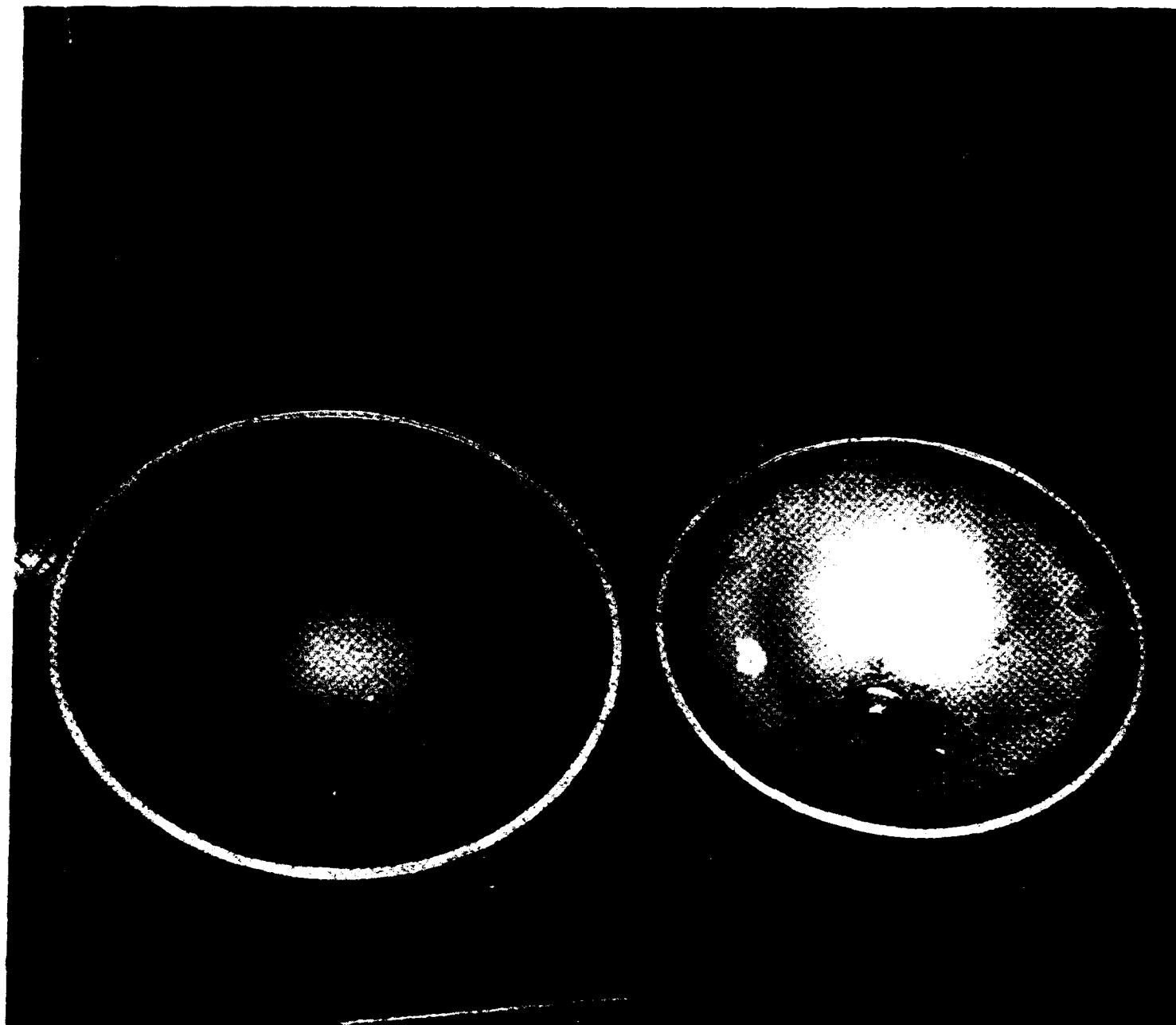
14A Fig. E-148
KEVLAR VESSEL TEST RV-15. P/N E4168. S/N 006. 20JUL89





TEST RV-14A, CUT APART POST TEST TANK, EXTERIOR
VIEW

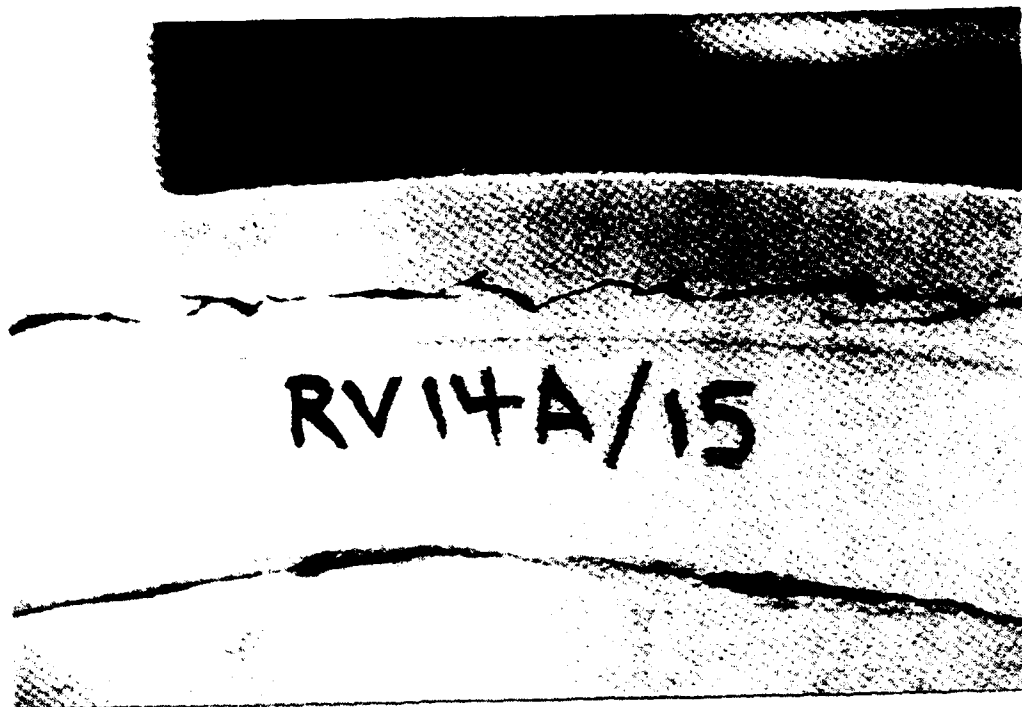
Fig. E-149
E-270



TEST RV-14A, CUT APART POST TEST TANK, INTERIOR VIEW

Fig. E-150

E-271



TEST RV-14A, POST TEST EMERITTLED GIRTH
CONTINUOUS CRACK

Fig. E-151



TEST RV-14A, POST TEST EMERITTLED GIRTH
CONTINUOUS CRACK

Fig. E-152

APPENDIX F - Full Scale Test Data Correlation

This appendix contains test data correlation examples and supporting measured pressure and fiber strain information.

Calculations given below show that the fiber strains resulting from the liner ductile, stable crack growth leak-before-burst (LBB) mode are small, and, therefore, unimportant, compared to the liner sudden unstable crack growth brittle failure mode.

F.1 Ductile Failure Mode

Figure F-1 illustrates the geometry for the case in which a ductile crack forms in the metal liner. The full tank pressure is suddenly applied to the overwrap over the area which becomes exposed. The centerline in this sketch denotes either an axis of symmetry, for a circular hole, or a plane of symmetry, for a linear crack.

For simplification of analysis, we replace the liner by the equivalent static pressure, P_w , it transmits to the fiberwrap boundary. From the results of Appendix A, we have,

$$\sigma_w = \frac{(R) P_w}{2 h_w} = \frac{(R)}{2 h_w} (P^* + P_i) \text{ --- (A-33), with}$$

initial stress pressure, P_i and incremental static fiber wrap stress pressure, P^* given by,

$$P_i = \frac{2 h_w \alpha_w \epsilon_i}{R} \text{ ... (A-34)}$$

$$P^* = \frac{p}{1 + \frac{h_M \alpha_M}{h_w \alpha_w}} \text{ ... (A-35)}$$

For typical numerical values,

$$h_M = .05, h_w = .23, \alpha_w = 6.76 \times 10^6,$$

$$\alpha_M = \frac{27 \times 10^6}{.7}, R = 7.64,$$

$\epsilon_i = .0035$ and $P = 4000$, we obtain the fiber wrap static equilibrium pressure,

$$P_w = P^* + P_i = \frac{4000}{1 + \frac{.05 \times 17/.7}{.23 \times 6.76}} +$$

$$\frac{2 \times .23 \times 6.76 \times 10^6 \times .0035}{7.64}$$

$$P_w = 1785 + 1425 = 3210 \text{ psig}$$

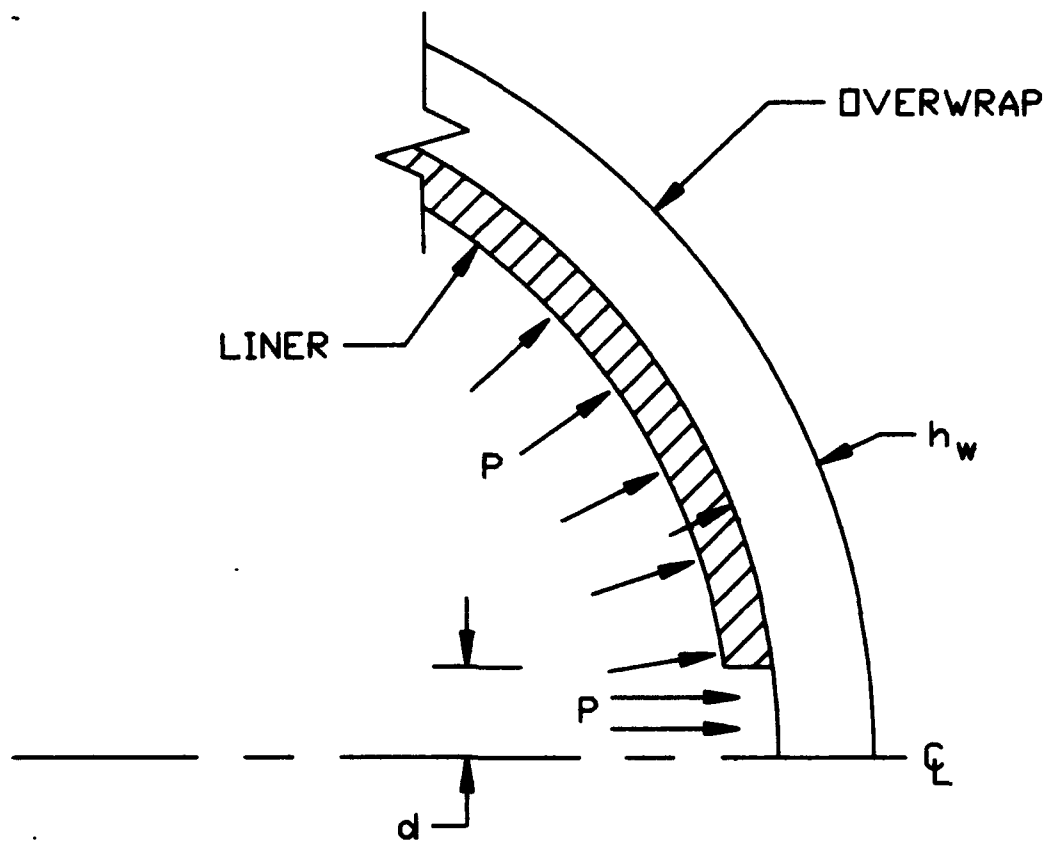


FIG. F-1 IDEALIZATION OF DUCTILE CRACK GEOMETRY

Computing now as an approximation, stresses and strains relative to equilibrium values, we define the problem as the effect of the sudden application of a pressure $P_M = P - P_w = 4000 - 3210 = 790$ psig to the exposed portion of the fiber wrap.

With this approximation, the simplified problem of a sudden stable ductile liner fracture is sketched on Figure F-2.

Assuming the liner remains attached to the fiber overwrap, we estimate the overwrap strains noting that if the crack opening is small compared to the liner thickness, the largest strains will be associated with shear. A force balance on the exposed piece of fiber overwrap gives the average shear strain across the thickness of the overwrap at a distance "d" from the centerline (Figure F-2) as $\gamma = \frac{\tau}{G} = \frac{P_M d}{G h_w}$ (linear crack) ... (A-36)

$$\gamma = \frac{P_M d}{2G h_w} \text{ (circular crack) ... (A-37)}$$

For a crack with an opening equal to the overwrap thickness ($2d = h_w$), for example we have for $G = 1.74 \times 10^6$ psi, $h_w = .23$ and $P_M = 790$ psi, static shear strains, γ , of .00023 in/in for a linear crack and .00011 in/in for a circular hole. These strains are very small compared to the static equilibrium strains in the fiber wrap, even if one assumes a maximum possible dynamic amplification factor of two on static shear strains.

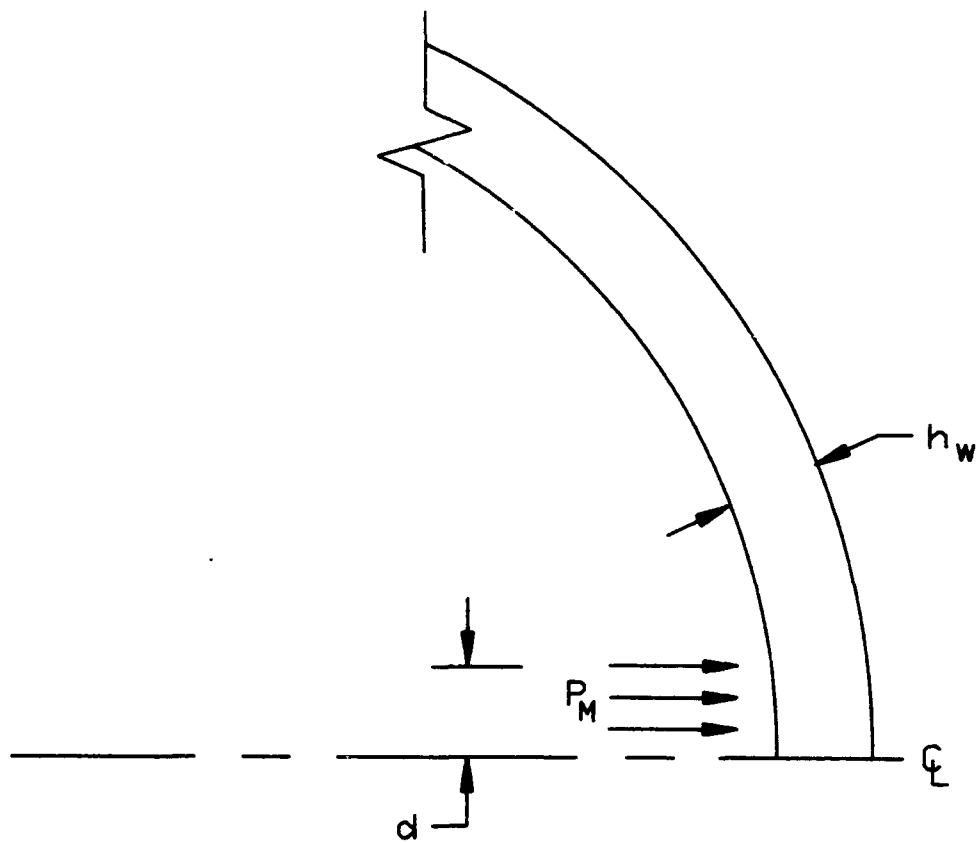


FIG. F-2 SIMPLIFIED CRACK GEOMETRY

F.2 Brittle Failure Mode

The critical liner brittle failure mode was analyzed and test data correlated using the two-dimensional PICES 2D finite difference transient computer code assuming as a worst case an instantaneous complete girth circumference brittle crack model. In addition, simplified lumped 1D spherically symmetric structural models were utilized. These 2D and 1D models have been discussed in detail in Appendix A.

F.2.1 PICES 2D Computer Program Data Correlation

PICES 2D computer runs were made for the brittle failure mode baseline tank (100% fiber thickness) and off-baseline fiber thickness tanks to assess the effects of fiber overwrap thickness, metal liner/fiber interface boundary condition ("slip" or "bond") and pressure, as well as to compare the theoretical PICES 2D results with applicable test data and the simplified 1D spherically symmetrical structural models.

F.2.2 Effect of Fiber Wrap Thickness

For a given fiber wrap thickness, the maximum fiber strains were found to be meridional at an angle of 20° from the pole where fiber thickness is minimum, as shown on Figure 2-15. In general, when comparing one fiber wrapped tank to another having the same type of wrap pattern, peak fiber strains are approximately proportional to the average lumped fiber thickness of each tank.

F.2.3 Effect of Liner/Fiber Interface Boundary Condition

The "slip" interface boundary condition (no friction and no cohesion) gave larger fiber strains, as shown on Figure 2-15, and correlated better with the test data compared to the "bond" interface boundary condition (infinite friction and infinite cohesion) case.

F.2.4 PICES 2D Results Compared to Test Data

The peak fiber strains computed by PICES 2D were reasonable, but conservative, since they were greater than the test as illustrated by the following data.

PICES 2D peak computed meridional strain for 4000 psig pressure was 17,600 micro-inch/inch, including a 3000 micro-in
inch
prestrain (Figure 2-14). The maximum delta meridional strain computed by PICES 2D was then $17600 - 3000 = 14600$ micro in.
inch

Typical measured maximum meridional delta micro strains were 10,600 - 11,900 and 10,600 for pressures of 3800 and 3700 psig, respectively, for tests RV-7 and RV-9 as given in Table F-1.

Taking strain proportional to pressure for small pressure changes, we project computed delta microstrains of $\frac{38}{40} \times 14600 =$
13,870 and $\frac{37}{40} \times 14600 = 13,505$, respectively, at 3800 and 3700

psig pressure. The PICES 2D computer model calculated strains are thus conservative which can be seen by comparing 13505 to 13870 computed delta microstrains with 10600 to 11900 measured delta microstrains. On the average then, PICES 2D computed fiber strains are 22% higher than measured values.

F.2.5 Comparison of PICES 2D Results With 1D Lumped Spherically Symmetric Model Predictions

The PICES 2D computed fiber strains were greater than those predicted by the simple 1D transient model as shown on Figure 2-14. In view of the good agreement between test results and the fiber strains predicted by the simple 1D model, as subsequently discussed in section F.2.6, and the higher computed fiber strains of the PICES 2D, subsequent test data correlation efforts using the PICES 2D computer code were stopped. Instead of modifying the PICES 2D model in the search for improved results, all subsequent test data efforts were performed using the simple 1D structural model(s) for program cost and schedule advantages.

F.2.6 Simple 1D Spherically Symmetric Transient Model Data

Correlation

Figures F-3 to F-6 and 2-17 are test data plots of typical fiber delta strains measured from the tank's prestrained state, i.e., total strain minus prestrain. Superposed on these plots are the delta fiber strains $(\epsilon_1 - \epsilon_i)$, $(\epsilon_2 - \epsilon_i)$ and $(\epsilon_{\max} - \epsilon_i)$ calculated by use of the simple 1D transient spherically symmetric model defined in Appendix A. Table F-1, constructed by utilizing the data of Figures F-3 to F-6 and 2-17, summarizes the comparison between measured and calculated fiber delta strains. It is seen that the agreement between the simple 1D analytic model theory and test data is reasonably good.

COMPARISON OF MEASURED AND CALCULATED TYPICAL DELTA FIBER STRAINS FOR 1D SPHERICALLY SYMMETRIC TRANSIENT MODEL

F-10

RV-7, SG5, WITH 2MS, 100MS, AND 10S TIME DIVISIONS

- SIMILAR TO ANALYTICAL MODEL.

OTHER RV-7 GAGES WITH SIMILAR RESPONSES ARE:

SG3, SG5, SG8, SG9, SG11, SG13, SG15, SG17,

SG18, SG22, SG23

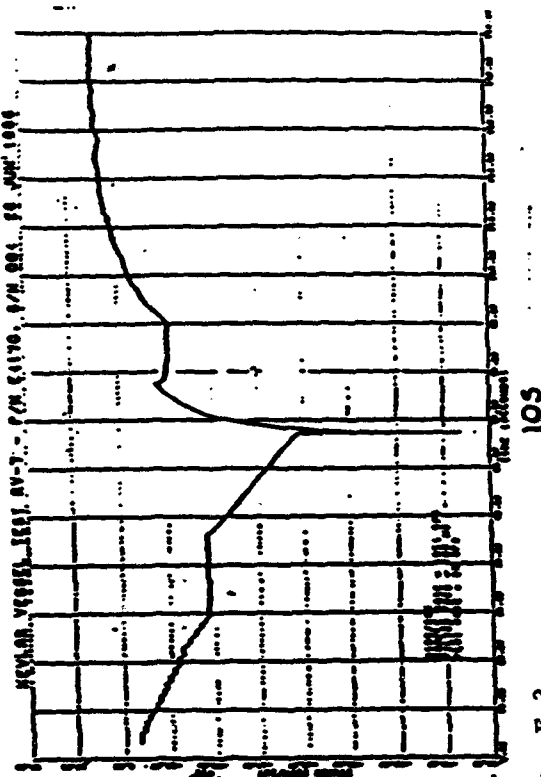
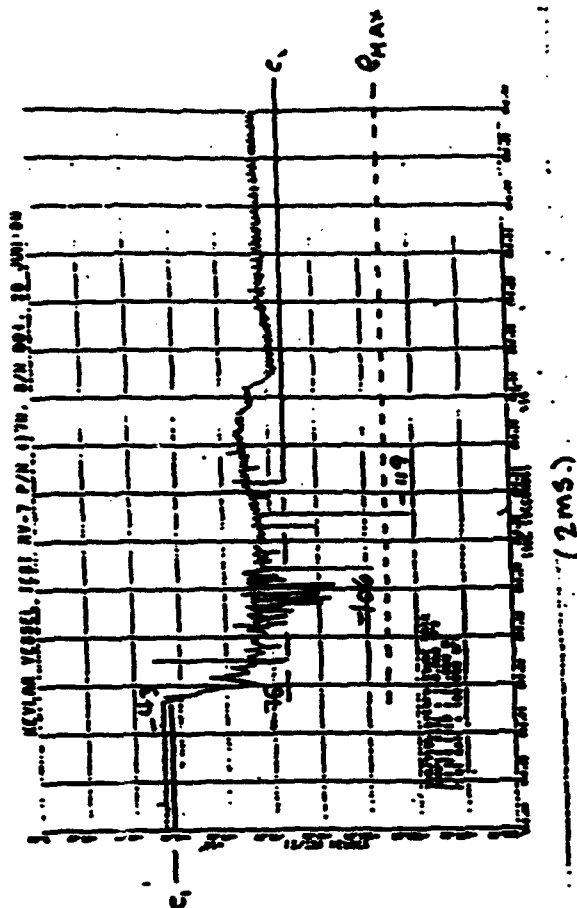
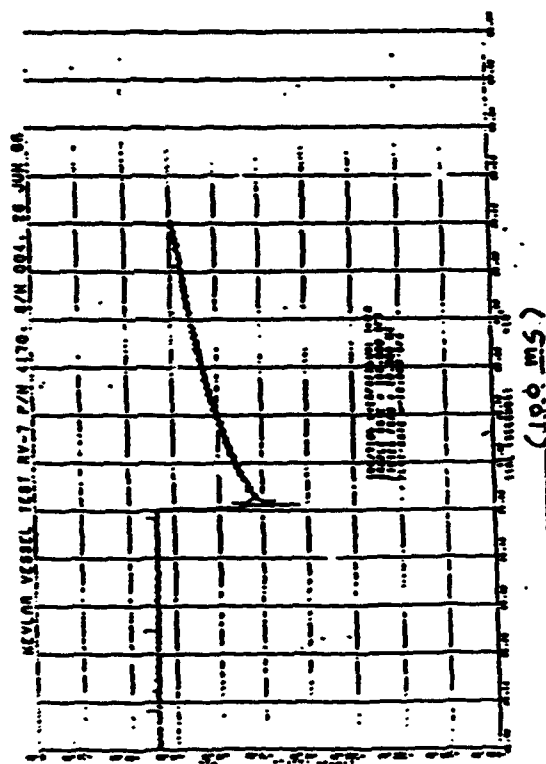


Fig. F-3



(10.0 MS)

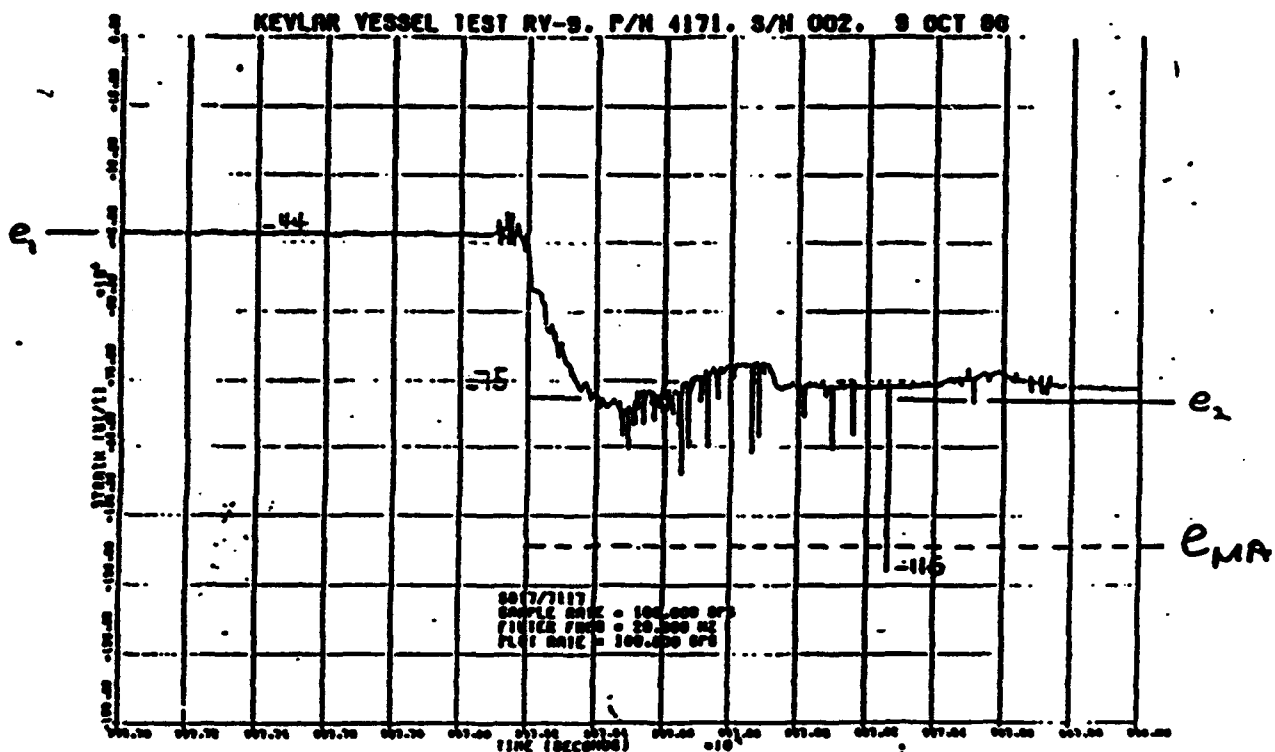


FIG. F-4

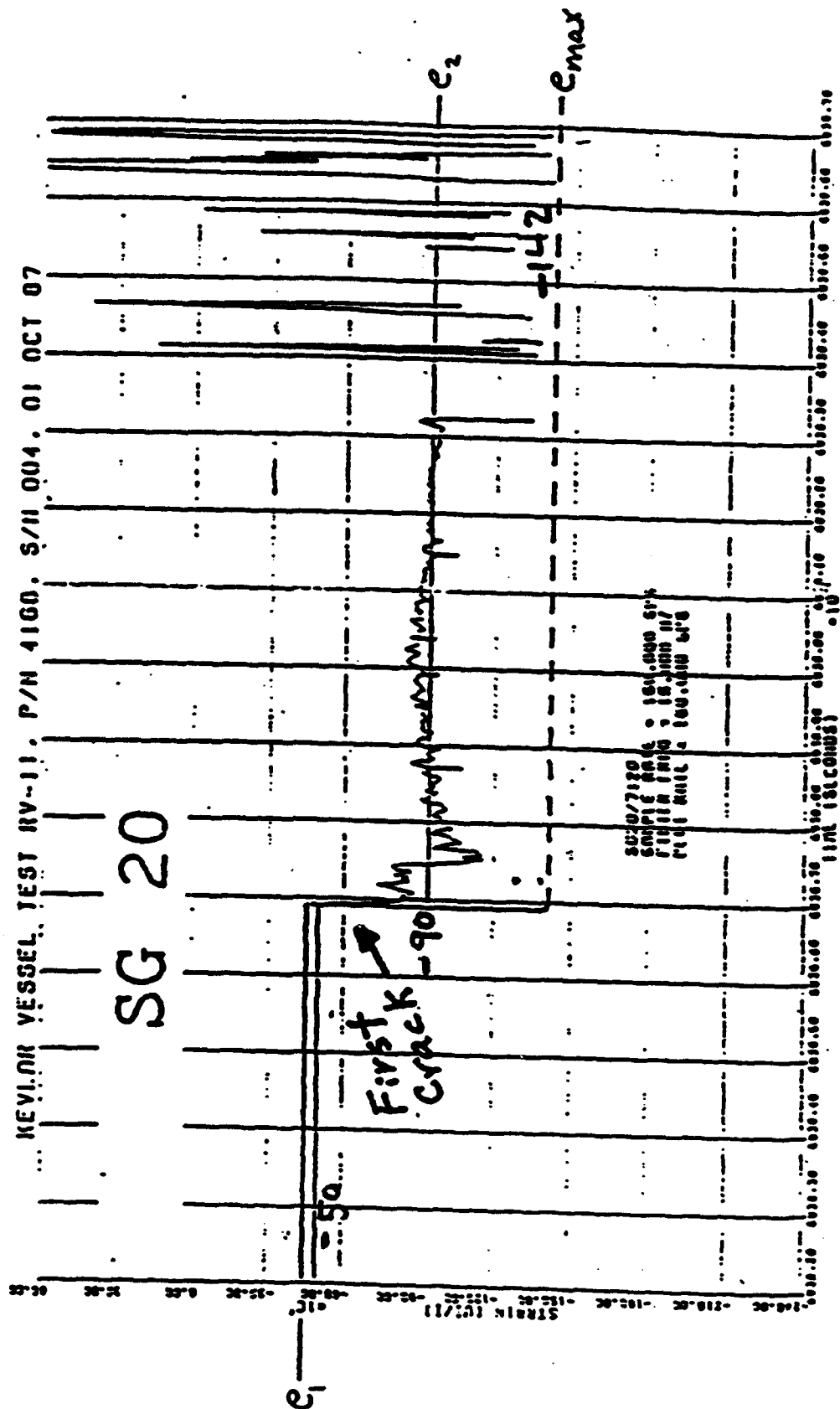


Fig. F-5

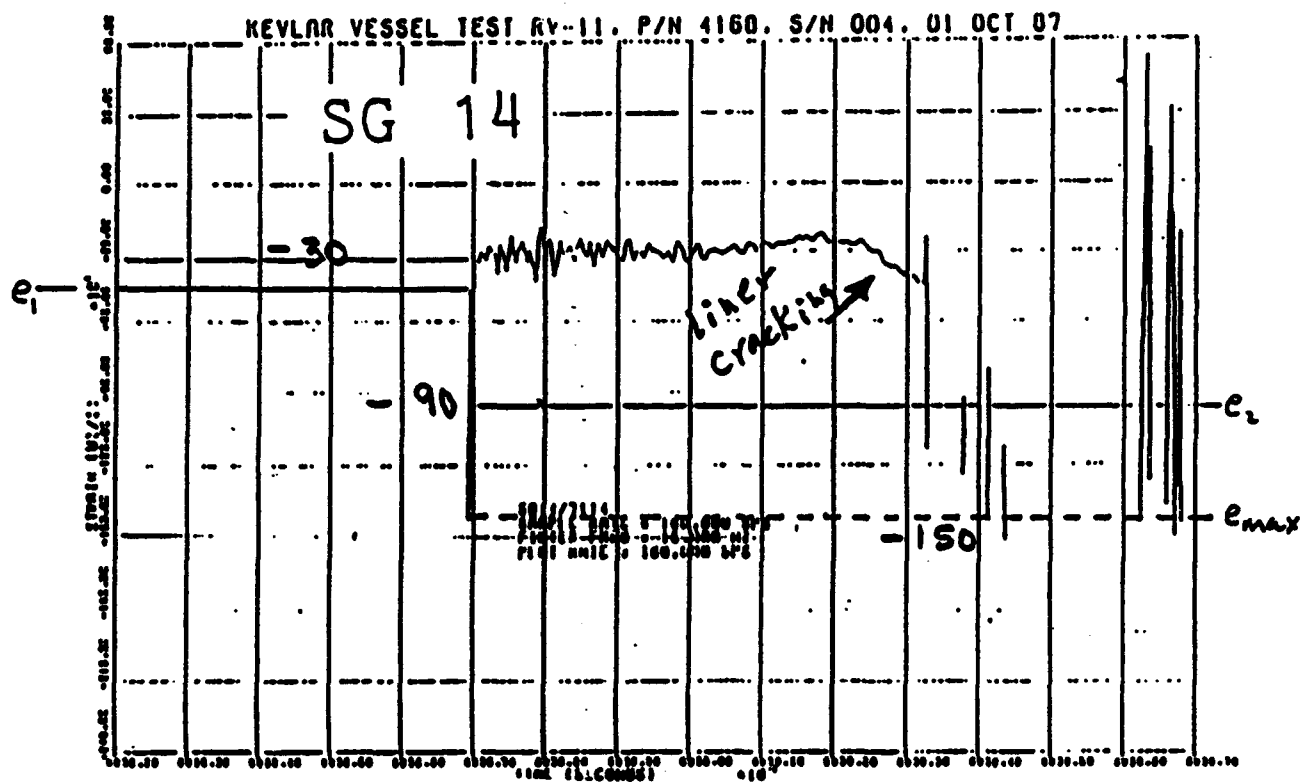


Fig. F-6

F.3 Determination of Effective Dynamic Amplification Factor For Liner Sudden Brittle Rupture Case

The one-dimensional (1D) model involving the concept that at sudden liner failure an additional pressure of dynamic amplification factor Φ times the equilibrium pressure the liner was carrying before failure is transferred to the fiber wrap, has been discussed in detail in Appendix A. Recasting those results in a form convenient for calculating dynamic amplification factor Φ from test data gives,

Fiber equilibrium strain increment,

$$\Delta\epsilon_{fo} = \frac{(RAP)}{E_f t_f} \frac{(k_f/k_M)}{1+k_f/k_M} \dots (A-38)$$

Fiber dynamic spike strain increment =

$$\Delta\epsilon_{fs} = \Phi \frac{(RAP)}{E_f t_f} \left(\frac{1}{1+k_f/k_M} \right) \dots (A-39)$$

Fiber strain increment = $(\epsilon_f - \epsilon_{fi}) = \Delta\epsilon_f =$

$$\Delta\epsilon_{fo} + \Delta\epsilon_{fs} = \frac{(RAP)}{E_f t_f} \left(\frac{1}{1+k_f/k_M} \right) \left\{ \frac{k_f}{k_M} + \Phi \right\} \dots (A-40)$$

Solving (A-39) and (A-40) for dynamic amplification factor Φ yields

$$\Phi = \frac{E_f t_f (1 + k_f/k_M) (\Delta \epsilon_{fs})}{\Delta PR} \dots (A-41) \text{ and}$$

alternatively,

$$\Phi = \frac{E_f t_f (1 + k_f/k_M) (\Delta \epsilon_f) - (k_f)}{\Delta PR \quad k_M} \dots (A-42)$$

Computations utilizing the test data for the critical liner girth embrittled mode and the local boss head weld embrittled mode in equation (A-41) and/or (A-42) gave values of dynamic amplification factor, Φ , in the range of 1.5 to 1.7. Typical calculations are given below.

F.3.1 Girth Weld HAZ Embrittled Mode Data Test RV-11

$$R = 7.64, t_M = .049, t_f = .13, \epsilon_i = .00425,$$

$$\Delta P = 3600, E_f = 19 \times 10^6, \frac{\Delta}{E_M} = \frac{27 \times 10^6}{.7},$$

$$\epsilon_f = .02 \text{ (fibers failed)}$$

$$k_f/k_M = \frac{19 \times .13/2}{17/.7 \times .049} = .6534 \text{ (see section A.3.2)}$$

$$\Delta \epsilon_f = \epsilon_f - \epsilon_i = .02 - .00425 = .01575$$

Using numerical values in (A-42) gives,

$$\Phi = \frac{.01575 (1.6534) \times 19000 \times 130}{7.64 \times 3600} - .6534 = 1.69$$

Test RV-7

$$R = 7.64, \tau_M = .044, \tau_f = .154, \Delta P = 3800,$$

$$E_f = 19 \times 10^6, E_M = \frac{27 \times 10^6}{.7}, \text{ spike } \Delta \epsilon_{fs} = .0083 \text{ (in/in)}$$

$$1 + k_f/k_M = 1 + 19 \times \frac{.154}{\frac{27 \times .044}{.7}} = 1.862$$

Substituting in (A-41) yields,

$$\Phi = \frac{.0083 \times 1.862 \times 19000 \times 154}{3800 \times 7.64} = 1.56$$

Test RV-9

$$R = 7.64, \tau_M = .053, \tau_f = .156, \Delta P = 3700,$$

$$E_f = 19 \times 10^6, E_M = \frac{17 \times 10^6}{.7}, \Delta \epsilon_{fs} = .009 \text{ (in/in)}$$

$$1 + k_f/k_M = 1 + 19 \times \frac{.156}{\frac{27 \times .053}{.7}} = 1.7249$$

Using (A-41) gives,

$$\Phi = \frac{.009 \times 19000 \times 156 \times 1.7249}{3700 \times 7.64} = 1.63$$

F.3.2 Boss/Head Weld HAZ Embrittled Mode Data

Test RV-12A

Membrane theory is not strictly applicable in the boss region since there are bending effects in the liner there.

Use of the extensional strain based fiber to metal

stiffness ratio, $k_f/k_M = \frac{E_f t_f / 2}{E_M t_M}$, defined in Appendix A, in

test data correlation is, therefore, somewhat questionable.

Instead, the approach to test data correlation is

to derive values of an effective k_f/k_M stiffness ratio

based on measured fiber strain data in the vicinity of

the embrittled boss/head weld heat affected zone (HAZ)

region. Noting that the fractions of the pressure carried by the metal and fiber are proportional to the ratio of its

stiffness to the sum of metal and fiber stiffness, one

proceeds as before to calculate the dynamic amplification

factor, ϕ . The calculations are given below.

From Figure E-121 (strain gage 2) in the boss/head weld embrittled area vicinity, the delta fiber strain prior to liner failure at 3750 psig is, $\Delta\epsilon_{fo} = 3500$ micro - in/in.

Substituting numerical values ($R = 10.3$, $E_f = 19 \times 10^6$, $t_f = .192$, $\Delta P = 3750$) into equation A-38 and solving for the effective fiber to metal stiffness ration, k_f/k_M , one obtains $k_f/k_M = .4938$.

Noting from Figure E-121 that the fiber delta strain spike at liner failure, $\Delta\epsilon_{fs} = (14,900 - 3500) = 11,400$ micro strain and using $k_f/k_M = .4938$ together with prior defined numerical parameters in equation A-41, gives the dynamic amplification faction, Φ , value, $\Phi = 1.61$.

Similar calculations utilizing test data from strain gage 1 (Figure E-119) for which $\Delta\epsilon_{fo} = 3400$ micro strain and $\Delta\epsilon_{fs} = 11,200$ micro strain gave a dynamic amplification factor of $\Phi = 1.56$.

APPENDIX G - DETAILED LIST OF FIGURES AND TABLES

This appendix contains a detailed list of figures and tables used to support and amplify the text of this report. For convenience of reference, the following scheme is used to aid figure/table ready identification/location.

1. In general, the first character (number or letter) of a figure or table number (e.g., 1-2, 2-3, A-1, C-2, etc.) identifies the report section or appendix in which it is located.
2. An exception is figure and table numbers with letters (A, B, C ... G) after the numerical digit (e.g., 3C) which refer to figures and/or tables in prior independently prepared documentation used to support this report text.

LIST OF FIGURES

<u>FIGURE NO.</u>		<u>PAGE</u>
1-1	OLYMPUS CRYOFORMED 301 S/S KEVLAR 49 OVERWRAP PRESTRESSED COMPOSITE PRESSURE VESSEL	1-2
1-2	CENTAUR CRYOFORMED 301 S/S KEVLAR 49 OVERWRAP PRESTRESSED COMPOSITE PRESSURE VESSEL	1-4
2-1	PRESTRESSED COMPOSITE TANK COMPONENTS AND REGIONS	2-2
2-2	6" ϕ KEVLAR 49 FIBER WRAP MATERIAL EVALUATION CYLINDER	2-4
2-3	SUB SCALE HYDROGEN EMBRITTLEMENT TEST MODES	2-5
2-4	GLOBALLY HYDROGEN EMBRITTLED PSC LINER AFTER TEST	2-7
2-5	POST TEST VIEW OF HYDROGEN EMBRITTLED ALL METAL TANK	2-8
2-6	NOTCH SHAPE, PRESSURANT TANK, 23" DIA	2-9
2-7	CENTER CRACKED TENSION PANEL	2-10
2-8	COMPACT TENSILE SPECIMEN	2-11
2-9	SCHEMATIC, TEST TANK INSTRUMENTATION	2-14
2-10	SKETCH, TEST SET-UP, AREA 1-52, D PAD	2-15
2-11	WITNESS PANELS SKETCH	2-17
2-12	DYNAMIC FIBER STRAIN SPIKE RV-7 TEST	2-19
2-13	INTENTIONAL "SURE FAIL" BRITTLE LINER RV-10 TEST TANK FRAGMENTS	2-20

LIST OF FIGURES

<u>FIGURE NO.</u>		<u>PAGE</u>
2-14	PISCES 2D VS 1D ANALYTIC MODEL COMPUTED STRAINS	2-23
2-15	TWO-DIMENSIONAL CALCULATION AT 4000 PSI, PEAK MERIDIONAL STRAIN VS. ANGLE	2-24
2-16	FIBER STRAIN VS. TIME-TEST RV-7, STRAIN GAGE NO. 6	2-25
2-17	FIBER STRAIN VS. TIME-TEST RV-9, STRAIN GAGE NO. 14	2-25
2-18	FIBER STRAIN VS TIME-TEST RV-11, STRAIN GAGES 4, 12, 20	2-26
2-19	FIBER STRAIN VS. TIME-TEST RV-11, STRAIN GAGES 2, 10, 18	2-27
2-20	KEVLAR OVERWRAPPED COMPOSITE SPHERE "FAIL SAFE" FIBER OPERATING STRESS VS. METAL OPERATING STRESS INCREMENT	2-29
2-21	FIBER OVERWRAPPED CYLINDER GEOMETRY AND STRESSES	2-32

LIST OF FIGURES

<u>FIGURE NO.</u>		<u>PAGE</u>
2-22	KEVLAR OVERWRAPPED COMPOSITE CYLINDER "FAIL SAFE" HOOP FIBER OPERATING STRESS VS. METAL HOOP OPERATING STRESS INCREMENT	2-33
A-1	BRITTLE LINER ANALYSIS	A-6
A-2	PISCES SHOCK-RESPONSE MODEL DEVELOPMENT	A-8
B-1	SPHERE MATERIAL EVALUATION	B-4
B-2	SUB-SCALE HYDROGEN EMBRITTLEMENT TEST MODES	B-5
B-3	SUB-SCALE HYDROGEN EMBRITTLEMENT VESSEL BURST TEST SCHEMATIC	B-6
E-1	TEST RV-4, TANK PRESSURE VS. TIME	E-45
E-2	TEST RV-4, FIBER STRAIN VS. TIME, STRAIN GAGE 1, 2, 3, 4	E-46
E-3	TEST RV-4, FIBER STRAIN VS. TIME, STRAIN GAGE 7, 8, 10, 11	E-47
E-4	TEST RV-4, FIBER STRAIN VS. TIME, STRAIN GAGE 12, 13, 14, 15	E-48
E-5	TEST RV-4, FIBER STRAIN VS. TIME, STRAIN GAGE 16, 17	E-49

LIST OF FIGURES

<u>FIGURE NO.</u>		<u>PAGE</u>
E-6	TEST RV-4A, TANK PRESSURE VS. TIME	E-50
E-7	TEST RV-4A, FIBER STRAIN VS. TIME, STRAIN GAGE 1, 2, 3, 4	E-51
E-8	TEST RV-4A, FIBER STRAIN VS. TIME, STRAIN GAGE 5, 6, 7, 8	E-52
E-9	TEST RV-4A, FIBER STRAIN VS TIME, STRAIN GAGE 9, 10, 11	E-53
E-10	TEST RV-4A, FIBER STRAIN VS. TIME, STRAIN GAGE 12, 13, 14, 15	E-54
E-11	TEST RV-4A, FIBER STRAIN VS. TIME, STRAIN GAGE 16, 17, 18, 19	E-55
E-12	TEST RV-4A, FIBER STRAIN VS. TIME, STRAIN GAGE 10, 21, 22, 23	E-56
E-13	AFAL TEST AREA 1-52	E-61
E-14	TEST TOWER CAMERA INSTALLATION	E-61
E-15	TANK MOUNTED IN TEST FIXTURE	E-62
E-16	TEST TANK STRAIN GAGE INSTRUMENTATION	E-62
E-17	STRAIN GAGE CLOSE UP VIEW	E-63
E-18	ACOUSTIC EMISSION PROBE INSTALLATION AND CHECK OUT	E-63

LIST OF FIGURES

<u>FIGURE NO.</u>		<u>PAGE</u>
E-19	VIEW OF TEST TANK, BIKINI GAGES AND WITNESS PANELS	E-63
E-20	TEST RV-5, TANK PRESSURE VS. TIME	E-71
E-21	TEST RV-5, FIBER STRAIN VS. TIME, STRAIN GAGE 2, 4	E-72
E-22	TEST RV-5, FIBER STRAIN VS. TIME, STRAIN GAUGE 5, 6, 8	E-73
E-23	TEST RV-5, FIBER STRAIN VS. TIME, STRAIN GAUGE 9, 10, 11	E-74
E-24	TEST RV-5, FIBER STRAIN VS. TIME, STRAIN GAUGE 20, 21, 22, 23	E-75
E-25	TEST RV-5, FIBER STRAIN VS. TIME, STRAIN GAUGE 16, 17, 18, 19	E-76
E-26	TEST RV-5, FIBER STRAIN VS. TIME, STRAIN GAUGE 12, 13, 14, 15	E-77
E-27	TEST RV-5, STRAIN GAGE LOCATIONS	E-78
E-28	TEST RV-5, POST TEST HYDROGEN EMBRITTLED LINER CRACKS, DIE PENETRANT ENHANCED	E-80
E-29	TEST RV-5, CLOSE UP OF POST TEST LINER DIE PENETRANT ENHANCED CRACKS	E-80

LIST OF FIGURES

<u>FIGURE NO.</u>		<u>PAGE</u>
E-30	TEST RV-7, INSTRUMENTED TANK MOUNTED IN TEST STAND	E-82
E-31	TEST RV-7, TANK PRESSURE VS. TIME	E-90
E-32	TEST RV-7, FIBER STRAIN VS. TIME, STRAIN GAUGE 4 (100 HZ, 1024 SPS).	E-91
E-33	TEST RV-7, FIBER STRAIN VS. TIME, STRAIN GAUGE 4 (20,000 HZ, 160,000 SPS)	E-92
E-34	TEST RV-7, FIBER STRAIN VS. TIME, STRAIN GAUGE 4 (20,000 HZ, 160,000 SPS PLOT RATE = 160,000 SPS)	E-93
E-35	TEST RV-7, FIBER STRAIN VS. TIME, STRAIN GAUGE 6 (100 HZ, 1024 SPS)	E-94
E-36	TEST RV-7, FIBER STRAIN VS. TIME, STRAIN GAUGE 6 (20,000 HZ, 160,000 SPS)	E-95
E-37	TEST RV-7, FIBER STRAIN VS. TIME, STRAIN GAUGE 6 (20,000 HZ, 160,000 SPS PLOT RATE = 160,000 SPS)	E-96
E-38	TEST RV-7, FIBER STRAIN VS. TIME, STRAIN GAUGE 12 (100 HZ, 1024 SPS)	E-97
E-39	TEST RV-7, FIBER STRAIN VS. TIME, STRAIN GAUGE 12 (20,000 HZ, 160,000 SPS)	E-98

LIST OF FIGURES

<u>FIGURE NO.</u>		<u>PAGE</u>
E-40	TEST RV-7, FIBER STRAIN VS. TIME, STRAIN GAUGE 12 (20,000 HZ, 160,000 SPS PLOT RATE = 160,000)	E-99
E-41	TEST RV-7, FIBER STRAIN VS. TIME, STRAIN GAUGE 16 (100 HZ, 1024 SPS)	E-100
E-42	TEST RV-7, FIBER STRAIN VS. TIME, STRAIN GAGE 16 (20,000 HZ, 160,000 SPS)	E-101
E-43	TEST RV-7, FIBER STRAIN VS. TIME, STRAIN GAUGE 16 (20,000 HZ, 160,000 SPS PLOT RATE = 160,000 SPS)	E-102
E-44	TEST RV-7, STRAIN GAUGE LOCATIONS	E-103
E-45	TEST RV-7, POST TEST VIEW OF TANK ON TEST STAND	E-106
E-46	TEST RV-7, CONTINUOUS GIRTH CRACKS HIGHLIGHTED BY DIE CHECK	E-108
E-47	TEST RV-7, CLOSE UP OF CONTINUOUS GIRTH CRACKS HIGHLIGHTED BY DIE CHECK	E-108
E-48	TEST RV-7, CONTINUOUSLY CRACKED EMERITTLED GIRTH RING	E-108
E-49	TEST RV-7, CONTINUOUSLY CRACKED EMERITTLED GIRTH RING	E-108
E-50	TEST RV-7 SEPARATED METAL RING	E-109

LIST OF FIGURES

<u>FIGURE NO.</u>		<u>PAGE</u>
E-51	TEST RV-7, SEPARATED METAL RING AND HEADS	E-109
E-52	TEST RV-7, REMOVED FIBER GIRTH RING AND FIBER HEAD PIECES	E-109
E-53	TEST RV-7, REMOVED FIBER HEADS	E-109
E-54	TEST RV-7, INSIDE VIEW, REMOVED FIBER HEADS AND GIRTH RING	E-110
E-55	SMALL LOOSE LINER FRAGMENT	E-111
E-56	TEST RV-9, INSTRUMENTED TANK IN WOODEN HANDLING STAND	E-113
E-57	TEST RV-9, CLOSE UP OF STRAIN GAUGES 12 TO 14	E-113
E-58	TEST RV-9, PRESSURE VS. TIME	E-121
E-59	TEST RV-9, PRESSURE VS. TIME	E-122
E-60	TEST RV-9, STRAIN VS. TIME, STRAIN GAGE 1, 100 HZ	E-123
E-61	TEST RV-9, STRAIN VS. TIME, STRAIN GAUGE 8, 100 HZ	E-124
E-62	TEST RV-9, STRAIN VS. TIME, STRAIN GAUGE 8, 20,000 HZ	E-125
E-63	TEST RV-9, STRAIN VS. TIME, STRAIN GAUGE 8, 20,000 HZ, 160,000 SPS	E-126

LIST OF FIGURES

<u>FIGURE NO.</u>		<u>PAGE</u>
E-64	TEST RV-9, STRAIN VS. TIME, STRAIN GAUGE 9, 100 HZ	E-127
E-65	TEST RV-9, STRAIN VS. TIME, STRAIN GAUGE 9, 20,000 HZ	E-128
E-66	TEST RV-9, STRAIN VS. TIME, STRAIN GAUGE 9, 20,000 HZ, 160,000 SPS	E-129
E-67	TEST RV-9, STRAIN VS. TIME, STRAIN GAUGE 10, 100 HZ	E-130
E-68	TEST RV-9, STRAIN VS. TIME, STRAIN GAGE 10, 20,000 HZ	E-131
E-69	TEST RV-9, STRAIN VS. TIME, STRAIN GAUGE 10, 20,000 HZ, 160,000 SPS	E-132
E-70	TEST RV-9, STRAIN GAUGE LOCATIONS	E-133
E-71	TEST RV-9, STRAIN GAUGE LOCATIONS	E-134
E-72	TEST RV-9, GIRTH CRACK, DIE CHECK ENHANCED	E-136
E-73	TEST RV-9, GIRTH CRACK, DIE CHECK ENHANCED	E-136
E-74	TEST RV-9, CUT FIBER SHELL, EXTERIOR VIEW	E-137
E-75	TEST RV-9, CUT FIBER SHELL, EXTERIOR VIEW	E-137
E-76	TEST RV-9, CUT SHELLS, FIBER/METAL INTERFACES	E-137
E-77	TEST RV-10, PRIOR TEST HYDROGEN EMBRITTLEMENT MODE	E-140

LIST OF FIGURES

<u>FIGURE NO.</u>		<u>PAGE</u>
E-78	TEST RV-10, CLOSE UP, VESSEL ON TEST STAND	E-140
E-79	TEST RV-10, VESSEL ON TEST STAND, BIKINI GAUGES, OVERPRESSURE TRANSDUCERS AND WITNESS PANELS	E-140
E-80	TEST RV-10, CLOSE UP OF STRAIN GAUGE AND THERMOCOUPLE INSTALLATION	E-140
E-81	TEST RV-10, VESSEL OUTLET PRESSURE	E-151
E-82	TEST RV-10, TANK PRESSURE	E-152
E-83	TEST RV-10, STRAIN VS. TIME, STRAIN GAUGE 15	E-153
E-84	TEST RV-10, STRAIN VS. TIME, STRAIN GAUGE 16	E-154
E-85	TEST RV-10, STRAIN VS. TIME, STRAIN GAGE 17	E-155
E-86	TEST RV-10, STRAIN VS. TIME, STRAIN GAGE 11	E-156
E-87	TEST RV-10, STRAIN GAUGE LOCATIONS	E-157
E-88	TEST RV-10, STRAIN GAUGE LOCATIONS	E-158
E-89	TEST RV-10, OVERPRESSURE VS. TIME, TRANSDUCER 5	E-159
E-90	TEST RV-10, OVERPRESSURE VS. TIME, TRANSDUCER 5, MAGNIFIED TIME SCALE	E-160
E-91	TEST RV-10, OVERPRESSURE VS. TIME, TRANSDUCER 3	E-161

LIST OF FIGURES

<u>FIGURE NO.</u>		<u>PAGE</u>
E-92	TEST RV-10, OVERPRESSURE VS. TIME, TRANSDUCER 3, MAGNIFIED TIME SCALE	E-162
E-93	TEST RV-10, POST TEST VIEW OF DAMAGED TEST STAND, BIKINI GAUGES, OVERPRESSURE TRANSDUCERS AND WITNESS PANELS	E-164
E-94	TEST RV-10, POST TEST CLOSE UP VIEW OF DAMAGED TEST STAND AND FIBER OVERWRAP FRAGMENTS	E-164
E-95	TEST RV-10, FIBER OVERWRAP FRAGMENT	E-164
E-96	TEST RV-10, FRAGMENT EMBEDDED IN WITNESS PANEL	E-164
E-97	TEST RV-10, POST TEST LINER FRAGMENT DEBRIS	E-165
E-98	TEST RV-10, LINER FRAGMENT	E-165
E-99	TEST RV-11, COMPOSITE TANK MOUNTED IN TEST STAND	E-168
E-100	TEST RV-11, STRAIN GAGE INSTALLATION	E-168
E-101	TEST RV-11, STRAIN GAGE INSTALLATION	E-168
E-102	TEST RV-11, TANK PRESSURE VS. TIME	E-185
E-103	TEST RV-11, TANK PRESSURE VS. TIME	E-186
E-104	TEST RV-11, STRAIN VS. TIME, STRAIN GAUGE 24	E-187
E-105	TEST RV-11, STRAIN VS. TIME, STRAIN GAUGE 6	E-188
E-106	TEST RV-11, STRAIN VS. TIME, STRAIN GAUGES 4, 12, 20	E-189

LIST OF FIGURES

<u>FIGURE NO.</u>		<u>PAGE</u>
E-107	TEST RV-11, STRAIN VS. TIME, STRAIN GAUGES 8, 16, 24	E-190
E-108	TEST RV-11, DIGITAL DATA, PRESSURE AND SG 24 VS. TIME	E-191
E-109	TEST RV-11, STRAIN GAUGE LOCATIONS STAND	E-192
E-110	TEST RV-11, POST TEST VIEW OF DAMAGED TEST STAND	E-195
E-111	TEST RV-11, FRAGMENT DISTRIBUTION	E-195
E-112	TEST RV-12, INSTRUMENTED TANK MOUNTED IN TEST STAND	E-197
E-113	TEST RV-12, POST TEST CLOSE UP VIEW OF TANK	E-199
E-114	TEST RV-12, POST TEST EMBRITTLED LINER BOSS REGION CRACKS	E-201
E-115	TEST RV-12A, PRE-TEST LINER HYDROGEN EMBRITTLEMENT MODE	E-206
E-116	TEST RV-12A, INSTRUMENTED TANK MOUNTED IN TEST STAND	E-206
E-117	TEST RV-12A, TEST AREA WITH CAMERA TOWER	E-207
E-118	TEST RV-12A, TANK PRESSURE VS. TIME	E-217

LIST OF FIGURES

<u>FIGURE NO.</u>		<u>PAGE</u>
E-119	TEST RV-12A, STRAIN VS. TIME, STRAIN GAUGE 1 (100 HZ)	E-218
E-120	TEST RV-12A, STRAIN VS. TIME, STRAIN GAUGE 1 (40,000 HZ)	E-219
E-121	TEST RV-12A, STRAIN VS. TIME, STRAIN GAUGE 2 (100 HZ)	E-220
E-122	TEST RV-12A, STRAIN VS. TIME, STRAIN GAUGE 2 (40,000 HZ)	E-221
E-123	TEST RV-12A, STRAIN VS. TIME, STRAIN GAUGE 24	E-222
E-124	TEST RV-12A, STRAIN VS. TIME, STRAIN GAUGE 4	E-223
E-125	TEST RV-12A, STRAIN VS. TIME, STRAIN GAUGE 14	E-224
E-126	TEST RV-12A, STRAIN VS. TIME, STRAIN GAUGE 16	E-225
E-127	TEST RV-12A, STRAIN VS. TIME, STRAIN GAUGE 6	E-226
E-128	TEST RV-12A, STRAIN VS. TIME, STRAIN GAUGE 8	E-227
E-129	TEST RV-12A, STRAIN VS. TIME, STRAIN GAUGE 5	E-228
E-130	TEST RV-12A, STRAIN GAUGE LOCATIONS	E-229
E-131	TEST RV-12A, STRAIN GAUGE LOCATIONS	E-230
E-132	TEST RV-12A, TEST CONSOLE ACTIVITY	E-231
E-133	TEST RV-12A, POST TEST VIEW OF FIBER DAMAGE	E-231
E-134	TEST RV-12A, POST TEST CLOSE UP VIEW OF FIBER DAMAGE	E-233

LIST OF FIGURES

<u>FIGURE NO.</u>		<u>PAGE</u>
E-135	TEST RV-12A, EMERITTLED BOSS HAZ LINER CRACKS	E-233
E-136	TEST RV-12A, CLOSE UP OF EMERITTLED BOSS HAZ LINER CRACKS	E-233
E-137	TEST RV-14, TANK PRESSURE VS. TIME	E-246
E-138	TEST RV-14, STRAIN VS. TIME, STRAIN GAUGE 15	E-247
E-139	TEST RV-14, STRAIN VS. TIME, STRAIN GAUGE 17E-141 STRAIN GAUGE LOCATIONS	E-248
E-140	TEST RV-14, STRAIN GAUGE LOCATIONS	E-249
E-141	TEST RV-14 STRAIN GAUGE LOCATIONS	E-250
E-142	TEST RV-14A, TANK PRESSURE VS. TIME	E-263
E-143	TEST RV-14A, STRAIN VS. TIME, STRAIN GAUGE 24	E-264
E-144	TEST RV-14A, STRAIN VS. TIME, STRAIN GAUGE 3	E-265
E-145	TEST RV-14A, STRAIN VS. TIME, STRAIN GAUGE 6	E-266
E-146	TEST RV-14A, STRAIN VS. TIME, STRAIN GAUGE 12	E-267
E-147	TEST RV-14A, STRAIN VS. TIME, STRAIN GAUGE 15	E-268
E-148	TEST RV-14A, STRAIN VS. TIME, STRAIN GAUGE 16	E-269
E-149	TEST RV-14A, CUT APART POST TEST TANK, EXTERIOR VIEW	E-270
E-150	TEST RV-14A, CUT APART POST TEST TANK, INTERIOR VIEW	E-271

LIST OF FIGURES

<u>FIGURE NO.</u>		<u>PAGE</u>
E-151	TEST RV-14A, POST TEST EMERITTLED GIRTH CONTINUOUS CRACK	E-272
E-152	TEST RV-14A, POST TEST EMERITTLED GIRTH CONTINUOUS CRACK	E-272
F-1	IDEALIZATION OF DUCTILE CRACK GEOMETRY	F-3
F-2	SIMPLIFIED DUCTILE CRACK GEOMETRY	F-5
F-3	TEST RV-7, SG5 WITH 2 MS, 100 MS AND 10S TIME DIVISIONS	F-11
F-4	TEST RV-9, SG17	F-12
F-5	TEST RV-11, SG 20	F-13
F-6	TEST RV-11, SG 14	F-14
1A	SPHERE MATERIAL EVALUATION SKC 11341	B-27
2A	SUBSCALE HYDROGEN EMERITTEMENT VESSEL BURST TEST SCHEMATIC	B-28
3A	SUBSCALE HYDROGEN EMERITTEMENT TEST MODES	B-29
4A	HYDROGEN EMERITTEMENT TEST 2 P/N D3912, S/N 4	B-31
5A	HYDROGEN EMERITTEMENT SUBSCALE TEST D3912 S/N 006	B-32
6A	HYDROGEN EMERITTEMENT SUBSCALE TEST D3912 MOD, S/N 006	B-33

LIST OF FIGURES

<u>FIGURE NO.</u>		<u>PAGE</u>
7A	HYDROGEN EMBRITTLEMENT SUBSCALE TEST D3912 MOD, S/N 006	B-34
8A	HYDROGEN EMBRITTLEMENT SUBSCALE TEST D3912 MOD, S/N 006	B-35
9A	HYDROGEN EMBRITTLEMENT SUBSCALE TEST D3912 MOD, S/N 3 HT 88019	B-36
10A	HYDROGEN EMBRITTLEMENT SUBSCALE TEST D3912 MOD, S/N 3 HT 88019	B-37
11A	HYDROGEN EMBRITTLEMENT SUBSCALE TEST D3912, S/N 3 HT 88019	B-38
12A	HYDROGEN EMBRITTLEMENT SUBSCALE TEST D3912, S/N 3 HT 88019	B-39
13A	HYDROGEN EMBRITTLEMENT SUBSCALE TEST D3912, S/N 3 HT 88019	B-40
14A	HYDROGEN EMBRITTLEMENT SUBSCALE TEST D3912, S/N 3 HT 88019	B-41
15A	LINER INDUCED FAILURE TEST	B-50
1B	CENTER CRACKED TENSION PANEL	C-12
2B	.5T - CT SPECIMEN ARDE	C-13
3B	11" ϕ CRYOFORMED 301 CRES SPHERE	C-17

LIST OF FIGURES

<u>FIGURE NO.</u>		<u>PAGE</u>
4B	11" Ø KEVLAR -49 OVERWRAPPED CRYOFORMED 301 CRES	C-18
5B	PRESSURANT TANK, 23" DIA	C-19
6B	PRESSURANT TANK, 23" DIA, INITIAL FLAW GEOMETRY	C-20
7B	LBB EVALUATION CRYOFORMED 301 CRES SPHERICAL TANK S/N 113, D = 23", FLAW IN WELD METAL	C-21
8B	I.D. CRACK AFTER LBB DEMONSTRATION, PRESSURANT TANK, 23" DIA	C-23
9B	LBB TEST, PRESSURANT TANK, 23" DIA	C-24
10B	BASE METAL (500X-ELECTROLYTIC OXALIC ACID ETCH)	C-25
11B	SINGLE PASS SQUARE BUTT WELD, MULTI-PASS MODIFIED U - PREP WELD (500X - ELECTROLYTIC OXALIC ACID ETCH)	C-26
1C	CENTER CRACKED TENSION PANEL DIMENSION IN INCHES	C-48
2C	CLIP GAGE ATTACHMENT SET UP FOR 6 INCH GAGE LENGTHS	C-49
3C	VIEW OF DSST GAGE AND TRAVELING STAGE MICROSCOPE FOR MEASURING SLOW-STABLE CRACK GROWTH	C-49
4C	1/2T COMPACT SPECIMEN	C-50
5C	REPRESENTATIVE LOAD-DISPLACEMENT RECORD, CTT PANEL	C-51

LIST OF FIGURES

<u>FIGURE NO.</u>		<u>PAGE</u>
6C	REPRESENTATIVE LOAD-DISPLACEMENT RECORD, COMPACT SPECIMEN	C-52
7C	MAGNIFIED VIEW OF CRACK TIP REGION AFTER CONSIDERABLE SLOW-STABLE CRACK EXTENSION	C-53
8C	COMPACT SPECIMEN AND CENTER CRACKED PANEL J_R - CURVES FOR UNAGED BASE METAL	C-54
9C	COMPACT SPECIMEN AND CENTER CRACKED PANEL J_R -CURVES FOR UNAGED BASE METAL	C-55
10C	COMPACT SPECIMEN AND CENTER CRACKED PANEL J_R - CURVES FOR UNAGED WELD METAL	C-56
11C	COMPACT SPECIMEN AND CENTER CRACKED PANEL J_R - CURVES FOR AGED WELD METAL	C-57
1D	CRACK PROPAGATION FOR LBB	C-107
2D	BASE METAL MICROSTRUCTURE (500X)	C-108
3D	WELD METAL MICROSTRUCTURE (500X)	C-109
4D	TYPICAL CRYOFORMED WELD CTC R-CURVE, 301 BASE METAL/308L WELD WIRE	C-109
5D	SPHERICAL SHELL CORRECTION FACTOR, $F_S(c)$	C-111

LIST OF FIGURES

<u>FIGURE NO.</u>		<u>PAGE</u>
6D	LEB EVALUATION FOR TANK S/N 104, D = 11 IN. FLAW IN BASE METAL	C-112
7D	LEB EVALUATION FOR TANK S/N 105, D = 11 IN, FLAW IN BASE METAL	C-112
8D	LEB EVALUATION FOR TANK S/N 003, D = 11 IN, FLAW IN WELD METAL	C-113
9D	LEB EVALUATION FOR TANK S/N 113, D = 23 IN, FLAW IN WELD METAL	C-113
10D	EDM CRACK STARTER NOTCH IN TANK S/N 113	C-114
11D	FLUID LEAKAGE AT $P_{MAX} = 4850$ PSI, TANK S/N 113	C-114
12D	BREAKTHROUGH OF CRACK ON ID OF TANK S/N 113	C-114
13D	FRACTURE SURFACE OF LEAKING CRACK, TANK S/N 113, EDM NOTCH ON O.D.	C-116
2-1E	6" ϕ CYLINDRICAL FIBER WRAPPED VESSEL	D-8
2-2E	PHOTO-TEST SET-UP	D-9
2-3E	PHOTO-VESSEL 030	D-10
2-4E	PHOTO-VESSEL 030	D-11
2-5E	PHOTO-VESSEL 028	D-12
2-6E	PHOTO-VESSEL 028	D-13

LIST OF FIGURES

<u>FIGURE NO.</u>		<u>PAGE</u>
2-7E	SCHEMATIC 6" Ø CYLINDER TEST SET-UP	D-15
3-1E	PRESSURE VS. HOOP STRAIN S/N 030 (GAGE C1)	D-17
3-2E	PRESSURE VS. HELICAL STRAIN S/N 030 (GAGE D2)	D-18
3-3E	PRESSURE VS. AXIAL STRAIN S/N 030 (GAGE L1)	D-19
3-4E	PRESSURE VS. HOOP STRAIN S/N 028 (GAGE C1, C2)	D-20
4-1E	CYLINDER FIBER WRAP, STRESSES, CONFIGURATION AND PRESSURE LOAD	D-24

LIST OF FIGURES

<u>FIGURE NO.</u>		<u>PAGE</u>
1F	SCHEMATIC TEST TANK INSTRUMENTATION	E-17
2F	STRAIN GAGE MOUNTING REQUIREMENTS	E-19
3F	BASIC STRAIN GAGE RECORDING SYSTEM	E-21
4F	MECHANICAL MEASUREMENT INSTRUMENTATION SYSTEM	E-22
5F	FOTONIC FIBEROPTIC NON-CONTACT SENSOR	E-24
6F	TEMPERATURE MEASUREMENT SYSTEM	E-26
7F	PIEZO ELECTRIC PRESSURE MEASUREMENT SYSTEM	E-28
1G	SKETCH, STRAIN GAGE MOUNTING	E-5

LIST OF TABLES

<u>TABLE NO.</u>		<u>PAGE</u>
E-1	16" ϕ AND 22" ϕ PSC VESSEL TEST MATRIX	E-34 TO E-36
B-1	SUB-SCALE HYDROGEN EMBRITTLEMENT TEST DATA	B-3
F-1	COMPARISON OF MEASURED AND CALCULATED TYPICAL DELTA FIBER STRAINS	F-10
1B	TEST MATRIX - SPECIMEN IDENTIFICATION	C-9
2B	SUMMARY DATA FROM R-CURVE TESTS OF CTT SPECIMENS	C-10
3B	SUMMARY DATA COMPARING OCT AND CT RESULTS	C-11
4B	ROOM TEMPERATURE FRACTURE TOUGHNESS DATA	C-16
5B	TEST PARAMETERS	C-22
6B	CYCLES TO LEAK	C-22
7B	SUSTAINED LOAD TESTS	C-22
8B	LEB VERIFICATION	C-22
1C	TEST MATRIX - SPECIMEN IDENTIFICATION	C-42
2C	SUMMARY DATA FROM R-CURVE TESTS OF CTT SPECIMENS	C-43

LIST OF TABLES

<u>TABLE NO.</u>		<u>PAGE</u>
3C	SUMMARY DATA COMPARING OCT AND CT RESULTS	C-44
4C	COMPARISON OF VISUAL VS COMPLIANCE INDICATED CRACK GROWTH AT SELECTED UNLOADING POINTS FOR OCT SPECIMENS	C-45
5C	COMPARISON OF VISUAL VS COMPLIANCE INDICATED CRACK GROWTH AT SELECTED UNLOADING POINTS FOR CT SPECIMENS	C-46
6C	FATIGUE PRECRACKING INFORMATION	C-47
1D	ROOM TEMPERATURE FRACTURE TOUGHNESS DATA	C-110
2D	TEST PARAMETERS	C-115
3D	CYCLES TO LEAK	C-115
4D	SUSTAINED LOAD TESTS	C-115
5D	LEB VERIFICATION	C-115